AN EXPERIMENTAL STUDY OF FRICTION BETWEEN SKIN AND NONWOVEN FABRICS

VASILEIOS ASIMAKOPOULOS

CONTINENCE AND SKIN TECHNOLOGY GROUP
DEPARTMENT OF MEDICAL PHYSICS AND BIOENGINEERING
UNIVERSITY COLLEGE LONDON

SUPERVISORS

PROF ALAN M. COTTENDEN
DR MARTIN E. FRY

THESIS SUBMITED FOR THE DEGREE OF DOCTOR OF PHILOSOPHY (PH.D) AT THE UNIVERSITY OF LONDON

Declaration

I, Vasileios Asimakopoulos, confirm that the work presented in this thesis is my own. Where information has been derived from other sources, I confirm that this has been indicated in the thesis.

Vasileios Asimakopoulos
26 August, 2013

Acknowledgements

I would like to express my gratitude to my supervisors Prof Alan Cottenden and Dr Martin Fry. I would like to thank especially Prof Alan Cottenden who stood by me and believed in me in times I doubted about myself. I never really understood the quotation from Alexander the Great: "*I am indebted to my father for living, but to my teacher for living well.*", until I met a teacher of his stature.

Without the help of my colleagues, Margaret Macaulay and Sabrina Falloon from Continence and Skin Technology Group who prepared the ethics committee application, helped with the recruitment of the participants and the conduction of the experiments, this project could not be completed. The personnel of the incontinence clinic of Prof Malone Lee of the first floor of Clerkenwell Building in Archway Campus and of Cheverton Lodge nursing home were also really helpful during the recruitment of the participants and conduction of my experiments. Most of all, I congratulate the volunteers for the volar forearm experiments, who accepted to participate in my research, holding themselves still in a chair, in many cases for more than two hours.

I also thank David Cottenden for his extremely valuable support during my project and Tal Hart, who I really doubt if he will ever understand how much he helped me.

Of course, I could not forget Raquel Santamarta, a favourite colleague for the first two years of my project and Mihaela Soric with whom I had the most exciting and passionate conversations.

During the last period of my project, Damon McNally contributed by processing the data of the volar forearm experiments, helping me to the better presentation of the graphs.

It would be ungrateful not to thank Derek Williams – Wynn of Polymer Systems Technology Ltd for spending several hours in his office and exchanging numerous emails with Prof Alan Cottenden and me, trying to understand the needs of my experiments and provide the suitable material which would satisfy the conditions the research demanded. Derek did everything, knowing he would not receive the proper compensation for his time; his only motivation was to help research.

Above all, I thank my family for their unconditional generosity and love during the struggles and joys of this project.

Abstract

Incontinence is a common health problem among the human population, especially the female population. Although there have been many efforts to deal with it in a sufficient way, for the incontinence sufferers there is no full cure. A way to deal with this large portion of incontinence sufferers is pads.

The continuous usage of pads creates some problems, though. The problems associated with skin are described by the term "Incontinence Associated Dermatitis", which includes all the diseases incontinence can induce in the skin. The most common cause of these diseases is friction between pads and skin.

In order to describe friction, Cottenden developed a mathematical model (Cottenden, 2010) for describing friction between a conformable sheet and a curved surface. Even though the general equation from this model is intractable, the model can be solved for specific surfaces, like cylinders and cones. Previous work has already validated the model for strips of nonwoven fabric on rigid convex prisms and low – half angle cones (Cottenden et al., 2008a). The aim of this project was to extend the validation to (i) large – half angle rigid cones (whose surfaces approximate to portions of the body); (ii) human volar forearms and (iii) highly compliant cylinders.

In the first part of the project I validated the model for an example nonwoven fabric on rigid (Plaster of Paris) cones with half angles of 25°, 35° and 45°. As predicted by the model, the data for all fabric footprints on all cones fell on the same master curve, within experimental error.

In the second part of the project, I used the volar forearms of young and older female participants. In this way I had the opportunity to test the model on real human skin (smooth and wrinkled) and different substrates (firm and flaccid tissues) as they varied between young and older subjects. Moreover, I observed the changing geometry of arms during experiments, especially the behaviour of – often wrinkled and flaccid – older arms and see how the model responded. I used strips of five different nonwoven fabrics (typical of those used to face pads) investigating not only how the substrate affected the model, but also how behaviour varied between fabrics. The agreement between experimental data and model predictions was excellent for all fabrics with all volar forearms, including the most wrinkled and flaccid.

In the third part of the project, I used the same five fabrics on compliant cylinders made of soft silicone membrane "skins". These cylinders helped me investigate how the model responded for extreme deformations (rucking) which were much greater than humans could have tolerated. Again, agreement between experiment and model was remarkably good.

In summary, all three blocks of experimental work provided further validation of Cottenden's model, increasing confidence that it can be used in future work to understand friction over the curved surfaces of the body and help develop products kinder to the skin.

Table of Contents

List of Tables

List of Figures

Notation

General

F	Force
T	Pulling force, identical to T_1 when convex prism approximates to cylinder
T_t	Tensometer force
m	Mass
g	Acceleration of gravity
μ	Coefficient of friction
μ_s	Coefficient of static friction
μ_d	Coefficient of dynamic friction
R^2	Correlation coefficient

Cones

Symbols as presented in Figure 3.1

T_0	Tension at the direction of pulling force of the compliant sheet from the trailing edge of cone surface to the pulling edge of the compliant sheet
T_{yy}	Tension at the direction of pulling force of the compliant sheet from the trailing edge of cone surface to the pulling edge of the compliant sheet
C_{yy}	Curvature of the fabric

Symbols as presented in Figure 3.4 and Figure 3.5

α	Cone half angle
S	Cone layout angle

Symbols as presented in Figure 3.14

T_1	Pulling force
T_2	Tension at the direction of the strip of fabric from the trailing edge of guide cylinder 1 to the trailing edge of cone surface
T_3	Tension at the direction of the strip of fabric from the triling edge of guide cylinder 1 to the trailing edge of cone surface
T_4	Tension at the direction of the stip of fabric from the trailing edge of guide cylinder 1 to the dead weight load
θ_1	Arc of angle of contact between the trailing edge of the cone to the direction of the dead weight mass and the perpendicular line to the strip on the cone.
θ_2	Arc of angle of contact between the trailing edge of the cone to the direction of the tensometer and the perpendicular line to the strip on the cone.
β_1	Arc of angle of contact between the strip of fabric and guide cylinder 1
β_2	Arc of angle of contact between the strip of fabric and guide cylinder 2

Symbols as presented in Figure 4.2

θ	Arc of angle of contact between the convex prism and the compliant sheet
φ	Angle between the pulling force and the horizontal as defined by the tensometer
α_m	Mean value of cone half angle
μ_p	True value of coefficient of friction of guide cylinders
μ'_p	Measured value of coefficient of friction of cylinders
β	Arc of angle of contact between strip of fabric and cylinder

Bending stiffness

Symbols as presented in Figure 4.4 and Figure 4.5

δ_{max}	Maximum deflection of strip of fabric
l	Length of strip of fabric under deflection
ω	Linear weight density
E	Young's modulus
I	Second moment of inertia
t	Thickness of cuboid of compliant material

Chapter 1 Introduction

The initial idea for this project came from a very common problem that particularly affects women, but also many men all over the world, incontinence. Even though is not a popular topic for study, incontinence is a wide spread problem in the global population, creating everyday problems for people of all ages, although the problem is more intense in elderly ages. For men this problem is less common than for women, but it does exist making the need of comforting the lives of millions of incontinence sufferers even more demanding.

In many cases the problem of incontinence can be treated through surgery or dealt with using psychotherapy, drugs or special techniques of making the function of pelvic organs more effective. Unfortunately, incontinence can often not be cured, so that many sufferers must manage their problem through catheters or incontinence pads.

Incontinence pads come in touch with the skin in the "pad area", which involves the genital and anal regions. Faeces or more frequently urine is in liquid or semi liquid form, causing the wetness of the pad and subsequently hydration of the parts of the skin that comes in touch with the pad.

Friction between pads and damp skin is the main cause of sore skin. Sore skin needs additional treatment, a factor that burdens the health systems of many countries with substantial expenses. A factor which shows the financial importance of incontinence for the health system is that the UK market for pads and appliances to contain incontinence is estimated at £143m, of which pads consume more than half (about 58%) (Altman et al., 2009), so everything that involves the facilitating of life of incontinence pad users is of high importance and of great financial significance.

Exactly this fact was the trigger for my project, while during my work I realised that even skin friction is an extremely interesting phenomenon, a few papers have been published; most of them from a purely academic interest, without assessing the needs of the real world. Initially, Professor Alan Cottenden started studying the phenomenon, in an attempt to understand it and improve the lives of incontinence sufferers. Rebecca Wong in her PhD thesis (Wong, 2008) assessed the methods of exploring skin friction and developed her own methodology for measuring it. Subsequently, David Cottenden in his PhD thesis developed a general model for investigating friction between fabrics and substrates, which he validated for simple geometries. This was the starting point for my work which aimed to test Cottenden's model for more complex geometries.

My project comprises three main blocks, each block successively testing Cottenden's model for a more complex situation. The first, presented in Chapter 3, tests the model for fabrics drawn over the surface of rigid large half – angle cones made of Plaster of Paris. Cones, because they simulate regions of human body, large half – angle because the model has already been validated for small half – angles (Karavokiros, 2007). Also, I use rigid cones to isolate the geometrical factor of the cone, excluding the complexity associated with compliant materials that may change shape significantly during an experiment.

Second, in Chapter 4 I test the model on human volar forearms, where I achieve two goals. First, I use real human skin and underlying soft tissues and I see how the model responds. Second, although forearms approximate to convex prisms, their geometry is not stable throughout the measurement: rucking changes the gross geometry of the fabric/skin interface and may also introduce rucks into the

skin. So, it is very interesting to observe the behaviour of the model when geometry does not stay constant throughout an experiment.

Third, in Chapter 5 I use compliant cylinders to test the model in extreme conditions of rucking. Throughout the experiments the cylinders deform heavily, but after the end of the run they return to their initial state. The core of the cylinders is made of silicone gel while I use as skin a low modulus silicone membrane for increased frictional properties. For better interpretation of my results I also construct a rigid cylinder covered with the same silicone membrane and I perform measurements on it.

Finally, in Chapter 6 I summarise my results, quoting the outcome of the experiments and suggesting future streams of research for investigating the phenomenon of skin friction further.

Skin friction is an extremely broad phenomenon which just in recent years started being studied more intensely. Few papers are published and purely about friction even fewer. There is a lot of potential in this particular field for future researchers and a lot of ground to cover in relation to other scientific fields.

Chapter 2 Literature review

2.1 Incontinence

Incontinence is the unintended loss of urine or stool. The two main consequences of incontinence are hygienic and social.

The main hygienic impacts are the ones which are relevant to the weakening of the function of skin as a barrier between the environment outside the human body and in the human body. A reason for this is the continuous hydration of skin. Moreover, frequent infections can happen due to the contact of urine or faeces with the skin, since they are responsible for incubating kinds of harmful bacteria like staphylococcus. Urgency incontinence can also cause falls which can lead to fracture and other morbidities (Charalambous and Triantafilidis, 2009).

Everybody can guess the social impacts of incontinence: embarrassment, loss of self – confidence and depression. Avoidance of any social events is the rule, while many incontinence sufferers tend to limit their social life within their residences (Charalambous and Triantafilidis, 2009).

2.1.1 Prevalence of incontinence

There are many studies indicating the prevalence of urinary incontinence. Around 5% of women under 65 suffer from daily urinary incontinence, and this number rises to 9% for those over 65 and 17% for women over 85. For men these figures are about half of those for women (Cottenden et al., 2008b).

Incontinence can often be cured by using behavioural therapy, drugs or surgery. On the other hand, the most common way of dealing with non – curable forms is to use pads.

2.1.2 Pads

Figure 2.1 shows photographs of the most popular kinds of incontinence pads.

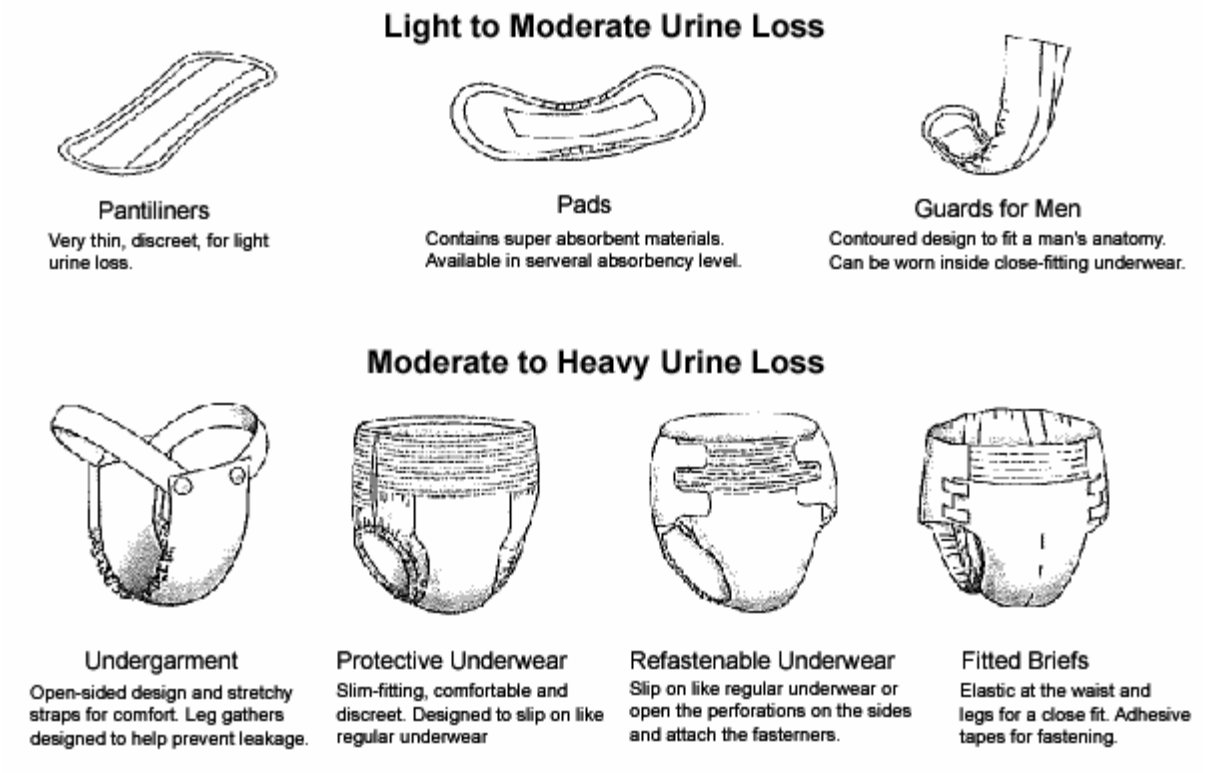

Figure 2.1: Different kinds of pads in the market (Diane Kaschak Newman, 2002)

As I show in Figure 2.1 there is a variety of absorbent products. Even though each of them is used for a different reason, they all have the same core structure: a water permeable sheet which comes in touch with the skin, an absorbent layer and a waterproof backing which seals the pad from the outer environment (Figure 2.2). The permeable sheet is usually made of nonwoven fabric and as I stated previously is the point of contact between the pad and the skin.

Figure 2.2: General structure of a pad

Companies prefer nonwoven fabrics as the permeable layer due to the very low quantity of polymer used in its production. Urine or faeces are usually in liquid form or have a high concentration of liquids. This causes increased wetness of the fabrics of the pads that leads to hydration of the skin. This hydration in relation to the friction caused by the movement of the incontinence sufferers is one of the main causes of incontinence associated dermatitis.

Incontinence associated dermatitis is the general term used to describe skin problems caused by incontinence: incontinence-associated dermatitis (IAD) is an inflammation of the skin that occurs when urine or stool comes into contact with perineal or perigenital skin (Gray et al., 2007).

2.1.2.1 Structure of stratum corneum

The skin layer which is in touch the pad is the stratum corneum. Skin is divided into two main layers, the epidermis and the dermis (Thibodeau and Patton, 2000). The outermost part of the skin is epidermis and in particular stratum corneum. So, at every frictional interaction with the skin, what really happens is the interaction of a surface with stratum corneum.

Its cells are filled with keratin and continually pushed to the surface of the epidermis. These dry, dead cells filled with keratin "flake off" by the thousands, and millions of epithelial cells reproduce every day to replace the millions shed (Thibodeau and Patton, 2000). Figure 2.3 shows a photomicrograph of the skin (Thibodeau and Patton, 2000), where the tough outer layer of the epidermis is shown.

Figure 2.3: Microscopic photograph of dermis, where I show the outer most part of stratum corneum

2.1.3 Hydration and skin

When the skin is occluded by pad materials, the stratum corneum becomes overhydrated, a fact which makes it sensitive to abrasion due to friction (Cottenden et al., 2008b). The lesions caused due to friction are the incentive for this project, since it is one of the main causes of skin lesions due to incontinence.

Until now I have mentioned skin and friction several times, without analysing friction. Friction is quite a general phenomenon, so the definition should be general as well. Friction is the force which opposes the initiation or sustaining of relative motion between two surfaces (a probe and a substrate) in contact (Figure 2.4). Static friction opposes the initiation of movement between two surfaces while dynamic friction impedes movement that is happening. Friction is characterised by the equation

$F=\mu N$, where for the friction force, N is the normal load and μ is the static (μ_s) or dynamic (μ_d) coefficient of friction, relevant to the nature of the material.

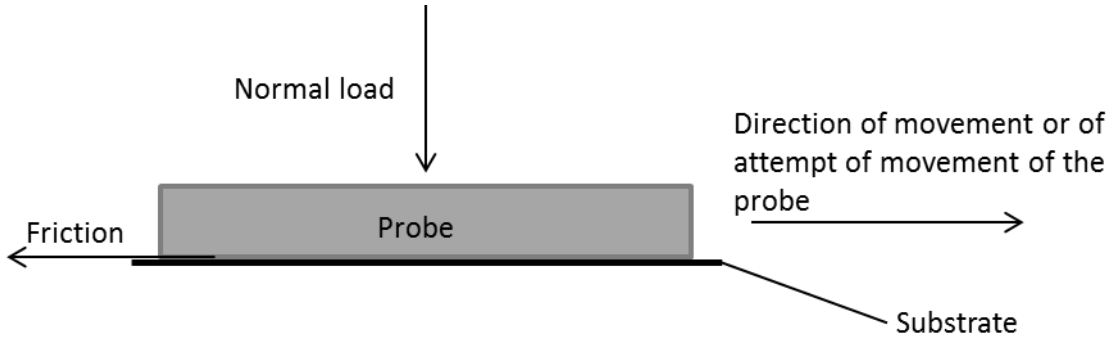

Figure 2.4: Direction of frictional force in relation to the direction of movement

Guillaume Amontons was the first who introduced empirical laws that describe the phenomenon of friction. Below I quote the famous three Amontons laws (Amontons, 1699).

The first law was initially investigated by Leonardo da Vinci and was later rediscovered by Amontons.

The force of friction is directly proportional to the applied load: $F=\mu N$. Where N is the normal load, μ the coefficient of friction, either static μ_s or dynamic μ_d and F is the frictional force.

The second law of friction is:

The force of friction is independent of the apparent area of contact.

This means that two bodies, regardless of their physical size or the nominal contact area, have the same coefficient of friction (Bhushan, 1999a). The only factors that affect friction are the normal load and the coefficient of friction μ.

The third law of friction was actually first discovered by Coulomb (Bhushan, 1999b)

The dynamic friction force is independent of the sliding velocity.

It is easy to understand that Coulomb makes the distinction between static and dynamic friction: static when there is not any motion but there is the attempt of motion between the interacting bodies; dynamic friction when there is motion between the interacting bodies.

Due to the importance of frictional interaction between skin and other materials like fabrics, experimental methods have been developed to investigate the frictional interaction.

2.2 Existing experimental methods for measuring skin friction

Skin friction, because the nature of the interacting surface is a complex phenomenon, researchers have come up with a variety of proposals to investigate it. In this section I am going to review the main ways skin friction has been studied.

I have recorded four main experimental methods of investigating friction on skin, on surfaces which simulate skin or just interesting frictional experimental methods that could be used in skin friction study. The first method is the method of linear pulls. In this case, there is movement in one direction. The second method is the reciprocating method, where there is counter movement. The third method is the rotational method, where the probe is usually placed at a stable point where it rotates. The fourth method is the curved pull method where the experimentalist investigates friction over the surface of a convex prism.

2.2.1 The linear pull method

The first and most simple method is the linear pull method. It is used when the experimentalist has the proper equipment and a reasonably large flat surface area to perform these measurements. A probe of the material of choice is pulled over the surface of the skin (surrogate). Because each measurement involves just one pass of one surface over the other, the tested surfaces are not worn out, so the experimentalist records the properties of the initial state of the surfaces.

Figure 2.5 presents how linear pulls take place.

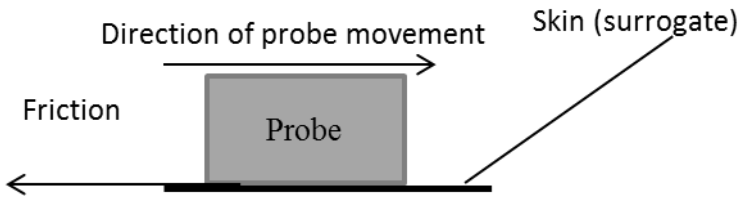

Figure 2.5: Linear pull frictional method

Below I quote the literature I read relevant to the linear pull method. I classify the published work according to the stable variables that characterise this method. So, I have the material and the geometry of the probe, the nature of the surface area they examine, the mode of application of the driving force, as well as the range of the normal load and the mode of application of it. Finally I quote the kind of examined friction through the coefficient of friction (static or dynamic).

Looking at Table 2.1 I can derive some valuable conclusions. The dominant probe shape is a sphere which has the advantage of smooth sensation on the experimental subject, but does not apply uniform pressure on the subject, over the whole of the tested area. My personal opinion is that the sled produces better results since it applies a more uniform pressure. About the geometrical properties of the presented work, I can state that in seven papers they use spheres or hemispheres, in one paper they use a cylinder and in two papers they use a sled. The counter surface is usually a skin site with the exception of the paper by Ramkumar et al (Ramkumar et al., 2004) that uses fabric. The driving force is usually supplied by a tensometer – like device, in one case (Comaish and Bottoms, 1971) static weights and a pulley used, while sometimes it is provided by the experimentalist or a participant, like

Derler et al (Derler et al., 2009a) who used the subject's strength; Darden et al (Darden and Schwartz, 2009) who used the volitional movement of the subject; and Ramahlo et al (Ramahlo, Szekeres and Fernandes, 2013) whose experiments were driven by hand. Normal load presents an impressive range from 0.015 to 1 N with the lowest value appearing in the work of Pailler-Mattei et al (Pailler-Mattei et al., 2007) and the highest value in the work of Ramahlo et al (Ramahlo, Szekeres and Fernandes, 2013). There is the exception of Derler et al (Derler et al., 2009a) who used the subject's weight and of Darden et al (Darden and Schwartz, 2009) where it was subject controlled. Finally, the experimentalists were usually interested either in dynamic friction or in both, static and dynamic friction. Notable is the exception of Nakajima et al (Nakajima and Narasaka, 1993) who was interested just in static friction.

Authors	Moving probe		Counter surface	Driving force	Normal load		μ_s or μ_d
	Material(s)	**Geometry**			**Range (N)**	**Source**	
Comaish and Bottoms (Comaish and Bottoms, 1971)	PTFE (fluon, teflon) or knitten nylon	Thin sheet	Mid-abdominal area (in vitro), dorsum, palm and mid tibia region (in vivo)	Static weights, pulley	?	Static weights	Both
Nakajima et al (Nakajima and Narasaka, 1993)	cotton, wool, silk, rayon, polyester and nylon fabrics	Half-cylinder 20mm long, 20 mm in diameter	Volar forearm (in vivo)	Tensometer-like device	$3x10^{-2}$-10^{-1}	Static weights	μ_s
Koudine et al (Koudine and Barquins, 2000)	Glass	Hemisphere	Forearm (in vivo)	Tensometer	Up to 0.1	Dead weight and pulley	Both
Asserin et al (Asserin et al., 1999)	Ruby	Sphere	Volar forearm (in vivo)	Tensometer	0.070	Static weights	Both
Egawa et al (Egawa et al., 2002)	Steel	20 parallel piano wires, 10 mm length, diameter 0.5 mm, total surface of 100 mm^2	Ventral forearm (in vivo)	Tensometer (KES-SE frictional analyzer)	0.244	Static weights	μ_d
Kondo et al (Kondo, 2002)	Cotton, wool, silk, rayon, polyester and	Contact area of 10 mm x 10 mm	Volar forarm (in vivo)	KES-SE (Frictional feel analyzer)	0.49 and 0.245	?	μ_d

Authors	Moving probe		Counter surface	Driving force	Normal load		μ_s or μ_d
	Material(s)	**Geometry**			**Range (N)**	**Source**	
	nylon fabrics						
Sivamani et al (Sivamani et al., 2003)	Stainless steel	Sphere, 10 mm diameter	Abdomen, dorsal skin of fingers (in vivo)	Tensometer	0.49 to 0.441	Static weights	μ_d
Ramkumar et al (Ramkumar et al., 2004)	Steel	Sled with contact area of 2000 mm^2	Fabric	Tensometer	0.393 to 0.883	Static weights	μ_d
Elkyat et al (Ahmed Elkyat, 2004)	PTFE, steel, glass	Sphere diameter of 10 mm	Volar forearm (in vivo), sil-flo, resin	Tensometer	0.105	Static weights	μ_d
Hong et al (Hong, Kim and Kang, 2005)	Sheepskin	Sled holder	Nonwoven fabrics	Tensometer	0.196	Static weights	μ_d
Pailler-Mattei et al (Pailler-Mattei et al., 2007)	Smooth steel	Sphere, 6.35 mm diameter	Inner forearm (in vivo)	Tensometer	0.015	Static weights	Both

Authors	Moving probe		Counter surface	Driving force	Normal load		μ_s or μ_d
	Material(s)	**Geometry**			**Range (N)**	**Source**	
Tang et al (Tang et al., 2008)	Polypropylene	Sphere, 10 mm diameter	Volar forearm (in vivo)	Tensometer	0.1 to 0.9	Static weights (?)	μ_d
Derler et al (Derler et al., 2009a)	Human Skin	Soft plantar skin (in vivo)	Rough ceramic surface, tri-axial force plate 800 mm x 400 mm	Subject's strength	Subject weight	Subject weight	μ_d
Darden and Schwartz (Darden and Schwartz, 2009)	Human Skin	Finger (in vivo)	3-axis dynamometer plate	Volitional movement of subject	Subject controlled	Subject controlled	μ_d
Ramahlo et al (Ramalho, Szekeres and Fernandes, 2013)	Five fabrics (with 82% polyamide and 18% elastane, with 100% polyester, with cotton, with silk and with wool)	Spherical surface of a radius of 26mm	Ventral face of forearm, palm	Driven by hand	0 to 1N	Hand driven (experimentalist)	μ_d

Table 2.1: Summary of the basic aspects of the published work using linear pull methods to measure friction between skin and fabrics, between skin and a counter surface, or between fabrics and a counter surface

2.2.2 Reciprocating method

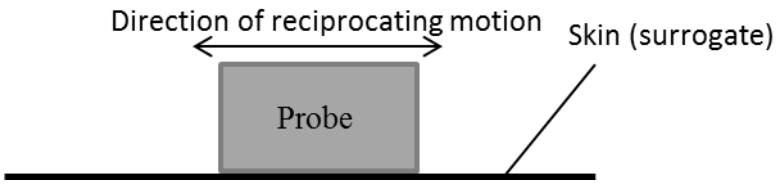

Figure 2.2.6: Reciprocating method with the reciprocating motion of the probe.

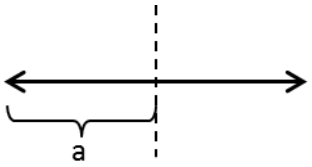

Figure 2.7: The length "a" presents the throw, while the arrows show the total length of the reciprocating movement

The reciprocating method is a version of the linear pull method, but in this case the motion is not unidirectional, but the probe "returns". Below I quote the literature relevant to the reciprocating method. I present, as before the material and the geometry of the probe, the tested surface, the throw (Figure 2.7) which is the distance the probe runs for each stroke. Also, I quote the range of the normal load and the mode of its application on the probe. Finally, I quote the kind of the investigated friction.

Very interesting is the geometry of the probe they usually used which is of spherical shape. In particular, in four papers they used a sphere and in one they used lenses, while in two papers they used a circular flat probe. In three papers they used as probes special sensing areas, while in two they used the finger. The counter surface was usually a skin site or another examined area covered in materials whose friction properties the experimentalists wanted to examine. Throw varied from 2.5 to 100 mm and also the frequency was from 0.333 to 1.0 Hz. Normal load varied a lot among the different studies, from 0.19 – 50 N, with the lowest value due to Kwiatkowska et al (Kwiatkowska et al., 2009) and the highest to Derler et al (Derler et al., 2009b). Finally the mode of application of the normal load was usually static weights or computer controlled, with the exception of Derler et al (Derler et al., 2009b) who used subjects' strength. The investigated kind of friction was either dynamic friction or both kinds, static and dynamic.

Authors	Moving probe		Counter surface	Throw (mm)	Frequency (Hz)	Normal load		μ_s or μ_d
	Material(s)	Geometry				Range (N)	Mode of application	
Naylor (Naylor, 1955)	Polyethylene, silver	8 mm diameter spheres	Anterior surface of tibia	±2.50	0.333	1.96	Static weights	μ_d
Sulzberger et al (Sulzberger et al., 1966)	Leathers, cloths, plastics	Spherical probe	Back, buttocks, shins, forearms, upper arms, thighs, palms, sole (in vivo)	?	0.42 - 17.3	2.1 - 11.3	Static weights	μ_d
Hills et al (Hills, Unsworth and Ive, 1994)	Corethium (lyophiized porcine skin)	25 mm diameter circular piece	14 prescribable bath emmolients, polymethylmathacrylate bath material	?	?	?	Static weights	Both
Derler et al (Derler, Schrade and Gerhardt, 2007)	Wool fabric	3-component dynamometer (Kistler 9254)	Lorica, polyurethane (PUR) and silicone	± 50 - 100	1.0 ± 0.3	3	Static weights	μ_d

Authors	Moving probe		Counter surface	Throw (mm)	Frequency (Hz)	Normal load		μ_s or μ_d
	Material(s)	Geometry				Range (N)	Mode of application	
Bertaux et al (Bertaux, Lewandowski and Derler, 2007)	Fabric sample	Circle 28.5 mm diameter	Lorica	± 12	0.75	3	Static weights	μ_d
Adams et al (Adams, Briscoe and Johnson, 2007)	Glass, Polypropylene (PP)	Lenses, (i) diameter 12 mm, curvature R=7.8 mm and (ii) diameter 25 mm, curvature R=20.7 mm	Volar forearm	± 90	?	2	Static weights	Both
Gerhardt et al (Gerhardt et al., 2008)	Metallic block with skin simulating materials	Sensing area of 60500 mm^2 (pressure sensitive film)	Skin (in vivo), supine and lateral position	?	1.25	Subject's weight	Computer controlled	Both
Derler et al (Derler et al., 2009b)	Skin (in vivo)	Index finger	Smooth and rough glass	?	0.333	Up to 50	Subject strength	μ_d

Authors	Moving probe		Counter surface	Throw (mm)	Frequency (Hz)	Normal load		μ_s or μ_d
	Material(s)	Geometry				Range (N)	Mode of application	
Kwiatowska et al (Kwiatkowska et al., 2009)	Smooth steel	Sphere of diameter 2 mm and 5 mm	Dry inner forearm skin	± 17.6	?	0.19 - 0.5	Static weights	Both
Shao et al (Shao, Childs and Henson, 2009)	Silicone in thin acrylic layer and silicone gel with elastomer	Finger (in vitro)	15 different sample surfaces on x-y motion table	?	?	?	Computer controlled	Both
Li et al (Li et al., 2012)	Acrylic resin	Hemisphere of 15mm diameter + 2.7mm thickness acrylic resin shell	Volar forearm	5	0.5	0.2 and 1	Computer controlled	μ_d

Authors	Moving probe		Counter surface	Throw (mm)	Frequency (Hz)	Normal load		μ_s or μ_d
	Material(s)	Geometry				Range (N)	Mode of application	
Gerhardt et al (Gerhardt et al., 2013)	Metallic block with skin simulating materials	Sensing area of 60500 mm^2 (pressure sensitive film)	Polyester fabric impregnated coated with low and high cross linked biopolymer network, impregnated with phytotherapeutic substances	20mm along the wet direction	3.1	5	Computer controlled	μ_d

Table 2.2: Summary of the basic aspects of the published work using the reciprocating method to measure friction between skin and fabrics, between skin and a counter surface, or between fabrics and a counter surface

2.2.3 Rotational method

Comaish et al (Comaish, Harborow and Hofman, 1973) initiated the rotational method, whose main characteristic was the probe of Figure 2.8. The advantages of this probe instead of using a sphere, for instance, is that under the condition that the annulus wall is thin, the experimentalist can assume that the linear velocity of any point on the interface between the annulus probe end and the substrate is approximately the same.

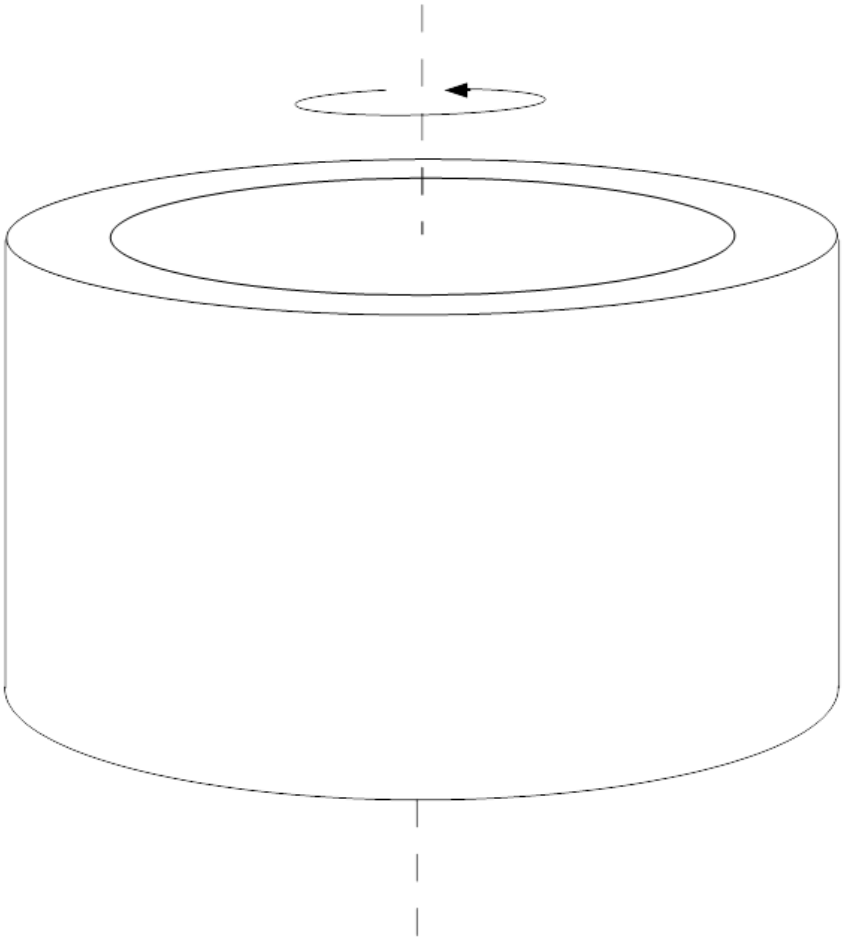

Figure 2.8: Annular ring which is used in the rotational method.

Veijgen et al (Veijgen, Masen and Heide, 2012) in his work used a cylindrical probe instead of an annular ring. The innovative point of this method is that it tried to measure not only the dynamic, but the static friction as well, which was defined as the value one second after movement starts. Both probe configurations, annular ring and cylindrical, calculate friction through the friction torque which is equal to the torque reaction from the drive (Comaish, Harborow and Hofman, 1973).

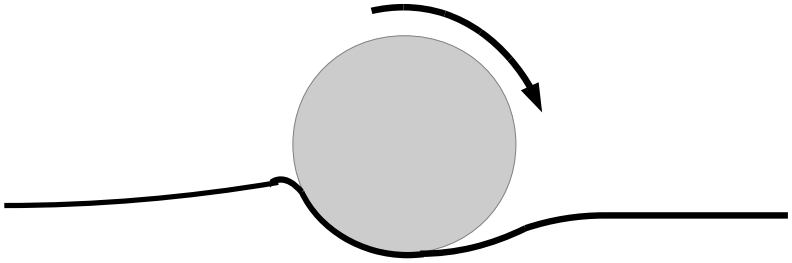

Figure 2.9: Cross section of cylindrical configuration used by Veijgen et al (Veijgen, Masen and Heide, 2012)

In the next page I quote the literature on the rotational method. For the rotational probe I describe the material and the rotational speed, I quote the nature of the counter surface, the range of the normal load and the way it was applied, and finally the kind of the investigated friction. The probe was always an annular ring, except in the paper of Lima et al (Lima et al., 2008) who used three contact points of equal distance from the axis of rotation with angular separations of 120°. The last two papers, of Veijgen et al (Veijgen, Masen and Heide, 2012) and Veijgen et al (Veijgen, Masen and Heide, 2013) used another apparatus whose basic component is a cylinder. I present the cross section of equipment in Figure 2.9. The probe was "dressed" with a material of interest to the research of the experimentalist. The rotation frequency used was between 0.0125 Hz and 2.5 Hz, with the lowest value appearing in Lima et al (Lima et al., 2008) work and the highest in Comaish et al (Comaish, Harborow and Hofman, 1973) work. The counter surface was always a skin site, except in the work of Lima et al (Lima et al., 2008) who used other fabrics or stainless steel. The range of the normal load, where specified, was 0.5 to 100 N, with the lowest values appearing in Veijgen et al papers (Veijgen, Masen and Heide, 2012), (Veijgen, Masen and Heide, 2013) and the highest in the Zhang et al (Zhang and Mak, 1999) paper.

Authors	Rotating probe			Counter surface	Normal load		μ_s or μ_d
	Shape	Material(s)	Rotational speed (Hz)		Range (N)	Source	
Comaish et al (Comaish, Harborow and Hofman, 1973)	Newcaslte friction meter (annular ring)	Steel, nylon, PTFE, a variety of fabrics and animal or vegetable tissue	2.5	Skin (in vivo)	1.96	Constant force spring	μ_d
Cua et al (Cua, Wilhelm and Maibach, 1990)	Newcastle friction meter (annular ring)	PTFE	2.5	Forehead (centre), postauricular, upper arm (inner middle third), volar and dorsal forearm (centre between wrist and elbow), palm (thenar aspect), abdomen (an inch above umbilicus), thigh (anterior, upper third), ankle (medial malleoli), upper back (scapula) and lower back	Constant normal load	Constant spring guided pressure	μ_d

Authors	Rotating probe			Counter surface	Normal load		μ_s or μ_d
	Shape	Material(s)	Rotational speed (Hz)		Range (N)	Source	
Zhang et al (Zhang and Mak, 1999)	Annular ring with outer diameter of 16 mm and inner diameter of 10 mm	Aluminium, nylon, silicone, cotton sock and pelite	0.42 to 1.042	Palm of hand, dorsum of the hand, anterior side of the forearm, posterior side of the forearm, middle anterior leg and middle posterior leg	25 to 100	Depends on the weight of the probe and the relative position of the rotary probe to the base plate	μ_d
Lima et al (Lima et al., 2008)	3 elements with a distance of 120º between them	Nonwoven fabrics	0.0125	Other fabrics or polished stainless steel	?	Dead weight at the top of the elements	μ_d

Authors	Rotating probe			Counter surface	Normal load		μ_s or μ_d
	Shape	Material(s)	Rotational speed (Hz)		Range (N)	Source	
Hendriks et al (Hendriks and Franklin, 2010)	Annular ring	PTFE and aluminium	Varies between 0.01 and 10	Arm, cheek	0.625	By adjusting the elongation of the spring of the measuring apparatus)	μ_d
Veijgen et al (Veijgen, Masen and Heide, 2012)	Cylinder of 20mm diameter and 10mm long	Solid stainless steel cylinder	0.05, 0.1, 0.4 and 0.5	Human skin in vivo	0.5 - 2	Spring based system inside the device	Both
Veijgen et al (Veijgen, Masen and	Cylinder of 20mm diameter and 10mm long	Stainless steel, aluminium, polyethylene and polytetrafluorethylene (cylinder)	0.05, 0.1, 0.4 and 0.5	Ventral forearm, dorsal forearm, index finger pad, dorsum hand	0.5 - 2	Spring based system inside the device	?

Authors	Rotating probe			Counter surface	Normal load		μ_s or μ_d
	Shape	Material(s)	Rotational speed (Hz)		Range (N)	Source	
Heide, 2013)							

Table 2.3: Summary of the basic aspects of the published work using the rotating method to measure friction between skin and fabrics, between skin and a counter surface, or between fabrics and a counter surface

2.2.4 Curved pull method

This method is about dragging a strip of fabric over a curved surface. In this method the curved surface is usually a finger or volar forearm, which approximates to a cylinder.

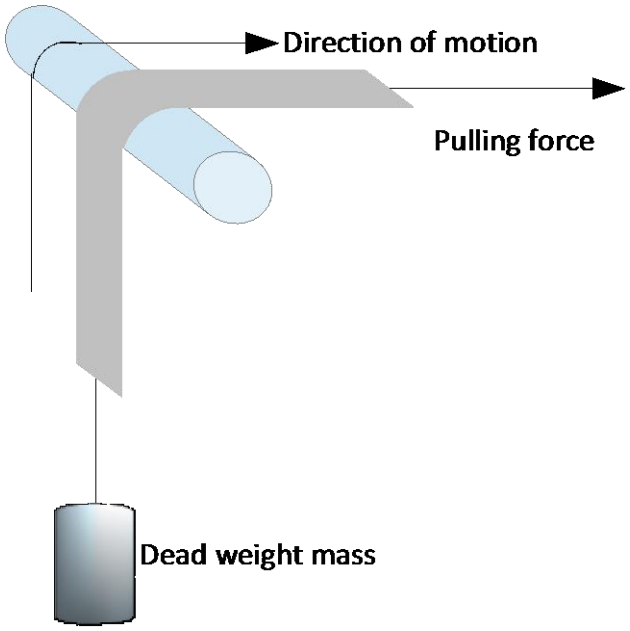

Figure 2.10: Shape simulating the curved pull method

Below I present the published work for the curved pull method. I present the two interacting materials (sliding material and skin site), and the mode of application of the pulling force. I also quote the dead weight mass (or equivalent). Note that it is not possible to quote a simple normal force as the interfacial pressure between the skin and fabric varies with angle around the curved surface. In the final column I quote the kind of the investigated friction.

The first column presents the authors and the second the compliant sheet materials that slide over the convex prisms. All of them are fabrics. The third column presents the skin site on which the measurements took place and were either the forearm or the finger. The mode of application was always a tensometer while the range of the dead weight load was from 0.049 to 0.98 plus the fabric weight. The mode of application of the force at the other edge of the strip of fabric was always a dead weight. The experimentalists of one paper (Gwosdow et al., 1986) examined the dynamic friction, while the experimentalists of the rest of the papers examined both kinds of friction.

Author	Material(s)	Counter surface	Mode of application of pulling force	Dead weight value(s)/ range (N)	μ_s or μ_d
Gwosdow et al (Gwosdow et al., 1986)	Worsted wool, brushed cotton, cotton, silk, linen, burlap	Volar forearm	Tensometer	0.98 + fabric weight	μ_d
Kenins (Kenins, 1994)	Cashmere, wool, polyester, cotton	Hairy forearm, glabrous finger skin (in vivo)	Tensometer	0.049 or 0.49 plus the weight of the strip fabric	Both
Wong (Wong, 2008)	Nonwoven fabric	Volar forearm	Tensometer	0 – 0.981	Both

Table 2.4: Summary of the basic aspects of the published work using the curved pull method to measure friction between skin and fabrics.

2.2.5 Comparative view of the experimental methods

Why are there four different ways of measuring skin friction, can't it be just one? The answer is that the four of them are necessary, depending on what the experimentalists want to study.

The linear pull method is ideal when the participant can provide a sufficient large flat area of skin or the counter surface has a wide enough area. It is preferred when the surface is sensitive and cannot stand too many measurements. With the right kind of probe both static and dynamic friction can be studied.

I can say that the reciprocating method is another form of the linear method, but the multiple strokes allow the derivation of much more information. The problem here is that the multiple strokes can wear out the examined surface, altering in this way the surface properties. So, the experimentalists need to pay attention where to apply this method, if they want to derive reliable results.

The rotational method is applied in cases where there is insufficient flat surface area to examine, so the experimentalists have to take advantage of just a very small area. The disadvantage of this method is that when a spherical or cylindrical probe is used, it does not offer a uniformal distribution of load. The advantage is that when it is used on a skin site, the value of dynamic friction is not affected by the viscoelastic properties of the skin.

Finally, there is the curved pull friction method. Linear and reciprocating methods bear results just on flat surfaces, while the rotational method is applied to just on one point of the surface. The curved pull method is the only method with which the experimentalists can test the friction properties of convex prism surfaces.

Each experimental method responds to the different requirements of each study. Linear and reciprocating methods are applied on flat surfaces, while the rotating method is applied in cases where there is limited surface area. The curved pull method is applied at the interface between compliant sheets and convex prisms, something innovative since it is the only method which allows measurements on curved surfaces.

A practical problem for the experimentalists is the speed of measurement, especially when they use participants who have limited available time. The most convenient method for the experimentalist and the participant as well is the rotating method, the measurements of which can take place at any available space, since the equipment is portable and does not demand a large surface area. The problem is that this method does not record static friction. Veijgen's et al (Veijgen, Masen and Heide, 2012) proposal is still interesting and remains to be further investigated.

Linear and reciprocating methods demand complicated equipment which means higher cost and the participant has to spend time to come to a selected place. Also the conduction of the experiments demands a relatively large surface area, a fact that adds another obstacle. The substantial difference between these two methods is that the reciprocating method can extract a lot more data than the linear, since it involves many more measurements.

The curved pull method demands a pulling device which is similar to the lineal method, so the limitations of the method are similar to the limitations of the linear method. What distinguishes this method is that it is used to measure friction on convex prisms and not on flat surfaces like the linear or reciprocating methods.

Overall, linear, reciprocating and curved pull methods demand sophisticated equipment, relatively large surface areas and subsequently are of high cost. On the other hand the majority of the rotating method papers use a device called the "Newcastle friction meter" or similar devices which are available commercially and at low cost. They do not demand a large surface area, a fact which makes the experiments fast and convenient for the participant and the experimentalist. The main minus of this method is that it cannot be used to measure static friction.

2.3 Theoretical models of friction

A variety of theoretical models have been developed to describe frictional phenomena. The first scientists who talked about this was Guillaume Amontons, a French physicist who named the empirical laws which characterise frictional interaction. Since then, many have developed mathematical models describing friction between varieties of surfaces. In this project I will concentrate on curved pull friction since it is the kind of method I will use in my experiments.

Amontons made the first attempt at a theoretical description of friction in 1699 and I present his empirical laws in §2.1.3. Since then a variety of models have been developed to characterise the frictional interaction on geometrical surfaces, each emphasising the aspects each scientist wants to describe. In the present project I am particularly interested in investigating friction on conical surfaces and cylinders and the best experimental method to achieve this is the curved pull method. Below I will summarise the basic aspects of the various models developed to describe friction on convex prisms, leaving the curved pull method until last.

2.3.1 Gwosdow contribution

The first mathematical model investigating friction according to the curved pull method is described by Gwosdow et al (Gwosdow et al., 1986). This group used an equation described by Shigley (Shigley, 1956) which describes the forces on the surface of drums. He was the first to use a mathematical model which characterises the friction on parts of a machine, something that always is of a great financial interest, to describe the frictional interaction on a volar forearm. A second paper investigating friction using the curved method is Kenins et al (Kenins, 1994), who investigated friction on forearms and fingers. The model describes the frictional interaction of the curved pull method (Figure 2.10) and the equation which is used is:

$$T_1 = T_2 e^{\mu\beta}$$ **Equation 2.1**

A cross section of Figure 2.10 but instead of pulling force and weight, T_1 and T_2 is presented in Figure 2.11.

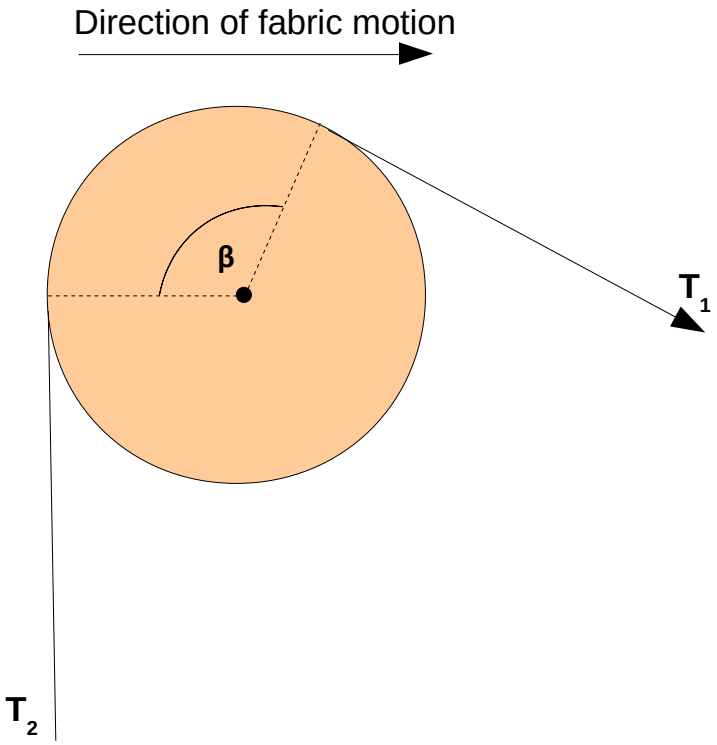

Figure 2.11: Cross section of Figure 2.10, where T_1 is the pulling force and T_2 is the dead weight, while β is the arc of angle of contact between the compliant sheet and the cylinder

Where T_1 is the pulling force and T_2 is the dead weight at the other end of the strip and β is the arc of angle of contact between the convex prism and the compliant sheet (with reference to Figure 2.10). Also, with this model the experimentalists can derive both static and dynamic friction.

In order to use this model, several assumptions have been made.

1. The "arm" has a cylindrical cross section
2. Amontons first law is obeyed (friction force is proportional to the normal load).
3. At the instant of slip the surface of the convex prism is incompliant and incompressible while the fabric needs to be inextensible with negligible bending modulus. Because the fabric is very thin, even though inextensible (of high modulus) we can assume that the bending modulus is very low.

Gowsdow's model was later developed by other researchers who were interested in performing measurements on convex prisms and whose work I mention in the next paragraphs.

2.3.2 Wong's, Cottenden's and Karavokiros' contribution

Rebecca Wong in her thesis (Wong, 2008) developed a methodology for conducting experiments on volar forearms, either in dry or in wet condition and she found that her data from measurements on young females agreed very well with Gwosdow's model despite volar forearms being only very approximately cylindrical. The methodology which I follow to conduct my experiments on the volar forearm Chapter 4 is the methodology developed by her (Dr Rebecca Wong).

David Cottenden in his thesis (Cottenden, 2010) pushed the mathematical model one step further by developing a mathematical model for describing frictional interaction between convex prisms (not just cylinders) and a compliant sheet. Initially he described the frictional interaction between cylindrical surfaces and a compliant sheet (similar to a strip of fabric), proceeding to the more complex phenomenon between convex prism surface and a compliant sheet. Finally, he evolved the model to describe friction between a general surface and a compliant sheet. He always used the same assumptions as Gwosdow (§2.3.1).

This mathematical model has been validated for cylindrical and elliptical prisms by an MSc student, Skevos Karavokiros. Part of his work has been published in the paper of Cottenden et al (Cottenden et al., 2008a) where the authors describe comparisons between the model and experimental data for rigid cylindrical and elliptical "arms" (Figure 2.12).

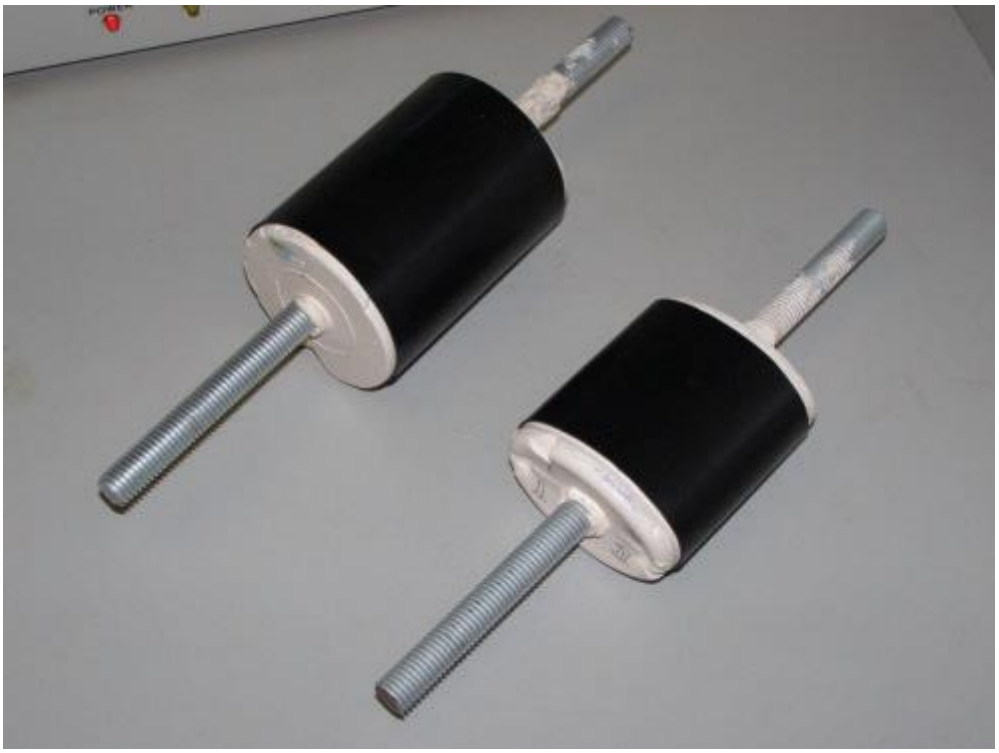

Figure 2.12: Cylindrical (left) and elliptical (right) prisms which were used by Cottenden et al (Cottenden et al., 2008a) to validate the model.

The model was also used by Karavokiros (Karavokiros, 2007) to study rigid cones with small – half – angle (Figure 2.14). He found that provided experiments were set up as Figure 2.13, data were well described by Gwosdow's Equation 2.1. For example, for a 12° half angle cone, the difference between Gwosdow's prediction and experimental data was about 10% (Cottenden and Cottenden, 2009). This explained why Wong found that data from her volar forearm which is within experimental method agreed well with Gwosdow's model.

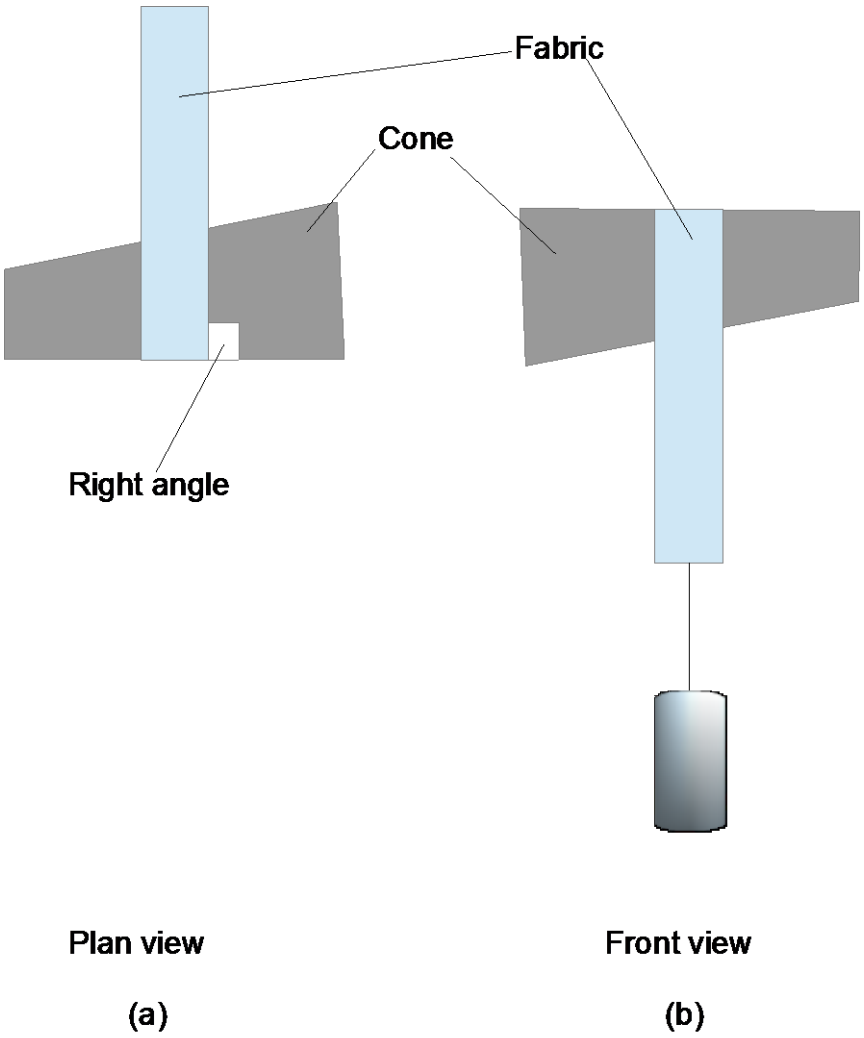

Figure 2.13: Plan and front view of a convex prism experiment

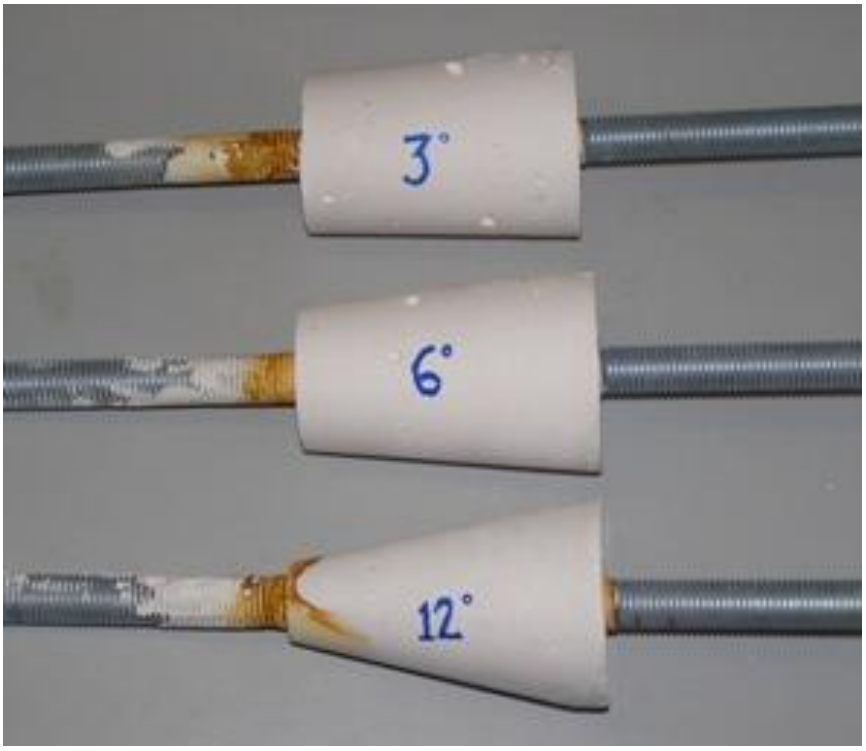

Figure 2.14: Cone prisms of half angles of 3°, 6° and 12°.

David Cottenden in his thesis (Cottenden, 2010) developed a mathematical model that describes friction between any surface and a conformable sheet. Although Cottenden's model does not necessitate any limitations in the surface of the prism, the occurring equation is intractable. The solution that came up is that the equation can be analytically tractable for many particular geometrical configurations.

The next step for validating this theoretical model is to proceed to more complex geometries, as the ones I will describe in the following paragraph.

So, to sum up, Cottenden's model has already been validated for convex prisms of cylindrical and elliptical cross sections, and for conical with low half – angles. In every case the geometry was rigid and simple. What remains is the validation of the model for large – half angle cones to test the model on human skin and try to find out whether the model stands when the conditions of §2.3.1 are not fully met.

2.4 Aims and objectives

Cottenden's convex prism model has been validated for rigid cylinders and prisms of elliptical cross section, and for young female volar forearms. The aim of my project was to test Cottenden's convex prism model and his general model in three new ways.

In the first way (Chapter 3) I tested Cottenden's general model by conducting experiments on rigid, large half – angle cones. Although Cottenden's general model is generally intractable, there is an analytical solution for conical surfaces providing a way of further testing the model for a geometry

which is both very different from a convex prism and clinically relevant (various body surfaces approximate to portions of large half – angle cone surface.

In the second way (Chapter 4) I test the Cottenden's model on volar forearms of young and elderly female participants. The volar forearms approximate to convex prisms but push the testing of the validation one step further since they provide a changing geometry throughout the experiment. Human volar forearms tend to deform (ruck), the volar forearms of the elderly participants more than the volar forearms of the young participants, due to the higher degree of flaccid substrate they have. This fact provides a variety of data that help test the model over a higher range of behaviours.

In the third way (Chapter 5) I pursue the highest possible degree of deformation. I use compliant cylindrical silicone arms that exhibit rucking in a degree I cannot achieve with the volar forearms of volunteers without extreme discomfort. The provided data help test the model in extreme conditions of derformation.

In the next chapter I start presenting my experiments on rigid large – angle cone prisms, investigating how the geometrical factor affects the studied mathematical model.

Chapter 3 Experiments on rigid cones

The first step of validating the mathematical model initiated by Dr David Cottenden in his PhD thesis (Cottenden, 2010) is isolating the geometrical properties of shapes and studying how the model behaves under these conditions. For this reason, I constructed cones with 45°, 35°, 25° and I conducted friction experiments on them, sliding a strip of nonwoven fabric according to the methodology described (§3.3.10). In the rest of the chapter I explain the path I followed until the completion of the experiments, which includes the discovery of the proper construction cone materials as well as the actual methodology of experimentation.

3.1 A few words about the mathematical model I seek to verify.

In his thesis, Dr David Cottenden (Cottenden, 2010) developed a mathematical model that describes the developing forces during the relative motion between two surfaces, based on Amonton's laws. A simplified version of this model that describes the frictional coupling on the surface of cones can be described by Equation 3.1 with reference to Figure 3.1:

$$T_{yy} = T_0 \exp\left(\int \mu(yy)\left|c_{yy}\right|dy\right) \quad \textbf{Equation 3.1}$$

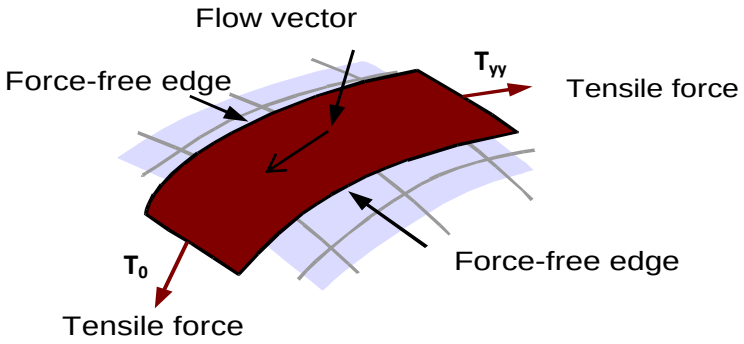

Figure 3.1: The tensile forces are represented by the T_0 and T_{yy}, while the flow vector represents the direction of the movement of the conformable sheet. (Courtesy of Dr David Cottenden)

According to Cottenden Equation 3.1 leads to Equation 3.2 for a strip of fabric dragged over the surface of a cone (Figure 3.2):

$$T_{yy} = T_0 \exp\left(\frac{1}{\tan\alpha}\int_{\theta_1}^{\theta_2}\left(\mu(\theta)\cos(\theta)d\theta\right)\right) \quad \textbf{Equation 3.2}$$

— T_{yy} and T_0 are the tensile forces at either end of the fabric strip ($T_{yy}>T_0$).
— θ_1 and θ_2 define the ends of the footprint of the fabric on the cone.
— $\mu(\theta)$ is the coefficient of friction between the fabric and the cone.

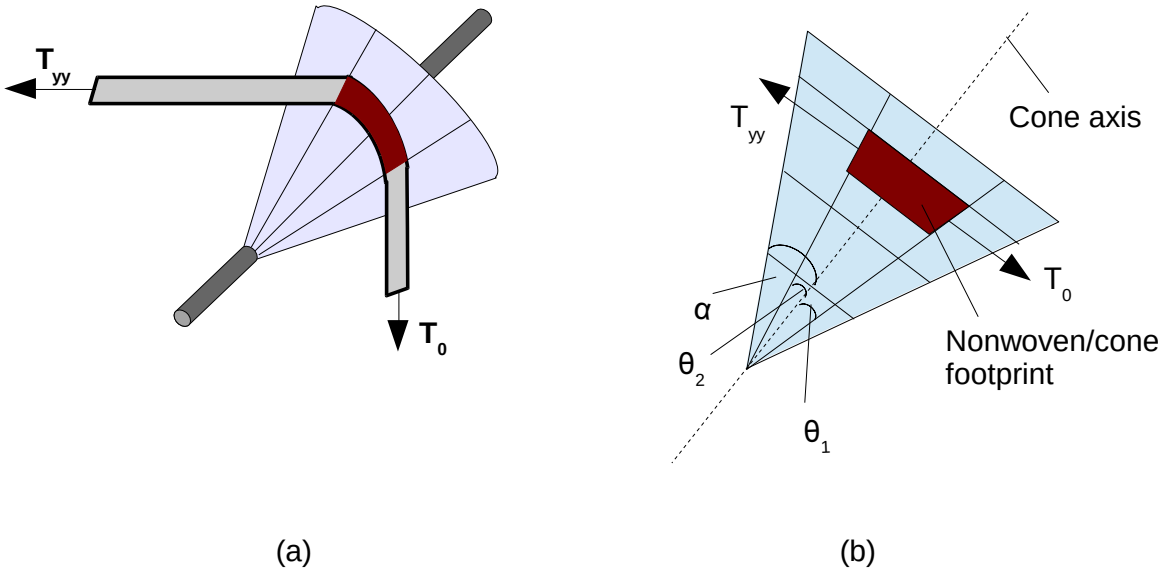

Figure 3.2: (a) Test configuration for fabric/cone experiments, (b) Plan view of the cone and fabric to show the key angles.

If μ is constant across the whole surface of the cone, Equation 3.2 simplifies to:

$$T_{yy} = T_0 \exp\left(\frac{\mu}{\tan\alpha}\left(\sin\theta_2 - \sin\theta_1\right)\right) \quad \textbf{Equation 3.3}$$

Rearranging, this becomes:

$$\ln\frac{T_{yy}}{T_0} = \mu\frac{\sin\theta_2 - \sin\theta_1}{\tan\alpha} \quad \textbf{Equation 3.4}$$

This means that if $\frac{\sin\theta_2 - \sin\theta_1}{\tan\alpha}$ is plotted against $\ln\frac{T_{yy}}{T_0}$ for a variety of T_0, θ_1 and θ_2 values for cones of a variety of α values, providing μ is constant across all points on the surface of all cones, all data should fall on a single straight line of gradient μ. This provides an elegant way of testing Cottenden's model (Cottenden, 2010).

To do this I designed and developed a suitable rig for holding cones, pulling nonwoven strips over their surfaces and measuring the various relevant forces and angles. Also, I made a set of cones and I tried to establish that the coefficient of friction between cone surface and nonwoven fabric strips was essentially the same for any test piece of a given nonwoven fabric and any of the surfaces of any test cones. I will describe the design, development and validation of a test rig to make the necessary measurements in the following sections.

3.2 Purpose of rigid cone experiments

In order to avoid the complicating factors of compliant materials I chose to make my cones from a rigid material so that their geometry would not change during an experiment. I chose to use Plaster of Paris for the simple reason it is cost efficient, I can find it very easily and in abundant quantities. As I will explain in the following paragraphs the main problem I faced is the covering material that has to exhibit uniform friction. I have to note that this procedure of finding the best material took a considerable amount of time during this research project, since it was difficult to find a material with uniform frictional properties.

So, summing up, the way I completed my work during this part of my PhD was, initially, to construct the rig that I used to adapt the contact angle between the cone and the strip of fabric each time I had to conduct an experiment. Second, find the proper covering material ("skin") that demonstrates uniform frictional properties, so I can attach it on the cones. Third, construct the cones of plaster of Paris and attach the proper "skin" material on the surface. Fourth, present and explain the experimental methodology I followed, and finally present the experimental results.

3.3 Methodology development

Crucial for extracting reliable results is the shaping of a robust methodology. This extremely important task of work is presented in this section.

3.3.1 Construction and description of the rig

The procedure I followed to complete each rigid cone experiment was identical and is precisely described in §3.3.2. Briefly, after I had constructed the cone, I placed it in the rig, presented in Figure 3.3, I used the strip of fabric corresponding to the tested cone and I started the experiments. Of course, before I conducted the experiment, I had to build the proper rig and this is what I present in the following paragraph.

When I work in the lab I always take into consideration the fact that the same equipment was being used by other researchers, so I should be able to assemble and disassemble my equipment quickly enough. So, in order to facilitate my experiments I decided to construct my rig on a trolley, which I could attach fast enough on the tensometer, pulling device which helped me conduct my experiments. This rig is presented in Figure 3.3 and its purpose is to measure the friction force opposing the motion of a strip of nonwoven fabric over the surface of a cone.

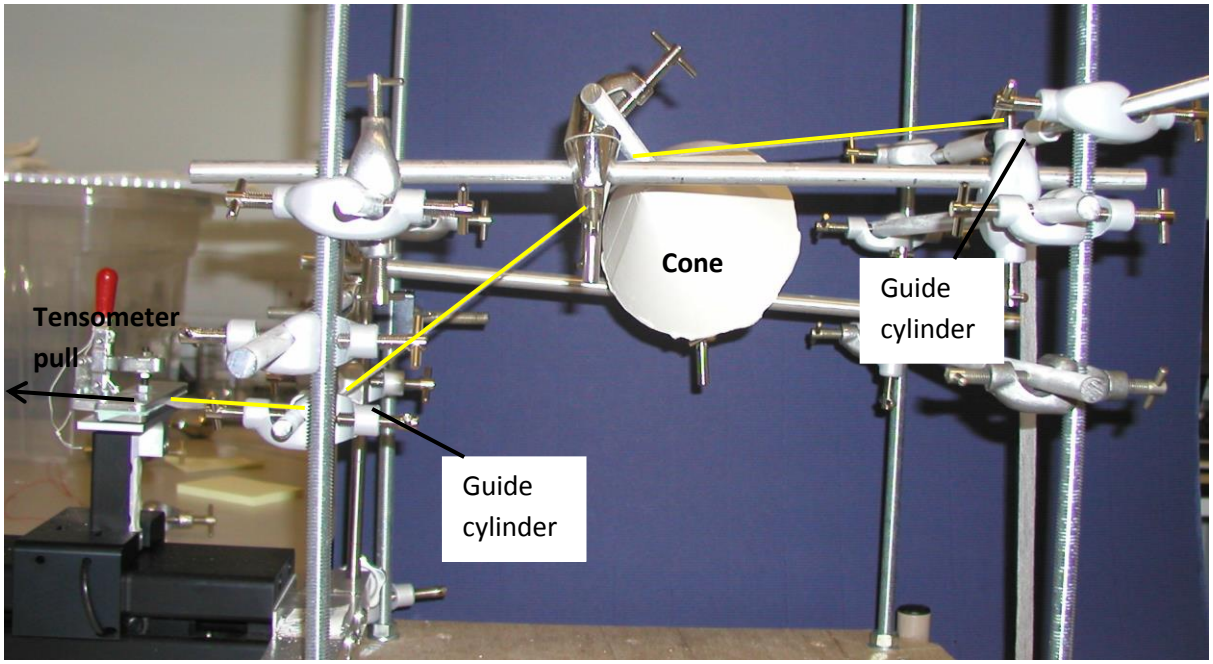

Figure 3.3: Photograph of the rig I used for the cone experiments

The line of the fabric is highlighted in yellow. The rig consists of four vertical studdings (length of 1m, diameter of 10mm) placed on a rectangular of dimensions 380 mm x 367 mm on a trolley, so the whole setup is easily moveable. On these four studdings I attach two rods and, subsequently, on these rods I attach the cone. In addition, two low friction guide rods were added to achieve the required path of the fabric strip through the apparatus, as discussed in §3.3.7.

3.3.2 Some facts about the used fabric

To complete this part of my project I needed to use a kind of nonwoven that I could find in abundance and was also cheap. This fabric existed in the lab and had already been used by a previous PhD student. It was of a kind typically used as the facing material on incontinence pads. I describe the properties of this fabric in Table 3.1.

Area density (gm^{-2})	17.0
Fibre polymer	Polypropylene
Bonding technique	Thermal calendered[1]
Manufacturer	Spun laid web
Optical micrographs	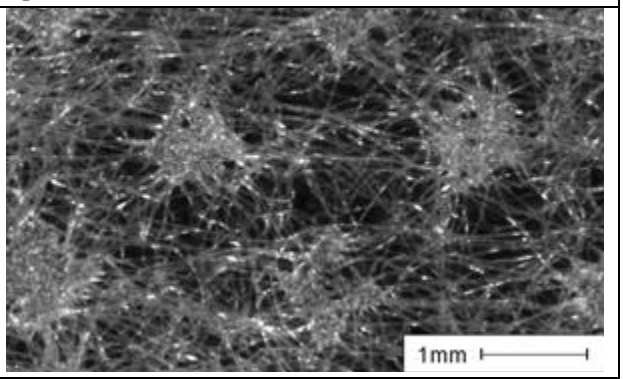

Table 3.1: Properties of the material used for friction experiments on cones nonwoven fabrics (Wong, 2008)

Each time I wanted to conduct experiments on a new cone, I cut a new strip of fabric that had the following dimensions: 995 mm x 30mm for the 45° and 35° cones and 1360mm x 30 mm for the 25° cones. The strips were relatively long because they needed to go through the whole length of the experimental setup, to be gripped by the tensometer head and to be attached to the dead weight at the other end of the strip.

3.3.3 Cone construction

Essential for my experiments is the accurate and precise construction of the cones. A random error at the cone angle is possible to have an effect at the final results.

Initially I constructed the mould made from polyethylene, a material which has very low surface energy so does not stick to the surface of the cone. I cut the mould at the proper layout angle which was derived by the equation:

$$S = 360 * sin(\alpha)$$ **Equation 3.5**

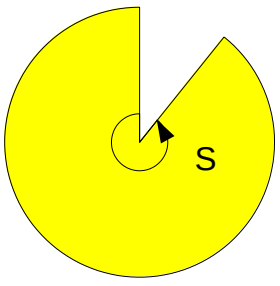

Figure 3.4: Layout angle on the mould.

[1] One or both calender rolls are heated to a temperature that allows the softening of the fibre. The fibre softens to form bonds with the other fibres.

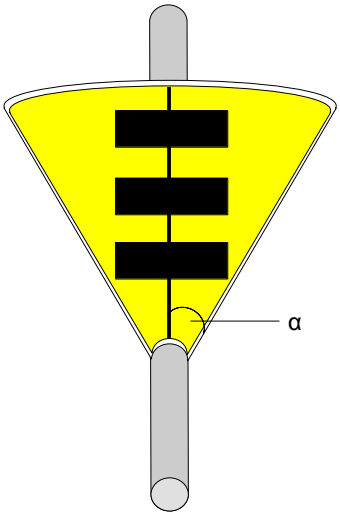

Figure 3.5: Mould of a cone, where α is the half cone angle.

Table 3.2 presents the half cone angles and the corresponding layout angles.

Half cone ange (α)	Layout angle (S)
45°	255°
35°	206°
25°	152°

Table 3.2: Correspondence between half cone angles and layout angles.

As axis for the cones I used studding of diameter of 10 mm. I prefer studdings to ordinary rod because the plaster of Paris is attached firmly on the thread without any danger of sliding. In my case, I mix the plaster of Paris with sufficient water to produce a mixture watery enough to last until I pour it into the mould (typically, 1.9 kg of plaster of Paris to each litre of water).

3.3.4 Cone angle verification

A problem that arises when I construct cones is that I don't know if they have the angle I set them to have, due to the fact they are handmade. For this reason I constructed a rig (Figure 3.6) to check their half angle.

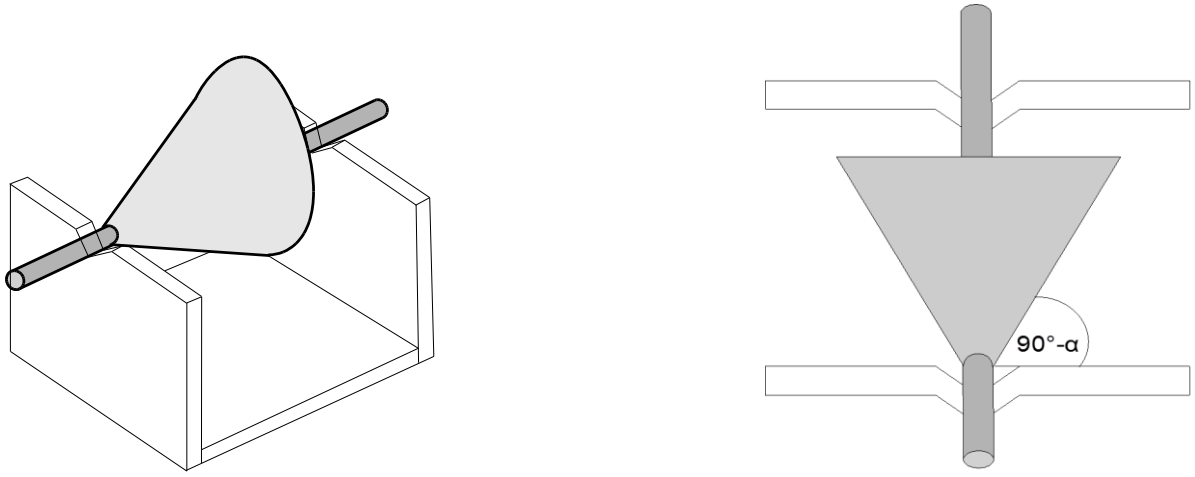

(a) **(b)**

Figure 3.6: (a) The diagram presents the setup of the cone in the half angle cone measuring rig I have constructed and (b) presents clearer the way I measure the half angle of a cone.

I took 7 – 12 measurements for each cone angle, each measurement at a different part of the cone. I present the results in Table 3.3.

Nominal cone angle (α)	Mean cone angle (α_m)	N	SD
25° (first cone)	24.6°	7	0.3°
25° (second cone)	25.6°	7	0.6°
35°	34.7°	10	1.2°
45°	45.0°	12	0.2°

Table 3.3: The ideal cone half angles, the mean (of 7-12 measurements) cone half angles and the error respectively as it results from successive measurements.

3.3.5 Using neoprene as cone surface material.

After constructing the cone, I needed to find and attach a suitable surface material. This material should have the uniform frictional properties across its surface, so data from friction experiments between the nonwoven test pieces and cone surfaces should fall on the same graph, for all fabric footprints on all cones, provided there is uniformity of friction. In Karavokiros' experiments (Karavokiros, 2007), with low angles cones, he achieved uniformity of friction using a neoprene sheet covering his cones. Therefore the search for a suitable surface material for the current work started with neoprene rubber.

As described by Karavokiros, I attached a sheet of neoprene by putting some PVA glue on the surface of the 35° plaster of Paris cone, which I manufacture as explained in §3.3.3 and then attached the neoprene as evenly as I could without any bumps. Preliminary experiments in which strips of the nonwoven were dragged over the surface of the 35° cone (using an early version of the method

described in §3.3.9) yielded very different values for the dynamic coefficient of friction, depended of the parts of the cone studied: range 0.34 – 0.59.

For this reason, I ran linear experiments along the neoprene surface of the cone to further explore its friction properties. I present the results of these experiments in Figure 3.7 and I conducted them with the setup shown in Figure 3.8. The problem arises from the fact that the lines don't coincide but they are parallel with a significance difference in the tensometer force.

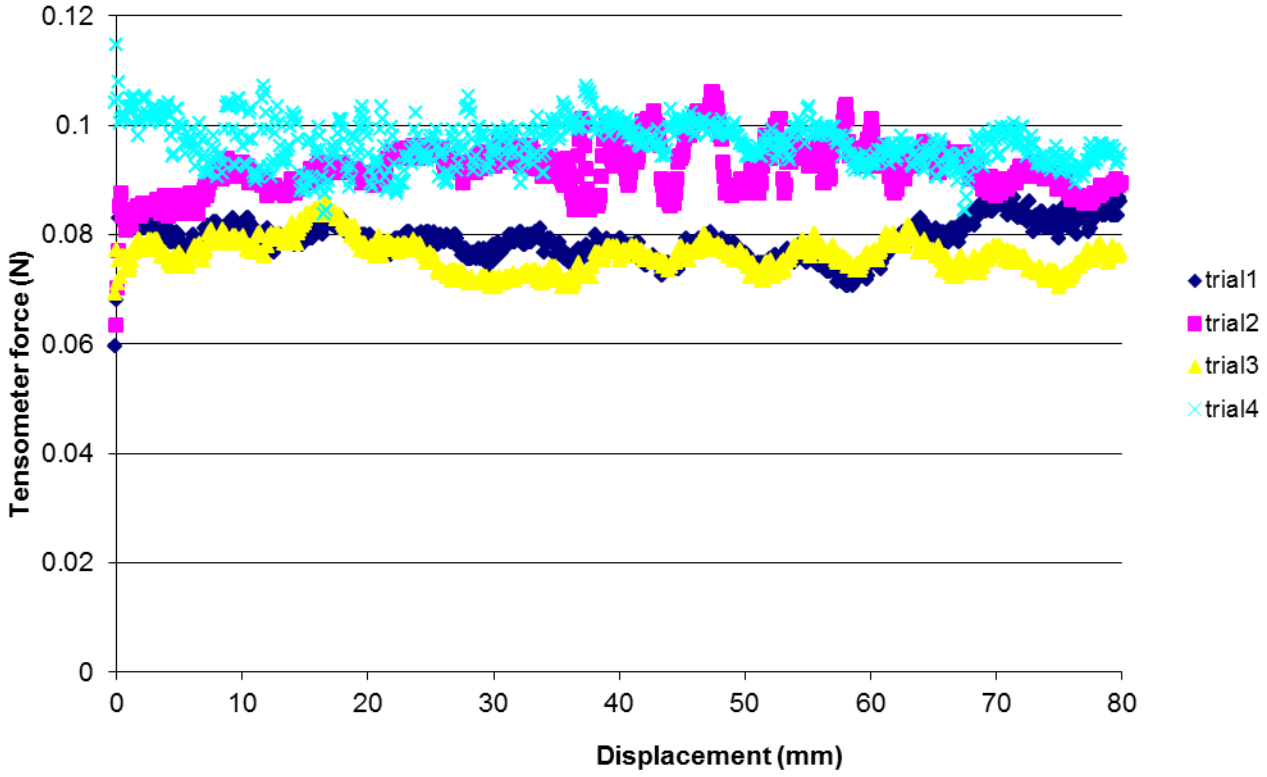

Figure 3.7: Result of linear experiments on the 35° cone covered with neoprene rubber sheet in four different paths, having a distance of 45° from each other.

I conducted these experiments by attaching a piece of nonwoven fabric on a cuboid piece of soft foam that could come in touch as a whole with the surface of the cone, no matter what the radius of curvature was. The piece of foam had dimensions of 10 x 10 mm, thickness of five mm.

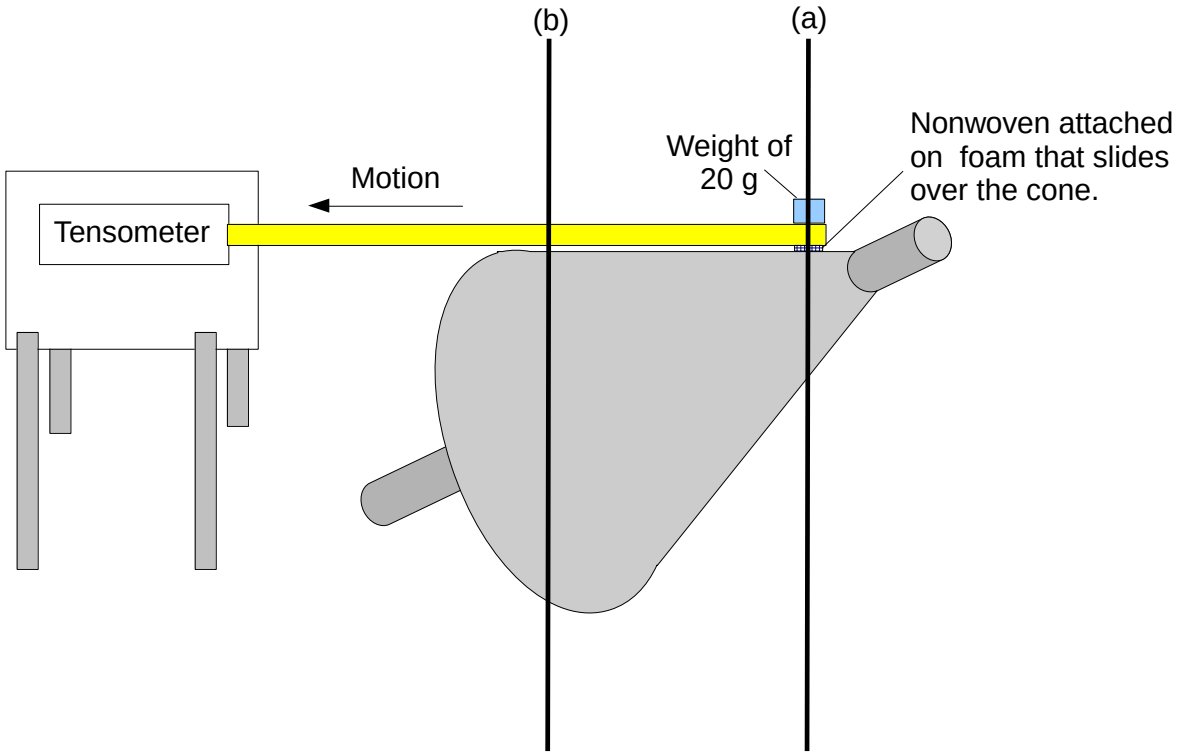

Figure 3.8: How the linear experiments are conducted over the surface of the cones.

The radius of curvature as shown in Figure 3.9 is larger when closer to the base and smaller when closer to the apex of the cone. This results from the fact that the distribution of the load on the cone will be different closer to the apex and different closer to the base of the cone. By saying this, I mean that the pressure closer to the apex will be higher in the centre of the cuboid foam, but closer to the base of the cone will be more uniform across the cuboid foam. Now, according to Amontons' law, the friction does not depend on the distribution of the load but on the total load I have. So, the friction should not depend on the radius of curvature, which is larger closer to the base and smaller closer to the apex of the cone. So, the frictional force would be the same no matter on which place of the cone the cuboid foam is.

I did not use a flat surface to study the frictional properties of plaster of Paris because the each mixture I make is different, so I wished to test exactly the one I used to construct the specific cone.

Figure 3.9: The (a) diagram presents the radius of curvature close to the Apex and the (b) diagram presents the radius of curvature close to the base of the cone.

Coming back to my linear experiments of Figure 3.8, I conducted them every 45° around the circumference of the cone, since I assumed that this angle would give me adequate coverage of the distribution of the frictional properties of the surface of the cone. The conclusion of my experiments is that the neoprene is not an adequate surface material. There can be a variety of reasons for this. First, it is old and dusty, something that could affect the measurements. Moreover, when I curve it, I may be causing filler particles to protrude, making the surface even rougher. I think these two factors make it inappropriate for my experiments.

3.3.6 Testing alternative cone surface materials

As I said previously, neoprene is not a suitable material to conduct my cone experiments. So, I started testing other materials as cone surface materials such as photographic paper. I conducted some linear experiments where I discovered I had isotropic properties. However, another problem arose, which was I could not apply it on the surface on the cone without creasing it or causing any bumps. For this reason I decided to abandon this surface material and test the bare surface of the cone.

This time the linear experiments were made across the surface of the cone in order to clarify whether the surface shares the same frictional properties. I repeated the linear experiments for the three half – angle cones, the 45°, 35° and 25° cone. The measurements were conducted setting a total displacement of 90mm and a crosshead velocity of 30mm/min or 0.0005m/s. There are five levels of comparison for the linear experiments across the bare surface cones:

1. At the same repeat, the variation of the friction force along the linear path.
2. Among different repeats of same experiments.
3. Among different experiments of almost the same path of the same cone. I say "almost" because I can never achieve exactly the same path, angle, position of the carriage in different experiments.
4. Among different paths of the same cone.
5. Among different cones.

From the comparison of the linear experiments some clarification was made. Initially, the first level of comparison was very good and the second was good since two repeats are never identical. The third level was quite good and the fourth level was satisfactory. The fifth level of comparison was satisfactory between the three cones, since the linear graphs produced a similar coefficient of friction. Overall, I can say that the bare surface is the material that fulfils all the conditions for becoming the subject of my experiments. In Figure 3.10, Figure 3.11, Figure 3.12 and Figure 3.13 I present the results of the linear pull experiments.

When I analysed the results of the linear experiments I find out the following coefficient of friction for each cone, for a total load of 28g: So for the 25° (first cone) I have a coefficient of friction of μ_d=(0.25±0.01) (Positions 3, 4 and 5), for the 25° (second cone) μ_d=(0.28±0.03) (Positions 2, 3, 4 and 5), for the 35° cone I have μ_d=(0.26±0.02) (Positions 1, 3, 4 and 6) and for the 45° cone I have μ_d=(0.29±0.01). These values were derived by dividing the received values from the tensometer with the used load which is 28g, while I excluded parts of the cone that exhibited frictional behaviour extremely high (usually parts close to the joint). It is easy to conclude that the linear experiments on the surface of plaster of Paris show almost isotropic frictional properties. As I observe from the linear experiments the coefficient of friction of the three cones is very similar to each other and almost

identical among different runs on the same cone. So, the curved pull experiments should give results that coincide for all the different cones made of the same material.

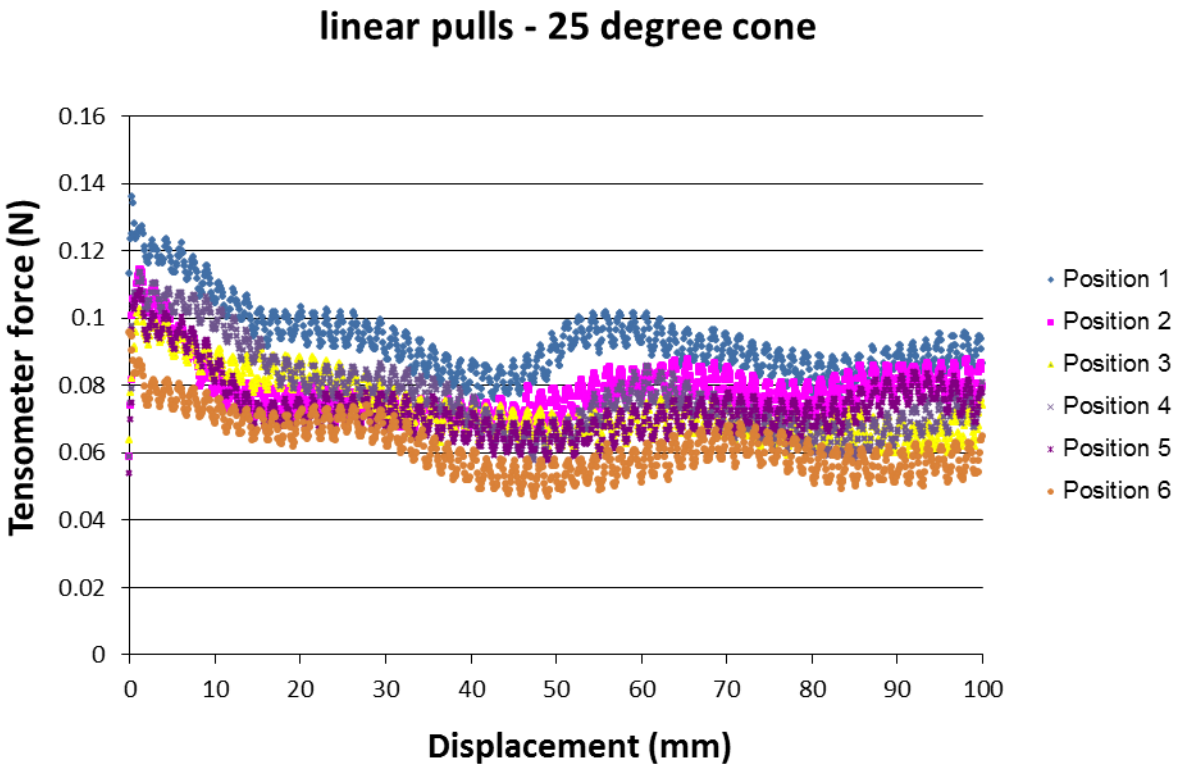

Figure 3.10: Results of linear pulls on 25° cone (first cone) from six different paths on the cone surface

The pitch of the thread of the tensometer I use to conduct the measurements is 2mm, while I can see that at Figure 3.10 at an interval of 10mm I have five peaks. That implies a direct relationship between the pitch of the thread and the high frequency that I can see in the graph, with each peak corresponding to a turn of the thread. An explanation of this could be that the nut which rotates on the driving shaft of the tensometer could catch dirt, or that this particular experiment was setup in a way that transmits the vibrations of the main trunk of the tensometer to the apparatus. Either way, this problem is not apparent in other force-displacement graphs.

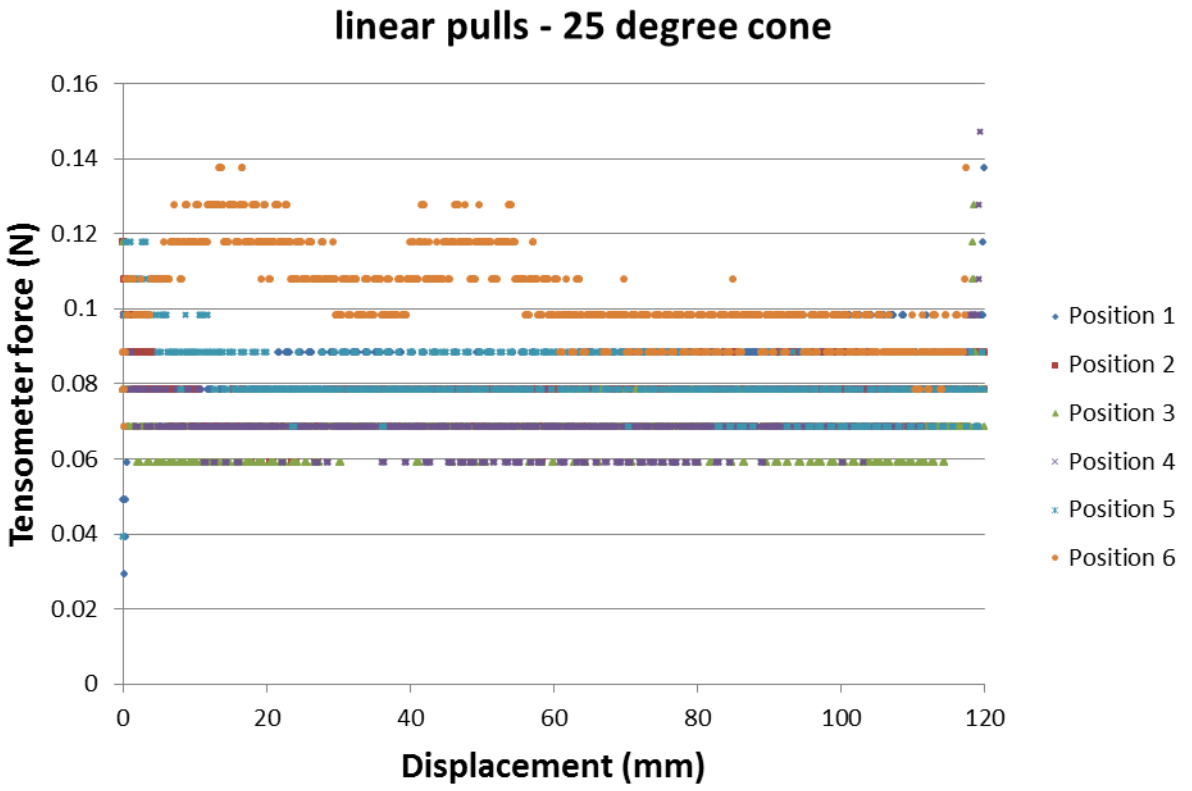

Figure 3.11: Results of linear pulls on 25° cone (second cone) from six different paths on the cone surface

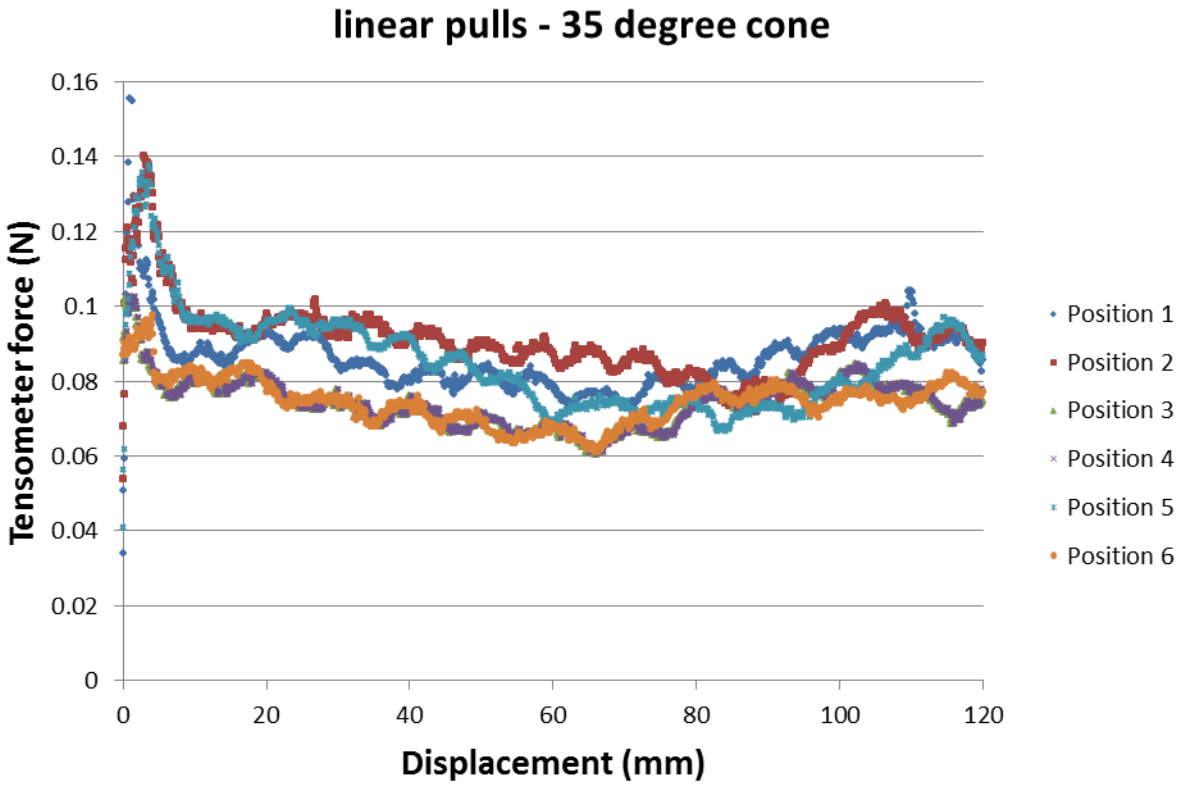

Figure 3.12: Results of linear pulls on 35° cone from six different paths on the cone surface.

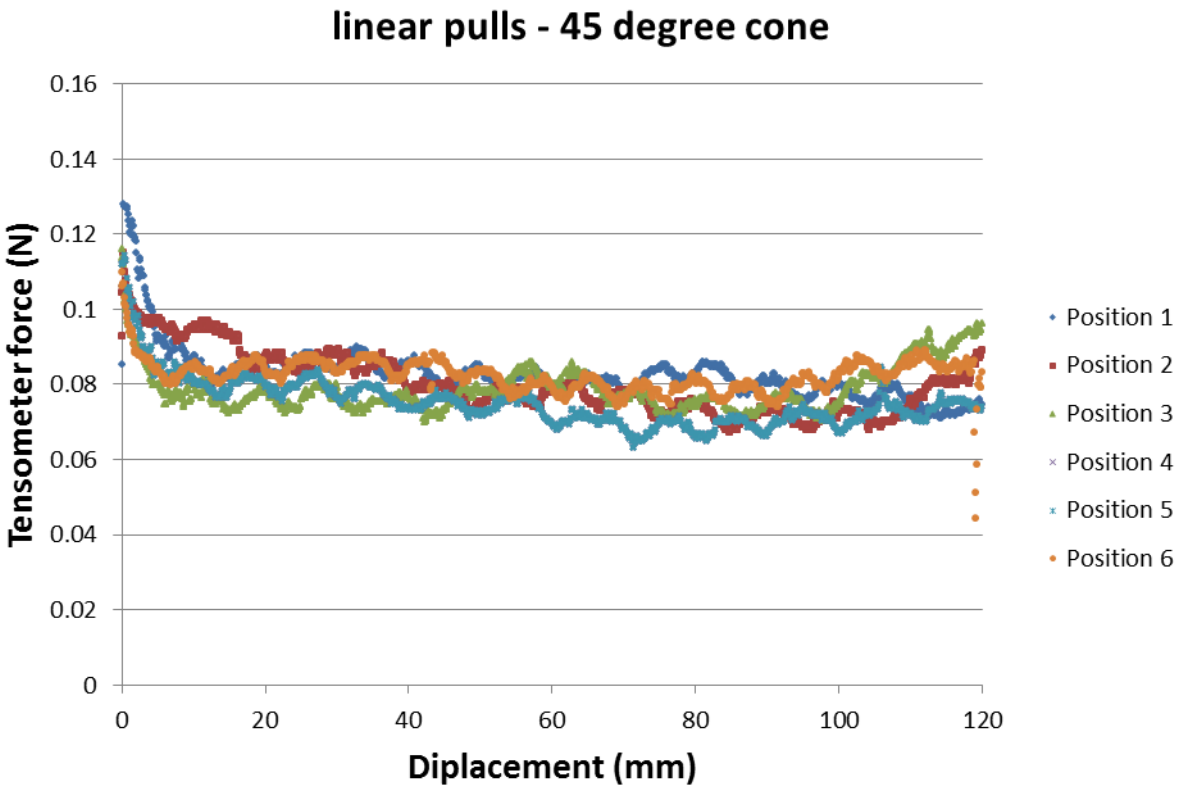

Figure 3.13: Results on linear pulls on 45° cone from six different paths on the cone surface.

3.3.7 Finding the best material for the guide cylinders

In order to conduct my main friction experiments some guide cylinders are crucial to direct my strip of fabric onto the cone surface. These guide cylinders need to have a small coefficient of friction, so the overall noise coming from them would not significantly affect the results that come from the cone surface. When I conducted my experiments, I tended to use many different portions of the cylinders. So, the guide cylinders needed to have uniformity of friction across the length and the circumference of the cylinder. If this did not happen and the friction varied across the cylinder, I would receive a lot of scatter in my results.

Initially, the cylinders were made of polypropylene and had an external diameter of 14 mm. First, I tested the polypropylene tubes for the coefficient of friction. The formula that I used to derive the value of the coefficient of friction was $T = mge^{\mu\beta}$, where T is the tensometer force, m is the mass of the deadweight on the free end of the fabric strip, and θ is the arc of angle of contact between the strip of fabric and the cylinder. For the polypropylene tubes I conducted experiments for seven different masses, for an angle of $\frac{\pi}{2}$ and the mean value of the coefficient of friction was 0.158.

So, the results of the coefficient of friction for the polypropylene cylinder showed that I could start some experiments with these cylinders. I conducted in total eight experiments with the 45° cone, 12

experiments with the 35° cone, and two experiments with the 25° cone, using always the bare surface cone as testing surface.

Unfortunately, the experiments did not bring the expected results, since they did not correspond to the same coefficient of friction. I investigated further the reasons of this and I saw that the polypropylene tubes had a coefficient of friction that varied along its length. So, I had to replace the polypropylene tubes with another material with a lower and more uniform coefficient of friction. For this reason I replaced the polypropylene white cylinders with other chromium plated brass cylinders that appear to have a lower coefficient of friction and an external diameter of 13 mm. Indeed, after conducting the experiments I found out a coefficient of friction of about 0.130, instead of 0.158 of the previous cylinders and a more uniform distribution of friction.

3.3.8 Description of the experimental procedure

Designing and developing the rig for friction measurements between cones and strips of nonwoven fabrics (Figure 3.14) involved addressing a number of constraints and practical issues of which the two most important were:

- Applying forces to the fabric.
- Arranging and measuring the different variables of the experiment θ_1, θ_2 and α (Equation 3.4)

The basic experimental device I used to conduct my experiments is called a tensometer. It is usually used to measure the strength of materials in industry and in this case it is a Diastron Miniature Tensile Tester 170 (MTT170). In my experiments I used it to measure the force applied to overcome the friction between the fabric and the guide cylinders and the cone surfaces, and the weights I have attached at the other end of the strip.

In each case I used a crosshead velocity of 30 mm/min ($5*10^{-4}$m/s) and a distance of around 120-130 mm. The crosshead moved horizontally, so I tried to keep the direction of the fabric, from the crosshead to the first cylinder horizontal. In this way, I did not introduce any component forces and also the direction of the fabric did not change as the crosshead moved further on the tensometer.

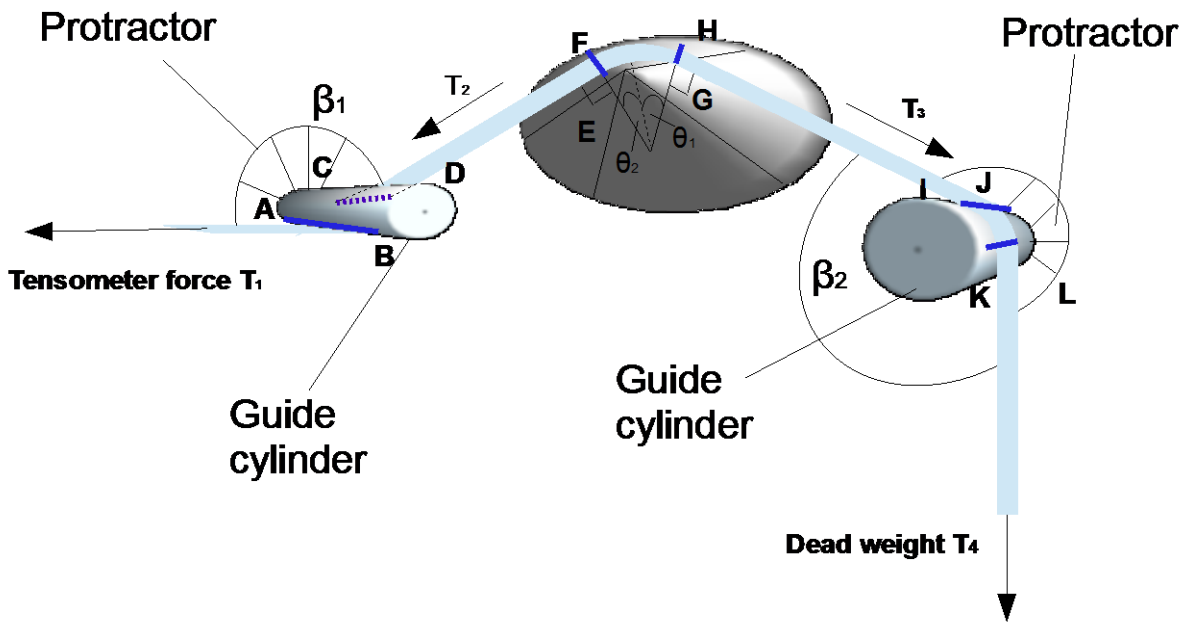

Figure 3.14: Diagram of the cone experiment setup, where I present the applying forces and the geometrical configuration.

3.3.8.1 Applying forces on the fabric

Equation 3.4 assumes only two forces on the fabric: tension (uniform across the width) parallel to the centre of the fabric strip and friction between the fabric and the cone. There are no lateral and no torsional forces on the fabric. I achieved that by dragging the piece of fabric along a geodesic on the cone surface (stays at the same place of the cone surface throughout the experiments), by applying tensile forces to the ends of the fabric strip, parallel to the strip centre line and by distributing uniformly the force across the fabric width. With this set up the fabric footprint of the cone is stable (unchanging) throughout the experiment as the strip slides over the cone. I have to signify here that because the fabric had a low shear modulus it was difficult to thread it in the test rig without distorting it, so introducing unintended stresses and strains. I tackled the problem by using a strip of paper (which had a higher shear modulus than the fabric) instead of the fabric strip to set up a particular experiment and measure the relevant angles. Once I had established the correct pathway with the paper strip and all angles measured (see §3.3.8.2), it was replaced with the fabric strip to run the experiments.

3.3.8.2 Arranging and measuring the variables θ_1, θ_2, tanα, β_1 and β_2.

From the previous paragraph I can infer that since the fabric footprint is constant throughout the experiment, I can measure the variables θ_1, θ_2 and tanα (Figure 3.2) at the beginning of the experiment and assume them not to change. Moreover, I built the cone around an axial rod, which was used to determine the cone position and orientation with the help of cone support rods and adjustable joints. I built the rig on a wheeled trolley which I clamped on the tensometer, while the tensometer had to be

clamped on the bench. This prevented movement between the tensometer and the cone throughout the experiments. Unfortunately, during our experiments there were three constraints:

(a) It is most convenient for the tensometer to be horizontal.
(b) The fabric should enter the tensometer horizontally so the tensometer reading equates to T_1 (Figure 3.14, Equation 3.10) throughout an experiment. Otherwise, the angle of the fabric to the horizontal where it enters the tensometer changes throughout the experiment as the crosshead moves further away from the cone, so changing the component of the tensometer reading which equated to T_1.
(c) The easiest way to apply tension to the other end of the fabric is with a dead weight, in a way that the force is vertically downwards.

I note that the set up described so far would allow experiments for only one pair of values for θ_1 and θ_2 for a given cone. To extend the range of the values of θ_1 and θ_2 that I could achieve I used guide cylinders. The orientation of the guide cylinders should be such as to avoid any lateral or torsional forces in the fabric. In order to do that, both guide cylinders had to be horizontal and perpendicular to the fabric centre line. Also, the lower surface of guide cylinder 1 had to be at the same height as the tensometer grips (so that the fabric entered the tensometer horizontally). By saying that, I mean that the leading edge of the fabric footprint of the cone (EF in Figure 3.14), has to be coplanar with the trailing edge of its footprint on guide cylinder 1 (CD, Figure 3.14). For the same reason (to avoid lateral and torsional forces) the trailing edge of the fabric footprint on the cone (GH, Figure 3.14) had to be coplanar with the leading edge of the second guide cylinder 2 (IJ, Figure 3.14).

In order to present clearly the points of contact of the fabric with the guide cylinders and the cone surface I quote the cross sectional view of the guide cylinders and the cone surface.

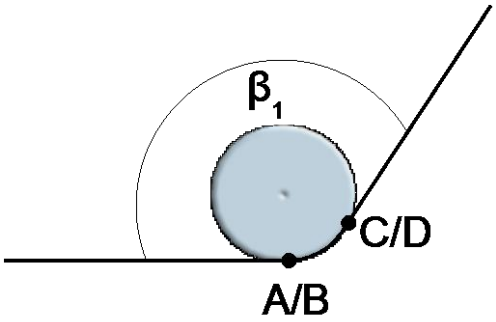

Figure 3.15: Cross sectional view of cylinder 1, where I present the angle β_1 and the points of contact between the fabric and the cylinder.

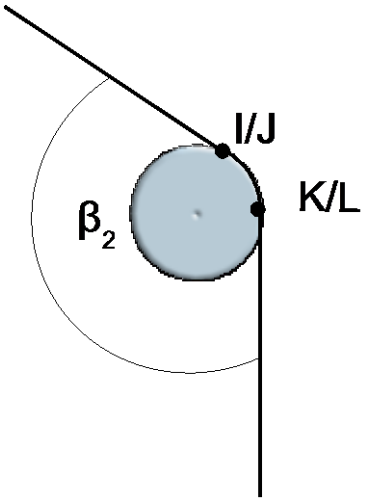

Figure 3.16: Cross sectional view of cylinder 2, where I present the angle β_2 and the points of contact between the fabric and the cylinder.

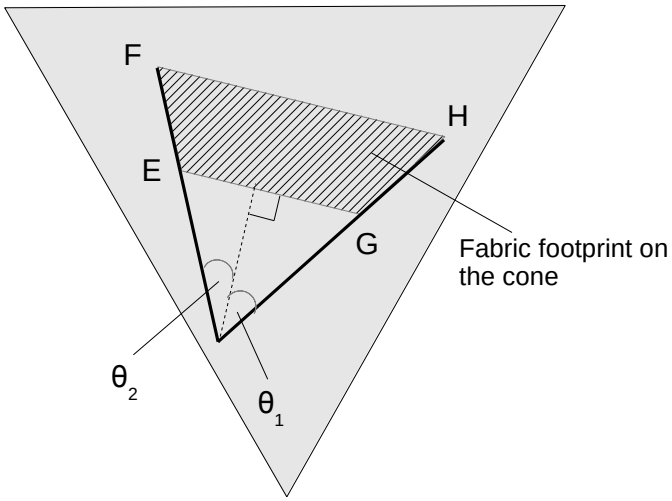

Figure 3.17: Cross sectional view of cone surface, where I show the area of contact between the cone surface and the strip of nonwoven fabric.

However, I should say that the introduction of the guide cylinders meant the tensometer reading was now affected by friction between the fabric and the guide cylinders as well as between the fabric and the cone. For that reason, corrections had to be made.

The relationship between the fabric tensions at either side of a guide cylinder are given by the equation that has been described by Gowsdow et al (Gwosdow et al., 1986):

$$T = T_0 e^{\mu\beta} \quad \textbf{Equation 3.6}$$

Where β is the angle of arc of contact between the cylinder and the fabric, T and T_0 are the fabric tensions ($T > T_0$) and μ_d is the static friction (Figure 3.18).

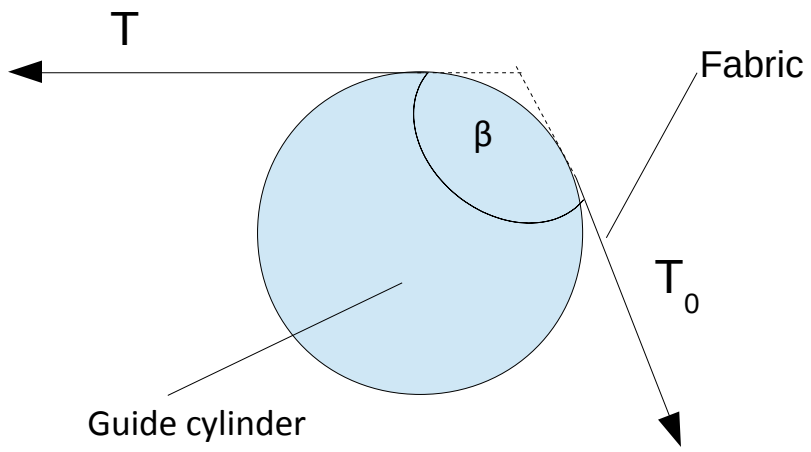

Figure 3.18: Interaction between fabric and guide cylinder (T> T_0)

I apply Equation 3.6 to guide cylinders 1 and 2 respectively:

$$T_2 = T_1 e^{-\mu_d \beta_1} \quad \textbf{Equation 3.7}$$

and

$$T_3 = T_4 e^{\mu_d \beta_2} \quad \textbf{Equation3.8}$$

I note that T_3 is bigger than T_4 and that T_2 is smaller than T_1. Combining the Equations 3.3, 3.7 and 3.8 I have:

$$\ln \frac{T_1 e^{-\mu_p \beta_1}}{T_4 e^{-\mu_p \beta_2}} = \mu \left(\frac{\sin\theta_2 - \sin\theta_1}{\tan\alpha} \right) \textbf{Equation 3.9}$$

Rearranging I have:

$$\ln\left(\frac{T_1}{T_4} e^{-(\mu_p \beta_1 + \mu_p \beta_2)} \right) = \mu \left(\frac{\sin\theta_2 - \sin\theta_1}{\tan\alpha} \right) \quad \textbf{Equation 3.10}$$

So, if I performed my experiments with different values of θ_1, θ_2, α, and I measured the values of T_4, T_1, θ_1, β_1, β_2 and μ_p. A plot of $\ln\left(\frac{T_1}{T_4} e^{-(\mu_p \beta_1 + \mu_p \beta_2)} \right)$ against $\mu \left(\frac{\sin\theta_2 - \sin\theta_1}{\tan\alpha} \right)$ for all data points from all cones should be a straight line with the gradient equal to μ, where μ is the coefficient of friction between the fabric and the cone surface.

Very crucial for my experiments was the measuring of β_1 and β_2 which are the arcs of angle of contact of the strip of fabric to the guide cylinders 1 and 2 respectively. I measured the arcs of angle of contact of the strip of fabric to the guide cylinders with the help of a paper strip, as discussed in §3.3.9.1. The way of measuring the arc of angle of contact of the two cylinders is by attaching a protractor to a disc and this disc to the cylinder (Figure 3.14), and laying on the surface of the cone a

sheet of paper from the Apex of the cone. The distance from this line to the line where the strip of paper lost contact with the cone in the direction of the tensometer defined the θ_2 angle and on the other side, at the line where it lost contact with the surface of the cone in the direction of the dead weight, defined the θ_1 angle (Figure 3.2).

3.3.9 Final detailed methodology

The final detailed methodology used to set up an experiment is given in the following list of steps (with reference to Figure 3.14).

1. Adjust guide cylinder 1 into horizontal position between the support rods with its lower surface at the same height as the grips of the tensometer.
2. Attach the cone onto the rig with the help of the support rods and adjustable joints.
3. Adjust the position and orientation of the cone so that what will be the trailing edge of the cone/paper footprint (EF) is coplanar with what will be the leading edge of the guide cylinder 1 / paper footprint (CD).
4. Adjust what will be the trailing edge of the guide cylinder 1 / paper footprint (IJ) so that it is coplanar with what will be the leading edge of the cone / paper footprint (GH).
5. Cut a strip of the test fabric 1.5 m long and 3 cm wide.
6. Cut a strip of paper with the same dimensions as the strip of fabric.
7. Put the strip of paper on the rig, ensuring that:
    a. Its length is at right angles to the tensometer and guide cylinder 1.
    b. It is horizontal between the grips of the tensometer and guide cylinder 1.
    c. It lies flat against the cone (it follows a geodesic path)
    d. Its length is perpendicular to guide cylinder 2.
8. Measure the angles of arcs of contact between the paper strip and the guide cylinders, β_1 and β_2, with the help of the attached protractors on the guide cylinders.
9. Measure the arcs of angles of contact between the strip of paper and the cone, θ_1 and θ_2, as described in §
   3.3.8.2 Arranging and measuring the variables θ1, θ2, tanα, β1 and β2..
10. Replace the strip of paper with the strip of test fabric.
11. Attach the dead weight to the free end of the fabric strip.
12. The experiments with the strip of fabric are ready to begin.

I repeated step 12 six times, each time with a different deadweight in order to complete a series of experiments with the same values of θ_1, θ_2, β_1 and β_2 for the cone being used.

3.4 Rigid cone results

In Figure 3.19 I present the results of the rigid cone experiments on the cones of 25° (cone 1), 25° (cone 2), 35° and 45°, where the data points fall close to a single regression line.

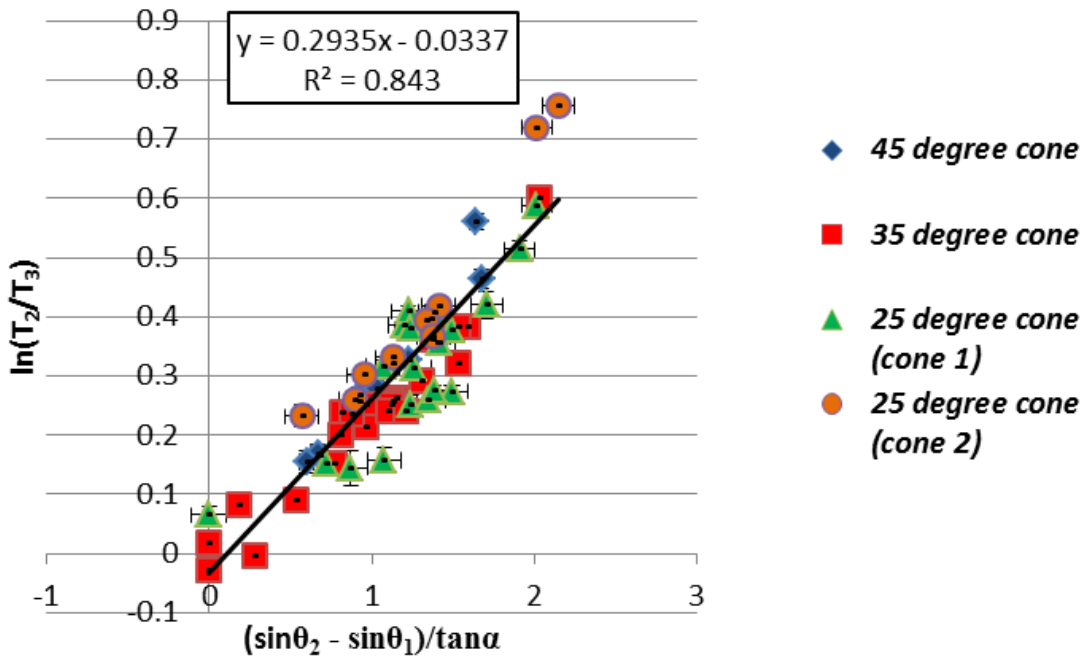

Figure 3.19: Results of cone angle experiments

The gradient of the regression line shows the overall coefficient of friction of the four cones. So, the values with the respective errors according to the least square method are: $\mu=0.293\pm0.016$, and for the offset I have: -0.03 ± 0.02. The mathematical model predicts that the offset should be zero, within experimental error. The negative value of the offset in this case probably comes due to the miscalculation of the coefficient of friction of the guide cylinders, which in this case may have been higher than the expected.

As I present in Figure 3.19, the results of four different cones constitute the total sum of the cone experiment results. If I analyse the results of each cone separately, for the 45° cone I obtain a $\mu=0.32\pm0.03$, and an offset of -0.05 ± 0.03.

For the 35° cone I obtain a $\mu=0.26\pm0.02$ and an offset of -0.02 ± 0.02

For the 25° first cone I obtain a $\mu=0.25\pm0.04$ and an offset of -0.01 ± 0.04

For the 25° second cone I obtain a $\mu=0.36\pm0.04$ and an offset of -0.05 ± 0.04.

As I see there are differences between the μ values for the different cones.

The trendline should go through the origin, so if I force the graph the correlation coefficient R^2 is 0.836 which is not so different from the 0.843 of the graph of Figure 3.19.

If I take a closer look at the graph I can see that I take measurements for approximately the same arc of angle of contact at the same cone but for different footprints. For the 45° cone, for the arc of angle of contact of 82° I have values of μ of 0.25 and 0.29. For the 35° cone, for similar arcs of angle of contact of 65° and 62° I have values of μ of 0.24 and 0.25. For the first 25° cone for the arcs of 54° and 51° I have values of 0.24 and 0.32, a relatively high difference, while for the second 25° cone for arcs of 25° and 27° I have values of 0.29 and 0.32. The high difference in the values of μ for the first 25° cone, led me to construct a second cone to crosscheck my results.

From the linear pull experiments I have found a maximum discrepancy between the results of the first 25° cone of 24%, with reference to the maximum value, while the quoted values show a discrepancy of 25%. About the second 25° cone, there is a discrepancy of 9%, while the maximum discrepancy was 25%. The results about the two 25° cones show that the difference of the μ values come within the margin of the predicted values from the linear pull measurements.

3.5 Discussion

The fact that the data points fall to a single regression line shows that the model is supported. Naturally, the different cones produced values of coefficient of friction which are close enough but not identical.

The range of μ I obtained was between 0.25 and 0.36. Many factors may have contributed to this difference of values. No matter how hard I try to manufacture cones of the same frictional properties, unfortunately I could not be as successful as I would like to be. Also the inhomogeneity of the fabric may have played an important role, since different strips of the fabric may have given different results. Moreover, the area of the fabric footprint on the cone in a given experiment is vital for the final results. If the area is bigger, the final result is more accurate because any small imperfections of the surface do not affect significantly the final outcome. In the next sections I analyse the potential error sources thoroughly.

3.5.1 Error analysis

From Figure 3.19 and from the different values of μ I quote in §3.4, I conclude there is a spread of data points, apparent from visual inspection of Figure 3.19. For this reason I perform an error analysis. I need to note that in this error analysis I take into consideration the error of the fraction F/mg ($=T_1/T_4$) that is derived from each experiment. In favour of better understanding, below I provide a graph (Figure 3.20) taken from one example experiment, where I make clear how the error arises. The gradient is 1.639 ± 0.015 and the offset 0.007 ± 0.012 according to the least squares method. In the same way I predict the error of every rigid cone experiment.

To conduct these experiments I assume that Amontons' laws stand. Exactly this graph of Figure 3.20 shows that since tensometer force and weight are proportional to each other, this assumption is correct, in accordance with Equation 3.1.

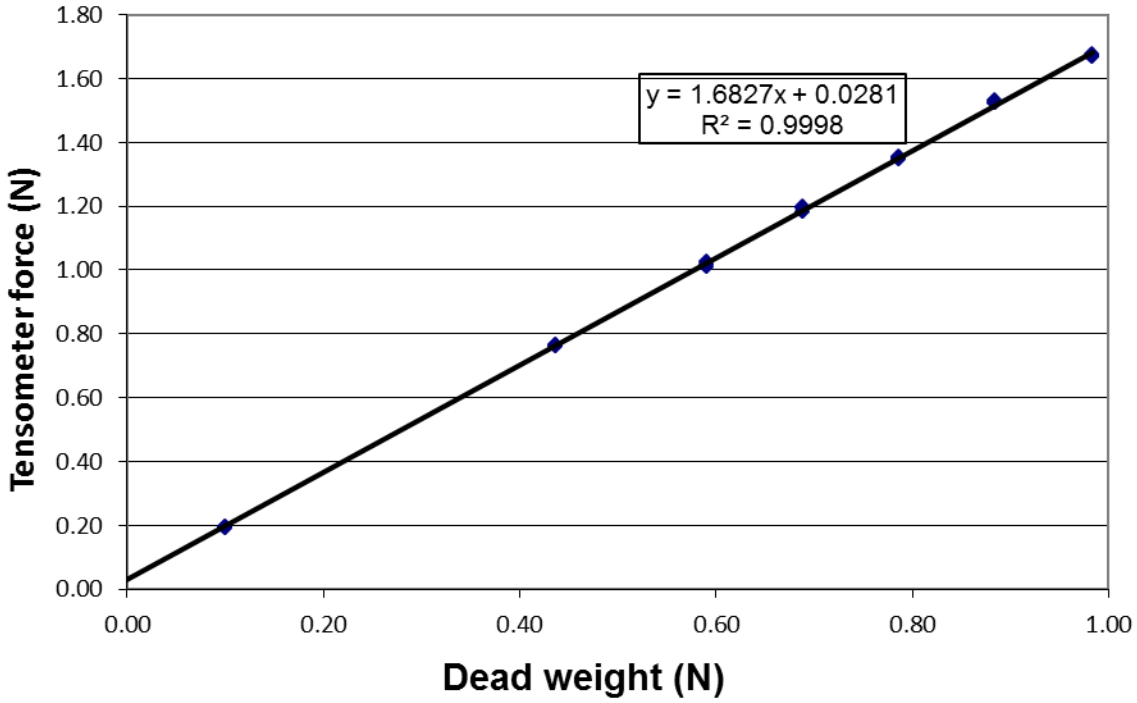

Figure 3.20: Graph of the tensometer force F against the deadweight mg for a rigid cone experiment.

The offset in the diagram of Figure 3.19 can have a variety of causes that are presented below:

1. I use a different strip of fabric each time, but the strip is worn out by usage, so there is a chance the coefficient of friction of the last experiments produces a slightly different value than the real one.
2. I should not forget the cones are handmade, so there are incurring errors as well. For example, the axial studding may not exactly be at the centre of the cone.
3. Also there can be errors in determining the angles θ_1, θ_2, as well as the angles β_1 and β_2.

Below follows an error analysis for the β_1 and β_2 angle that will investigate how the arcs of angle of contact of the fabric on the chromium – plated brass cylinders change in relation to the arc of angle of contact $\theta_1 + \theta_2$ of the cones.

I plot a graph of: $\beta_1+\beta_2=f(\sin\theta)$ **Equation 3.11**

The way to do this is to develop further Equation 3.3 with the help of the two dimensional figure of the rig that is presented in Figure 3.21.

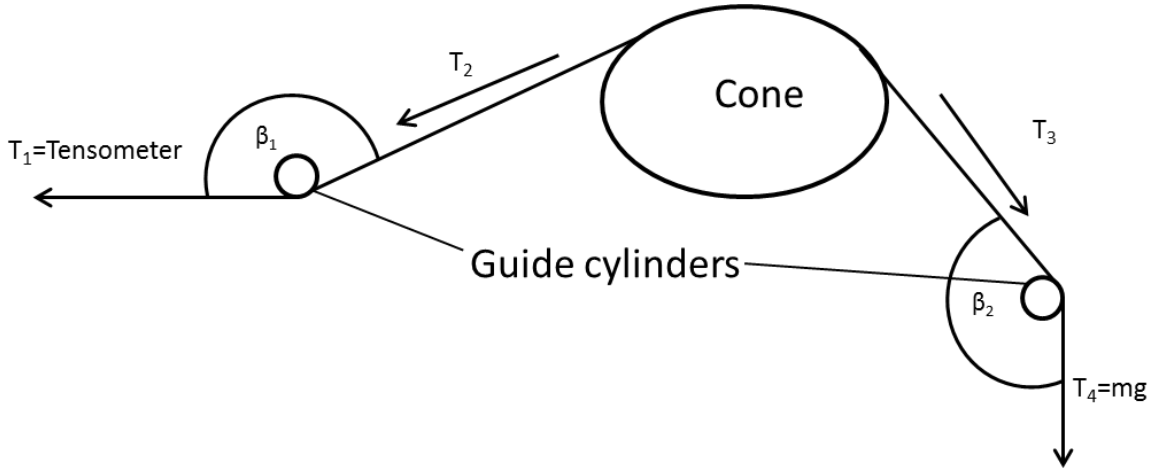

Figure 3.21: Two dimensional figure of the rig (see Figure 3.14 for 3D rig)

If I replace in Equation 3.3: $T_{yy} = Fe^{-\mu'_p \beta}$ **Equation 3.12**

and $T_0 = mge^{-\mu'_p \beta}$ **Equation 3.13**

where μ'_p is the coefficient of friction of the pipes, common for both of them.

So I have:

$$F = e^{\mu'_p(\beta_1+\beta_2)} mge^{\frac{\mu}{\tan\alpha}[\sin\theta]_{\theta_1}^{\theta_2}} \quad \textbf{Equation 3.14}$$

$$\ln F = \mu_p(\beta_1+\beta_2) + \ln[mg] + \mu\left[\frac{[\sin\theta]_{\theta_1}^{\theta_2}}{\tan\alpha}\right] \quad \textbf{Equation 3.15}$$

$$\beta_1+\beta_2 = \frac{\mu}{\mu_p}\left[\frac{[\sin\theta]_{\theta_2}^{\theta_1}}{\tan a}\right] - \frac{1}{\mu_p}\ln\left(\frac{F}{mg}\right) \quad \textbf{Equation 3.16}$$

If now we suppose that $\beta_1 + \beta_2$ is given by a formula of the form $(\beta_1+\beta_2) = \gamma\left[\frac{\sin\theta}{\tan\alpha}\right]_{\theta_1}^{\theta_2}$ then we have:

$$(\beta_1+\beta_2) = \frac{\mu}{\mu_p}\left[\frac{\sin\theta}{\tan a}\right]_{\theta_1}^{\theta_2} - \frac{1}{\mu_p}\ln\frac{F}{mg} \quad \textbf{Equation 3.17}$$

The following graph (Figure 3.22) presents the graphs that correspond to each half cone angle α, based on Equation 3.17.

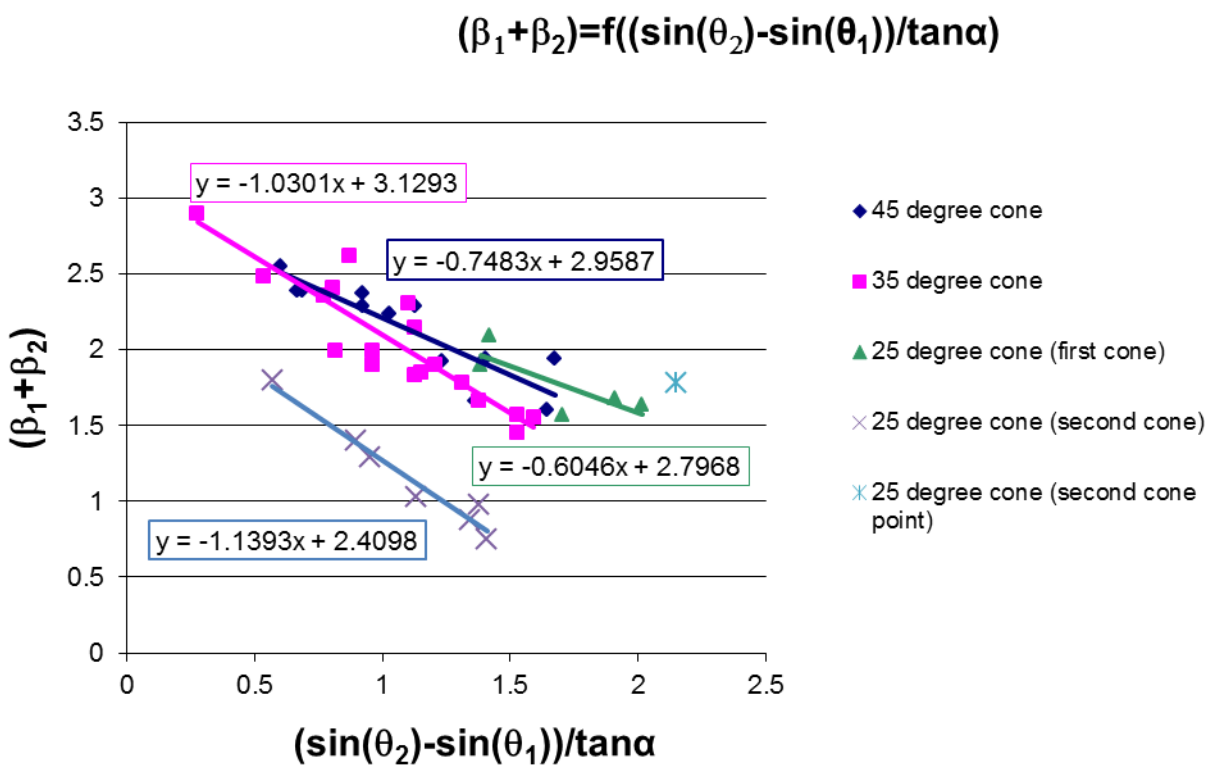

Figure 3.22: Variation of $(\beta_1+\beta_2)=f\left(\frac{\sin\theta_2-\sin\theta_1}{\tan\alpha}\right)$

So, for the 25° first cone the precise equation is:

$$(\beta_1+\beta_2)=-0.6046\left[\frac{\sin\theta}{\tan\alpha}\right]_{\theta_1}^{\theta_2}+2.7968 \quad \textbf{Equation 3.18}$$

For the 25° second cone:

$$(\beta_1+\beta_2)=-1.1393\left[\frac{\sin\theta}{\tan\alpha}\right]_{\theta_1}^{\theta_2}+2.4098 \quad \textbf{Equation 3.19}$$

For the 35° cone:

$$(\beta_1+\beta_2)=-1.0301\left[\frac{\sin\theta}{\tan\alpha}\right]_{\theta_1}^{\theta_2}+3.1293 \quad \textbf{Equation 3.20}$$

For the 45° cone:

$$(\beta_1+\beta_2)=-0.7483\left[\frac{\sin\theta}{\tan\alpha}\right]_{\theta_1}^{\theta_2}+2.9587 \quad \textbf{Equation 3.21}$$

As I can observe from Figure 3.22, the smaller the difference of the sines is ($\sin\theta_2 - \sin\theta_1$), the bigger the sum of the angles ($\beta_1+\beta_2$). This practically means that when the angles θ_1 and θ_2 have similar

values, the noise from the guide cylinders friction is proportionally big. Therefore, the larger the arc of angle of contact between the cone surface and the strip of fabric, in relation to the sum ($\beta_1+\beta_2$), the more reliable the results are.

3.5.2 Analysis of error bars, offset and slope deviation

In the graph of Figure 3.19 I present the results of the rigid cone experiments. What follows is an analysis of the error bars that accompany each data point of the graph.

The sum of ($\beta_1+\beta_2$) has an overall error of about two degrees. I also assumed that the θ_1 and θ_2 have individually an error of about two degrees and the error of half angle cone α is defined in

Table 3.3. For the error of tanα of the cones 25° (first cone), 25° (second cone), 35° and 45° I have the values I present in Table 3.4.

Cone angle (α)	**Mean cone angle (α_m)**	**SD (α)**	**SD (tanα))**
25° (first cone)	24.6	0.3	0.006
25° (second cone)	25.6°	0.6°	0.012
35°	34.7°	1.2°	0.02
45°	45.00°	0.16°	0.004

Table 3.4: The cone angles with the corresponding errors of the tanα

So, the total error of $\boldsymbol{\mu}$ is given from Equation 3.22.

$$\delta\mu = \sqrt{\Sigma_i \Delta_i^2} \qquad \textbf{Equation 3.22}$$

Where Δ_i are:

$$\Delta\theta_1 = \frac{\partial\mu}{\partial\theta_1}\delta\theta_1 \qquad \textbf{Equation 3.23}$$

$$\Delta\theta_2 = \frac{\partial\mu}{\partial\theta_2}\delta\theta_2 \qquad \textbf{Equation 3.24}$$

$$\Delta_{F/mg} = \frac{\partial\mu}{\partial\left(\frac{F}{mg}\right)}\delta\left(\frac{F}{mg}\right) \qquad \textbf{Equation 3.25}$$

$$\Delta_{\beta_1+\beta_2} = \frac{\partial\mu}{\partial(\beta_1+\beta_2)}\delta(\beta_1+\beta_2) \qquad \textbf{Equation 3.26}$$

$$\Delta\mu_p = \frac{\partial\mu}{\partial\mu_p}\delta\mu_p \qquad \textbf{Equation 3.27}$$

$$\Delta\alpha = \frac{\partial\mu}{\partial\alpha}\delta\alpha \qquad \textbf{Equation 3.28}$$

From the above equations the error of the ratio *F/mg* is very small since the tensometer force and the mass (and subsequently the weight) are well defined. So Equation 3.25 is not taken into consideration.

During the effort of adding the error in the graph, I understood that I have to calculate the error of each axis respectively. To be more precise what I represent on the vertical axis is:

$$A = \ln\left(\frac{T_1}{T_4} e^{-\left(\mu_p \beta_1 + \mu_p \beta_2\right)}\right) = \ln\left(F / mg\right) - \left(\beta_1 + \beta_2\right)\mu_p \quad \textbf{Equation 3.29}$$

And what I represent on the horizontal axis is:

$$B = \frac{\left[\sin\theta\right]_{\theta_1}^{\theta_2}}{\tan\alpha} \quad \textbf{Equation 3.30}$$

So, for the error bars of the vertical axis:

$$\delta \mathrm{A} = \sqrt{\left(\frac{\partial \mathrm{A}}{\partial\left(\beta_1 + \beta_2\right)} \delta\left(\beta_1 + \beta_2\right)\right)^2 + \left(\frac{\partial \mathrm{A}}{\partial \mu_p} \delta \mu_p\right)^2} \quad \textbf{Equation 3.31}$$

For the error bars of the horizontal axis:

$$\delta \mathrm{B} = \sqrt{\left(\frac{\partial \mathrm{B}}{\partial \theta_1} \delta\theta_1\right)^2 + \left(\frac{\partial \mathrm{B}}{\partial \theta_2} \delta\theta_2\right)^2 + \left(\frac{\partial \mathrm{B}}{\partial \alpha} \delta\alpha\right)^2} \quad \textbf{Equation 3.32}$$

So, with these two equations (3.31 and 3.32) I calculate the value for the error bars for each point in Figure 3.19.

3.5.3 Sources of errors

The results of the cone experiments spread across four different cones and I need to say that the spread of the results for each cone is significantly different. I identify several reasons that cause this effect and I quote them below:

- The cone of 45° has bigger surface area compared with the 25° cone, so I can characterise the tensometer force that I record as a "weighted average" from a larger number of samples, though more credible. As I assume, the 45° cone has a larger surface area than the 25° cone, so its results are more consistent.
- For the 45° cone I use a larger amount of material, a fact that prevents the appearing of bubbles when I mix the Plaster of Paris with water. As I observed, the phenomenon of air mixing with the rest of the mixture (plaster of Paris with water) is more intense with the smaller cones where I use smaller quantities. This has a result of producing bubbles on the surface of the cone that disturbs the homogeneity of the cone.

Another factor that can confuse the researcher who tries to interpret the results is the offset of Figure 3.19. As I can see from the initial Equation 3.2 on which this study is built, it does not have the intercept that appears in the experimental data, so the question of why it appears has to be answered. This offset suggests that some of the initial assumptions are not quite met. The bending modulus of the fabric is not exactly zero, so the tensometer has to apply an initial force to bend the fabric. Also, the fabric is not entirely inextensible, but a stretching occurs throughout the experiment, especially before sliding occurs. Another point which can affect the results in that the fabric is not placed precisely along a geodesic, so there is lateral movement on the cone. Finally, no matter how much I would like to, the surface of the cone is not completely homogeneous, which means another factor of error adds up.

3.6 Conclusion

In this chapter I present my work for high angle cones. The R^2 for Figure 3.19 is 0.843, an impressive number considering I have worked on four different cones. As I show in Figure 3.20 Amontons' laws are generally followed, while even though the strip of fabric is neither inextensible nor it has zero bending modulus, the model shows a satisfactory behaviour. So, the model works for high angle cones.

In the next chapter I test the model on volar forearms. Volar forearms are convex prisms of compliant substrate, while human skin adds a pinch of pragmatism to the model.

Chapter 4 Experiments on volar forearms

In Chapter 3 I dealt with rigid cones which present an idealised geometry, smooth surface and essentially zero deformation. The nonwoven exhibited negligible deformation and the model responded well.

In this chapter I push the validation one step further by using the volar forearms of participants with some essential differences to the rigid cones. Human forearms are distinguished by their compliant substrates, the surface wrinkling, the rucking deformation throughout the experiments and the sometimes substantial deformation of the nonwoven strip.

The major question waiting to be asked is how the model responds to a compliant geometry and sometimes far from smooth surfaces. To examine this I performed experiments on the volar forearms of 17 female participants, 10 above 65 years old and 7 below 65 years old using the configuration shown in Figure 4.1. The main difference between these groups is the substrate of the volar forearm. In the case of the young group the substrate was firm while in the older group it was more flaccid and the surface often heavily wrinkled. I have to note that most of the times I use female participants because I want a glabrous surface, which I can easily find on women, even though men with the same characteristics are welcome.

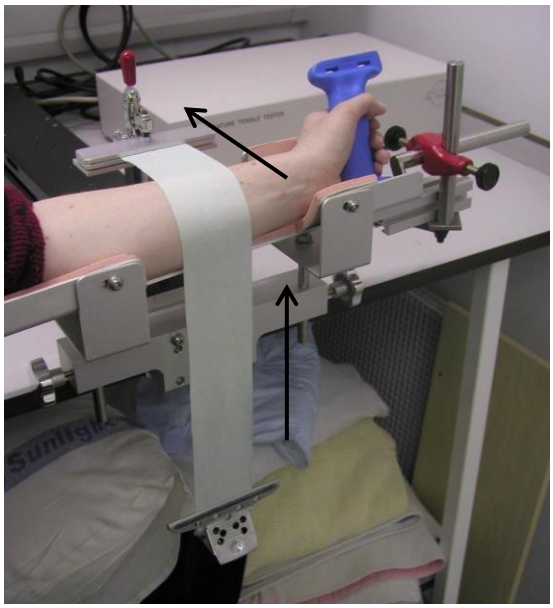

Figure 4.1: Setup used for volar forearm experiments (courtesy of Wing Kei Rebecca Wong.)

When I study compliant structures, a variety of deformations is happening throughout the experiments, which of course will be mentioned, and crucial for the conduction and the analysis of the experiments are the properties of the fabrics, so I will quote their properties and dedicate a section for their further study.

What I try to do in this chapter is validate the theoretical model for even more complex geometries, so a review of the model is necessary before I report the results.

4.1 Theoretical model

In the previous chapter I validated Cottenden's model on rigid cones, by isolating the geometrical factor and observing how it affects the model. In this chapter the shape of the arm approximates to a convex prism and the model collapses to the equation (Cottenden et al., 2008a):

$$T_1 = T_4 e^{\mu\theta}$$ **Equation 4.1**

From which I derive the coefficient of friction:

$$\mu = \frac{1}{\theta} \ln \frac{T_1}{T_4}$$ **Equation 4.2**

Where θ is the arc of angle of contact, tensometer force and dead weight are the forces that are presented in Figure 4.2. The tensometer force must be sufficient to initiate and sustain slippage, so that is possible to calculate the static coefficient of friction μ_s and the dynamic coefficient of friction μ_d. Ideally, the arc of angle of contact between the volar forearm and the strip of fabric is $\frac{\pi}{2}$, so the tensometer force coincides with the pulling force. Otherwise, I have to calculate the θ angle as presented in Figure 4.2, where in Equation 4.2 instead of tensometer force T_4 I use the pulling force T_1.

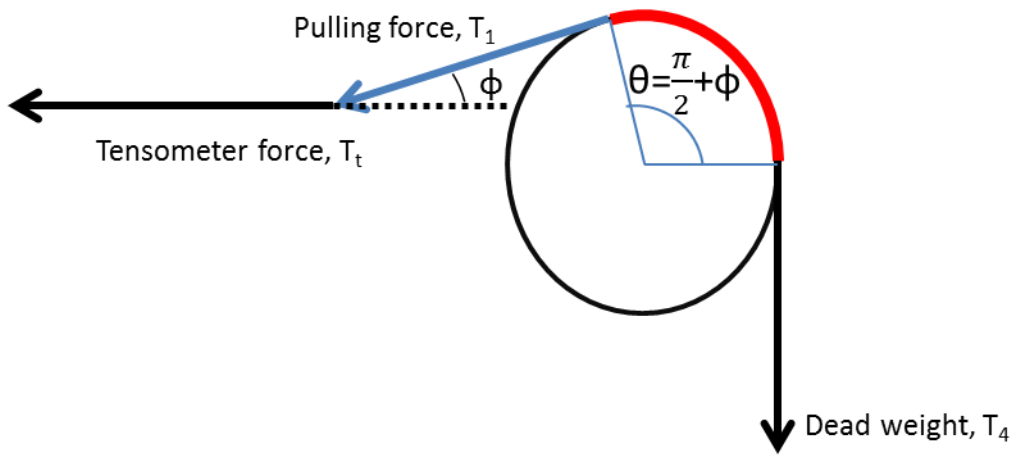

Figure 4.2: Cross section of a volar forearm and the applied forces, where φ is the angle between the horizontal and the strip of the fabric.

What I present in Figure 4.2 is the common case of forces in my experiments. I understand the direction of pulling force by the direction of the strip of fabric, since the pulling force is applied by the strip of fabric. I need to say that φ and subsequently θ might change by up to 2° during each measurement as the tensometer crosshead moves up to two degrees, a difference which I have incorporated in my error calculations. I placed the tensometer at a horizontal position, so the applied tensometer force had always a horizontal direction.

Below I present the equation from which I derive the pulling force, T_1.

$$T_1 = \frac{T_t}{\cos\phi} \quad \textbf{Equation 4.3}$$

The arc of angle of contact between the fabric and the volar forearm is:

$$\theta = \frac{\pi}{2} + \phi \quad \textbf{Equation 4.4}$$

In practice φ never exceeded 2° and so corrections were not applied since the error was too small relative to experimental noise to justify the work.

The materials as well as the method I used to validate the model follow.

4.2 Material and methods

I conducted my experiments using a selection of five nonwoven fabrics which I analysed further and an experimental setup which I also present in the following sections.

4.2.1 Nonwoven selection

We used a set of fabrics that were provided by SCA Hygiene, a selection of fabrics commonly used in incontinence pads and other hygiene products. The main characteristics of these fabrics are presented in Table 4.1, where PET is polyethylene terephthalate, PP is polypropylene and PE is polyethylene. The symbolism S/C bico means surface/core bicomponent.

Nonwoven code	Bonding technique	Fiber polymer(s)	Area density (gm^{-2})
SF03	Carded; Spunlaced	PET 100%	50
SF14	Carded	PP 95% Cotton 5%	30
SF17	Spunbond	PP	17
SF18	Spunbond	PE/PP S/C bico 30/70	15
DC06	?	PP	17

Table 4.1: Fabric characteristics

These fabrics with the experimental setup comprise the equipment I used to conduct the volar forearm experiments.

4.2.3. Experimental setup

In Figure 4.1 I present the experimental setup used for these experiments. As I show the forearm is stabilised in an armrest, while the participant sits comfortably on an armchair. During the measurements the participant grips loosely the armrest handle, an action which helps the participant stabilise her arm at the desired position.

Moreover, the experimental setup involves three cameras, one in front of the arm, one above of the arm and one at the side of the arm (Figure 4.3). The cameras in front and above of the arm provide interesting views of the deformation of the arm throughout the experiment on the top and on the front of the arm. The camera at the side of the arm provides interesting information about the angle between the strip of the fabric and the horizontal, information which helps me calculate the coefficient of friction using φ angle from Equation 4.3 and Equation 4.4. In order to make it easier we place a grid at the other side of the arm to calculate efficiently the possible deviation of the fabric from the horizontal (Figure 4.3).

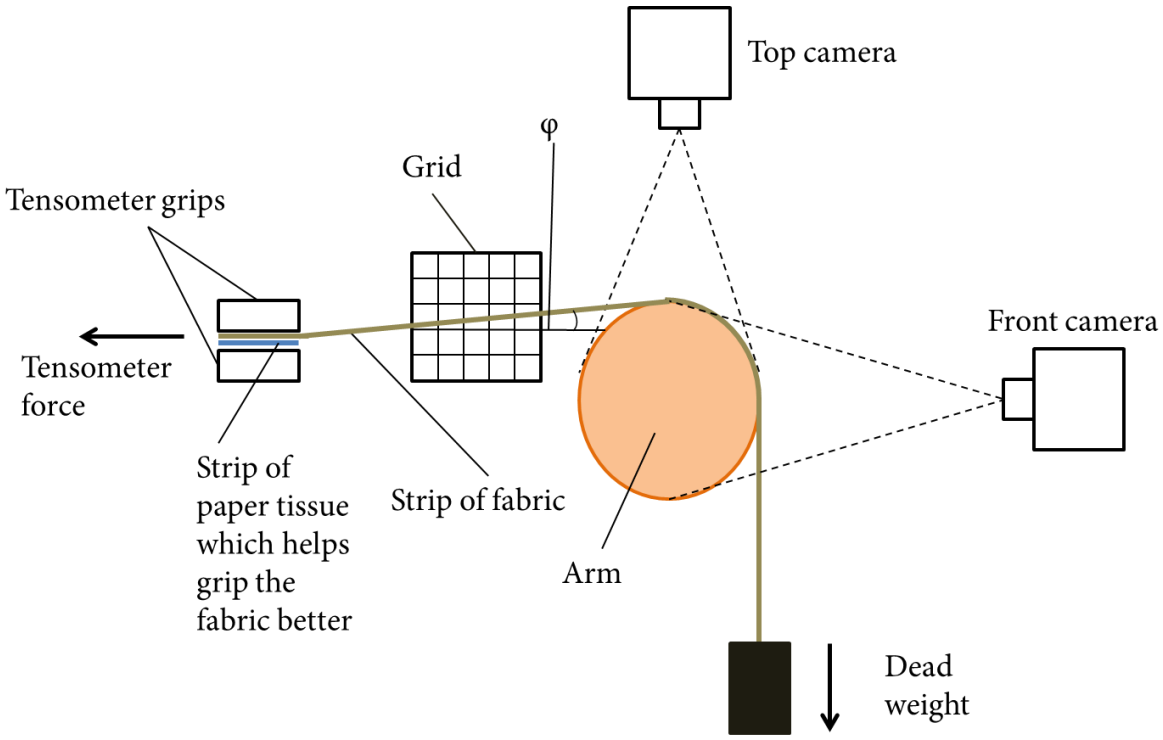

Figure 4.3: Arrangement of cameras in volar forearm experiments. A third camera (not shown) was placed on the opposite side of the fabric to the grid so that φ could be measured.

The complicated structure of Figure 4.3 is followed by a complicated method necessary to conduct each experiment. Since I conducted the experiments on participants, the methodology should be well defined, easily understood and approved by the national research ethics service.

4.3 Experimental process and selection of data (as described in the submitted protocol)

As it is easily understood, crucial for this part of the project was the careful selection of volunteers and the setup of an experimental process from which I could derive reliable data. These are the parts of the project I try to develop in this section. As I mentioned in the introductory section, to perform proper experiments I need hairless skin which can be mainly found on the volar forearm of women, though men cannot be excluded. I use the volar forearm because it is easily accessible, so convenient for both, experimentalists and participants. For this reason I and one of my colleagues, with whom we were conducting the experiments, applied for ethical approval at NRES committee London – Stanmore (REC Reference: 11/LO/1324, see Appendix A for details). The full application is given is Appendix A. The volunteers for our experiments were UCL students, patients of a collaborating incontinence clinic and residents of the Cheverton Lodge nursing house. The measurements on the volar forearm of the participants recruited from UCL and the incontinence clinic could take place in an environmentally controlled room (ECR) of stable temperature (23°C) and relative humidity (50%) in our laboratory, so we preferred the participants who could come to our premises. When we realised we could not recruit the necessary number of frail subjects to participate in our experiments we transferred our equipment to Cheverton Lodge nursing home where we could test many participants in a limited period of time. Since the residents of Cheverton Lodge were too frail to come to our premises, we had to conduct our measurements in space provided by the nursing house, relying heavily on Cheverton Lodge's staff and director, Ms Mary Rabbitt.

4.3.1 Why we choose different age groups?

For our experiments we recruited participants of two age groups: seven in the age range of 18-64 years and ten who were 65+ years old. So, by testing a variety of participants of different ages I could access a range of volar forearm types, from firm and smooth to flaccid and wrinkled. So, I have in total 17 participants, testing five fabrics on each participant, each fabric using five different dead weight masses and most of the times for each dead weight I conducted two measurements. This approximates a total of 850 frictional measurements which as it is easily understood demands further processing.

4.3.2 Structure of a measurement session

In this section we define the structure of a measurement session in two different – but at the same time – very similar parts.

- The participants who come into the ECR.
- The participants of the nursing house.

In §4.3.3 I present the detailed methodology of conduction of the experiments.

4.3.3 Methodology of volar forearm friction experiments

Below I present the detailed methodology we followed to conduct each experiment in the ECR:

1. Welcome the participant in the lab, ask if she wishes to visit the toilet and accompany her to the ECR.
2. Wait half an hour for the acclimatization period, where we explain the procedure and we ask her to sign the consent form in case she has not signed it.
3. At the end of the acclimatization period we measure the trans epidermal water loss (TEWL) to see if skin humidity affects the experiments.
4. Adjust the volar forearm so that the top surface is at the same height as the tensometer crosshead. In this way the fabric between the top of the volar forearm and the tensometer is horizontal
5. Verify that the top of the volar forearm is as horizontal as possible from the elbow to the wrist to avoid lateral fabric slippage during measurements.
6. Verify the whole structure is stable.
7. Adjust the nonwoven strip, ensuring that:
    (a) It is at right angle to the tensometer pull direction and the volar forearm surface.
    (b) It is horizontal between the grips of the tensometer crosshead and top surface of the volar forearm
    (c) It lies flat against the volar forearm.
8. Mark the "path" which the fabric follows on the volar forearm either using strips of special non-allergic sticky tape or erasing pen marks to either side of the intended fabric footprint to make sure I always use the same part of the volar forearm for the measurements.
9. Focus the front view and top view camera to record the deformations of the volar forearm and the movement of the fabric. At the same time, apply the focus of the side camera to record the angle between the strip of fabric and the horizontal.
10. Attach the dead weight mass to the free end of the fabric strip.
11. The experiments are ready to begin.

The experiments in the nursing home followed the same methodology, with the exception they did not take place in a room with a controlled environment, so there was no need for an acclimatization period. All the measurements started directly from step three.

I repeated the experiments for the five different dead weights I used, 10g, 20g, 30g, 50g and 70g in random order, having two repeats for each dead weight mass. We ended up with these values for several reasons. First, we needed the highest value to be high enough to test the validity of the model, without altering the structure of the fabric or causing significant disturbance to the participant. Second, we needed a good range of dead weights to help us have a clear photograph of the behaviour of the mathematical model we wanted to test. In the tensometer settings, I used a different maximum tensometer force each time, depending on the dead weight. The maximum force I setup had a range from 0.98N to 2.45N. I always set the lowest maximum tensometer force to complete the measurement for the simple reason that it has an impact on precision, since more pixels correspond to a smaller force. The sliding speed in the volar forearm experiments was 150 mm/min (= 0.0025 m/s) and the maximum displacement was 50 mm, according to previous work described by Rebecca Wong (Wong, 2008). Previous work conducted for a PhD thesis (Cottenden, 2010) proved that with this speed we could achieve reliable results. At the same perspective, we conducted some preliminary experiments from which we concluded that the displacement was about right and combined credible results with the least possible disturbance for the participant. All the experiments were conducted with

the help of the experimental device Diastron Miniature Tensile Tester 170 (MTT170) of Diastron limited. Finally, the testing fabrics of the experiments where five fabrics (Table 4.1). The dimension of each tested strip was 30 mm x 450 mm. The width was wide enough to minimise any changing of the properties due to strains applied, while the fabric should be long enough to allow the conduction of each experiment, by being long enough to cope with the crosshead displacement and short enough, so it did not impede the change of dead weight masses between experiments, and the weight of the fabric should not affect the measurements. I present further calculations for this issue in §4.4.7.2

The tensometer produced graphs of tensometer force against displacement. Tensometer force is the horizontal component of the pulling force which coincides with the pulling force when the arc of angle of contact is $\theta = \frac{\pi}{2}$. Displacement is the movement of tensometer crosshead. So, a tensometer trace or a tensometer graph presents the variation of the pulling force, or its horizontal component, as the tensometer pulls the fabric across the volar forearm for a particular length.

In the next two paragraphs I describe thoroughly the broader procedure from the recruitment to the conduction of the experiments in the ECR and in the nursing house.

4.3.3.1 Experiments in environmentally controlled room

In the case of the UCL employees and students we raised informative posters explaining how valuable their participation would be and if they are interested they can contact us. About the candidates recruited from the incontinenence clinic, they were initially approached by a member of staff who explained to them what was the purpose of our research and if they showed interest we were called to provide more thorough information by explaining the procedure of the measurements and providing the necessary information sheets. After at least 24 hours we contacted by telephone the candidates to ask if they wanted to participate in our measurements and in common we arranged a convenient time.

Upon the arrival, the participants were asked if they wished to visit the lavatory, so they will not feel the need to do so throughout the experiments. We accompanied them to the ECR where they were offered a refreshment and a snack if they wished. In the first half hour they acclimatized themselves in the ECR and signed the consent form, while we placed their arm in the armrest in such a way where the top of the volar forearm was level and levelled to the tensometer to ensure that φ is 0 (Figure 4.1). We marked the middle third of the volar forearm on which we were going to perform the measurements with two thin non allergic sticky strips. At the end of the half hour we took a photograph of the arm of the participant and we measured the skin hydration by measuring the trans epidermal water loss (TEWL) of the volar forearm, using a Vapometer, before and after the completion of the experiment. The photograph was taken to ensure the good state of the arm throughout the experiment, as we were going to compare it with another photograph at the end of the measurements. Measurement of the hydration level was necessary to compare the coefficient of friction to the hydration levels (how damp the skin was) between the different participants.

4.3.3.2 Experiments in the nursing house

Prior to the visit in the nursing house, my colleagues and I visited Cheverton Lodge when we were applying for ethical approval to inform the manager (Ms Mary Rabbitt) about our research and ask whether she was willing to help us. The manager should know about our research since she was the one who was going to inform the relatives of the residents about the research in which they were going to participate. After we obtained ethical approval we visited the nursing house several weeks prior to the experiments to talk to the manager and to the candidates, to whom we provided with information sheets and consent forms. The candidates should be in full mental health to participate in our measurements, otherwise there was the danger of harming them during the experiments. A few days before we went to the nursing home to conduct our experiments, we went to collect the consent forms and see the residents who agreed to participate in our experiments.

Notable is the fact that the participants of the nursing home came with the assistance of a nurse and were sitting in a wheel chair. The setup used for the experiments in the nursing house was the same as the setup in the ECR except for the fact that the measurements did not take place in an environmentally controlled room, but in a room provided by the administration of the nursing house. The experiments took place on the 21st and 22nd of May of 2012. The temperature had a range of 23.3 °C to 25.5 °C and relative humidity of 44% to 50%; that is close to the 23°C and 50% of our ECR.

4.3.4 Bending stiffness

When the data for volar forearm measurements were analysed, it became apparent that the results may have been influenced by the bending stiffness of the fabric which was assumed to be negligibly small in the theoretical model. Accordingly, the bending stiffness of the fabrics was measured as follows.

4.3.4.1 Experimental setup

Initially I designed and constructed the experimental setup that I use to find the bending stiffness of each material. I placed the strip of fabric I want to study between a flat piece of wood that has its surface that comes in touch with the fabric covered with paper to avoid adhesive affects, and the bench. I need to say that the fabrics bend under their own weight. Figure 4.4 shows the kind of deformation of the strip of fabric I want to achieve.

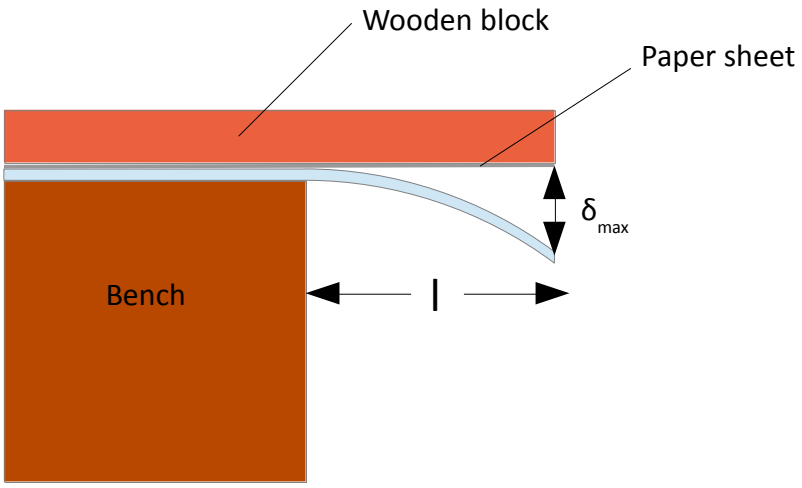

Figure 4.4: Deflection of fabric under each own weight

The way that each experiment took place was by sliding the wooden block a certain length (l) off the edge of the bench. After I gradually reduced the length (l) using my hands to move the board, recording each time the length and the corresponding deflection of the fabric δ_{max}. For this reason I attached a ruler at the side of the board to help me record the length and one ruler at the tip of the board to record the deflection (Figure 4.5). The deflection was recorded by a camera, with the help of which I could measure the deflection with an accuracy of 0.1 mm.

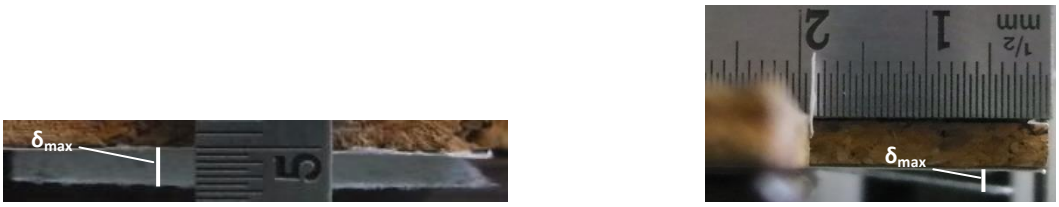

(a) (b)

Figure 4.5: Photograph (a) a front view of the setup with the help of which I measured the deflection δ_{max} of the fabric and photograph (b) presents a lateral view of the setup with the help of which I measured the length of the fabric under deflection l.

The bending modulus of the fabric was derived by the beam theory for uniform load, where the deflection at the end is given by the formula (Gere, 2004):

$$\delta_{max} = \frac{\omega l^4}{8EI} \quad \textbf{Equation 4.5}$$

So the bending stiffness is:

$$EI = \frac{\omega l^4}{8\delta_{max}} \quad \textbf{Equation 4.6}$$

Where $\boldsymbol{l}$ is the length of the fabric, $\boldsymbol{\omega}$ is the linear weight density (the weight per unit length of the strip) of the fabric and $\boldsymbol{\delta}_{max}$ is the deflection at the end of the beam. *E* is the Young's modulus of the material and *I* is the second moment of inertia. The product *EI* is the bending stiffness.

In the next section I quote the successive steps I follow to conduct each measurement.

4.3.4.2 Methodology

The detailed methodology I used was simple but at the same time very tedious:

1. I cut a strip with dimensions of 30mm x 100 mm, a length which I found convenient.
2. I attach it on the lower side of the wooden block I use, on a piece of paper that I have attached on the board to avoid fibres catching on the surface.
3. I place the fabric 1 mm from the edge of the board to avoid adhesion effects. The fabric is placed at right angles to the edge of the board, having towards the board the 3 mm side.
4. I extend the wooden block and fabric at the edge of the bench until δ_{max} is about XX mm
5. I reduce the length in steps, each time recording the length of the fabric and the corresponding deflection.

I used three strips of each fabric and I repeated the procedure twice for the first strip and once for the remaining two strips. In this way I tested the repeatability of the method on the same strip and across different strips of the same fabric. About the test pieces, I had 5 different fabrics of DC06, SF03, SF14, SF17 and SF18 (Table 4.1).

Having described the methodology I used to conduct my experiments, it is time to proceed to the presentation of the results.

4.4 Results

For simplicity I start my analysis of results from volar forearm friction experiments by using a representative of the below 65 years old group, participant MM03 and a representative of the above 65 years old group, participant DJ10 who had an especially flaccid arm and participant HJ07 who combined boney arm and flaccid tissues. For both of them I present the results I achieved using fabric SF03 which exhibited the simplest behaviour. I also show graphs for fabric SF17 and participant RJ05 who generated the highest coefficient of friction of all participants. I then present the tensometer graphs for the rest of the fabrics for these participants.

In the nested structures of the tensometer graphs I provide photographs of the arms corresponding to some points of the graphs. The (a) photographs correspond to the front view camera and the (b) photographs to the top view camera. The arrows label the direction of movement of the fabric.

Before presenting the graphs, I first establish below a nomenclature for the different tissue and fabric behaviours observed.

4.4.1 Effects on skin and fabric during the experiments

Deformation in the volar forearms is described as wrinkling and rucking. Notable is the fact that the difference between wrinkling and rucking is hardly distinguishable. I can define that wrinkling is the state of the skin which pre-exists my experiments, while rucking is the result of shear forces applied on the skin. One photograph presented in Figure 4.6 shows the wrinkled skin of participant DJ10 of my experiments, while in Figure 4.7 I present rucking under the shear forces applied by the tensometer. In order to make the change more obvious I present a photograph under the 10g dead weight where I can barely see any rucking in (i) and under 70g dead weight in (ii) where rucking is obvious.

Figure 4.6: Wrikled skin of volar forearm of participant DJ10

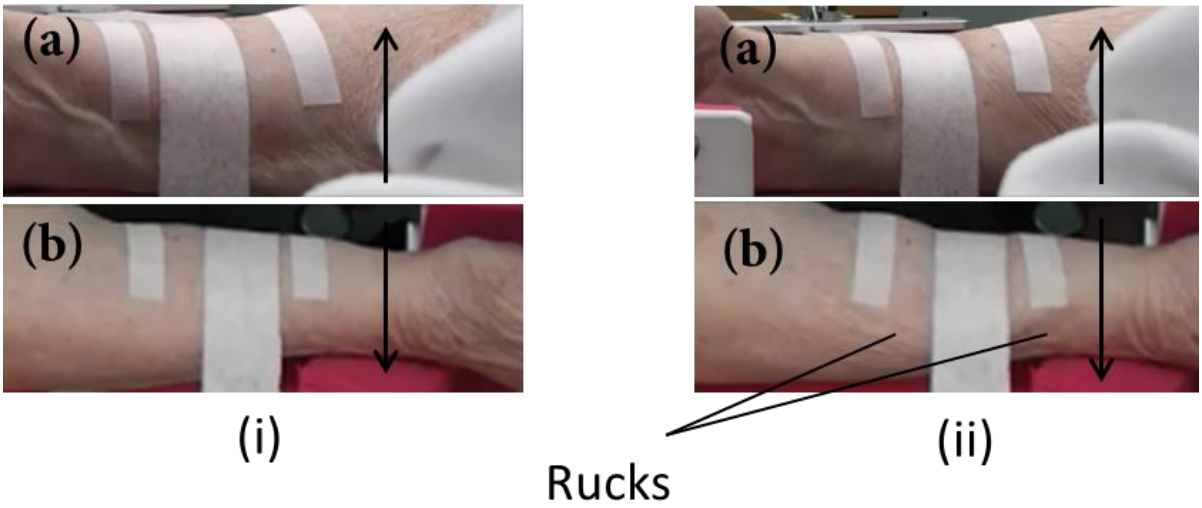

Figure 4.7: In these photographs of participant DJ10 and fabric SF03 I present (i) the state of the fabric and the tissue under 10g of dead weight, on photograph (ii) under 70g of dead weight. Where (a) is the front view camera and (b) is the top view camera, while the arrows show the direction of motion of the fabric.

In younger participants though, I did not observe either wrinkling or rucking, just indentation on the skin under the fabric pressure (Figure 4.8). Extreme rucking is apparent if I compare the photographs (i) and (ii) of Figure 4.7 and especially the front view photographs. Rucking appeared on older and

younger participants under the influence of high shear forces. Naturally, it was more intense on older participants, while we could barely see it on young participants.

Throughout the experiments I observed two different shapes of the fabric tangent to the skin: concave and flat (causing just minor indentation). I present these two phenomena in Figure 4.8, where at the photographs corresponding to 10g dead weight (i) I can see just the indentation phenomenon, while at the photograph of 70g dead weight (ii) I observe the concave effect from the front view camera (a) and deep indentation from the top view camera (b). I should say I observed rarely the effect of concave deformation on young participants, while it was common on older participants due to the flaccid tissues. In most of the young participants the only phenomenon I observed was indentation, where the fabric was level on the volar forearm, even under the higher dead weights.

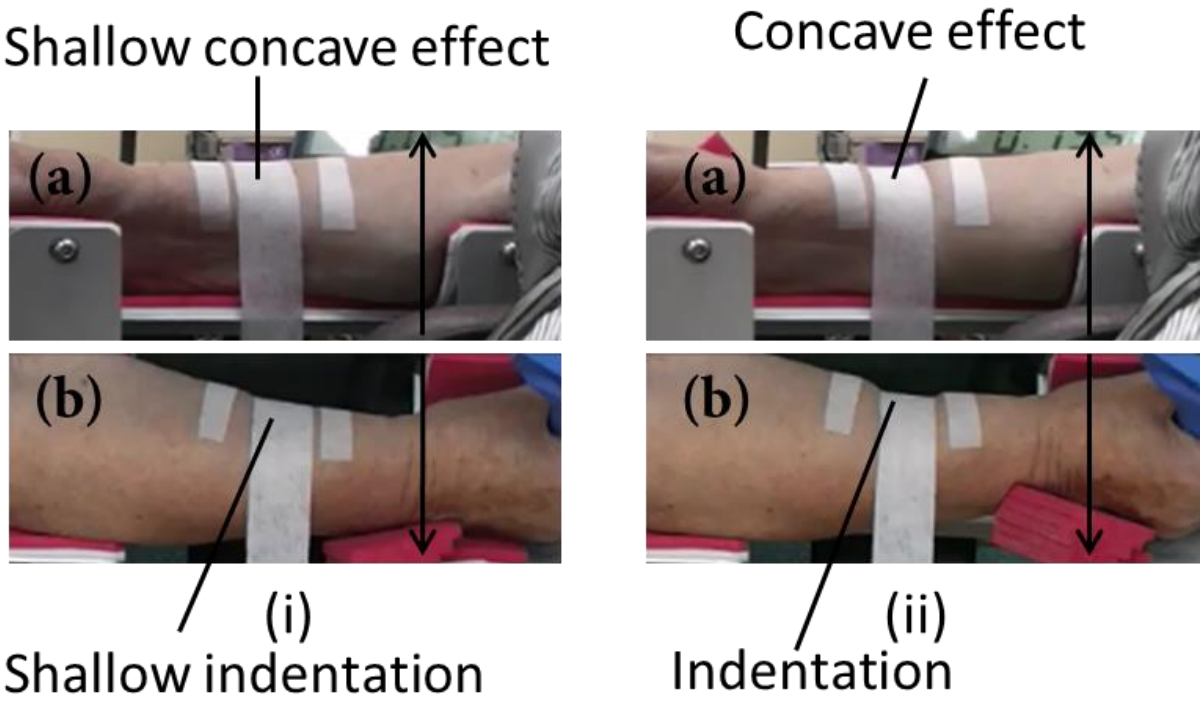

Figure 4.8: Photographs front (a) and top (b) view of participant's MD08 volar forearm under the weight of 10g (i) and under the dead weight of 70g (ii). Again, the arrows show the direction of movement of the fabric.

4.4.2 Experimental results of participant MM03

A complete set of tensometer curves of all volar forearm friction experiments is presented in Appendix B, while selected examples are presented here.

In Figures 4.9 – 4.11 tensometer graphs and photographs are presented for participant MM03 (who belongs to the group of below 65 years old participants) and fabric is SF03, which produces some of the simpler graphs. In the next paragraph I will try to illustrate changes at the geometry of the interface throughout the experimental procedure.

At the beginning I carefully placed the strip of fabric on the forearm and I waited for the tensometer crosshead to start moving. At the initial stage I did not see any slippage between the fabric and the skin, just shear movement of the skin. This deformation can be seen on the graph as the initial steep part of the curve. Finally, the deformation reaches a maximum which corresponds to the maximum tensometer force. At this point sliding starts between the fabric and skin and abruptly the tensometer force falls to a lower value, which remains roughly constant for the rest of the experiment. At this stable value the coefficient of friction also stays stable and the value I calculate corresponds to the dynamic coefficient of friction. The coefficient of friction which corresponds to the highest tensometer force is the static coefficient of friction.

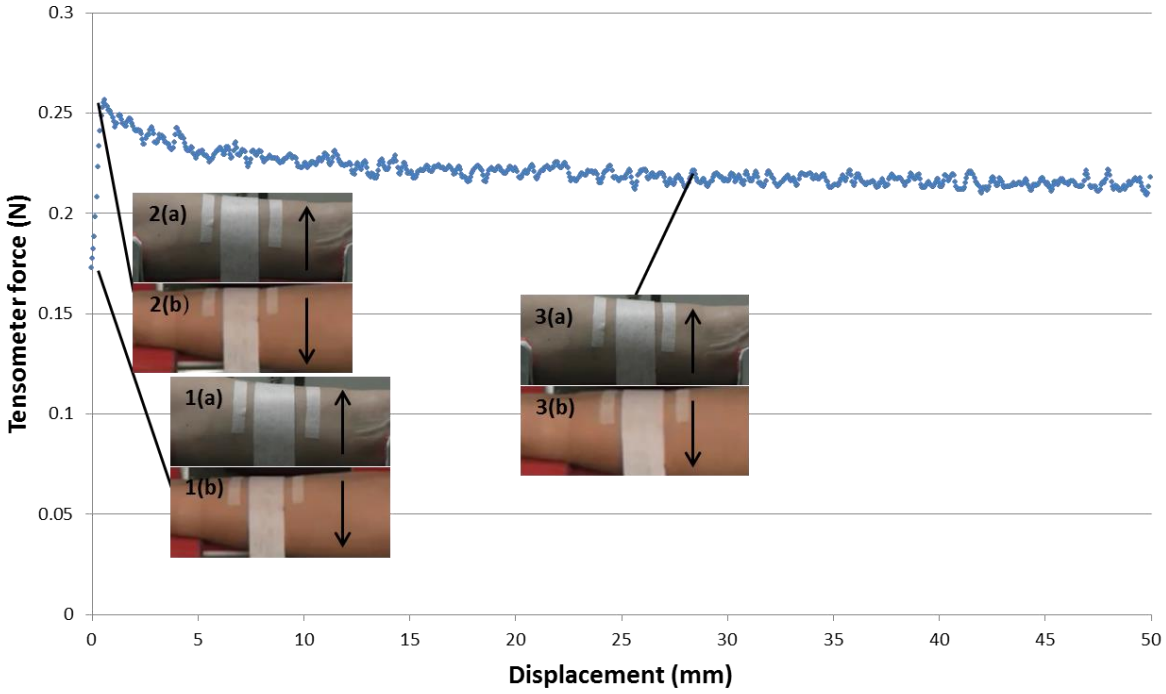

Figure 4.9: Tensometer graph of participant MM03 for fabric SF03 for the dead weight of 10g, where (a) front view camera and (b) top view camera.

Figure 4.9 shows photographs of the skin at three different points of the experiment. There is very little deformation or rucking.

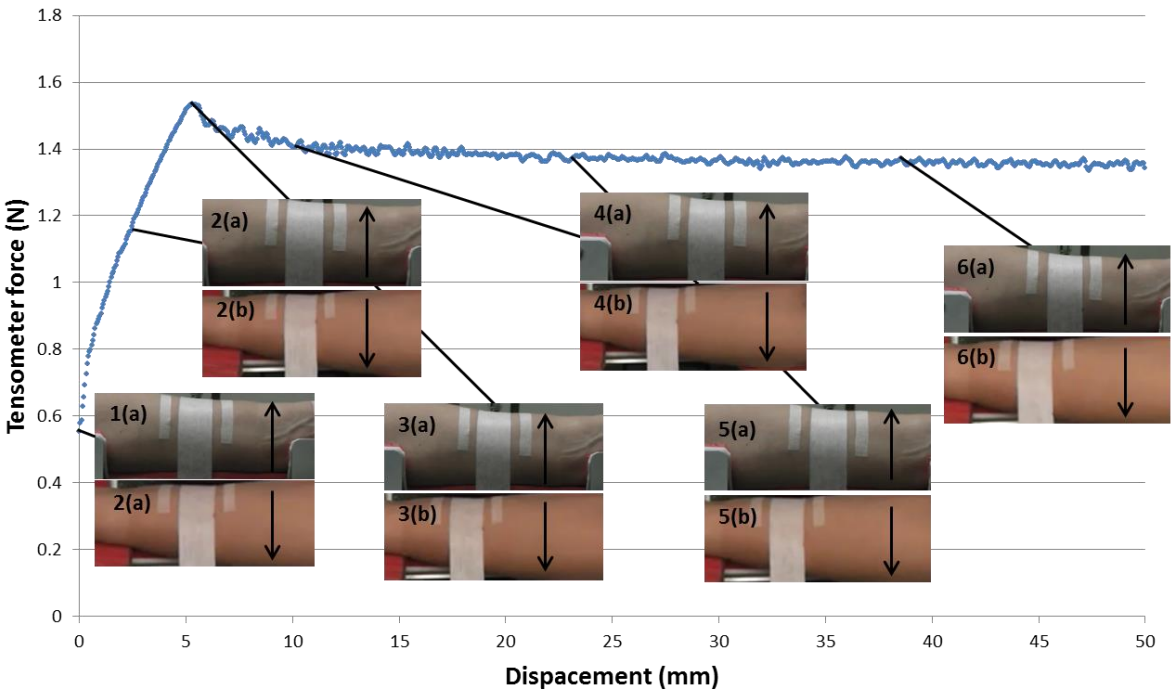

Figure 4.10: Tensometer graph of participant MM03 for fabric SF03 for the dead weight of 70g, where (a) front view camera and (b) top view camera.

Under the dead weight of 70g the volar forearm shows more deformation and in Figure 4.10 I tried to present the skin's appearance at various relevant points of the graph.

The first set of photographs show the state of the arm as the tensometer force increases. At the peak of the graph, sliding starts occurring and a faint indentation is now visible. At the plateau of the graph when sliding finally occurs, indentation is also visible and identified in photographs 4, 5 and 6.

Below I present all the tensometer graphs that correspond to the various dead weight masses I use to complete the experiment of fabric SF03 on participant MM03.

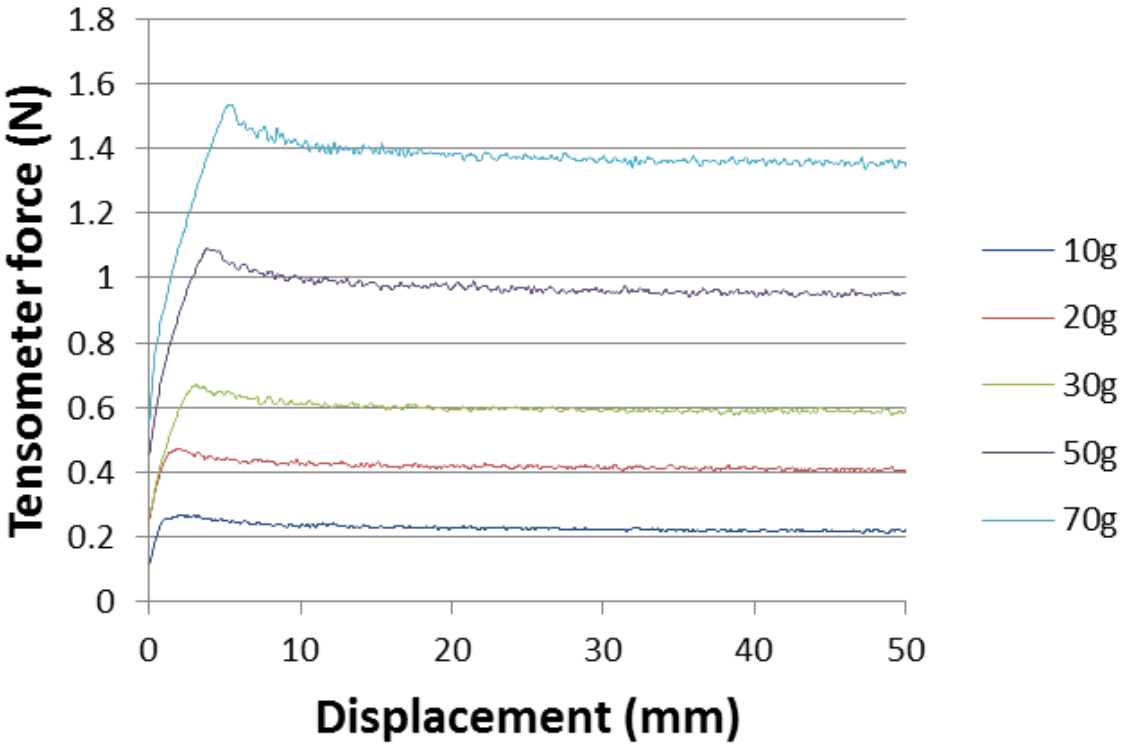

Figure 4.11: Tensometer graphs of fabric SF03 over the volar forearm of participant MM03

As I present in Figure 4.11, it is clear that bigger dead weight results in higher tensometer forces, which is completely normal according to Equation 4.1. Moreover, the graphs show the equilibrium plateau was reached relatively quickly, which means that for this particular participant the deformation of the volar forearm is not great. This will be analysed further in the discussion section. I need to mention that the part of each graph before it reaches its peak signifies the part of the curve where deformation is the dominant effect, while after the peak sliding becomes the dominant effect. From Figure 4.11 I show that the highest deformation happens under the dead mass weight of 70g and the smallest deformation under the 10g dead weight mass.

The graphs lead to a linear graph of pulling force against dead weight with an extraordinarily high R^2 value of 0.99 (Figure 4.12), as predicted by Cottenden's model (Cottenden, 2010).

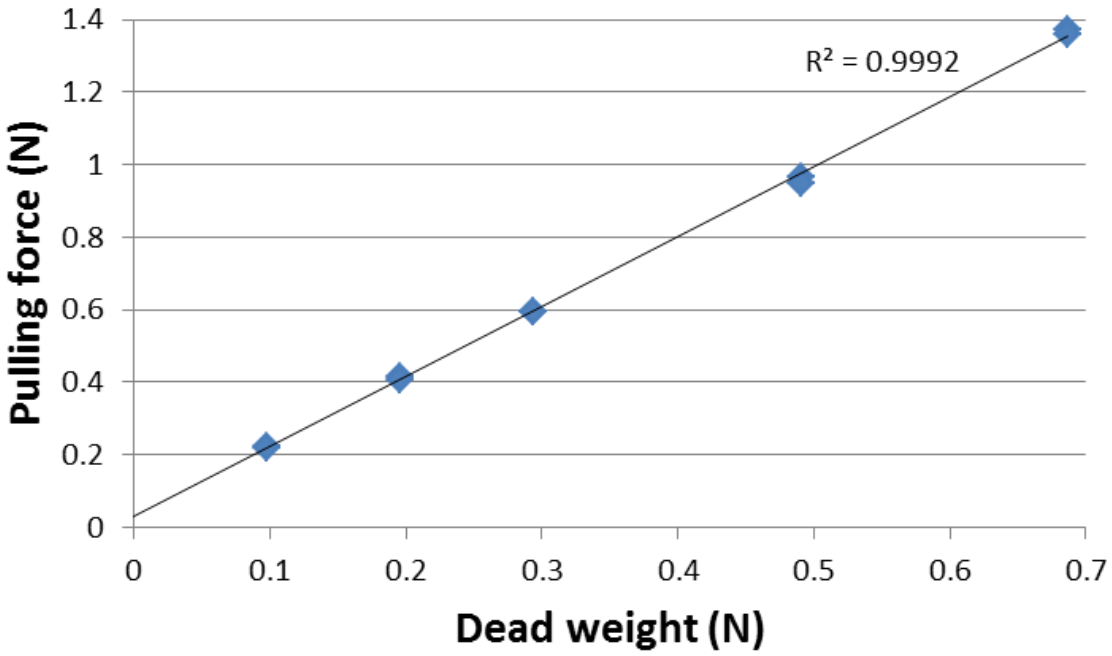

Figure 4.12: Graph of pulling force against dead weight of fabric SF03 on participant MM03. There are ten data points, two for each participant.

For every series of measurements of every fabric I have a graph of pulling force against dead weight similar to the graph I quote in Figure 4.12. The positive intercept which appears is not predicted by the mathematical model, but I intend to analyse this further in §4.5.3.1.

As I mentioned earlier, SF03 is not the only fabric I experimented with. Below I quote the tensometer graphs for the rest of the fabrics for MM03.

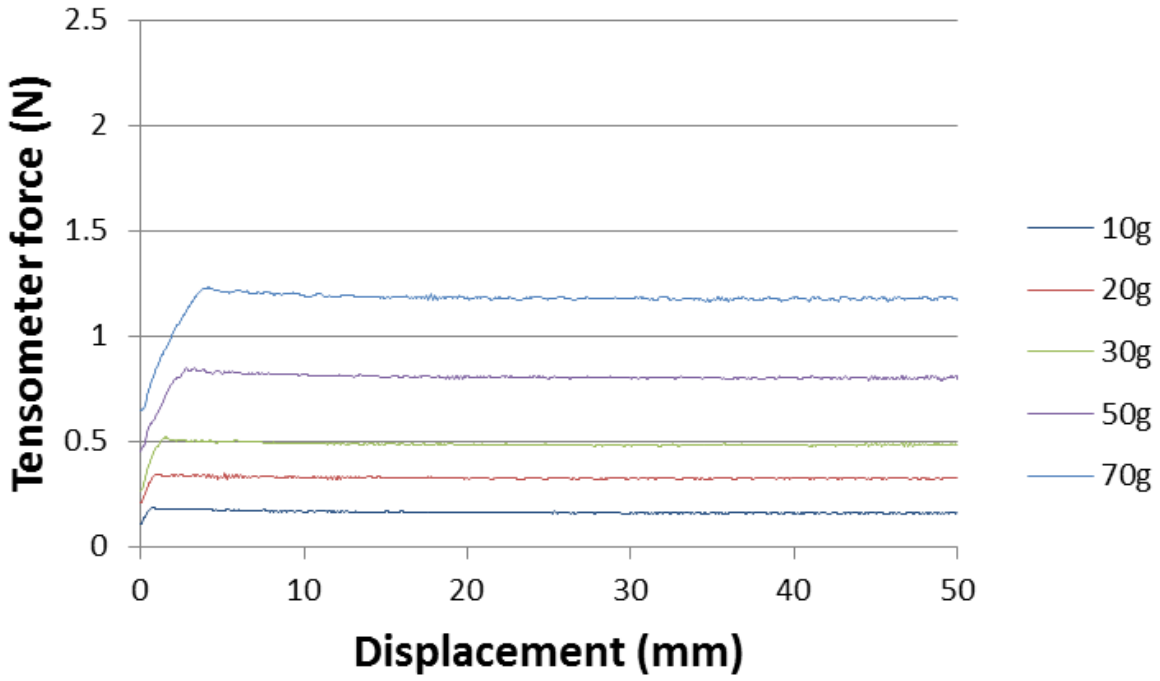

Figure 4.13: Tensometer graphs of fabric DC06 on participant MM03

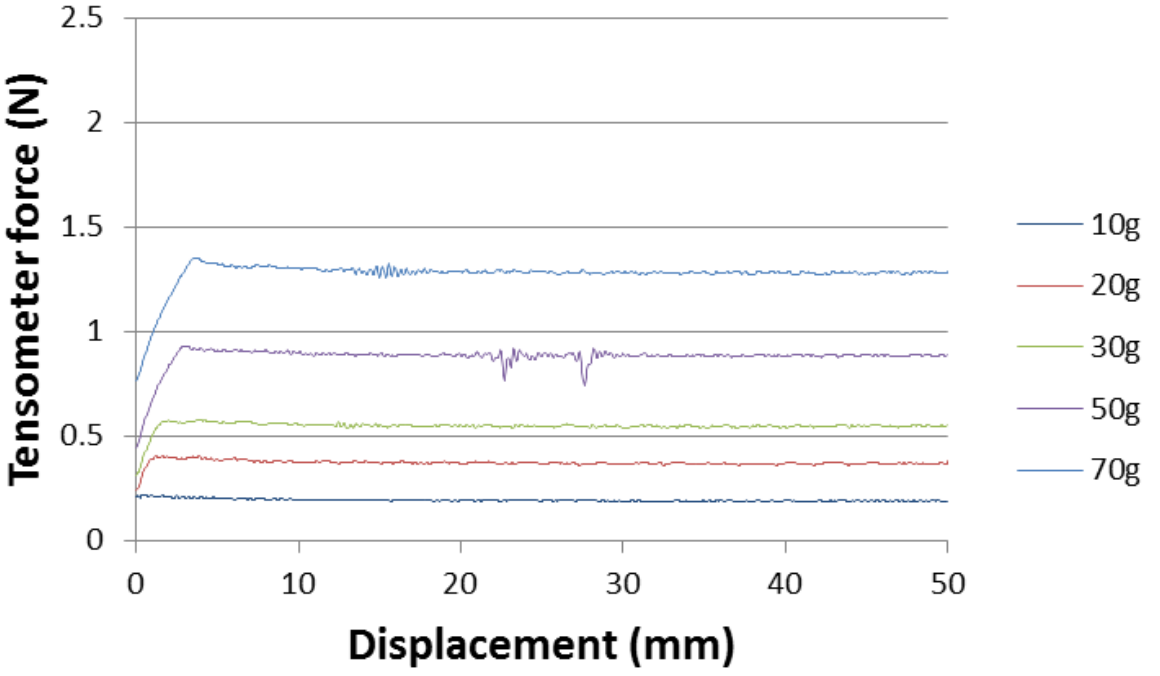

Figure 4.14: Tensometer graphs of fabric SF14 on participant MM03

At the line corresponding to the 50g the data show that the participant moved twice between 20 and 30 mm, since these disruptions do not exist on any other graphs.

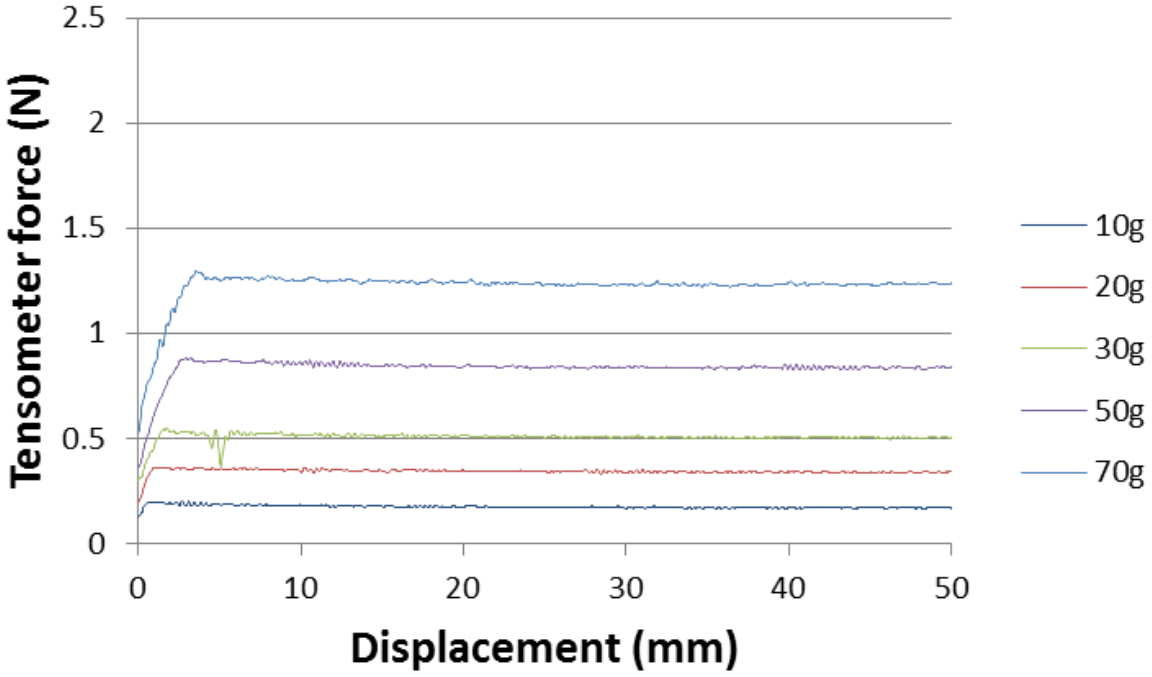

Figure 4.15: Tensometer graphs of fabric SF17 on participant MM03

In Figure 4.15 the line for the 30g show that participant moved in the distance between and 10 mm. The rest of the graphs do not show any unusual behaviour.

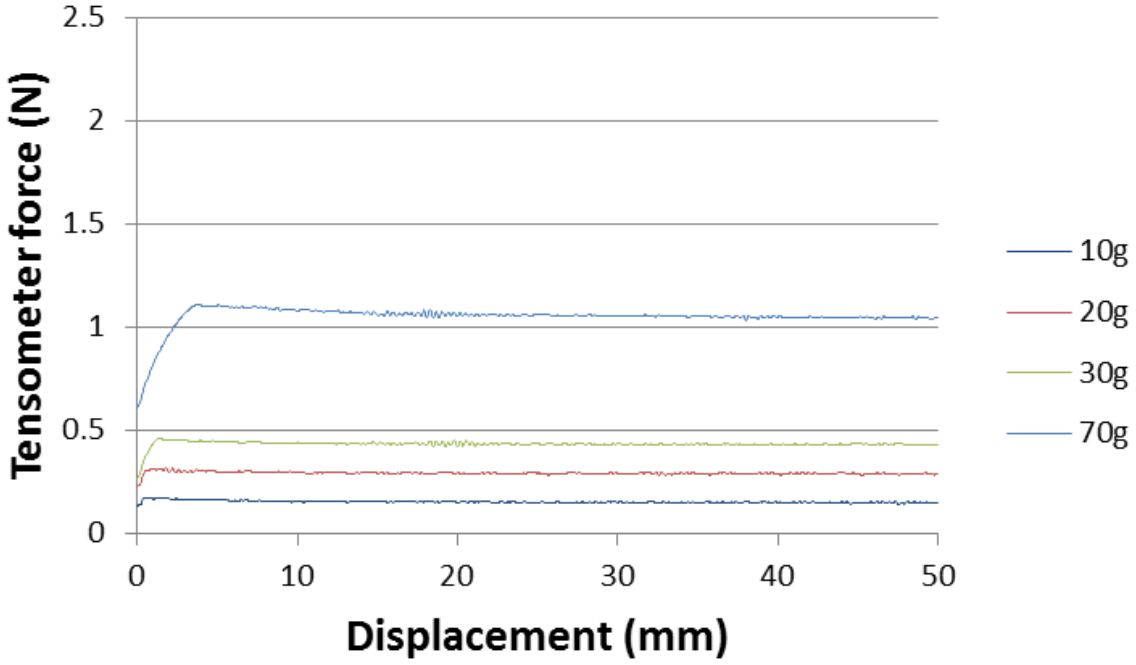

Figure 4.16: Tensometer graphs of fabric SF18 on participant MM03

Due to mistakes during the experimental process (I did not use the correct dead weight mass) it was not possible to extract the data for the 50g dead weight mass. The rest of the dead weight masses are

displayed thoroughly though. As I show the static friction is a bit higher than the plateau which represents dynamic friction.

The previous results came up from measurements on a participant who belongs in the group below 65 years old, so has firm underlying tissues and not wrinkled skin. Below I present another participant from the group of over 65 years old with more flaccid tissue and wrinkled skin.

4.4.3 Experimental results of participant DJ10

Below I show the results from the experiments on fabric SF03, on a much older participant, DJ10. This first graph (Figure 4.17) corresponds to a 10g tensometer graph. The photographs of a particular point show the deformation of the fabric and the arm during the whole experiment.

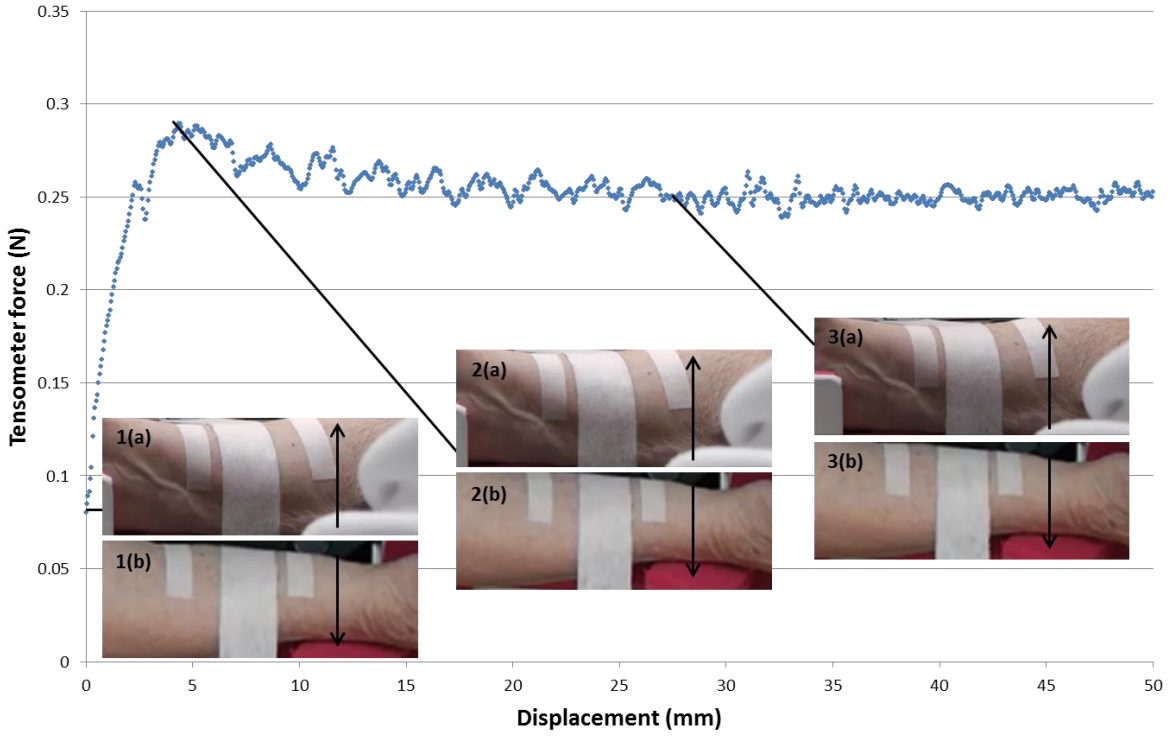

Figure 4.17: Tensometer graph of 10g dead weight of participant DJ10 in experiments with fabric SF03, where (a) front camera view and (b) top camera view.

As I mentioned for the previous participant, I don't observe any significant deformations, so more photographs than one seem pointless.

Below I present the graph of 70g dead weight on participant DJ10 using fabric SF03.

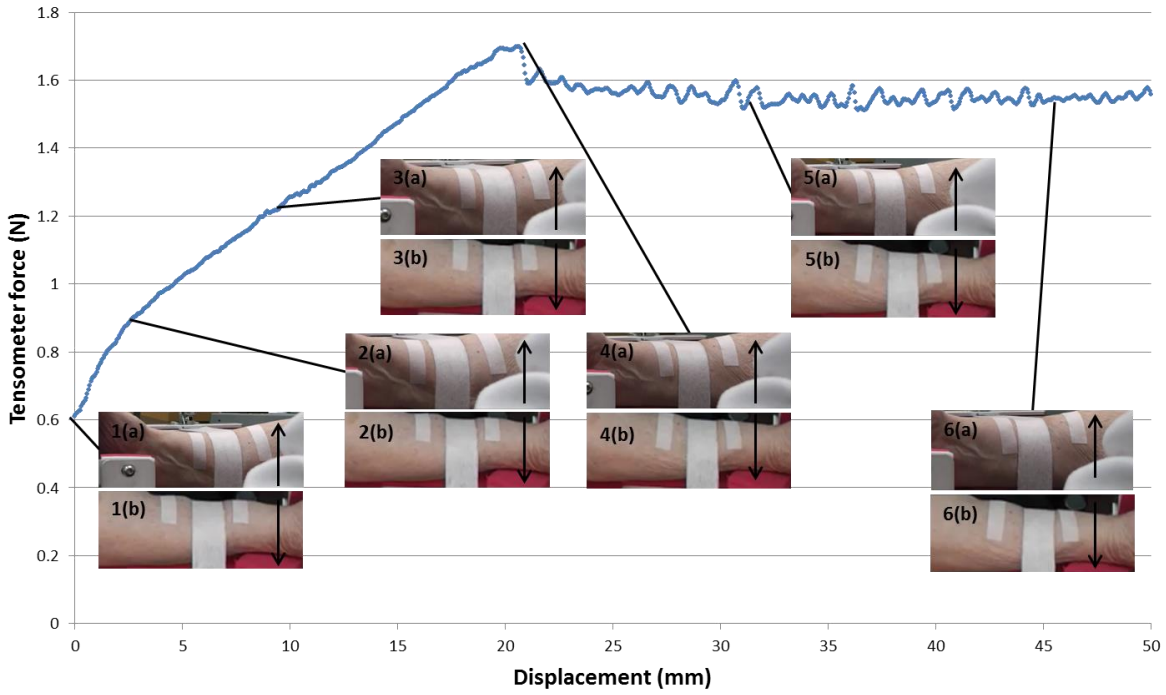

Figure 4.18: Tensometer graph of 70g dead weight of participant DJ10 in experiments with fabric SF03, where (a) front camera view and (b) top camera view.

As before I tried to present all the changes in the volar forearm condition and correlate them with the changes of the graph. At the beginning of the graph I observe just indentations, but as I show progressively rucking appears from photographs 4, from shallow rucking in photograph 3, to clearly obvious rucking of photograph 6.

Below I present the tensometer graphs of all the experiments of fabric SF03 on participant DJ10.

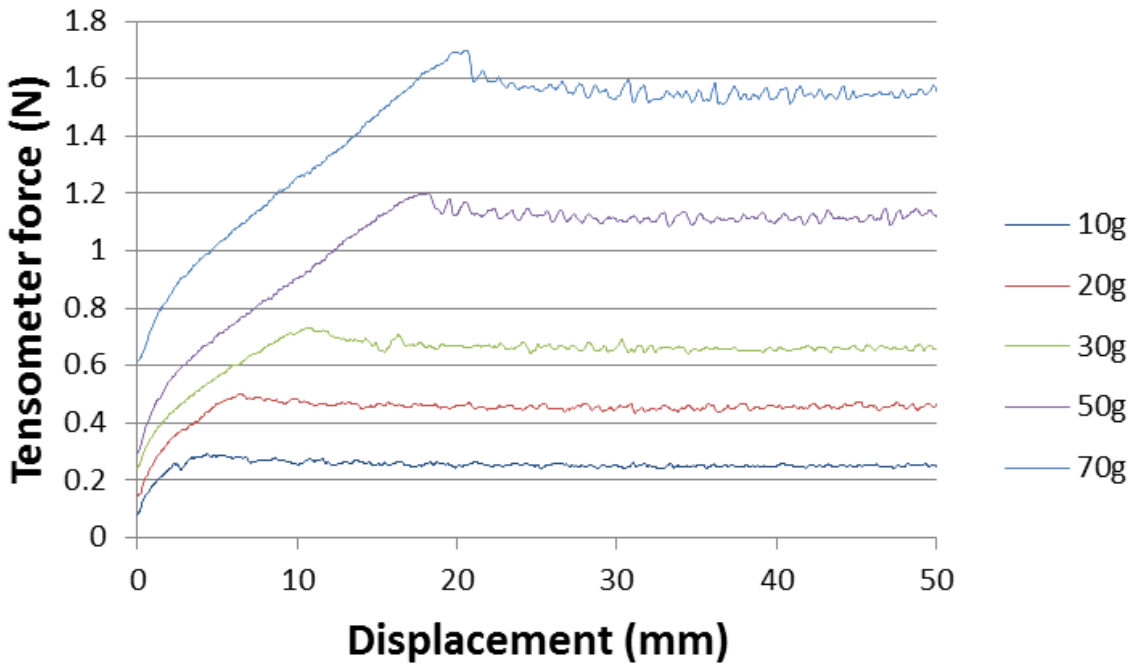

Figure 4.19: Tensometer graphs of fabric SF03 on participant DJ10 which correspond on different dead weights

Again, as I present it is obvious that bigger dead weights correspond to higher tensometer forces. The main difference Figure 4.11 is that it takes a greater displacement for the tensometer force to reach the plateau, which is completely normal since the wrinkled skin and the flaccid tissue is susceptible to more severe deformation. Notable is the fact that the bigger the dead weight mass the more severe the deformation is. If I compare the graph of the 10g to the graph of 70g, remarkable is the difference in deformation. For the 70g, tensometer force reaches its peak at 20 mm, while at the 10g it takes less than 5 mm.

Below I present the graph of pulling force against dead weight of fabric SF03 on participant DJ10.

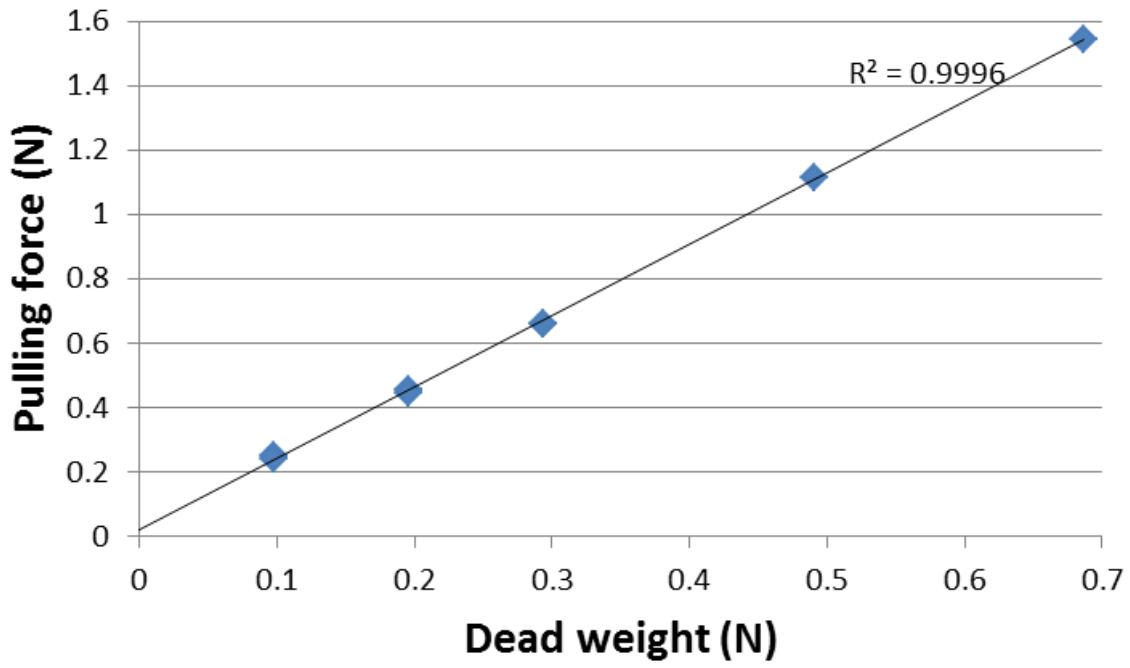

Figure 4.20: Linear graph of pulling force against weight of fabric SF03 against participant DJ10.

Commenting for Figure 4.20 is the same as for commenting for Figure 4.12: the correlation factor, R^2, is once more extremely high, as for participant MM03.

Below I present the tensometer graphs forDJ10 for the rest of the fabrics I examined.

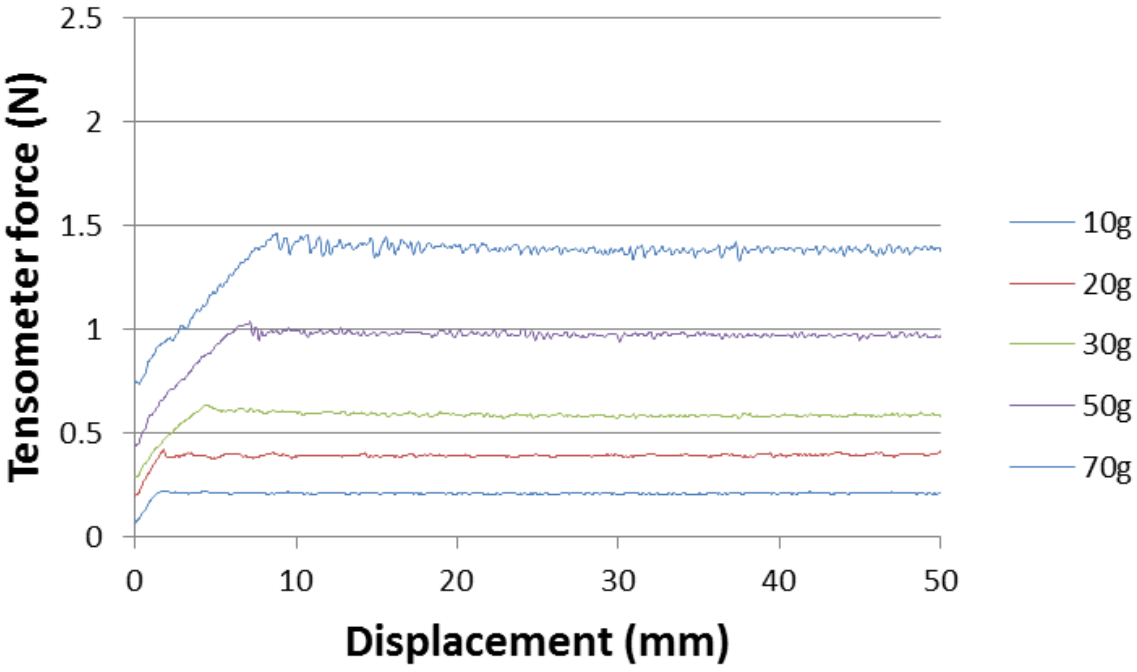

Figure 4.21: Tensometer graphs of fabric DC06 on participant DJ10

In Figure 4.21 the tensometer graphs of 50g and 70g presents more movement artefacts in comparison to the first three graphs.

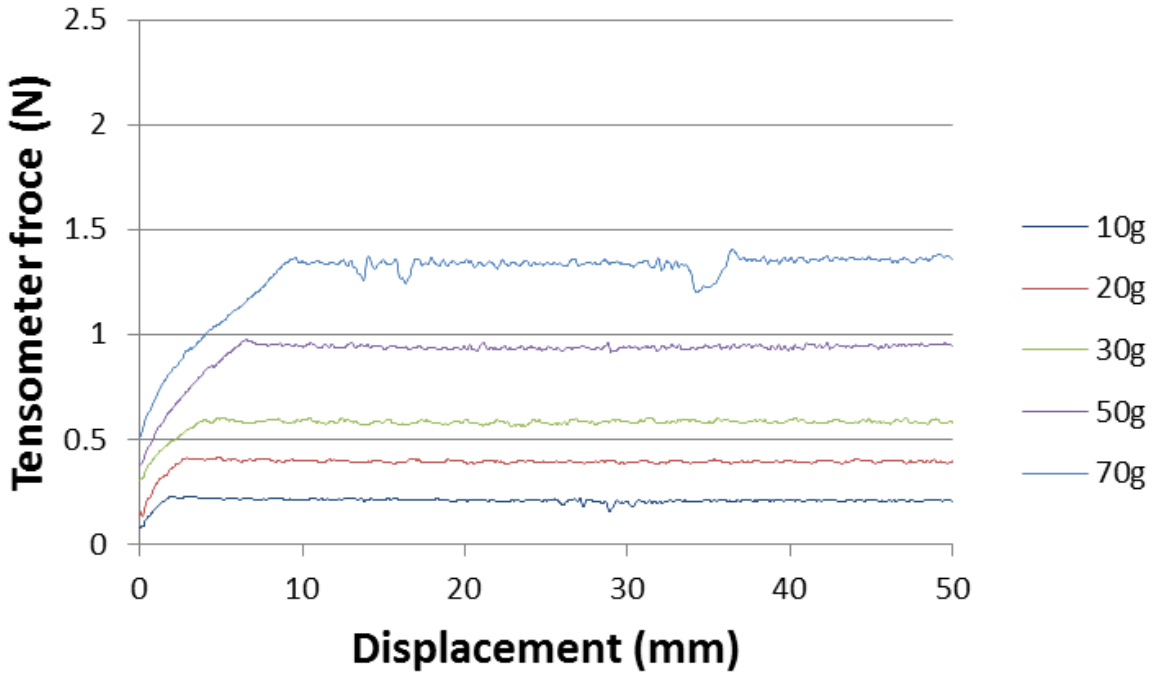

Figure 4.22: Tensometer graphs of fabric SF14 on participant DJ10

The disturbances at the graph of 70g show that participant moved during the measurements between 10 and 20mm and between 30 and 40mm.

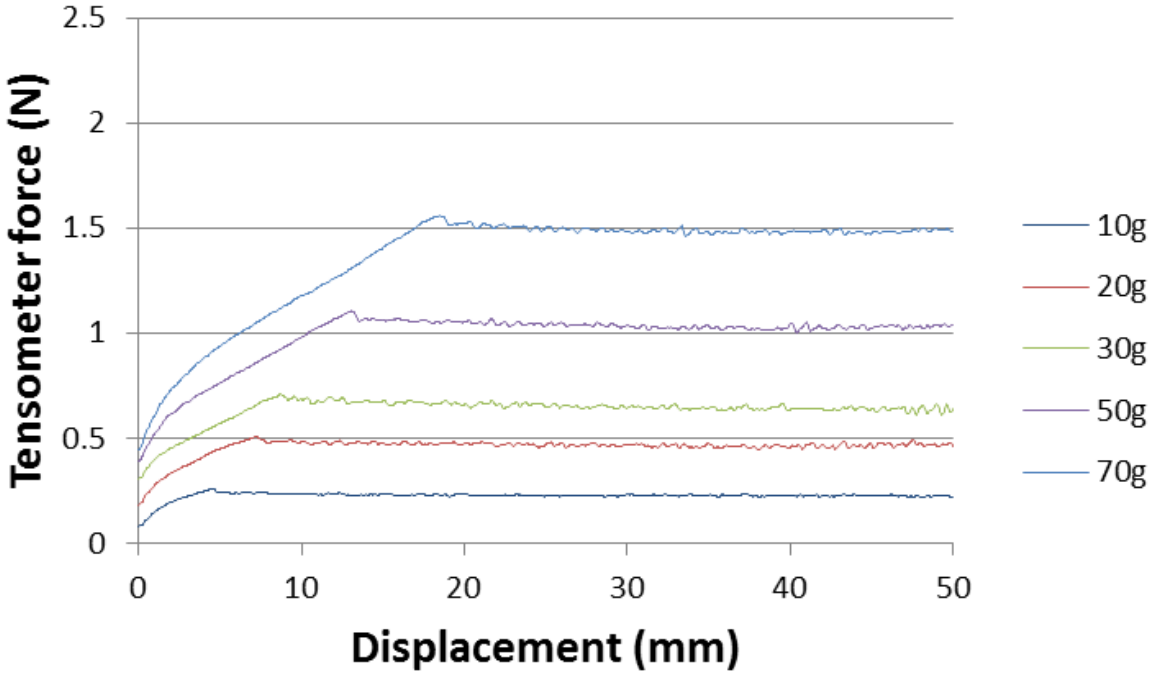

Figure 4.23: Tensometer graphs of fabric SF17 on participant DJ10

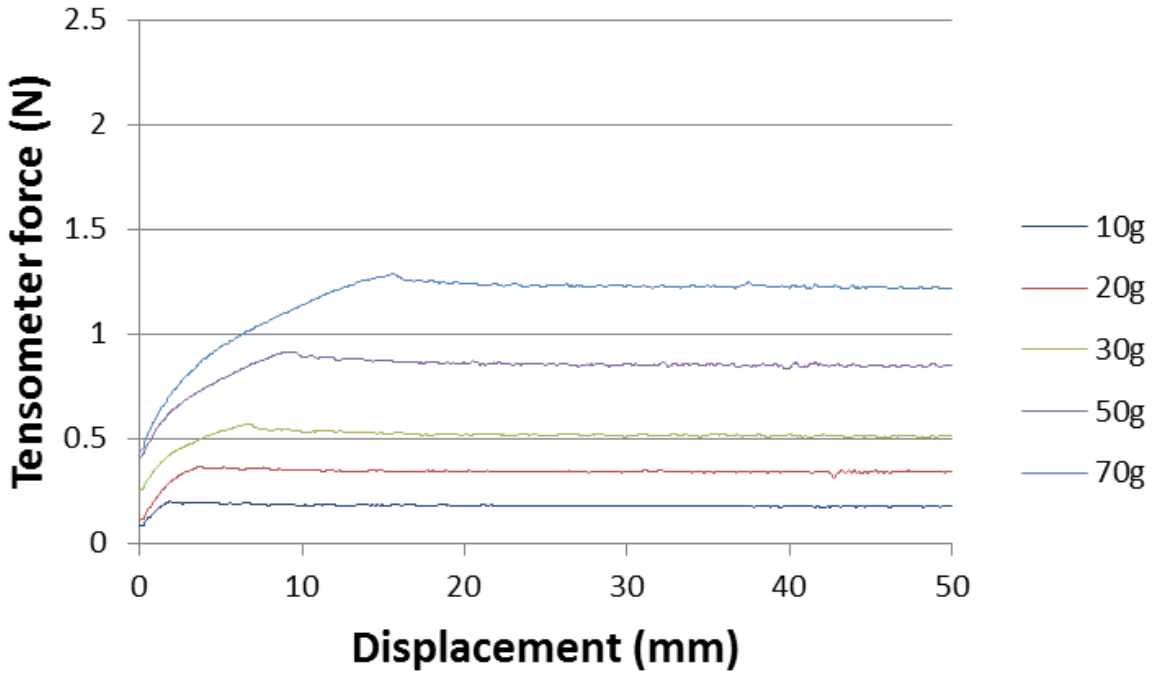

Figure 4.24: Tensometer graphs of fabric SF18 on participant DJ10

Tensometer graphs for fabric SF18 show that they reach "smoothly" the peak force of static friction, in comparison to the tensometer graphs for fabric SF17, where the uphill part of the curves is more abrupt. In §4.4.4 I continue with the data for participant HJ07.

4.4.4 Experimental results of participant HJ07

Participant HJ07 provided a boney volar forearm and I thought it would be very interesting to present the results of fabric SF03 on this participant, in an analogous way to the previous results. So, for the lighter dead weight mass I present the following graph.

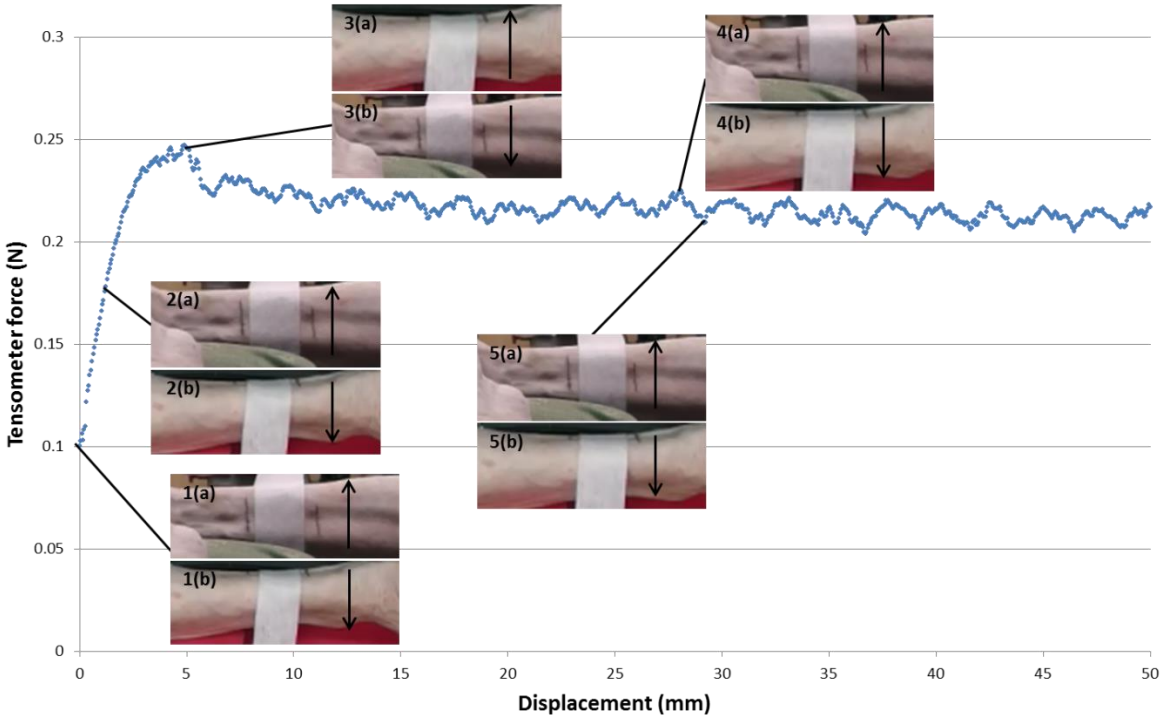

Figure 4.25: Tensometer graph of participant HJ07 for the dead weight mass of 10g, where (a) front view camera and (b) top view camera.

In Figure 4.25 I present several photographs of the volar forearm during the experiment, and particularly I show a photograph without deformation, a photograph where the dominant effect of the experiment is deformation (2), a photograph at the highest value of the graph and a photograph at the highest (4) and lowest (5) point of the minor stick – slip phenomenon I observe.

"Stick – slip" is the phenomenon where there is a succession between static and dynamic friction, or between the effects of sticking and slipping.

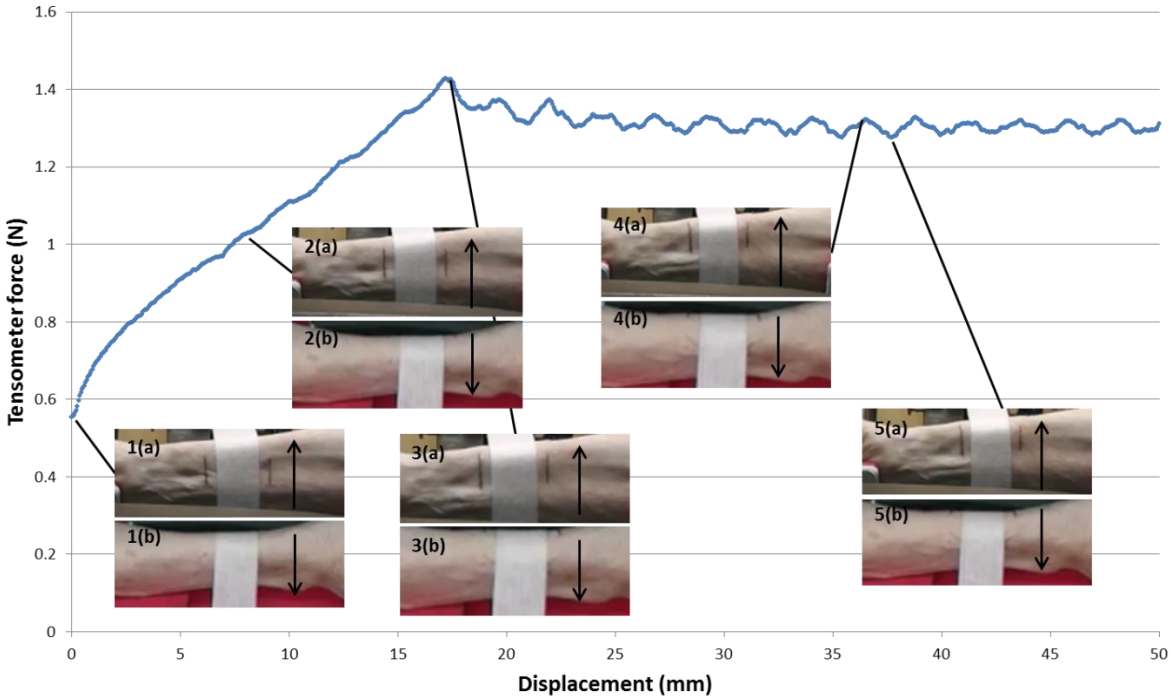

Figure 4.26: Tensometer graph of participant HJ07 for the dead weight of 70g, where (a) front view camera and (b) top view camera.

Again, as in the previous graph I present a photograph at the initial point of the graph (1), a photograph where the dominant phenomenon is deformation (2), a photograph at the peak of the graph (3) and photographs (4) and (5) at the highest and lowest point of the stick slip phenomenon.

In the following photograph I present the tensometer graphs of fabric SF03 on participant HJ07.

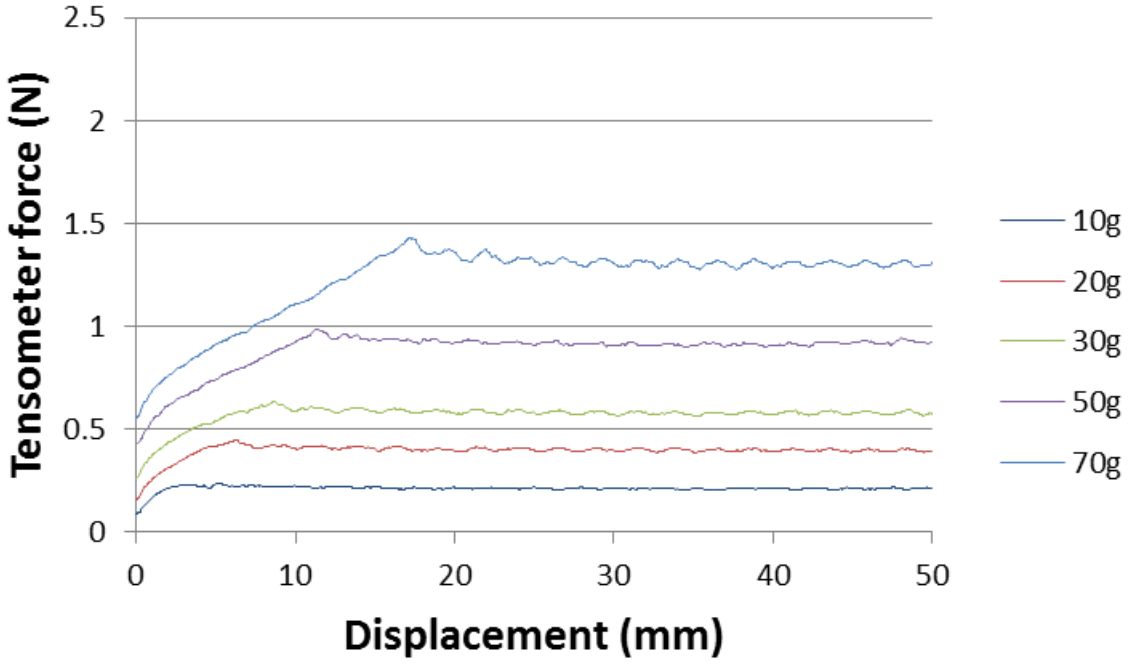

Figure 4.27: Tensometer graphs of fabric SF03 on participant HJ07

Even though the arm is considered the most boney, from the plateau of the graphs of Figure 4.27 I derive the pulling force value and I plot the graph of pulling force against dead weight of Figure 4.28.

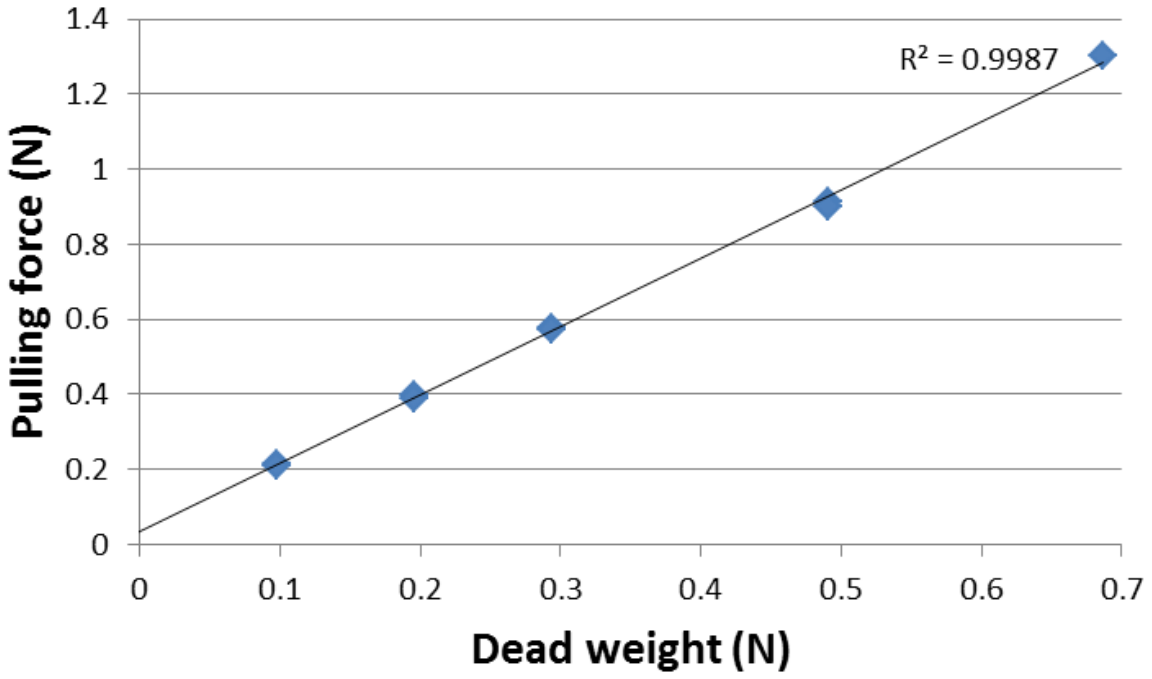

Figure 4.28: Graph of pulling force against dead weight of fabric SF03 on participant HJ07

The impressive linearity is the main characteristic of all the plots of pulling force against dead weight.

The tensometer graphs between participant HJ07 and the rest of the fabrics follow.

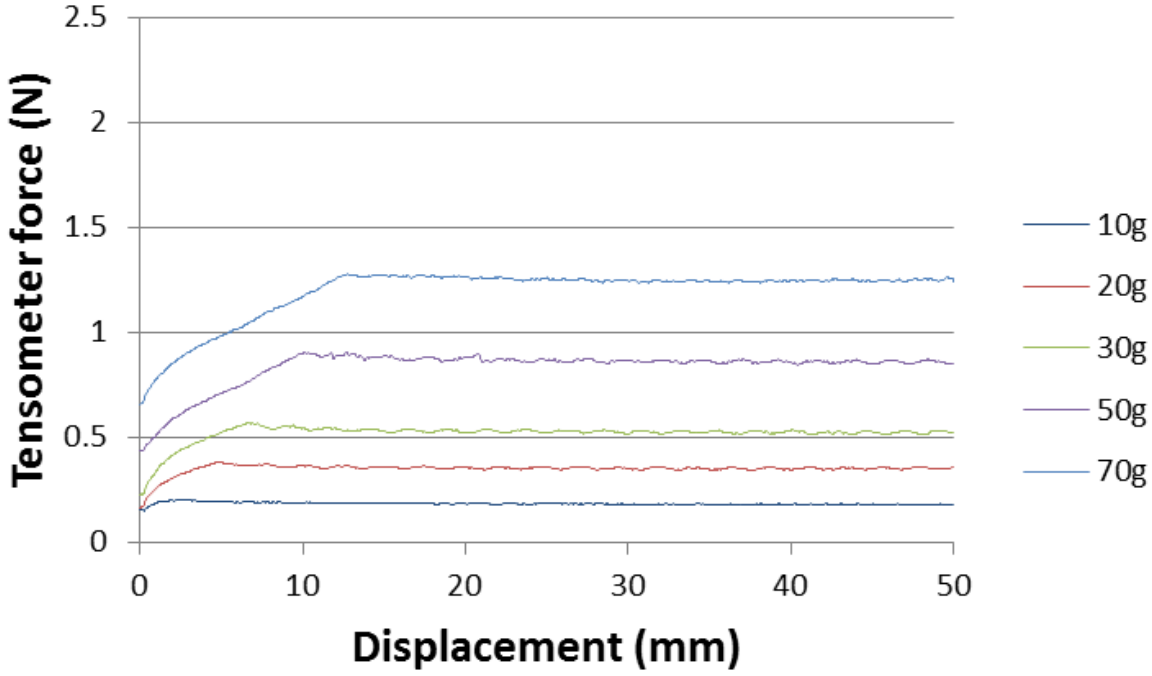

Figure 4.29: Tensometer graphs of fabric DC06 on participant HJ07

In Figure 4.29 obvious is the relatively big deformation of the arm which in the case of the 70g graph reaches 12mm of displacement.

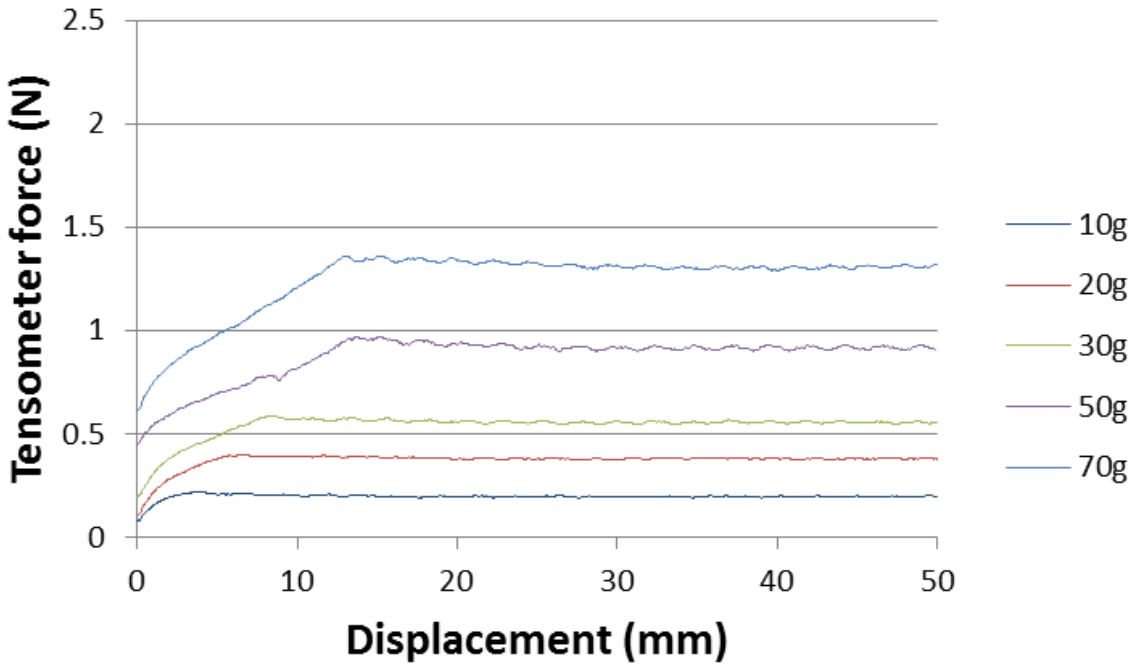

Figure 4.30: Tensometer graphs of fabric SF14 on participant HJ07

The displacement is in Figure 4.30 relatively big as well.

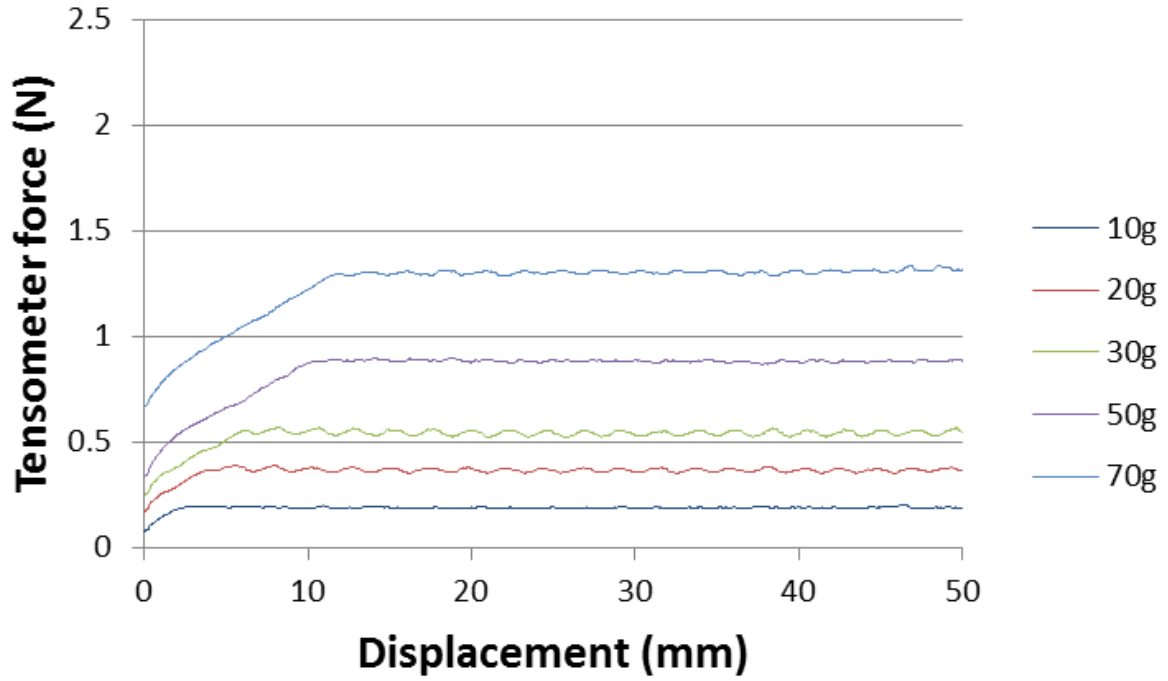

Figure 4.31: Tensometer graphs of fabric SF17 on participant HJ07

As in the previous graphs, the deformation in Figure 4.31 is impressive.

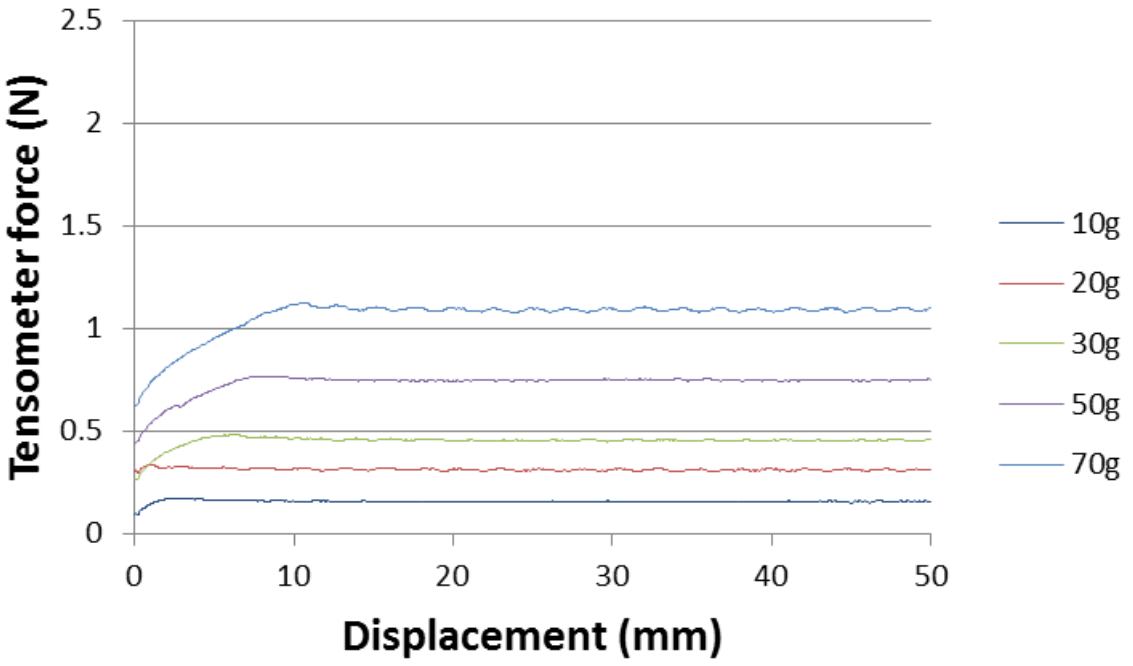

Figure 4.32: Tensometer graphs of fabric SF18 on participant HJ07

The data generated from these graphs produce the coefficient of friction which is presented for all the experiments in Table 4.2.

4.4.5 Presentation of experimental results of every participant

In Table 4.2 I present the coefficient of friction of every participant for every fabric with the corresponding standard deviation. The calculation of standard deviation is relatively easy. For every linear graph of every experiment I derive the slope and the intercept with their corresponding standard deviations. I use these standard deviations and the error of the calculation of the φ angle which I set at two degrees to calculate the standard deviation of the coefficient of friction.

Code	Age (years)	μ									
		DC06		SF03		SF14		SF17		SF18	
LC16	28	0.333	(0.011)	0.382	(0.010)	0.374	(0.012)	0.355	(0.011)	0.252	(0.010)
MS04	28	0.369	(0.012)	0.470	(0.013)	0.413	(0.011)	0.414	(0.013)	0.268	(0.010)
KG13	30	0.396	(0.011)	0.410	(0.010)	0.391	(0.011)	0.390	(0.011)	0.264	(0.010)
CB18	45	0.431	(0.013)	0.466	(0.011)	0.420	(0.010)	0.447	(0.014)	0.290	(0.010)
MM03	51	0.325	(0.010)	0.397	(0.010)	0.370	(0.010)	0.357	(0.011)	0.261	(0.008)
AD02	57	0.409	(0.012)	0.470	(0.090)	0.430	(0.011)	0.429	(0.012)	0.292	(0.009)
RJ05	60	0.513	(0.023)	0.607	(0.014)	0.571	(0.014)	0.554	(0.023)	0.373	(0.013)
HJ07	72	0.359	(0.011)	0.369	(0.011)	0.369	(0.011)	0.379	(0.016)	0.277	(0.014)
DA15	73	0.447	(0.011)	0.456	(0.011)	0.416	(0.011)	0.450	(0.012)	0.312	(0.010)
MG12	76	0.442	(0.013)	0.411	(0.012)	0.435	(0.012)	0.459	(0.013)	0.315	(0.011)
JJ09	79	0.351	(0.013)	0.407	(0.013)	0.388	(0.013)	0.359	(0.014)	0.283	(0.010)
SF06	81	0.493	(0.014)	0.512	(0.013)	0.476	(0.011)	0.481	(0.018)	0.357	(0.012)
MH17	84	0.465	(0.012)	0.455	(0.012)	0.445	(0.011)	0.489	(0.013)	0.337	(0.011)
MT14	89	0.430	(0.013)	0.430	(0.010)	0.396	(0.011)	0.454	(0.014)	0.323	(0.011)
DJ10	91	0.429	(0.011)	0.499	(0.012)	0.417	(0.013)	0.466	(0.017)	0.363	(0.011)
MD08	93	0.466	(0.018)	0.514	(0.014)	0.465	(0.012)	0.489	(0.013)	0.338	(0.012)
AB11	95	0.354	(0.011)	0.371	(0.011)	0.363	(0.009)	0.414	(0.021)	0.263	(0.011)
mean		0.413	(0.069)	0.449	(0.060)	0.420	(0.049)	0.434	(0.076)	0.304	(0.037)

Table 4.2: Coefficient of friction between participants and fabrics with the respective error in brackets

In Figure 4.33 show the coefficient of friction for every participant and for each fabric pictorially.

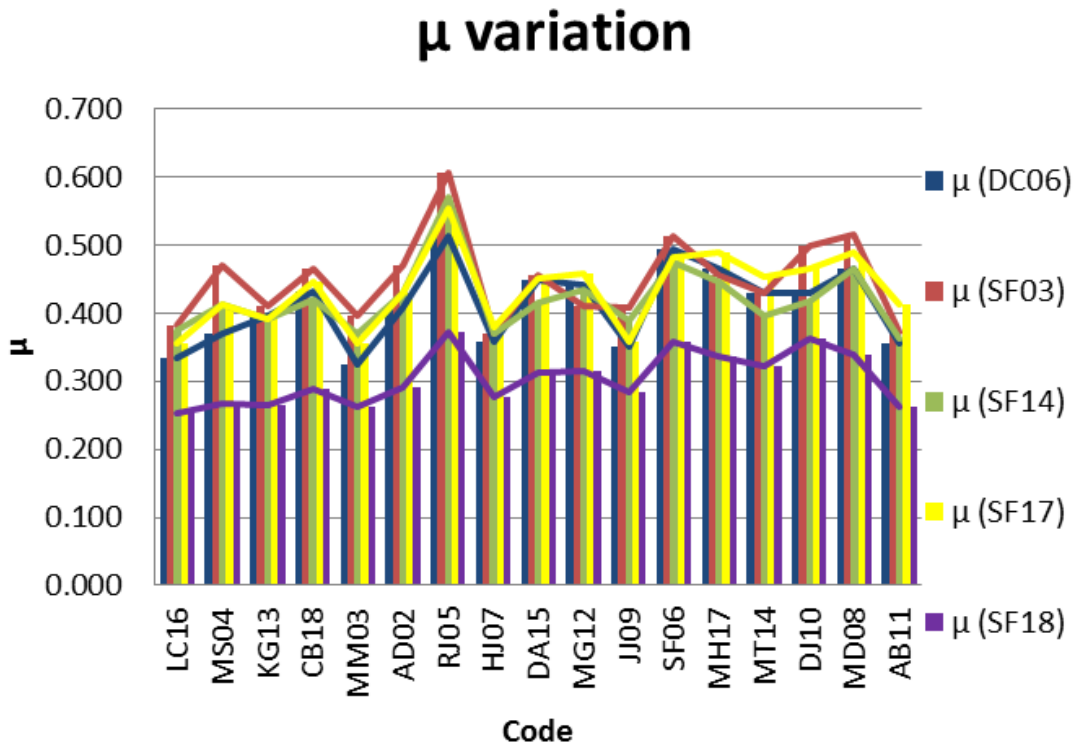

Figure 4.33: Variation of μ of each fabric against every participant. The participants are arranged in order of increasing age from LC16 to AB11.

Below I quote the graphs for each fabric, where at the vertical axis I have the values of μ and at the perpendicular axis I quote the code of each participant, where the position of each code is proportional to the age of the participant.

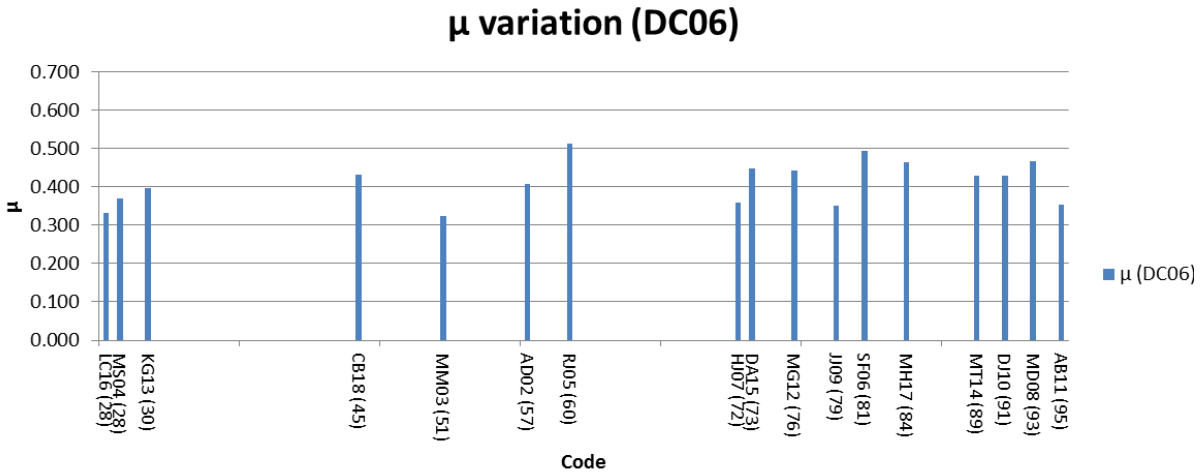

Figure 4.34: Variation of μ of fabric DC06 against every participant, while in brackets I show the age of each participant.

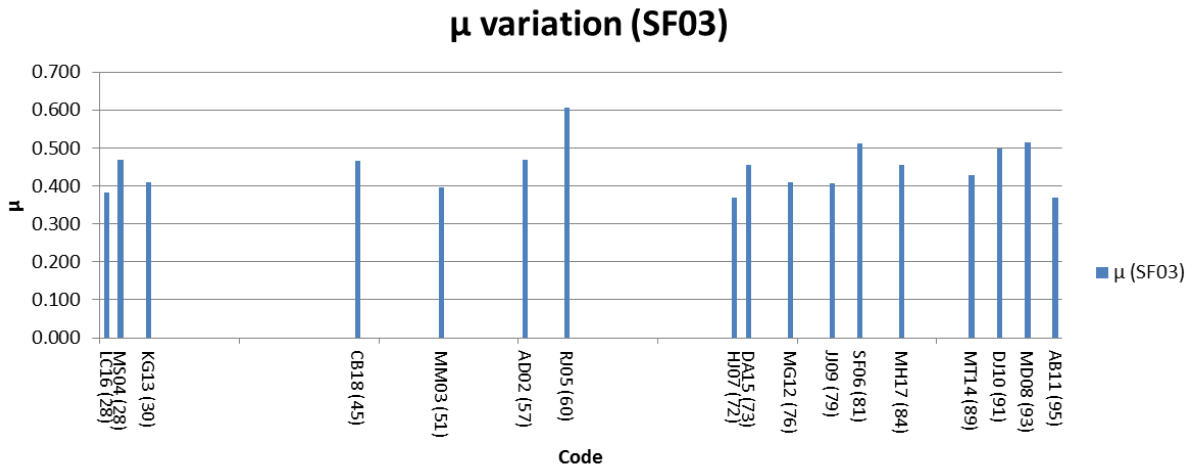

Figure 4.35: Variation of μ of fabric SF03 against every participant, while in brackets I show the age of each participant.

.

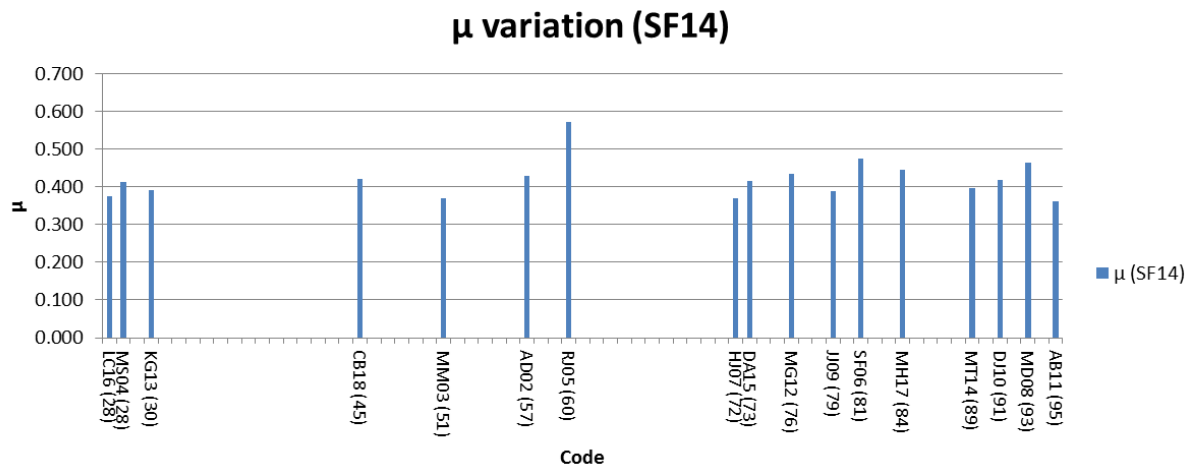

Figure 4.36: Variation of μ of fabric SF14 against every participant, while in brackets I show the age of each participant.

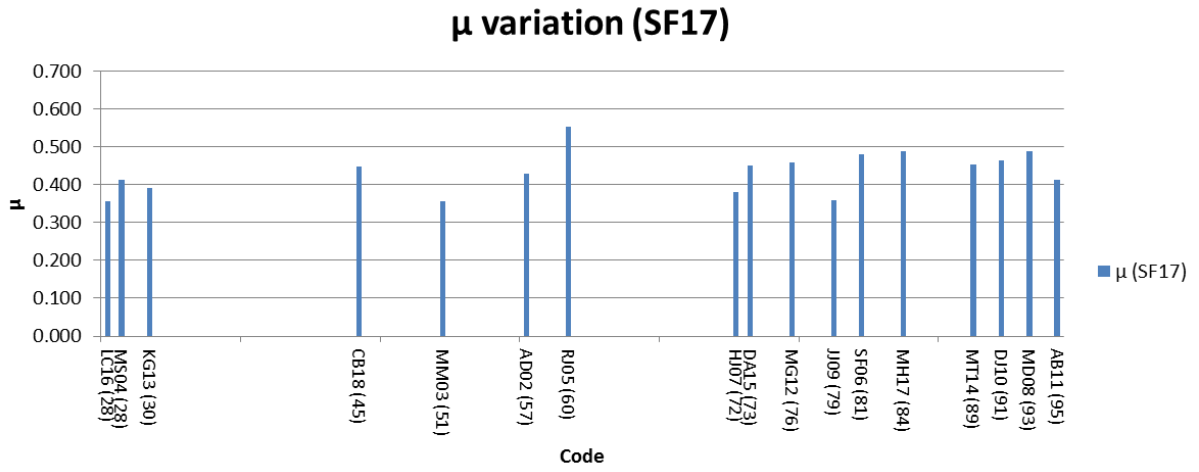

Figure 4.37: Variation of μ of fabric SF17 against every participant, while in brackets I show the age of each participant.

.

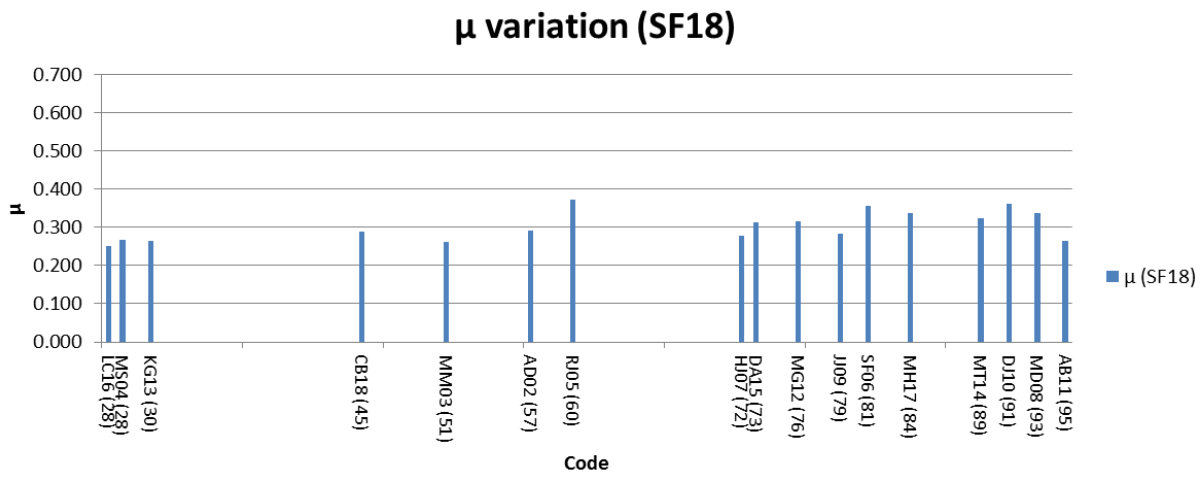

Figure 4.38: Variation of μ of fabric SF18 against every participant, while in brackets I show the age of each participant.

.

From Figure 4.33 to 4.38 it is clear that participant RJ05 presents the highest coefficient of friction and especially with fabric SF17. I can also see that the coefficient of friction is independent of the participant's age and each fabric appears similar coefficient of friction on approximately every participant. Fabric SF18 has the lowest coefficient of friction while the rest of the other fabrics appear very similar values. However, for most of the participants, fabric SF03 has the highest coefficient of friction.

Along with the tensometer experiments we undertook some measurements of trans epidermal water loss (TEWL) before and after the experiments. This measures the water vapour flux density from the skin and shows how hydrated the skin is. The device we used to measure TEWL is the Vapometer. I present the results of the TEWL measurements in Table 4.3.

Code	Age (years)	TEWL ($gm^{-2}h^{-1}$)	
		Before	After
LC16	28	2.235	3.643
MS04	28	2.989	2.291
KG13	30	2.847	1.723
CB18	45	1.870	0.801
MM03	51	3.343	2.982
AD02	57		
RJ05	60	2.376	1.940
HJ07	72	2.411	1.498
DA15	73	1.725	1.567
MG12	76		
JJ09	79	1.914	2.892
SF06	81	0.738	0.842
MH17	84	0.842	1.580
MT14	89	3.153	2.787
DJ10	91		
MD08	93	3.899	4.656
AB11	95		

Table 4.3: Measurements of TEWL before and after the friction experiments. The higher values of TEWL for each participant are highlighted in orange

As I show in Figure 4.39, Figure 4.40 and Table 4.3 there is no correlation between coefficient of friction and TEWL readings. Participants JJ09 and MD08 whose TEWL readings after the experiments were higher than before were in the room of conduction of the experiments in the time window 11 – 1, on the 21st and 22nd of May of 2012 respectively. On the 21st the recorded temperature was around 25°C and on the 22nd around 23°C. I did not observe the same difference in TEWL for the other participants at the same time of day, which suggests these particular participants where just rather tense during the measurements. Participants SF06 and MH17 travelled to the laboratory using public transport. About the time they arrived in the laboratory, the outside temperature was around 14°C and 18°C respectively while the temperature in the ECR was around 23°C. So this temperature difference could be a reason for the higher TEWL after the experiments, while the tension during the experiments could be another. Participant LC16 came from the incontinence clinic neighbouring to our premises where the temperature was similar to the temperature of the ECR. So, the higher TEWL probably came from the fact she was probably tense during the experiments.

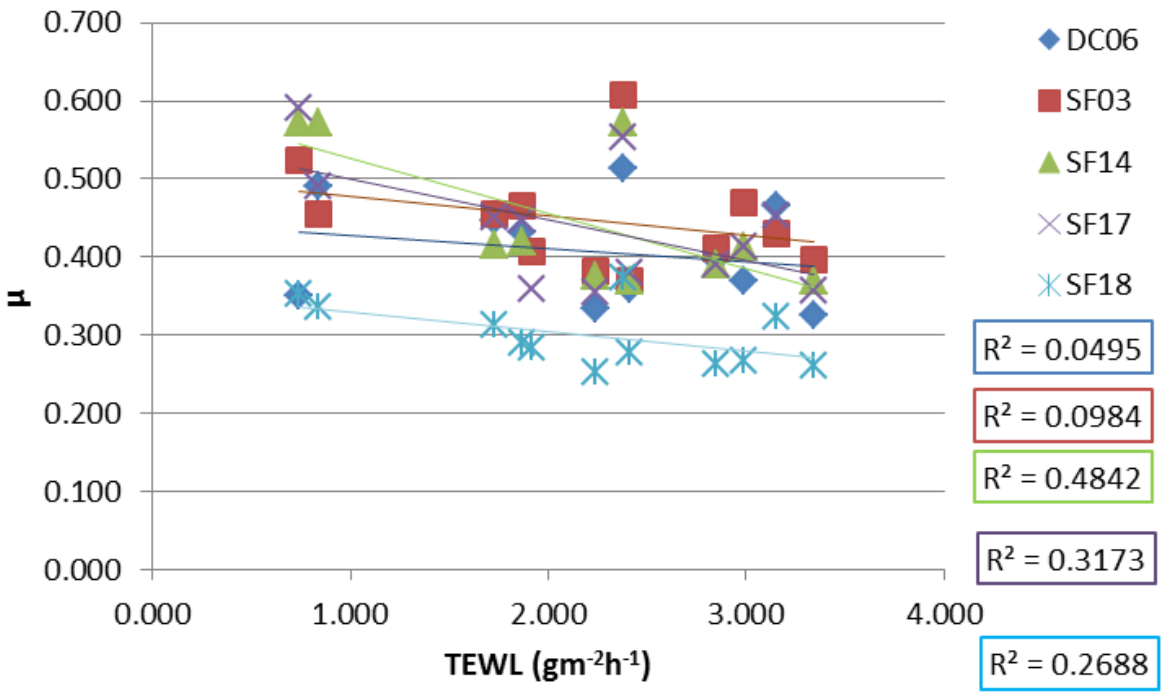

Figure 4.39: Graph presenting the variation of the coefficient of friction against values of TEWL before the experiments.

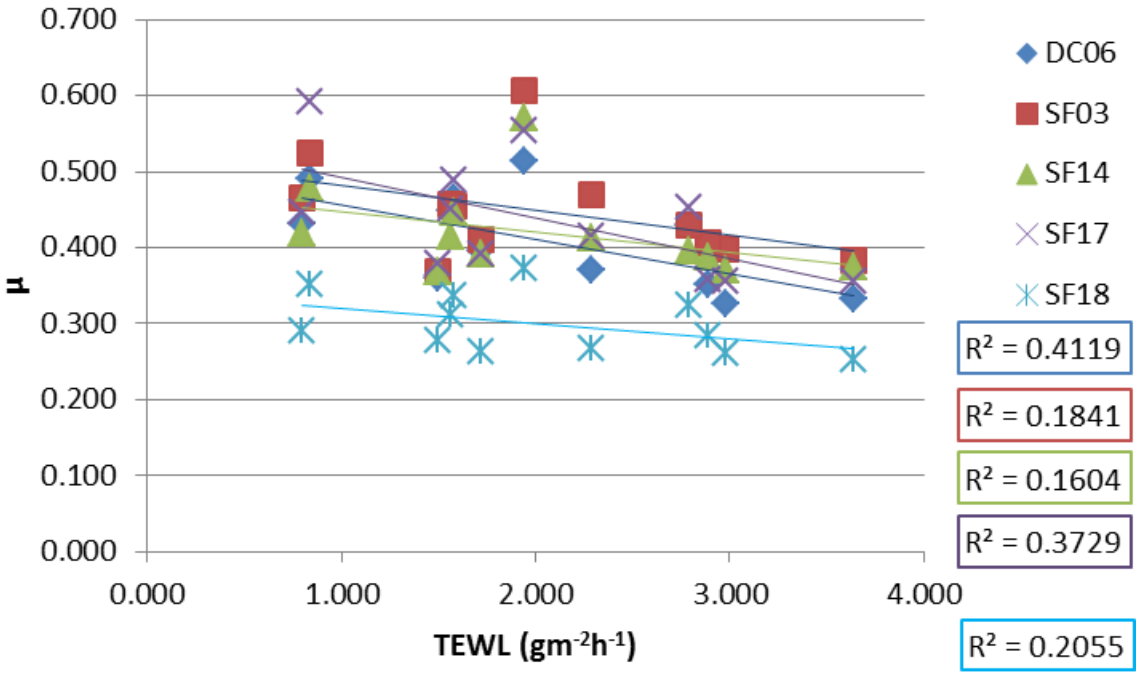

Figure 4.40: Graph presenting the variation of the coefficient of friction against values of TEWL after the experiments

As I show from Figure 4.39 and Figure 4.40 there is a weak relationship between the TEWL and the coefficient of friction μ. Even though the correlation factor, R^2, has a very low range from 0.0495 to

0.4842, which means the data points have a relatively big scatter, the trendlines show the general tendency to decrease the μ as TEWL increases, which means more humid skins have a lower coefficient of friction.

4.4.6 Analysis of stick – slip phenomenon

Some participants appear a frictional phenomenon known as stick – slip. Fully developed stick – slip was observed for only two fabrics (SF17 and DC06) for two participants (RJ05 and SF06). In §4.4.6.1 and §4.4.6.2 I analyse these experiments.

4.4.6.1 Experiments on participant RJ05

Due to the high coefficient of friction of participant RJ05, I decided to present the data of the experiments of fabric SF17 on the volar forearm of participant RJ05. The following Figure 4.41 presents the 10g tensometer graph.

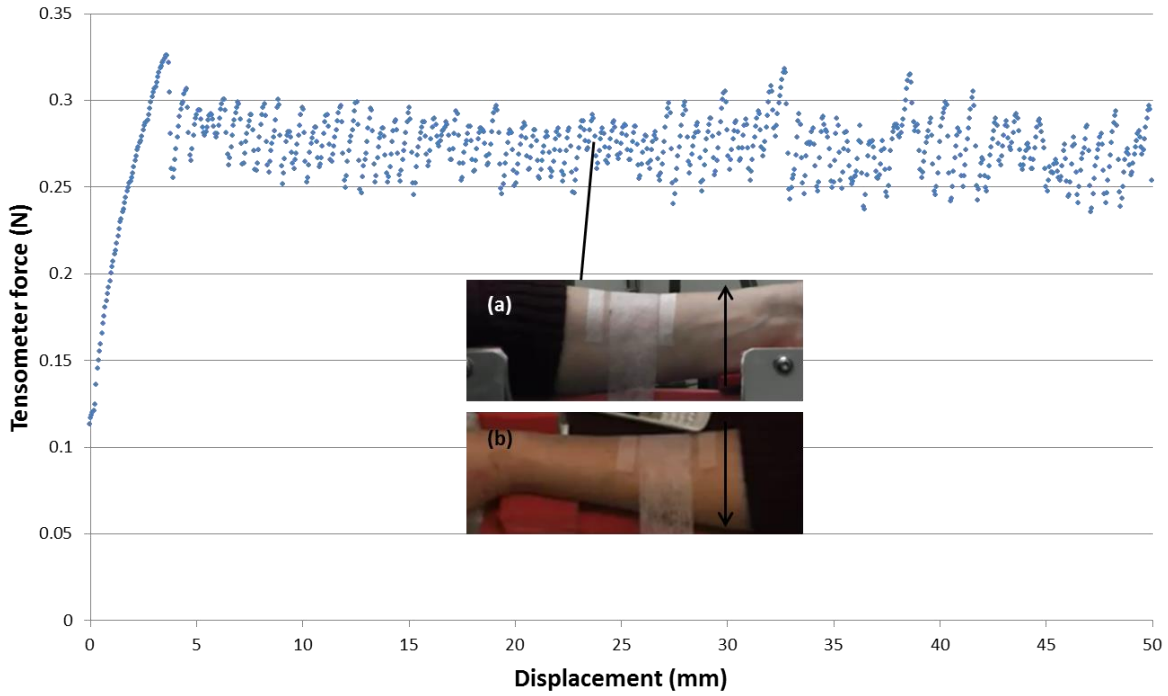

Figure 4.41: Tensometer graph and photographs of the frictional experiment of 10g of fabric SF17 on participant RJ05

Subsequently, I present the 70g tensometer graph.

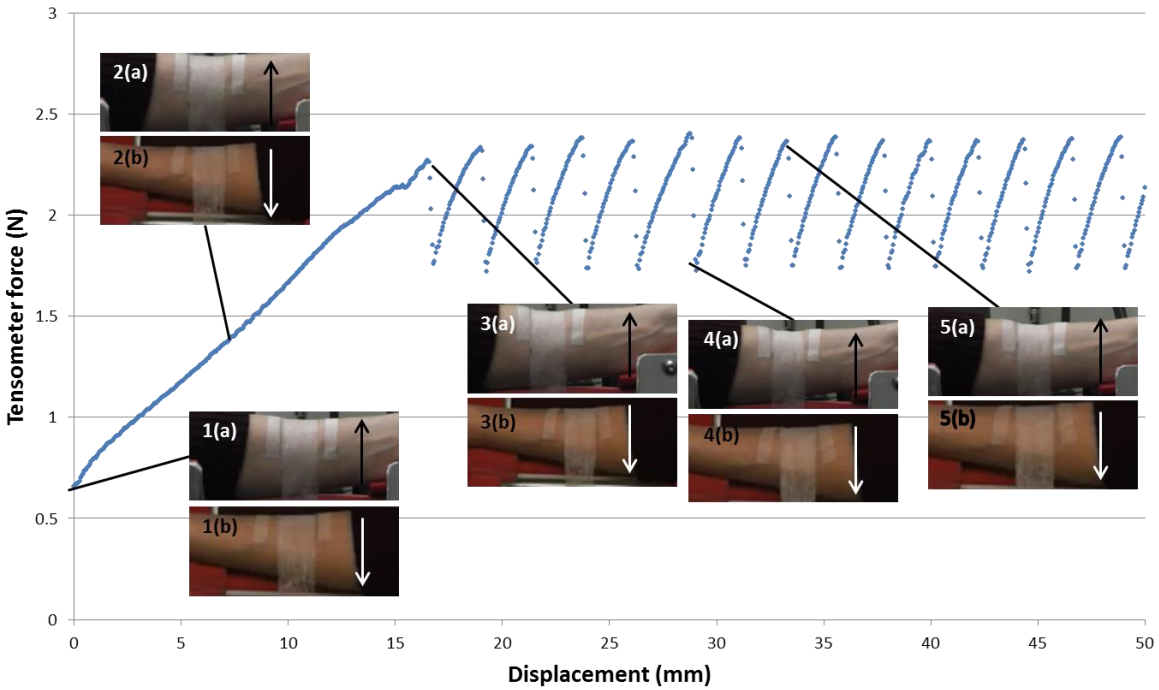

Figure 4.42: Tensometer graph and photographs of the frictional experiment of 70g of fabric SF17 on participant RJ05

Impressive is the stick – slip effect obvious at the "plateau" of the graph which is even more obvious in the following graph where I present a collection of the graphs of the fabric SF17 on participant RJ05.

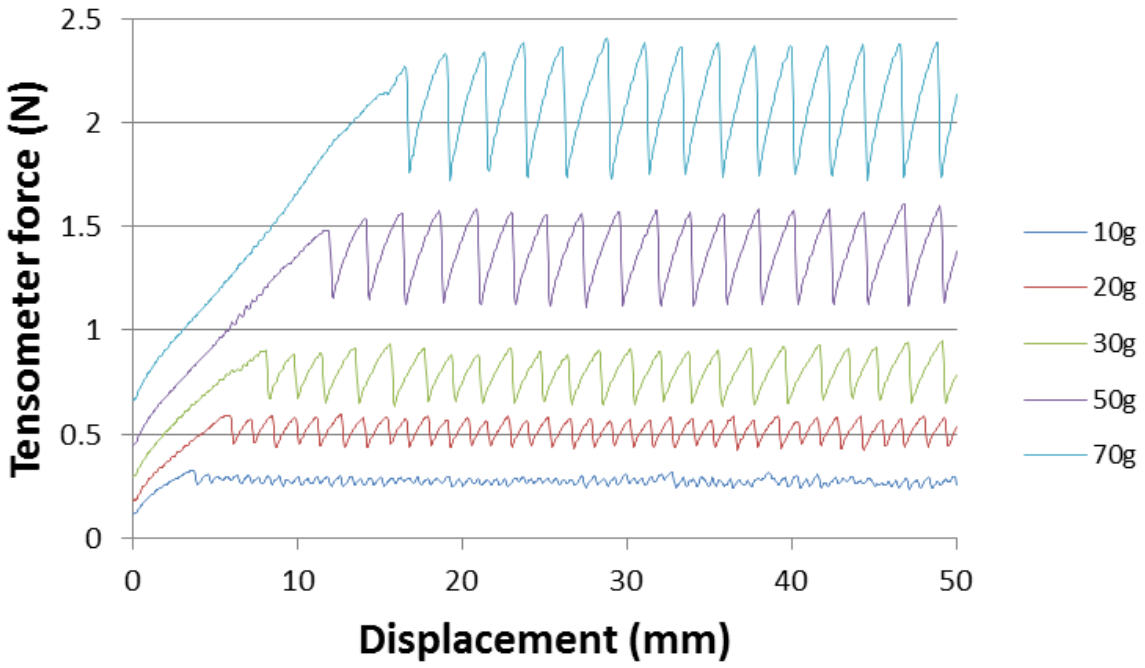

Figure 4.43: Tensometer graphs of fabric SF17 on participant RJ05

The stick – slip effect becomes more intense as the dead weight increases, reaching its highest intensity at the 70g. When stick slip phenomenon appears, the arising question is which values I will

take into consideration, the values similar to photograph 4 or the values similar to photograph 3 of Figure 4.42. In the following graph of pulling force versus dead weight, present the calculations using both sets of values for all the dead weight masses except the 10g where the phenomenon is not so obvious.

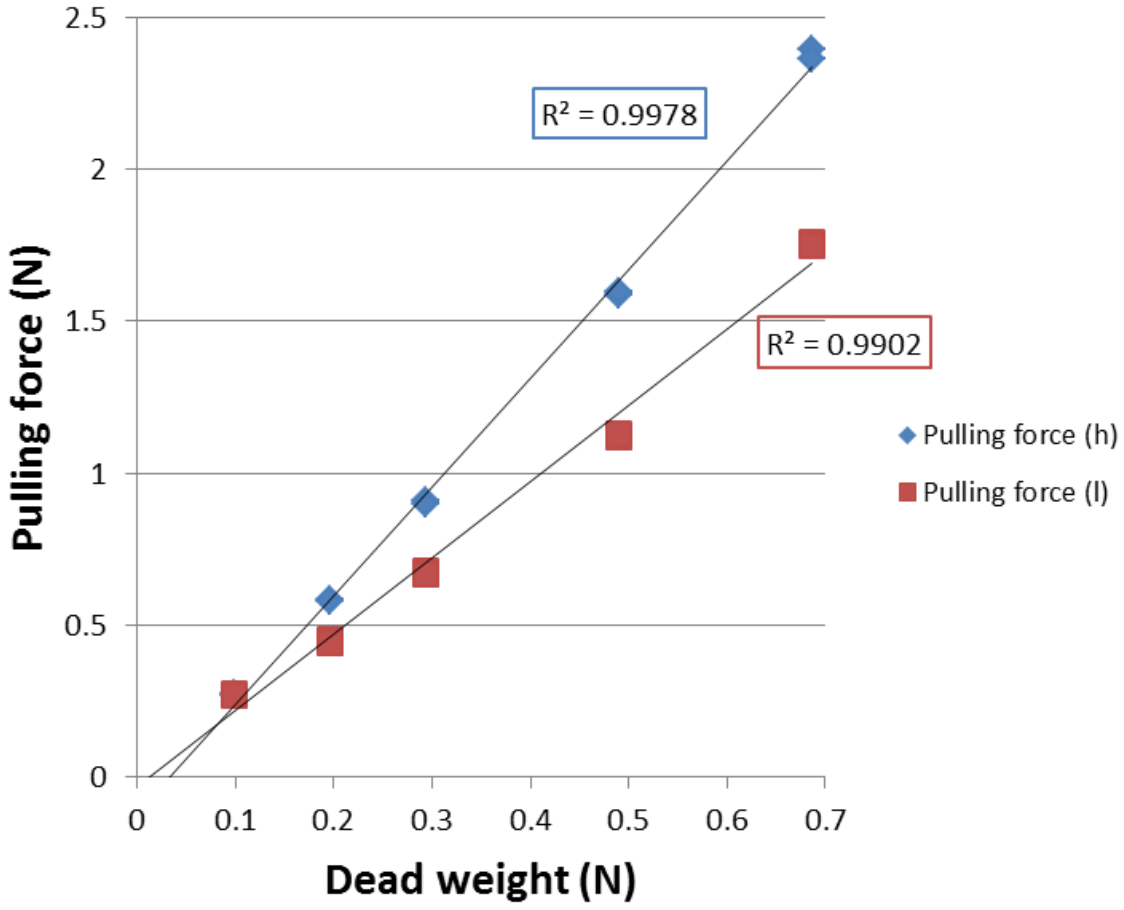

Figure 4.44: Graph of pulling force against weight of fabric SF17 on participant RJ05

As Figure 4.44 shows, both sets of values present linear plots. Now if we take into consideration that stick – slip is like multiple friction experiments, probably the lower set of values is the most credible one. The reason is that generally static friction is higher than dynamic, so the lower value is closer to the plateau which usually characterises dynamic friction values. So, every time I observe this phenomenon, this is the set of data I will use for the derivation of my results. Interesting is the fact that if I take a closer look at the points of Figure 4.44, I can see that they shape of the graphs they form are not a straight lines but a shallow curve.

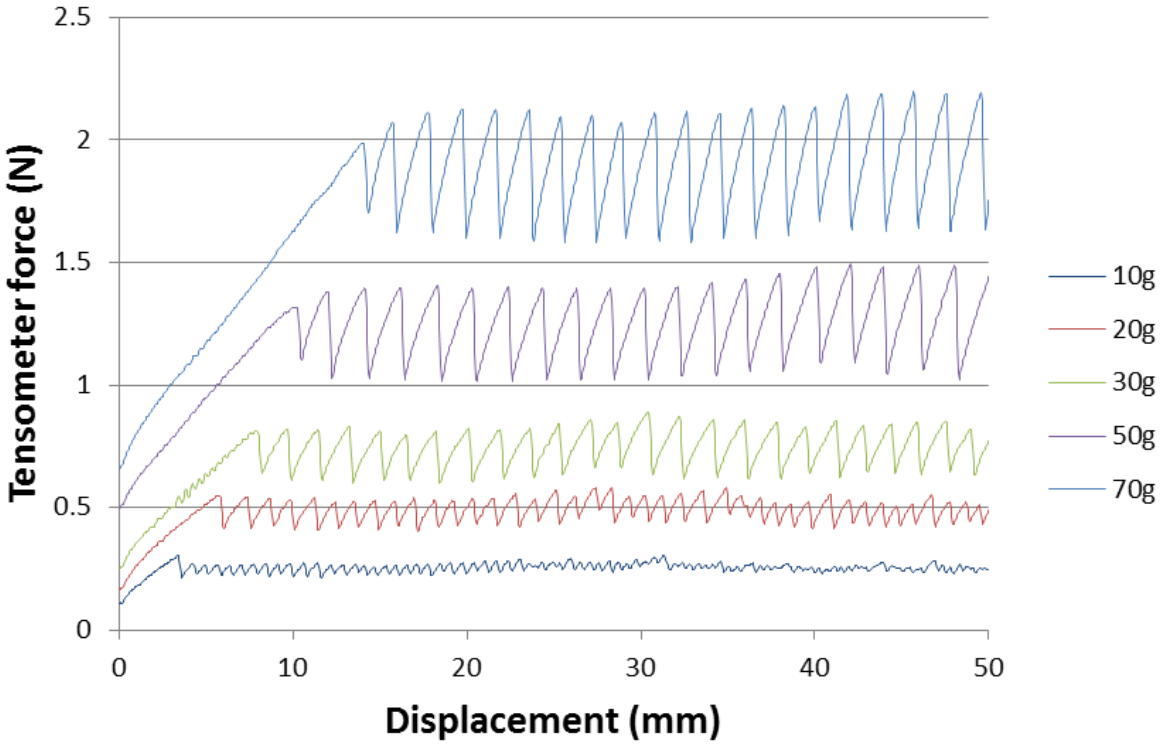

Figure 4.45: Tensometer graphs of fabric DC06 on participant RJ05

From Figure 4.45 I derive the data to plot the graph of pulling force against dead weight between participant RJ05 and fabric DC06 which I present in Figure 4.46.

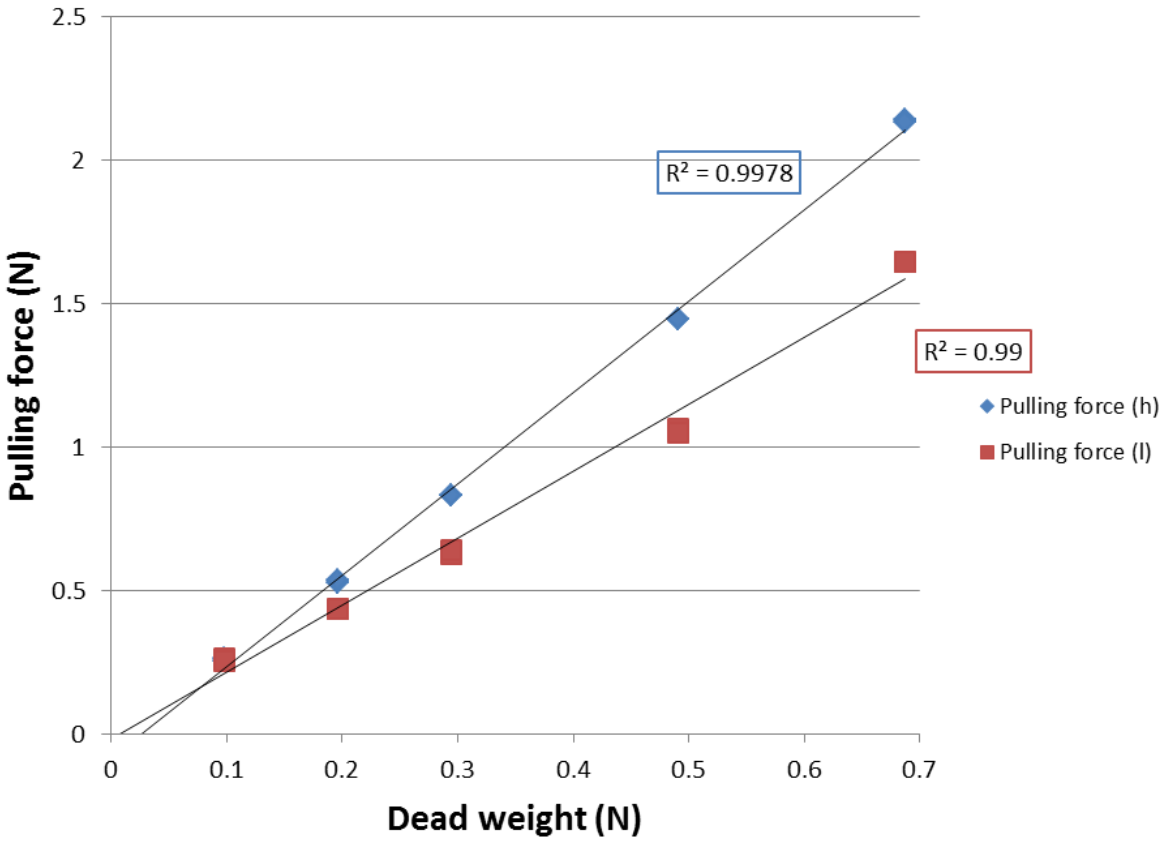

Figure 4.46: Graph of pulling force against weight of fabric DC06 on participant RJ05. Where (h) are the values corresponding to the higher part of the stick slip and (l) to the lower part

The graph is similar to Figure 4.46 where the two data sets create "open scissors". As before, for the derivation of the coefficient of friction I'll use the "red" data set. Again, especially the red points of the graph do not form a straight line but a "shallow" curve.

In Figure 4.47 and Figure 4.48 I present the tensometer graphs of SF14 and SF18 on participant RJ05.

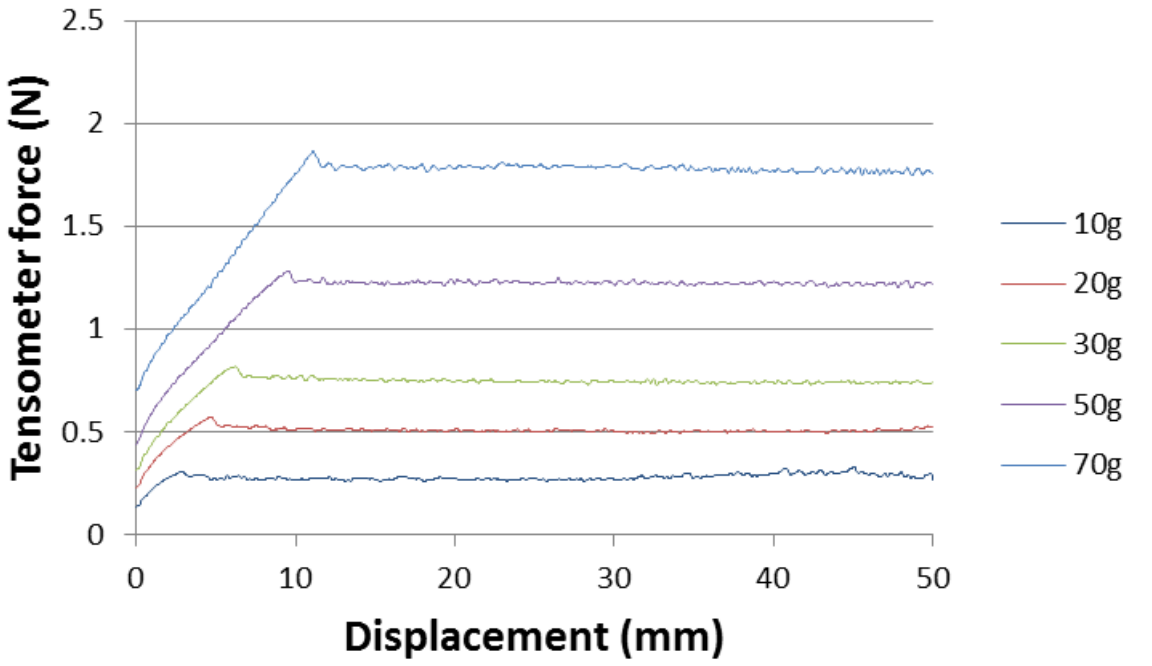

Figure 4.47: Tensometer graphs of fabric SF14 on participant RJ05

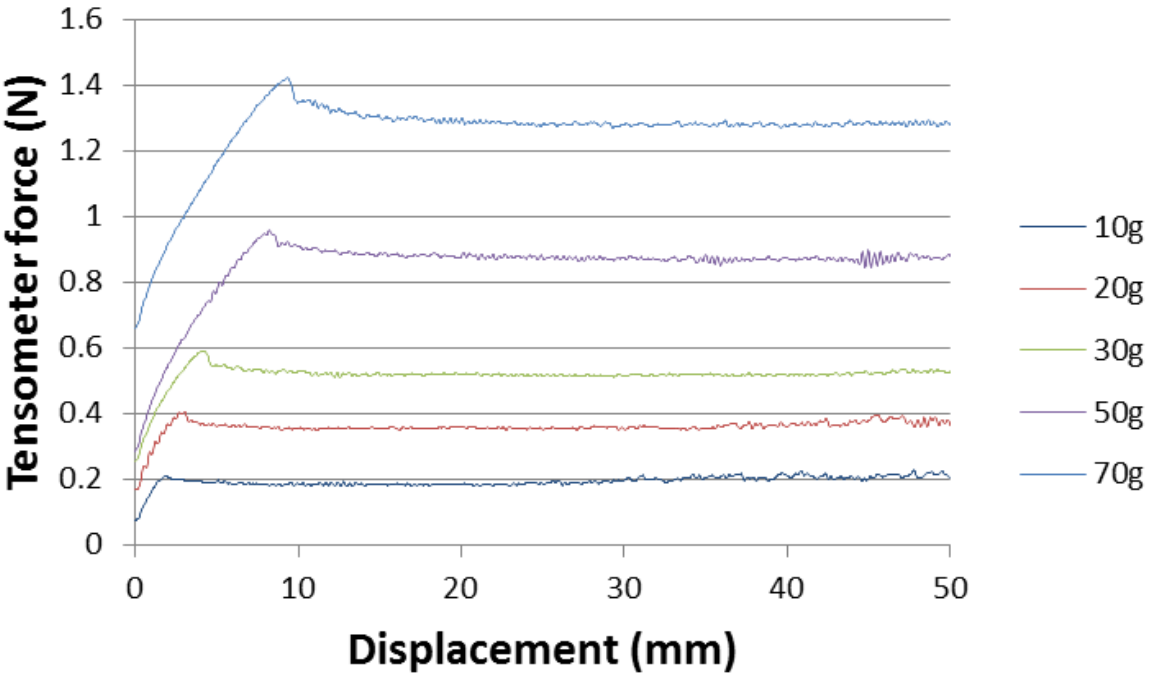

Figure 4.48: Tensometer graphs of fabric SF18 on participant RJ05

4.4.6.2 Experiments on participant SF06

Participant RJ05 was not the only participant to exhibit the stick – slip phenomenon. SF06 is another participant on whom I observe this phenomenon, and particularly with fabric SF17. I present the tensometer graphs which show the stick – slip phenomenon in Figure 4.49.

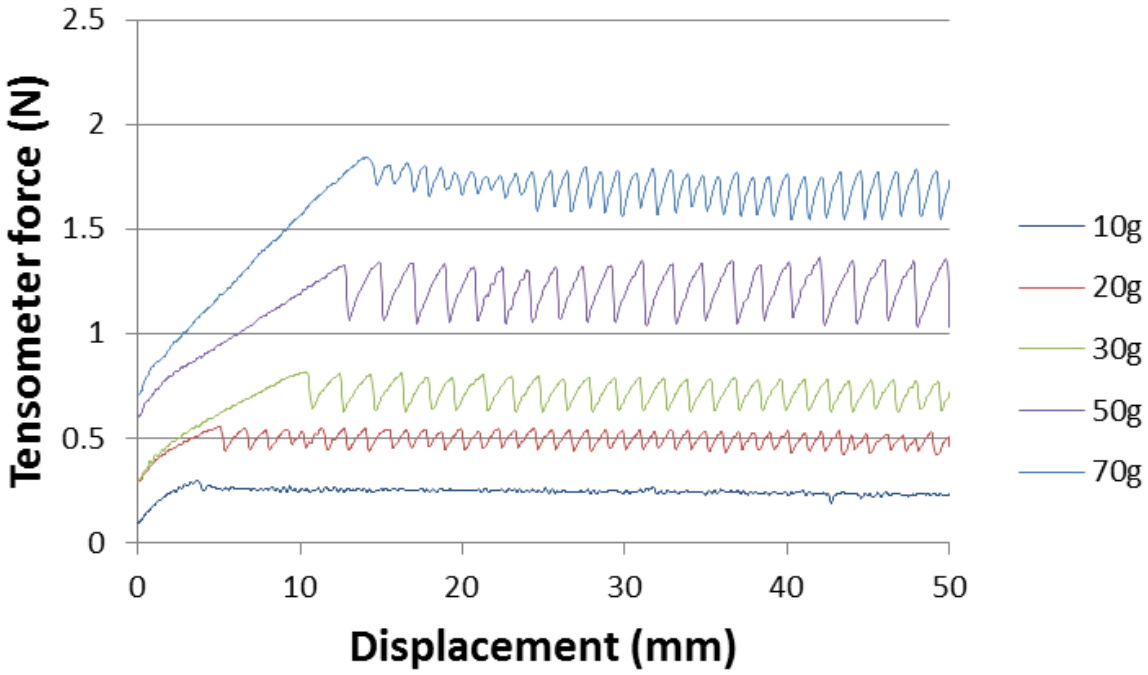

Figure 4.49: Tensometer graphs of fabric SF17 on participant SF06

Below I present the pulling force against weight of the two sets of data which come up from the derived data from Figure 4.49.

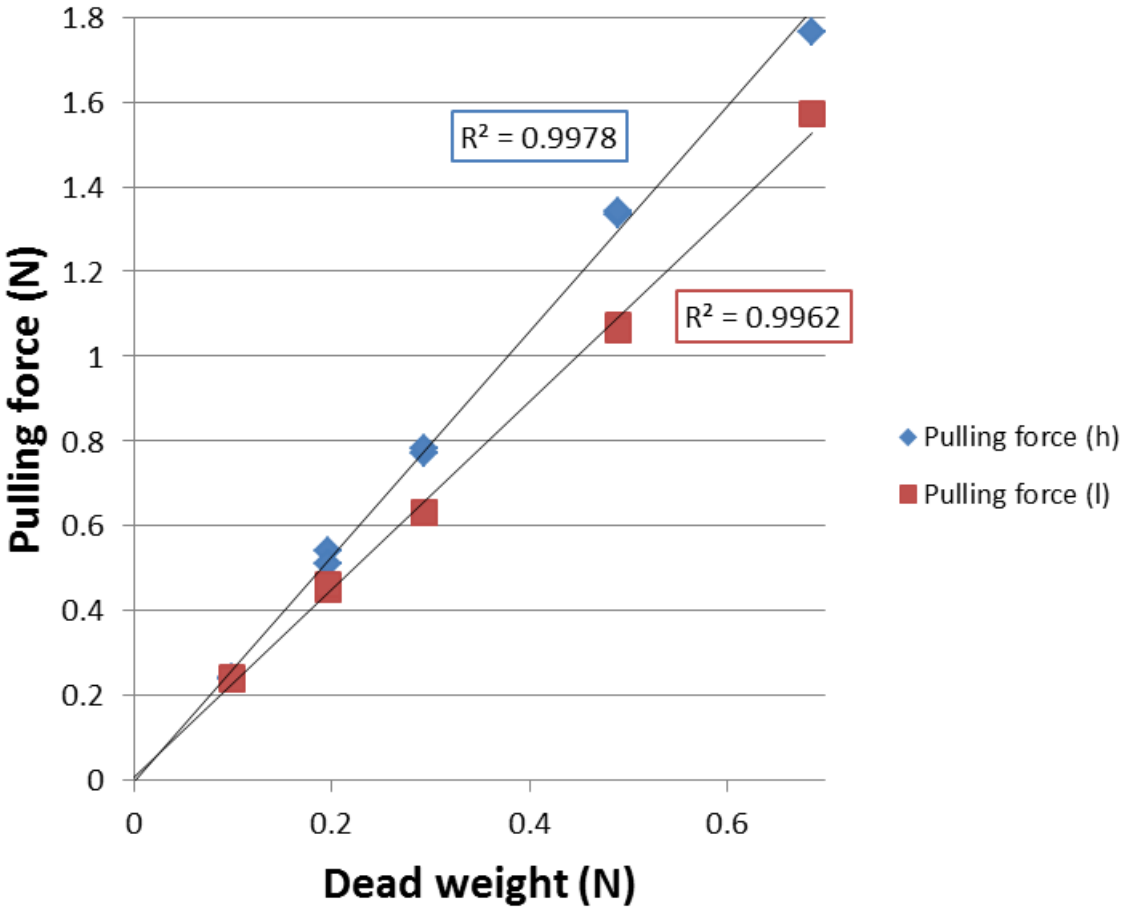

Figure 4.50: Graph of pulling force against weight of fabric SF17 on participant SF06. Where (h) are the values corresponding to the higher part of the stick slip and (l) to the lower part

As in participant RJ05, the plots of fabric SF17 on participant SF06 create "open scissors", the data from which I derive the coefficient of friction, are those which correspond to the "low" values.

4.4.7 Correlation between volar forearm results and bending stiffness

As predicted by Cottenden's model dead weight and dynamic friction force were highly linearly correlated for all fabrics and participants. However the model predicts graphs of friction force against dead weight passing through the origin, whereas most experimental graphs had positive intercepts (Table 4.4). In most of the cases intercept falls within the barriers of experimental error, while in red I show the cases where intercept is twice the size of the experimental error. So, I cannot find any significant discrepancy between the results and the model predictions.

Code	Age (years)	Intercept (N)									
		DC06		SF03		SF14		SF17		SF18	
LC16	28	-0.010	(0.014)	0.025	(0.011)	0.001	(0.015)	-0.014	(0.015)	0.001	(0.012)
MS04	28	-0.008	(0.015)	0.026	(0.014)	0.015	(0.011)	-0.009	(0.019)	0.014	(0.011)
KG13	30	-0.004	(0.014)	0.033	(0.011)	0.012	(0.013)	0.014	(0.013)	0.011	(0.014)
CB18	45	-0.020	(0.021)	0.022	(0.013)	0.008	(0.014)	-0.030	(0.022)	-0.014	(0.014)
MM03	51	-0.015	(0.013)	0.028	(0.011)	0.005	(0.012)	-0.017	(0.016)	-0.010	(0.008)
AD02	57	-0.001	(0.017)	0.048	(0.011)	0.018	(0.014)	-0.005	(0.015)	0.016	(0.009)
RJ05	60	-0.022	(0.049)	0.027	(0.015)	-0.00008	(0.020)	-0.031	(0.052)	-0.005	(0.020)
HJ07	72	0.0004	(0.012)	0.034	(0.014)	0.010	(0.013)	-0.003	(0.023)	-0.001	(0.019)
DA15	73	-0.019	(0.016)	0.032	(0.014)	0.004	(0.017)	-0.005	(0.019)	0.003	(0.013)
MG12	76	0.020	(0.017)	0.034	(0.014)	0.027	(0.013)	0.010	(0.017)	0.015	(0.013)
JJ09	79	-0.023	(0.019)	0.037	(0.017)	-0.003	(0.020)	-0.008	(0.021)	-0.010	(0.012)
SF06	81	-0.004	(0.020)	0.061	(0.017)	0.014	(0.008)	0.009	(0.0321)	-0.009	(0.017)
MH17	84	0.0008	(0.016)	0.071	(0.014)	0.024	(0.012)	0.012	(0.018)	-0.004	(0.013)
MT14	89	0.003	(0.018)	0.044	(0.009)	0.026	(0.013)	-0.002	(0.023)	0.018	(0.015)
DJ10	91	0.004	(0.010)	0.018	(0.010)	0.012	(0.015)	0.020	(0.024)	-0.003	(0.011)
MD08	93	0.006	(0.030)	0.052	(0.023)	0.012	(0.015)	0.003	(0.018)	0.008	(0.017)
AB11	95	-0.005	(0.016)	0.027	(0.016)	0.011	(0.011)	-0.020	(0.041)	-0.002	(0.015)
mean		-0.006	(0.011)	0.036	(0.014)	0.012	(0.009)	-0.004	(0.014)	0.002	(0.010)

Table 4.4: Intercept of the linear plot of pulling force against dead weight for each fabric and for every participant. In brackets I present the corresponding standard deviation. In red are the intercept values which are higher than twice the size of standard deviation.

Furthermore, intercepts appear to be greater for the (subjectively) stiffer fabrics, a fact which led me to examine the bending stiffness of each fabric.

4.4.7.1 Bending stiffness results

I tested five fabrics in total, but for the calculations of the bending stiffness I need the linear density of the fabric weight. The finding of the linear density is a common way for characterising fabrics. It was calculated by weighing the strips of fabrics I was going to use, dividing the weight by the length of the fabric and multiply the outcome by g. The results are in Table 4.5.

Name	Linear weight density ω (N/m)	
	mean	SD
SF03	0.0138	0.0005
SF14	0.00978	0.00015
SF17	0.0043	0.0002
SF18	0.0044	0.0003
DC06	0.0053	0.0009

Table 4.5: Weight linear density of each fabric and the corresponding error.

So, after a series of experiments for each fabric, I derived the corresponding numbers for the bending stiffness which are presented below.

Fabric	Bending stiffness EI ($10^{-9}Nm^2$)	
	Mean	SD
DC06	54	9
SF03	860	30
SF14	260	5
SF17	8.3	0.5
SF18	19.7	1.4

Table 4.6: Bending stiffness of each fabric with the corresponding error.

So, according to the data of Table 4.4 and Table 4.6 there is a direct correlation between the intercept and the bending modulus. Higher bending modulus means stiffer fabric, which seems to be the reason which leads to the appearance of intercepts.

If I plot the bending stiffness against the intercept I take the plot of Figure 4.46 I present below.

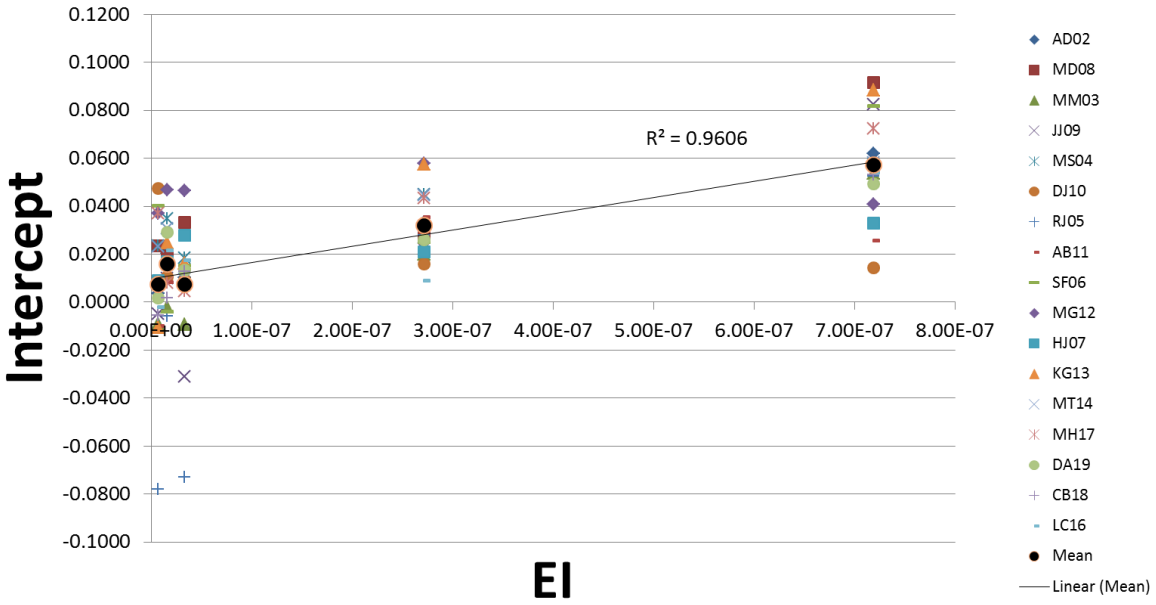

Figure 4.51: Linear graph of intercept (of the graphs of pulling force against weight) against bending stiffness EI of each fabric.

As I show in Figure 4.51 the intercept has a tendency to increase as bending stiffness increases. This shows a clear dependency between intercept and bending stiffness, the higher the bending stiffness is the higher the intercept appears.

4.4.7.2 Impact of fabric weight on intercept

Another possible source of intercept could be the weight of each fabric. This is because the weight of the vertical part of fabric strips (Figure 4.1) adds to the dead weight force. Previously in Table 4.5, I mentioned the linear density of each fabric from which I can derive the weight of the vertical component of the fabric, between the dead weight mass and the volar forearm. This length is between 20 cm and 23 cm for all participants. The next Table 4.7 presents the contributing mass and the weight accordingly. As I show, the "heaviest" fabric is SF03 which contributes a value of 0.345g or an error of 3.45% to the 10g dead weight mass. Of course the length which contributes to the measurements progressively reduces as the tensometer crosshead moves for 50mm throughout each experiment, ending up to a length of 18cm and a dead weight mass of 0.270g. Cottenden's model (Cottenden, 2010) assumes that this fabric weight is negligible and these measurements show that this assumption is valid, even for the lightest dead weight and densest fabric.

Nonwoven code	Area density (gm^{-2})	Dead weight mass (g) for length of 20 cm - 23 cm
SF03	50	0.300 - 0.345
SF14	30	0.180 - 0.207
SF17	17	0.102 - 0.117
SF18	15	0.090 - 0.104
DC06	17	0.102 - 0.117

Table 4.7: Dead weight mass which contributes to each friction experiment.

I need to mention that this intercept does not affect the calculation of μ since the only required element is the ratio of pulling force over dead weight.

4.4.7.3 Fact about linearity of plots of pulling force against dead weight

Interesting is the fact the plot of the pulling force against dead weight shows tremendous linearity, which was anticipated since Equation 4.1 shows that these two figures (T_1 and T_4) are proportional. In the following Table 4.8 I present the correlation coefficient of pulling force against dead weight of every fabric against every participant.

Code	Age (years)	Correlation coefficient R^2				
		DC06	SF03	SF14	SF17	SF18
LC16	28	0.9987	0.9992	0.9986	0.9984	0.9986
MS04	28	0.9985	0.9991	0.9993	0.9979	0.9988
KG13	30	0.9988	0.9993	0.9990	0.9990	0.9983
CB18	45	0.9977	0.9992	0.9990	0.9975	0.9983
MM03	51	0.9987	0.9992	0.9990	0.9983	0.9995
AD02	57	0.9982	0.9993	0.9990	0.9988	0.9993
RJ05	60	0.9900	0.9988	0.9986	0.9902	0.9974
HJ07	72	0.9994	0.9987	0.9997	0.9982	0.9987
DA15	73	0.9988	0.9991	0.9984	0.9982	0.9987
MG12	76	0.9985	0.9989	0.9990	0.9984	0.9986
JJ09	79	0.9973	0.9982	0.9975	0.9970	0.9987
SF06	81	0.9982	0.9989	0.9997	0.9962	0.9981
MH17	84	0.9988	0.9990	0.9993	0.9985	0.9987
MT14	89	0.9982	0.9996	0.9990	0.9974	0.9982
DJ10	91	0.9997	0.9996	0.9992	0.9983	0.9995
MD08	93	0.9976	0.9995	0.9989	0.9986	0.9981
AB11	95	0.9991	0.9991	0.9996	0.9944	0.9988
mean		0.9980	0.9991	0.9990	0.9974	0.9986

Table 4.8: Correlation coefficient of every friction experiment I have conducted on volar forearms

The impressively high correlation coefficient declares the validity of the mathematical model I try to validate. All the values for R^2 are above 0.99, an impressive fact that proves the robustness of the model.

4.5 Analysis of the results

The analysis of the results will happen in several axes. How the coefficient of friction of different fabrics varies for the same participant, the coefficient of friction of the same fabric for different participants for the same and different age groups, and finally how bending stiffness affects the intercept.

4.5.1 Comparison of μ for different fabrics.

The fabric with the highest coefficient of friction against skin was SF03, presenting a mean of 0.449, followed by SF17 which had a mean of 0.434 (Table 4.2). The fabric with the lowest coefficient of friction was SF18 with 0.304.

With reference to Table 4.1, I cannot see any strong correlation between the structure of the fabric and the coefficient of friction.

4.5.2 Comparison of tensometer graphs of the same fabric on the same participant

As I show in the results section, in Figure 4.11 and Figure 4.19 for fabric SF03, the static friction reaches its peak much more quickly with the lower dead weight masses than the higher ones. Not only this, but in the lower masses, the value of the static friction is similar to the value of the dynamic friction, in comparison to the 50g and 70g masses where the peak of static friction is significantly higher than the value of dynamic friction. However, for the rest of the fabrics, I cannot witness such a difference between static and dynamic friction. Fabric DC06, SF14, SF17 and SF18 show very small or no difference between static and dynamic friction. If there is a case of flaccid tissue, there is a small but obvious difference between static and dynamic friction. In case of firm volar forearm this difference is many times imperceptible.

4.5.3 Graphs of pulling force against dead weight

All the graphs of pulling force against dead weight present a linear plot. All the experiments of every participant produce a linear graph, showing in this way the remarkable stability of the theoretical model, as I have already mentioned in §4.4.7.3.Below in §4.5.3.1 I analyse the intercept which appears at every linear graph in the following section.

4.5.3.1 Intercept

From Equation 3.1 I can see that the pulling force is directly proportional to the dead weight, so the graph of pulling force against dead weight is a linear plot going through the origin. Of course, the true

experimental data never go through the origin and the question that arises is whether the intercept lies within the bounds of experimental error. As I can see from the intercept data of Table 4.4 some of the intercept values of the linear graphs are not covered within the experimental error. In order to find the source of intercept I conducted some experiments investigating the bending stiffness of each fabric the results of which are presented in §4.4.7. Most of the intercept values which are not covered from the experimental error correspond to fabric SF03 which had the highest bending stiffness. This suggests that the tensometer had to apply additional force to bend the fabric, a factor which is not included in Cottenden's model, creating in such a way the intercept. There is one more case with fabric SF14 and participant MG12. SF14 is the fabric with the second highest bending modulus which justifies the appearance of intercept.

4.5.4 Skin deformation during measurements

The main reason I chose to work with two different age groups is the different behaviour of the skin and the underlying tissue. The younger group had firm volar forearm, while the older showed a flaccid behaviour. In particular, if I compare the graphs shown in Figure 4.11 and Figure 4.19, I can see that the static friction reaches its peak much quicker on participant MM03 than on participant DJ10. I can also see that deformation is smallest for the lower dead weight mass (10g) and biggest for the highest dead weight mass (70g). To be more precise, for the dead weight mass of 70g, the graph of MM03 reaches its peak within 5mm, while for DJ10 the required space is 19mm. The comparison of these two numbers shows the degree of deformation which is much bigger for the older participants. At this point I have to add that flaccid tissue is independent of the shape of the arm. Measurements on participant HJ07 showed that for the dead weight mass of 70g, sliding occurs after 16.5 cm. This number which is closer to the number of DJ10 is an indication of similarity in the behaviour of older participants.

From the volar forearm graphs that I generated, the most steep initial part of the curve was shown by participant MM03 for fabric SF14 and the least steep initial part was shown by participant HJ07 for fabric SF03. The gradient of participant MM03 for this case for the graph for the 70g deadweight is 0.17 N/mm, while the gradient for participant HJ07 is 0.044 N/mm, much less than the gradient for MM03.

4.5.5 "Stick and slip" and friction experiments

As I have already mentioned earlier in three cases I have stick and slip, but in some cases I have a phenomenon which is between the stick and slip and the usual wave form of the graphs which is caused by the noise of the experimental setup. I present a typical stick and slip graph in Figure 4.42 and a graph which is not clearly stick and slip in Figure 4.52. As you can see in this graph, the variations between high and low value are very small, so small that I cannot clearly judge if it is stick and slip phenomenon. On the other hand, the variations are very abrupt which leads me to the conclusion this is not the usual wavy form which I meet in many of my experiments. On the other hand, the usual wavy form is presented by Figure 4.9 and Figure 4.10 where a minor fluctuation due to the "noise" produced by the equipment is visible. Interesting is the fact that even when I had the stick – slip phenomenon the correlation coefficient was again incredibly high, higher than 0.99, something which proves for one more time how robust the model is. Also throughout all of my

experiments I did not witness significant deformation (lateral and longitudinal) of the fabric, while I saw impressive rucking of the volar forearm throughout my experiments.

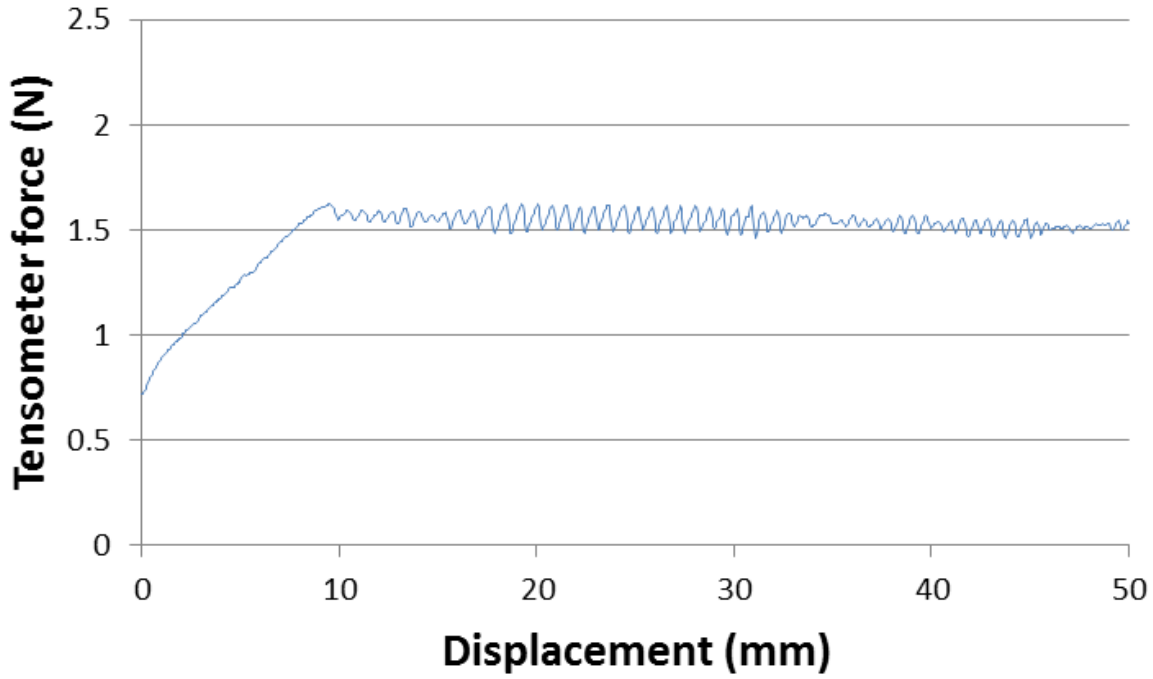

Figure 4.52: Tensometer graph of fabric DC06 over participant SF06 of dead weight mass of 70g

4.5.6 Skin as countersurface

By analysing these results I should not forget that in the case of volar forearm experiments I did not use as countersurface artificial materials, but the real actual human skin. The skin site I chose was the volar forearm since it is hairless and simulates the parts of the body where the skin is hairless as well. The tensometer graphs I derived are extremely "smooth", without any artefacts, a fact which is not so common in the other parts of my project where I use surrogate surfaces. The problem of the compliancy of the arm is not visible in the graphs and it does not create any inconsistency in the results. This fact is even more important considering the experiments were "in vivo" and not "in vitro". Overall, I feel the need to say that nature is much better at creating materials with ideal properties than man.

In the next chapter I am going to push the validation one step further by using cylindrical model arms. These arms show extreme rucking which is impossible to produce on a volar forearm. Additionally, due to the high forces applied on the fabric I have stretching and narrowing of the strip of fabric. It will be interesting to investigate how the model responds under these conditions.

Chapter 5 Experiments on compliant cylinders

Every step of my project pushes the validation of the mathematical model one step further. In the rigid cones section I tried to validate the model on rigid cones, just changing the half cone angle, isolating in this way the geometrical factor. During the volar forearm section I deal with compliant substrate with wrinkled surface, while in this chapter I focus on modelling volar forearms in which I could produce more extreme deformations than volunteers could tolerate.

I used compliant arms of cylindrical shape. In order to compare them to each other, I constructed a rigid cylinder and had two more compliant cylinders constructed. These three cylinders were of successive degrees of compliancy (one softer than the other, while the first cylinder was rigid) providing in this way different degree of mechanical behaviour.

5.1 Preliminary experiments

In this part of the project I try to discover the materials which exhibit the desired behaviour. The sought materials should generate the greatest possible deformation, while at the same time they should demonstrate sliding, so I can generate the dynamic coefficient of friction. These properties can be generated by materials which have a high degree of compliancy, while their surface is covered by a high friction material which intensifies the desired compliancy.

Below I present some of the materials which I tested and compared but they did not exhibit the desired behaviour, so I had to discard them.

One of the combinations I tested was latex sheet (from **FOUR D RUBBER CO LTD,** type of latex sheet: **SUPATEX YELLOW**) as skin with polyurethane foam as substrate. The combination of these two materials should simulate the range of behaviour I observe in the volar forearms, but in higher degree. In other words I want to see the effects of deformation (rucking), while after a point allowing slippage to calculate the coefficient of dynamic friction. I conducted a series of experiments since these materials were easily accessible in the market, but unfortunately they did not generate the expected result. The sticky surface of the yellow latex sheet produced a too high coefficient of friction, causing the rupture of the strip of fabric at high loads. The other substrate that I tested was gelatin solution (VWR, BDH, PROLABO, product 24350.262) in various formulations. Unfortunately again, all the formulations that I tested, produced unsatisfactory results. During the experiments all the cylinders ruptured on their surface under high loads which extended to the core of the cylinder. In order to deal with the brittleness of the gel I incorporated a layer of cotton wool. In this case I managed to eliminate the rupture, but the cylinder still did not produce the desired deformation, so I had to discard this kind of material as well.

5.2 Main experiments

In this section I describe the final choice of materials I used to conduct the experiments, as well as the additional experiments to explore further the properties of these materials.

5.2.1 Materials

The solution about the materials I was seeking for, came from a company based in High Wycombe. I and my supervisor contacted the company and talked on the phone to Mr Derek Williams – Wynn, the manager of the company. He was very willing to help us, even though he was not going to make any profit from it, but he was satisfied for helping research. He sent us a variety of silicone rubber materials, some of which were too stiff, while some others were so compliant that it was impossible to retain the shape of a cylinder. Also, some materials gave us the impression that after each experiment they could not be restored to their initial shape, so I could not use them for successive measurements. We arranged a visit to the premises of the company, where Mr Williams – Wynn welcomed us and helped us decide which where the best materials to use. We ended up with two different silicone gels and two different silicone membranes. From these membranes I used the one which had the highest coefficient of friction. The combination of two different gel arms with the chosen membrane offered two different degrees of deformation, one higher than the other, so I could test the model in a greater range of behaviour, both of them more extreme than the exhibited behaviour in the volar forearms.

After we chose the materials we mailed to the company studdings of length of 500mm and diameter of 10mm to use as the cylinder core. With these studdings, we ordered two cylindrical arms of Gel-8250 and Gel-8170 with caps at both ends, diameter of 60mm and length of 200mm. We also ordered low modulus silicone membrane, according to the description of Mr Derek Williams – Wynn **CSM82-4905-10**, with which I wrapped each cylinder. I chose this specific membrane because less "rigid" (low modulus) materials seem to have a higher coefficient of friction, achieving in a better way the desirable objectives of intense deformation.

The structure of each cylinder was as follows:

- The cylinder made of Gel-8170 had caps at both ends, the length of the cylinder without the caps was 150 mm and the length with the caps was 215 mm. The diameter of the cylinder with the studding was 63 mm.
- The cylinder made of Gel-8250 had a length of 230 mm with the caps and a length of 190 mm without the caps. The diameter with the studding was 63 mm.
- The rigid cylinder I tested was made of ABS and had a diameter of 70 mm and a length of 254 mm. I need to emphasize on the fact that I placed three membranes on the rigid cylinder, two (number two and three) with the same orientation and one (number one) close to the edge of the cylinder, with perpendicular orientation. The width of membrane number one was 67 mm, of number two was 75 mm and of number three was 80 mm. The length of the cylinder was 251 mm and its diameter 69 mm.
- At the centre of the rigid cylinder I had placed a studding to grip it steadily in the setup, while I filled the cylinder with plaster of Paris to make the structure steady.
- As core for each cylindrical arm there was a studding with a length of 500 mm and diameter of 10 mm.
- Silicone membrane CSM82-4905-10 had a thickness of 0.25mm.

Below in Figure 5.1 I present a descriptive figure of the compliant cylinders.

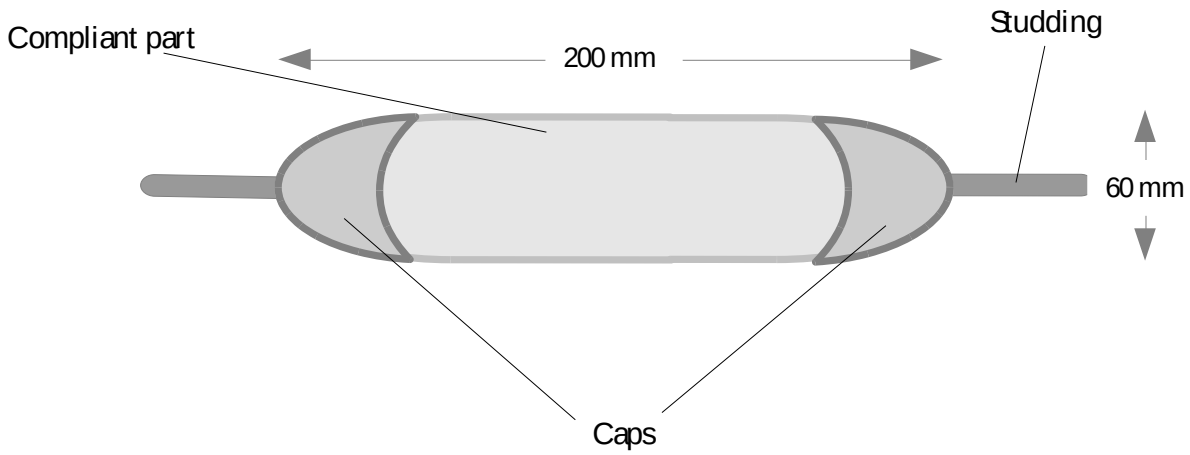

Figure 5.1: Diagram of a compliant arm.

After I took the cylinder out of the cast and measured its dimensions, I applied on its surface the low modulus membrane which the group supplied for my experiments. I adjust the dimensions of the sheet to the dimensions of the surface of the cylinder with extra caution not to create any air bubbles or fold the membrane on itself, disturbing in such a way the smoothness of the surface.

Penetration value shows how deep I can "go" in the material without causing permanent distortions, while I analyse the shear modulus and the compression modulus in §5.2.2.

5.2.2 Further investigation of gel mechanical properties

Nusil technology did not provide the value for shear modulus in Table 5.1, but I measured it with a cuboid of material using a rig I constructed (Figure 5.2). I created a board on which I attached a polyethylene sheet that does not allow the gel to stick, so leaving any debris. In such a way the board can be reused by testing more sticky materials. On this board I placed the cuboid. On the top of the cuboid I placed a level metal sheet, on which I put a dead weight mass of 100g for better contact with the cuboid piece of gel. The cuboid I wanted to test had dimensions 50mm x 50mm x 15mm. I attached both boards at both square sides of 50mm x 50mm. I was very careful to place both boards in parallel in order to avoid compressive components. The crosshead speed was 30mm/min(=0.0005m/s).

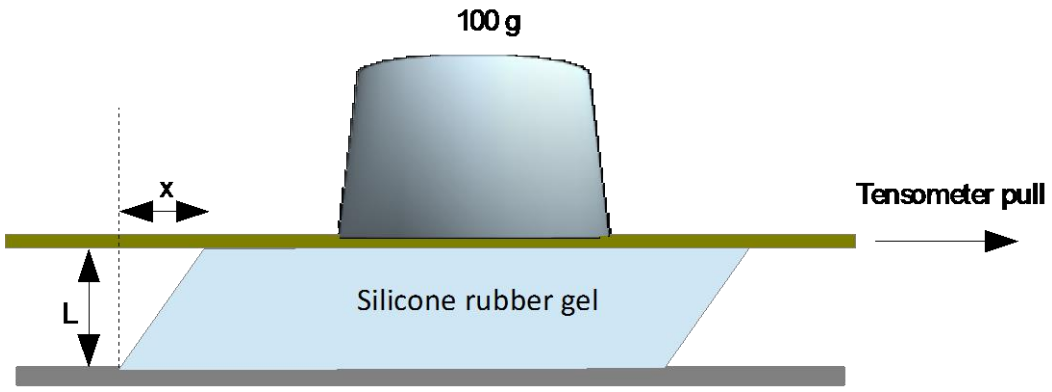

Figure 5.2: Diagram of shear modulus experiments.

These experiments produced a linear plot, from the slope of which I could derive the shear modulus. In the following Figure 5.3 I show the graphs from which I derive the shear modulus for Gel-8170 and Gel-8250.

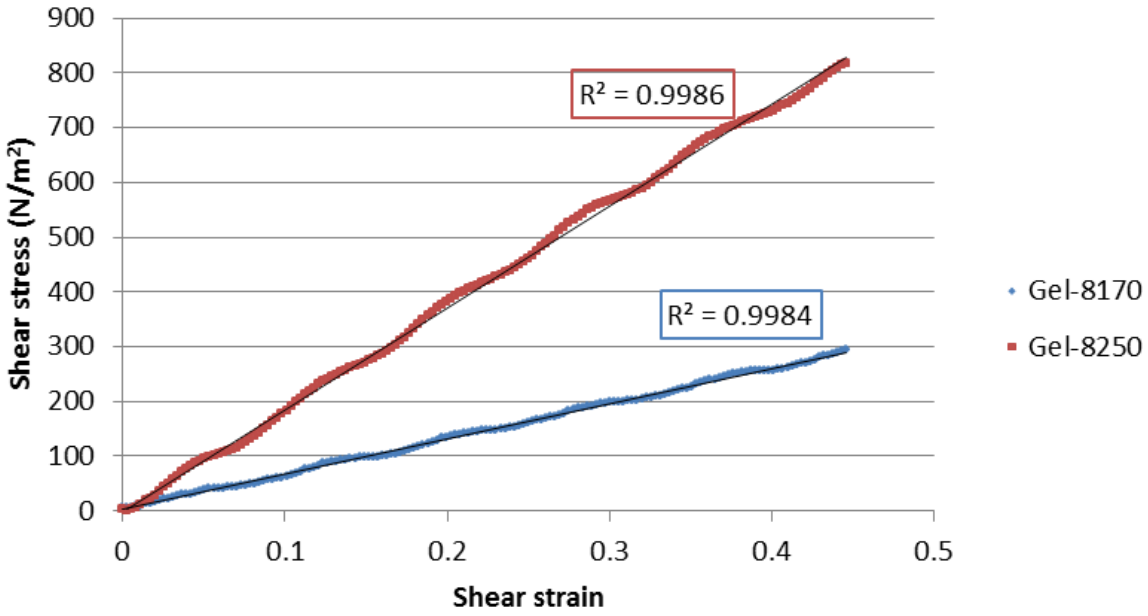

Figure 5.3: Graph for Gel-8170 and Gel-8250 produced by the shear modulus experiments, as they are presented in Figure 5.2.

From Figure 5.3 I can see that the data points have a "wavy" form. This could happen due to the minor vibrations of the gels throughout the experiments or due to the sliding of the lower surface of cuboid which is supposed to stay still. The high correlation coefficient in both cases declares I can derive the shear modulus with satisfactory accuracy. It is clear that the shear modulus for Gel-8250 is higher than that of Gel-8170, which translates to higher compliancy for Gel-8170 than for Gel-8250. I present the calculated values in Table 5.1.

To derive the compression modulus I conducted another series of experiments by compressing each gel between two parallel boards of wood (Figure 5.4). The gel is laid on a polyethylene sheet which as

in the shear modulus experiments, has low surface energy. The crosshead speed was 50mm/min(=0.000833m/s).

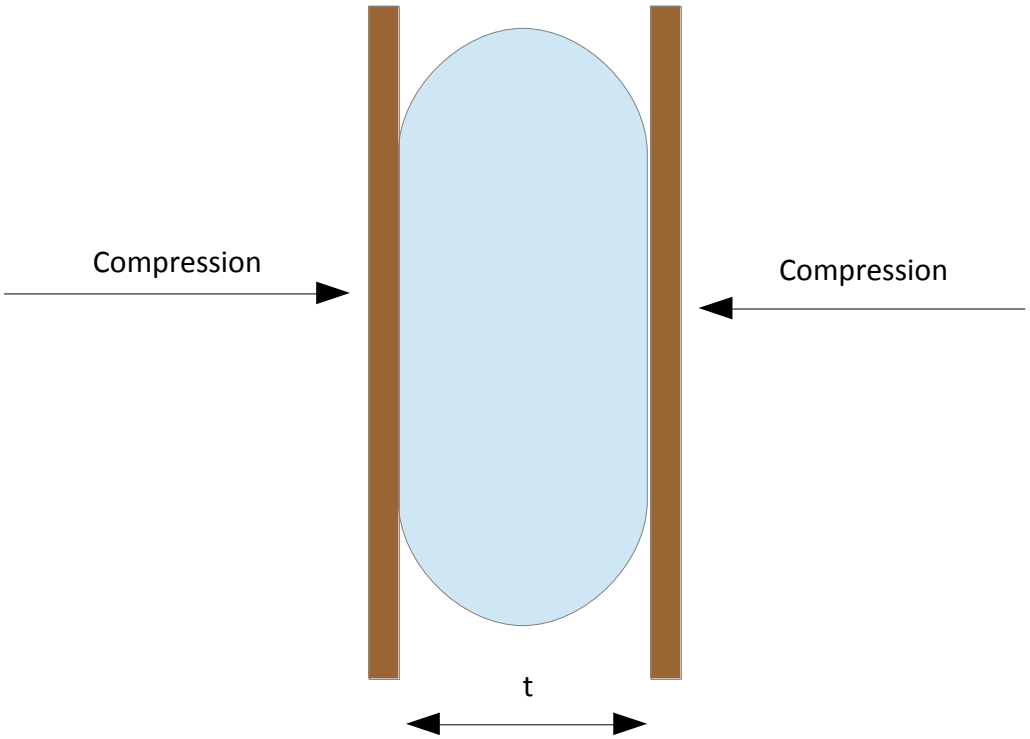

Figure 5.4: Diagram of the compression modulus experiments.

Below I present the plots generated from the experiments for Gel-8170 and Gel-8250.

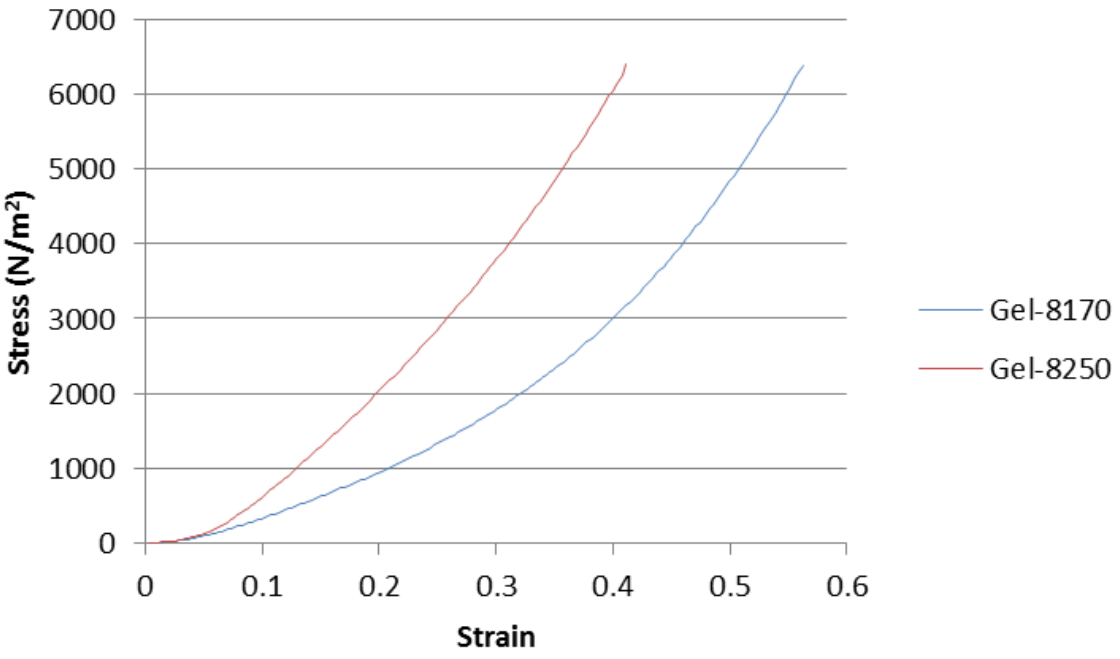

Figure 5.5: Stress – strain curve for the compression modulus of Gel-8170 and Gel-8250

As I can see from Figure 5.5: Stress – strain curve for the compression modulus of Gel-8170 and Gel-8250 compression modulus which is the gradient of stress over strain is characterised by a curve. This means I cannot derive a sole value for the material, but for a certain strain I can find the corresponding stress. Another outcome of the curve is that for Gel-8250 higher stress values are achieved for lower strain than for Gel-8170. This fact indicates lower compression modulus for Gel-8170 than Gel-8250, which means by applying more pressure on Gel-8170 I can cause more deformation.

The maximum compression I observed during the experiments from the Gel-8250 experiments was 2.5mm and from Gel-8170 experiments 9mm. This corresponds to a strain of 0.12 for Gel-8250 and 0.42 for Gel-8170. With regard to Figure 5.5 the compression modulus for Gel-8250 is 11,751Pa and for Gel-8170 is 10,600Pa.

5.2.3 Strip deformation

Throughout the experiments on compliant substrate I did not observe deformation just on the cylinder, but on the fabric as well. Sometimes, the tensions on the fabrics were so large that I observed lateral and longitudinal deformation of such a degree, that in some cases the strip of fabric wss converted to a cord. So, the tensometer had to apply force, not only to deform the cylinder and cause sliding, but to deform the fabric as well.

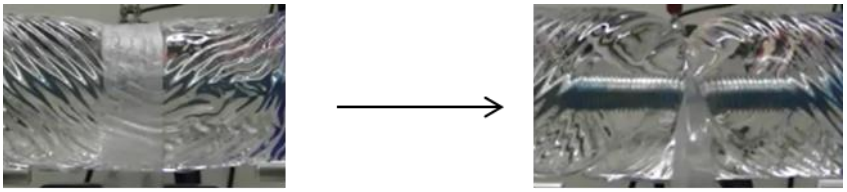

Figure 5.6: Strip of fabric on the compliant arm without deformation (a), with substantial lateral deformation (b).

What follows is the presentation of some key mechanical properties of the gel materials.

5.2.3 Mechanical properties of gel materials

Table 5.1 shows some key properties of the silicone materials.

	Penetration (mm) (manufacturer's data)	**Shear modulus (Pa)**	**Compression modulus (Pa)**
Gel-8250	4.0-4.5	1,860 (5)	7658 (343)
Gel-8170	7.5-7.6	644 (2)	7773 (124)

Table 5.1: The gel types I used as a substrate material with the corresponding mechanical properties, where brackets there is the SD.

5.2.4 Methodology

The procedure I follow to complete each experiment was very similar to the one that was followed for the volar forearm experiments, just much simpler since in this case I examine cylinders, while previously it was human subjects. Below I present the steps I followed:

1. Adjust the top surface of the cylinder to the same height as the tensometer crosshead.
2. Verify the cylinder is horizontal.
3. Verify the whole structure is stable.
4. Adjust the nonwoven strip, ensuring that:
    (a) Its length is at right angles to the tensometer.
    (b) It lies flat against the cylinder.
5. Attach the dead weight to the free end of the fabric strip.
6. The experiments are ready to begin.

I followed the steps for every different strip of fabric I attached. The setup which I used for the conduction of these experiments was very similar to the one used for the volar forearm experiments, presented in Figure 4.1.

5.2.5 Settings

During preliminary experiments I noticed that the total displacement of 50 mm that I had set for the volar forearm experiments was not sufficient for the compliant arm experiments. The main reason was that the tensometer had to overcome the deformation of the compliant arm and perform sliding which would enable me to calculate the dynamic coefficient of friction. Due to the high degree of the achieved deformation, the total of 50mm was not enough, so I used the maximum displacement the experimental equipment offers, 140mm.

For these reasons I changed the total displacement to 140 mm, but I kept the velocity to 50 mm/min or 0.00083m/s, the same as the one used for the rigid cone experiments. The dead weight masses that I used had a range of 10g to 70g. For each dead weight mass I used a different maximum tensometer force in the tensometer settings. The maximum tensometer force had a range of 6.86N to 11.76N. The main reason for changing the maximum force for different measurements was that different maximum lead to different resolution in the tensometer graphs. So, by inputting the lowest maximum force I achieved the highest possible resolution.

For the rigid cylinder the dead weight masses remained the same, but the maximum tensometer force in the settings slightly changed, having a range from 4.9N to 9.8N. The values were a bit lower than the ones for the compliant arms, since the rigid cylinder did not deform so much. So, there was no need to consume extra force to decouple sliding from deformation.

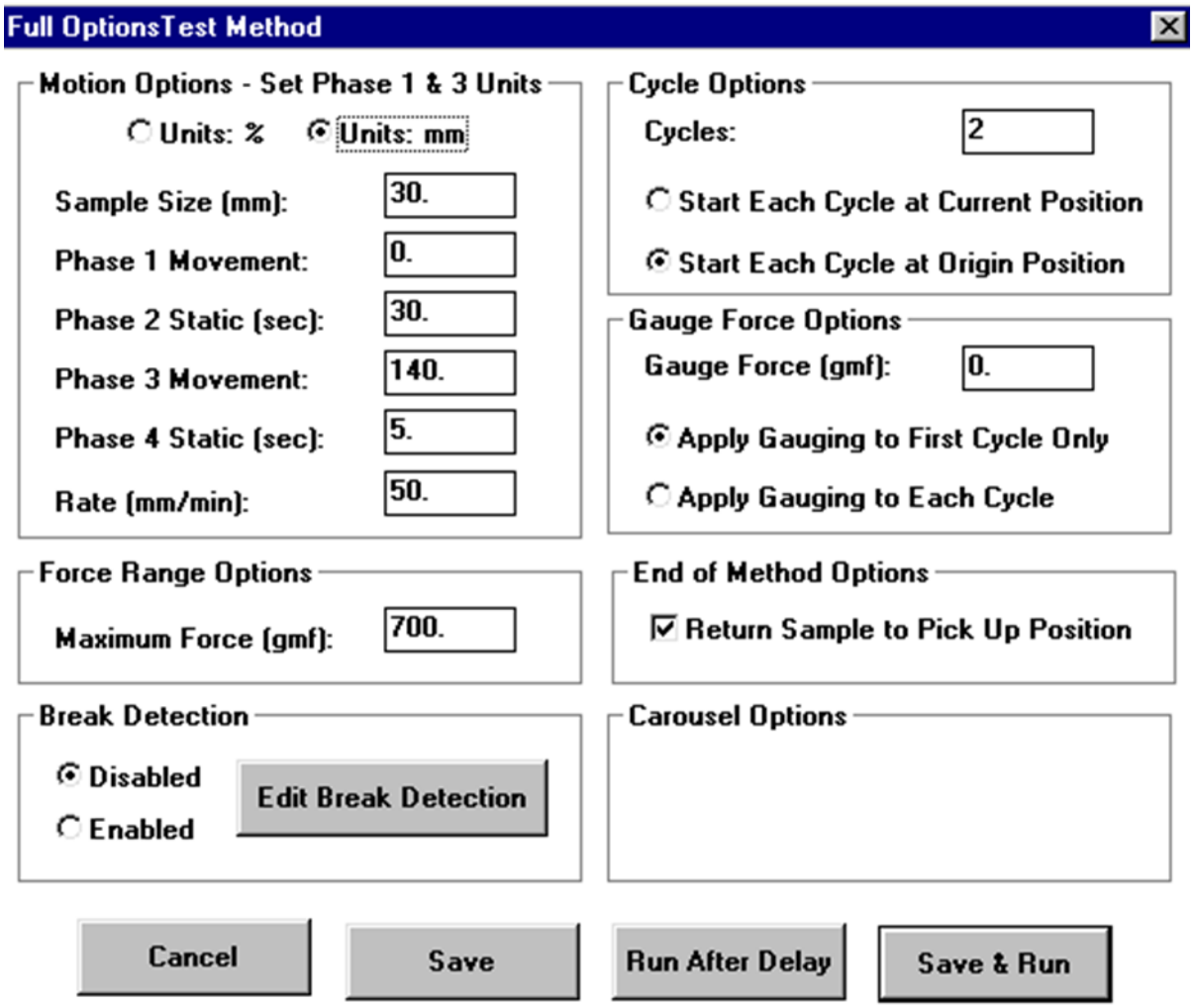

Figure 5.7: Photograph of the tensometer software

With reference to Figure 5.7, for these experiments, for Phase 1, I input 0 mm which means I did not want the tensometer to start moving right after I pressed the button to start the measurements. For Phase 2, I input 30 s, which was the necessary time to place and align the fabric before the measurement started. For Phase 3, I input 140 mm which was the displacement I wanted the tensometer to conduct, in this case the highest achievable by the tensometer. In Phase 3, I set 5 s, which meant that after the completion of each measurement the tensometer crosshead had to remain still for 5 s. If the crosshead started returning immediately after the measurement to the initial position, there was the danger of sliding on the test surface. For this reason, I set this small interval to help me displace the strip of fabric. The highest tensometer force that I mentioned earlier is the maximum force that Figure 5.7 presents.

5.3 Results

I conducted experiments on two compliant arms; one made of Gel-8250 and another made from the more compliant material, Gel-8170. I was able to extract the coefficient of friction for all the fabrics

on the cylinder of Gel-8250, but not all of them on the cylinder of Gel-8170 since the tensometer could not generate a high enough force to initiate slip with all fabrics. A full set of friction curves is given in Appendix C.

5.3.1 Experimental results of fabric SF03 on cylinder Gel-8250

When I started each measurement I placed very carefully the strip of fabric on the cylinder. When the crosshead started moving, applying shear stress on the cylinder, I initially observed rucking which becomes more and more extreme. After gross deformation reached each peak, sliding was initiated, followed by a plateau of each graph since the tensometer force was relatively stable.

In the graphs below I show the tensometer graphs for dead weights of 10g and 70g for compliant arm Gel-8250. For the graph of 10g I present Figure 5.8.

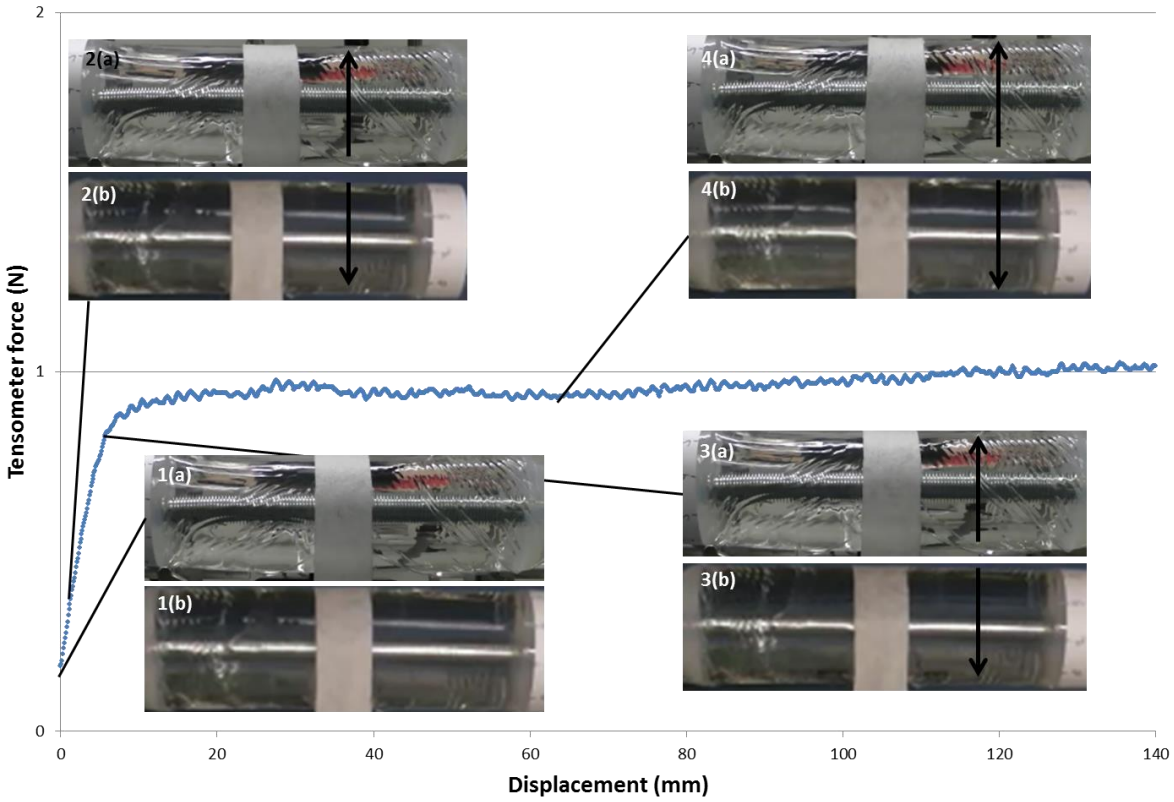

Figure 5.8: Tensometer graph of dead weight mass of 10g for SF03 on cylinder Gel-8250 with the corresponding photographs. At the upright corner of each photograph I show the number of the photograph, where (a) is the front view of the cylinder, (b) is the top view camera, while the arrow shows the direction of movement of the fabric.

As I show, with difficulty I can see any changes on the fabric or on the arm throughout the experiment. If I observe very carefully the front view of photographs 1 and 3 I can see the shaping of a minor indentation of concave form.

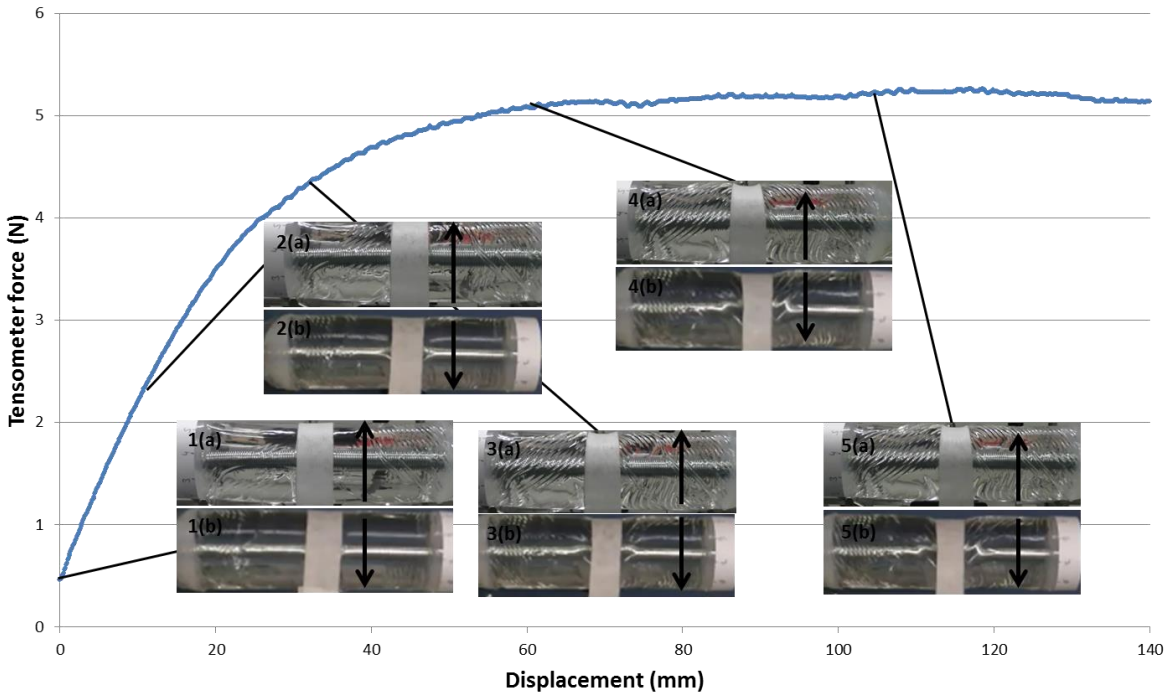

Figure 5.9: Tensometer graph of friction experiment of 70g of fabric SF03 on Gel-8250, the (a) photographs present the front view of the camera and the (b) photographs present the top view of the cylinder. The arrows show the direction of movement of the fabric.

From the photographs of Figure 5.9 it is obvious the gradual formation of an indentation which has concave shape at the front view camera and indentation from the top view camera. Since there is no peak identifying where is the maximum static friction value, after which sliding starts, the starting point of the plateau with the mean on which I calculate the dynamic coefficient of friction, corresponds to photographs 4. Moreover, the gradual narrowing of the fabric is visible throughout the measurement.

Below I present the series of tensometer graphs that correspond to the fabric SF03 on cylindrical arm Gel-8250.

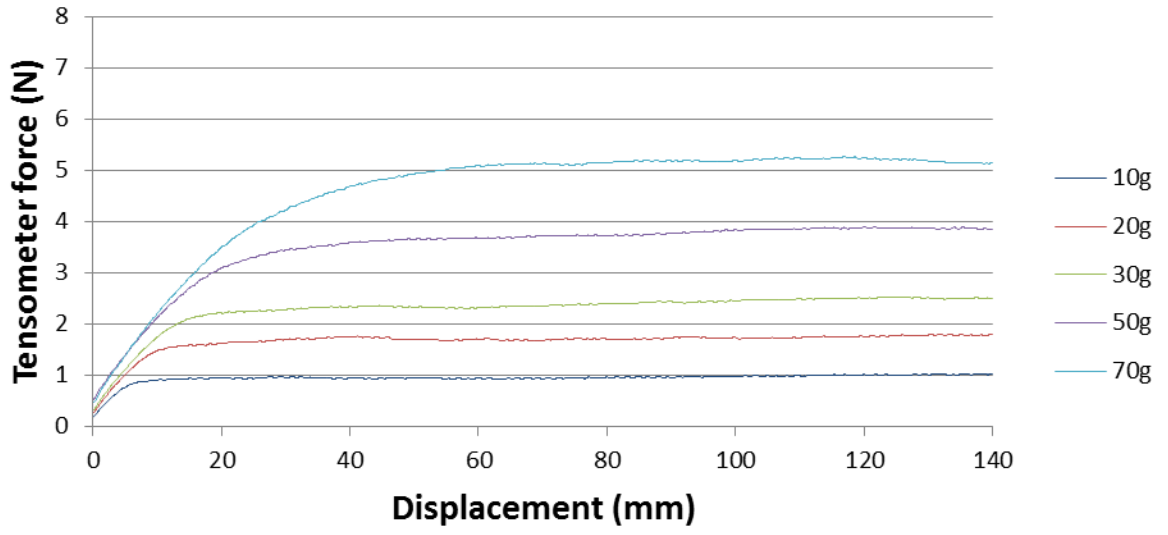

Figure 5.10: Tensometer graphs of fabric SF03 over cylinder Gel-8250

In Figure 5.10 I present the tensometer graphs which correspond to every dead weight I used. As the graphs show, the pulling force, which in the case of the compliant cylinder measurements is the same with the tesnometer force, for each dead weight is derived by the plateau of each graph, which is extremely obvious in these graphs.

From the five different graphs I can plot the pulling force as a function of dead weight for this specific series of experiments (Figure 5.11).

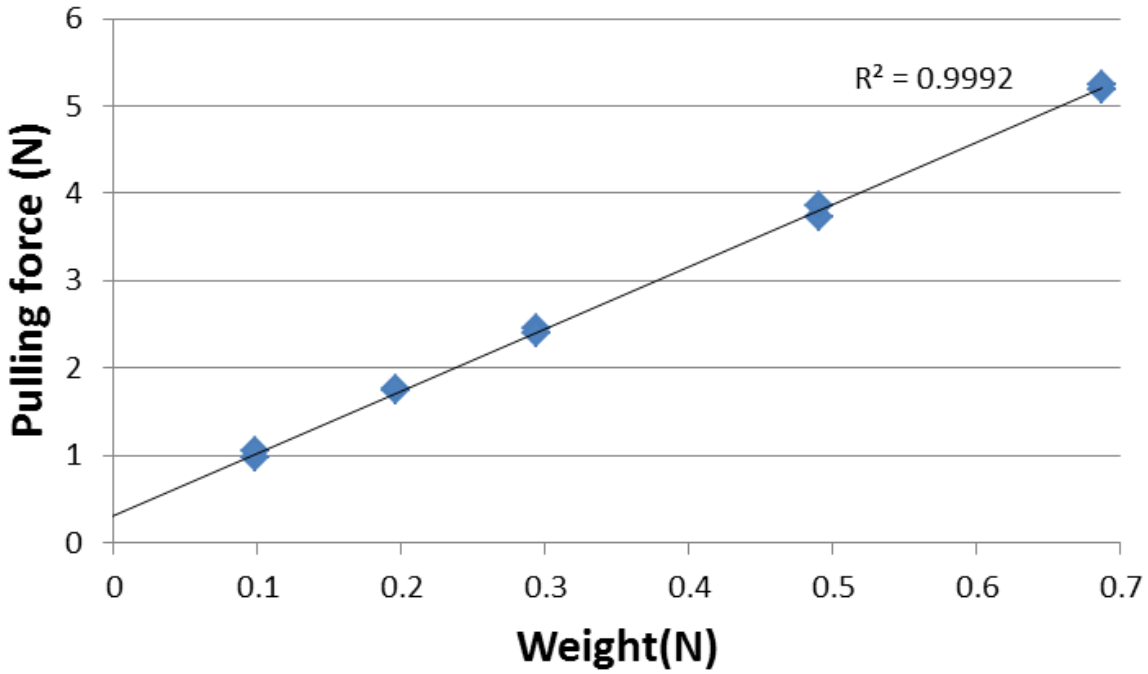

Figure 5.11: Graph of pulling force against dead weight of fabric SF03 on cylinder made of Gel-8250

For each dead weight mass I conduct two measurements, the results of which I incorporate in every linear graph I quote. From the above graph I can see that the pulling force is directly proportional to the dead weight, as the model predicts (Equation 4.1), but there is a positive intercept.

5.3.2 Experimental results of fabric DC06 on Gel-8250

Each fabric had different characteristics and responded differently in each experiment. In the case of DC06, it was not just the cylinder which deformed, but there was impressive lateral deformation of the fabric on the cylinder. Moreover, the tensometer force gradually reached a plateau, without achieving an overall maximum force for the static friction.

In Figure 5.12 I show the tensometer graph of 10g of fabric DC06 on cylinder Gel-8250.

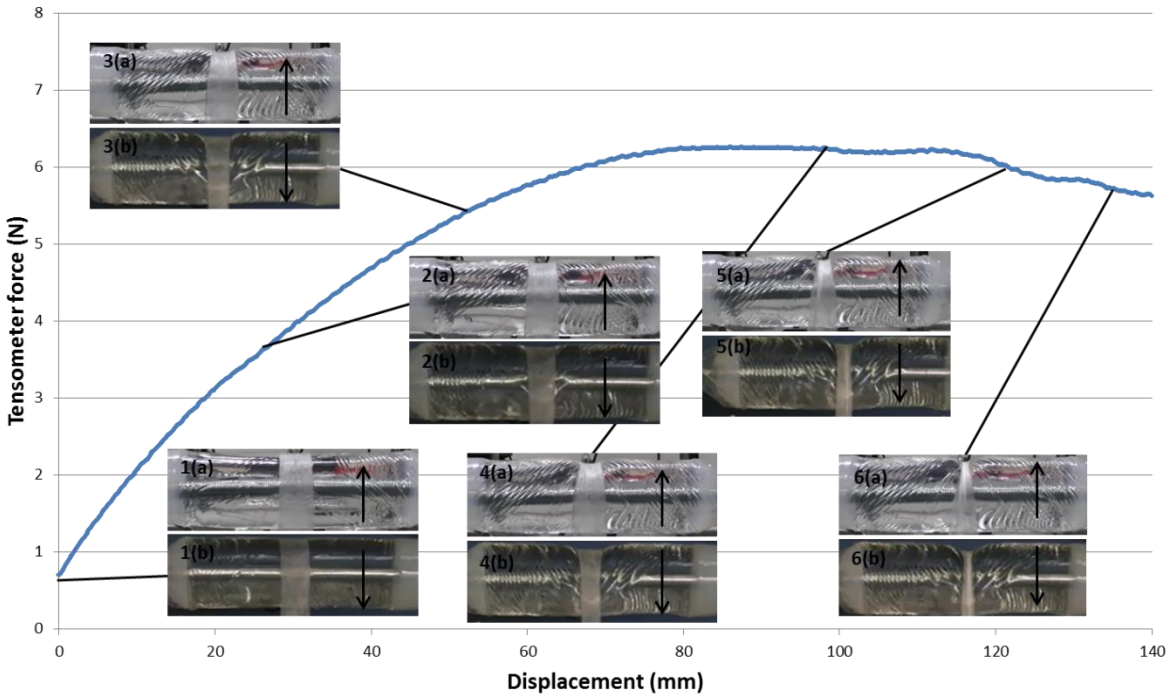

Figure 5.12: Tensometer graph of friction experiment of 10g of fabric DC06 on Gel-8250, the (a) photographs present the front view of the cylinder and the (b) photographs present the top view of the cylinder. The arrows show the direction of movement of the fabric.

Even though it is difficult to see any deformation on the cylinder or on the fabric, it is obvious that after photograph 4 there is the shaping of a concave effect from the front view and indentation from the top view. From photograph 4 to photograph 6 there is not any significant change in deformation, which seems to remain the same. Slippage between the fabric and the gel starts at 29.2 mm.

Below I present the 70g tensometer graph.

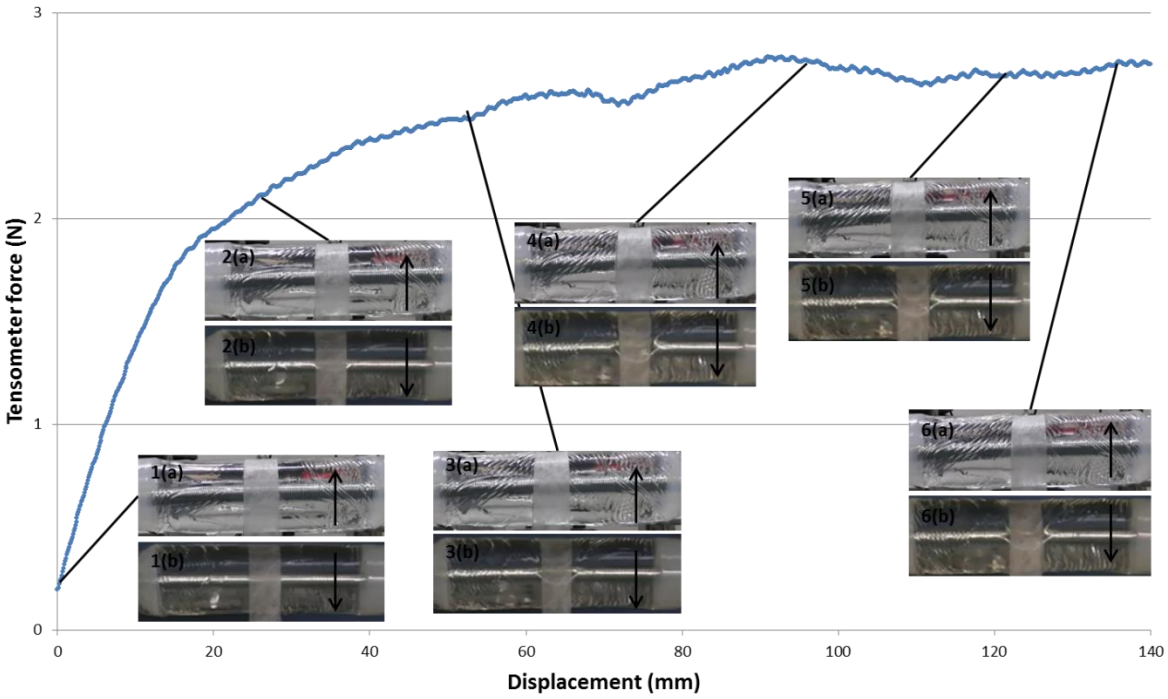

Figure 5.13: Tensometer graph of friction experiment of 70g of fabric DC06 on Gel-8250, the (a) photographs present the front view of the camera and the (b) photographs present the top view of the cylinder. The arrows show the direction of movement of the fabric.

There is a big difference between Figure 5.12 and Figure 5.13. While in Figure 5.12 is difficult to see even minor deformation, in Figure 5.13 the fabric is constantly deforming. Photographs 2 and 3 present concave effect and identation, while in photograph 4(a) there is an obvious tuck across the length of the fabric. This tuck becomes more and more obvious and in photograph 6 the lateral contraction of the strip is so intense that is close to forming a string. The slippage started where the horizontal part of the graph starts, at around 80 mm. At the last part of the plateau after the 120 mm, the shape of the fabric gradually started changing and the strip converted to a string.

Below I present all the tensometer graphs of fabric DC06 over cylinder Gel-8250.

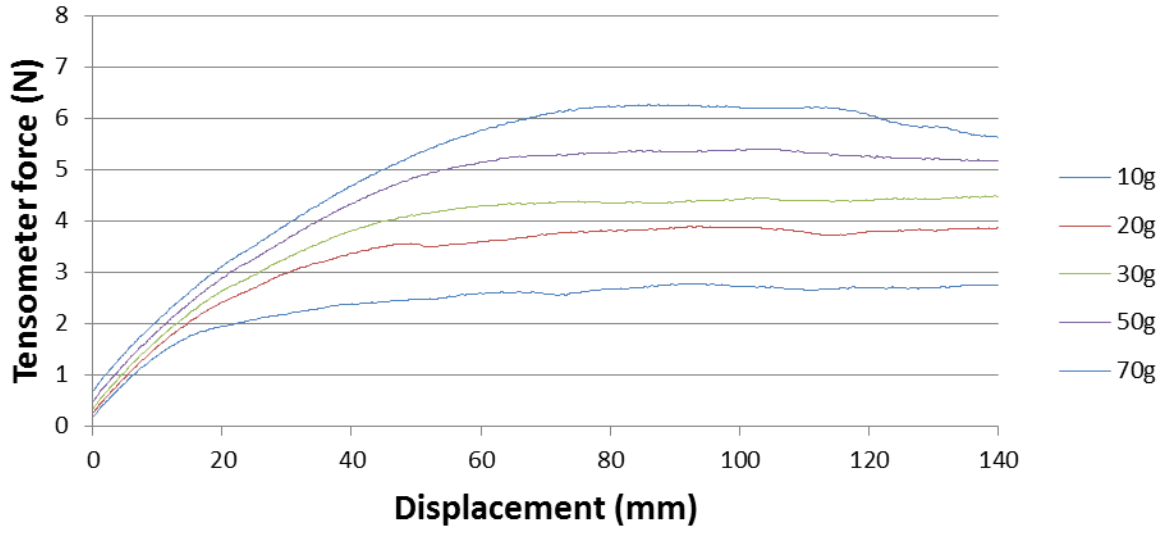

Figure 5.14: Tensometer graphs of fabric DC06 over cylinder Gel-8250

As I show in Figure 5.14 for the first four curves the plateau seems stable, while the tensometer force has the same value as the value of static friction. Curves for 10g and 20g are quite similar appearing at two points of plateau a tensometer force low. The curve for 70g has lower forces after the point corresponding to 115mm, dropping from 6.2N to 5.7N. I calculated the values from which I derive the coefficient of dynamic friction for each dead weight mass using the horizontal part of each graph which follows the steep part of the graph that corresponds to the deformation of the cylinder.

From the tensometer graphs of Figure 5.14 I derive the graph of pulling force against dead weight which I present in Figure 5.15.

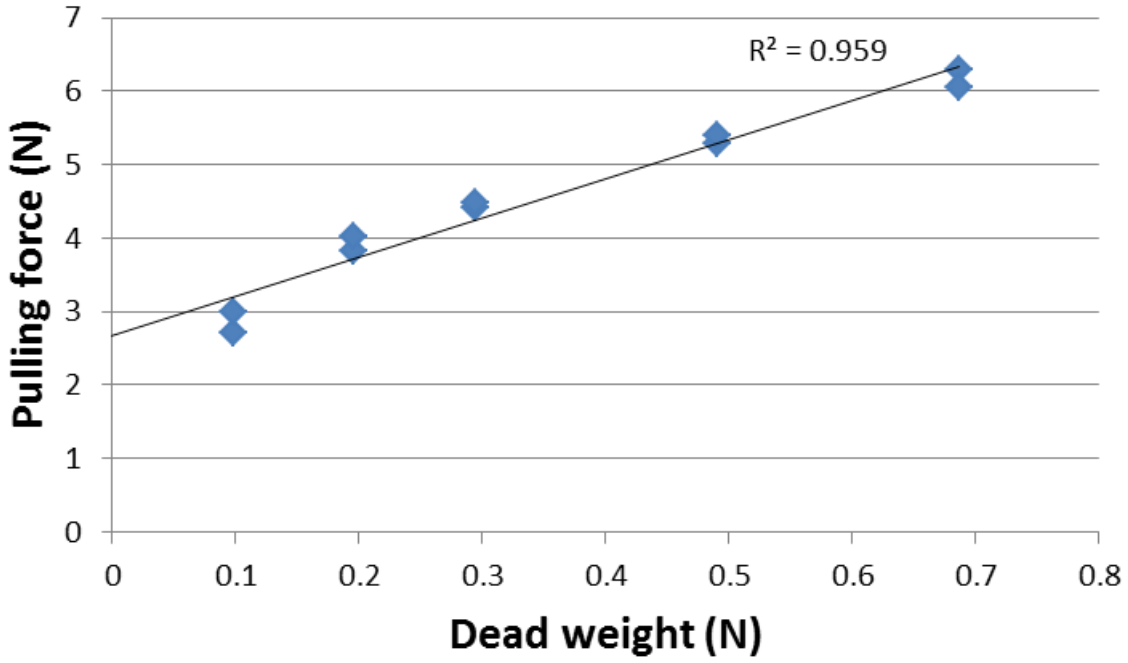

Figure 5.15: Graph of pulling force against dead weight of fabric DC06 on cylinder made of Gel-8250

The linearity of Figure 5.15 is obvious and once again proves the validity of the model. On the other hand there is a big intercept which will be analysed in the discussion part. Interestingly, the points of the graph which correspond to the dead weight mass of 10g do not coincide in the same linear line that characterises the rest of the points. If I take into account these points the first part of the line is a curve converting to a line to the last four points of the graph.

5.3.3 Tensometer graphs of fabrics SF14, SF17 and SF18 on cylinder Gel-8250

Even though I chose to present in more detail the results of SF03 and DC06, the rest of the five fabrics appeared results which vary to each other, a fact which proves different materials appear different results.

In this section I quote the tensometer graphs which correspond to the rest of the fabrics.

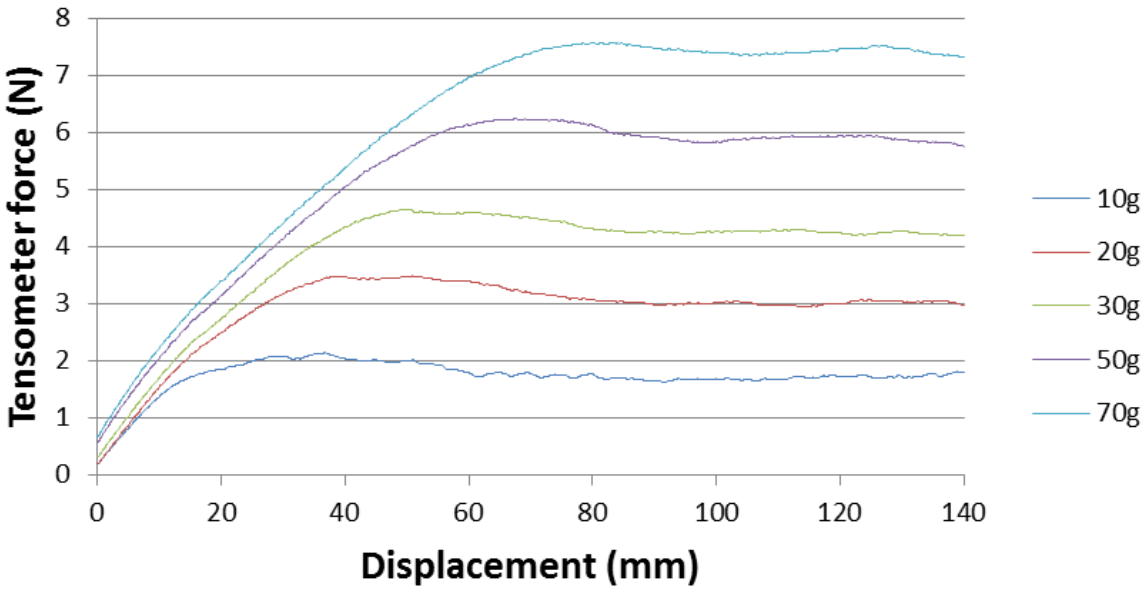

Figure 5.16: Tensometer graphs of fabric SF14 over cylinder Gel-8250

The graphs of Figure 5.16 are very similar to each other. Characteristic is the length of displacement required to reach the plateau for each dead weight mass, with the longest displacement, the one for the 70g.

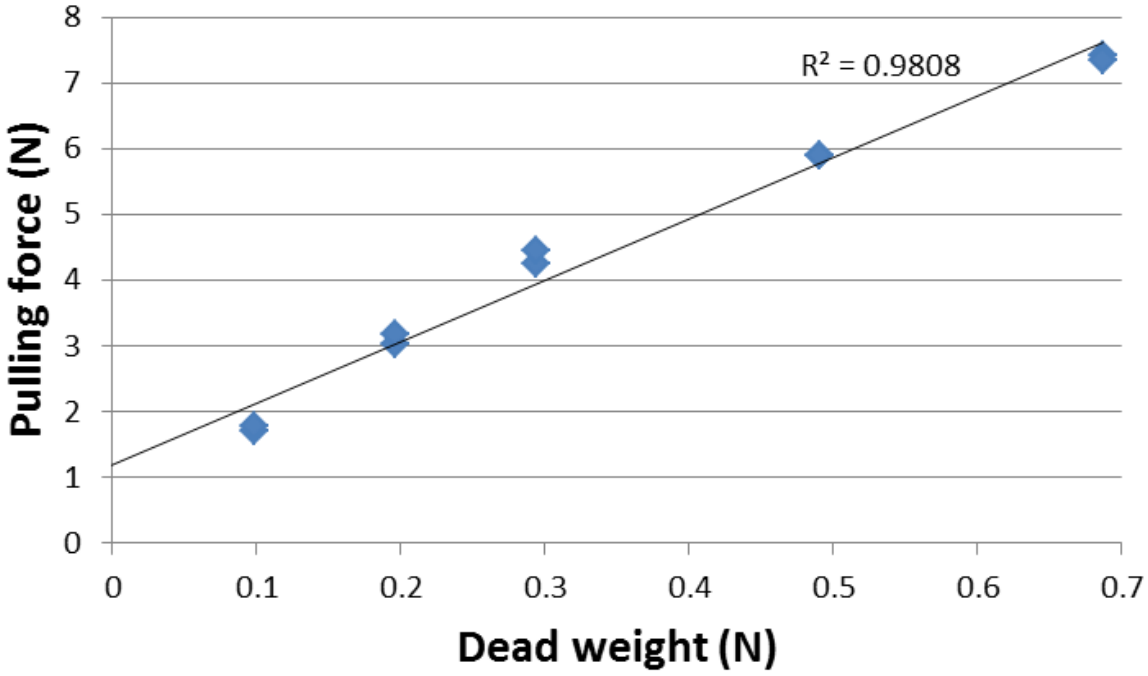

Figure 5.17: Graph of pulling force against dead weight for fabric SF14 on cylinder Gel-8250

As I show in Figure 5.17, even though the correlation coefficient R^2 is impressively high, the three points that correspond to the dead weight loads of 30g, 50g and 70g align to a straight line that curves down to the points that correspond to the dead weight loads of 10g and 20g.

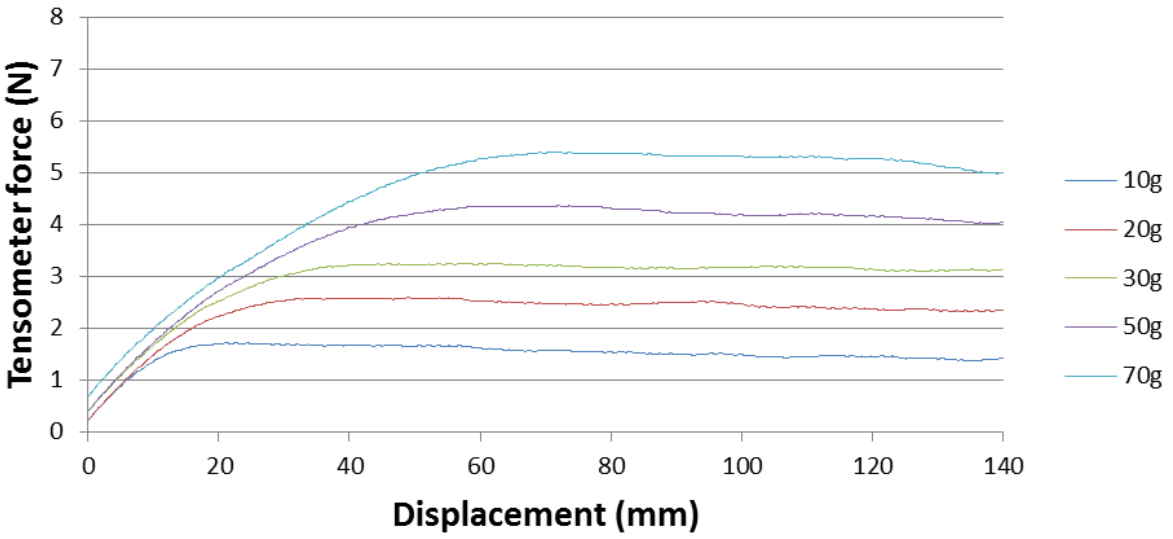

Figure 5.18: Tensometer graphs of fabric SF17 over cylinder Gel-8250

As I can see from Figure 5.18 the deformation for the 70g graph reached 60mm at slip, while for the 10g it was 15mm. Also the values for the peak of each graph are similar to the values of the plateau.

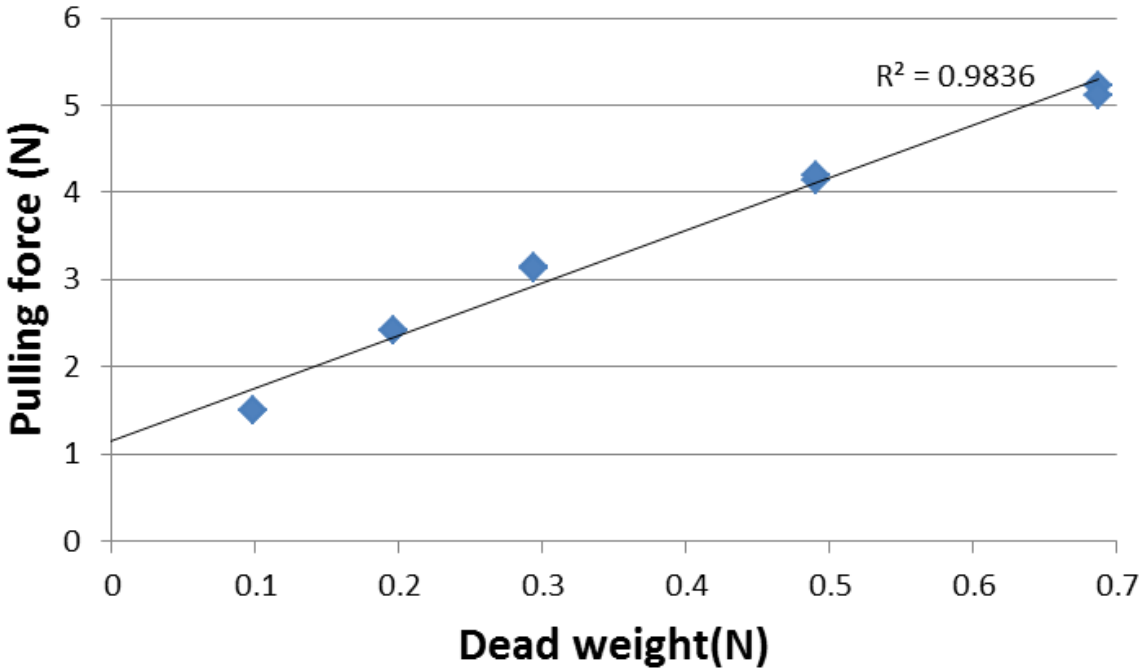

Figure 5.19: Graph of pulling force against dead weight for fabric SF17 on cylinder Gel-8250

On Figure 5.19 apply the same comments that I mentioned for Figure 5.17.

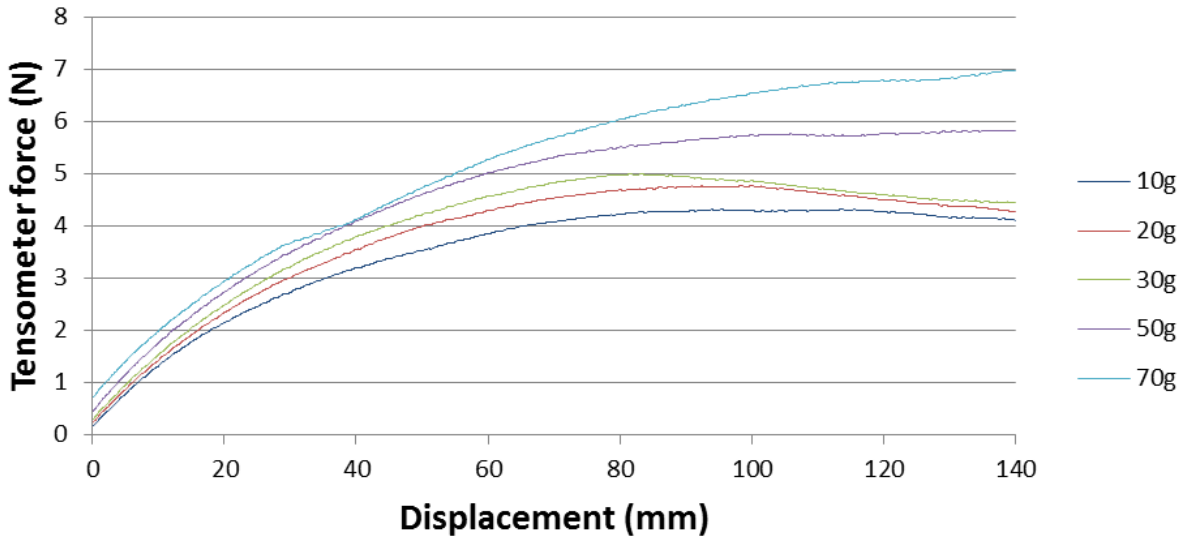

Figure 5.20: Tensometer graphs of fabric SF18 over cylinder Gel-8250

In the case of Figure 5.20 is difficult to trace the plateau, since the graphs have a shape of a curve which faintly reaches a plateau and never reach a peak. The deformation for the 10g curve reaches the 80mm while for the 70g curve seems to reach the 120mm.

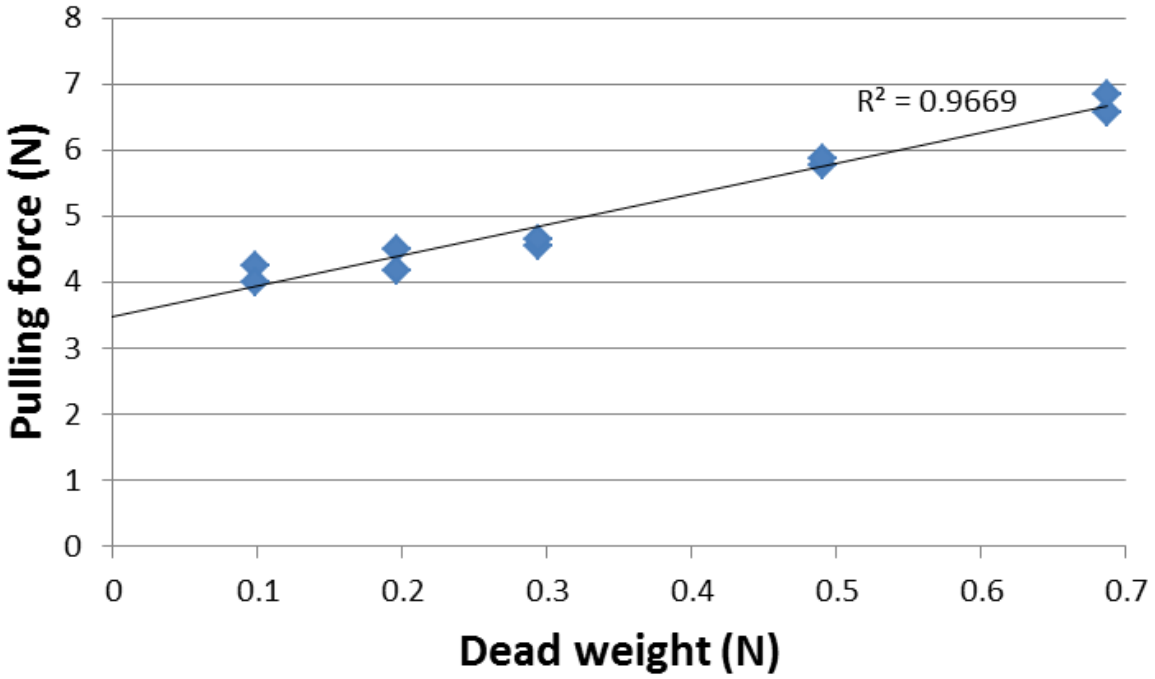

Figure 5.21: Graph of pulling force against dead weight for fabric SF18 on cylinder Gel-8250

Figure 5.21 appears a regression line which is straight within the experimental error

Below, I continue with the experimental results on cylinder Gel-8170.

5.3.4 Experimental results of fabric SF03 on Gel-8170

Until now I presented the results of the experiments on Gel-8250. In this Section I push the validation one step further going to the even more compliant arm of Gel-8170. Now I will have the opportunity to study the model's behaviour in even more extreme conditions. I start with fabric SF03.

I continue the presentation of my experimental results with the presentation of the tensometer graph of 10g of fabric SF03

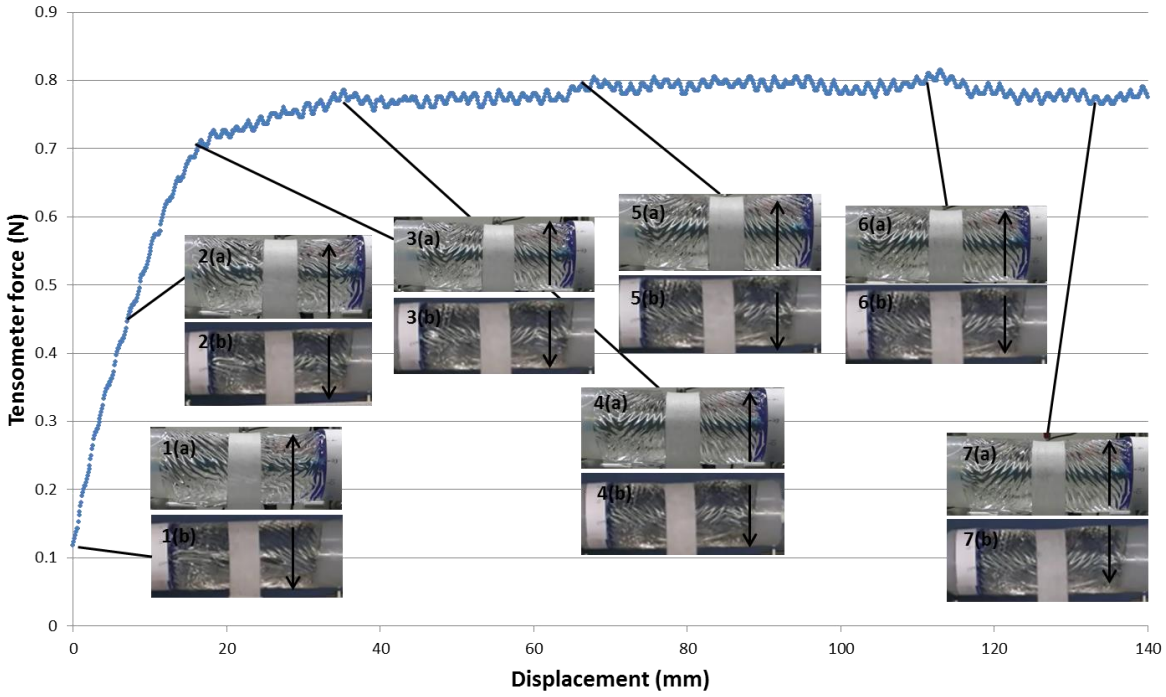

Figure 5.22: Tensometer graph of friction of 10g dead weight mass experiment of fabric SF03 on cylinder made of Gel-8170.

At the beginning I can see that the strip of fabric is in full contact with the cylinder (photograph 1) with zero deformation. This does not seem to change until photograph 6 where I start observing a very shallow concave deformation. This deformation becomes even deeper in photograph 7, while does not seem to be so deep in photograph 6.

About the experiments with the rest of the dead weight masses I could not observe any sliding in the 70g tensometer graph, so I derived the μ using the results from the 10g, 20g, 30g and 50g tensometer. Bellow, I will show the 50g and the 70g tensometer graph, trying to explain the differences between these two.

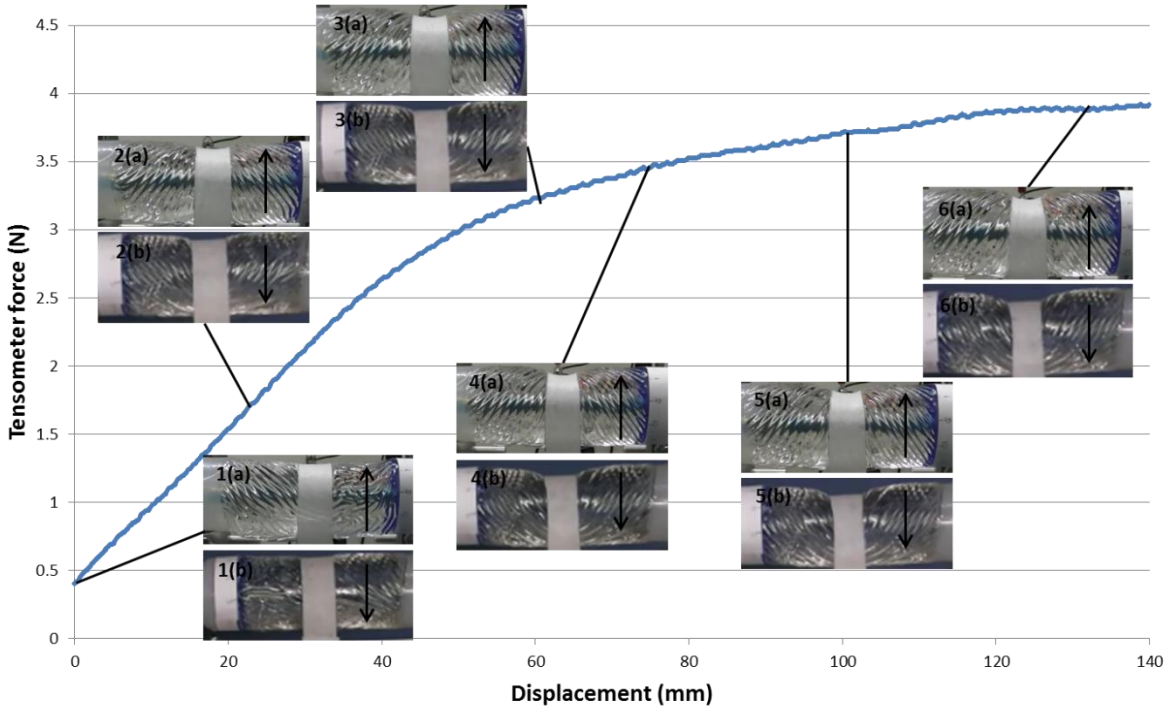

Figure 5.23: Tensometer graph of friction of 50g dead weight mass experiment of fabric SF03 on cylinder made of Gel-8170.

In Figure 5.23 the fabric at the beginning succeeds full contact with the cylinder and the deformation progressively increases as the tensometer force increases. Finally, I observe the deepest deformation of photograph 6 which is of concave shape from the front view and just indentation from the top view.

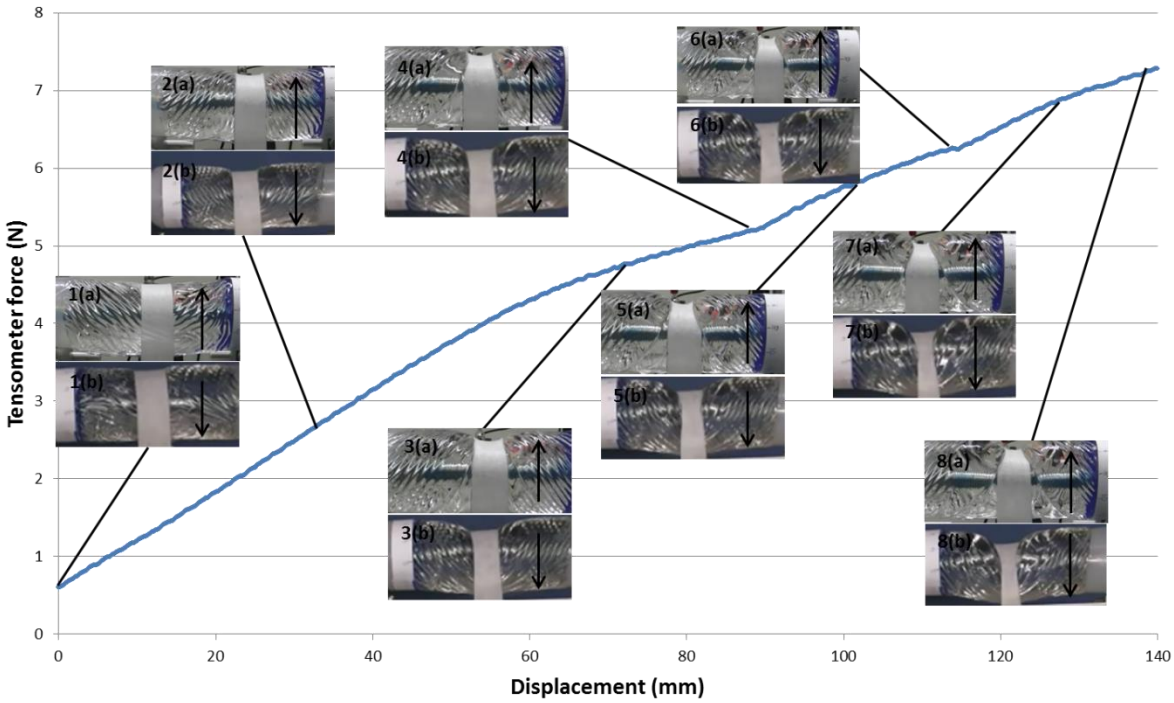

Figure 5.24: Tensometer graph of friction of 70g dead weight mass experiment of fabric SF03 on cylinder made of Gel-8170.

In Figure 5.24 from photograph 1 to photograph 6 I see a continuous deformation. I need to say that from photograph 5 onwards, the fabric seems to obtain its current state without showing any further deformation, which means the dominant deformation mode is the rucking of the cylinder surface.

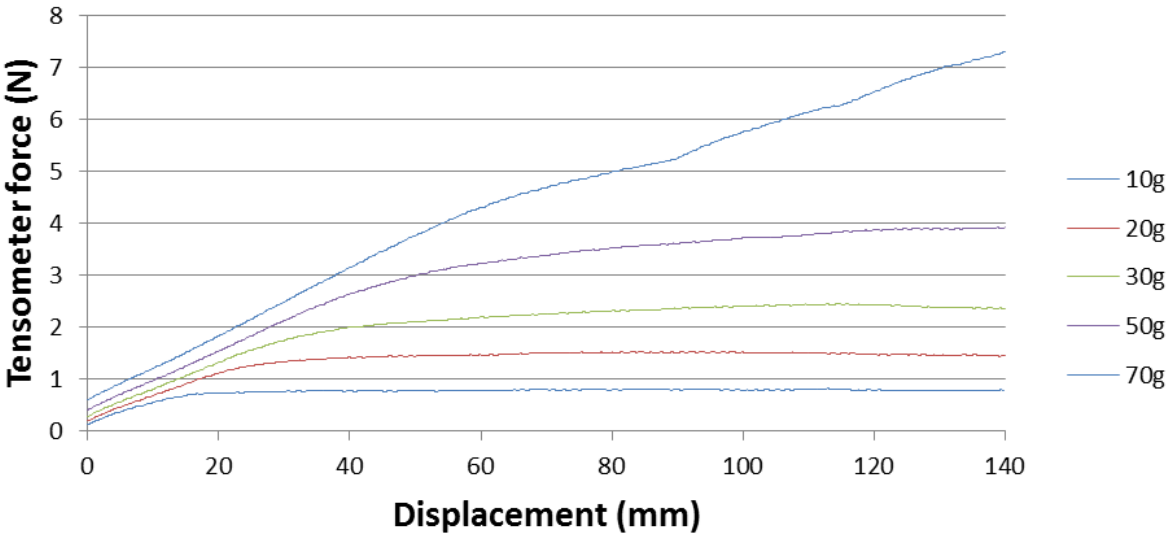

Figure 5.25: Tensometer graphs of fabric SF03 over cylinder Gel-8170

In Figure 5.25 I present the graphs for every dead weight. The coefficient of friction for this experiment was extracted from the graphs which exhibit a plateau. That means that I take into consideration all the graphs except for the highest one which correspond to 70g dead weight, as I have already said.

Since I conduct my experiments on cylindrical shapes, the formula characterising the coefficient of friction is Equation 4.1. From this equation you can see that the tensometer / pulling force is directly proportional to the dead weight, so the graph of pulling force versus dead weight for every experiment should be a straight line.

In order to generate the coefficient of friction in every experiment I plot the pulling force against dead weight, which in every case is a straight line that should go through the origin. Figure 5.26 presents an example of this plot.

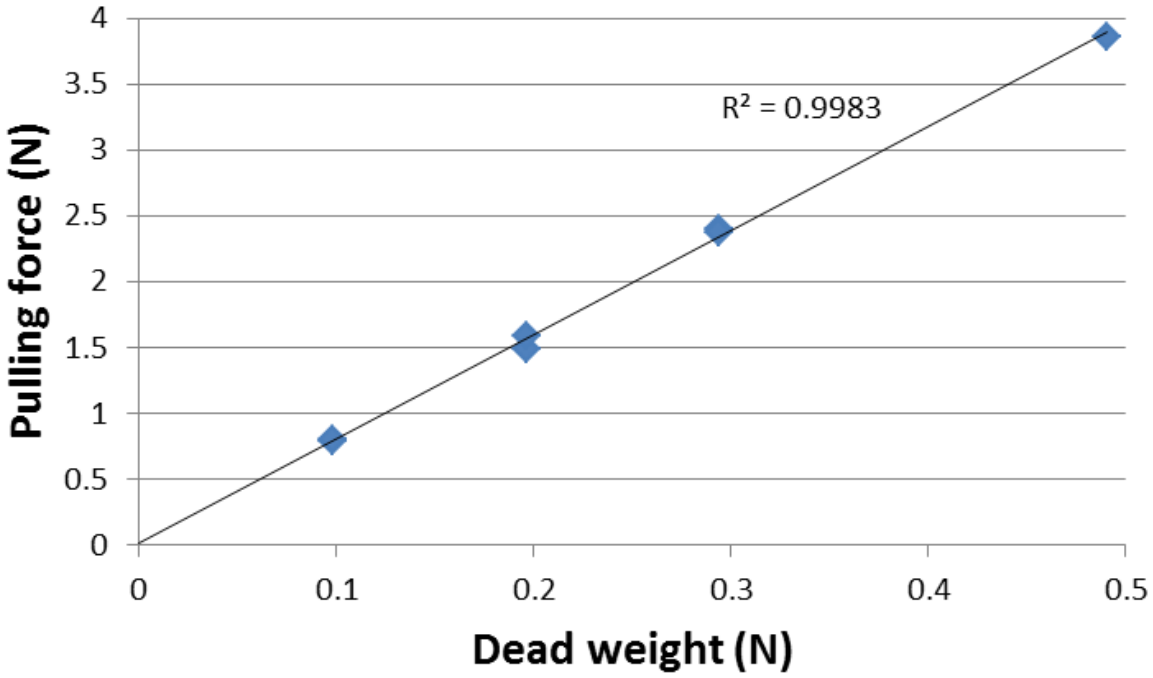

Figure 5.26: Graph of pulling force against weight of fabric SF03 on cylinder arm of Gel-8170

From Figure 5.26 I can see that this line is straight, with a remarkably high correlation coefficient.

Another fabric that appears very interesting frictional and deformative properties is DC06, which I am going to analyse in the following section.

5.3.5 Experiments of DC06 on cylinder Gel-8170

Interesting is to see how fabric DC06 behaved on Gel-8170. Apart from cylinder deformation, the fabric deformed so much that it turned into a string at the dead weight mass of 70g.

In this section I will present the graphs of 10g and 70g of DC06 over cylinder Gel-8170.

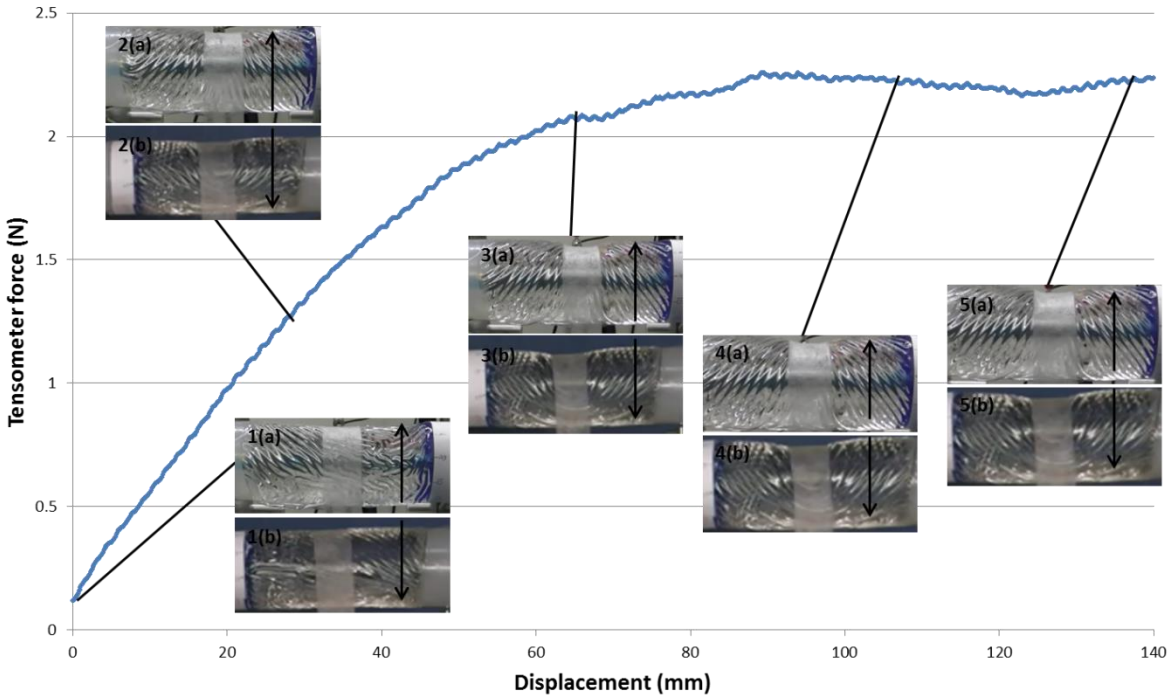

Figure 5.27: Tensometer graph of 10g dead weight mass experiment of fabric DC06 on cylinder made of Gel-8170.

As I show in Figure 5.27, initially there was no deformation as the tensometer crosshead had not started moving yet. In photograph 2 some identation is appearing in the top view photograph, while in photograph 3 indentation in the top view photograph is even more intense and a concave affect has started appearing in the front view photograph. Finally photographs 4 and 5 seem to be quite similar, presenting the most intense indentation and concave effect.

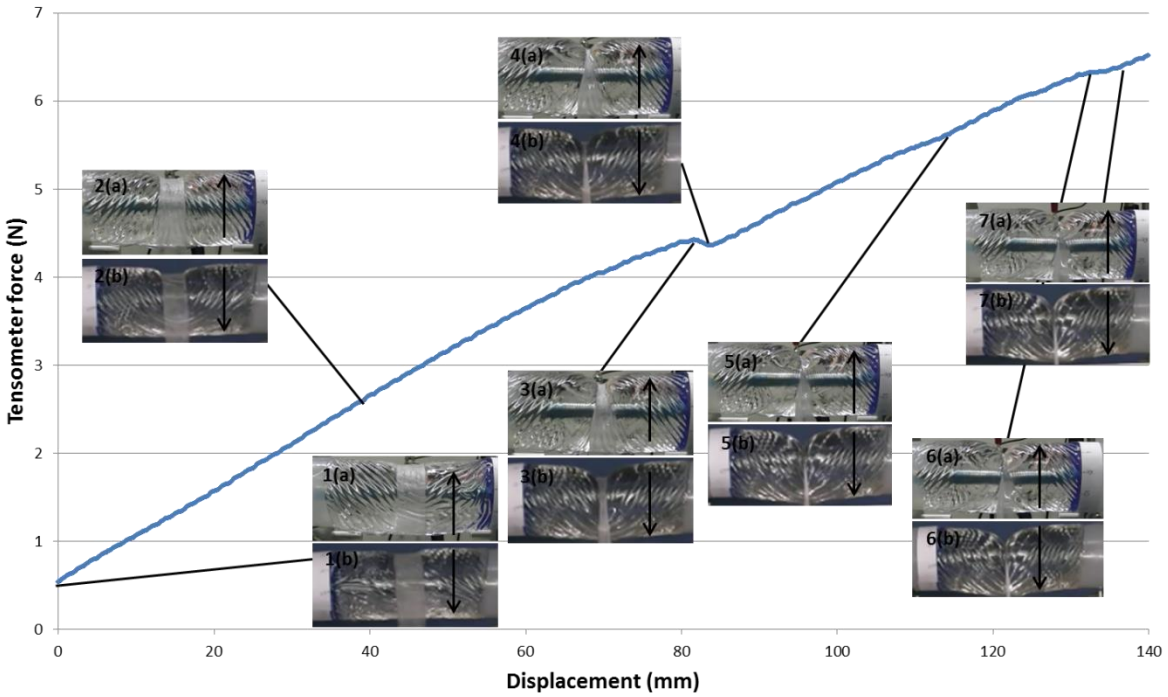

Figure 5.28: Tensometer graph of 70g dead weight mass experiment of fabric DC06 on cylinder made of Gel-8170.

In Figure 5.28 the successive photographs I quote, show a continuous deformation of the arm and the fabric, without succeeding sliding, as the form of the graph indicates. As I show, between photographs 5 and 6 the strip is becoming a cord. In the final photographs 6 and 7 the strip of fabric has reached the maximum lateral deformation since it is transforming to a cord.

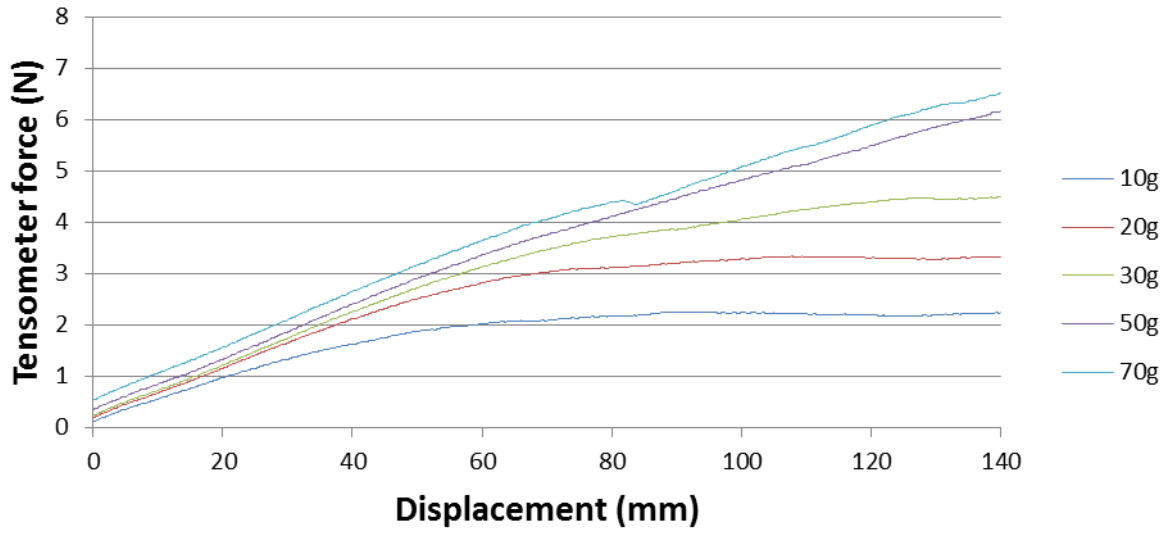

Figure 5.29: Tensometer graph of fabric DC06 over cylinder Gel-8170.

From Figure 5.29 it can be seen that experiments with dead weight masses of 50g and 70g never reached a plateau, so I calculated the coefficient of friction from the three first dead mass weights of 10g, 20g and 30g.

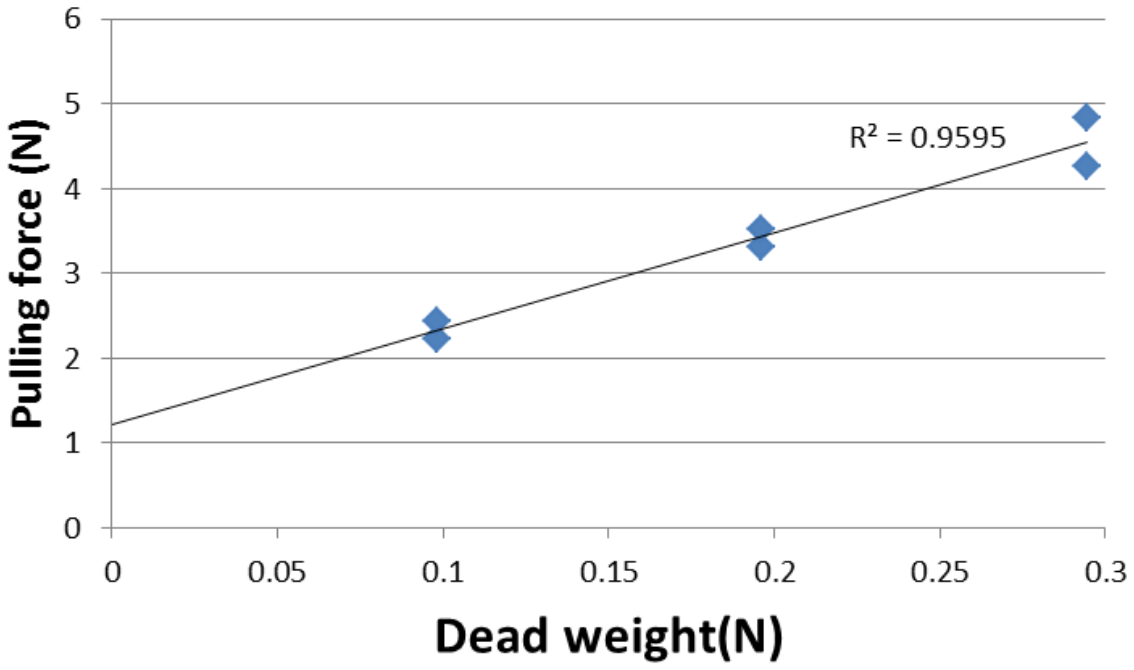

Figure 5.30: Graph of pulling force against dead weight for fabric DC06 on cylinder Gel-8170

The three points of Figure 5.30 produce a coefficient of friction, but not so credible as the five points of the most of the other experiments for the other fabrics. Notable is the fact that the two data points that correspond to the dead weight of 30g do not coincide.

As the graphs in Figure 5.11 and Figure 5.26 show the compliance of the arm does not affect the derivation of the coefficient of friction; as long I can produce sliding, I can extract the coefficient of friction of each surface.

5.3.6 Tensometer graphs of SF14, SF17 and SF18 on cylinder Gel-8170

In the sections quoting results on Gel-8250 I choose to analyse just two of the fabrics and just quote the rest of the results. Similarly, about Gel-8170 I choose to analyse the results about SF03 and DC06 and simply quote the rest of the results.

In this section I present the tensometer graphs of the fabrics I do not analyse thoroughly.

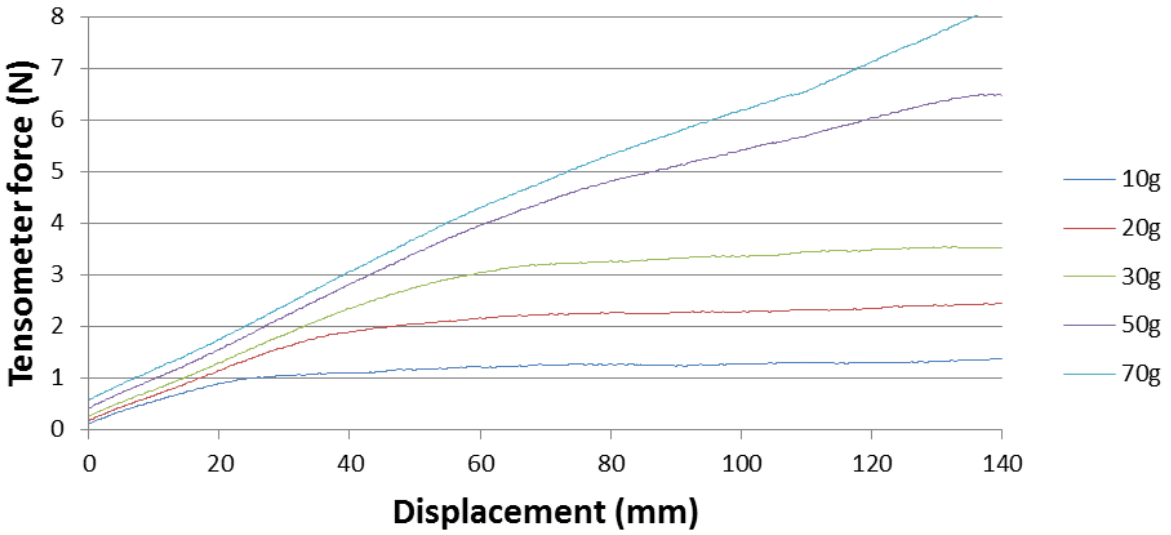

Figure 5.31: Tensometer graph of fabric SF14 over cylinder Gel-8170

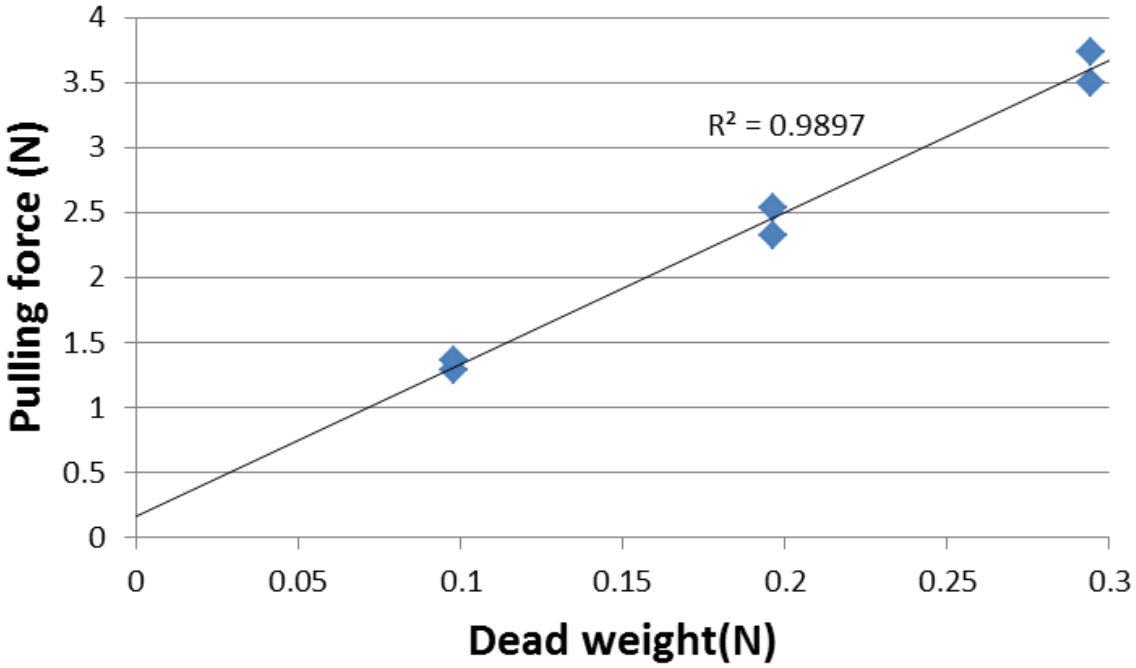

Figure 5.32: Graph of pulling force against dead weight for fabric SF14 on cylinder Gel-8170

In Figure 5.32, as the dead weight increases the dinstance between the data points of the same dead weight tend to increase.

As I present in Figure 5.31, the graphs corresponding to the dead weight masses of 10g, 20g and 30g present a plateau which shows higher values than the value of static friction which is at around 25mm for the 10g graph and around 65mm for the 65mm. The graphs of 50g and 70g do not show any sliding at all, just deformation.

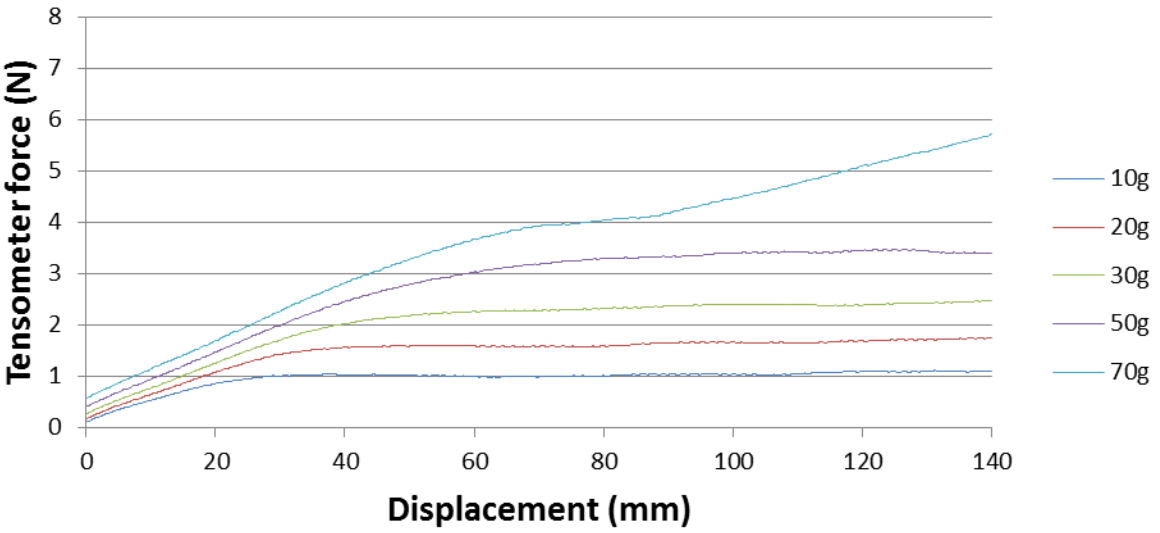

Figure 5.33: Tensometer graph of fabric SF17 over cylinder Gel-8170

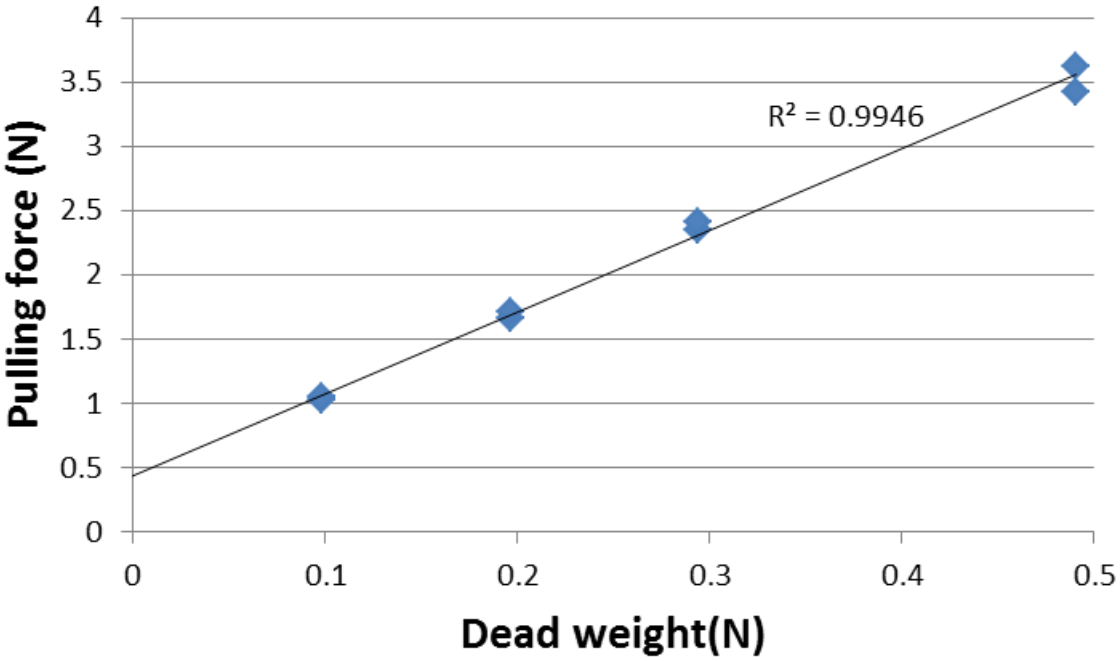

Figure 5.34: Graph of pulling force against dead weight for fabric SF17 on cylinder Gel-8170

In Figure 5.34 I show that I derive the coefficient of friction from the first four data points, the last of which, again, has two distinct data points.

For the first four graphs of Figure 5.33 the plateau has the same value for the tensometer force. The graph of 70g seems to have a constant deformation. Between 70mm and 90mm seems to stabilise, but after the 90mm the cylinder keeps deforming. For the 50g graph, at around 70mm the deformation stops and sliding starts, while at the 10g this starts at around 30mm.

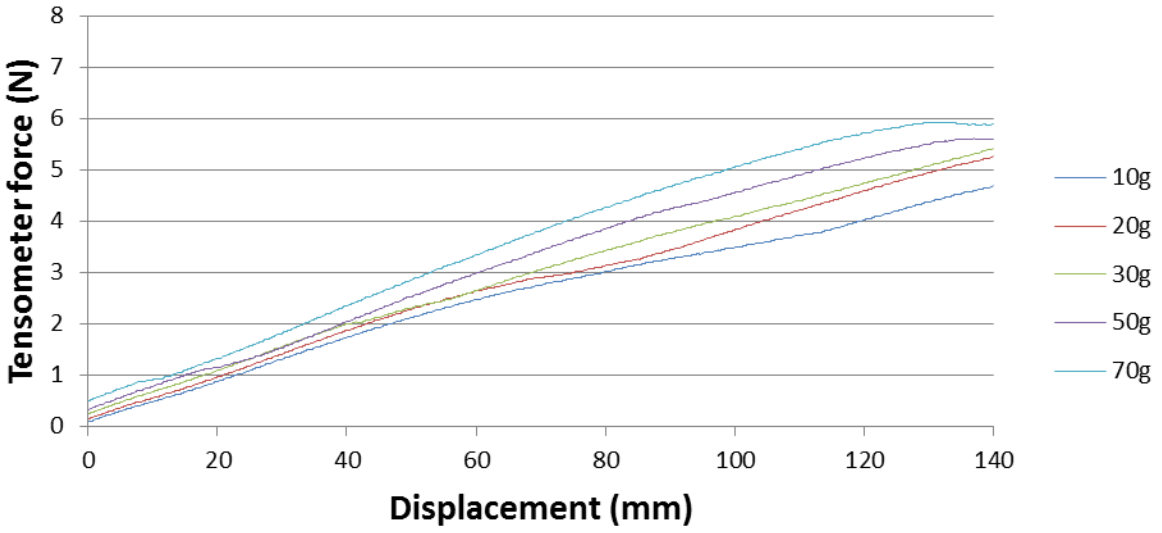

Figure 5.35: Tensometer graph of fabric SF18 over cylinder Gel-8170

In Figure 5.35 the only described phenomenon is deformation. Since there is not any plateau, I cannot derive the coefficient of friction.

5.3.7 Cylindrical rigid arms

In order to compare three different degrees of compliance I attach the same silicone membrane I used on the compliant arms on a rigid cylinder. Since there is not any deformation I did not use the cameras. Below I quote the tensometer graphs of all the fabrics of the membranes 1 and 3 which had different orientations. I also show the linear plots of fabric SF03 which presents the stick – slip phenomenon.

5.3.7.1 Fabric SF03 on cylindrical arms

Below I will present the results of fabric SF03 on membranes 1 and 3. Notice the impressive stick – slip phenomenon.

5.3.7.1.1 Fabric SF03 on the 1st membrane

Below I present the graphs for fabric SF03.

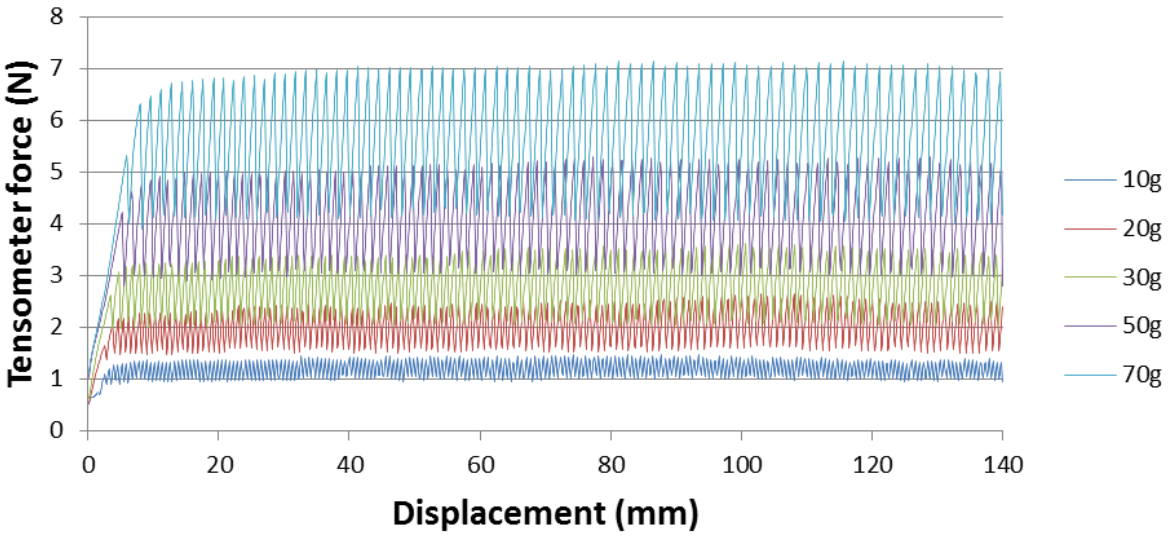

Figure 5.36: Tensometer graphs of fabric SF03 over rigid cylinder with the 1st membrane

As it is easy to see from Figure 5.36 there is a very intense stick and slip phenomenon. I cannot distinguish static friction from dynamic friction since the stick – slip phenomenon is so obvious, but I can say the plateau which is characterised by the mean of the stick – slip is pretty stable. From the high and the low values I receive two different linear plots which I present in the following graph.

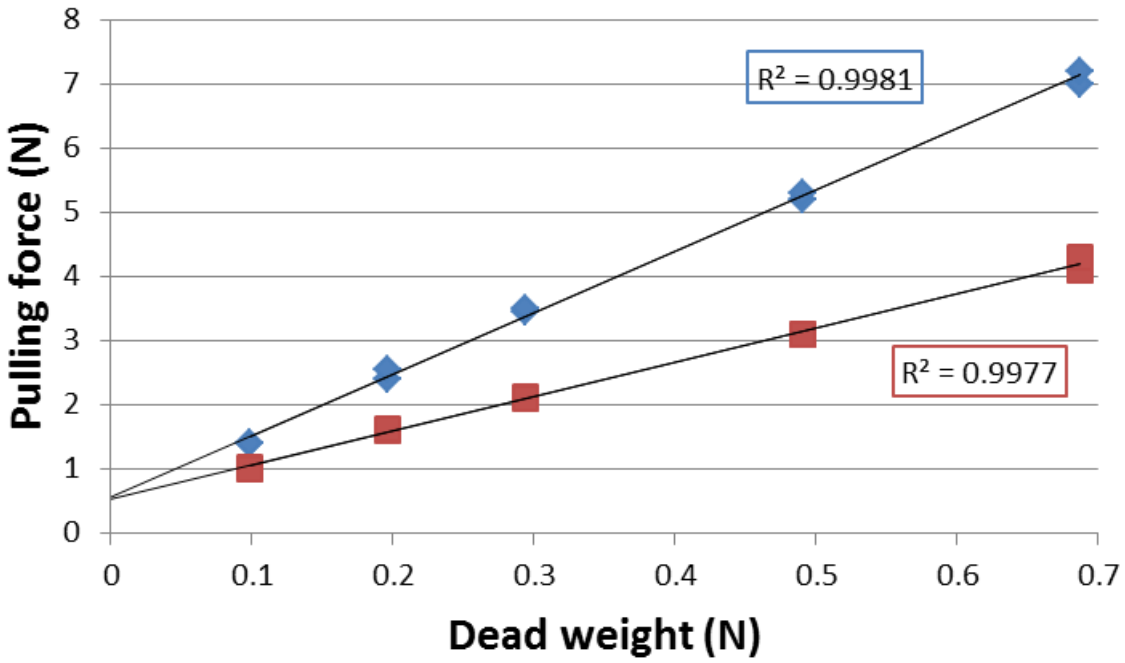

Figure 5.37: Linear plots of fabric SF03 over a rigid cylinder using the 1st membrane. The values of the blue points incur from the high values of the stick slip phenomenon and of the red points of the low values.

In Figure 5.37 I can see the scissors shape of the linear plot which is characteristic of the stick slip phenomenon, but in the case of the compliant arms is not slightly curved like the ones I saw in the volar forearms (Figure 4.44,Figure 4.46 and Figure 4.50). The values which give a coefficient of

friction are the ones which correspond to the low peak of the graphs, since it is probably closer to the plateau values.

5.3.7.1.2 Fabric SF03 on the 3rd membrane

Below I present the tensometer graphs for the 3rd membrane

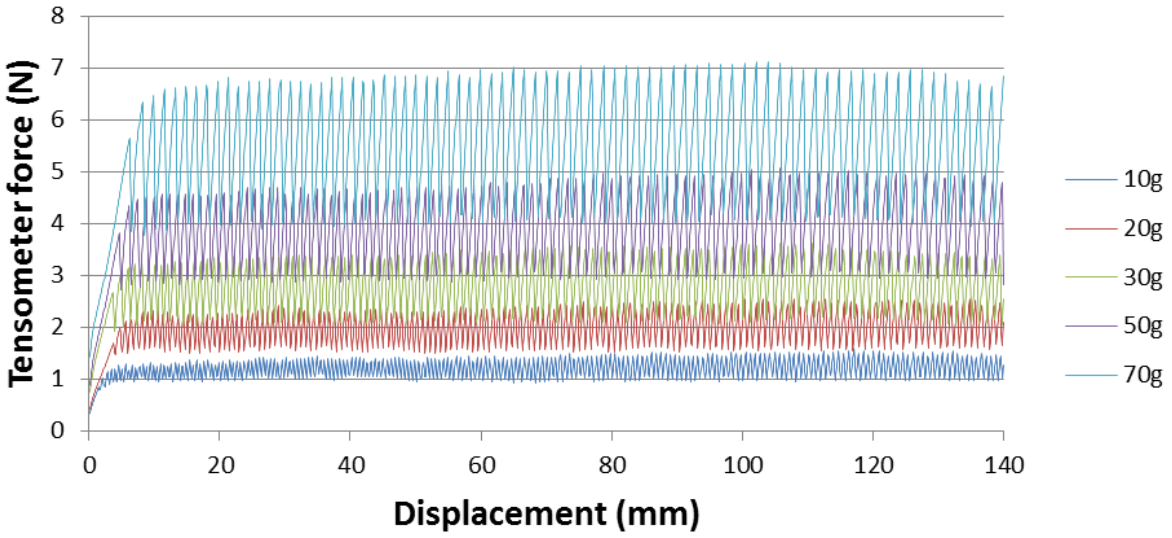

Figure 5.38: Tensometer graphs of fabric SF03 over rigid cylinder with the 3rd membrane

The observed stick slip phenomenon is very similar to the presented of Figure 5.36. Exactly this fact means that the linear plot present in Figure 5.39 will be very similar to the linear plot of Figure 5.37.

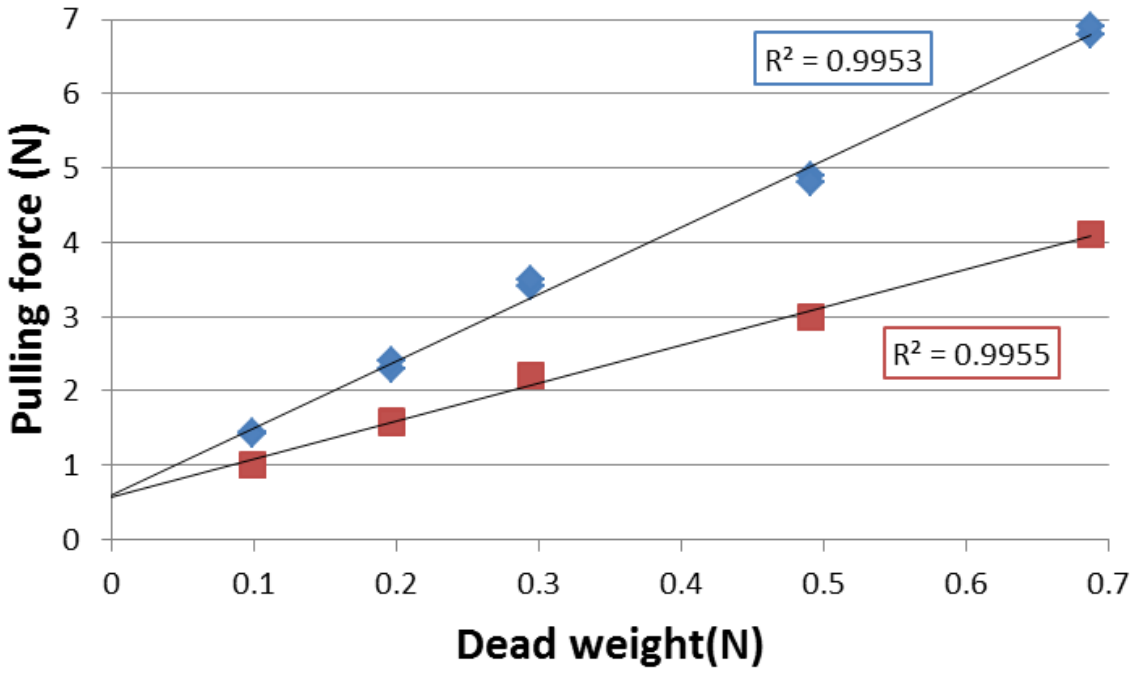

Figure 5.39: Linear graphs corresponding to the tensometer graphs of Figure 5.38

Again in Figure 5.39 I see the scissors phenomenon that I see in every stick – slip phenomenon. Impressive is the fact that always the intercept seems to appear very similar values for the high and low values of the stick slip.

5.3.7.2 Tensometer graphs on the 1st membrane

Below I present the tensometer graphs of the rest of the fabrics on the 1st membrane. Each set of tensometer graphs produces a linear plot similar to the linear plot already presented.

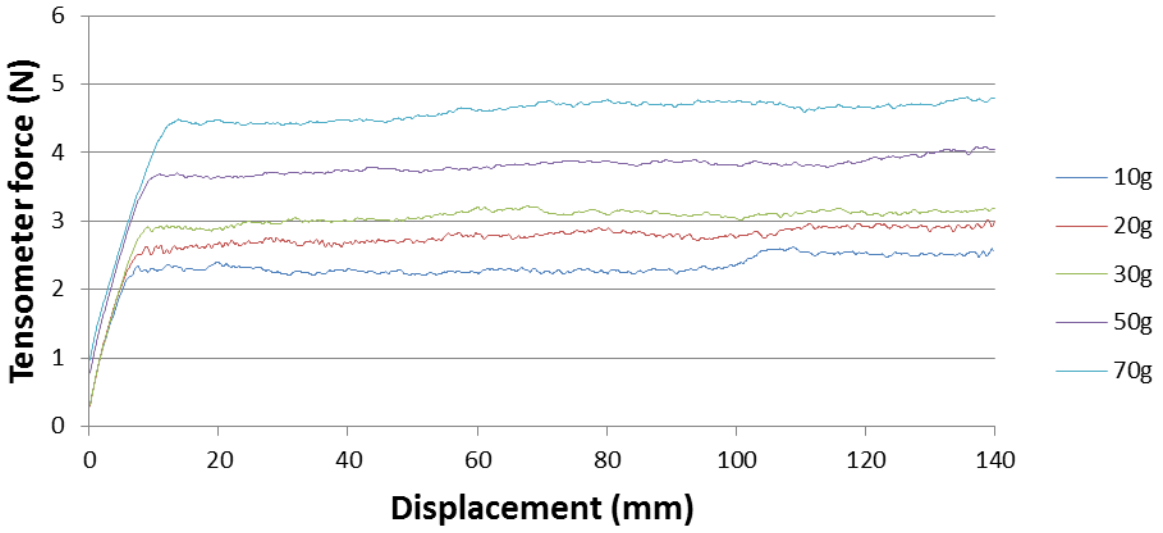

Figure 5.40: Tensometer graphs of fabric DC06 over rigid cylinder with the 1st membrane

In Figure 5.40 I can characterise as maximum static friction the point where the plateau starts. On the other hand, the plateau does not have a stable value but the tensometer force has a tendency to increase with displacement.

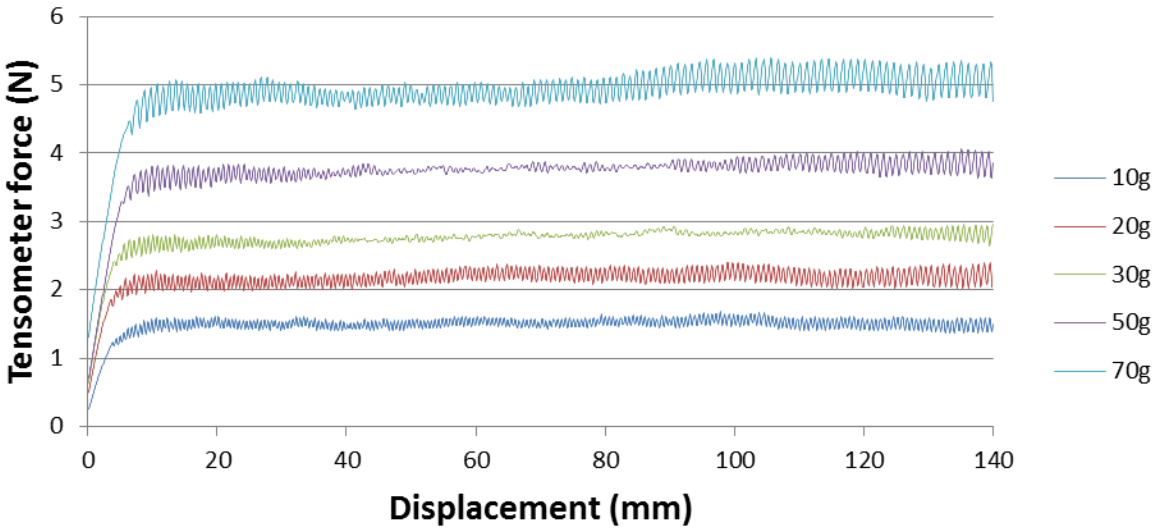

Figure 5.41: Tensometer graphs of fabric SF14 over rigid cylinder with the 1st membrane

Fabric SF14 shows a minor stick slip phenomenon. Impressive in the fact that for the curves of 30g and 50g the middle of the graph does not show any stick – slip, but the beginning and the end of the plateau do. The graphs for 10g, 20g and 70g show a full stick – slip phenomenon. In case I can define as static friction the point where the plateau starts, static friction has approximately the same value as the dynamic friction. The 70g graph seems to follow a faint uphill trend after the 95mm.

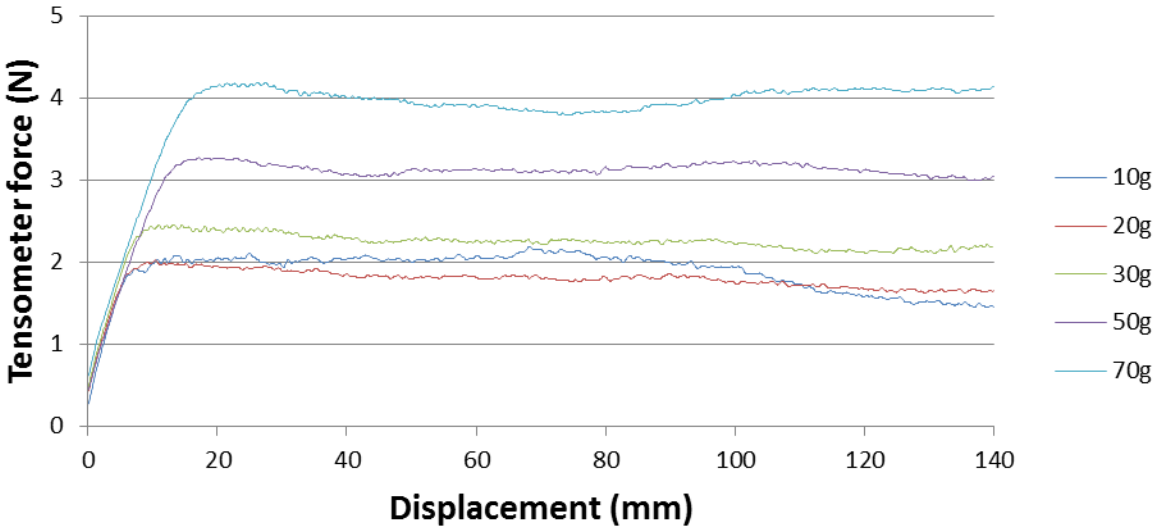

Figure 5.42: Tensometer graphs of fabric SF17 over rigid cylinder with the 1st membrane

The graphs presented in Figure 5.42 are similar to those presented in most other experiments. I have to note though, the graphs for the 10g and 20g are very close at the beginning of the plateau, at the middle is approaching the level of the 30g graph, while towards the end the curve of the 20g goes below the curve for 10g. The plateau of 70g appears a wavy shape, having the lowest point at around 80mm. Static friction presents a value at around the level of the mean.

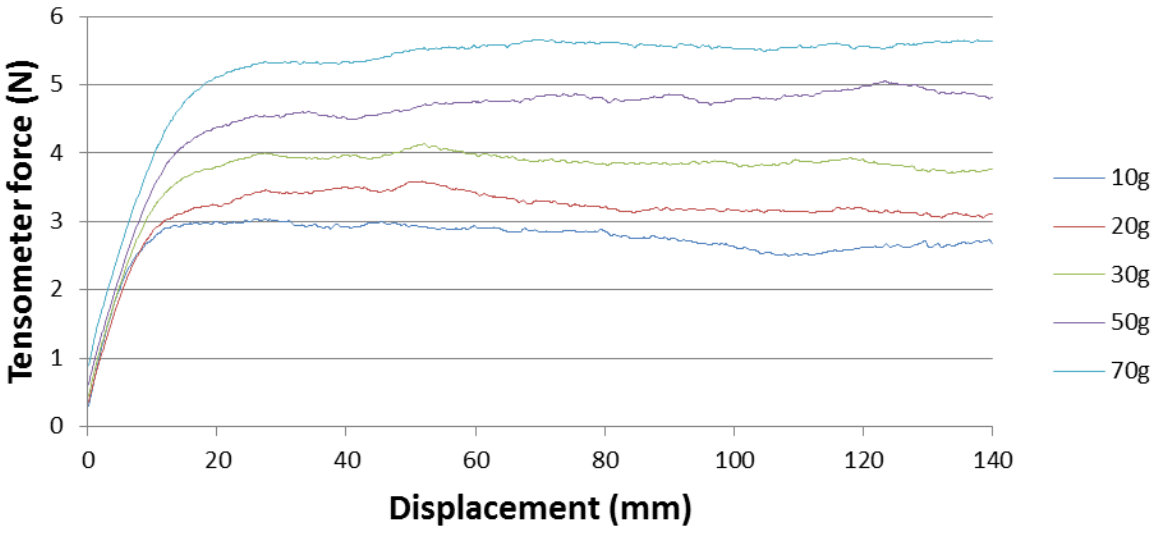

Figure 5.43: Tensometer graphs of fabric SF18 over rigid cylinder with the 1st membrane

In Figure 5.43 static friction seems to have a different value in every graph in relation to the dynamic friction. In the graphs of 50g and 70g is has a lower value than the mean of dynamic friction, while at the 20g and 30g there is a peak at around 55mm. After this point the graphs follow downhill direction. At the 10g graph, after the 18mm when the static friction reaches its highest point the plateau is stable with a downhill tendency after the 50mm.

5.3.7.3 Tensometer graphs on the 3rd membrane

Below I quote all the graphs for the 3rd membrane

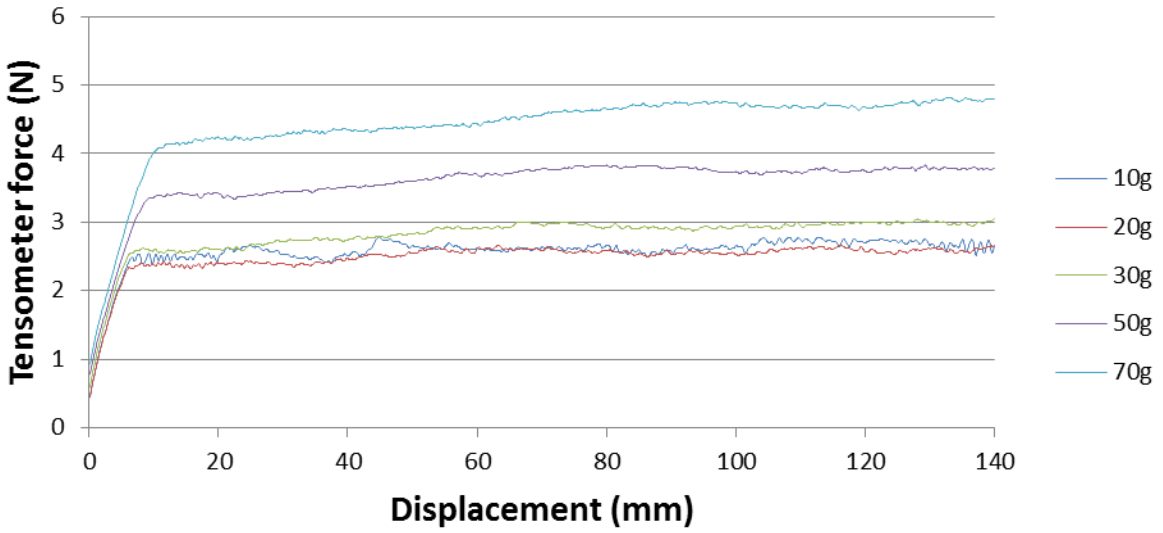

Figure 5.44: Tensometer graphs of fabric DC06 over rigid cylinder the 3rd membrane

As I can see from Figure 5.44 the plateau reaches its highest point at around 5mm to 10mm while it appears an uphill tendency. Notable is that the 10g graph shows a "jump" at around 105mm.

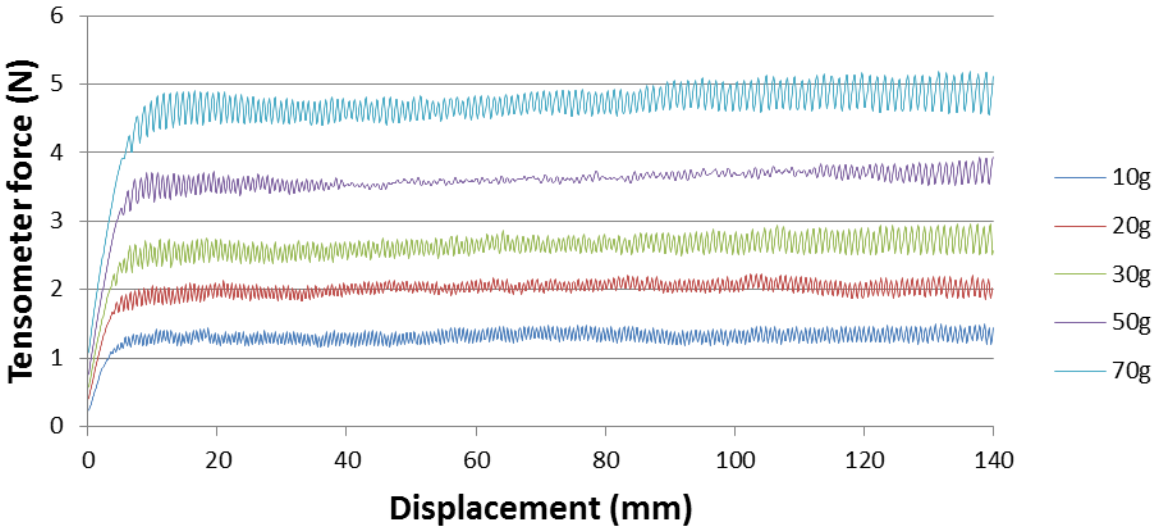

Figure 5.45: Tensometer graphs of fabric SF14 over rigid cylinder with the 3rd membrane

In Figure 5.45 there is a stick – slip phenomenon, as in Figure 5.41. The main difference though is that in this case just the graph of 50g appears stick slip just in the beginning and in the end of plateau and not in the middle, while in Figure 5.41 the graphs of 30g and 50g appear this behaviour. Static friction seems to be at the same level as the dynamic friction.

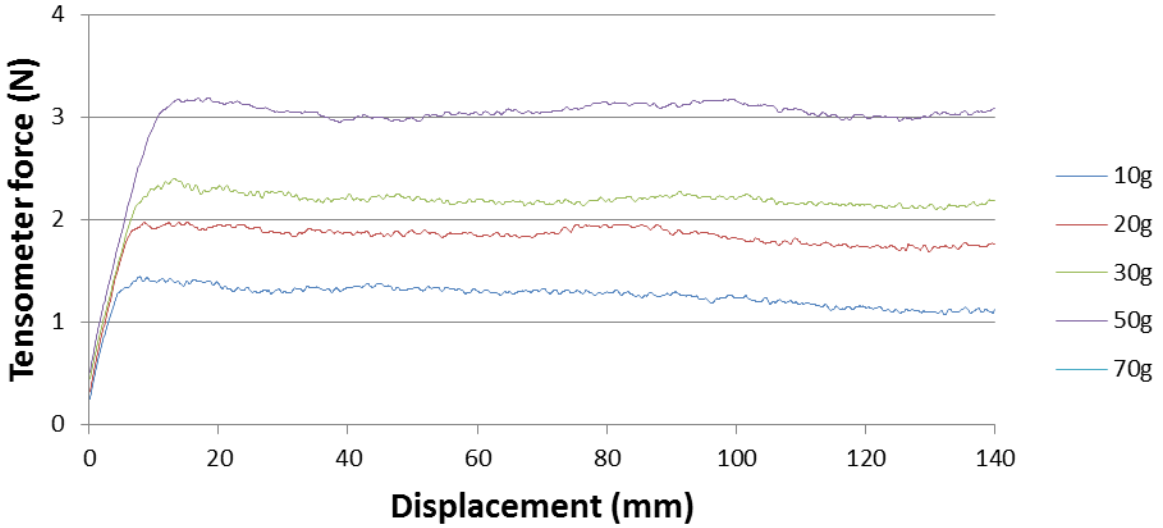

Figure 5.46: Tensometer graphs of fabric SF17 over rigid cylinder with the 3rd membrane

Figure 5.46 does not present the graph of 50g. This happens because the strip of fabric did not stand the strains and ruptured. So, I extracted the coefficient of friction from the four initial curves. Static

friction presents a value which is higher than the mean of the plateau, while the plateau does not show a stable value.

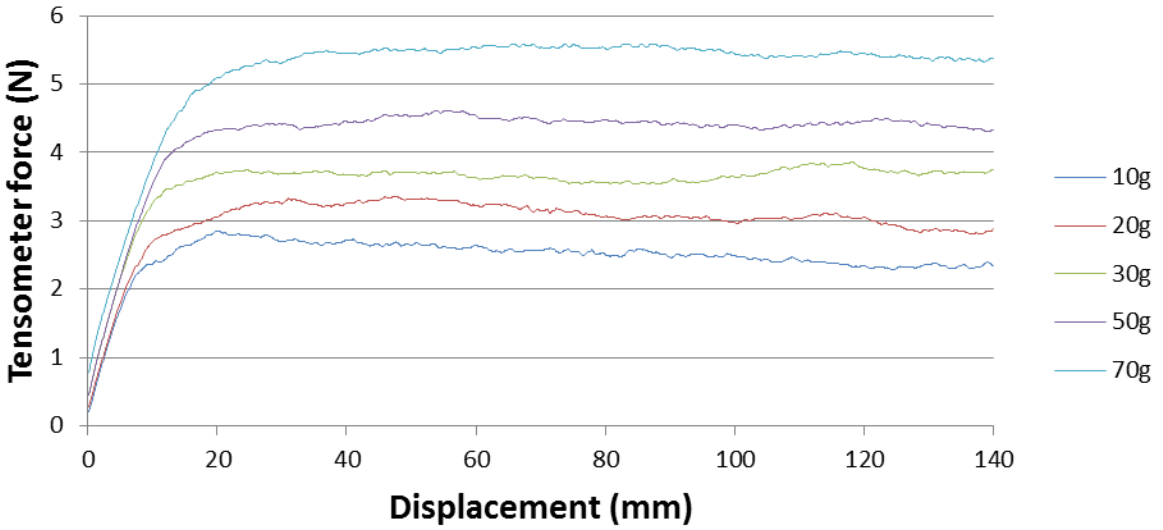

Figure 5.47: Tensometer graphs of fabric SF18 over rigid cylinder with the 3rd membrane

Static friction reaches its peak between 20mm and 30mm. For the graphs of 70g and 50g static friction has the same value as the dynamic. At the 30g graph dynamic friction has a peak at the 120mm, the 20g graph has a downhill direction after 60mm while the static friction of the 10g graph is higher than dynamic friction since plateau follows a downhill direction.

5.4 Discussion

As I can see from the presentation of the results, different arms produce different coefficient of friction, dependent on the substrate of the arm, even though all have the same skin. Also, the graph of pulling force against dead weight should be a straight line without intercept according to the model, but in most of the cases intercept does appear, so the causes of this need to be investigated.

5.4.1 Concentrated results

Table 5.2 summarises the coefficient of friction of the rigid membrane and of the two compliant arms.

Core		μ_d				
		DC06	SF03	SF14	SF17	SF18
Compliant	Gel-8250	1.06 (0.05)	1.24 (0.03)	1.41 (0.04)	1.13 (0.04)	0.97 (0.05)
	Gel-8170	1.51 (0.07)	1.30 (0.03)	1.53 (0.05)	1.15 (0.03)	-
Rigid	1st membrane	0.851 (0.015)	1.289 (0.017)	1.117 (0.016)	0.89 (0.06)	1.01 (0.02)
	2nd membane	0.89 (0.03)	1.25 (0.02)	1.123 (0.017)	0.89 (0.02)	0.99 (0.04)
	3rd membrane	0.85 (0.05)	1.25 (0.02)	1.106 (0.019)	0.95 (0.02)	0.99 (0.03)
mean		1.03 (0.25)	1.27 (0.03)	1.25 (0.17)	1.00 (0.13)	0.992 (0.014)

Table 5.2: Results of coefficient of friction on the three membranes on the rigid cylinder and on the two cylindrical compliant arms.

The results of Table 5.2 are presented in a clearer way in Figure 5.48.

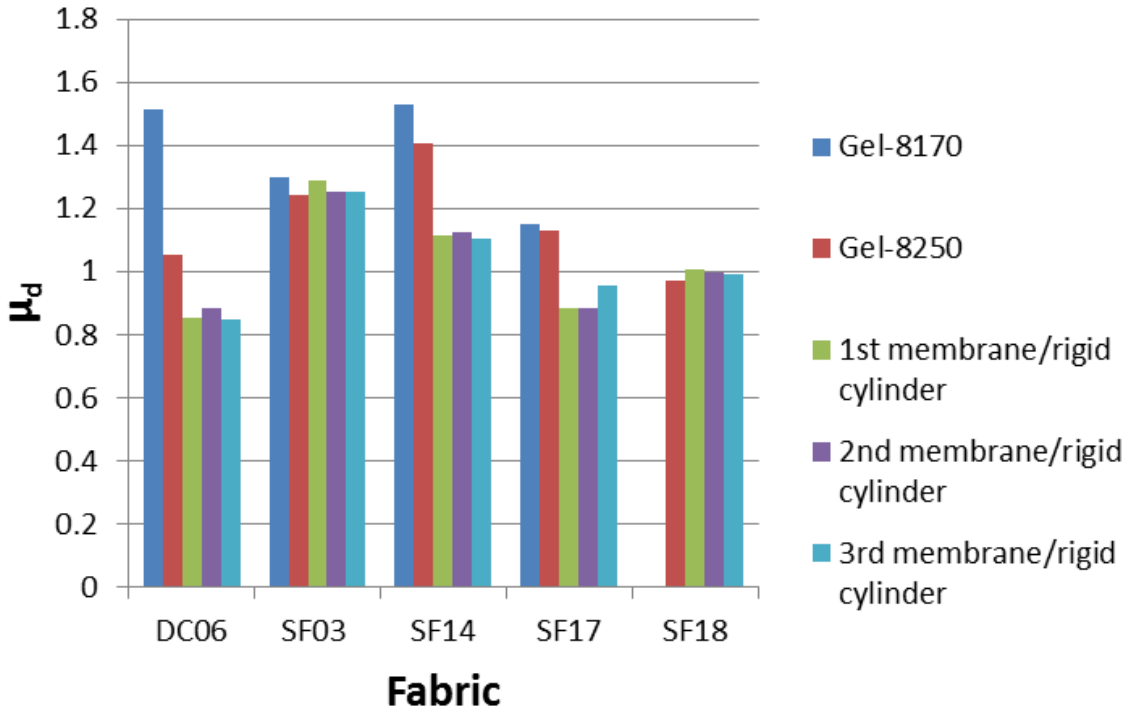

Figure 5.48: μ variation of cylindrical arms.

From the graph above (Figure 5.48) I can see that the coefficient of friction between each fabric and the membrane has a different value depending on the substrates. Fabric SF14 appears to have the highest coefficient of friction for the arms of Gel-8170 and Gel-8250, while on the rigid cylinder SF03 appears stick – slip, which is a different frictional behaviour. Fabric SF03 yields the same coefficient of friction on all the surfaces, no matter what the substrate is, something I see for fabric SF18 as well. Notable is the fact that on Gel-8170 arm the friction experiments with fabric SF18 did not show any sliding and the only effect was deformation, so I did not manage to extract the value of dynamic friction.

About the experiments from which I managed to derive a coefficient of friction, the correlation coefficient R^2 of every linear plot of pulling force against dead weight is presented in Table 5.3.

Core		R^2				
		DC06	SF03	SF14	SF17	SF18
Compliant	Gel-8250	0.959	0.999	0.981	0.984	0.967
	Gel-8170	0.960	0.998	0.990	0.995	-
Rigid	1st membrane	0.997	0.998	0.998	0.938	0.992
	2nd membane	0.987	0.998	0.997	0.995	0.975
	3rd membrane	0.958	0.996	0.996	0.995	0.988

Table 5.3: Correlation coefficient of the linear plots of pulling force against dead weight

As I show in Table 5.3 the correlation coefficient shows the high degree of validity of the mathematical model I want to verify, no matter the compliancy of the cylinder.

Normally, the coefficient of friction should be the same at all cases, since according to the second Amontons law the friction force is independent of the apparent contact area. So, something is happening at the interface that is changing the nature of the materials which come in touch. In order to make things clearer I have identified three factors:

1. As first factor I identify the stresses that are applied on the fabrics during the experiments. These stresses lead to the narrowing of the fabric which in some cases is converted to a string, something that could change the nature of the material.
2. Second, the structural shape of the fabric as it slides over a compliant cylinder is different from strip to strip at the same kind of fabric. So, different strip of the same kind of fabric could produce results with a considerable standard deviation.
3. Third, the compliant arms have the property of rucking in high degree. As a result, the membrane tends to fold on itself during the experiments which could alter the frictional properties of the surface of the cylinder (membrane) making it stickier.

As I can see from the results, fabrics SF14 and SF03 show the highest coefficient of friction, while SF17 and SF18 give similar values. Fabric DC06 gives the lowest value except for cylinder Gel-8170 which gives the second highest coefficient of friction. Overall, fabric SF17 gives the lowest coefficient of friction and fabric DC06 the second lowest.

Especially in the case of DC06 the fabric changes from strip to string, something that might be changing the nature of the material, while from SF17 and SF14 can just be justified from the higher frictional forces at the interface. The rest of the fabrics do not show significant changes between the different cylinders, which means that the conditions remain the same between the different substrate materials.

5.4.1.1 Predictions for dead weight masses of cylinder Gel-8170

Due to the high compliance of the cylinder, I conducted the derivation of coefficient of friction using data of less than five dead weight masses. In this section I try to predict the required tensometer force to achieve sliding for the higher dead weight masses.

In order to derive the coefficient of friction, necessary is the linear relationship between pulling force and dead weight mass. From this linear relationship I derive a formula from which I can extract the tensometer force for every given dead weight. About the formulae that follow, where y is the pulling force and x is the dead weight mass. In the case of these experiments the pulling force coincided with the tensometer force.

For fabric DC06 the formula is

$$y = 11.331x + 1.2076 \qquad \textbf{Equation 5.1}$$

So, for the 50g I have a tensometer force of 6.765N and for the 70g, 8.989N.

For the fabric SF03 I have

$$y = 7.9135 + 0.0128 \qquad \textbf{Equation 5.2}$$

For the 70g I have 5.447N.

For the fabric SF14 I have

$$y = 11.708x + 0.1587 \quad \textbf{Equation 5.3}$$

For the 50g I have 5.901N and for 70g I have 8.198N

For the fabric SF17 I have

$$y = 6.3517x + 0.4417 \quad \textbf{Equation 5.4}$$

For the 70g I have 4.803N.

Unfortunately the total displacement of 140mm was not enough to achieve these values which correspond to the plateau of the tensometer curves.

5.4.2 Comparison of μ of different fabrics

As I show in Table 5.2 the three membranes which I have attached on the rigid cylinder produce the same values for μ, a fact which states that no matter what the orientation of the fabric is, the frictional properties they demonstrate are the same. On the other hand the value μ on the cylinder of Gel-8250 is even higher and the values on the cylinder made of Gel-8170 appear the highest values of all the cylinders. If I take into consideration the fact that Gel-8170 is more compliant than Gel-8250, it is obvious that compliancy affects the value of μ. According to Amontons laws, the apparent contact area does not affect the value of μ. This means that throughout these experiments what probably happens is a change of the nature of the materials at the interface.

During the experiments the rucks due to the compliancy of the materials create more resistance because of the curved nature of the cylinder (flatter surface, higher friction value). As a result, I have greater deformation of the strip of fabric as it is described in §5.2.3. This deformation causes bigger strains which alter the nature of the fabric, which can contribute to the change of μ.

5.4.3 Tensometer graphs of the same fabric on the same gel arm

Looking at the tensometer graphs the first thing I see is the movement artefacts which do not affect the shape of the curve though. When I compare the graphs of 10g to 70g, I see that the degree of the arm deformation is much bigger at the 70g than the 10g. Notable similarity has the shape of the curve which in most of the cases has the same shape, no matter how big the dead weight mass is, a fact which declares the series of the events happening throughout the experiments are the same on each cylinder, no matter how big the dead weight mass is. The only thing that changes with the dead weight mass is the scale of the events.

5.4.4 Analysis of intercept appearance

In the following table I present the intercept of the linear graphs (pulling force against dead weight mass) of every experiment I have conducted on cylindrical arms.

Core		Intercept (N)				
		DC06	SF03	SF14	SF17	SF18
Compliant	Gel-8250	2.7 (0.2)	0.32 (0.04)	1.2 (0.3)	1.15 (0.16)	3.47 (0.18)
	Gel-8170	1.2 (0.5)	0.01 (0.07)	0.2 (0.3)	0.44 (0.10)	-
Rigid	1st membrane	1.97 (0.04)	0.53 (0.07)	1.03 (0.05)	1.2 (0.2)	2.28 (0.09)
	2nd membane	2.12 (0.12)	0.61 (0.08)	1.03 (0.07)	1.28 (0.06)	2.46 (0.16)
	3rd membrane	1.95 (0.17)	0.59 (0.11)	0.92 (0.08)	0.89 (0.06)	2.16 (0.11)
mean		2.0 (0.5)	0.4 (0.2)	0.9 (0.4)	1.0 (0.3)	2.6 (0.6)

Table 5.4: Intercept values of experiments on cylindrical arms.

At first glance on the table I can see that if I compare the values of the different fabrics I observe, even though they vary among the different cylinders, among each other they seem to behave the same. So, fabric SF18 shows the highest intercept, while fabric SF03 shows the lowest intercept, except on the arm Gel-8170, where I do not have any data for SF18. For this arm, SF14 exhibits the lower value and SF03 the highest.

If I compare Table 5.4 with Table 4.6 which presents the bending stiffness of each fabric, I can observe that the intercept is not related to the size of the bending stiffness. This indicates that other mechanisms dominate, which are possibly the subject of a future project. These mechanisms can be the force spent by the tensometer to deform the fabric before it starts sliding on the cylinder or the deformation induced on the cylinder before the sliding. As I show in Table 5.4, the biggest intercepts appear on fabrics DC06 and SF18. From the scope of the cylinders, cylinder of Gel-8250 and the rigid cylinder appear the highest intercepts, while the values of intercept appear on cylinder of Gel-8170 are quite smaller. Exactly this fact is what shows the less compliant a cylinder is, the more likely is to appear a bigger value of intercept.

5.4.5 Cylinder deformation during measurements

I use three different cylinders with different compliance. The rigid cylinders do not show any deformation at all, the cylinder of Gel-8250 shows deformation and the cylinder of Gel-8170 shows the highest deformation of all. Now, if I examine the coefficient of friction μ in relation to the compliance I see the more compliant a cylinder is, the higher the coefficient of friction it produces. On the other hand compliance in not relevant to the appearing intercept.

In order to survey the results better I examine the cylinder – fabric system as one. When the cylinder does not deform, all the force of the tensometer before the initiation of the sliding is absorbed by the fabric. On the other hand, in the case of the compliant arms, all the energy is absorbed by a combination of fabric and cylinder deformation. Since the highest values of intercept correspond to the less compliant arms, I assume that the intercept value depends on the deformation of the fabric just before the initiation of the sliding.

5.4.6 Overall graph evaluation

If I examine the derived graphs along the perpendicular axis of the tensometer force I can see that static friction usually has a value equal or higher than the dynamic friction, depending highly of the compliancy of the cylinder. Sometimes dynamic friction appears higher values than the static friction, and possibly the main reason is that deformation of cylinder and fabric coexists with sliding. This is especially obvious at the last part of the measurements and on cylinder Gel-8170 which has greater compliancy.

Another phenomenon which I can trace on the perpendicular axis is that the tensometer curves do not start from the zero point, but somewhat higher. This height represents the minimum force the tensometer has to apply to initiate movement of the crosshead and usually is equal to the dangling dead weight mass. Sometimes, when I was applying the fabric onto the cylinder, I stretched it a bit instead of just placing it, so the tensometer has to apply a slightly higher force than the dangling weight.

On the other hand, along the displacement axis I observe the rapid rise of the curve at its initial stage as deformation takes place, while when coefficient of friction stabilizes the graph follows the shape of a plateau (level, while I can distinguish some movement artefacts). Apart from the equipment noise, another source of artefacts is that the fabric is not a homogeneous material, since the texture is not the same along its length, so the coefficient of friction does not stay stable. Also the continuous deformation of the fabric and the arm, even in a lower degree, affects the shape of the curve at the later plateau stage, a fact I realise since the plateau in most of the cases is not entirely flat.

At the graphs regarding the pulling force against displacement, the points corresponding to different weights, usually don’t align so well as in the volar forearm experiments, probably because the plateau of the compliant arm cylinders is not so clear as the plateau of the volar forearm experiments.

Chapter 6 Conclusions and future work

There are millions of incontinence sufferers who use pads. The continuous use of pads can lead to the appearance of a skin disease called incontinence associated dermatitis, the main cause of which is friction between the skin and the pad coverstock material which is nonwoven fabric.

This project was initially conceived to validate a mathematical model describing friction at the interface between convex prisms and nonwoven fabrics. It is a combination of different fields of science, physics, mechanical engineering, material science and physiological measurements. The complexity of the project intrigues great interest, not only for its outcomes but for the different streams of future work it generates.

6.1 Outcomes of the project

Initially I want to validate a mathematical model for friction between convex prisms and a compliant sheet, based on the work of Gwosdow et al (Gwosdow et al., 1986) which was further evolved by David Cottenden (Cottenden, 2010). The model had already been validated for simple geometries of convex prisms of circular and elliptical cross section, while it remained to be validated for more complex geometries. In this project I validated the model for more complex geometries.

I started from using the surface of high half angle conical shapes since cones approximate parts of human body and I tried to examine whether the values of the coefficient of friction in various parts of the cone coincide on the same line in the master graph (Figure 3.19) for all the cones I experimented with. If I examine the results of each cone separately with the results of the linear experiments, I can see that the results are within the bounds of experimental errors. The only cone for which this does not happen is the second 25° cone. A variety of reasons can cause this. The coefficient of friction from the linear experiments is derived from certain positions, while the positions which were not taken into account correspond to the region close to the joint, or regions that produce different frictional behaviour from the rest of the cone surface. Due to the small surface area of 25° cone, sometimes these areas cannot be avoided, producing results out of the expected. No matter of these deviations, the results did present agreement in a high degree, showing that pulling force is proportional to dead weight in agreement with Cottenden's model.

Second, I addressed the more complicated scenario of dragging a fabric over a compliant substrate, human volar forearms. Two were the difficulties of this block of work. First the counter surface of volar forearms was not incompressible and inextensible, something that Cottenden's model assumes to stand and second the counter surface is human skin, a living tissue which varies from participant to participant. Additionally, the gross geometry of the interface changes throughout the experiment, initiating local changes like rucking. Also, the applied pressure from the strip on the volar forearm causes a different deformation at the interface (on the volar forearm and the fabric), depending on the volar forearm and the fabric. Moreover, I tested how different fabrics respond to the experiments and I tested five different kinds of fabric. I discovered that the bending modulus of the fabrics does have an effect on the results of the experimental process; results in offsets in the linear graphs of pulling force against dead weight that correlate to the size of the bending modulus. Of course, I should not forget that in the case of volar forearms I experiment on real human skin, testing the model in the surface where fabrics are applied in real conditions. The tensometer graphs for each participant

produced graphs of pulling force against dead weight of high correlation coefficient, a fact that shows how good the model works on real skin. Finally, at each experiment I conducted on every participant, no matter if she was a young or an elderly participant, the pulling force was proportional to dead weight, proving once more that the model stands. Another interesting conclusion that came up from the experiments is that the coefficient of friction did not seem to vary with the age of the participants.

The third block of my work is the most interesting part of the project since there is not any similar reference in the literature review. I use compliant cylinders made of silicone gel and a high friction membrane. In this way I pushed the validation of the model even further, causing extreme deformations not only on the convex prism which has the shape of a cylinder but on the strip of fabric as well. With the help of the high friction membrane, I applied on the strips of fabric high forces causing the narrowing and the stretching of the fabric and changing even further the gross geometry of the interface. In quite a few cases the strip was converted to a cord under the influence of high loads. I have to note that the skin use in all the experiments was the same, but what was different was the substrate. As I showed the results differed significantly for the same fabric across a range of cylinders, a fact which underlines how important the substrate is for the friction phenomenon. Notable is the fact that the fabric bending modulus did not seem to influence the offset of the linear graph of pulling force against dead weight.

During the three blocks of work I have made the assumption that fabric is a homogeneous material. This is quite inaccurate since it is a fluffy and a relative inhomogeneous material, a fact that does not seem to affect the credibility of the model which seems to produce credible results. Nonwoven fabrics are very thin, relatively inextensible but drape well. In simple words the fabric fulfils the conditions of the model as it is described in the literature review, which states that the compliant sheet needs to be inextensible, incompressible with a low bending modulus.

The three streams of work I describe take the validation of the model one step further, successively validating the model for more complex geometries, from rigid to compliant models. I assess several issues, observing how geometrical factors (rigid geometry) and how the changing geometry throughout the measurements affect the model. Even though I conducted the experiments in pragmatic conditions which are different from the ideal theoretical conditions, the model seems to respond well, producing results where the pulling force is proportional to dead weight, though possible to generate the coefficient of friction.

This work is just one of the first steps of exploring the phenomenon of friction on skin. New possible streams of work for even a more robust validation of the model are proposed in the following section.

6.2 Future work

This project has validated Cottenden's model but generated many questions that can possible be the subject for future projects. Four are mainly the future work directions I have traced, the foundations of which are laid on the current project.

Every graph of pulling force versus dead weight comes with an offset, which the model does not predict. The offset is more obvious at the third part of the project, for the experiments with the compliant arms, where the applied forces are larger, but it appears in every part of the project. I propose several explanations in the compliant cylinders section, like the change of the nature of the

test materials throughout the measurement, but it has to be thoroughly assessed to provide a satisfactory analysis.

Avery interesting subject for investigation arises from the experiments of the volar forearm section and of the compliant arm section. For the same countersurface, different fabrics give different values for the coefficient of friction. So, necessary is to relate the structure of the fabrics to the frictional properties.

Throughout the volar forearm experiments there is compression of the volar forearm of the participants as the fabrics slide over their arms. This way, a very fascinating set of data results that is relevant to the compliance of the muscles of each participant, a problem which also demands further investigation.

Another possible direction would be the validation of the model on different convex prism shapes instead of cylindrical and conical arms. An idea is a rigid shape of an hourglass (Figure 6.1) that approximates even more the shape of parts of human body. The muscle between two joints under pressure tends to contract, taking the form of an hourglass, so this shape could be the next logical step after a cone. Even though it is not a convex prism, the fabric is compliant enough to achieve full contact at the instant of slip.

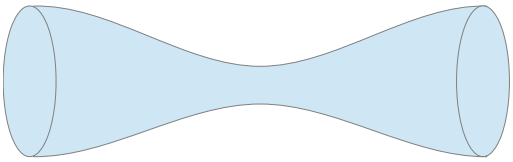

Figure 6.1: Shape of hourglass which approximates to muscles under contraction between joints

A cylinder with furrows and ridges will be another useful idea. One of the conditions I have accepted for the model is that the Amontons laws stand. One of Amontons laws is that friction is independent of the area of contact. So, by using a surface similar to the surface of Figure 6.2 on a cylindrical core (similar to a gear wheel), the shape of the interface between the strip of compliant sheet and this surface will be a cylinder, but without occurring full contact in the way it would if I used cylinder with circular cross section, but the shape of the interface between the slip and the fabric will be circular. In this way I can test the validity of the relationship of Amontons law with the theoretical model and simulate heavily wrinkled/rucked surfaces

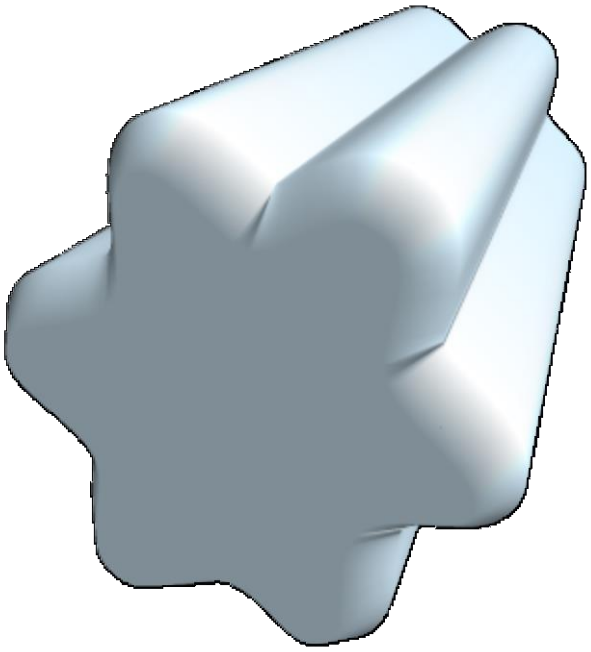

Figure 6.2: shape similar to a wheeled gear

Another possible project stream is that instead of conducting experiments on the volar forearm, in a possible project the scientists could use other parts of the human body, like the buttocks and the inner side of the thighs. Since a great application of nonwoven fabrics is incontinence products, measurements on the skin sites of these regions can give even more useful results. Also, I conducted the experiments on dry skin, so skin in various degrees of wetness in the anal and genital region can be another possible experimental stream. A project on the wet skin of volar forearm is already being performed by another PhD student.

In the third part of my project I used cylinders of various compliances to test the mathematical model. The next possible steps are constructing a replica of buttocks or the genital area of silicone and perform friction measurements on them. Replica is not necessary to simulate the pad area, but any part of the body the experimentalists wish to study.

In my experiments I used as compliant sheet nonwoven fabrics, while experimentalists could use other kinds of fabrics, made of a variety of materials, like silk, wool or of synthetic origin and woven in different styles. Additionally, they could investigate not only their frictional properties, but their tactile and comfort properties. The use of different kinds of fabric could help discover how different kinds of fabrics with different properties affect the model.

Overall, this project pushes the validation of a mathematical model that describes friction between skin and fabrics one step further and initiates several streams of work which could add to the credibility of the model. A complete model that describes the friction between skin and fabrics could lead to the design of more comfortable incontinence products, facilitating the life of millions of incontinence pad wearers. It is easily understood that the mathematical model this study validates, can be used for any tests of compliant sheet on relatively rigid convex prisms, so this model has a broad spectrum of applications.

APPENDIX A

Application submitted for ethics committee approval for volar forearm work

In order to conduct the experiments on human subjects I needed to apply for ethical approval which was submitted to and approved by from London Stanmore Research Ethics Committee. In this application I reassured the ethical committee that I was going to perform the measurements on the volar forearm of young and elder participant, as long as I had their consent or the consent of the next of kin, in case they were able to consent for themselves, and they were fully aware of the experimental process and the reason they were participating in these experiments.

The study was completed under the supervision of Prof Alan Cottenden and in collaboration with Sabrina Falloon, another PhD student. The application was written with the significant help and guidance of Margaret Macaulay (research nurse) and Sabrina Falloon.

The measurements took place either in the Environmentally Controlled Room of our laboratory, or in the nursing house of Cheverton Lodge where the elderly participants were. People who participated were the personnel of the lab, patients of an incontinence clinic we are collaborating with and residents of the Cheverton Lodge nursing house. I should mention that Margaret Macaulay transported the experimentalists and their equipment to and from the nursing home and also assisted significantly in communication with the participants.

The application for ethical approval is constituted by my CV, the cover letter, the protocol, the online form, the information sheets for the UCL personnel, the patients of the incontinence clinic and the residents of the nursing house and the respective consent forms. The application also includes any other relevant documents demanded by the ethics committee.

Protocol for a study of friction between skin and nonwoven fabrics

Vasileios Asimakopoulos[1], Alan Cottenden[1], James Malone-Lee[2], Mary Rabbitte[3]

[1]Department of Medical Physics & Bioengineering, University College London, UK
[2]Department of Medicine, University College London, UK
[3]Cheverton Lodge Care Home

20 July 2011, version 2.2

Full title of study An experimental study of friction between skin and nonwoven fabrics.
Short title Friction between skin and nonwoven fabrics
Chief investigator Prof. Alan Cottenden
Co-investigators Miss Sabrina Falloon, Mr Vasileios Asimakopoulos
Sponsor University College London

Abstract

Wearers of incontinence pads and sanitary towels frequently experience skin abrasion due to friction. The Continence and Skin Technology Group has worked for some years to develop techniques for measuring this friction *in vivo*. In order to deepen our understanding of how this friction works, we now need to conduct a study on real skin *in vivo*.

This study will involve performing some mechanical tests on a *relatively* hairless area of the forearm of volunteers with nonwoven coverstock fabrics. There will of course be interaction between the participants and investigators, but no identifiable information will be included in the study. All participants will have given informed consent before taking part in the study.

Contents

1 Introduction

The work described in this document involves measuring friction between nonwoven fabrics (similar to tea bag material and commonly used against the skin in incontinence pads) and the volar forearm of adults of different ages. It is the latest of a series of *in vivo* and *ex vivo* experimental studies, having the overall aim of understanding and modelling friction between incontinence pads and skin, so paving the way for the development of more skin-friendly products. The proposed work will use methodologies developed and successfully used in earlier studies, giving a high level of confidence that it will yield fruitful data.

1.1 Background

Approximately five million people in the UK are known to be incontinent of urine, and the prevalence is anticipated to increase further as the growing population ages [1]. Whilst many sufferers can be at least partially cured, the significant minority who cannot be fully cured require products to manage their condition. The most common product type is absorbent pads, but can lead to skin damage, often in the form of Incontinence Associated Dermatitis (IAD), of which friction is a major contributor.

The friction mechanisms that occur here must first be identified and modelled before products can be improved to be less damaging to the skin.

So far, many clinical studies have been carried out to determine the prevalence, severity, duration and location of IAD in incontinent nursing home populations [2]. A methodology has been developed for measuring friction between nonwoven fabrics and volar forearm skin [3] - skin on the underside of the lower arm, commonly used as a proxy for the diaper area of the skin. Mechanisms of friction between nonwoven fabrics and a skin surrogate (Lorica Soft) have also been investigated and significant progress has been made toward identifying them [4].

In a current study, I aim to validate a theoretical model developed to understand the friction mechanisms between skin and nonwoven fabrics. I initially tested the model mathematically on cones made from plaster of Paris that present uniform frictional properties. Then I adapted the model by making cylinders from different kinds of foam to test the geometrical aspects of the model (wrinkling and rucking). The next step is to make friction measurements on human skin to compare with those made on surrogate arms. Results from tests with the plaster of Paris cones and the foam models will be validated against results from tests on human skin in this work.

1.2 Aims and objectives

The aim of this study is to validate the findings of the friction mechanism work done so far with *in vivo* measurements on volar forearm skin. This will involve measuring friction force between nonwoven fabrics and volar forearm on people of different ages and genders, using a range of nonwoven fabrics and pressures.

The methods for obtaining these data are described in §2.2. Experiments relating to these objectives must give an indication of the extent to which the mechanisms and rules identified are common to all people. Consequently, the individuals who participate will vary in age, and if possible, should vary in ethnicity and gender so that any important features that are identified

can be established as likely universal, or not. However, though this would be desirable, it is not of primary importance for the present project.

2 Methodology

This section describes all procedures and methods that will be employed in the execution of this work, including the identification of subjects, obtaining consent, the recruitment of participants (§2.1), and the experimental methodologies for making measurements on volar forearm skin (§2.2). The timing of different stages in the recruitment of subjects and the experiments are given in §2.4.

2.1 Identification of subjects and consent

This study will involve working with volar forearm skin *in vivo*. The volar forearm is a fairly flat and hairless part of the body and is easily accessible for taking measurements. This makes it well suited to our experiments: in this exploratory work it is more important that skin is uniform and simple than that it is from the diaper area.

Criteria for *inclusion* in this study are as follows.

- The participant is aged 18 (years) or over.
- The participant has little or no hair on their volar forearms - see fig1.

Criteria for *exclusion* from this study are as follows:

- The participant is under 18 years old.
- The participant has hairy volar forearms - see fig1.
- The participant has an active skin condition that makes the surface of their skin rougher than it would normally be (e.g. eczema, psoriasis).
- The participant has a known allergy to nonwoven fabrics.

Volunteers will be sought from outpatients of the Incontinence Clinic of Whittington Health NHS, residents of Cheverton Lodge Care Home, students and staff from the Clerkenwell Building, and students and staff from UCL.

2.1.1 Incontinence clinic participants

Identification and initial contact with prospective participants will be made by their doctor, Prof James Malone-Lee (JML), in routine appointments with his patients, during which he will give them an information sheet to read. The patient will then be asked if they would like to speak to an investigator – Sabrina Falloon (SF) or Vasileios Asimakopoulos (VA) will explain the study further and answer any questions they may have. The patient will be given at least 24 hours to consider their decision. If they are happy to participate, the patient should contact one of the investigators. The participant will come to the 3rd floor of the Clerkenwell Building on an arranged date when an investigator will go through the details of the study again with them and the consent form will be signed. Some participants may take part in the experiment on the same day as one of their future outpatient appointments. However, if a participant comes outside their usual appointment, transport will be arranged or travel expenses will be reimbursed.

2.1.2 Nursing home participants

This same process applies to residents of the nursing home, except that the general manager, Mary Rabbitte (MR), will identify and make the initial contact with potential participants, and consent will be obtained in the home rather than the Clerkenwell Building.

2.1.3 Students and staff participants

All students and staff from the Clerkenwell Building will be invited to participate by poster adverts and will receive information sheets on request; students and staff of UCL will receive their invitation in a generic e-mail with an attached PIS. They will all need to contact the investigators to register their interest in participation in the study and direct all their questions to them. They will also be required to sign consent forms in the same way as other participants.

Recruitment will continue until sufficient data have been gathered; the number of participants needed is expected to be about 20, and will not exceed 30. The participants will be split equally into two groups (18-64 yrs and 65 yrs +), but no precise figure is possible due to the exploratory nature of this work.

Figure 1: Image of forearm skin: people with MORE hair on the *underside* of their forearm than shown in the photo above will NOT be considered for participation in the study.

2.2 Experimental methodology

The experimental methodology presented here is the mainly result of work by Rebecca Wong (WKRW) on volar forearm skin. WKRW did very similar experiments but she focused on young female subjects, whereas in this study, people of all ages (above 18) and both genders are considered. Methodology used by WKRW has been adapted to address the aims set out in §1.2. All reasonable measures have been taken to anticipate any issues that may arise. The experimental methods required to achieve the objectives stated in §1.2 are detailed below.

2.2.1 Dry friction

Most measurements will take place on the participant's volar forearm in an environmentally (temperature and humidity) controlled room in the Department of Medical Physics and Bioengineering, UCL Archway Campus. It is not essential for the dry skin friction measurements to be taken in there, so measurements made at the nursing homes will not be affected by the

lack of environment control. However, for convenience, measurements will be taken in the department for all other participants.

For consistency: Baseline measurements of trans-epidermal water loss (TEWL) on the volunteers' arm will be taken with an evaporimetry device in order to help us to make conclusions about the friction values produced by their skin with nonwoven fabrics. This is because we know that skin hydration affects friction values and some people's skin may naturally lose water at a faster rate than others' [5]. The instrument used is non-invasive and consists of a small probe, which will be placed gently on the skin and will remain in position for approximately 3 minutes for baseline measurements.

In the nursing home, the temperature of the room will also be measured, using a standard commercially available room thermometer, so that these friction measurements can be fairly compared with those made in the environmentally controlled room.
Photographs of the volunteers' arm will be taken in order to characterise the surface wrinkling and topography of the skin. This will be performed in good lighting conditions with a high-resolution digital camera.

For skin friction measurements: The skin friction measurements will be carried out using a piece of equipment called a Tensometer (MTT175 Miniature Tensile Tester, Dia-Stron Ltd.), which has an armrest to position and support the participant's arm. A strip of nonwoven fabric (similar to the stay-dry topsheet of a pad) with a light weight (no more than 100g) attached will be pulled across the skin by the Tensometer, while the same machine measures the force required to do this and the distance the material moves.

Skin friction measurements will be taken on the volunteers' dry arm under various loads and repeated at least three times. Each friction test will be video recorded in order to demonstrate any gross physical differences between participants' skin in the study. Photographs will also be taken of the participant's volar forearm before and after the measurements.

2.3 Health and safety

Both investigators have had the appropriate training and experience to use the equipment (described in this protocol) proficiently, and have tested this method on models many times.

There is a very low chance that participants may present with reddening of the skin or a rash as a result of contact with the nonwoven fabric, but should this persist or occur repeatedly, medical advice will be sought. A similar study (involving the same measurements with the same materials) has been carried out successfully with no sign of adverse skin reactions.
The arm rest was specifically designed to support an arm comfortably and the chair on which the participant sits will be adjusted to suit the comfort of the individual. (The chair will have a backrest, armrests and adjustable height for both safety and comfort.)

No significant health and safety issues are raised by this study. Typical laboratory risks still apply - such as chemical, mechanical and electrical hazards - but this will be managed by good laboratory practice. Chemicals are stored safely in locked cupboards and participants will not come into direct contact with any dangerous electrical equipment.

2.4 Projected timing

The purposes of this section are to clarify the timings of participant recruitment and experiment completion, and to give an approximate guide to the start and end dates of the work. This work

is expected to start immediately after ethics approval has been obtained. Participants will be recruited throughout the study from all 'groups' (i.e. incontinence clinic, nursing home, students and staff from Clerkenwell Building, students and staff from UCL). Students and staff in the Clerkenwell Building are most available to receive information and will therefore most likely be recruited first, having been given a PIS. All potential participants will have had a period of at least 24 hours to consider whether or not to take part. This means that experiments may go ahead the following day for Clerkenwell Building staff and student participants.

Patients from JML's clinic will have a longer period between first receiving information and actually taking part. This depends on the gap between appointments (typically 8-12 weeks), as some patient participants will prefer to take part on the same day as an appointment for their convenience. However, those who prefer not to do this can participate sooner. Investigators will travel to the nursing home to take measurements on residents there, in which case the time between residents receiving information and participating will depend mainly on the daily schedule at the home. While it is not possible to specify an end date for this study, the work will continue until at least the minimum amount of data has been collected from the minimum number of participants. It is estimated that it will take up to the end of September 2012.

3 Ethics

This study involves interaction between the investigators and participants prior to, during and sometimes after experiments. This is because all participants will need to arrange a time and date with the investigators for the friction measurements to be taken, and this may need to be repeated.

In consequence of this, the primary ethical requirement is to obtain informed consent from participants. As described in §2.1, this will be managed collectively by the investigator and the prospective participant's doctor or nursing home staff using materials prepared by us. At least 24 hours will be given to the prospective participants in which to consider the information, before they are given the opportunity to take part when written consent is sought (§2.1).

The data obtained by the experiments will have an alphanumeric code and will be entirely untraceable to the participant, but will be kept on password-secure computers. Minimal personal details will be kept in separate files containing information such as gender, ethnicity, and age of the participant, as well as a general description of the condition of the skin. These files will also be stored on password-secure computers in either the laboratory or office, both of which have code-locked doors. Our practice with experimental data of this type is to keep them in long term storage for 20 years with personal data in separate files.

4 Expertise

Prof. Alan Cottenden is a Medical Physicist with over 25 years' experience working on incontinence technology. He has managed, directed, or participated in around 25 clinical trials of incontinence products and clinical studies involving *in vivo* measurements on skin.

Mary Rabbitte is the manager of Cheverton Lodge Care Home and has been working with nursing home residents for more than 10 years.

Vasileios Asimakopoulos is a PhD student in the Continence and Skin Technology Group, a joint venture of the departments of Medical Physics & Bioengineering and Medicine at UCL. His previous training is in physics and biomedical engineering. His first supervisor is Alan Cottenden.

Sabrina Falloon is a PhD student in the Continence and Skin Technology Group, a joint venture of the departments of Medical Physics & Bioengineering and Medicine at UCL. Her previous training is in medical engineering. Her first supervisor is Alan Cottenden.

Prof. James Malone-Lee is Professor of Medicine at University College London, and has been working on incontinence for about 25 years. In this time he has overseen 15 clinical trials, and has considerable experience in this respect.

References

[1] Thomas, S., Billington, A. and Getliffe, K. (2004). Improving continence services a case study in policy influence. *Journal of Nursing Management.* **12**(4), pp. 252-257

[2] Abrams, P., Cardozo, L., Khoury, S. and Wein, A. eds. (2009). *Incontinence: 4th International Consultation on Incontinence, Paris July 5-8, 2008.* 4th Ed. Health Publication Ltd.

[3] Wong, W. K. R. (2008). A study of evaporation and friction on hydrated forearm skin [PhD thesis]. University College London.

[4] Cottenden, D. J. (2010). A multiscale analysis of frictional interaction between human skin and nonwoven fabrics [PhD thesis]. University College London.

[5] Warrier, A.G., Kligman, A. M., Harper, R. A., Bowman, J. and Wickett, R.R. (1996). A comparison of black and white skin using noninvasive methods. *J. Soc. Cosmet. Chem.* **47**, pp. 229-240

University College London
Department of Medical Physics and Bioengineering
Continence & Skin Technology Group

Archway Campus
Clerkenwell Building
Highgate Hill
London
N19 5LW
England

University College London Continence & Skin Technology Group study into friction between volar forearm skin and nonwoven fabrics

Participant Information Sheet: Students & staff

(1 August 2011 Version 1.4)

What is the purpose of this study?

People who use sanitary towels or incontinence pads sometimes get sore skin caused by friction (rubbing) against the surface of the pads. We need to understand how this friction occurs in order to develop pads which are kinder to the skin.

The purpose of this study is to find out how the friction between the skin and the fabric which forms the surface of the pads works.

Who is organising and funding the study?

This study is organised by research staff at University College London. The study is funded by SCA Hygiene Products AB (a pad manufacturer) and University College London.

Why have I been chosen?

We need up to 30 volunteers to take part in this study. We know that different people's skin reacts differently to fabrics, therefore we need to measure friction on men and women of different ages. These tests will tell us if some fabrics cause more friction than others. This knowledge will ultimately help pad manufacturers to develop pads that are kinder to the skin.

What types of experiments will you be doing?

The experiments we will be doing will measure the force needed to make fabric slide over your skin. You will be asked to sit with your arm supported on an arm rest as shown in the photograph below. The fabric will be pulled gently and slowly across your arm by a device called a tensometer. Each test will take less than one minute and will be repeated several times. You will be asked to keep your arm as still as possible during the tests.

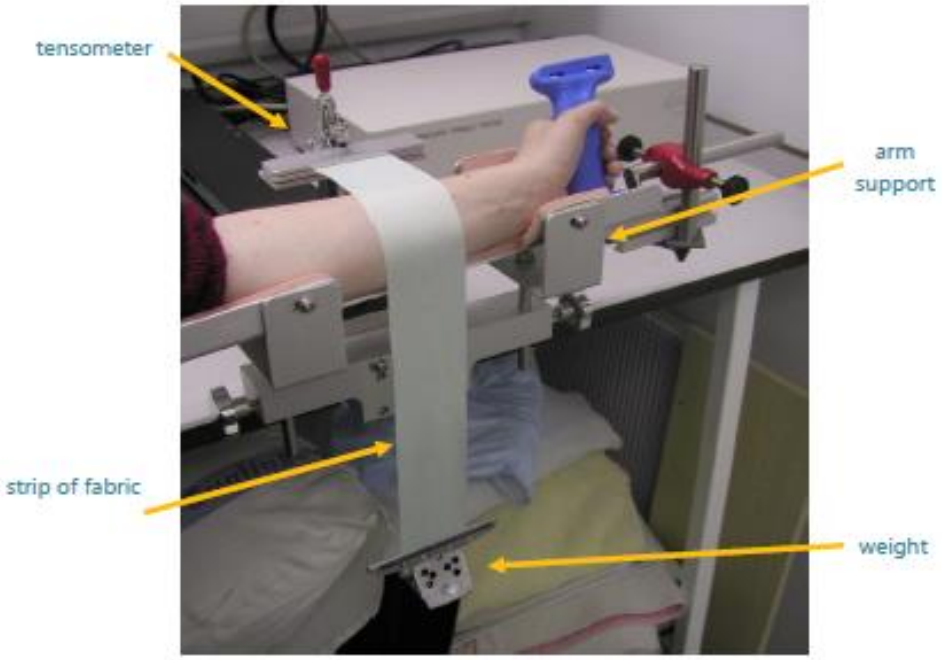

We will also measure water loss from your skin which can affect friction.

We may need to dampen your skin and/or the fabric as we would like to know more about the effect of moisture on friction.

A photograph of your arm will be taken before and after each test. A video record will be made as the strips of fabric are being pulled across your arm. Only your forearm, the fabric and equipment will in the shot. It will not be possible to see your face.

Skin moisture can be affected by how relaxed or excited you feel, so reading material and videos will be provided to help you relax during the tests. You are also welcome to read a book or magazine, or watch a DVD of your own choice.

In total the tests will take approximately two hours including breaks. Depending on the results obtained, we may have to repeat the tests at a later date; this would be no later than 6 months after the initial tests. It is unlikely that you will be required to participate for a third time.

The tests will be done at our department (see address at the top of page 1). If you are not already expecting to come to the Archway Campus on the day that you participate, your travel costs will be reimbursed.

Do I have to take part?

No, you do not have to take part. You do not have to give a reason.

What if I change my mind?

You are free to change your mind and withdraw from the study at any time up to or during your participation.

What are the possible disadvantages or risks of taking part?

If your skin is sensitive to the fabrics, you may experience some minor irritation where the fabric touches your skin. There are no other anticipated risks or side effects associated with taking part in this study.

What are the possible benefits of taking part?

There are no immediate or direct benefits to you from taking part. Longer term, you and/or others may benefit from any improvements to fabrics that are used in incontinence pads and sanitary towels as a result of this study.

Confidentiality

Your participation in this study will not involve accessing any of your medical information. Results from this study will be made anonymous so they cannot be linked to you.

What will happen to the results of the study?

Results from the study will be published widely (in print/conferences) but will be completely anonymous and untraceable back to you. Your personal details will be stored securely and separately from the results gathered from the tests in accordance with the University's policy. A summary of the results will be sent to you after the completion of the work.

What happens if something goes wrong?

If you have a concern about any aspect of this study, you should ask to speak to the researchers who will do their best to answer your questions (contact details at the end of this document). If you remain unhappy and wish to complain formally, please contact the Chief Investigator, Professor Alan Cottenden, who will forward your complaint to the appropriate person. You can contact him at:

3rd floor, Clerkenwell Building
Highgate Hill
London
N19 5LW
Tel: 020 7288 5670

Who has reviewed the study?

The study has received ethics approval from the London Stanmore Research Ethics Committee.

What happens next?

Any questions you may have should be answered satisfactorily by the researchers. If you wish to take part, you will be asked to sign a consent form. You will be given a copy of the signed consent form.

Thank you very much for your help.

Sabrina Falloon
Tel: 020 7288 3771
E-mail: sabrina.falloon.10@ucl.ac.uk

Vasileios Asimakopoulos
Tel: 020 7288 5150
E-mail: v.asimakopoulos@ucl.ac.uk

University College London
Department of Medical Physics and Bioengineering
Continence & Skin Technology Group

Archway Campus
Clerkenwell Building
Highgate Hill
London
N19 5LW
England

University College London Continence & Skin Technology Group study into friction between volar forearm skin and nonwoven fabrics

Participant Information Sheet: Outpatients

(1 August 2011 Version 1.5)

What is the purpose of this study?

People who use sanitary towels or incontinence pads sometimes get sore skin caused by friction (rubbing) against the surface of the pads. We need to understand how this friction occurs in order to develop pads which are kinder to the skin.

The purpose of this study is to find out how the friction between the skin and the fabric which forms the surface of the pads works.

Who is organising and funding the study?

This study is organised by research staff at University College London. The study is funded by SCA Hygiene Products AB (a pad manufacturer) and University College London.

Why have I been chosen?

We need up to 30 volunteers to take part in this study. We know that different people's skin reacts differently to fabrics, therefore we need to measure friction on men and women of different ages. These tests will tell us if some fabrics cause more friction than others. This knowledge will ultimately help pad manufacturers to develop pads that are kinder to the skin.

What types of experiments will you be doing?

The experiments we will be doing will measure the force needed to make fabric slide over your skin. You will be asked to sit with your arm supported on an arm rest as shown in the photograph below. The fabric will be pulled gently and slowly across your arm by a device called a tensometer. Each test will take less than one minute and will be repeated several times. You will be asked to keep your arm as still as possible during the tests.

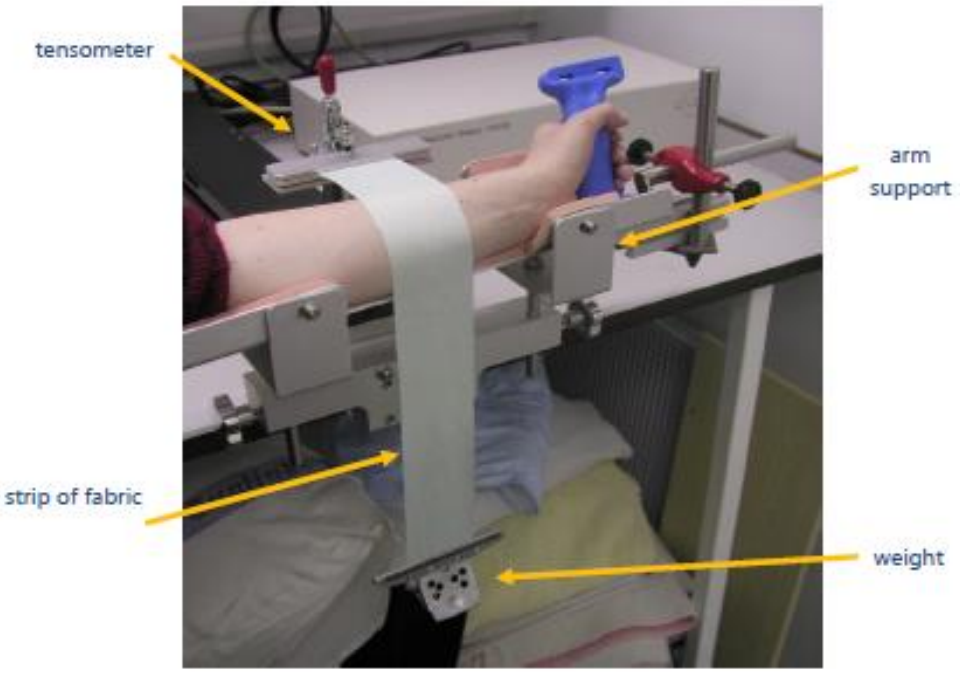

We will also measure water loss from your skin which can affect friction.

We may need to dampen your skin and/or the fabric as we would like to know more about the effect of moisture on friction.

A photograph of your arm will be taken before and after each test. A video record will be made as the strips of fabric are being pulled across your arm. Only your forearm, the fabric and equipment will in the shot. It will not be possible to see your face.

Skin moisture can be affected by how relaxed or excited you feel, so reading material and videos will be provided to help you relax during the tests. You are also welcome to read a book or magazine, or watch a DVD of your own choice.

In total the tests will take approximately two hours including breaks. Depending on the results obtained, we may have to repeat the tests at a later date; this would be no later than 6 months after the initial tests. It is unlikely that you will be required to participate for a third time.

The tests will be done at our department on the 3rd floor of the Clerkenwell Building. We will arrange the tests for a day that is convenient for you. This could be when you are coming to see Professor Malone-Lee. If it does not coincide with a clinic appointment, we will pay your travel costs.

Do I have to take part?

No, you do not have to take part. You do not have to give a reason and it will not affect your care in any way.

What if I change my mind?

You are free to change your mind and withdraw from the study at any time up to or during your participation.

What are the possible disadvantages or risks of taking part?

If your skin is sensitive to the fabrics, you may experience some minor irritation where the fabric touches your skin. There are no other anticipated risks or side effects associated with taking part in this study.

What are the possible benefits of taking part?

There are no immediate or direct benefits to you from taking part. Longer term, you and/or others may benefit from any improvements to fabrics that are used in incontinence pads and sanitary towels as a result of this study.

Confidentiality

Your participation in this study will not involve accessing any of your medical information. Only your name and age will be passed to us from the outpatients staff. Results from this study will be made anonymous so they cannot be linked to you. Your GP will be informed of your participation in the study **only** if you consent to this.

What will happen to the results of the study?

Results from the study will be published widely (in print/conferences) but will be completely anonymous and untraceable back to you. Your personal details will be stored securely and separately from the results gathered from the tests in accordance with the University's policy. A summary of the results will be sent to you after the completion of the work.

What happens if something goes wrong?

If you have a concern about any aspect of this study, you should ask to speak to the researchers who will do their best to answer your questions (contact details at the end of this document). If you remain unhappy and wish to complain formally, you can do this through the NHS Complaints Procedure (or Private Institution). Details can be obtained from the hospital.

Who has reviewed the study?

The study has received ethics approval from the London Stanmore Research Ethics Committee.

What happens next?

Any questions you may have should be answered satisfactorily by the researchers. If you wish to take part, you will be asked to sign a consent form. You will be given a copy of the signed consent form.

Thank you very much for your help.

Sabrina Falloon
Tel: 020 7288 3771
E-mail: sabrina.falloon.10@ucl.ac.uk

Vasileios Asimakopoulos
Tel: 020 7288 5150
E-mail: v.asimakopoulos@ucl.ac.uk

University College London
Department of Medical Physics and Bioengineering
Continence & Skin Technology Group

Archway Campus
Clerkenwell Building
Highgate Hill
London
N19 5LW
England

University College London Continence & Skin Technology Group study into friction between volar forearm skin and nonwoven fabrics

Participant Information Sheet: Nursing Home Residents

(1 August 2011 Version 1.6)

What is the purpose of this study?

People who use sanitary towels or incontinence pads sometimes get sore skin caused by friction (rubbing) against the surface of the pads. We need to understand how this friction occurs in order to develop pads which are kinder to the skin.

The purpose of this study is to find out how the friction between the skin and the fabric which forms the surface of the pads works.

Who is organising and funding the study?

This study is organised by research staff at University College London. The study is funded by SCA Hygiene Products AB (a pad manufacturer) and University College London.

Why have I been chosen?

We need up to 30 volunteers to take part in this study. We know that different people's skin reacts differently to fabrics, therefore we need to measure friction on men and women of different ages. These tests will tell us if some fabrics cause more friction than others. This knowledge will ultimately help pad manufacturers to develop pads that are kinder to the skin.

What types of experiments will you be doing?

The experiments we will be doing will measure the force needed to make fabric slide over your skin. You will be asked to sit with your arm supported on an arm rest as shown in the photograph below. The fabric will be pulled gently and slowly across your arm by a device called a tensometer. Each test will take less than one minute and will be repeated several times. You will be asked to keep your arm as still as possible during the tests.

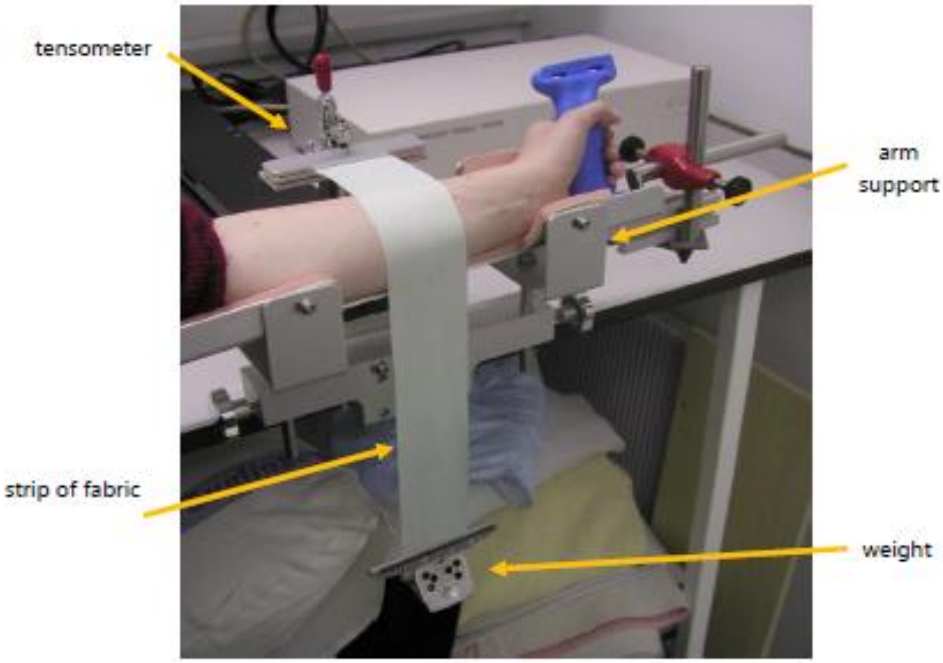

We will also measure water loss from your skin which can affect friction.

A photograph of your arm will be taken before and after each test. A video record will be made as the strips of fabric are being pulled across your arm. Only your forearm, the fabric and equipment will in the shot. It will not be possible to see your face.

Skin moisture can be affected by how relaxed or excited you feel, so reading material and videos will be provided to help you relax during the tests. You are also welcome to read a book or magazine, or watch a DVD of your own choice.

In total the tests will take approximately two hours including breaks. Depending on the results obtained, we may have to repeat the tests at a later date; this would be no later than 6 months after the initial tests. It is unlikely that you will be required to participate for a third time.

The tests will be done at Cheverton Lodge Nursing Home. You will not have to leave the nursing home to take part in this study.

Do I have to take part?

No, you do not have to take part. You do not have to give a reason and it will not affect your care in any way.

What if I change my mind?

You are free to change your mind and withdraw from the study at any time up to or during your participation.

What are the possible disadvantages or risks of taking part?

If your skin is sensitive to the fabrics, you may experience some minor irritation where the fabric touches your skin. There are no other anticipated risks or side effects associated with taking part in this study.

What are the possible benefits of taking part?

There are no immediate or direct benefits to you from taking part. Longer term, you and/or others may benefit from any improvements to fabrics that are used in incontinence pads and sanitary towels as a result of this study.

Confidentiality

Your participation in this study will not involve accessing any of your medical information. Only your name and age will be passed to us from your nursing home manager. Results from this study will be made anonymous so they cannot be linked to you. Your GP will be informed of your participation in the study **only** if you consent to this.

What will happen to the results of the study?

Results from the study will be published widely (in print/conferences) but will be completely anonymous and untraceable back to you. Your personal details will be stored securely and separately from the results gathered from the tests in accordance with the University's policy. A summary of the results will be sent to you after the completion of the work.

What happens if something goes wrong?

If you have concerns about any aspect of this study, please contact one of the researchers (see details below). If you are unhappy with the way you have been dealt with, or in the unlikely event that you suffer any harm, please speak to your nursing home manager.

Who has reviewed the study?

The study has received ethics approval from the London Stanmore Research Ethics Committee.

What happens next?

Any questions you may have should be answered satisfactorily by the researchers. If you wish to take part, you will be asked to sign a consent form. You will be given a copy of the signed consent form.

Thank you very much for your help.

Sabrina Falloon
Tel: 020 7288 3771
E-mail: sabrina.falloon.10@ucl.ac.uk

Vasileios Asimakopoulos
Tel: 020 7288 5150
E-mail: v.asimakopoulos@ucl.ac.uk

UCL Department of Medical Physics and Bioengineering
Continence & Skin Technology Group

Archway Campus
3rd floor, Clerkenwell Building
Highgate Hill
London
N19 5LW

University College London Continence & Skin Technology Group study into friction between volar forearm skin and nonwoven fabrics

Participant consent form: Students & staff – confidential

(prepared 1 August 2011, Version 1.5)

Chief Investigator's name: Alan Cottenden

Chief Investigator's address: Continence & Skin Technology Group, Third Floor, Clerkenwell Building, Highgate Hill, London N19 5LW

To be completed by the participant:

Please initial the box:

1. I have read the participant information sheet (version 1.4, dated 01/08/2011) about the study that was given to me. ☐
2. I have been given enough information about the study and all my questions have been given a satisfactory answer. ☐

_____ _____

Member of staff providing information Position

3. I understand that my participation is voluntary and that I am free to withdraw at any time without giving any reason, without my medical care or legal rights being affected. ☐
4. I consent to audio visual recordings and photographs of my forearm being taken for this study. ☐
5. I agree to take part in the study. ☐

Participant:

Signature: _____

Print name: _____

Date: _____

Person taking consent:

Signature: _____

Print name: _____

Position: _____

Date: _____

When complete: one copy for participant; original to go in study notes.

UCL Department of Medical Physics and Bioengineering
Continence & Skin Technology Group

Archway Campus
3rd floor, Clerkenwell Building
Highgate Hill
London
N19 5LW

University College London Continence & Skin Technology Group study into friction between volar forearm skin and nonwoven fabrics

Participant consent form: Outpatients – confidential

(prepared 1 August 2011, Version 1.8)

Chief Investigator's name: Alan Cottenden

Chief Investigator's address: Continence & Skin Technology Group, Third Floor, Clerkenwell Building, Highgate Hill, London N19 5LW

To be completed by the participant:

Please initial the box:

1. I have read the participant information sheet (version 1.5, dated 01/08/2011) about the study that was given to me. ☐
2. I have been given enough information about the study and all my questions have been given a satisfactory answer. ☐

_____ _____

Member of staff providing information Position

3. I understand that my participation is voluntary and that I am free to withdraw at any time without giving any reason, without my medical care or legal rights being affected. ☐
4. I consent to audio visual recordings and photographs of my forearm being taken for this study. ☐
5. I agree to the investigators sending a letter to my GP about my participation.* ☐
6. I agree to take part in the study. ☐

*Giving consent to this part is not required for participation in the study.

Participant:

Signature: _____

Print name: _____

Date: _____

Person taking consent:

Signature: _____

Print name: _____

Position: _____

Date: _____

When complete: one copy for participant; one copy to go in participant's medical records; original to go in study notes.

UCL Department of Medical Physics and Bioengineering
Continence & Skin Technology Group

Archway Campus
3rd floor, Clerkenwell Building
Highgate Hill
London
N19 5LW

University College London Continence & Skin Technology Group study into friction between volar forearm skin and nonwoven fabrics

Participant consent form: Nursing Home Residents – confidential

(prepared 1 August 2011, Version 1.5)

Chief Investigator's name: Alan Cottenden

Chief Investigator's address: Continence & Skin Technology Group, Third Floor, Clerkenwell Building, Highgate Hill, London N19 5LW

To be completed by the participant: Please initial the box:

1. I have read the participant information sheet (version 1.6, dated 01/08/2011) about the study that was given to me. ☐
2. I have been given enough information about the study and all my questions have been given a satisfactory answer. ☐

_____ _____
Member of staff providing information Position

3. I understand that my participation is voluntary and that I am free to withdraw at any time without giving any reason, without my medical care or legal rights being affected. ☐
4. I consent to audio visual recordings and photographs of my forearm being taken for this study. ☐
5. I agree to the investigators sending a letter to my GP about my participation.* ☐
6. I agree to take part in the study. ☐

*Giving consent to this part is not required for participation in the study.

Participant:

Signature: _____

Print name: _____

Date: _____

Person taking consent:

Signature: _____

Print name: _____

Position: _____

Date: _____

When complete: one copy for participant; one copy to go in participant's care notes; original to go in study notes.

University College London
Department of Medical Physics & Bioengineering

3rd Floor, Clerkenwell Building
Archway Campus
Highgate Hill
London
N19 5LW

Continence and Skin Technology Group study of friction between nonwoven fabrics and human skin

Volunteers needed!

TO ALL **STAFF AND STUDENTS**:

We are two PhD students carrying out a study on friction between human skin and nonwoven fabrics (the kind used as coverstocks on incontinence pads, diapers and sanitary towels) in order to better understand interaction between the two. It is anticipated that the results of this study will contribute to the improvement of nonwoven fabrics, making them more 'skin-friendly'.

We need 10 volunteers **between the ages of 18 and 64 years** to take part and we are hoping that you will be one of them! Your participation would involve sitting in a our lab while we make measurements on your volar forearm (underside of your lower arm). *See photograph below.* This would be done in no more than two 2-hour sessions and you are welcome to bring a book or DVD to pass the time!

If you are interested in taking part, **please contact one of us in person, by phone or by e-mail and ask for an information sheet!**

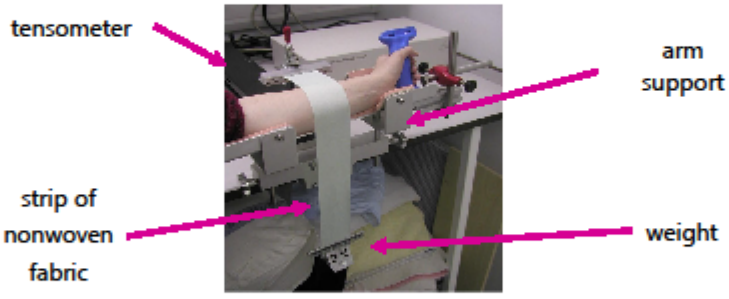

Many thanks,
Sabrina and Vasileios

020 7288 3771 - sabrina.falloon.10@ucl.ac.uk / 020 7288 5150 - v.asimakopoulos@ucl.ac.uk

Version 1.2, 20 July 2011

Participant Involvement Flowchart

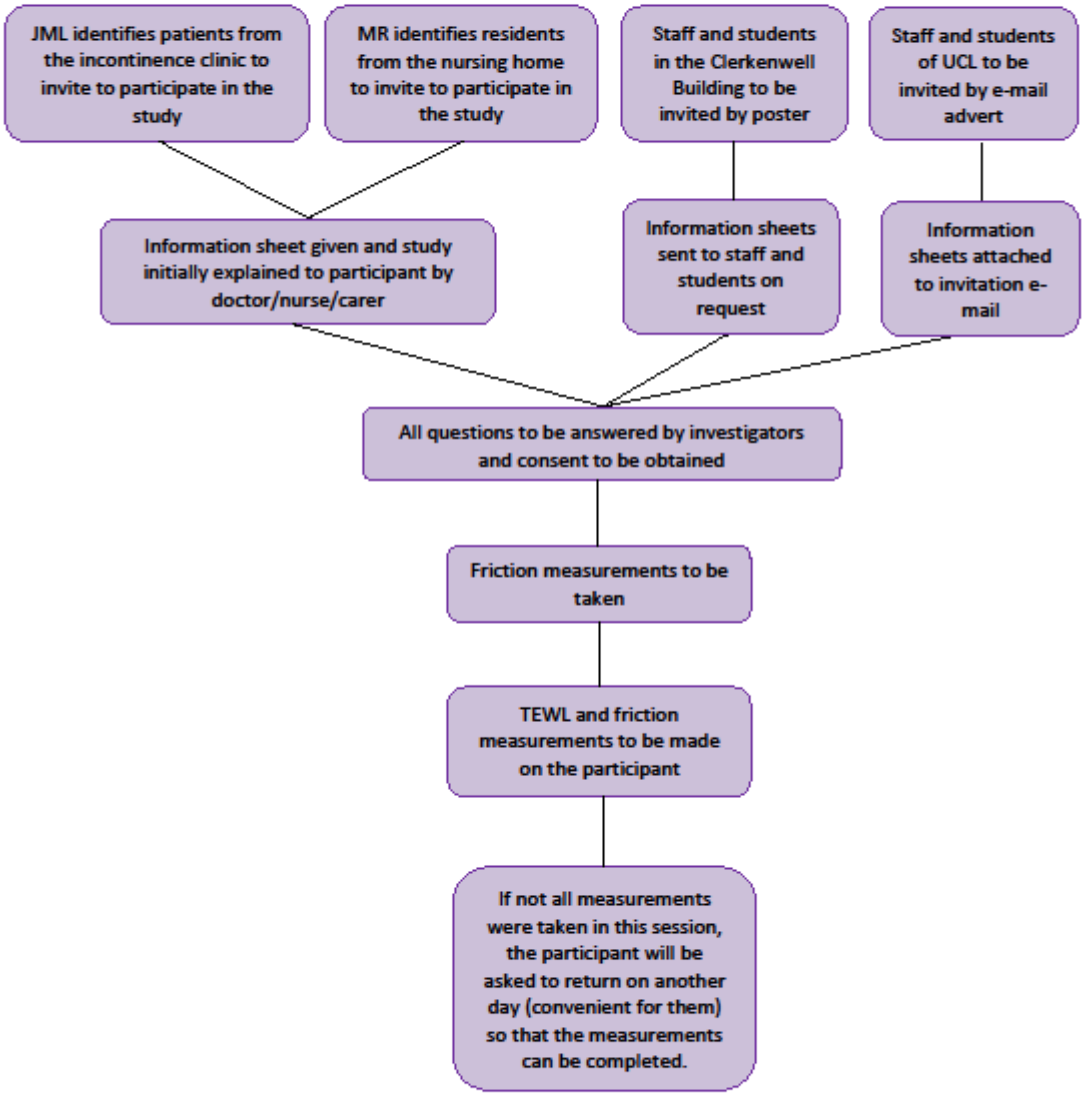

UNIVERSITY COLLEGE LONDON
DEPARTMENT OF MEDICAL PHYSICS AND BIOENGINEERING

Continence and Skin Technology Group
3rd Floor, Clerkenwell Building
Archway Campus
Highgate Hill
London
N19 5LW

<<GP NAME>>
<<GP ADDRESS>>

<<DATE>>

Version 1.3

Re.: <<PATIENT NAME>> - Notification of participation in a study of friction between volar forearm skin and nonwoven fabrics

Dear *<<GP NAME>>*,

The above named patient has consented to take part in a study on friction at the interface of volar forearm skin and nonwoven fabrics (the kind routinely used as coverstocks on incontinence pads, diapers and sanitary towels). This study is being carried out by the Continence and Skin Technology Group at University College London as part of two individual PhD projects. It is funded by UCL and SCA Hygiene Products AB in Sweden, and has been approved by London Stanmore Research Ethics Committee.

Each participant will have a strip of nonwoven fabric pulled across their volar forearm by a Tensometer (pulling machine), while a computer simultaneously measures friction forces between the fabric and skin. All procedures are non-invasive and participants are free to withdraw from the study at any time.

Please do not hesitate to contact either of the investigators for any further information or if you have any concerns regarding your patient's participation.

Thank you for your support in this venture.

Yours sincerely,

Sabrina Falloon, MEng, AMIMechE
PhD Student / Investigator

Tel: 020 7288 3771
E-mail: sabrina.falloon.10@ucl.ac.uk

Vasileios Asimakopoulos, BSc, MSc
PhD Student / Investigator

Tel: 020 7288 5150
E-mail: v.asimakopoulos@ucl.ac.uk

Version 1.2

Dear all,

We are two PhD students carrying out a study on friction between human skin and nonwoven fabrics (the kind used as coverstocks on incontinence pads and sanitary towels) in order to better understand interaction between the two. It is anticipated that the results of this study will contribute to the improvement of nonwoven fabrics, making them more 'skin-friendly'.

We need 10 volunteers **between the ages of 18 and 64 years** to take part and we are hoping that you will be one of them! Your participation would involve coming to the **Archway Campus** of UCL and sitting in a room while we make measurements on your volar forearm (underside of your lower arm). This would be done in no more than two 2-hour sessions and you are welcome to **bring a book or DVD** to pass the time!

All travel costs will be **reimbursed** and refreshments will be provided! If you are interested in taking part, **please read the information sheet** attached to this e-mail and then send an e-mail to sabrina.falloon.10@ucl.ac.uk or v.asimakopoulos@ucl.ac.uk, or call one of the numbers at the bottom of this message.

Many thanks,

Sabrina and Vasileios

Continence & Skin Technology Group
Archway Campus
University College London
+44(0)20 7288 3771 / +44(0)20 7288 5150

NHS
National Research Ethics Service

NRES Committee London - Stanmore
Northwick Park Hospital
Room 019, Level 7 Maternity Block
Watford Road
Harrow
Middlesex
HA1 3UJ

Telephone: 020 8869 3020
Facsimile: 020 8869 5222

12 September 2011

Prof Alan Cottenden
Senior Lecturer
University College London
3rd Floor, Clerkenwell Building
Archway Campus, Highgate Hill
London
N19 5LW

Dear Professor Cottenden

Study title: **An experimental study of friction between skin and nonwoven fabrics.**
REC reference: **11/LO/1324**

The Research Ethics Committee reviewed the above application at the meeting held on 01 September 2011. Thank you, Miss Falloon and Mr Asimakopoulos for attending to discuss the study.

Ethical opinion

The Committee's discussion and comments on this application are identical to your previous application also submitted for this REC meeting. Both applications being very similar.

In discussion, the Committee noted the following ethical issues.

The Committee noted that the recruitment would be carried out by the nursing home manager. There was concern that there ought not to be any coercion of this potentially vulnerable group.

It was noted that the insurance ran out in August 2011. The Committee would require an updated version.

Some general comments were made. The Committee wondered whether in the case of this study it was necessary to inform the GP. Also the Committee questioned why there would be a 6 month follow-up. Some members felt that there was an assumption that participants will want to participate in both the wet and dry friction, maybe some participants would only want to participate in one aspect.

The issues raised above were discussed with you and your students upon you joining the meeting.

The Committee highlighted to you that both students could have applied with one

application as the differences in the work were small.

The Committee asked about whether the time stated to hydrate the skin was enough and whether perhaps the wetting solution could be made slightly acid. You explained that infact it was alkaline conditions rather than acid conditions which caused more skin damage. It was useful for the Committee to be reminded of this.

The Committee asked if it was really necessary to inform the participants' GP. Miss Falloon explained that this was an option and they had offered it out of courtesy. The Committee was content with this.

The Committee asked why you needed to do a 6 month follow-up. Miss Falloon explained that this was not a follow-up as such simply that they had made provision for up to 6 months for participants to come back and have the measurements done again if they hadn't succeeded for any reason the first time. For example if the participants had become tired, not felt well etc. The Committee was content with this.

Members asked if the participants could move their forearm freely while the measurements were being done. Miss Falloon explained that this would not be the case and the participants would need to keep the arm still to eliminate other variables. The Committee also asked why some participants were going to have repeat measurements. Miss Falloon explained that this was to obtain more consistency in the data. The Committee was content with this.

The Committee suggested that perhaps the researchers could try the friction on themselves to get a feel for it. Miss Falloon explained that they had intended to do this.

The issue of possible coercion in the nursing homes was discussed with the researchers. You explained that the research team had a good relation with the nursing home which would be involved in the study and they would ensure proper consenting procedures. You also reassured the Committee that only those who could consent for themselves would be included in the study.

One member also asked if you had factored in the possible effects on skin of exposure to the sun. You had not thought of this. The Committee suggested that you could be mindful of this as it could make the skin a bit more sensitive.

The Committee asked if the participants would be consented once or twice. You said that the consenting would be done only once. The Committee agreed too that this was sensible.

The Committee highlighted to you that the renewed insurance document would be required for the records.

The members of the Committee present gave **a favourable ethical opinion** of the above research on the basis described in the application form, protocol and supporting documentation, subject to the conditions specified below.

Ethical review of research sites

NHS Sites

The favourable opinion applies to all NHS sites taking part in the study, subject to management permission being obtained from the NHS/HSC R&D office prior to the start of the study (see "Conditions of the favourable opinion" below).

Conditions of the favourable opinion

The favourable opinion is subject to the following conditions being met prior to the start of the study.

Management permission or approval must be obtained from each host organisation prior to the start of the study at the site concerned.

Management permission ("R&D approval") should be sought from all NHS organisations involved in the study in accordance with NHS research governance arrangements.

Guidance on applying for NHS permission for research is available in the Integrated Research Application System or at http://www.rdforum.nhs.uk.

Where a NHS organisation's role in the study is limited to identifying and referring potential participants to research sites ("participant identification centre"), guidance should be sought from the R&D office on the information it requires to give permission for this activity.

For non-NHS sites, site management permission should be obtained in accordance with the procedures of the relevant host organisation.

Sponsors are not required to notify the Committee of approvals from host organisations

Additional Condition:

The Committee would require the renewed insurance document for the record, as it had expired in August 2011 .

It is responsibility of the sponsor to ensure that all the conditions are complied with before the start of the study or its initiation at a particular site (as applicable).

You should notify the REC in writing once all conditions have been met (except for site approvals from host organisations) and provide copies of any revised documentation with updated version numbers. Confirmation should also be provided to host organisations together with relevant documentation

Approved documents

The documents reviewed and approved at the meeting were:

Document	*Version*	*Date*
Advertisement	Poster	20 July 2011
Advertisement	Email: 1.2	20 July 2011
Covering Letter		01 August 2011
Evidence of insurance or indemnity		
GP/Consultant Information Sheets	1.3	01 August 2011
Investigator CV		21 July 2011
Letter from Sponsor		15 July 2011
Other: Letter Re: Self-funding		01 August 2011
Other: CV Sabrina Falloon		20 July 2011
Other: CV James Malone-Lee		21 July 2011
Other: CV Mary Rabitte		
Other: Letter of support from academic supervisor		17 June 2011

Participant Consent Form: Outpatients' Consent form	1.8	01 August 2011
Participant Consent Form: Nursing home residents' Consent form	1.5	01 August 2011
Participant Consent Form: Students and staff Consent form	1.5	01 August 2011
Participant Information Sheet: Outpatients' PIS	1.5	01 August 2011
Participant Information Sheet: Nursing home residents' PIS	1.6	01 August 2011
Participant Information Sheet: Research participants' PIS	1.4	01 August 2011
Protocol	2.2	20 July 2011
REC application		02 August 2011
Summary/Synopsis	1.2	20 July 2011

Membership of the Committee

The members of the Ethics Committee who were present at the meeting are listed on the attached sheet.

Statement of compliance

The Committee is constituted in accordance with the Governance Arrangements for Research Ethics Committees (July 2001) and complies fully with the Standard Operating Procedures for Research Ethics Committees in the UK.

After ethical review

Reporting requirements

The attached document "After ethical review – guidance for researchers" gives detailed guidance on reporting requirements for studies with a favourable opinion, including:

- Notifying substantial amendments
- Adding new sites and investigators
- Notification of serious breaches of the protocol
- Progress and safety reports
- Notifying the end of the study

The NRES website also provides guidance on these topics, which is updated in the light of changes in reporting requirements or procedures.

Feedback

You are invited to give your view of the service that you have received from the National Research Ethics Service and the application procedure. If you wish to make your views known please use the feedback form available on the website.

Further information is available at National Research Ethics Service website > After Review

11/LO/1324 **Please quote this number on all correspondence**

With the Committee's best wishes for the success of this project

Yours sincerely

[redacted]

APPENDIX B

Library of tensometer curves from all friction measurements on volar forearms

This appendix contains the tensometer curves for all the volar forearm friction experiments described in Chapter 4. These were five fabrics (SF03, SF14, SF17, SF18 and DC06) and 17 test subjects. The title of each graph has the form of PPPP_AA_FFFF, where PPPP is the code of each participant, AA is the age of each participant and FFFF is the code of the fabric of each participant. For most subjects two repeat measurements were made for each dead weight load, for each fabric (first and second run).

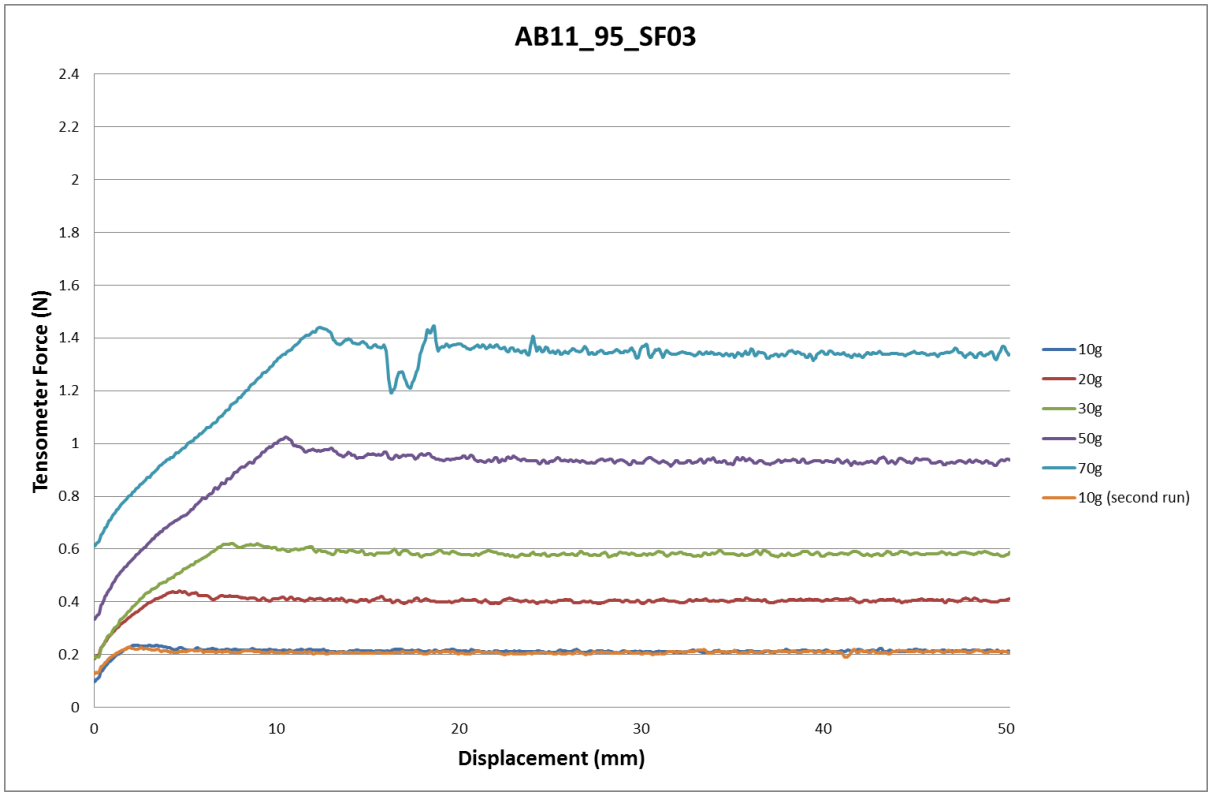
AB11_95_SF03
Tensometer Force (N)
Displacement (mm)
0
0.2
0.4
0.6
0.8
1
1.2
1.4
1.6
1.8
2
2.2
2.4
0
10
20
30
40
50
10g
20g
30g
50g
70g
10g (second run)

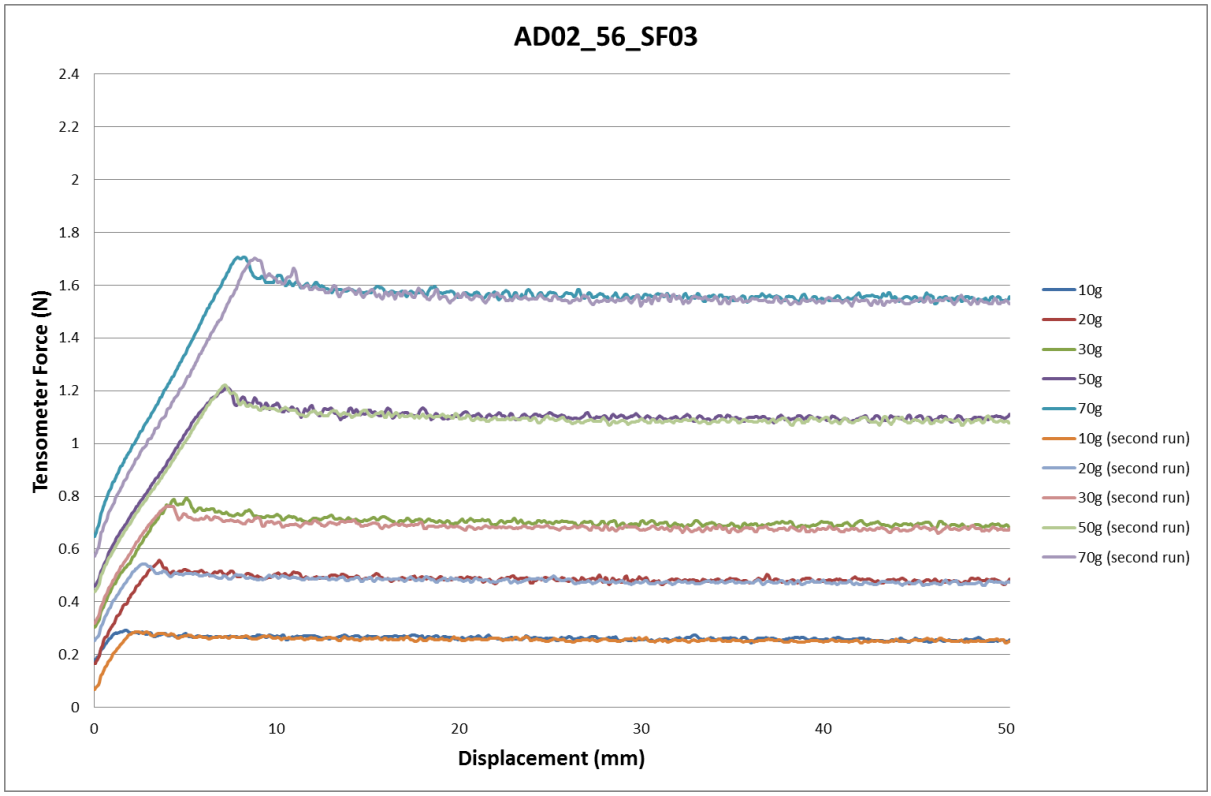
AD02_56_SF03
Tensometer Force (N)
Displacement (mm)
0
0.2
0.4
0.6
0.8
1
1.2
1.4
1.6
1.8
2
2.2
2.4
0
10
20
30
40
50
10g
20g
30g
50g
70g
10g (second run)
20g (second run)
30g (second run)
50g (second run)
70g (second run)

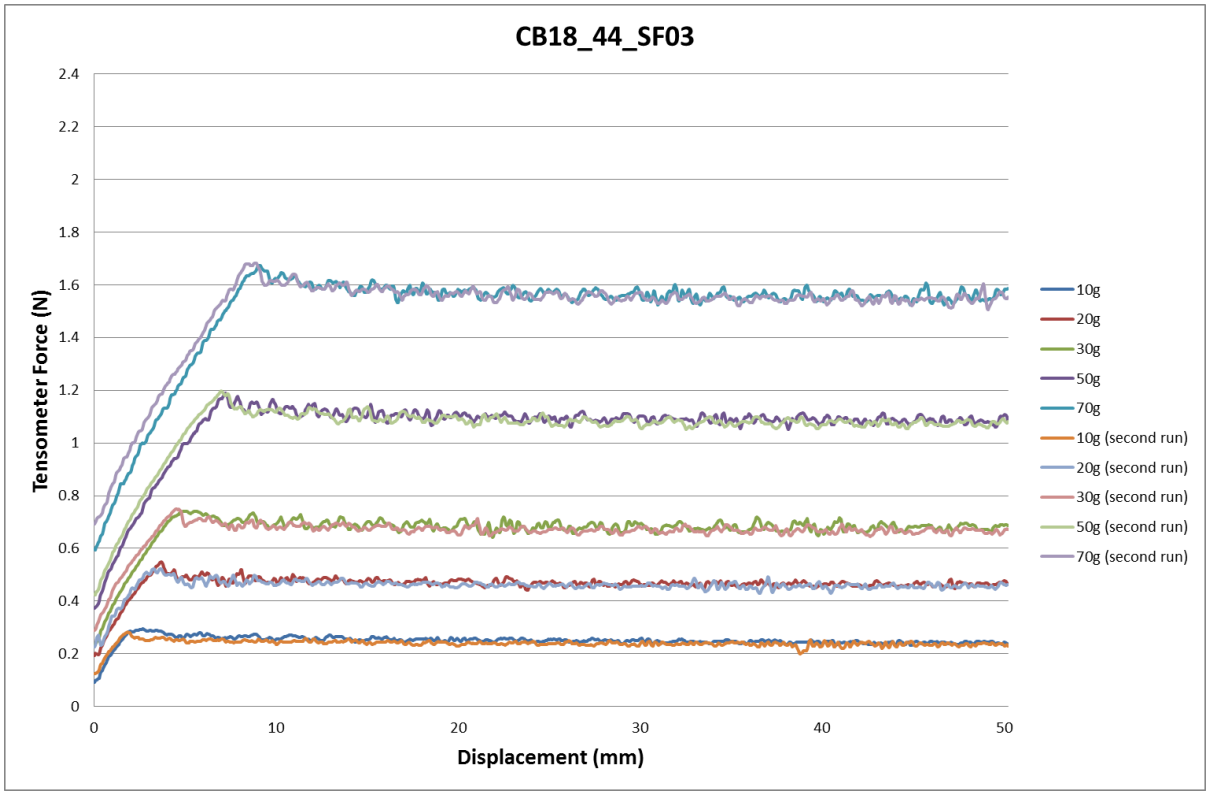
CB18_44_SF03
Tensometer Force (N)
Displacement (mm)
0
0.2
0.4
0.6
0.8
1
1.2
1.4
1.6
1.8
2
2.2
2.4
0
10
20
30
40
50
10g
20g
30g
50g
70g
10g (second run)
20g (second run)
30g (second run)
50g (second run)
70g (second run)

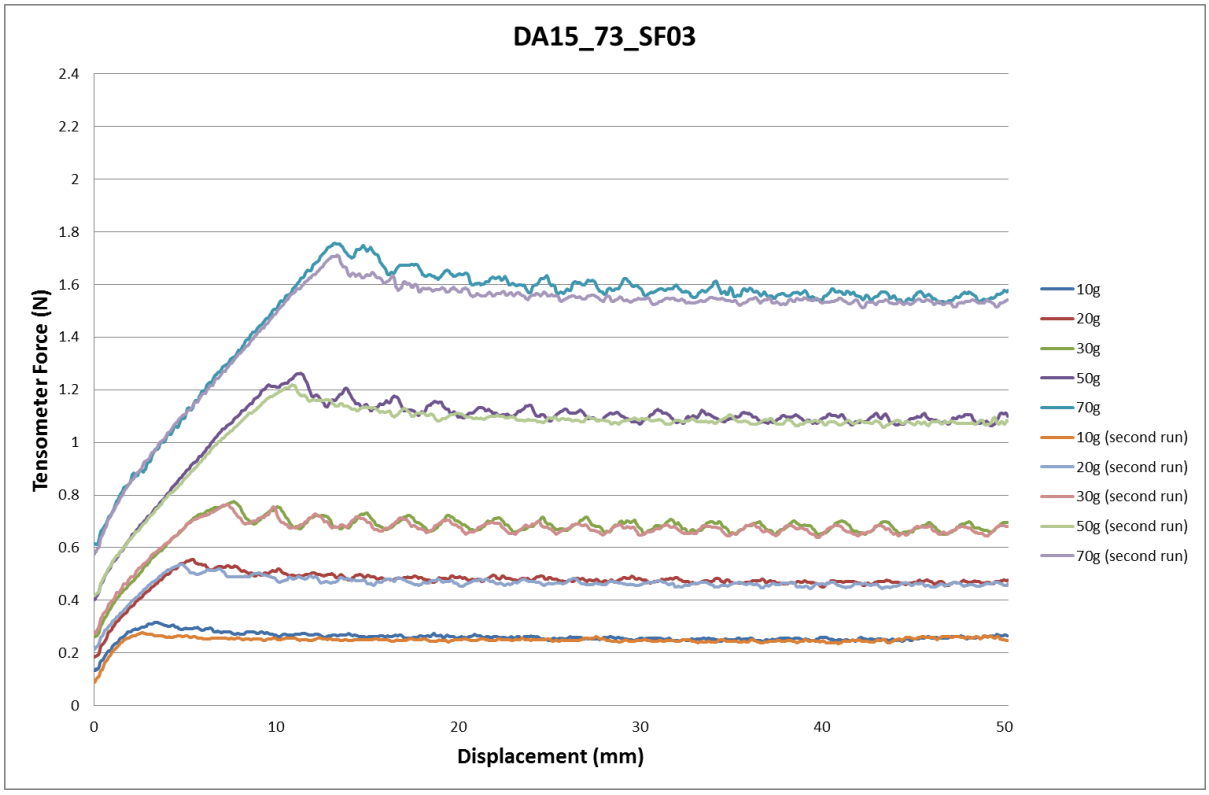
DA15_73_SF03
Tensometer Force (N)
Displacement (mm)
0
0.2
0.4
0.6
0.8
1
1.2
1.4
1.6
1.8
2
2.2
2.4
0
10
20
30
40
50
10g
20g
30g
50g
70g
10g (second run)
20g (second run)
30g (second run)
50g (second run)
70g (second run)

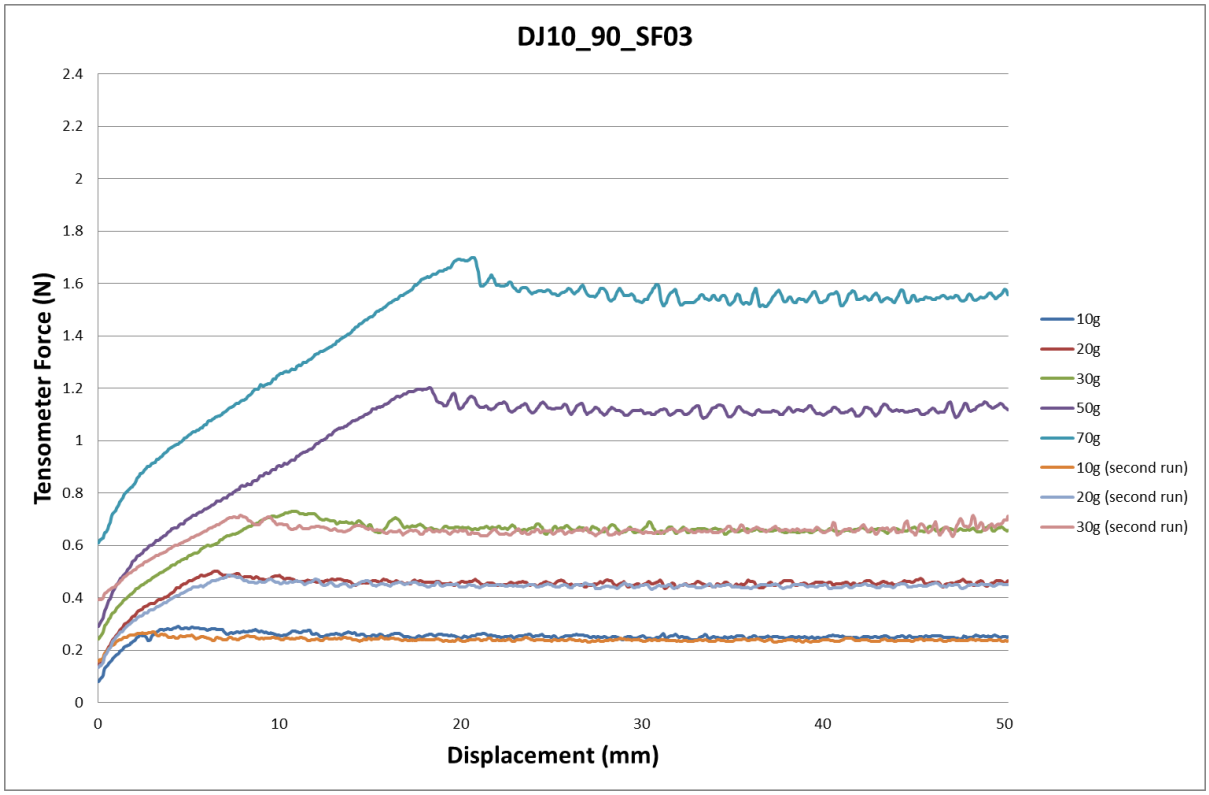
DJ10_90_SF03
Tensometer Force (N)
Displacement (mm)
0
0.2
0.4
0.6
0.8
1
1.2
1.4
1.6
1.8
2
2.2
2.4
0
10
20
30
40
50
10g
20g
30g
50g
70g
10g (second run)
20g (second run)
30g (second run)

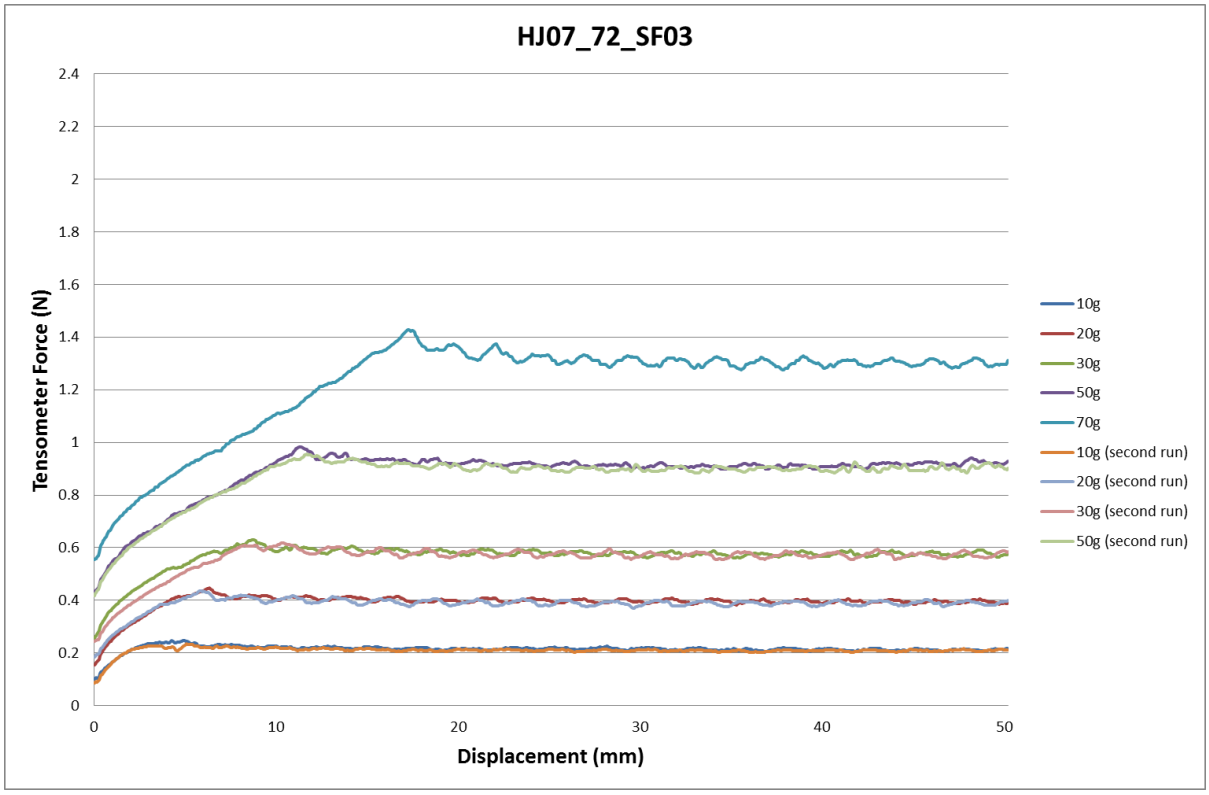
HJ07_72_SF03
Tensometer Force (N)
Displacement (mm)
0
0.2
0.4
0.6
0.8
1
1.2
1.4
1.6
1.8
2
2.2
2.4
0
10
20
30
40
50
10g
20g
30g
50g
70g
10g (second run)
20g (second run)
30g (second run)
50g (second run)

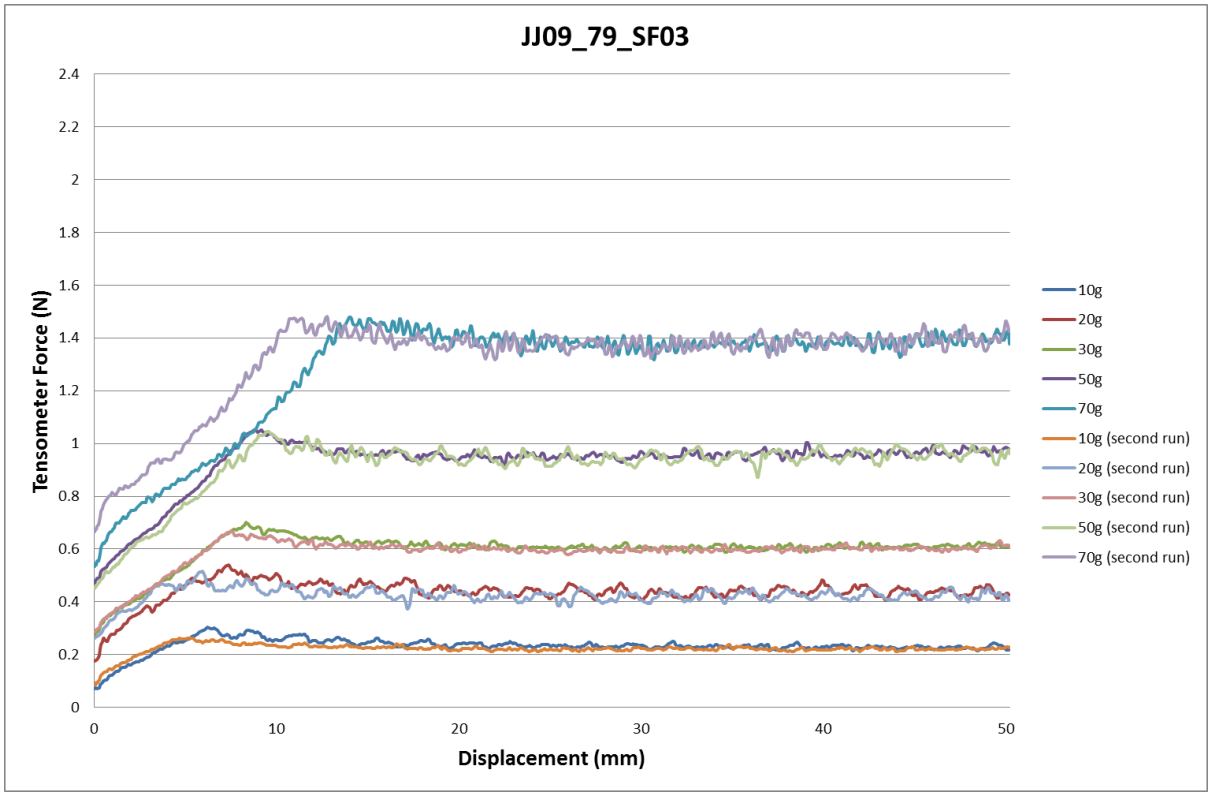
JJ09_79_SF03
Tensometer Force (N)
Displacement (mm)
0
0.2
0.4
0.6
0.8
1
1.2
1.4
1.6
1.8
2
2.2
2.4
0
10
20
30
40
50
10g
20g
30g
50g
70g
10g (second run)
20g (second run)
30g (second run)
50g (second run)
70g (second run)

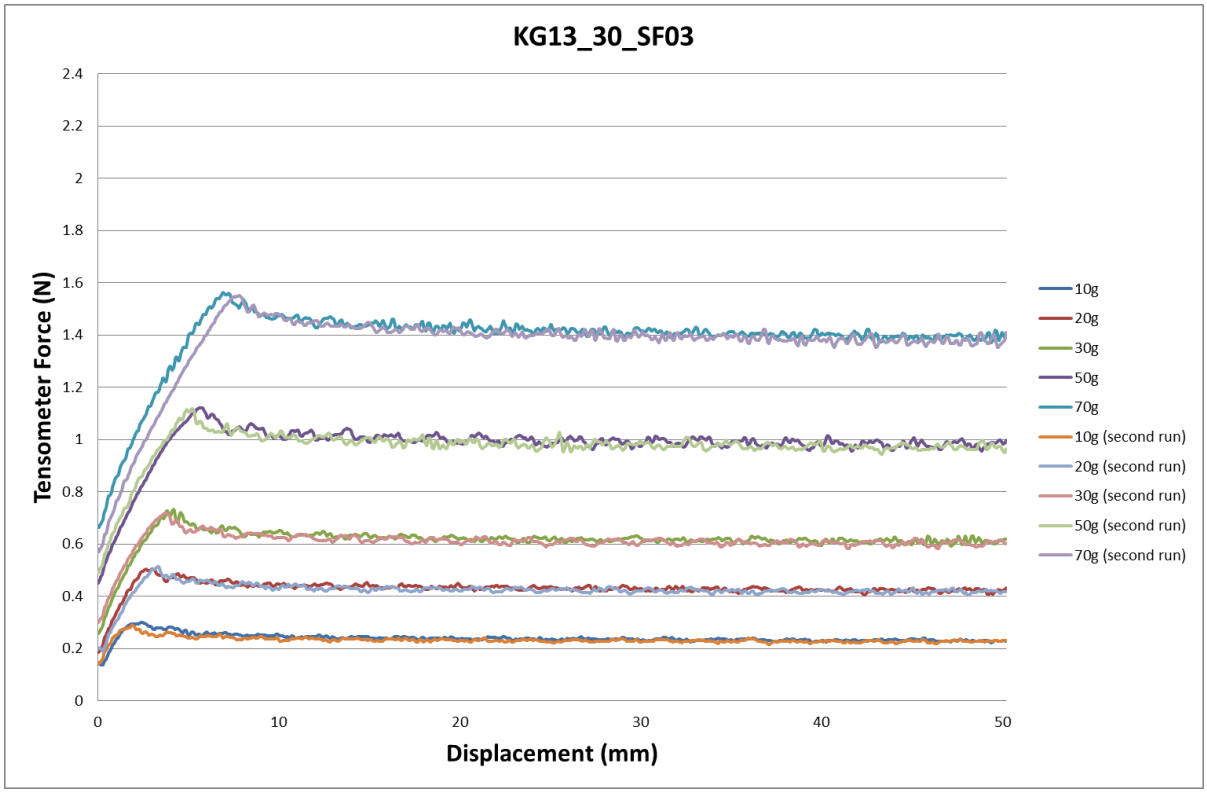
KG13_30_SF03
Tensometer Force (N)
Displacement (mm)
0
0.2
0.4
0.6
0.8
1
1.2
1.4
1.6
1.8
2
2.2
2.4
0
10
20
30
40
50
10g
20g
30g
50g
70g
10g (second run)
20g (second run)
30g (second run)
50g (second run)
70g (second run)

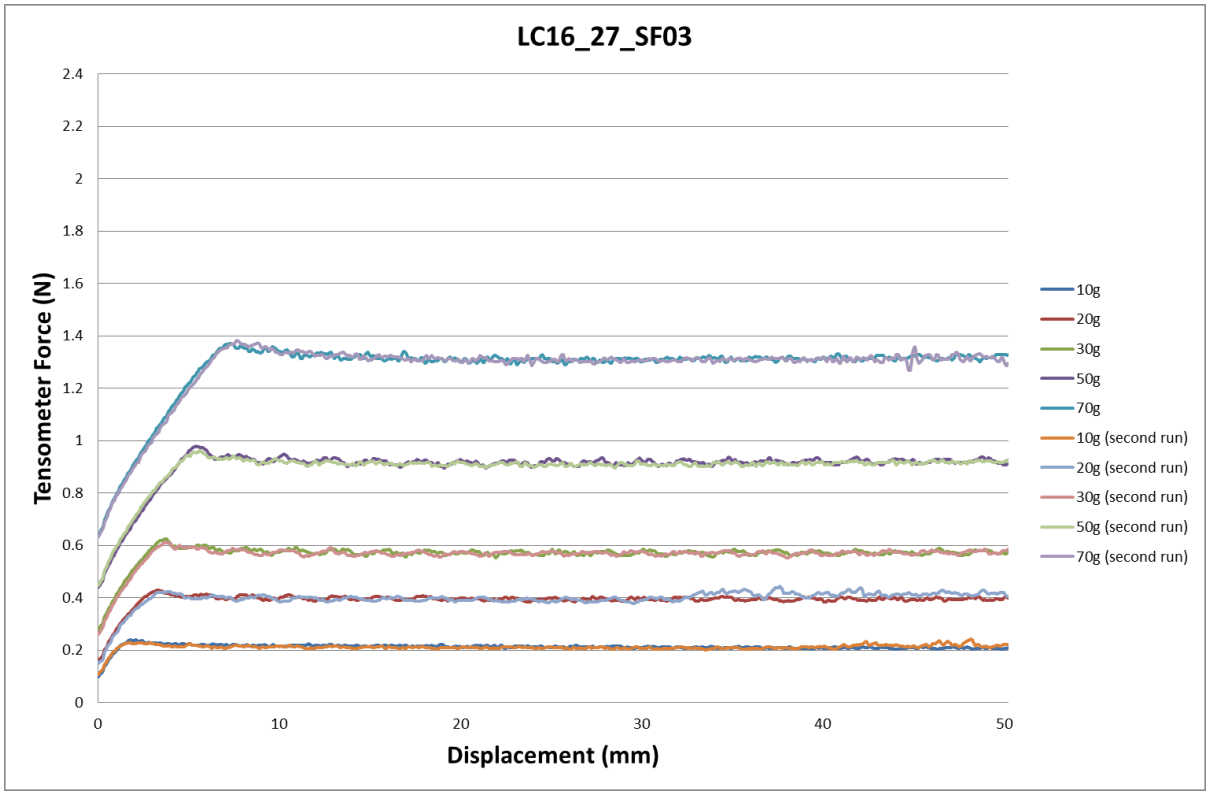
LC16_27_SF03
Tensometer Force (N)
Displacement (mm)
0
0.2
0.4
0.6
0.8
1
1.2
1.4
1.6
1.8
2
2.2
2.4
0
10
20
30
40
50
10g
20g
30g
50g
70g
10g (second run)
20g (second run)
30g (second run)
50g (second run)
70g (second run)

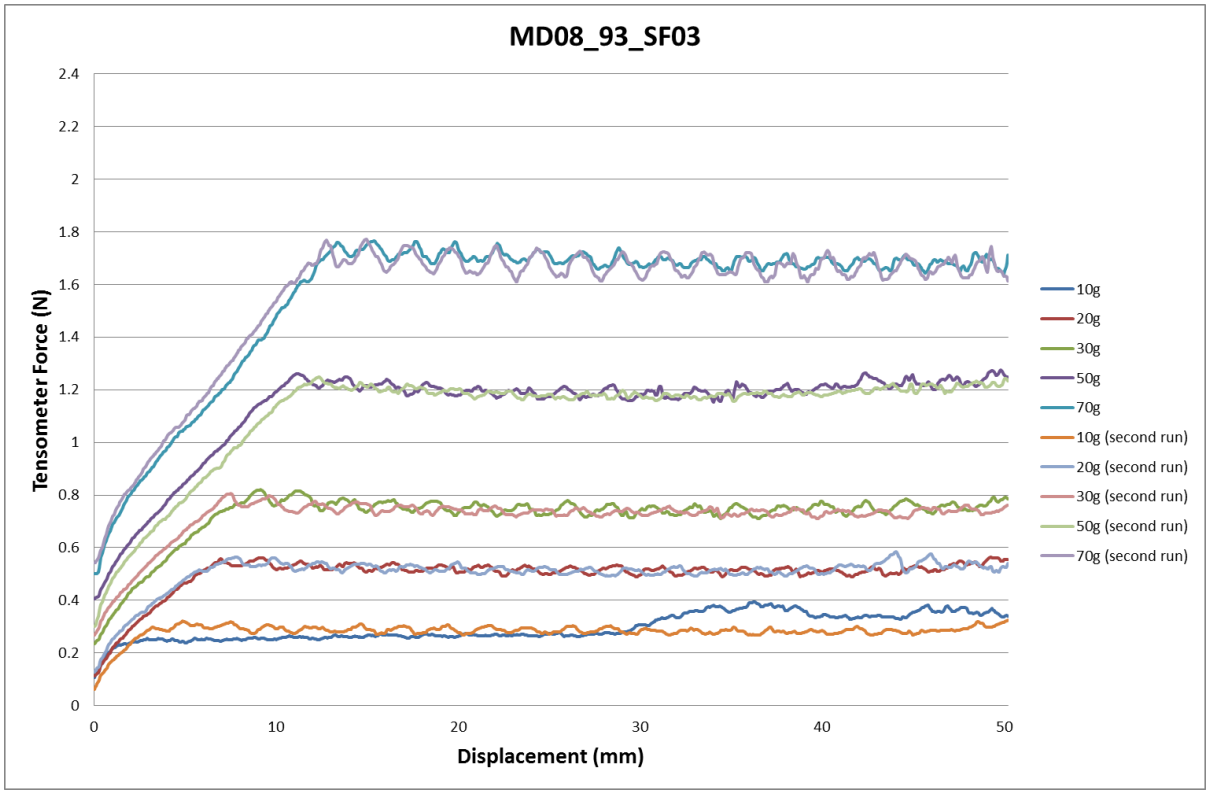
MD08_93_SF03
Tensometer Force (N)
Displacement (mm)
0
0.2
0.4
0.6
0.8
1
1.2
1.4
1.6
1.8
2
2.2
2.4
0
10
20
30
40
50
10g
20g
30g
50g
70g
10g (second run)
20g (second run)
30g (second run)
50g (second run)
70g (second run)

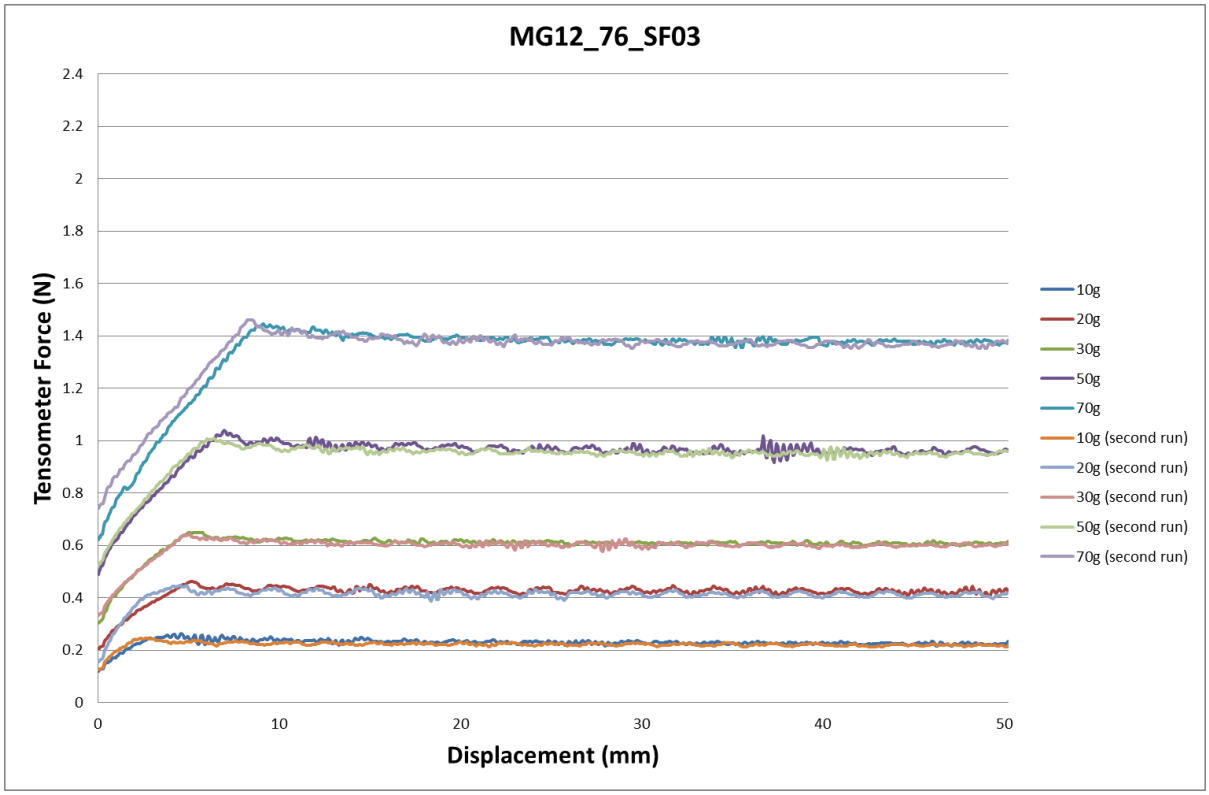
MG12_76_SF03
Tensometer Force (N)
Displacement (mm)
0
0.2
0.4
0.6
0.8
1
1.2
1.4
1.6
1.8
2
2.2
2.4
0
10
20
30
40
50
10g
20g
30g
50g
70g
10g (second run)
20g (second run)
30g (second run)
50g (second run)
70g (second run)

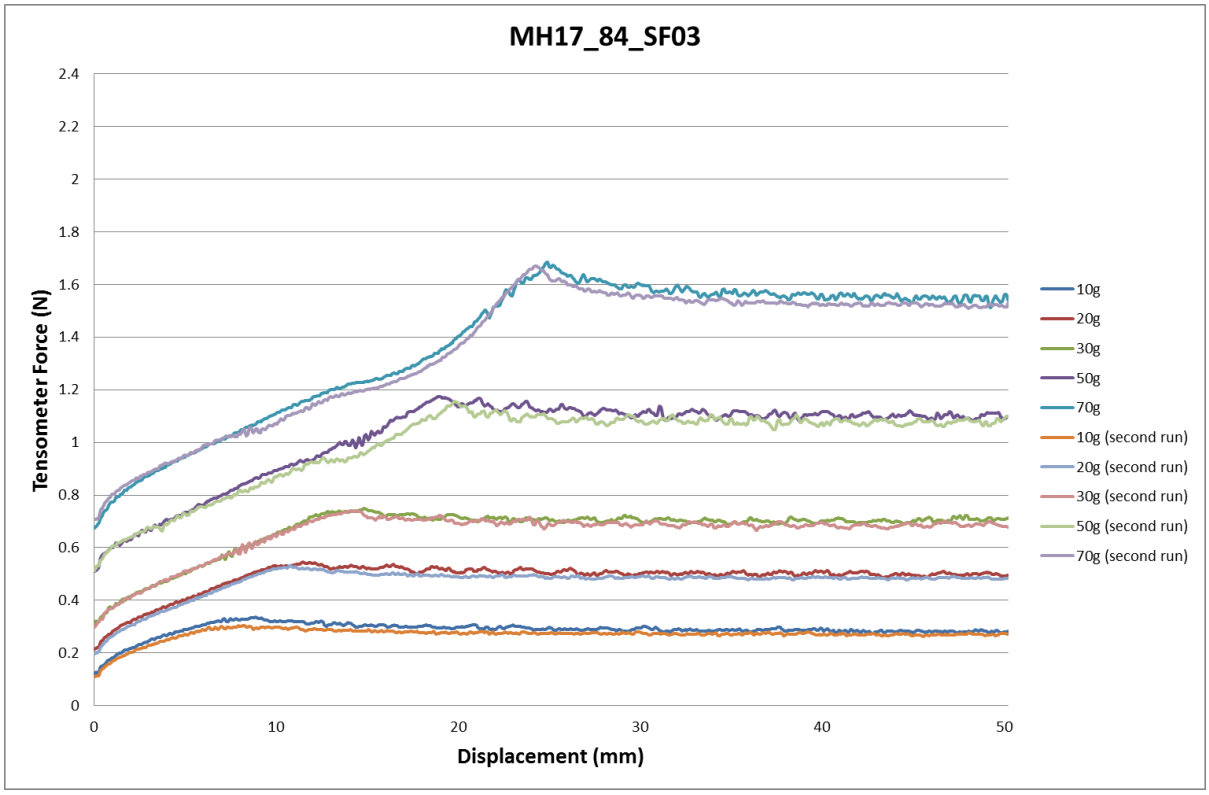
MH17_84_SF03
Tensometer Force (N)
Displacement (mm)
0
0.2
0.4
0.6
0.8
1
1.2
1.4
1.6
1.8
2
2.2
2.4
0
10
20
30
40
50
10g
20g
30g
50g
70g
10g (second run)
20g (second run)
30g (second run)
50g (second run)
70g (second run)

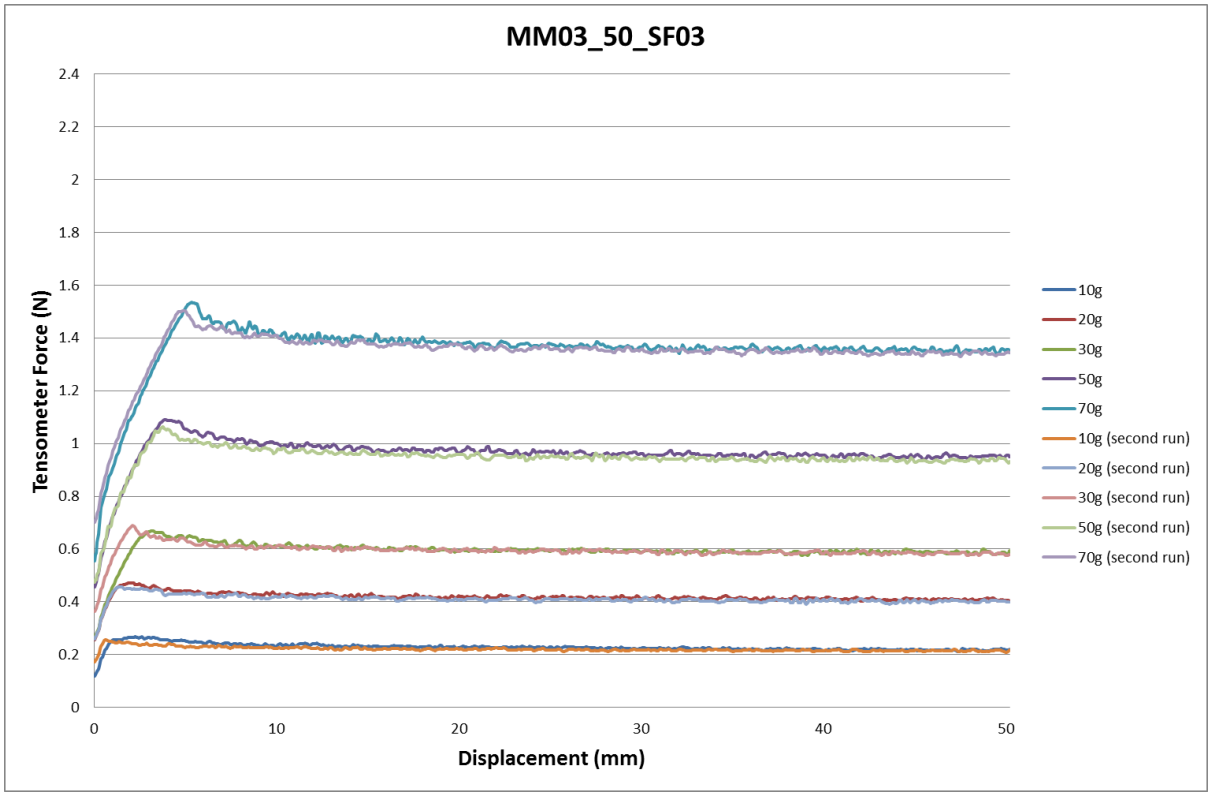
MM03_50_SF03
Tensometer Force (N)
Displacement (mm)
0
0.2
0.4
0.6
0.8
1
1.2
1.4
1.6
1.8
2
2.2
2.4
0
10
20
30
40
50
10g
20g
30g
50g
70g
10g (second run)
20g (second run)
30g (second run)
50g (second run)
70g (second run)

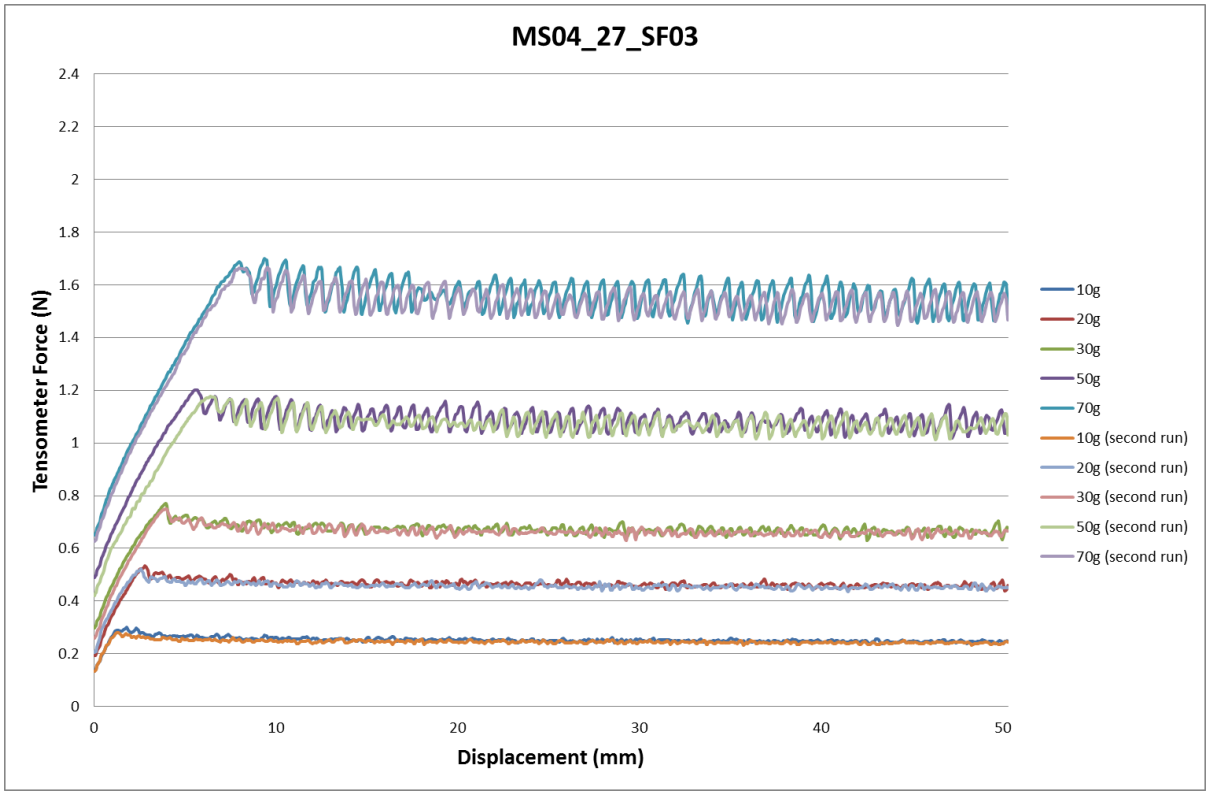
MS04_27_SF03
Tensometer Force (N)
Displacement (mm)
0
0.2
0.4
0.6
0.8
1
1.2
1.4
1.6
1.8
2
2.2
2.4
0
10
20
30
40
50
10g
20g
30g
50g
70g
10g (second run)
20g (second run)
30g (second run)
50g (second run)
70g (second run)

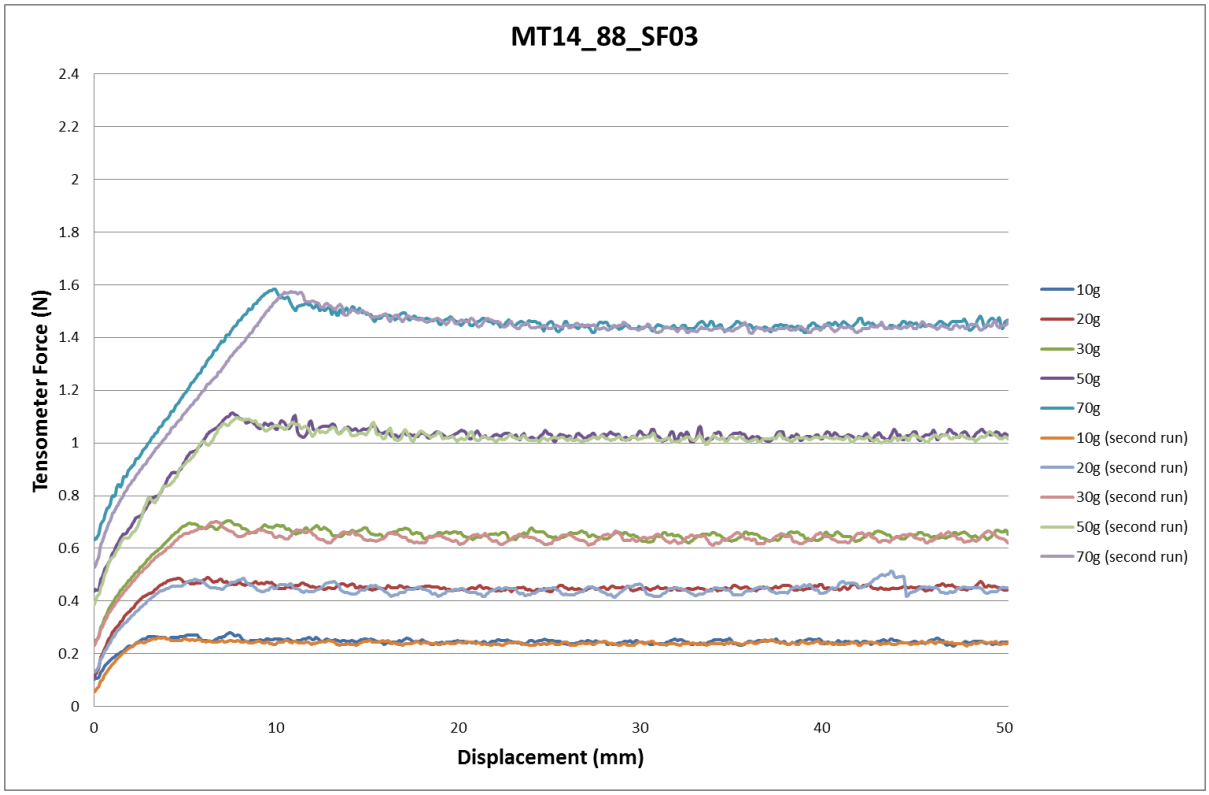
MT14_88_SF03
Tensometer Force (N)
Displacement (mm)
0
0.2
0.4
0.6
0.8
1
1.2
1.4
1.6
1.8
2
2.2
2.4
0
10
20
30
40
50
10g
20g
30g
50g
70g
10g (second run)
20g (second run)
30g (second run)
50g (second run)
70g (second run)

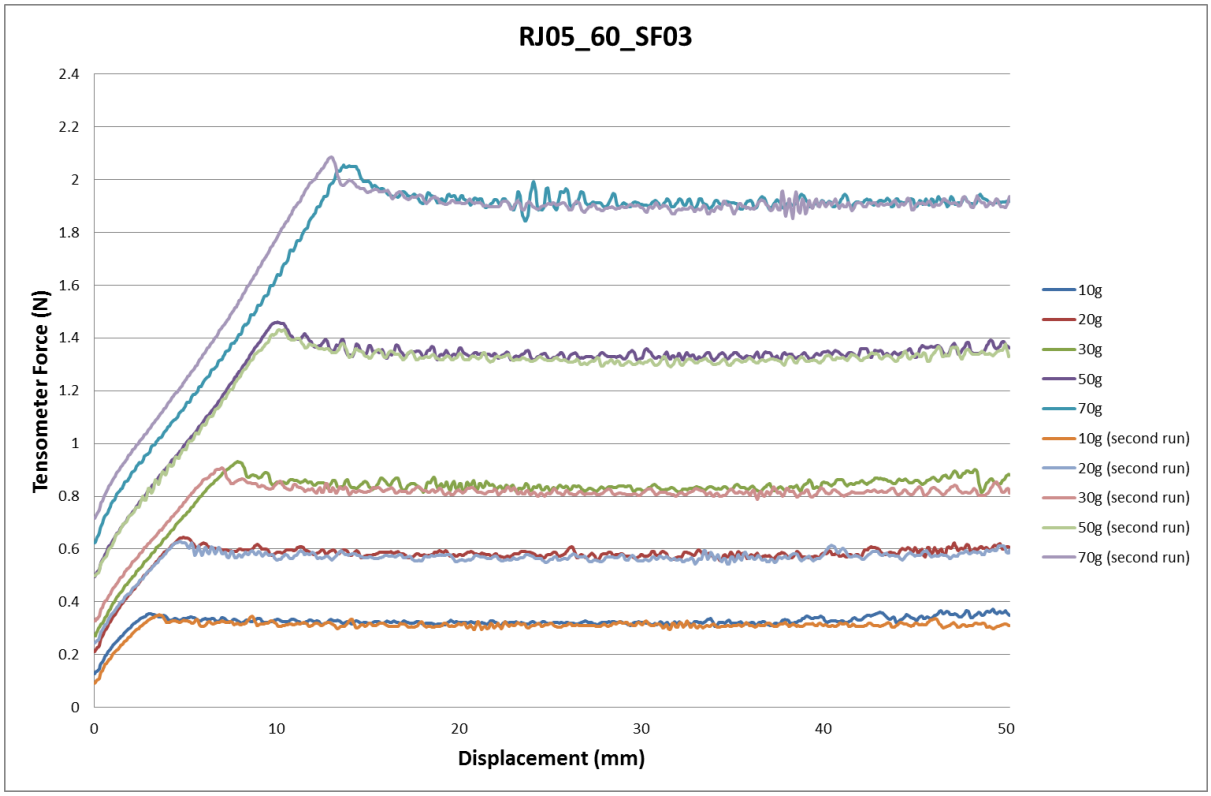
RJ05_60_SF03
Tensometer Force (N)
Displacement (mm)
0
0.2
0.4
0.6
0.8
1
1.2
1.4
1.6
1.8
2
2.2
2.4
0
10
20
30
40
50
10g
20g
30g
50g
70g
10g (second run)
20g (second run)
30g (second run)
50g (second run)
70g (second run)

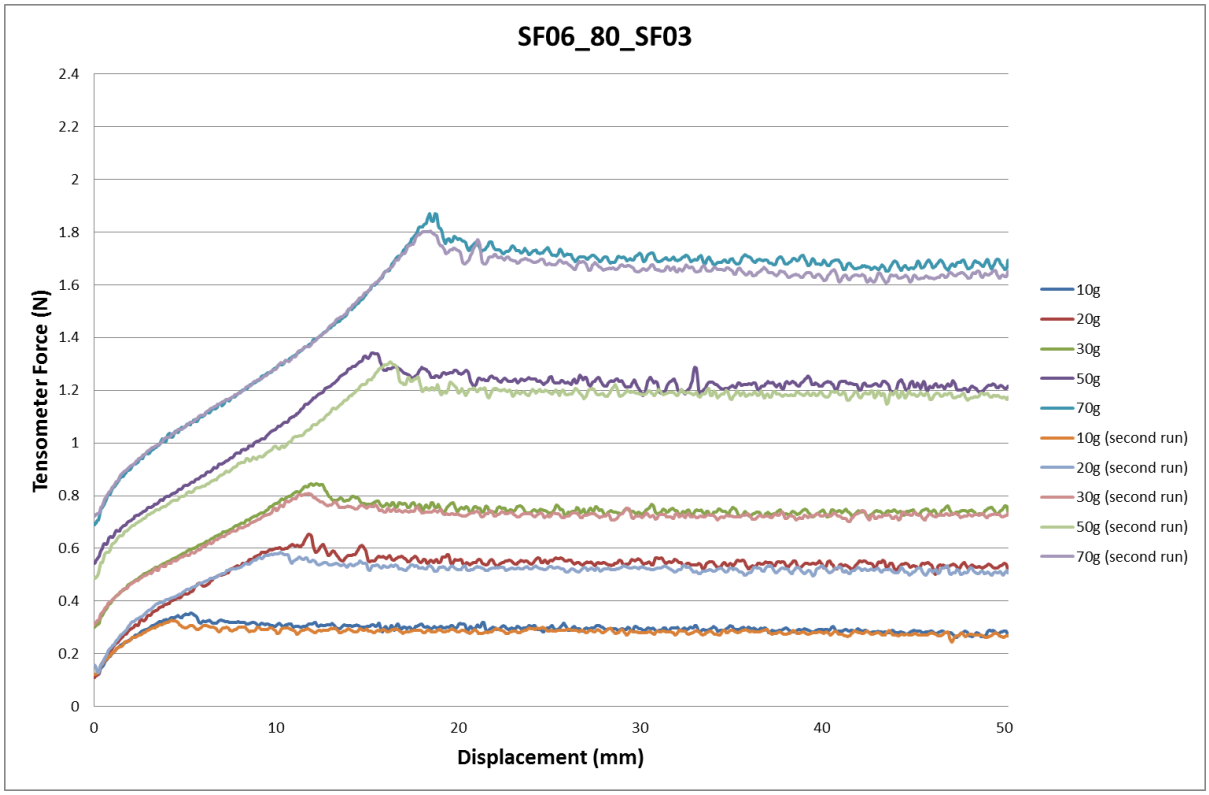
SF06_80_SF03
Tensometer Force (N)
Displacement (mm)
0
0.2
0.4
0.6
0.8
1
1.2
1.4
1.6
1.8
2
2.2
2.4
0
10
20
30
40
50
10g
20g
30g
50g
70g
10g (second run)
20g (second run)
30g (second run)
50g (second run)
70g (second run)

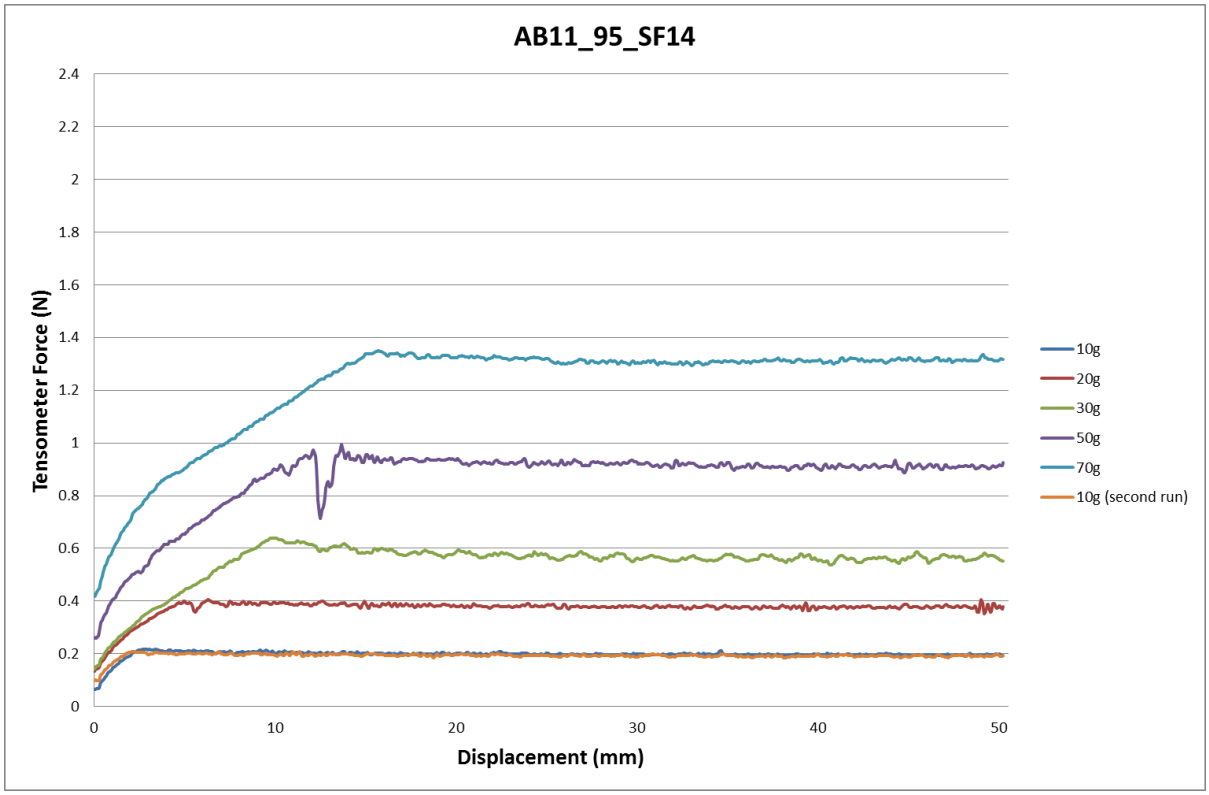
AB11_95_SF14
Tensometer Force (N)
Displacement (mm)
0
0.2
0.4
0.6
0.8
1
1.2
1.4
1.6
1.8
2
2.2
2.4
0
10
20
30
40
50
10g
20g
30g
50g
70g
10g (second run)

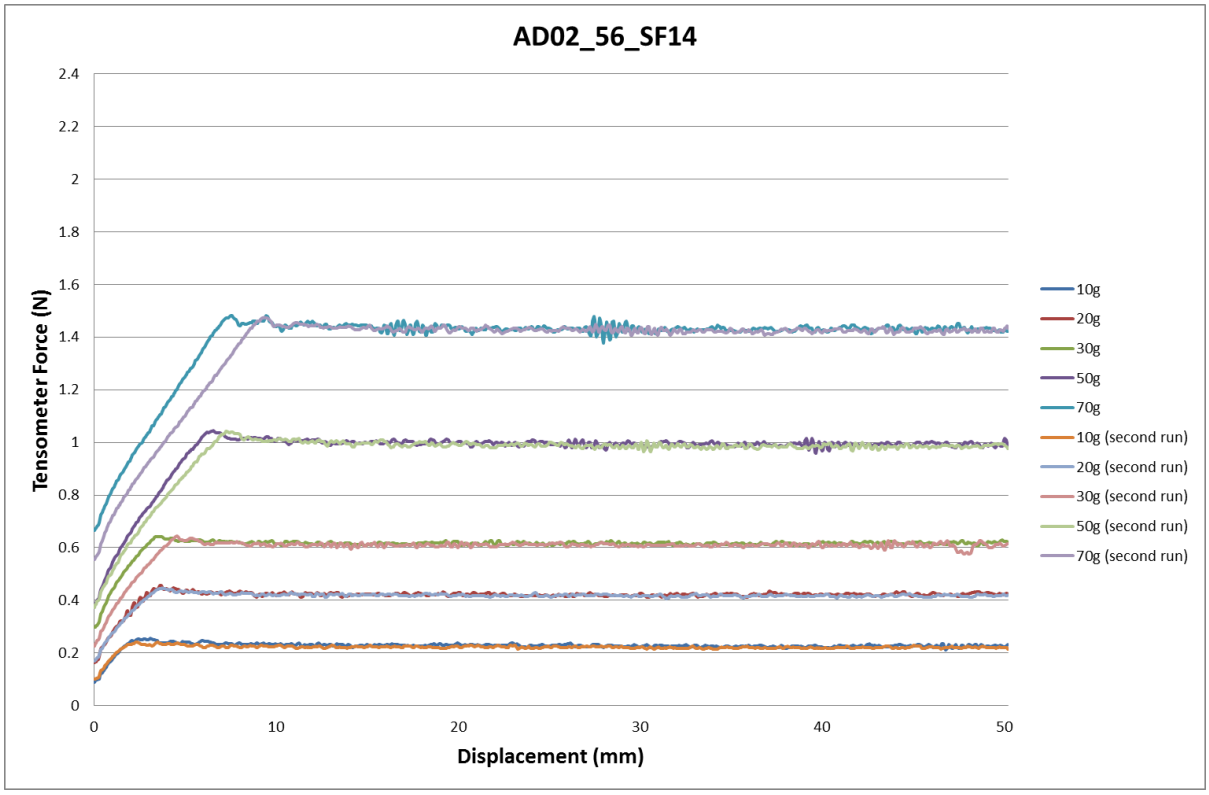
AD02_56_SF14
Tensometer Force (N)
Displacement (mm)
0
0.2
0.4
0.6
0.8
1
1.2
1.4
1.6
1.8
2
2.2
2.4
0
10
20
30
40
50
10g
20g
30g
50g
70g
10g (second run)
20g (second run)
30g (second run)
50g (second run)
70g (second run)

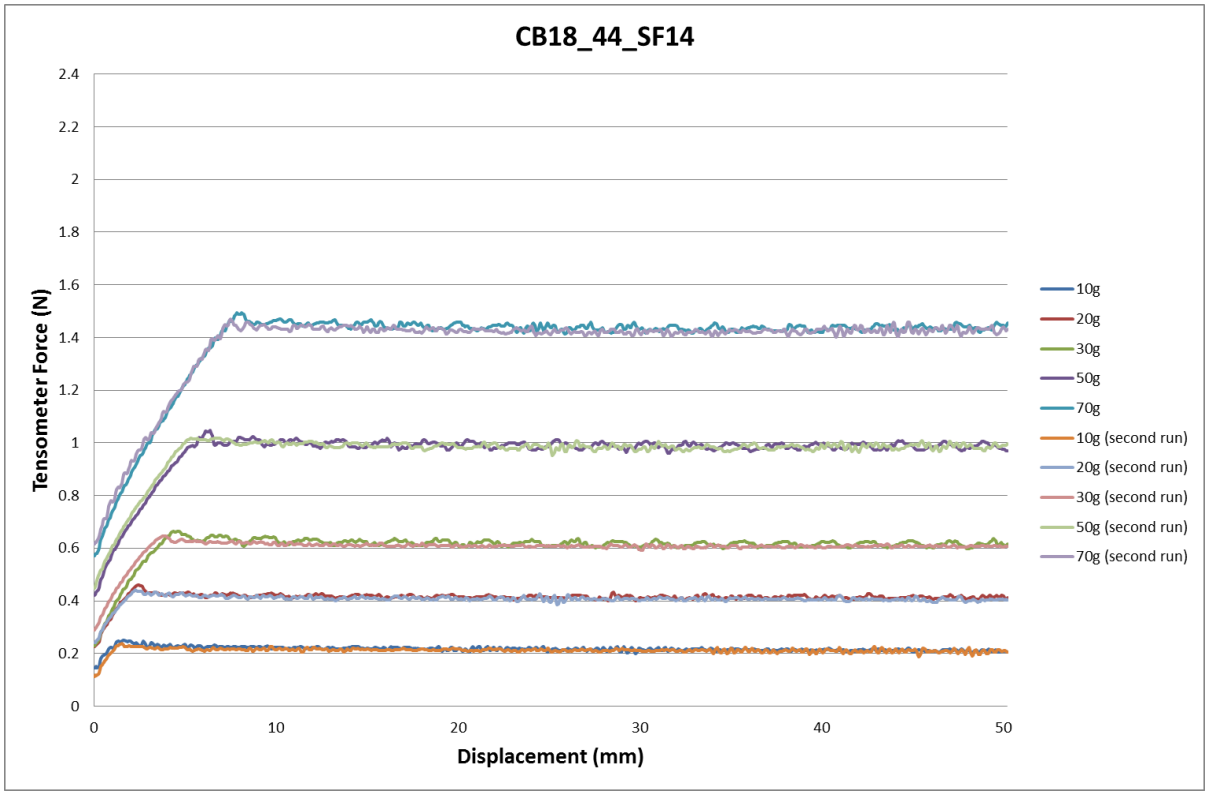
CB18_44_SF14
Tensometer Force (N)
Displacement (mm)
0
0.2
0.4
0.6
0.8
1
1.2
1.4
1.6
1.8
2
2.2
2.4
0
10
20
30
40
50
10g
20g
30g
50g
70g
10g (second run)
20g (second run)
30g (second run)
50g (second run)
70g (second run)

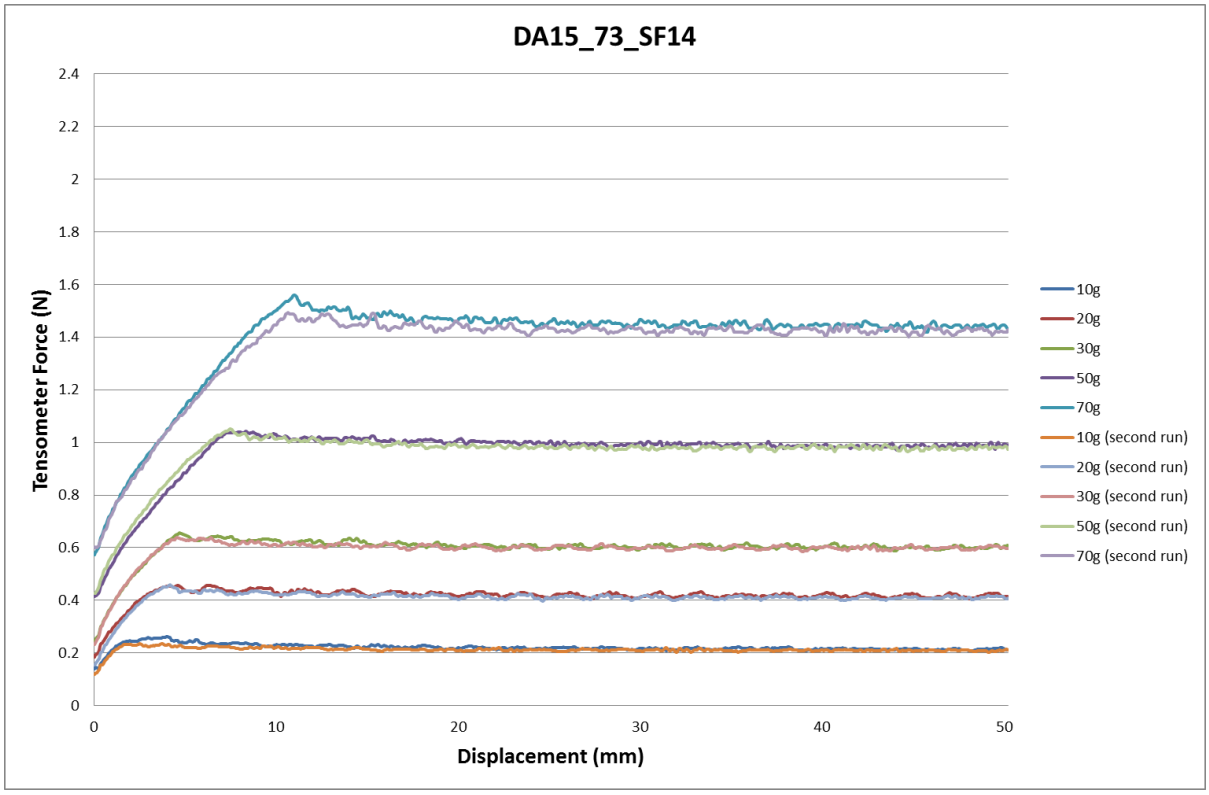
DA15_73_SF14
Tensometer Force (N)
Displacement (mm)
0
0.2
0.4
0.6
0.8
1
1.2
1.4
1.6
1.8
2
2.2
2.4
0
10
20
30
40
50
10g
20g
30g
50g
70g
10g (second run)
20g (second run)
30g (second run)
50g (second run)
70g (second run)

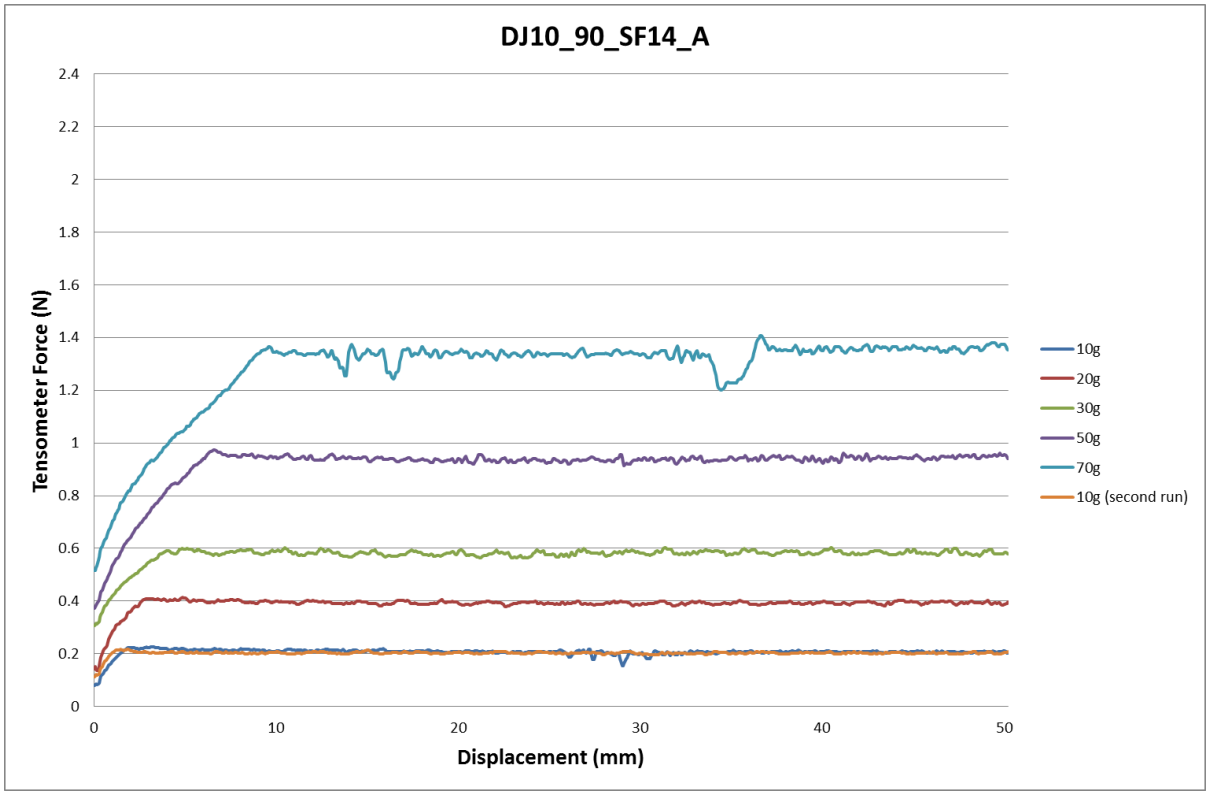
DJ10_90_SF14_A
Tensometer Force (N)
Displacement (mm)
0
0.2
0.4
0.6
0.8
1
1.2
1.4
1.6
1.8
2
2.2
2.4
0
10
20
30
40
50
10g
20g
30g
50g
70g
10g (second run)

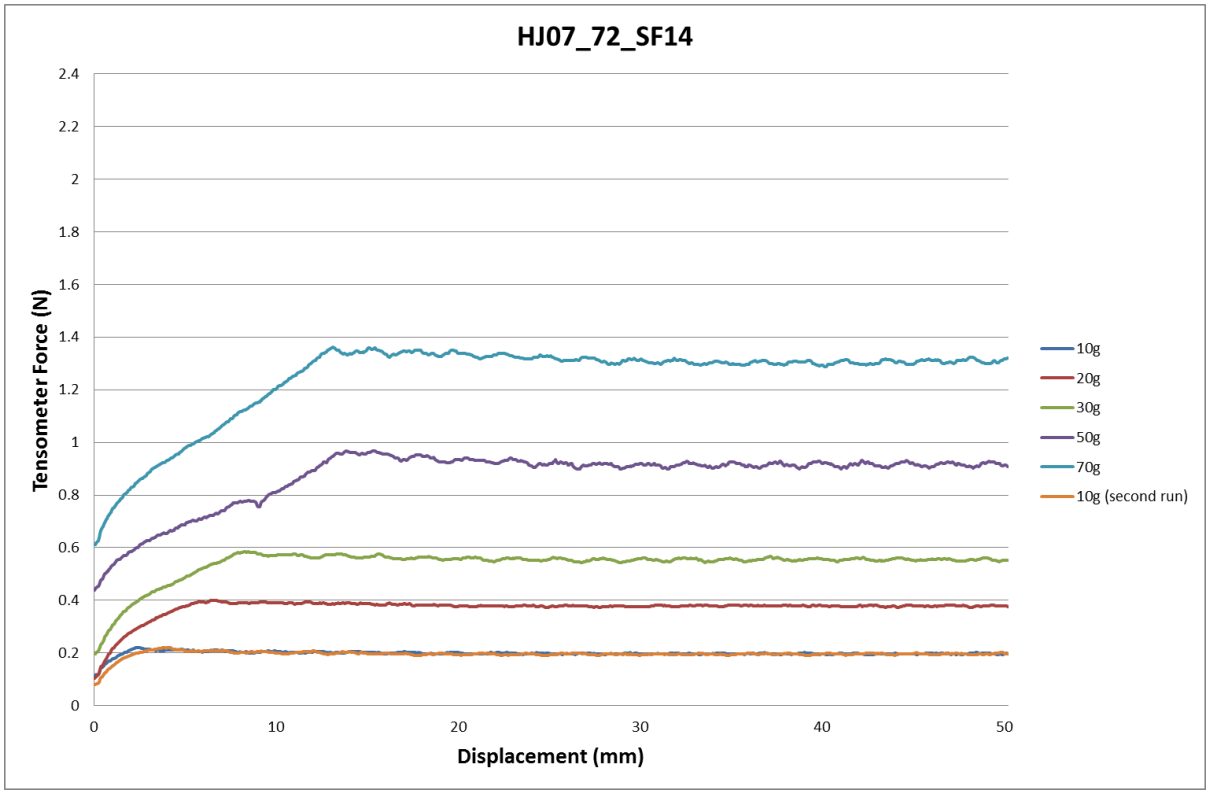
HJ07_72_SF14
Tensometer Force (N)
Displacement (mm)
0
0.2
0.4
0.6
0.8
1
1.2
1.4
1.6
1.8
2
2.2
2.4
0
10
20
30
40
50
10g
20g
30g
50g
70g
10g (second run)

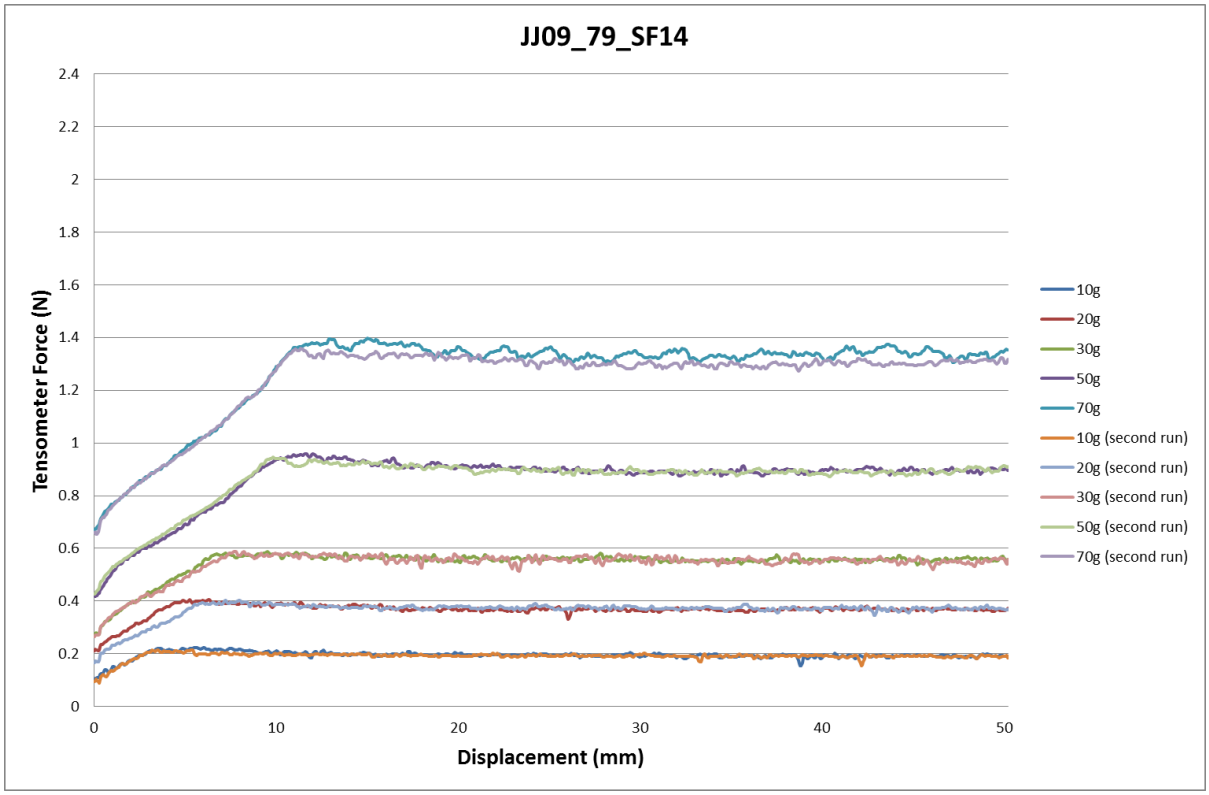
JJ09_79_SF14
Tensometer Force (N)
Displacement (mm)
0
0.2
0.4
0.6
0.8
1
1.2
1.4
1.6
1.8
2
2.2
2.4
0
10
20
30
40
50
10g
20g
30g
50g
70g
10g (second run)
20g (second run)
30g (second run)
50g (second run)
70g (second run)

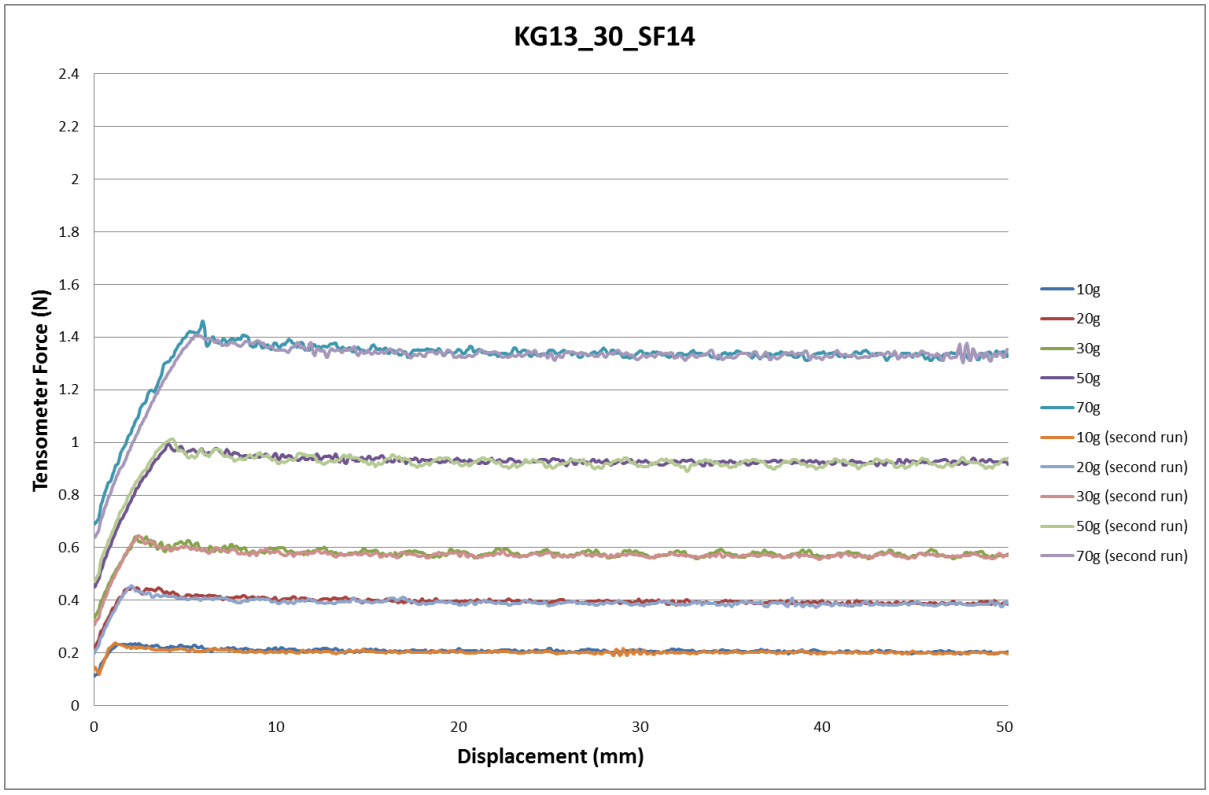
KG13_30_SF14
Tensometer Force (N)
Displacement (mm)
0
0.2
0.4
0.6
0.8
1
1.2
1.4
1.6
1.8
2
2.2
2.4
0
10
20
30
40
50
10g
20g
30g
50g
70g
10g (second run)
20g (second run)
30g (second run)
50g (second run)
70g (second run)

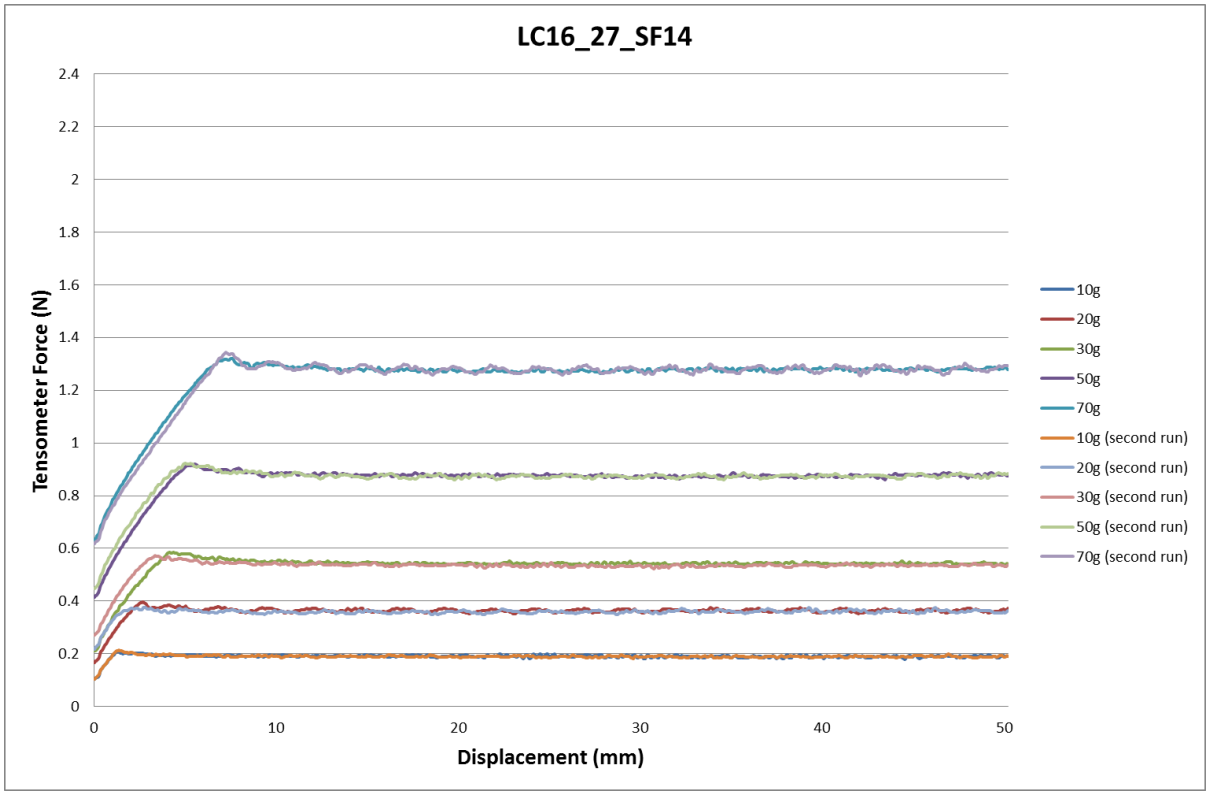
LC16_27_SF14
Tensometer Force (N)
Displacement (mm)
0
0.2
0.4
0.6
0.8
1
1.2
1.4
1.6
1.8
2
2.2
2.4
0
10
20
30
40
50
10g
20g
30g
50g
70g
10g (second run)
20g (second run)
30g (second run)
50g (second run)
70g (second run)

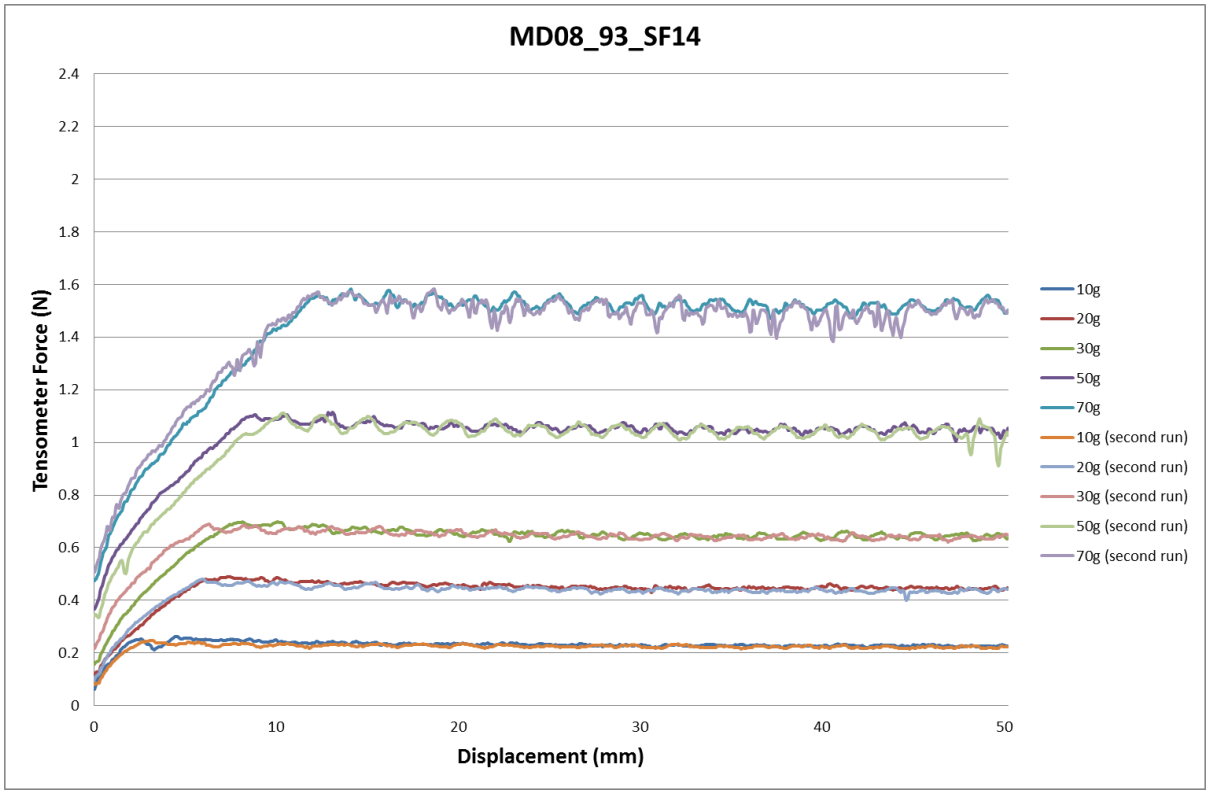
MD08_93_SF14
Tensometer Force (N)
Displacement (mm)
0
0.2
0.4
0.6
0.8
1
1.2
1.4
1.6
1.8
2
2.2
2.4
0
10
20
30
40
50
10g
20g
30g
50g
70g
10g (second run)
20g (second run)
30g (second run)
50g (second run)
70g (second run)

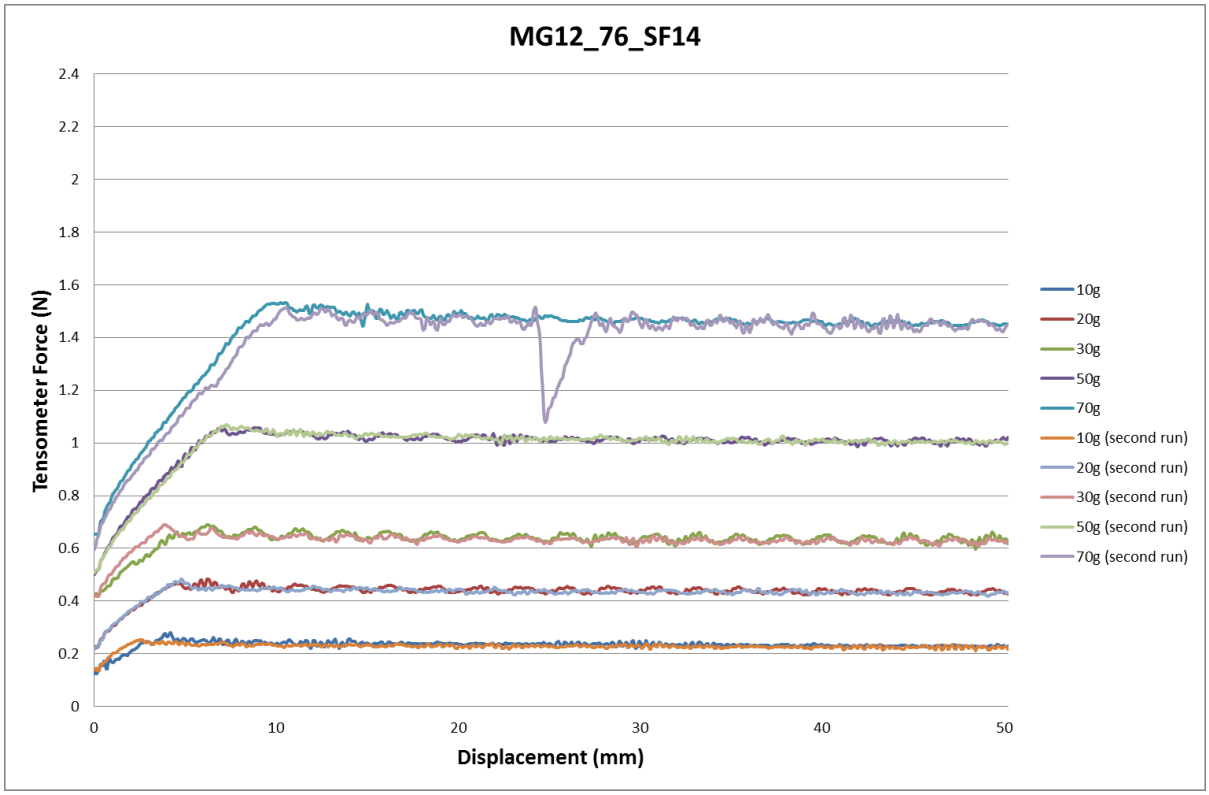
MG12_76_SF14
Tensometer Force (N)
Displacement (mm)
0
0.2
0.4
0.6
0.8
1
1.2
1.4
1.6
1.8
2
2.2
2.4
0
10
20
30
40
50
10g
20g
30g
50g
70g
10g (second run)
20g (second run)
30g (second run)
50g (second run)
70g (second run)

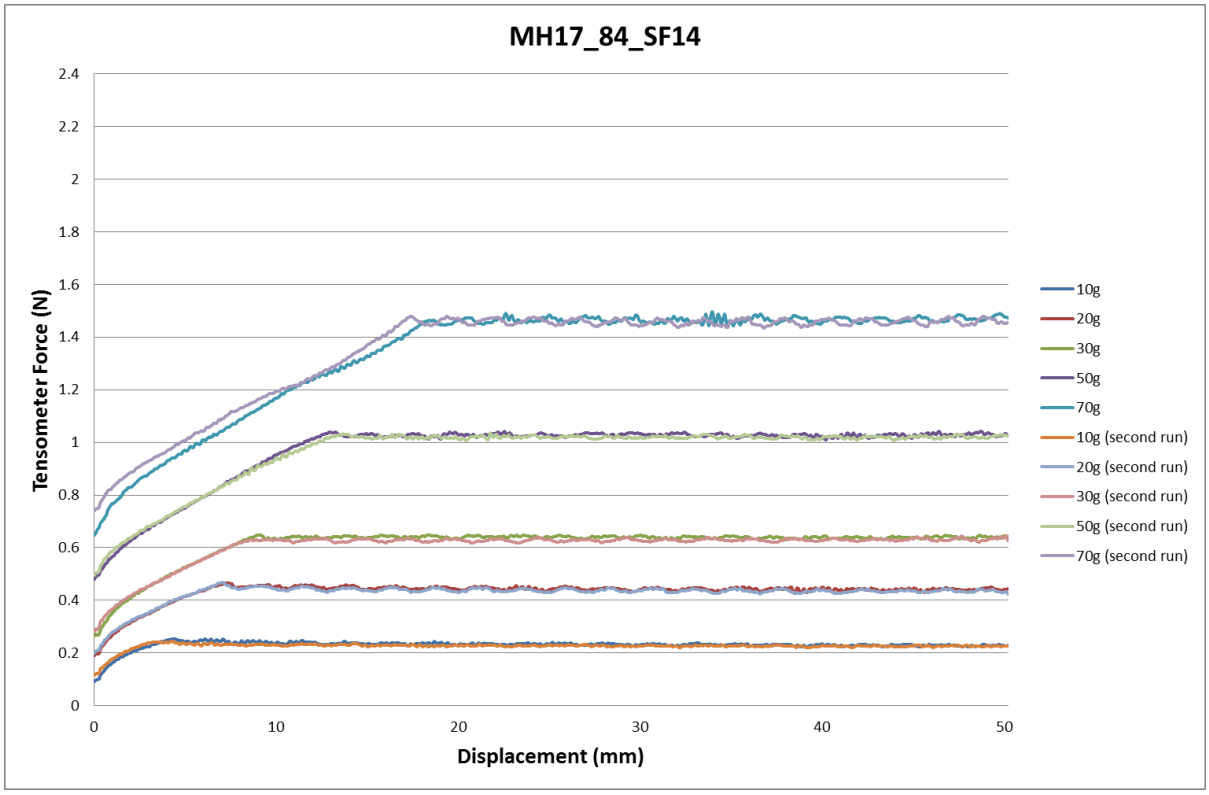
MH17_84_SF14
Tensometer Force (N)
Displacement (mm)
0
0.2
0.4
0.6
0.8
1
1.2
1.4
1.6
1.8
2
2.2
2.4
0
10
20
30
40
50
10g
20g
30g
50g
70g
10g (second run)
20g (second run)
30g (second run)
50g (second run)
70g (second run)

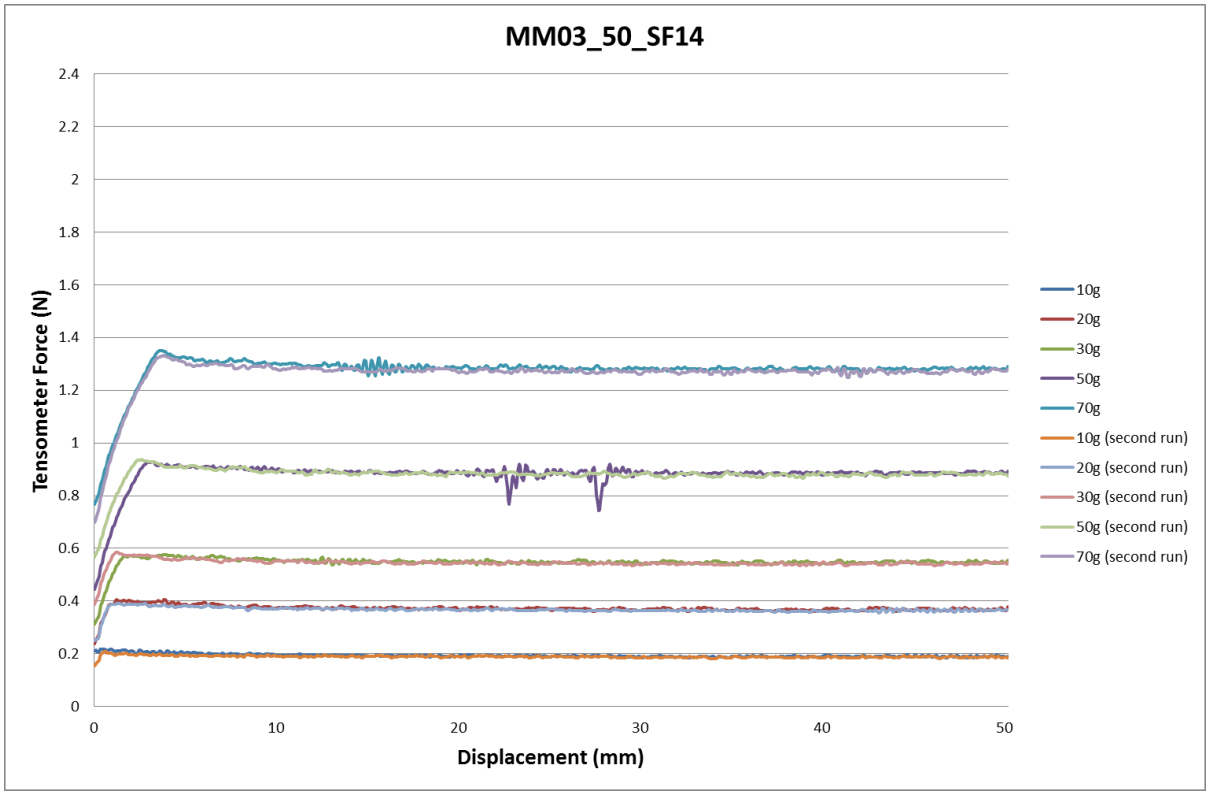
MM03_50_SF14
Tensometer Force (N)
Displacement (mm)
0
0.2
0.4
0.6
0.8
1
1.2
1.4
1.6
1.8
2
2.2
2.4
0
10
20
30
40
50
10g
20g
30g
50g
70g
10g (second run)
20g (second run)
30g (second run)
50g (second run)
70g (second run)

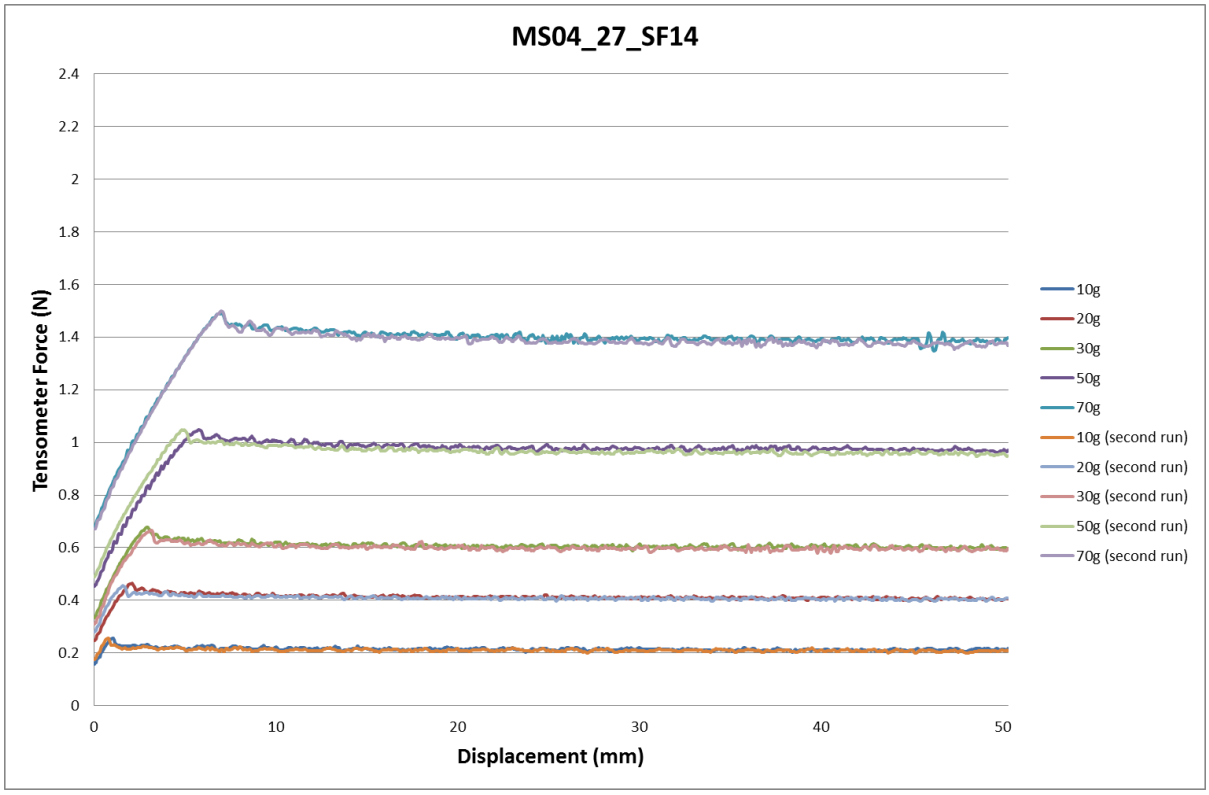
MS04_27_SF14
Tensometer Force (N)
Displacement (mm)
0
0.2
0.4
0.6
0.8
1
1.2
1.4
1.6
1.8
2
2.2
2.4
0
10
20
30
40
50
10g
20g
30g
50g
70g
10g (second run)
20g (second run)
30g (second run)
50g (second run)
70g (second run)

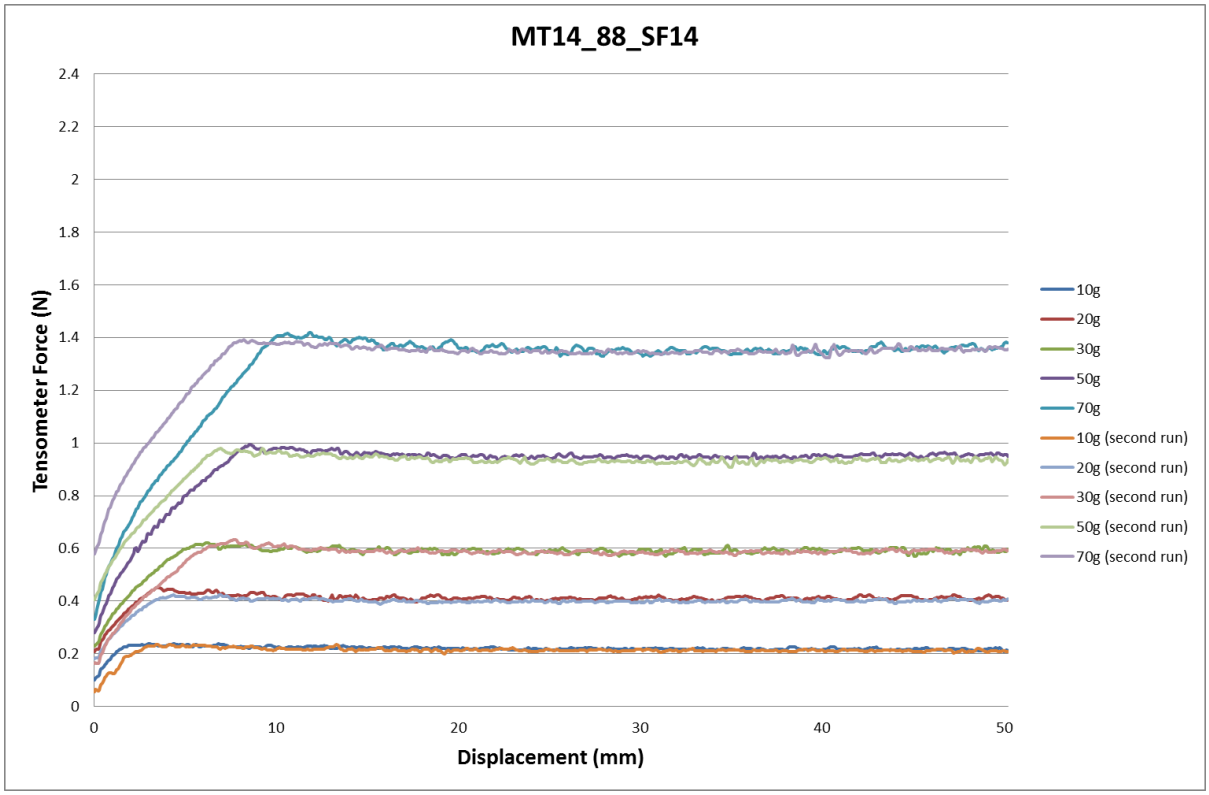
MT14_88_SF14
Tensometer Force (N)
Displacement (mm)
0
0.2
0.4
0.6
0.8
1
1.2
1.4
1.6
1.8
2
2.2
2.4
0
10
20
30
40
50
10g
20g
30g
50g
70g
10g (second run)
20g (second run)
30g (second run)
50g (second run)
70g (second run)

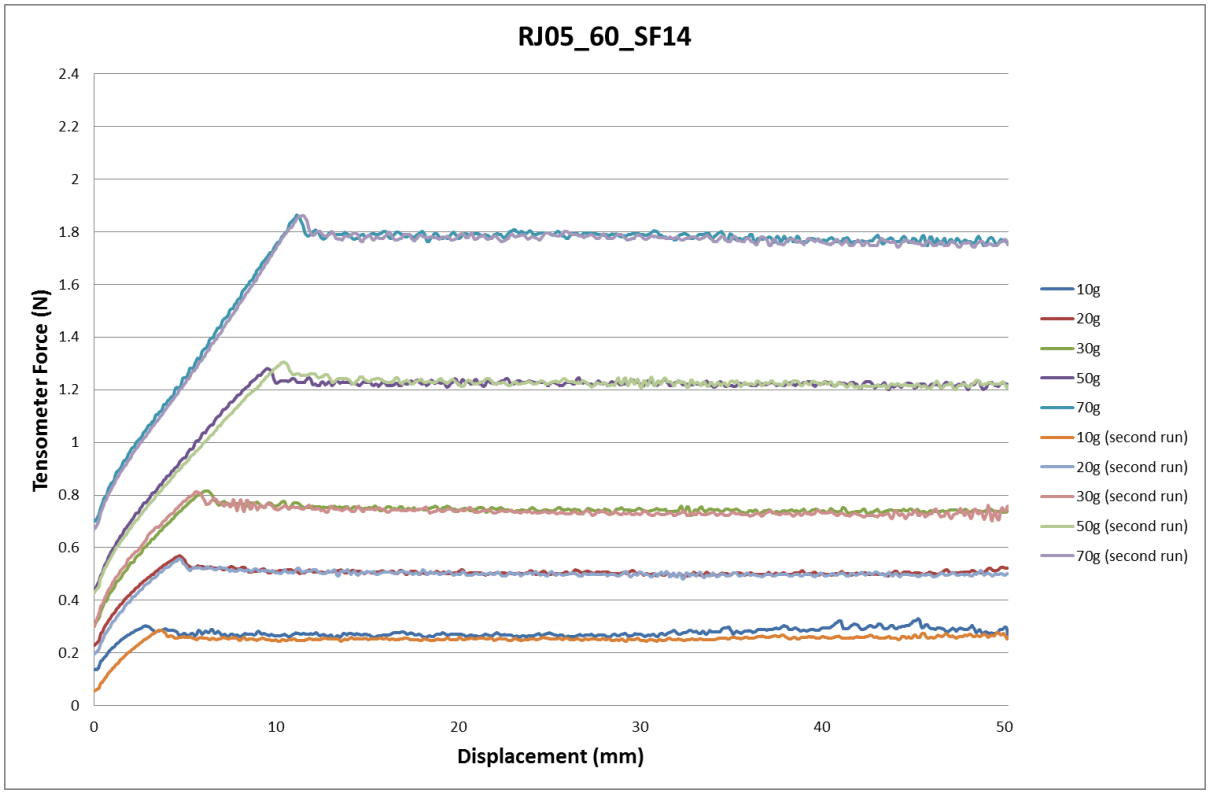
RJ05_60_SF14
Tensometer Force (N)
Displacement (mm)
0
0.2
0.4
0.6
0.8
1
1.2
1.4
1.6
1.8
2
2.2
2.4
0
10
20
30
40
50
10g
20g
30g
50g
70g
10g (second run)
20g (second run)
30g (second run)
50g (second run)
70g (second run)

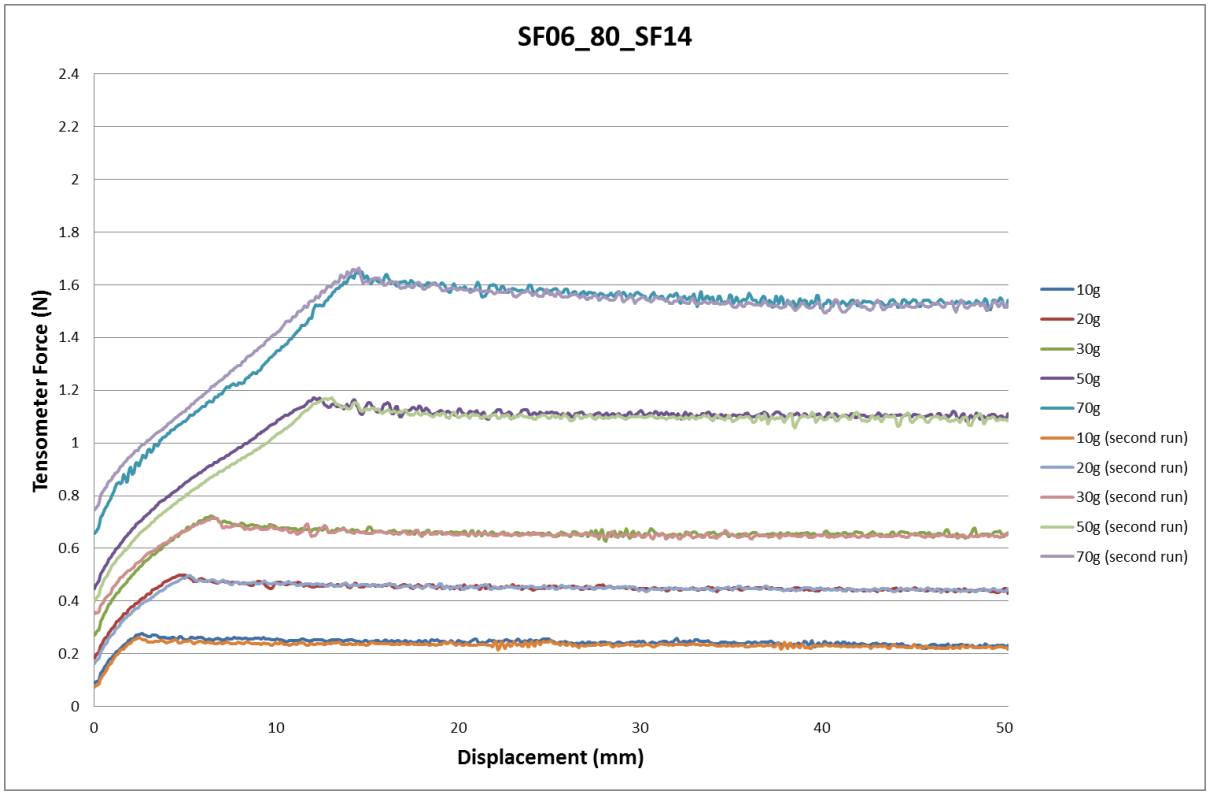
SF06_80_SF14
Tensometer Force (N)
Displacement (mm)
0
0.2
0.4
0.6
0.8
1
1.2
1.4
1.6
1.8
2
2.2
2.4
0
10
20
30
40
50
10g
20g
30g
50g
70g
10g (second run)
20g (second run)
30g (second run)
50g (second run)
70g (second run)

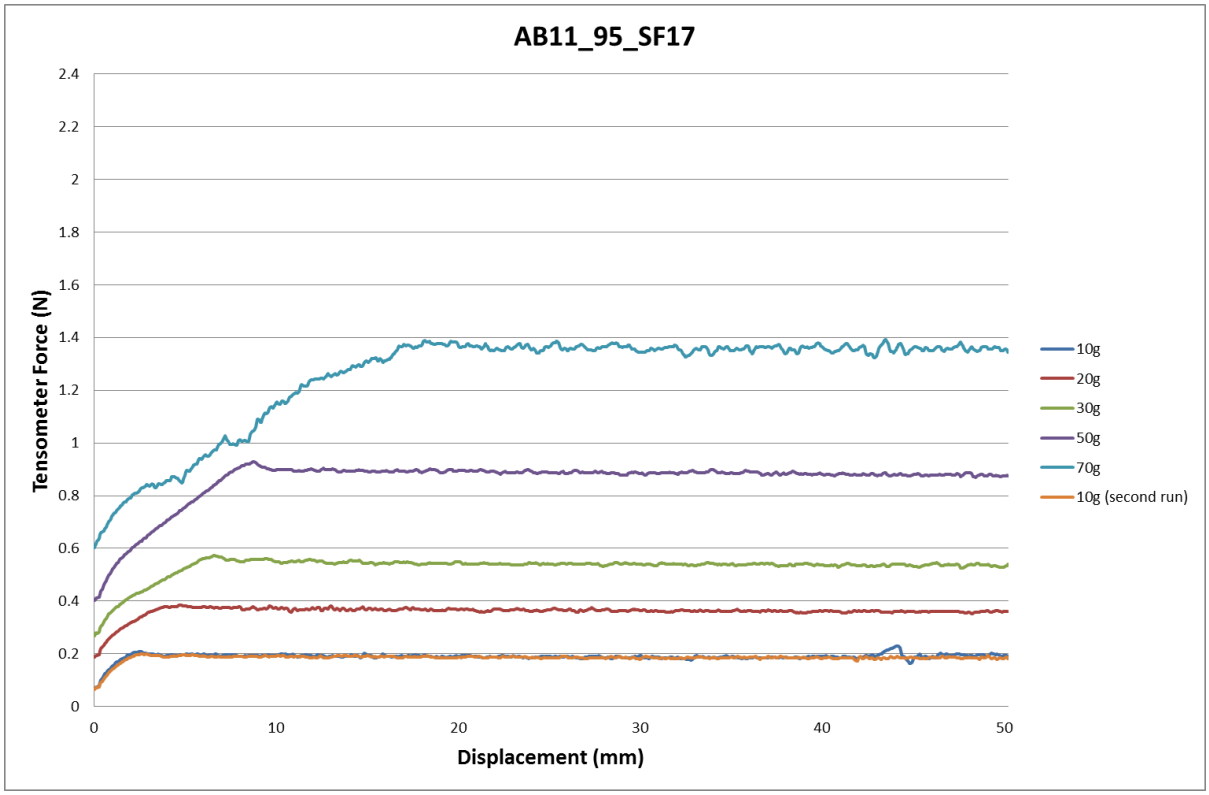
AB11_95_SF17
Tensometer Force (N)
Displacement (mm)
0
0.2
0.4
0.6
0.8
1
1.2
1.4
1.6
1.8
2
2.2
2.4
0
10
20
30
40
50
10g
20g
30g
50g
70g
10g (second run)

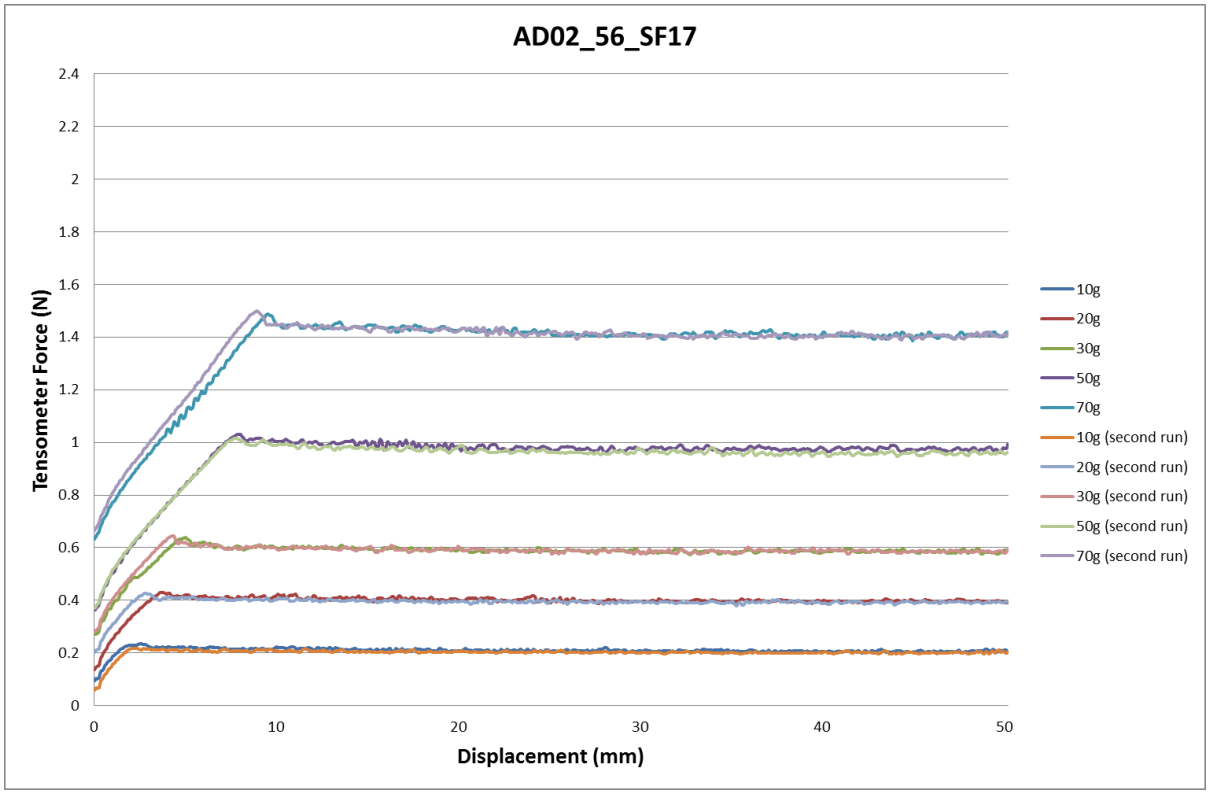
AD02_56_SF17
Tensometer Force (N)
Displacement (mm)
0
0.2
0.4
0.6
0.8
1
1.2
1.4
1.6
1.8
2
2.2
2.4
0
10
20
30
40
50
10g
20g
30g
50g
70g
10g (second run)
20g (second run)
30g (second run)
50g (second run)
70g (second run)

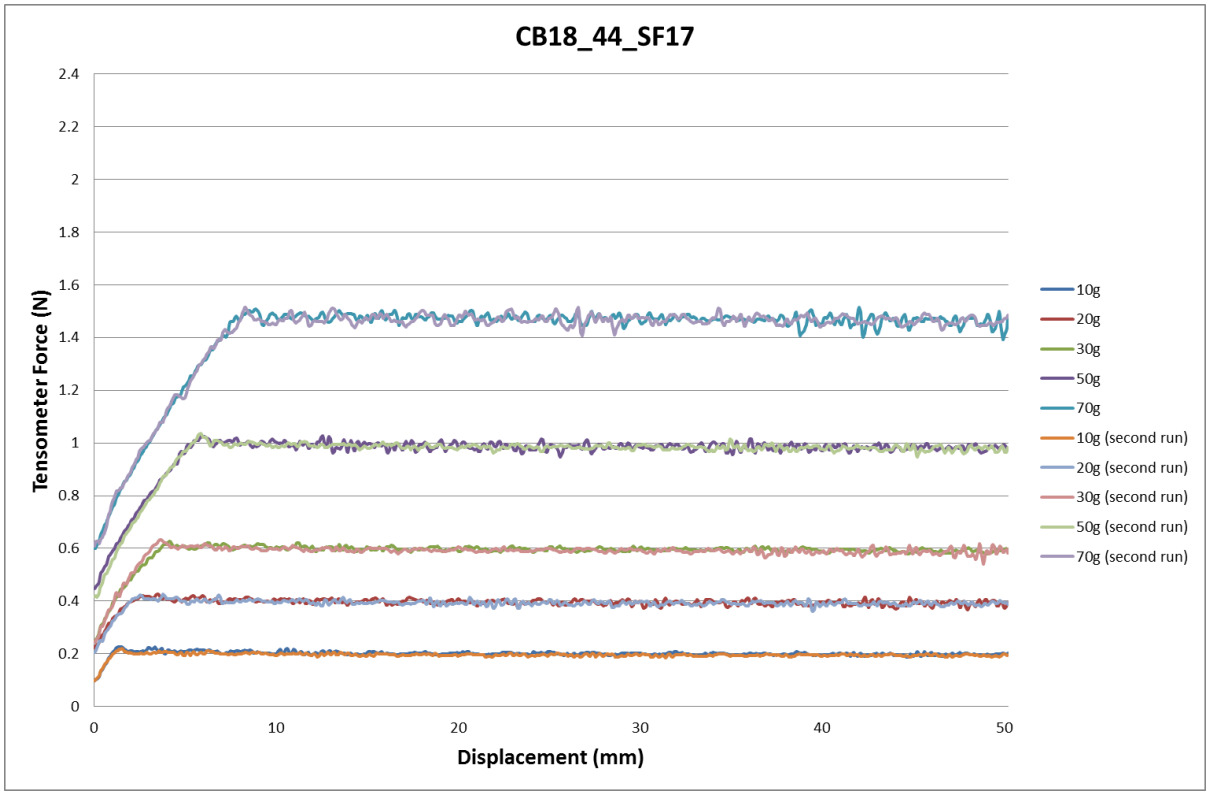
CB18_44_SF17
Tensometer Force (N)
Displacement (mm)
0
0.2
0.4
0.6
0.8
1
1.2
1.4
1.6
1.8
2
2.2
2.4
0
10
20
30
40
50
10g
20g
30g
50g
70g
10g (second run)
20g (second run)
30g (second run)
50g (second run)
70g (second run)

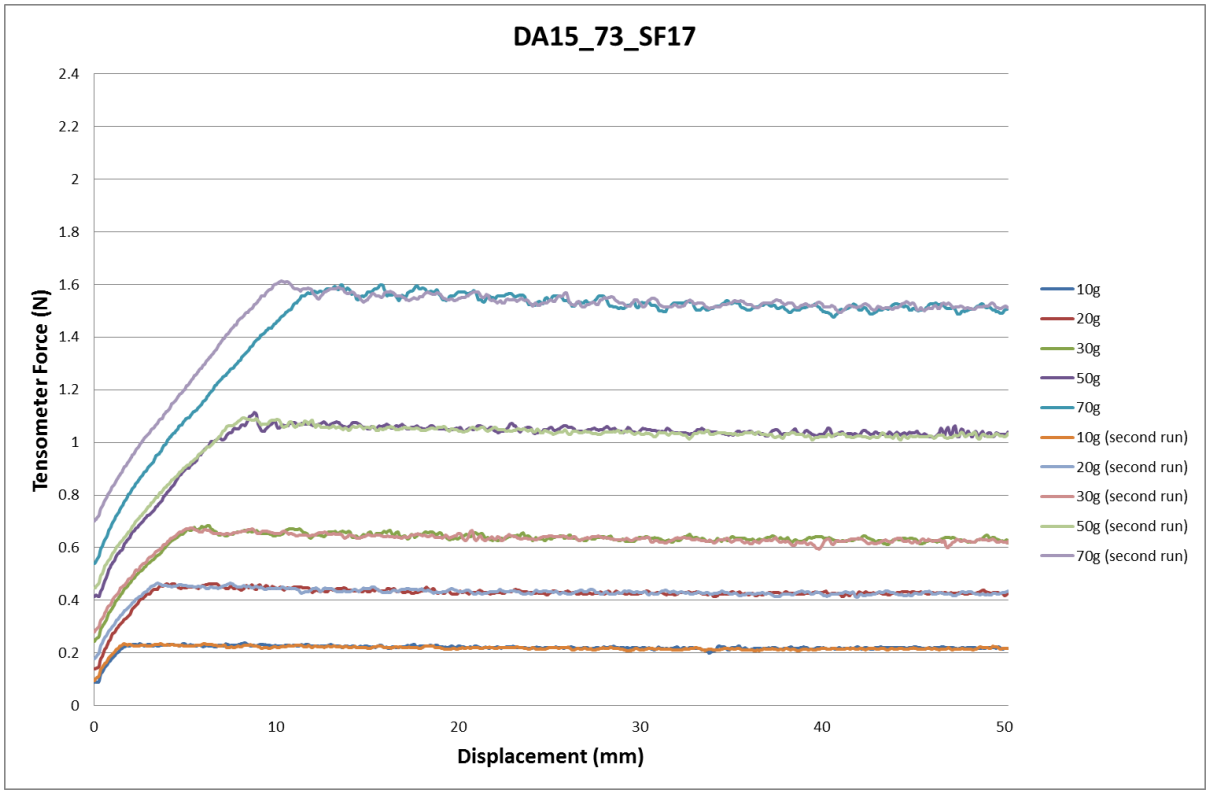
DA15_73_SF17
Tensometer Force (N)
Displacement (mm)
0
0.2
0.4
0.6
0.8
1
1.2
1.4
1.6
1.8
2
2.2
2.4
0
10
20
30
40
50
10g
20g
30g
50g
70g
10g (second run)
20g (second run)
30g (second run)
50g (second run)
70g (second run)

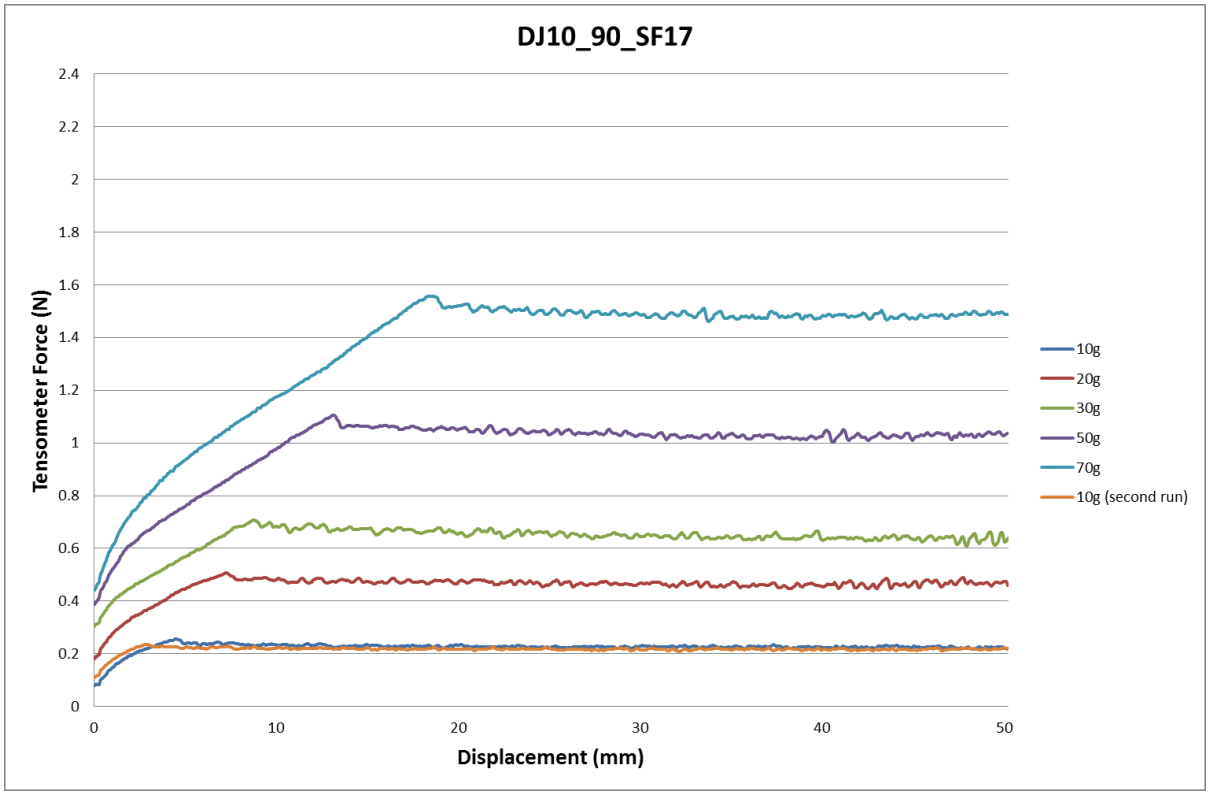
DJ10_90_SF17
Tensometer Force (N)
Displacement (mm)
0
0.2
0.4
0.6
0.8
1
1.2
1.4
1.6
1.8
2
2.2
2.4
0
10
20
30
40
50
10g
20g
30g
50g
70g
10g (second run)

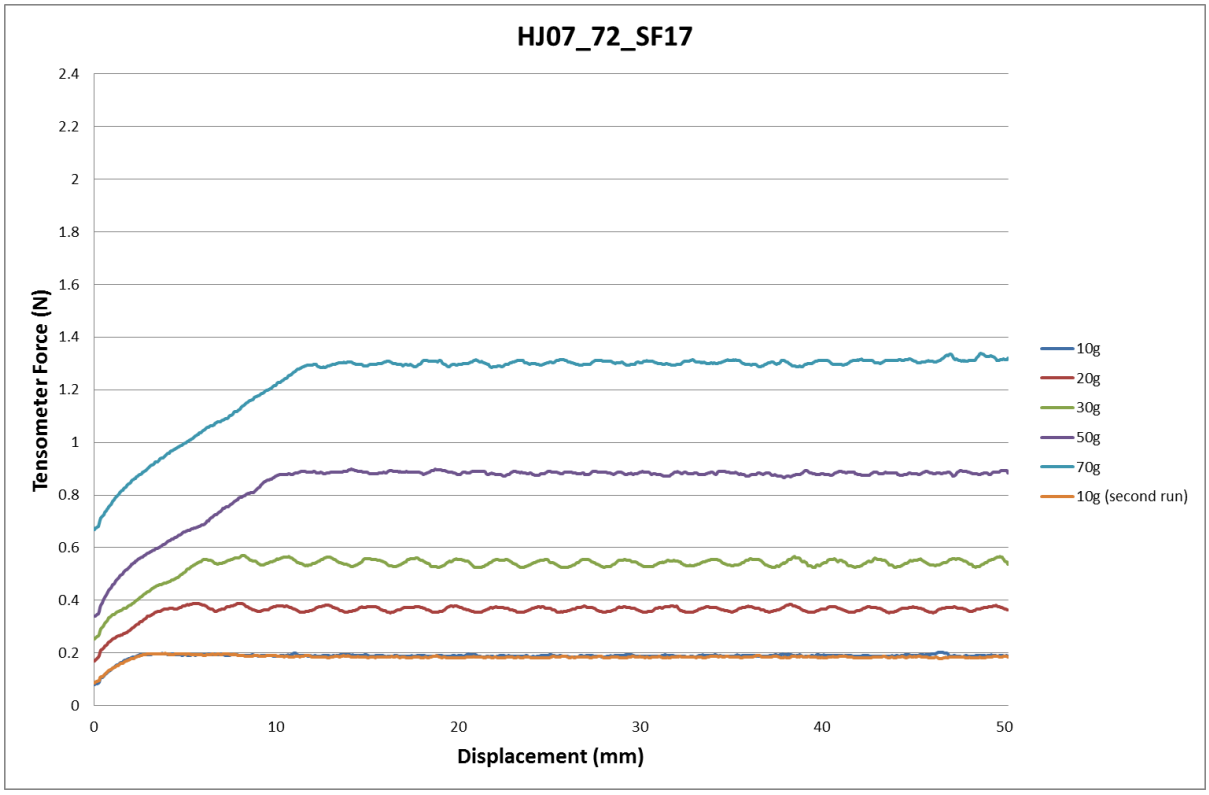
HJ07_72_SF17
Tensometer Force (N)
Displacement (mm)
0
0.2
0.4
0.6
0.8
1
1.2
1.4
1.6
1.8
2
2.2
2.4
0
10
20
30
40
50
10g
20g
30g
50g
70g
10g (second run)

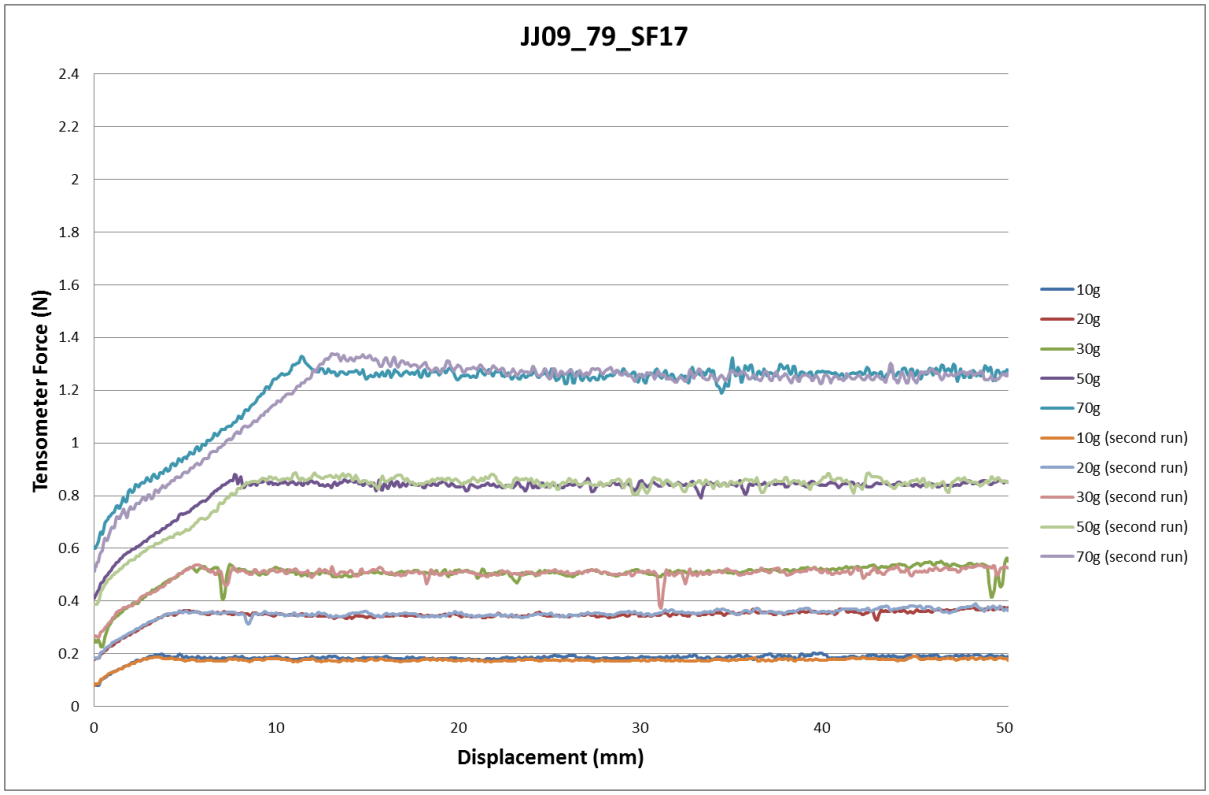
JJ09_79_SF17
Tensometer Force (N)
Displacement (mm)
0
0.2
0.4
0.6
0.8
1
1.2
1.4
1.6
1.8
2
2.2
2.4
0
10
20
30
40
50
10g
20g
30g
50g
70g
10g (second run)
20g (second run)
30g (second run)
50g (second run)
70g (second run)

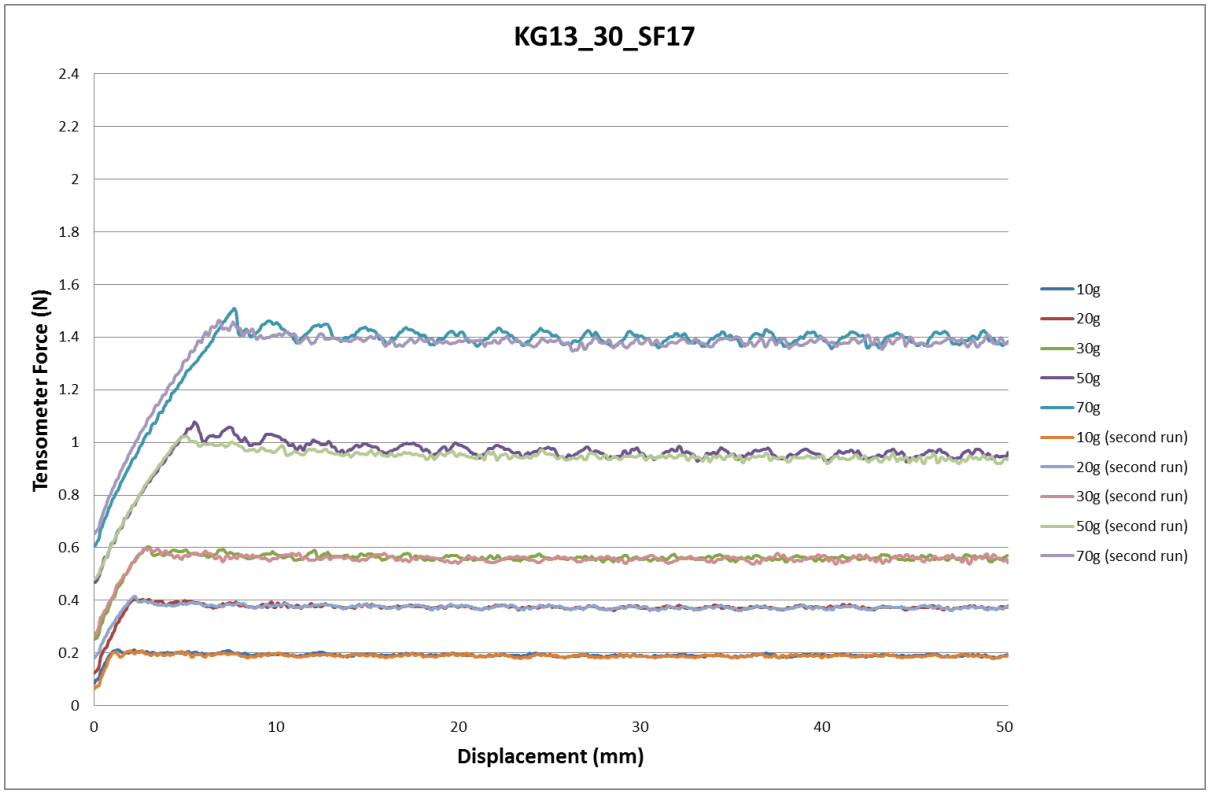
KG13_30_SF17
Tensometer Force (N)
Displacement (mm)
0
0.2
0.4
0.6
0.8
1
1.2
1.4
1.6
1.8
2
2.2
2.4
0
10
20
30
40
50
10g
20g
30g
50g
70g
10g (second run)
20g (second run)
30g (second run)
50g (second run)
70g (second run)

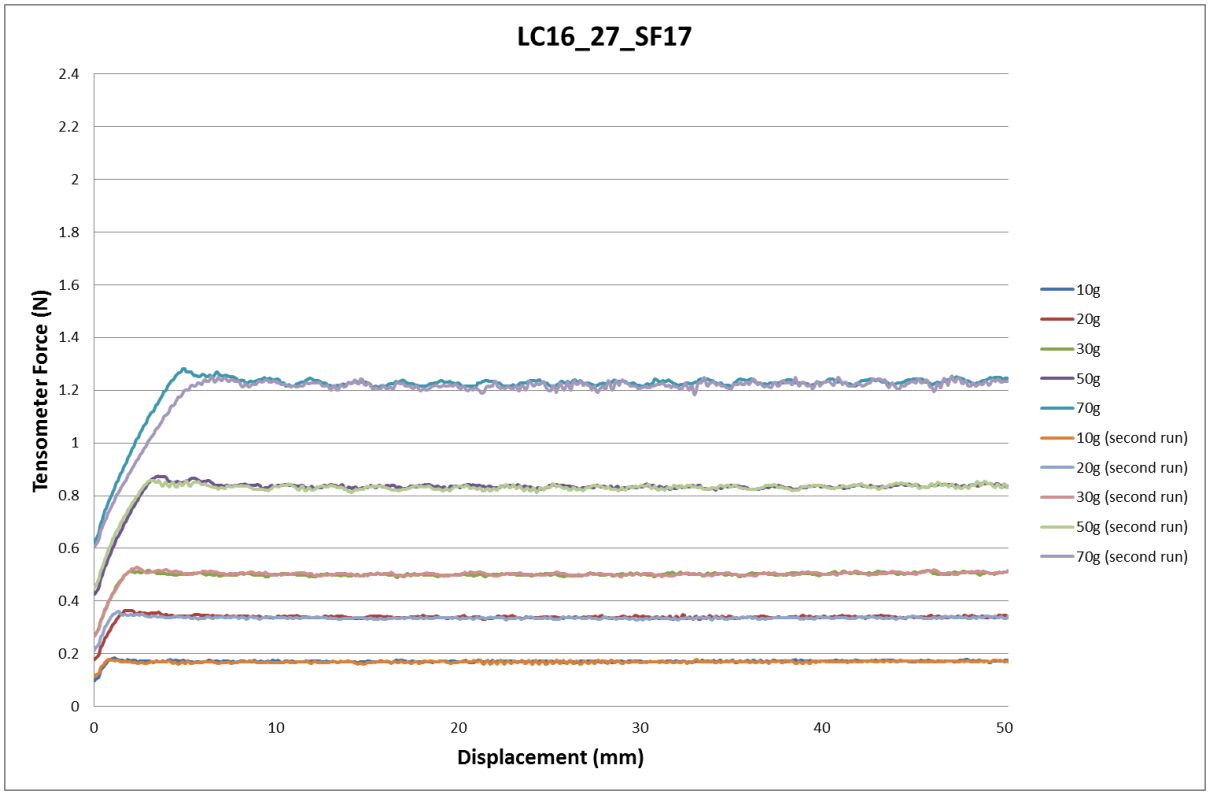
LC16_27_SF17
Tensometer Force (N)
Displacement (mm)
0
0.2
0.4
0.6
0.8
1
1.2
1.4
1.6
1.8
2
2.2
2.4
0
10
20
30
40
50
10g
20g
30g
50g
70g
10g (second run)
20g (second run)
30g (second run)
50g (second run)
70g (second run)

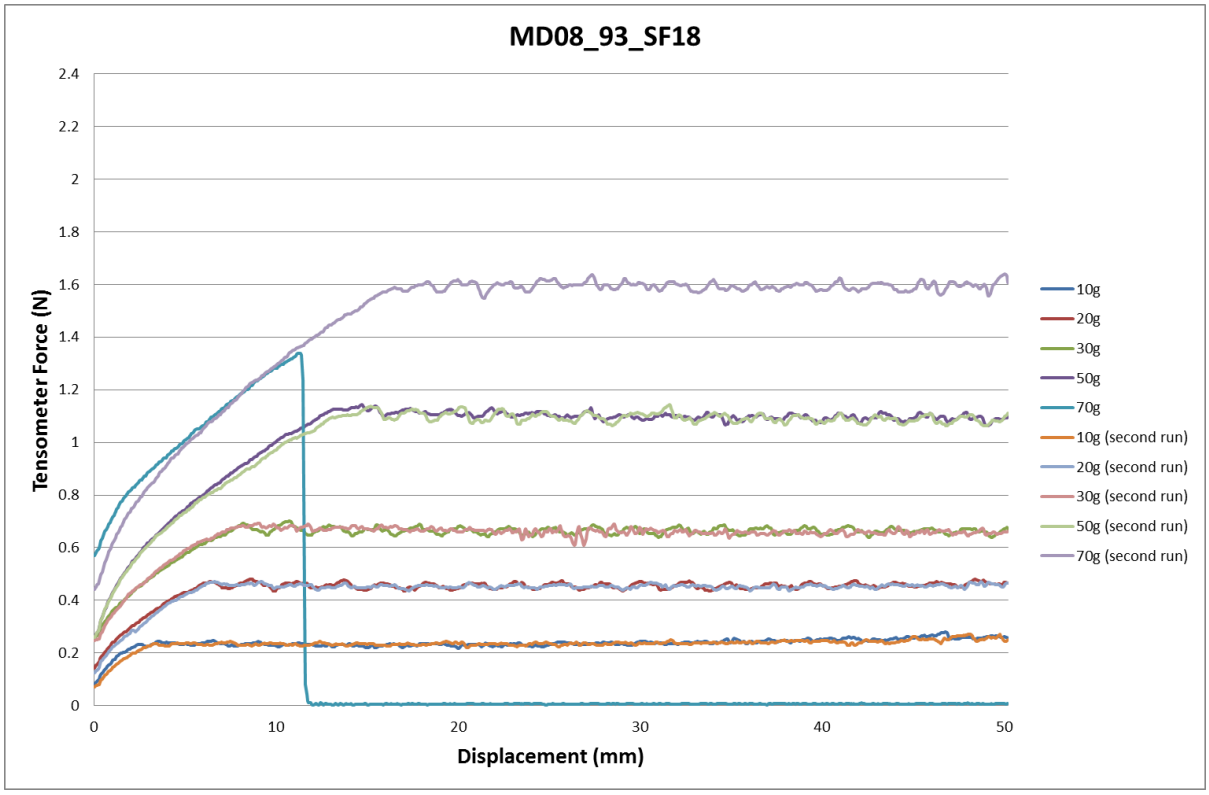
MD08_93_SF18
Tensometer Force (N)
Displacement (mm)
0
0.2
0.4
0.6
0.8
1
1.2
1.4
1.6
1.8
2
2.2
2.4
0
10
20
30
40
50
10g
20g
30g
50g
70g
10g (second run)
20g (second run)
30g (second run)
50g (second run)
70g (second run)

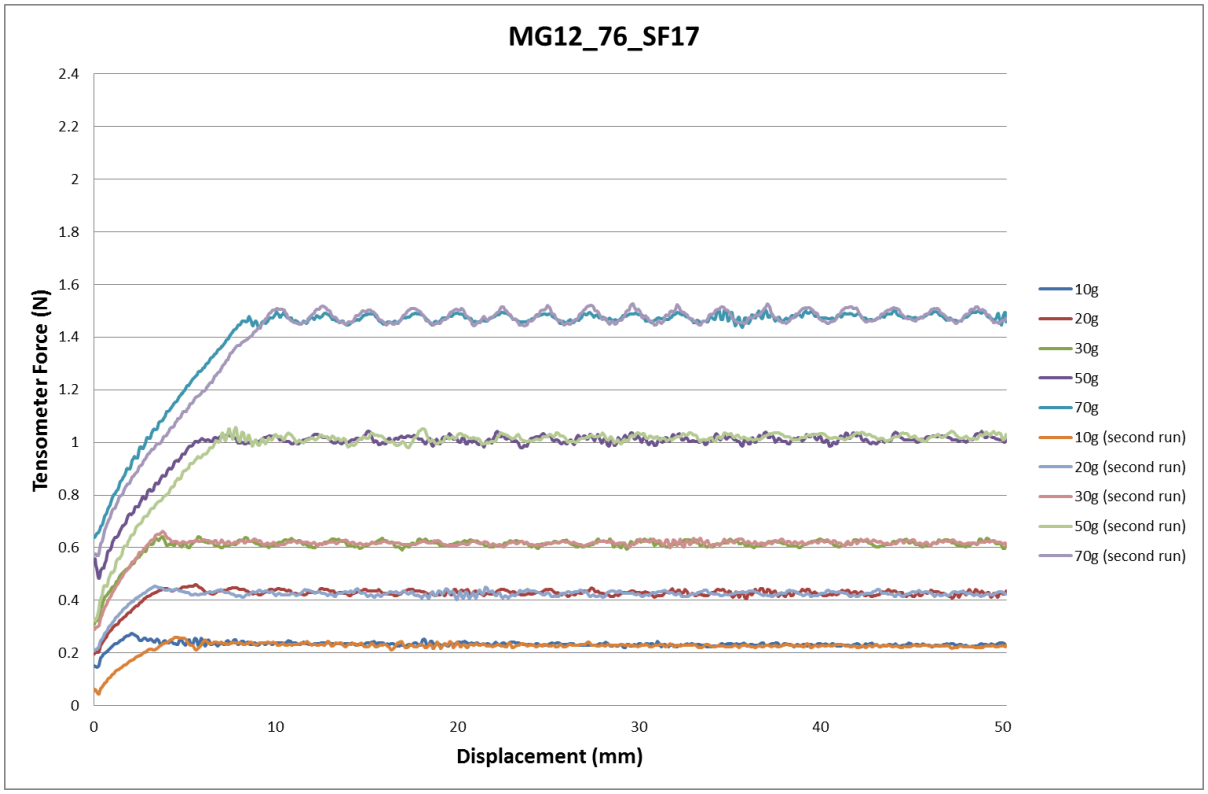
MG12_76_SF17
Tensometer Force (N)
Displacement (mm)
0
0.2
0.4
0.6
0.8
1
1.2
1.4
1.6
1.8
2
2.2
2.4
0
10
20
30
40
50
10g
20g
30g
50g
70g
10g (second run)
20g (second run)
30g (second run)
50g (second run)
70g (second run)

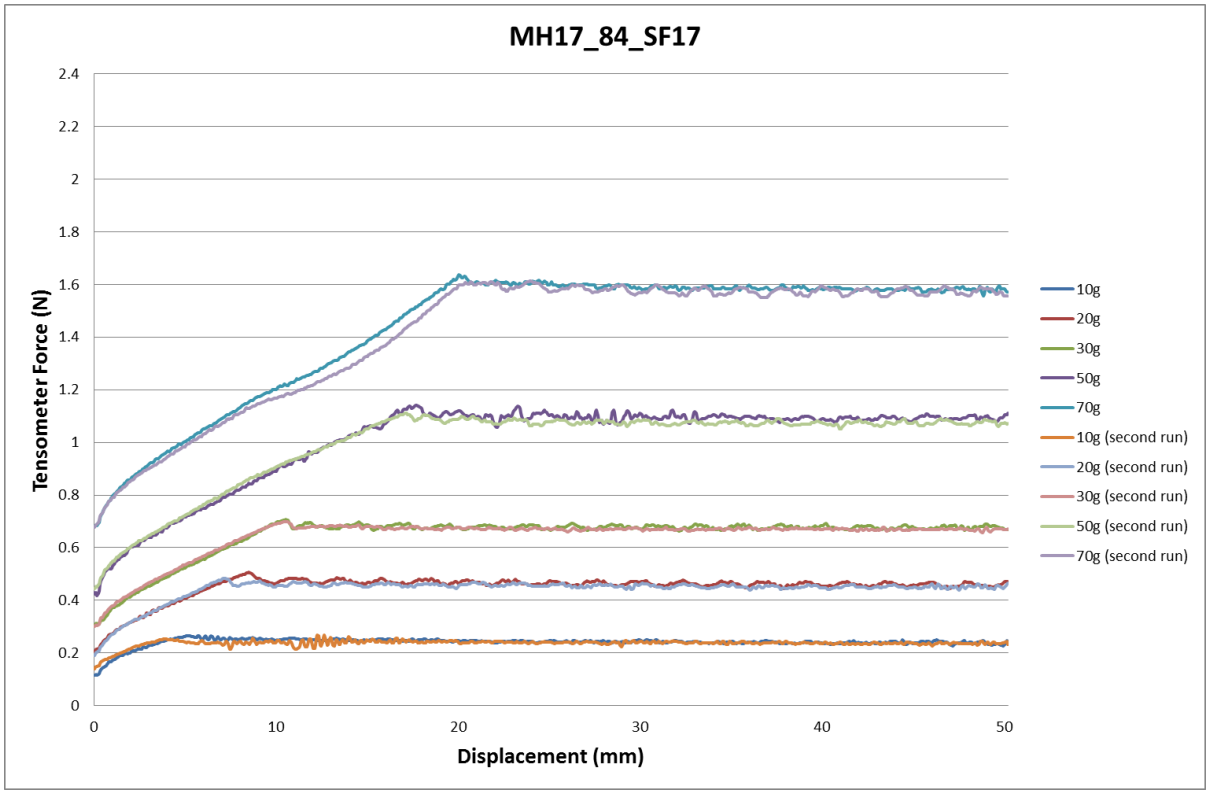
MH17_84_SF17
Tensometer Force (N)
Displacement (mm)
0
0.2
0.4
0.6
0.8
1
1.2
1.4
1.6
1.8
2
2.2
2.4
0
10
20
30
40
50
10g
20g
30g
50g
70g
10g (second run)
20g (second run)
30g (second run)
50g (second run)
70g (second run)

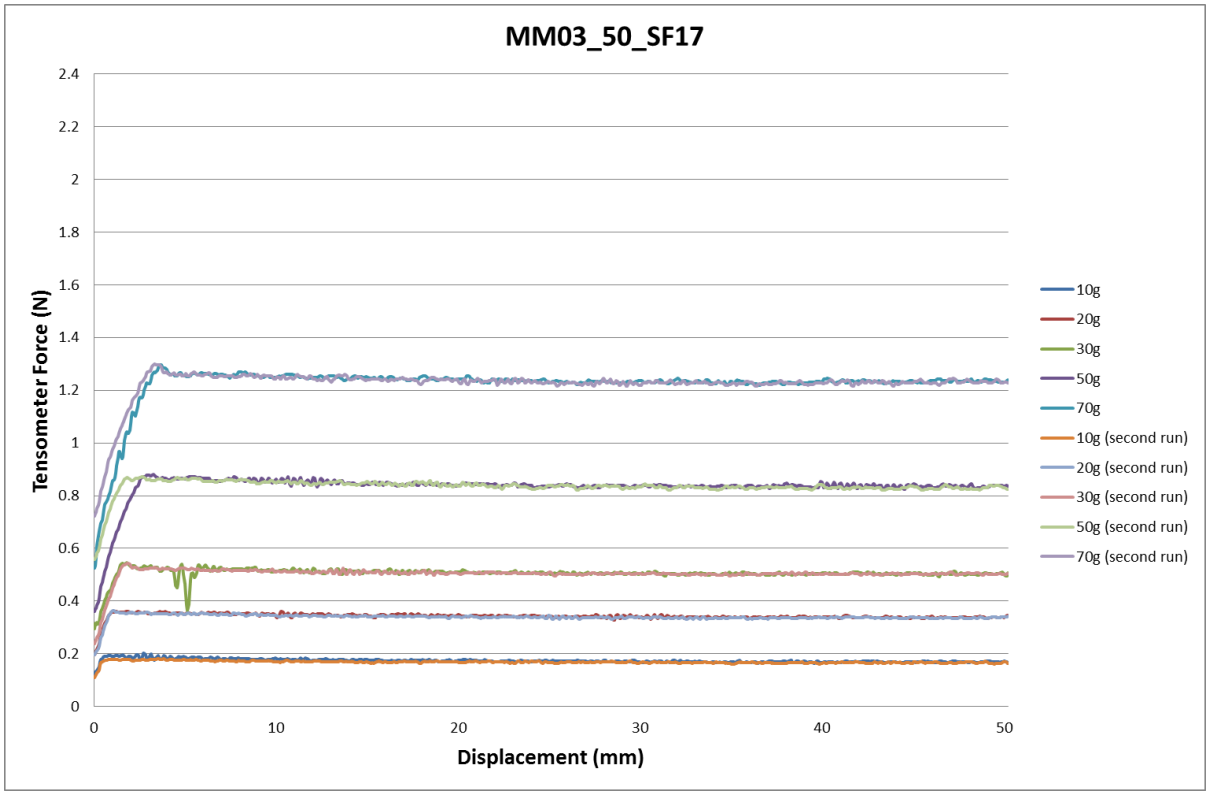
MM03_50_SF17
Tensometer Force (N)
Displacement (mm)
0
0.2
0.4
0.6
0.8
1
1.2
1.4
1.6
1.8
2
2.2
2.4
0
10
20
30
40
50
10g
20g
30g
50g
70g
10g (second run)
20g (second run)
30g (second run)
50g (second run)
70g (second run)

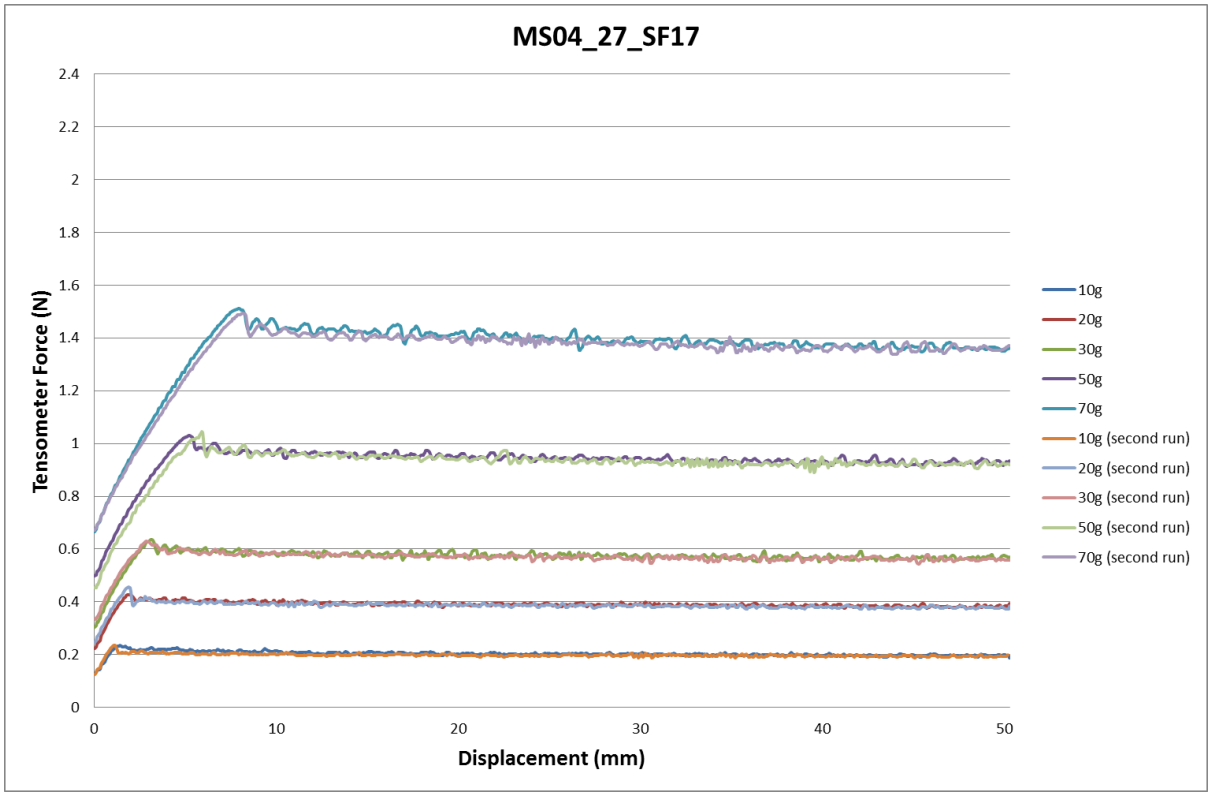
MS04_27_SF17
Tensometer Force (N)
Displacement (mm)
0
0.2
0.4
0.6
0.8
1
1.2
1.4
1.6
1.8
2
2.2
2.4
0
10
20
30
40
50
10g
20g
30g
50g
70g
10g (second run)
20g (second run)
30g (second run)
50g (second run)
70g (second run)

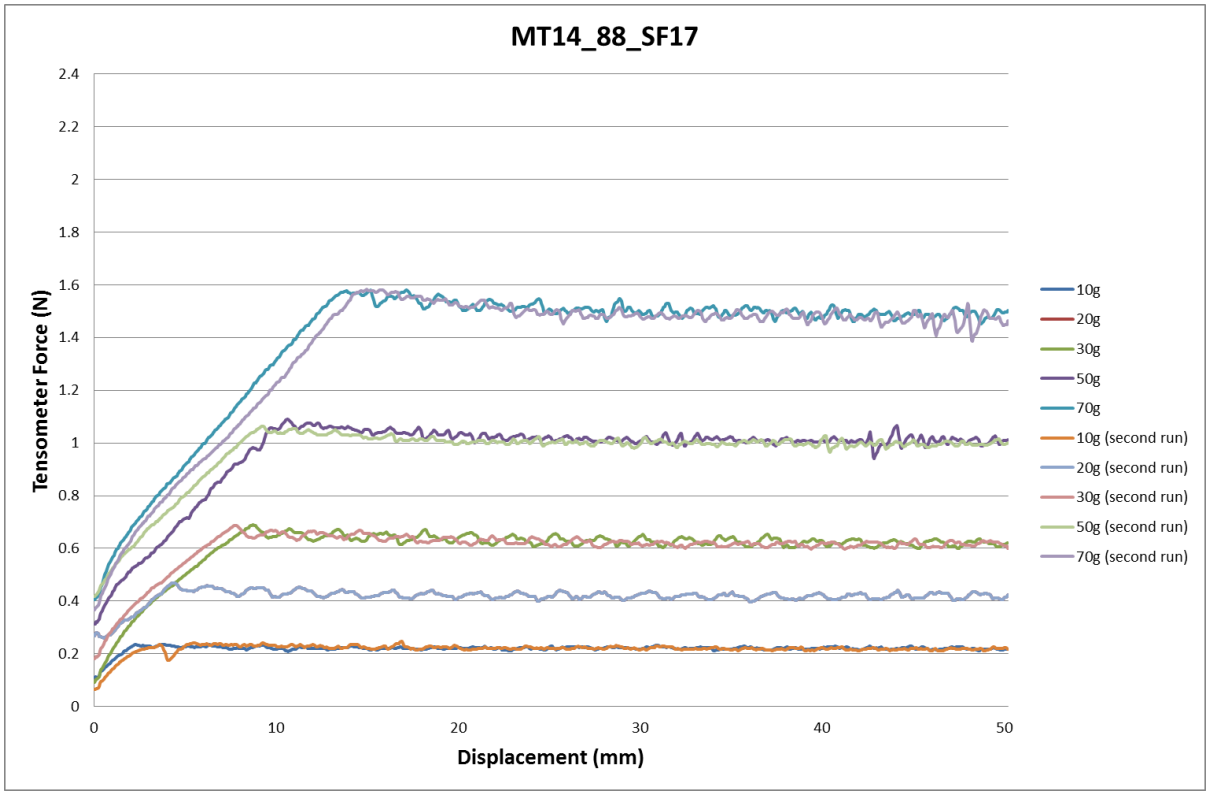
MT14_88_SF17
Tensometer Force (N)
Displacement (mm)
0
0.2
0.4
0.6
0.8
1
1.2
1.4
1.6
1.8
2
2.2
2.4
0
10
20
30
40
50
10g
20g
30g
50g
70g
10g (second run)
20g (second run)
30g (second run)
50g (second run)
70g (second run)

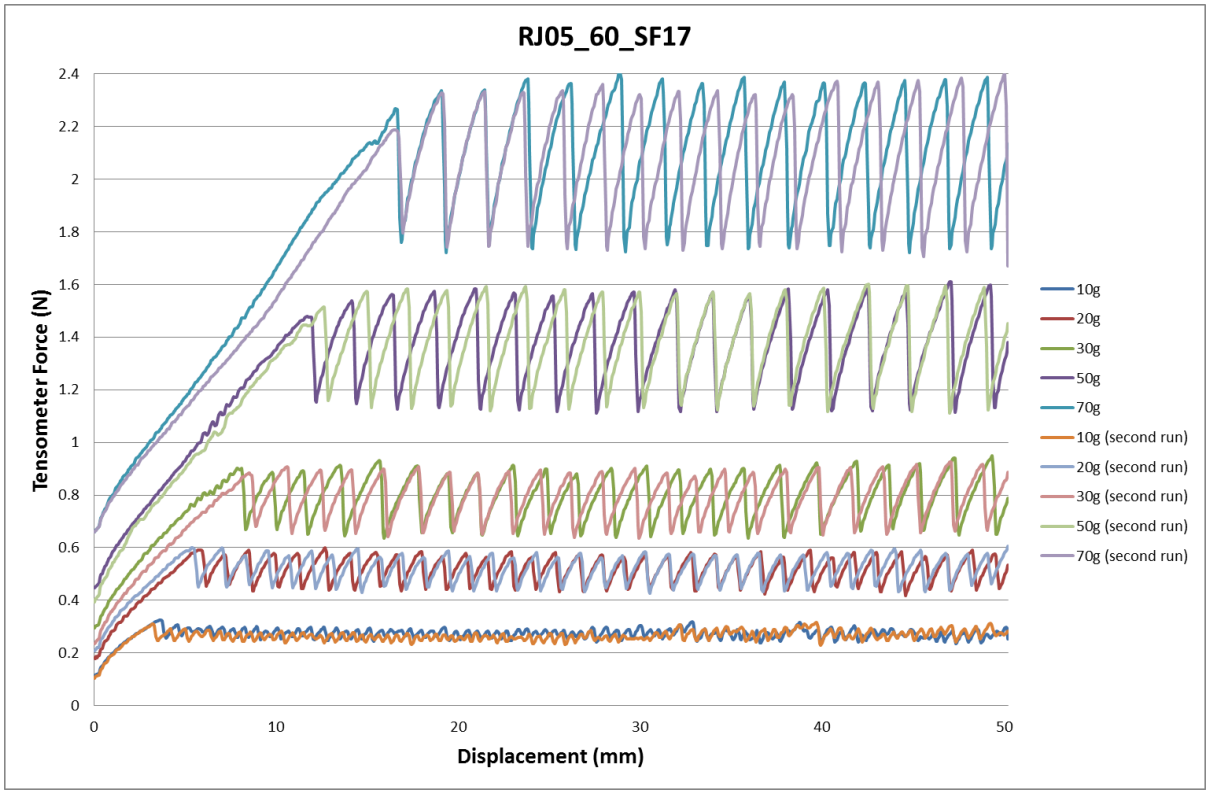
RJ05_60_SF17
Tensometer Force (N)
Displacement (mm)
0
0.2
0.4
0.6
0.8
1
1.2
1.4
1.6
1.8
2
2.2
2.4
0
10
20
30
40
50
10g
20g
30g
50g
70g
10g (second run)
20g (second run)
30g (second run)
50g (second run)
70g (second run)

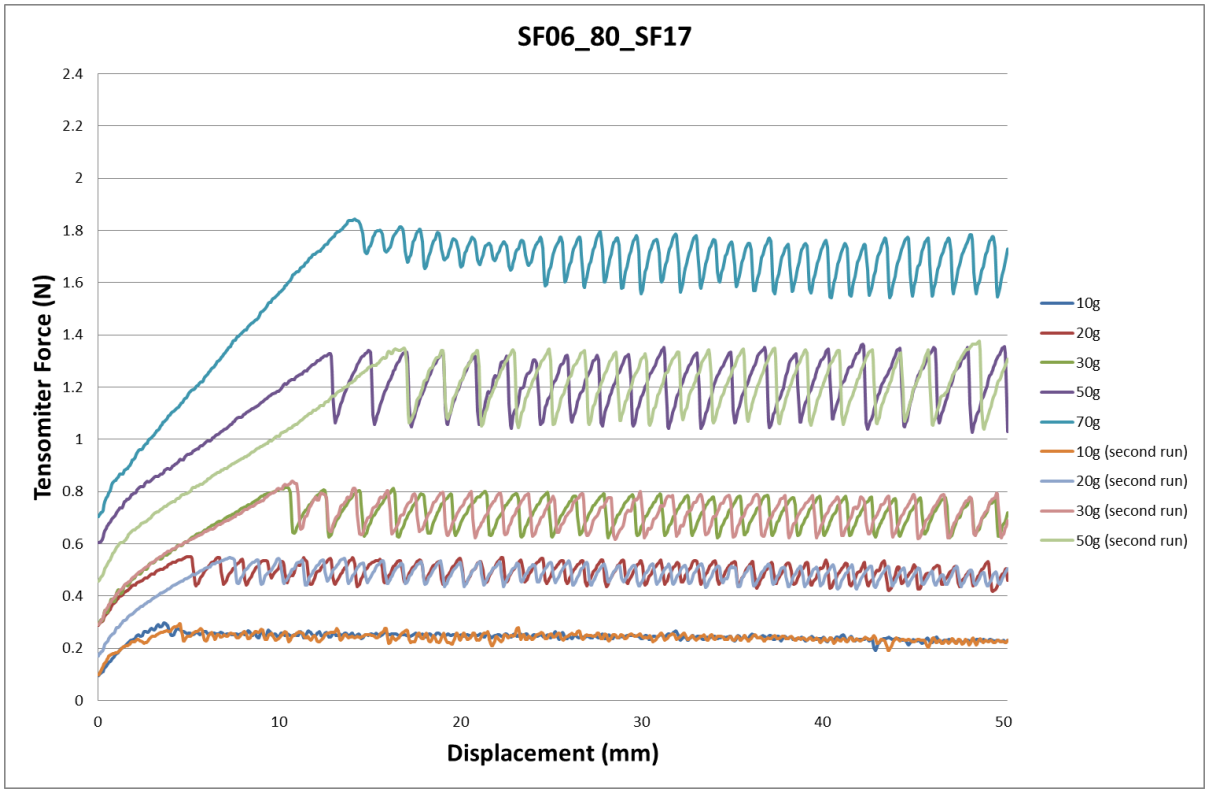
SF06_80_SF17
Tensomiter Force (N)
Displacement (mm)
2.4
2.2
2
1.8
1.6
1.4
1.2
1
0.8
0.6
0.4
0.2
0
0
10
20
30
40
50
10g
20g
30g
50g
70g
10g (second run)
20g (second run)
30g (second run)
50g (second run)

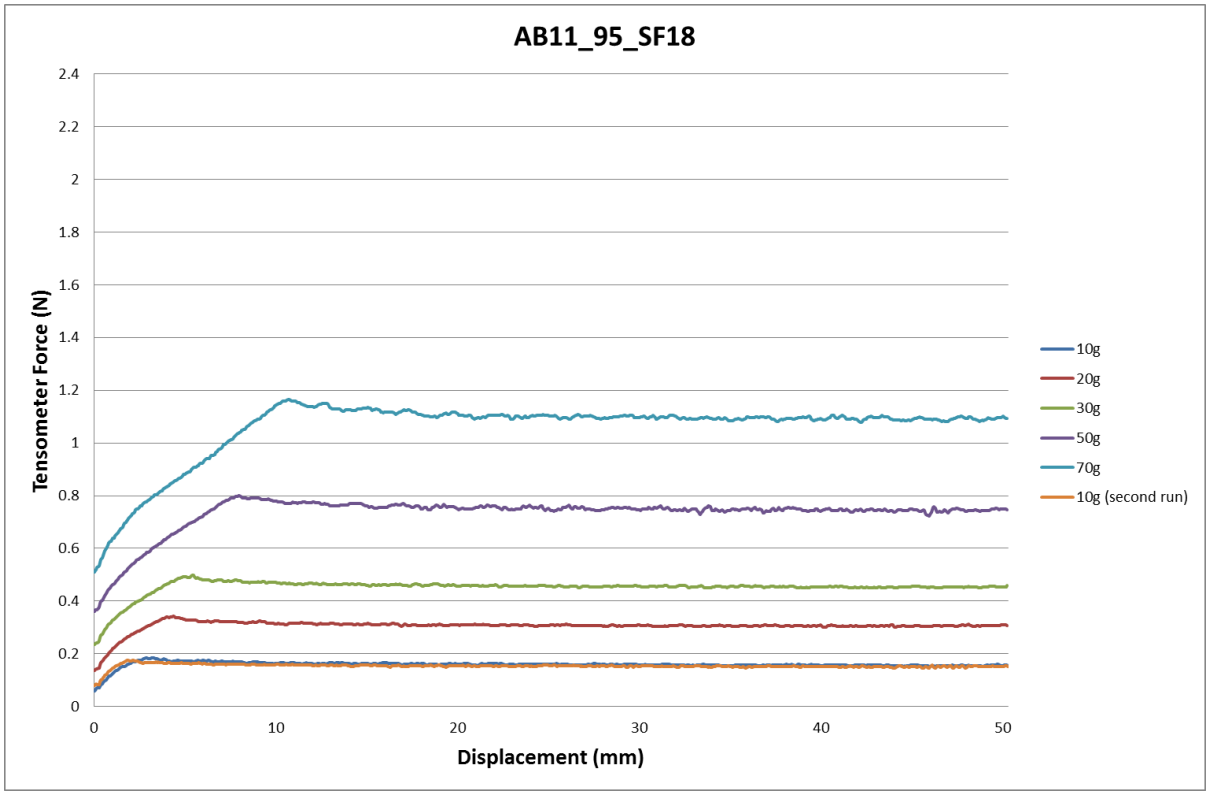
AB11_95_SF18
Tensometer Force (N)
Displacement (mm)
0
0.2
0.4
0.6
0.8
1
1.2
1.4
1.6
1.8
2
2.2
2.4
0
10
20
30
40
50
10g
20g
30g
50g
70g
10g (second run)

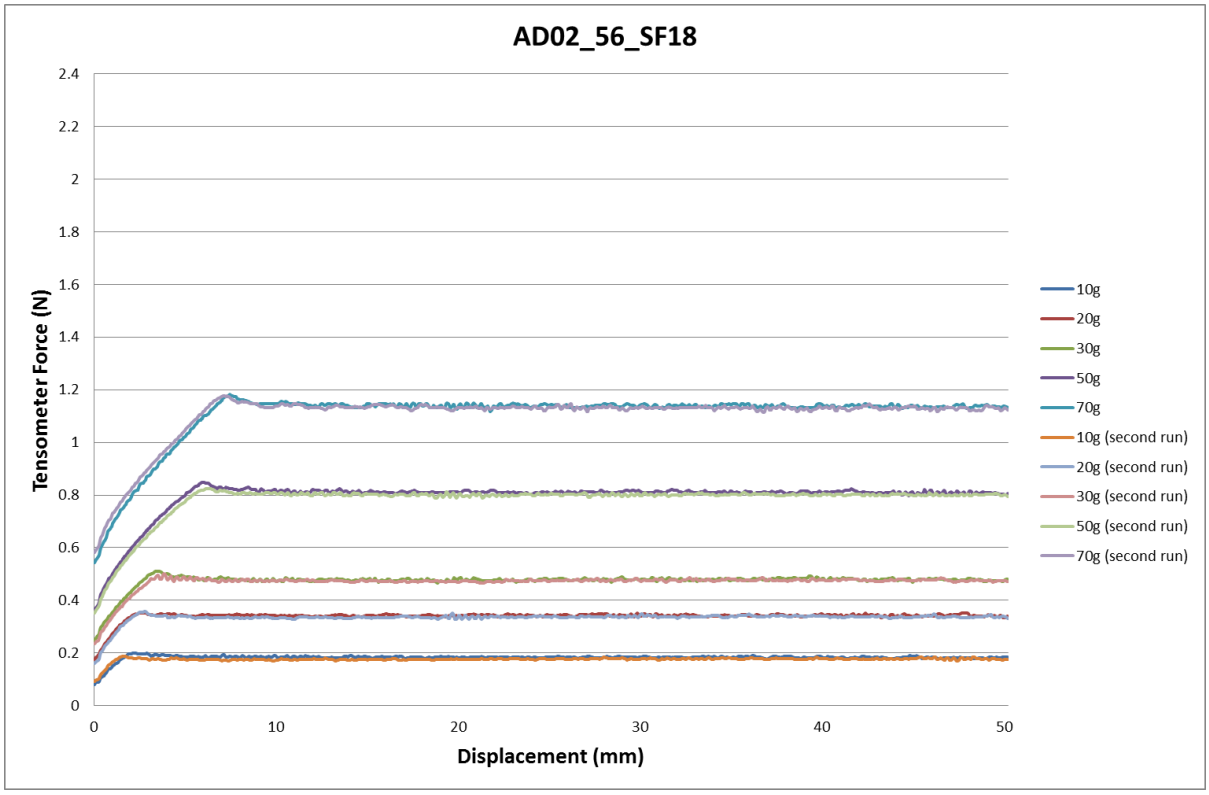
AD02_56_SF18
Tensometer Force (N)
Displacement (mm)
0
0.2
0.4
0.6
0.8
1
1.2
1.4
1.6
1.8
2
2.2
2.4
0
10
20
30
40
50
10g
20g
30g
50g
70g
10g (second run)
20g (second run)
30g (second run)
50g (second run)
70g (second run)

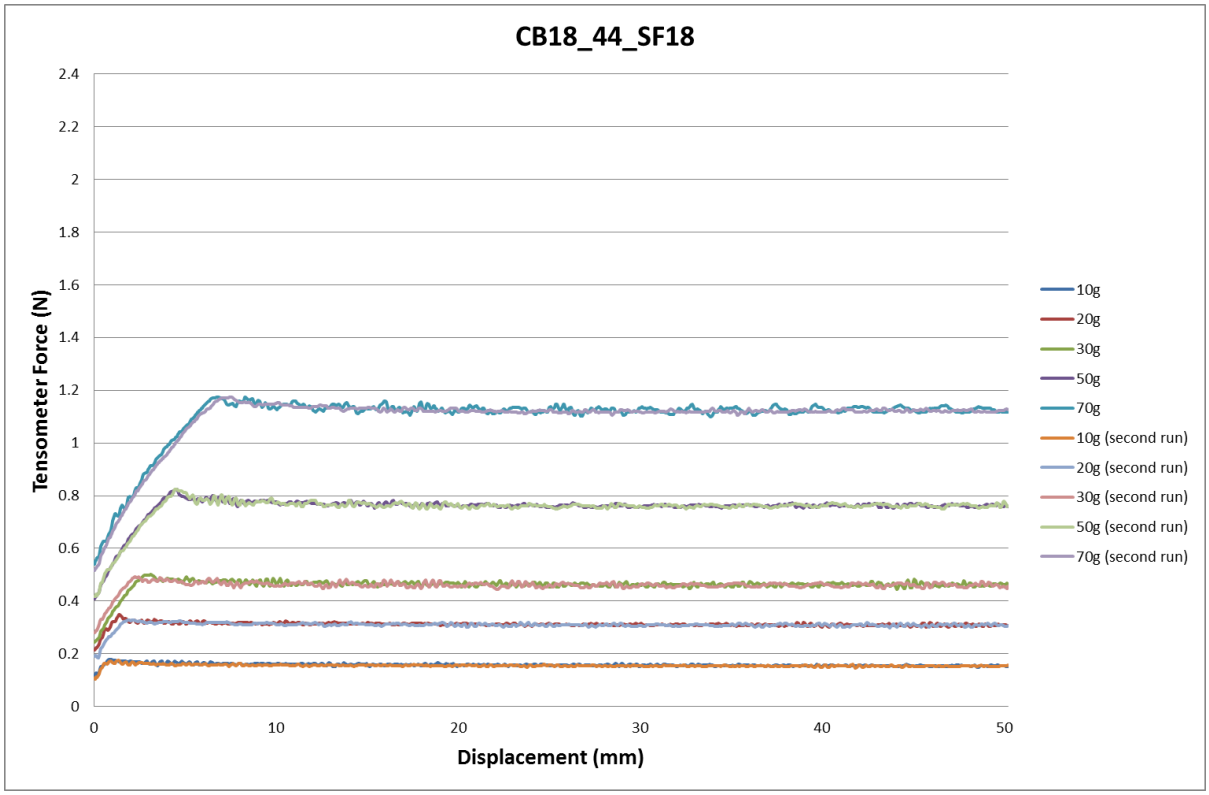
CB18_44_SF18
Tensometer Force (N)
Displacement (mm)
0
0.2
0.4
0.6
0.8
1
1.2
1.4
1.6
1.8
2
2.2
2.4
0
10
20
30
40
50
10g
20g
30g
50g
70g
10g (second run)
20g (second run)
30g (second run)
50g (second run)
70g (second run)

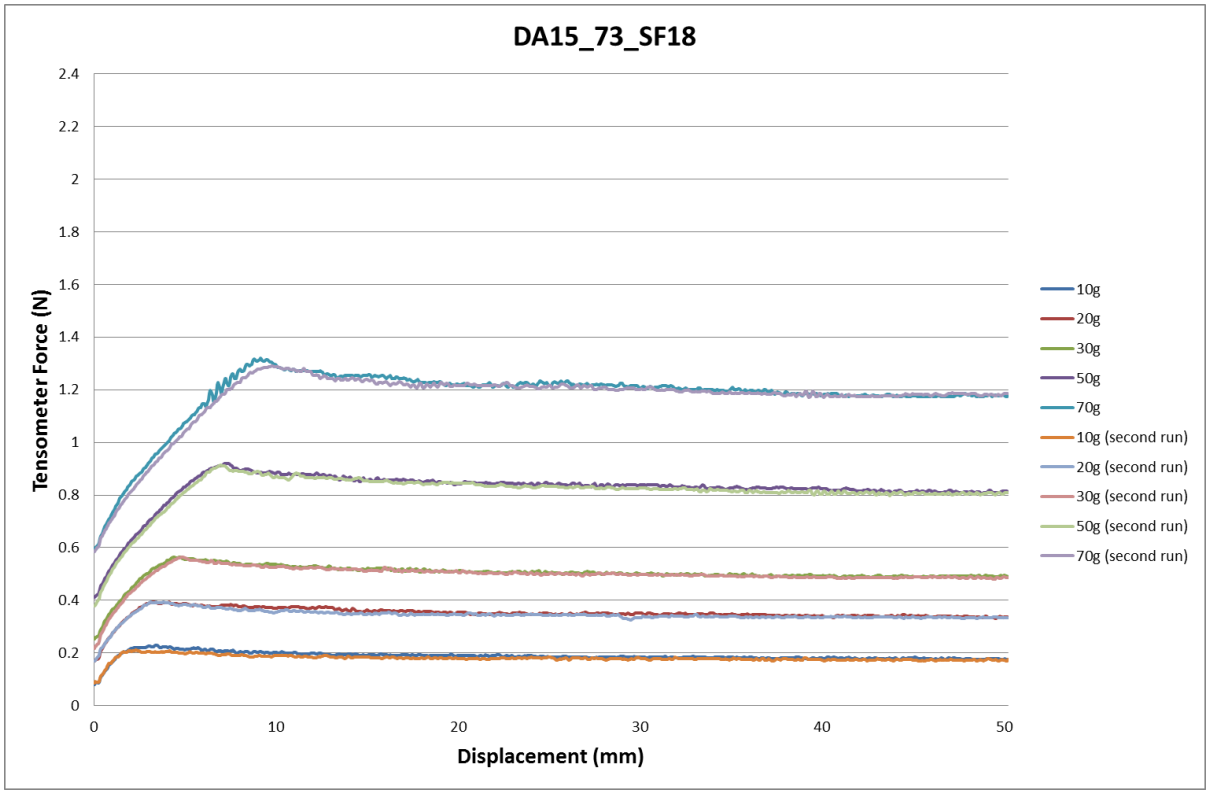
DA15_73_SF18
Tensometer Force (N)
Displacement (mm)
0
0.2
0.4
0.6
0.8
1
1.2
1.4
1.6
1.8
2
2.2
2.4
0
10
20
30
40
50
10g
20g
30g
50g
70g
10g (second run)
20g (second run)
30g (second run)
50g (second run)
70g (second run)

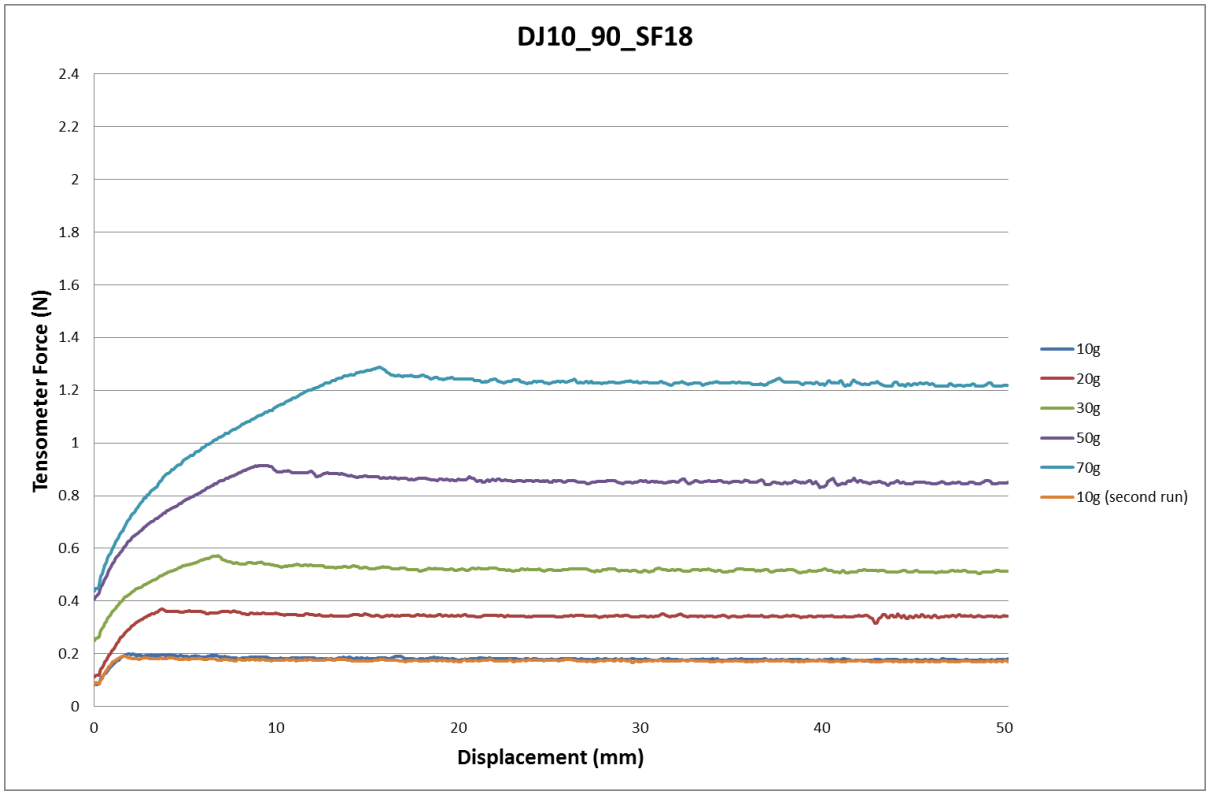
DJ10_90_SF18
Tensometer Force (N)
Displacement (mm)
0
0.2
0.4
0.6
0.8
1
1.2
1.4
1.6
1.8
2
2.2
2.4
0
10
20
30
40
50
10g
20g
30g
50g
70g
10g (second run)

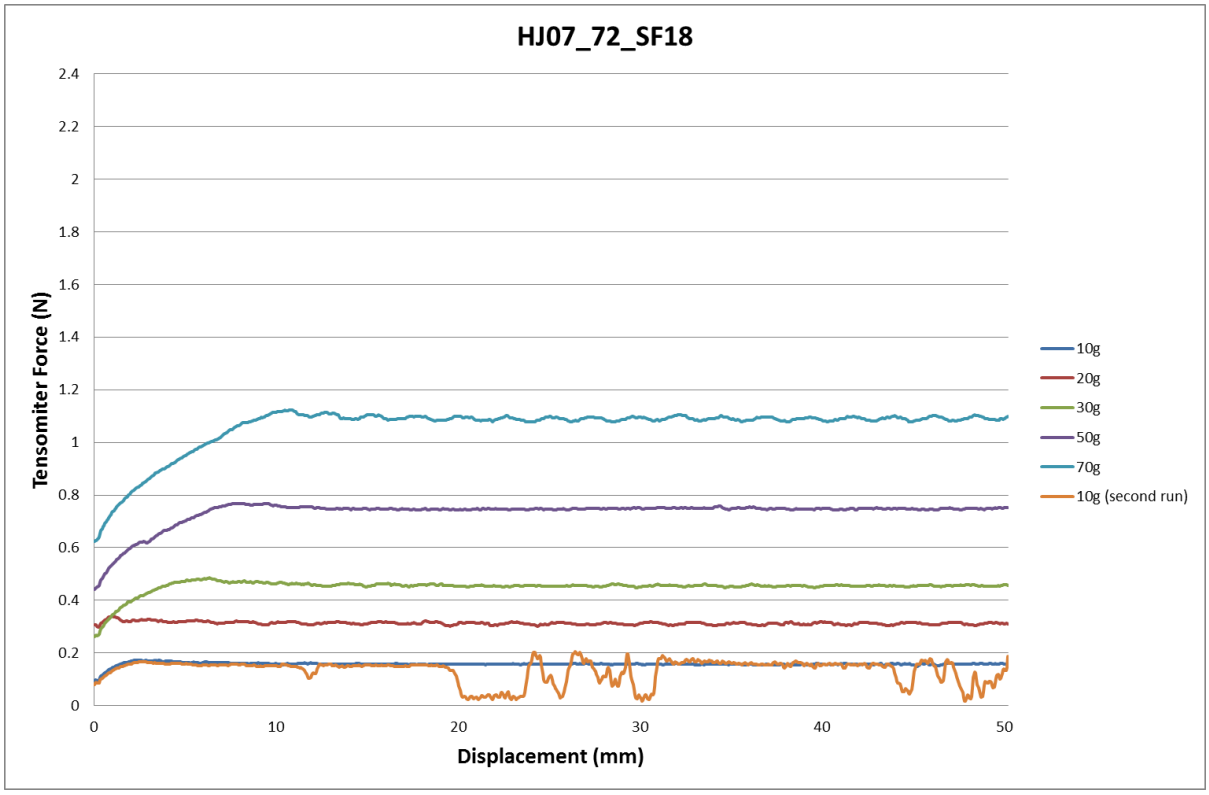
HJ07_72_SF18
Tensomiter Force (N)
Displacement (mm)
0
0.2
0.4
0.6
0.8
1
1.2
1.4
1.6
1.8
2
2.2
2.4
0
10
20
30
40
50
10g
20g
30g
50g
70g
10g (second run)

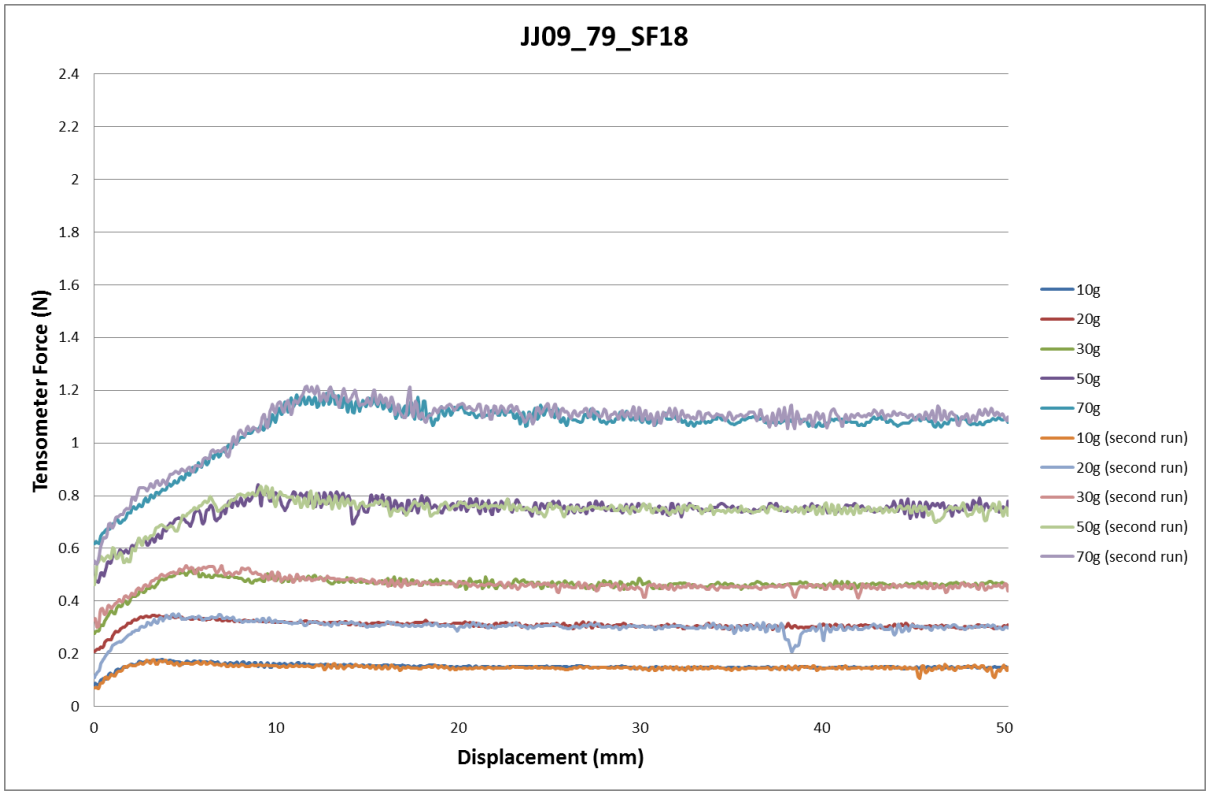
JJ09_79_SF18
Tensometer Force (N)
Displacement (mm)
0
0.2
0.4
0.6
0.8
1
1.2
1.4
1.6
1.8
2
2.2
2.4
0
10
20
30
40
50
10g
20g
30g
50g
70g
10g (second run)
20g (second run)
30g (second run)
50g (second run)
70g (second run)

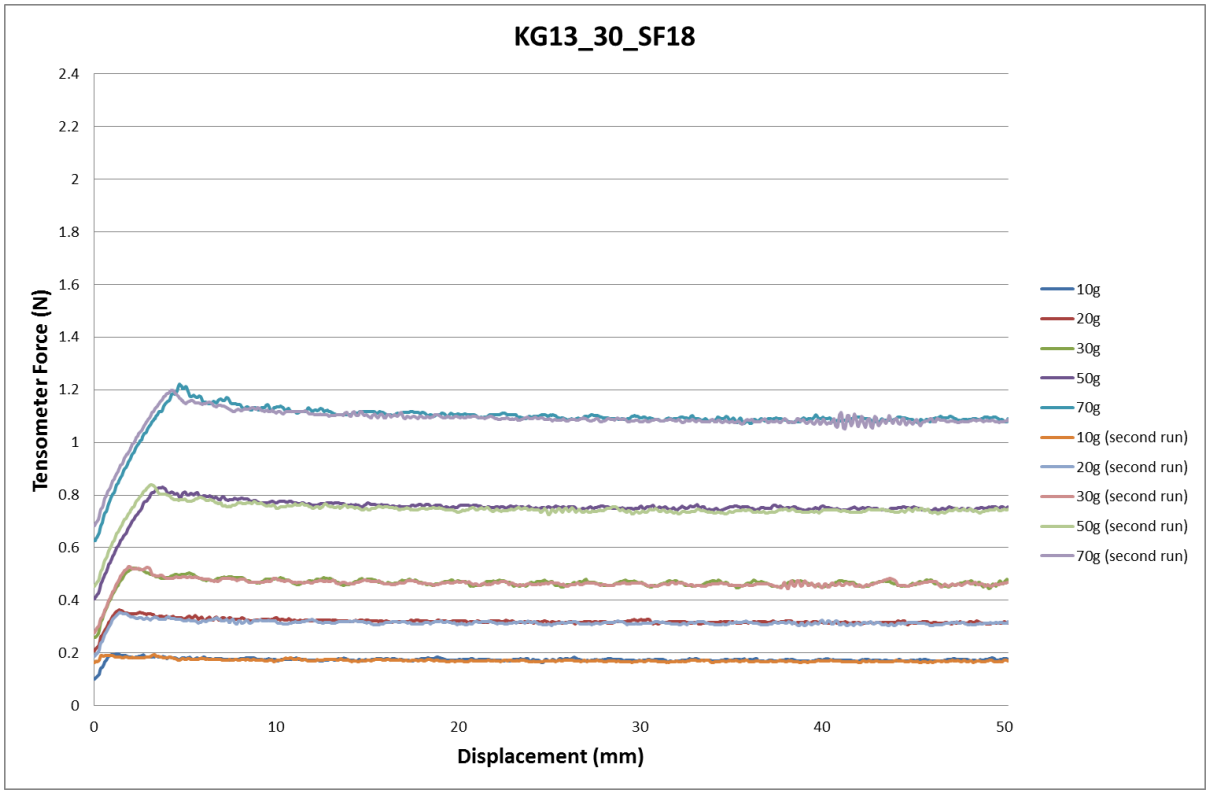
KG13_30_SF18
Tensometer Force (N)
Displacement (mm)
0
0.2
0.4
0.6
0.8
1
1.2
1.4
1.6
1.8
2
2.2
2.4
0
10
20
30
40
50
10g
20g
30g
50g
70g
10g (second run)
20g (second run)
30g (second run)
50g (second run)
70g (second run)

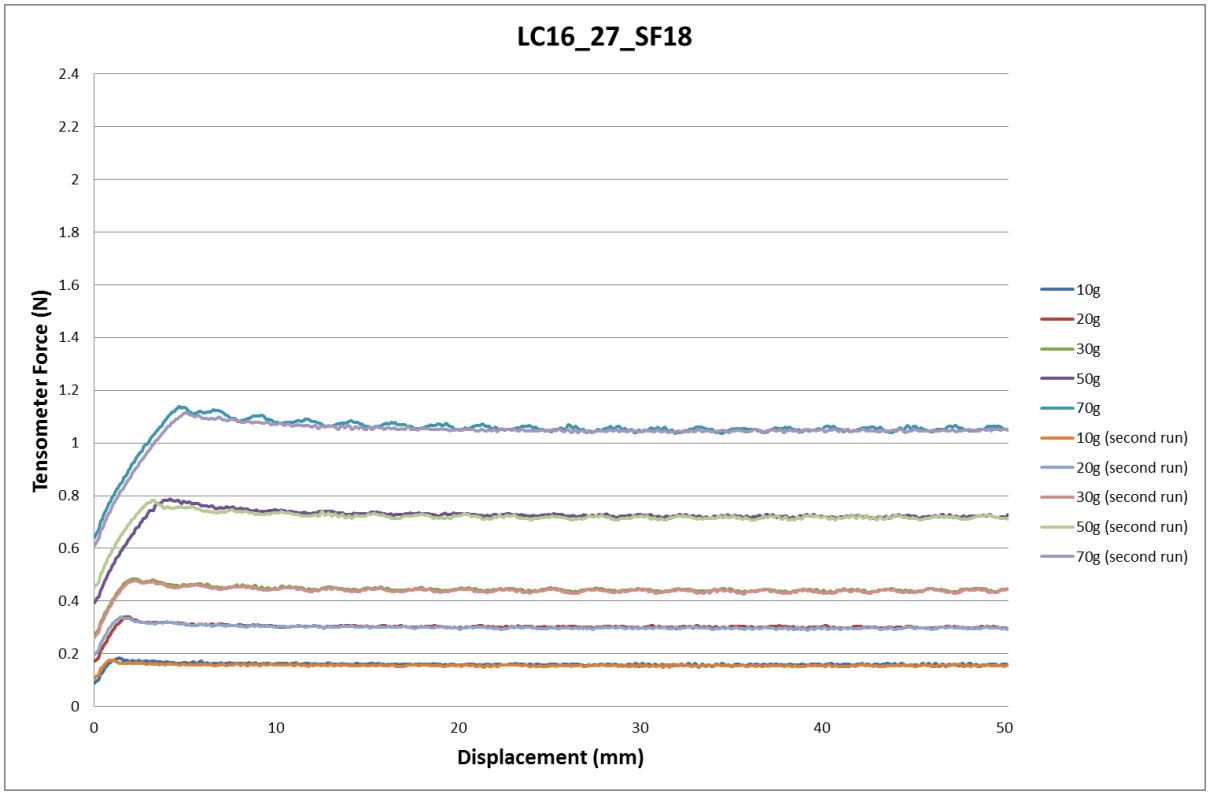
LC16_27_SF18
Tensometer Force (N)
Displacement (mm)
0
0.2
0.4
0.6
0.8
1
1.2
1.4
1.6
1.8
2
2.2
2.4
0
10
20
30
40
50
10g
20g
30g
50g
70g
10g (second run)
20g (second run)
30g (second run)
50g (second run)
70g (second run)

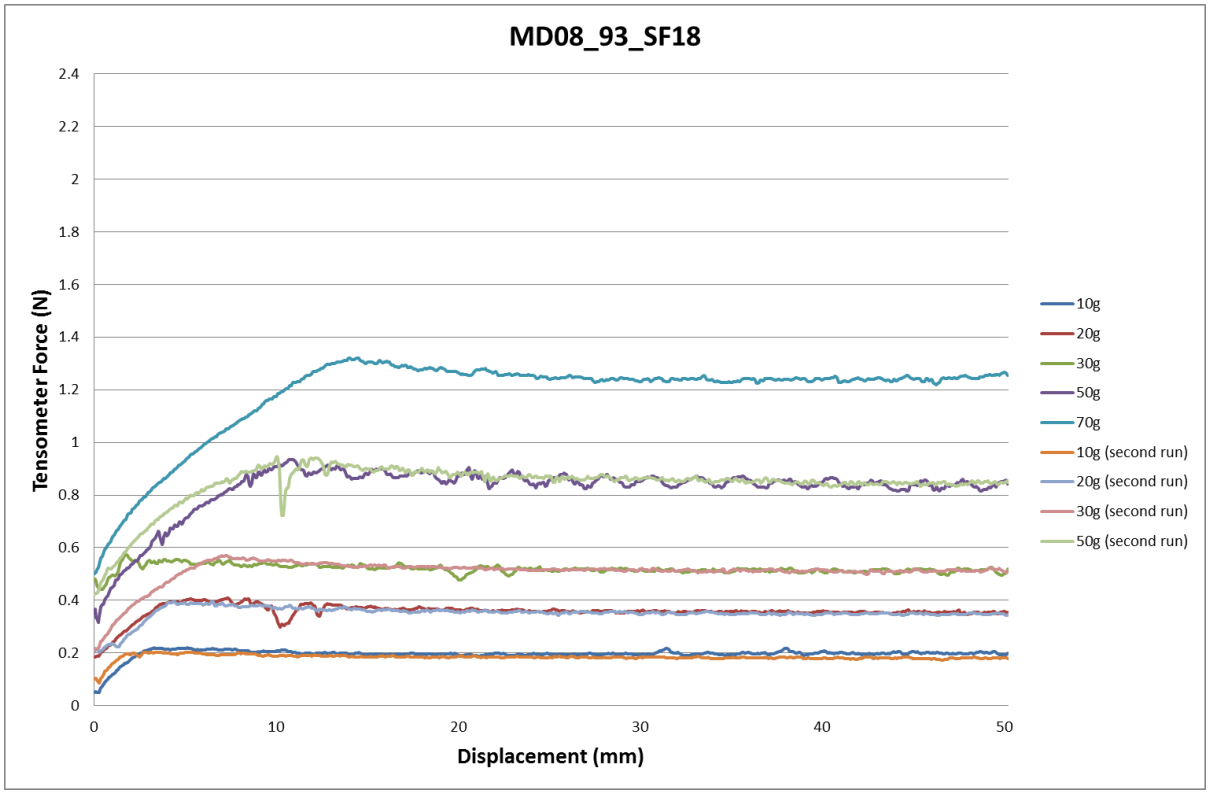
MD08_93_SF18
Tensometer Force (N)
Displacement (mm)
0
0.2
0.4
0.6
0.8
1
1.2
1.4
1.6
1.8
2
2.2
2.4
0
10
20
30
40
50
10g
20g
30g
50g
70g
10g (second run)
20g (second run)
30g (second run)
50g (second run)

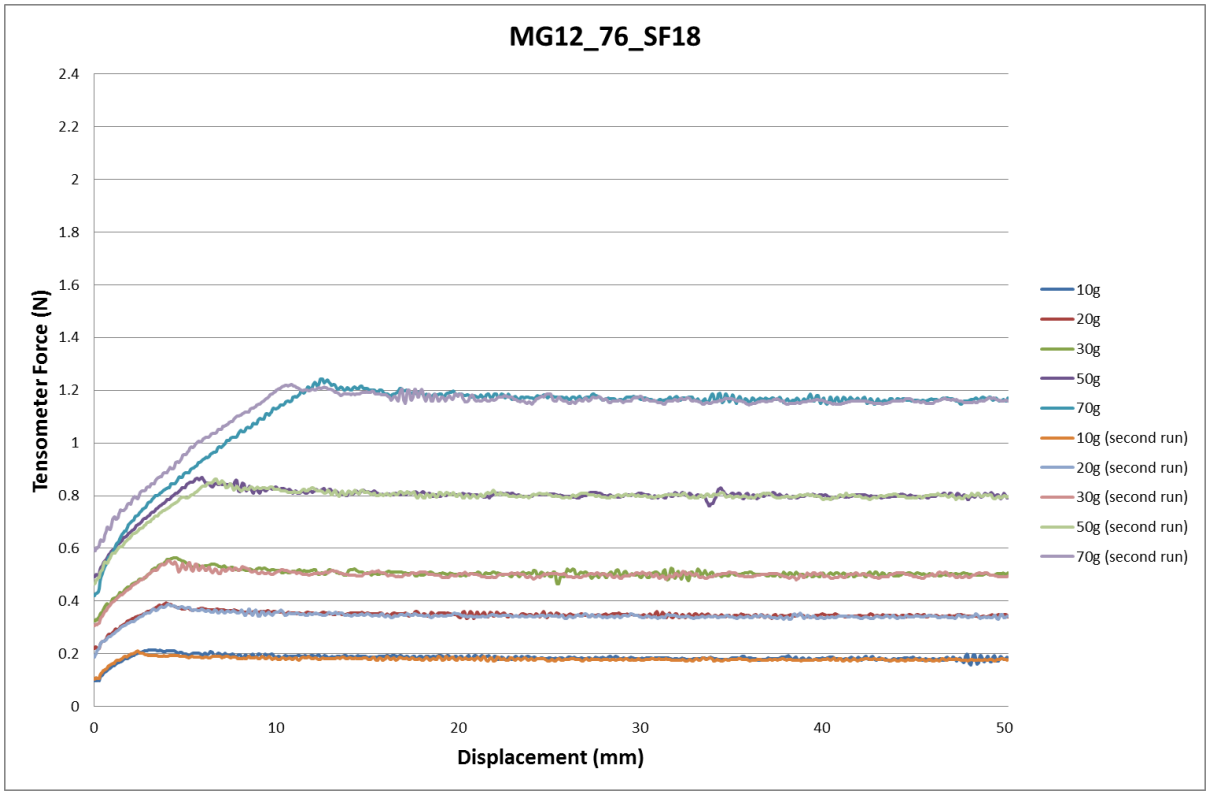
MG12_76_SF18
Tensometer Force (N)
Displacement (mm)
0
0.2
0.4
0.6
0.8
1
1.2
1.4
1.6
1.8
2
2.2
2.4
0
10
20
30
40
50
10g
20g
30g
50g
70g
10g (second run)
20g (second run)
30g (second run)
50g (second run)
70g (second run)

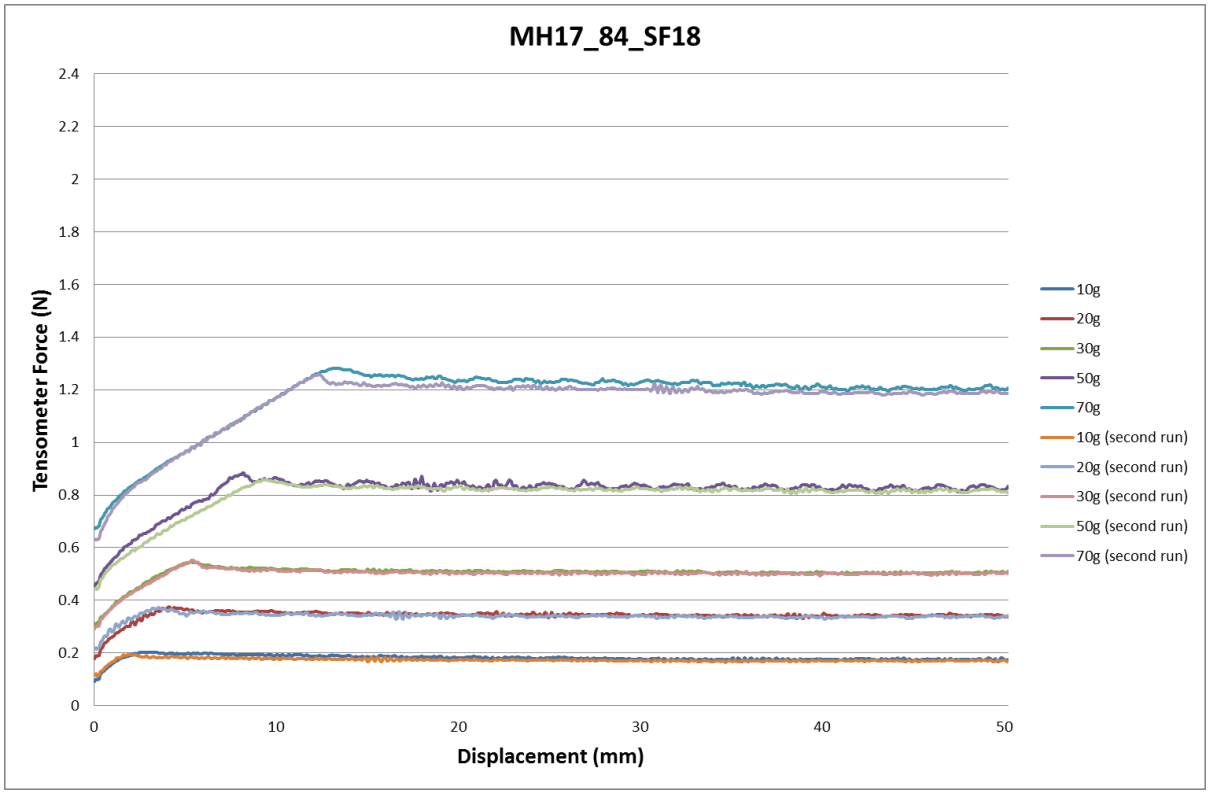
MH17_84_SF18
Tensometer Force (N)
Displacement (mm)
0
0.2
0.4
0.6
0.8
1
1.2
1.4
1.6
1.8
2
2.2
2.4
0
10
20
30
40
50
10g
20g
30g
50g
70g
10g (second run)
20g (second run)
30g (second run)
50g (second run)
70g (second run)

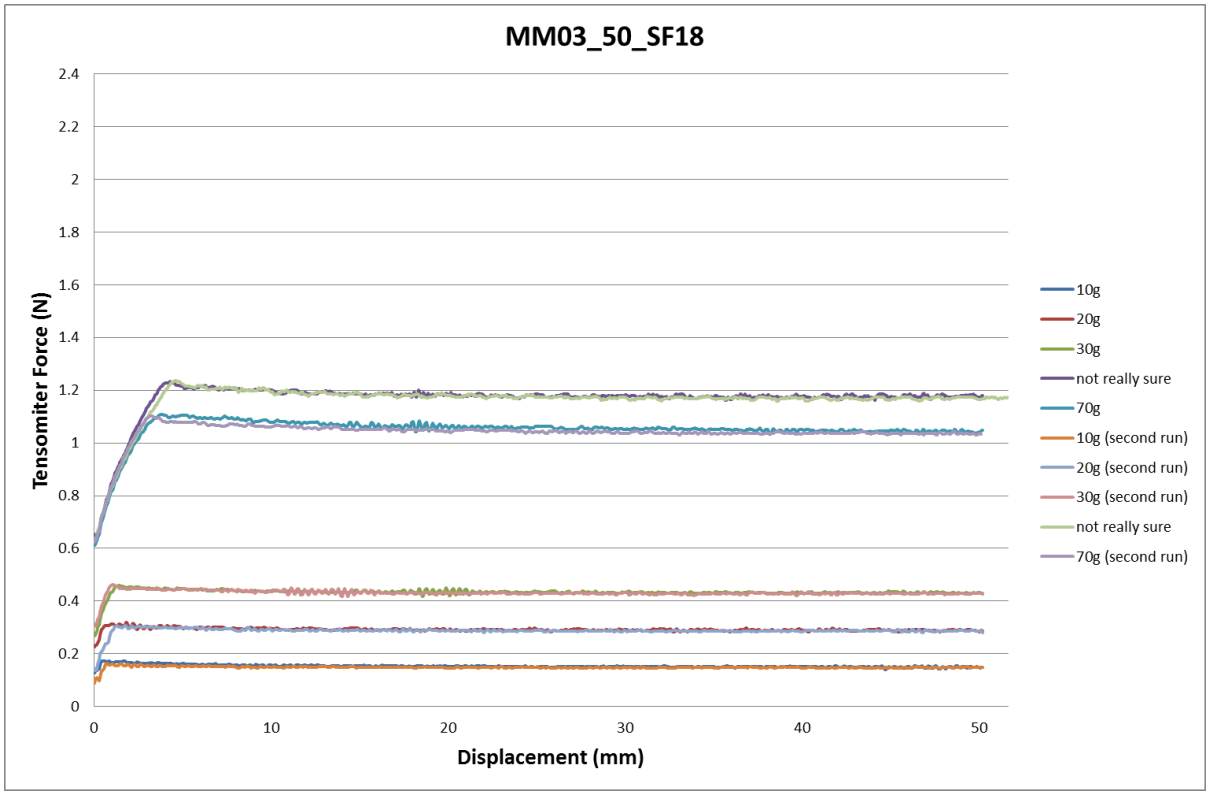
MM03_50_SF18
Tensomiter Force (N)
Displacement (mm)
0
0.2
0.4
0.6
0.8
1
1.2
1.4
1.6
1.8
2
2.2
2.4
0
10
20
30
40
50
10g
20g
30g
not really sure
70g
10g (second run)
20g (second run)
30g (second run)
not really sure
70g (second run)

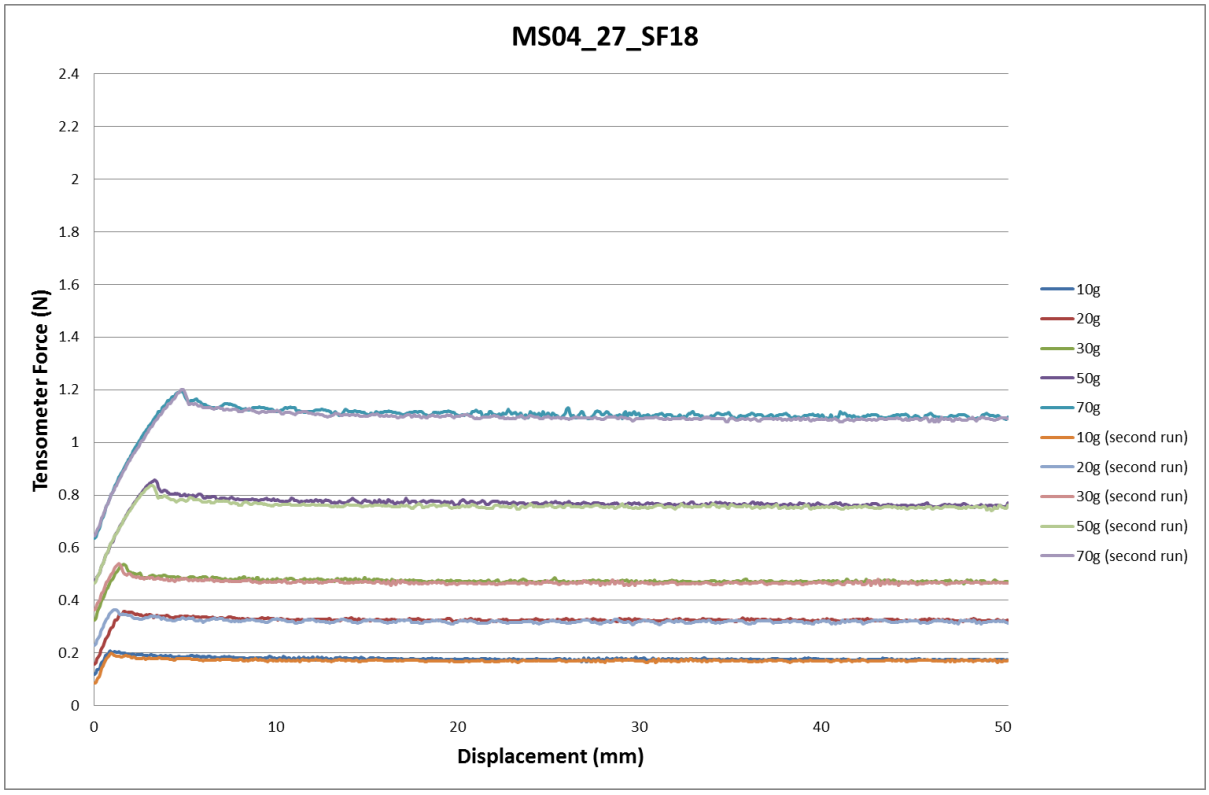
MS04_27_SF18
Tensometer Force (N)
Displacement (mm)
0
0.2
0.4
0.6
0.8
1
1.2
1.4
1.6
1.8
2
2.2
2.4
0
10
20
30
40
50
10g
20g
30g
50g
70g
10g (second run)
20g (second run)
30g (second run)
50g (second run)
70g (second run)

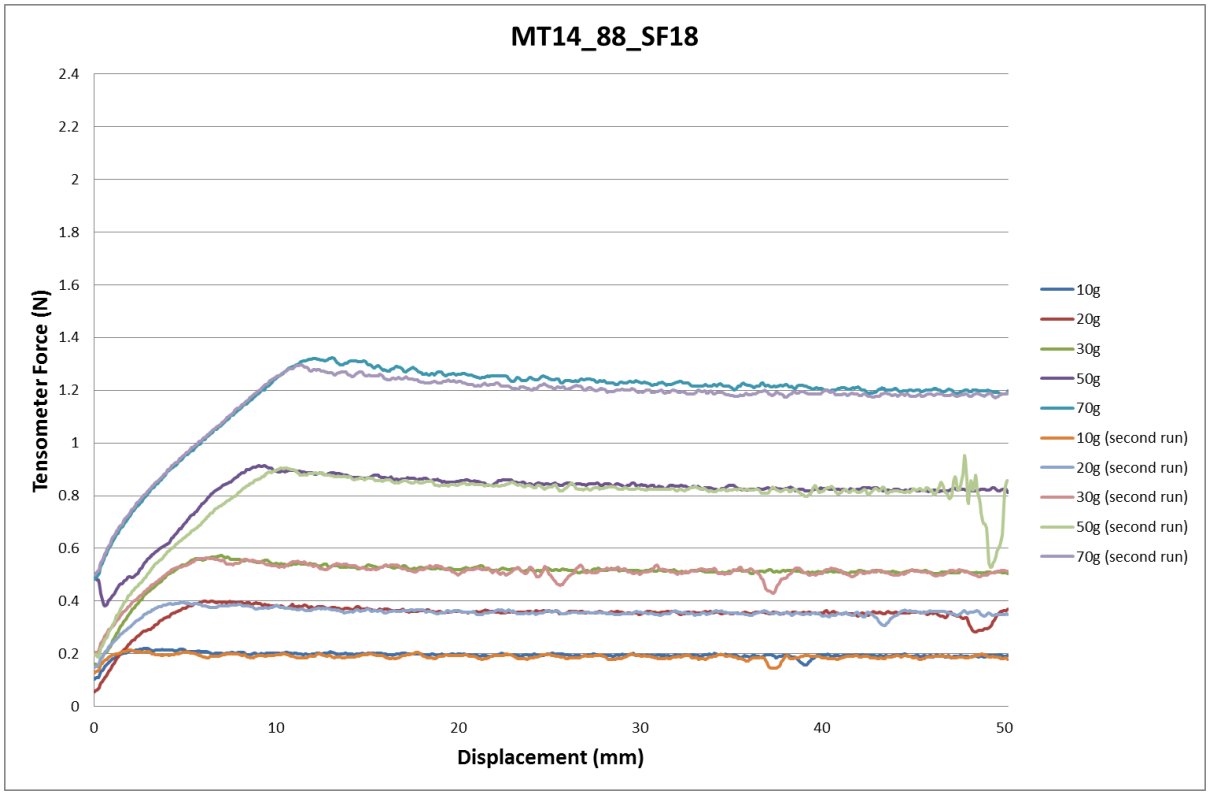
MT14_88_SF18
Tensometer Force (N)
Displacement (mm)
0
0.2
0.4
0.6
0.8
1
1.2
1.4
1.6
1.8
2
2.2
2.4
0
10
20
30
40
50
10g
20g
30g
50g
70g
10g (second run)
20g (second run)
30g (second run)
50g (second run)
70g (second run)

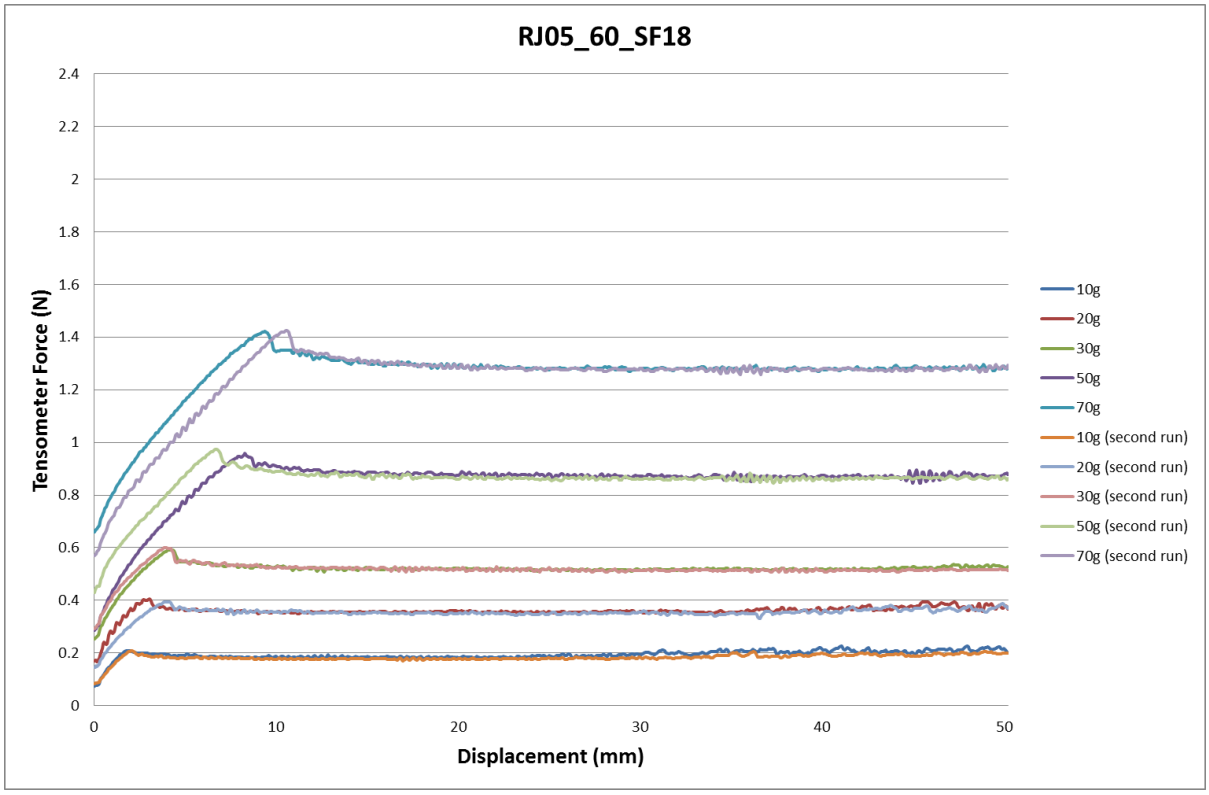
RJ05_60_SF18
Tensometer Force (N)
Displacement (mm)
0
0.2
0.4
0.6
0.8
1
1.2
1.4
1.6
1.8
2
2.2
2.4
0
10
20
30
40
50
10g
20g
30g
50g
70g
10g (second run)
20g (second run)
30g (second run)
50g (second run)
70g (second run)

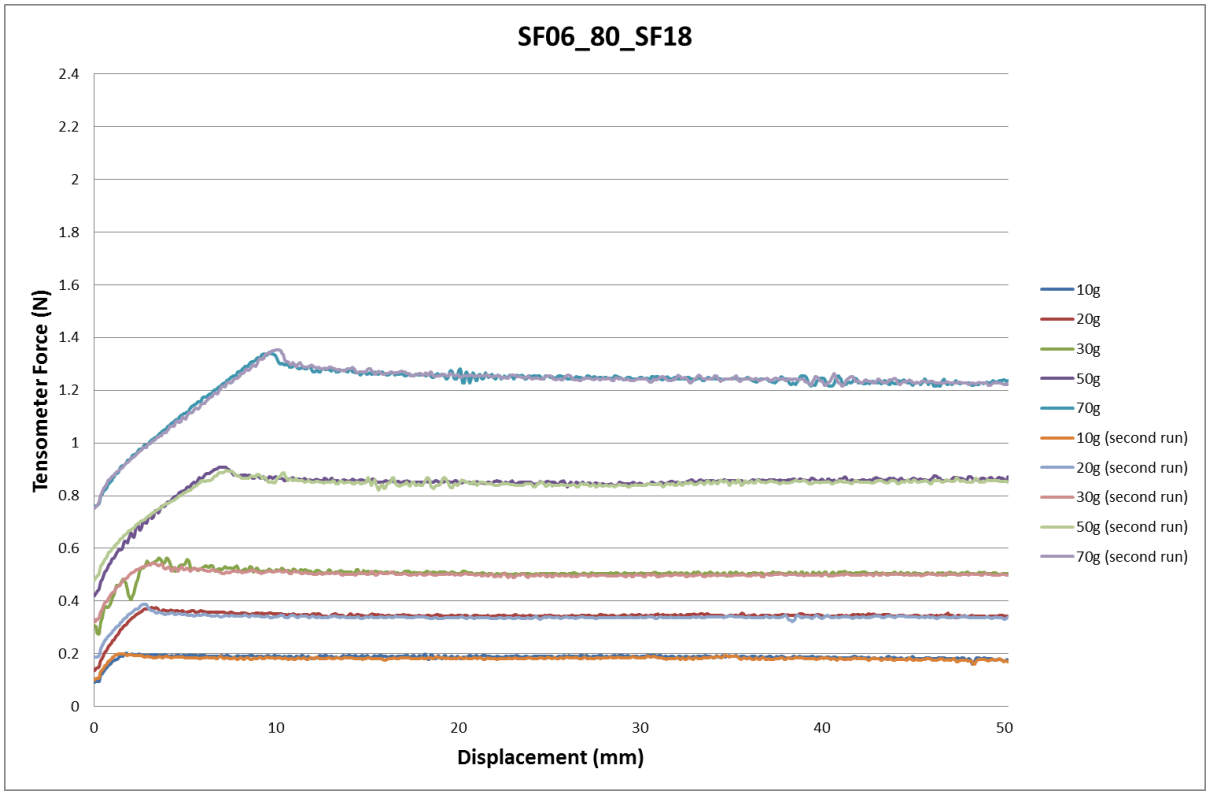
SF06_80_SF18
Tensometer Force (N)
Displacement (mm)
0
0.2
0.4
0.6
0.8
1
1.2
1.4
1.6
1.8
2
2.2
2.4
0
10
20
30
40
50
10g
20g
30g
50g
70g
10g (second run)
20g (second run)
30g (second run)
50g (second run)
70g (second run)

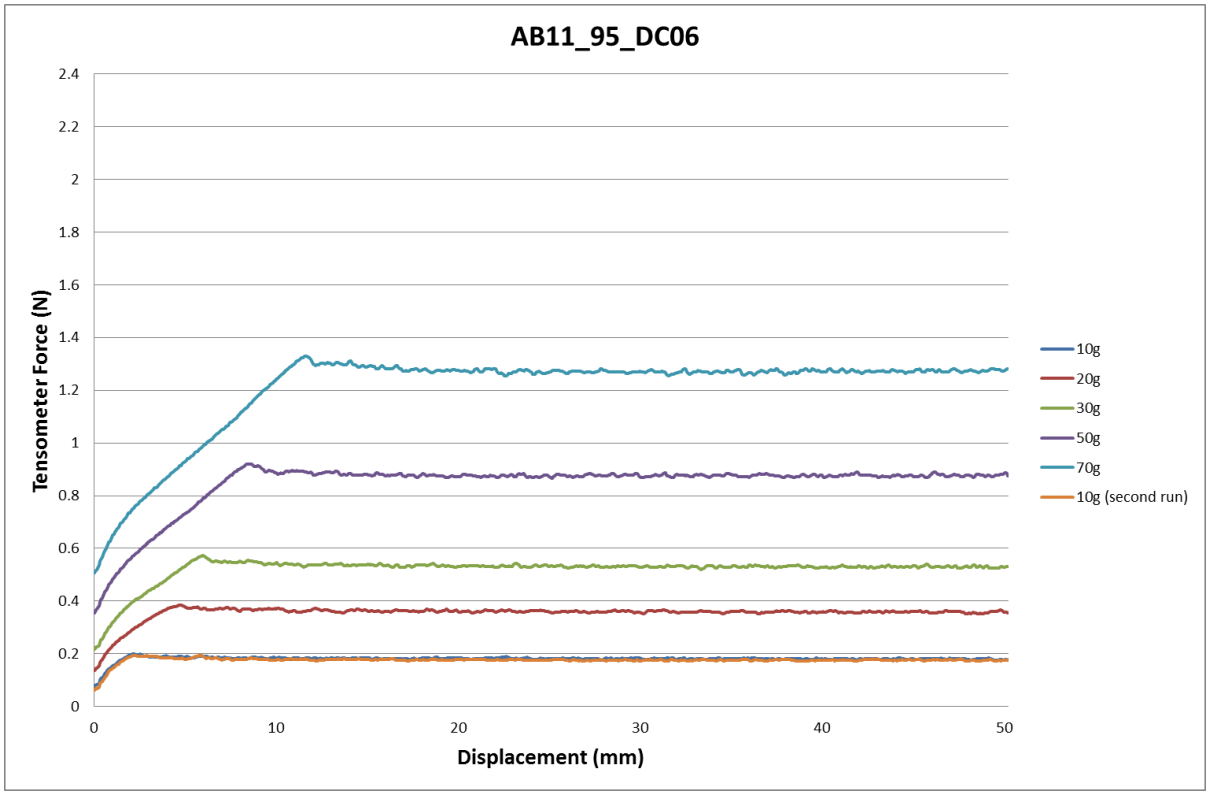
AB11_95_DC06
Tensometer Force (N)
Displacement (mm)
0
0.2
0.4
0.6
0.8
1
1.2
1.4
1.6
1.8
2
2.2
2.4
0
10
20
30
40
50
10g
20g
30g
50g
70g
10g (second run)

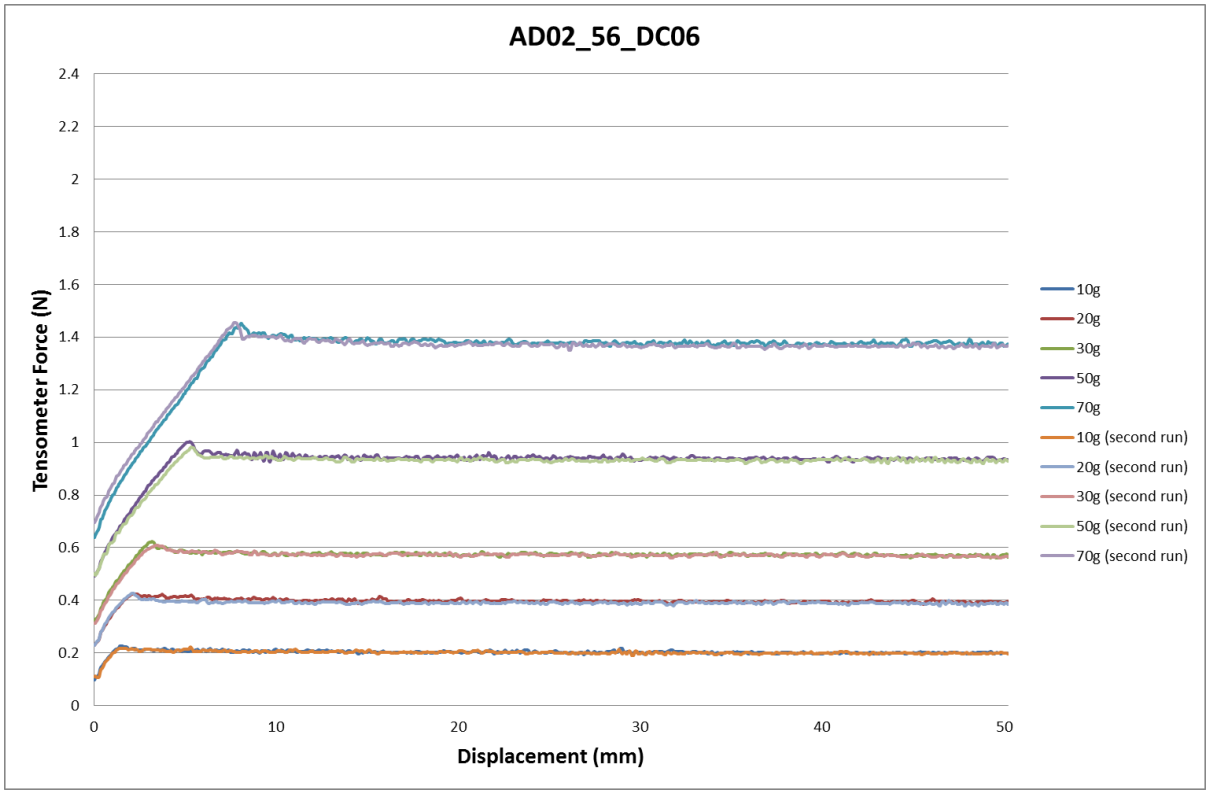
AD02_56_DC06
Tensometer Force (N)
Displacement (mm)
0
0.2
0.4
0.6
0.8
1
1.2
1.4
1.6
1.8
2
2.2
2.4
0
10
20
30
40
50
10g
20g
30g
50g
70g
10g (second run)
20g (second run)
30g (second run)
50g (second run)
70g (second run)

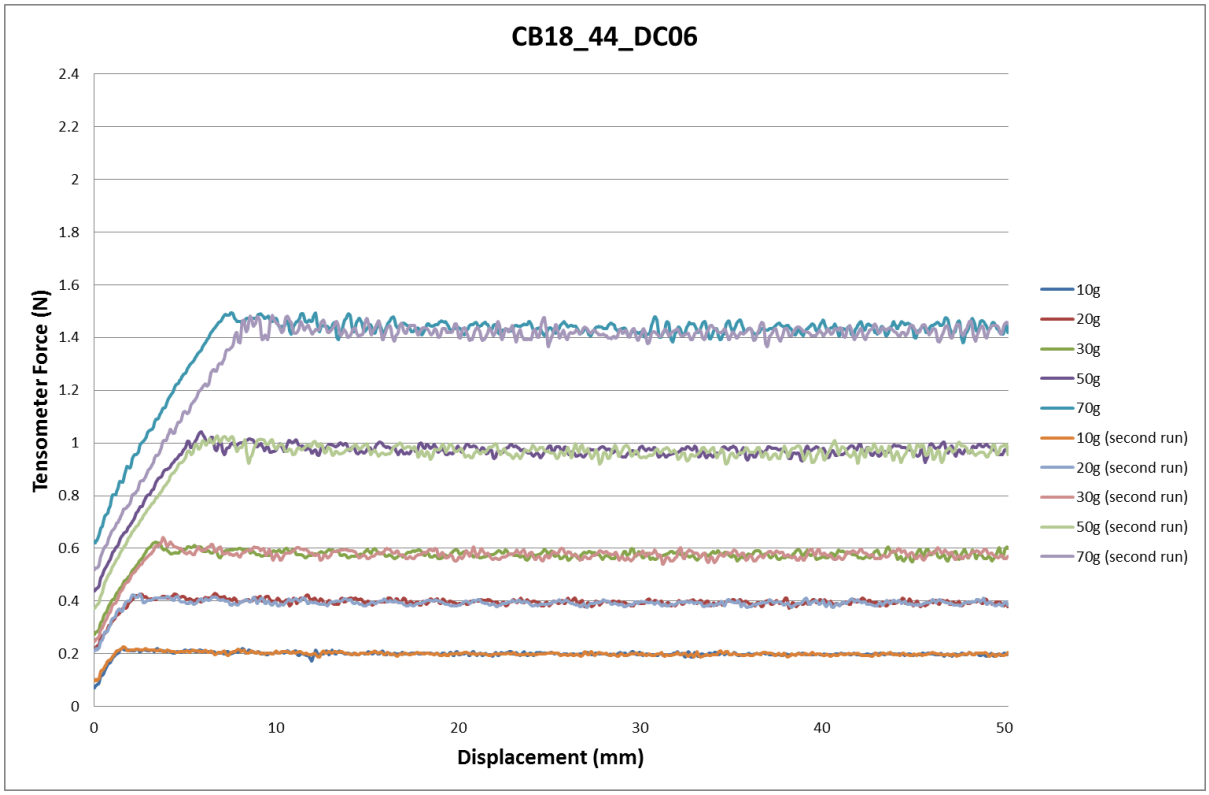
CB18_44_DC06
Tensometer Force (N)
Displacement (mm)
0
0.2
0.4
0.6
0.8
1
1.2
1.4
1.6
1.8
2
2.2
2.4
0
10
20
30
40
50
10g
20g
30g
50g
70g
10g (second run)
20g (second run)
30g (second run)
50g (second run)
70g (second run)

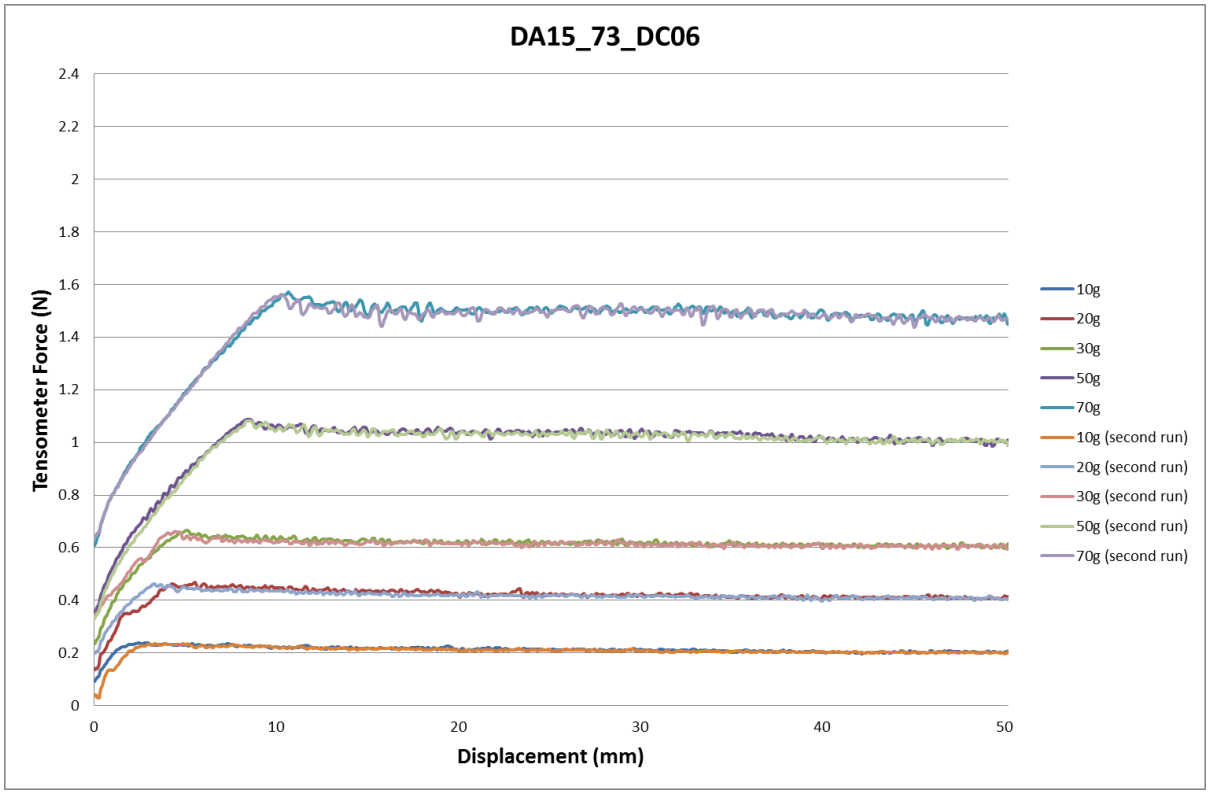
DA15_73_DC06
Tensometer Force (N)
Displacement (mm)
0
0.2
0.4
0.6
0.8
1
1.2
1.4
1.6
1.8
2
2.2
2.4
0
10
20
30
40
50
10g
20g
30g
50g
70g
10g (second run)
20g (second run)
30g (second run)
50g (second run)
70g (second run)

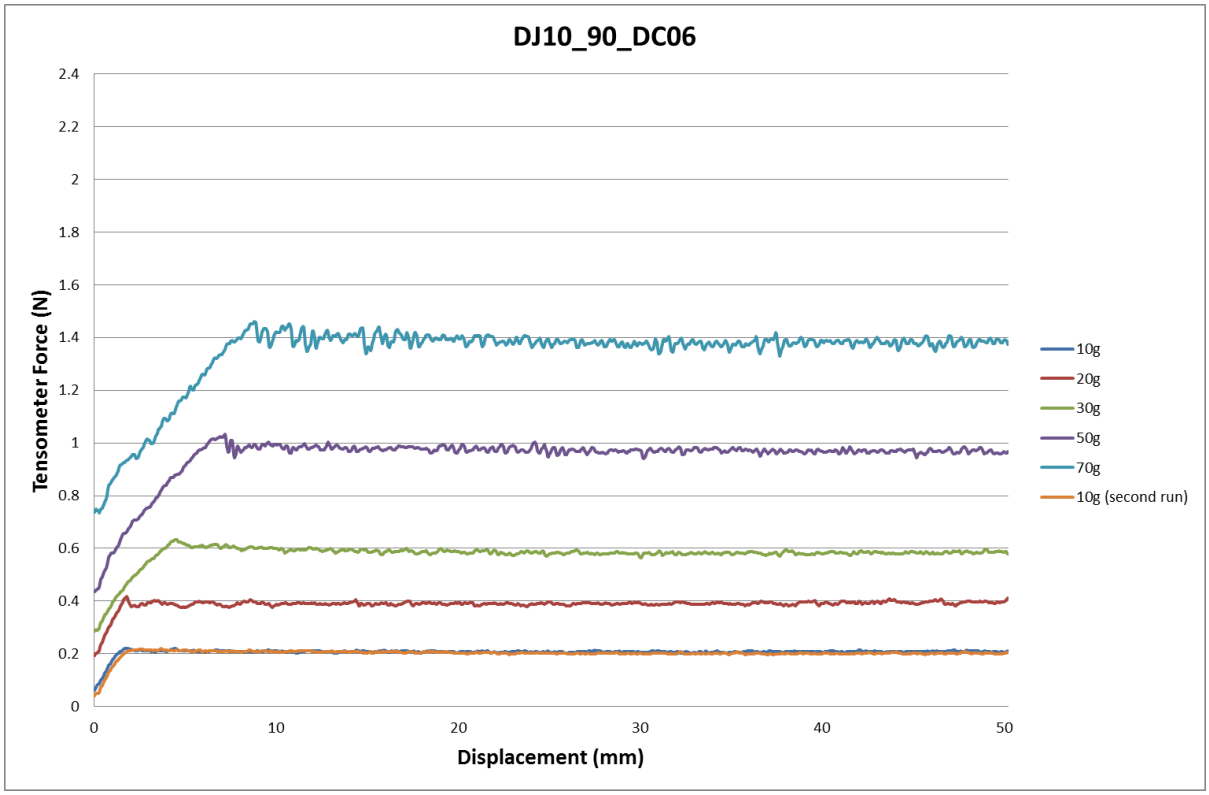
DJ10_90_DC06
Tensometer Force (N)
Displacement (mm)
0
0.2
0.4
0.6
0.8
1
1.2
1.4
1.6
1.8
2
2.2
2.4
0
10
20
30
40
50
10g
20g
30g
50g
70g
10g (second run)


HJ07_72_DC06
Tensometer Force (N)
Displacement (mm)
0
0.2
0.4
0.6
0.8
1
1.2
1.4
1.6
1.8
2
2.2
2.4
0
10
20
30
40
50
10g
20g
30g
50g
70g
10g (second run)

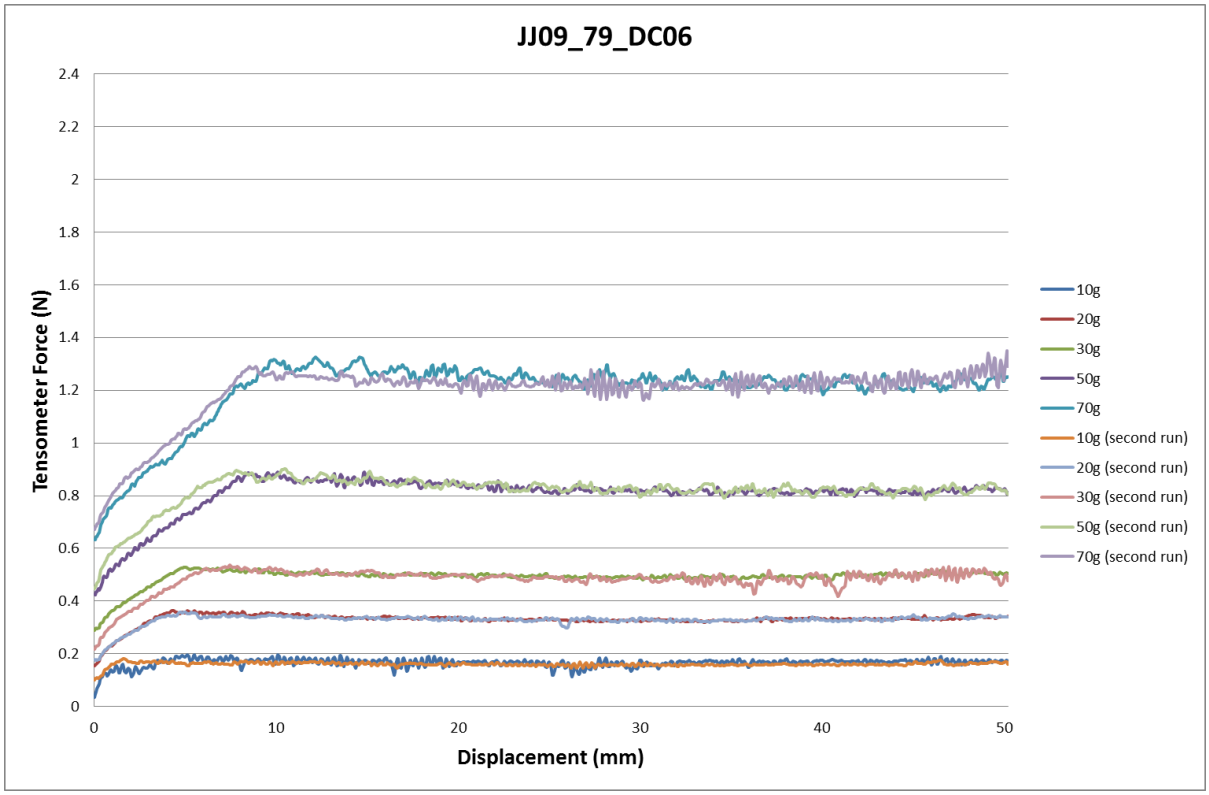
JJ09_79_DC06
Tensometer Force (N)
Displacement (mm)
0
0.2
0.4
0.6
0.8
1
1.2
1.4
1.6
1.8
2
2.2
2.4
0
10
20
30
40
50
10g
20g
30g
50g
70g
10g (second run)
20g (second run)
30g (second run)
50g (second run)
70g (second run)

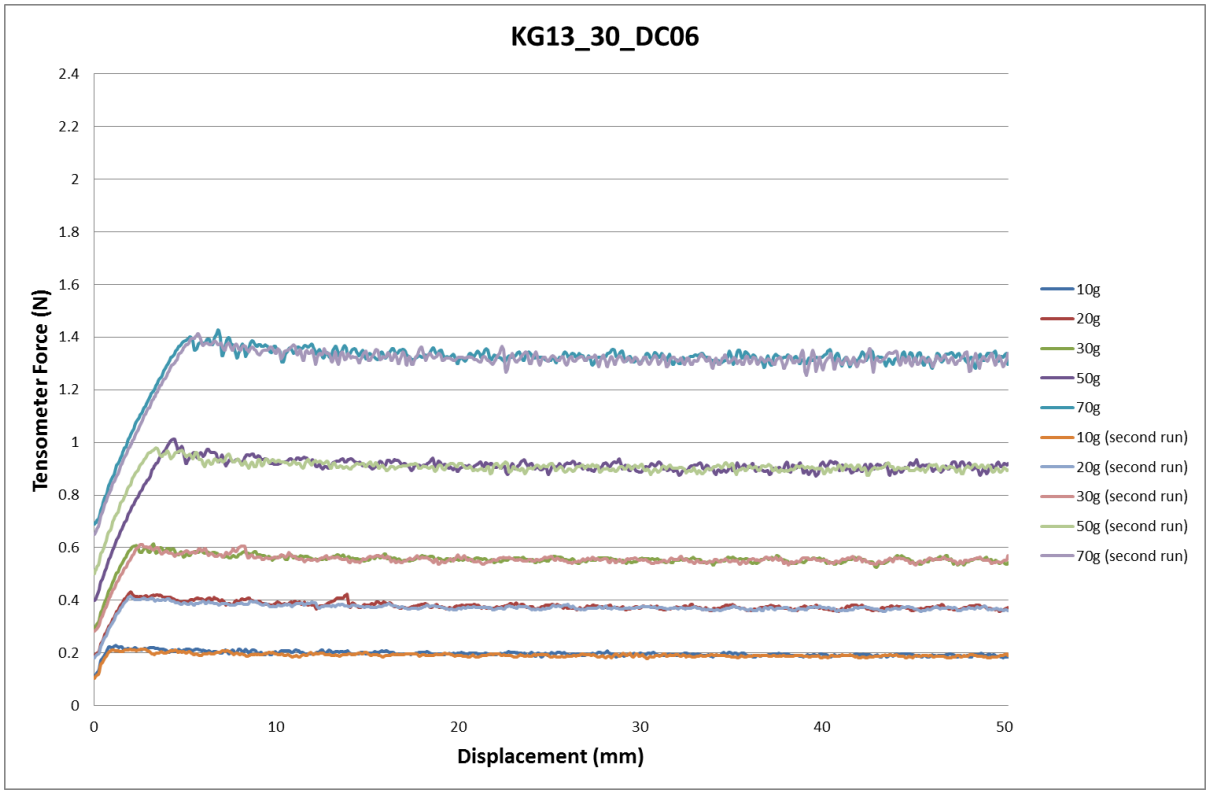
KG13_30_DC06
Tensometer Force (N)
Displacement (mm)
0
0.2
0.4
0.6
0.8
1
1.2
1.4
1.6
1.8
2
2.2
2.4
0
10
20
30
40
50
10g
20g
30g
50g
70g
10g (second run)
20g (second run)
30g (second run)
50g (second run)
70g (second run)

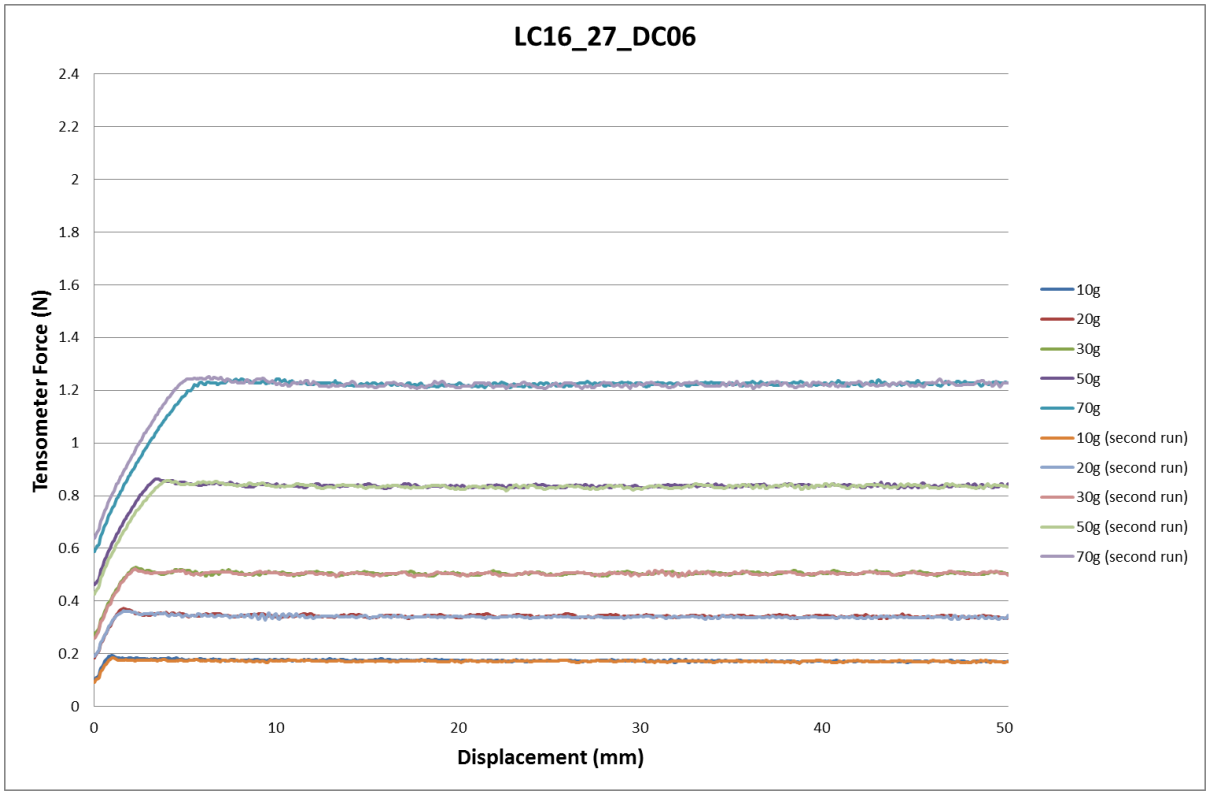
LC16_27_DC06
Tensometer Force (N)
Displacement (mm)
0
0.2
0.4
0.6
0.8
1
1.2
1.4
1.6
1.8
2
2.2
2.4
0
10
20
30
40
50
10g
20g
30g
50g
70g
10g (second run)
20g (second run)
30g (second run)
50g (second run)
70g (second run)

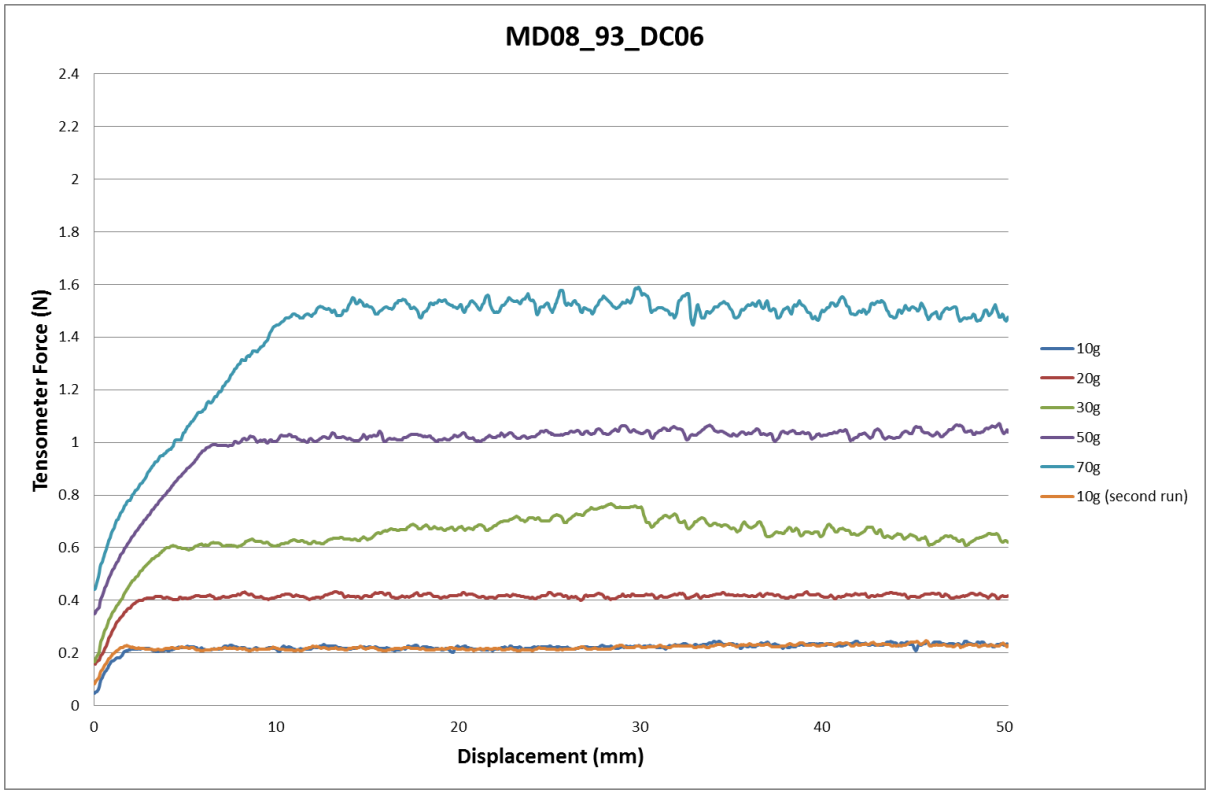
MD08_93_DC06
Tensometer Force (N)
Displacement (mm)
0
0.2
0.4
0.6
0.8
1
1.2
1.4
1.6
1.8
2
2.2
2.4
0
10
20
30
40
50
10g
20g
30g
50g
70g
10g (second run)

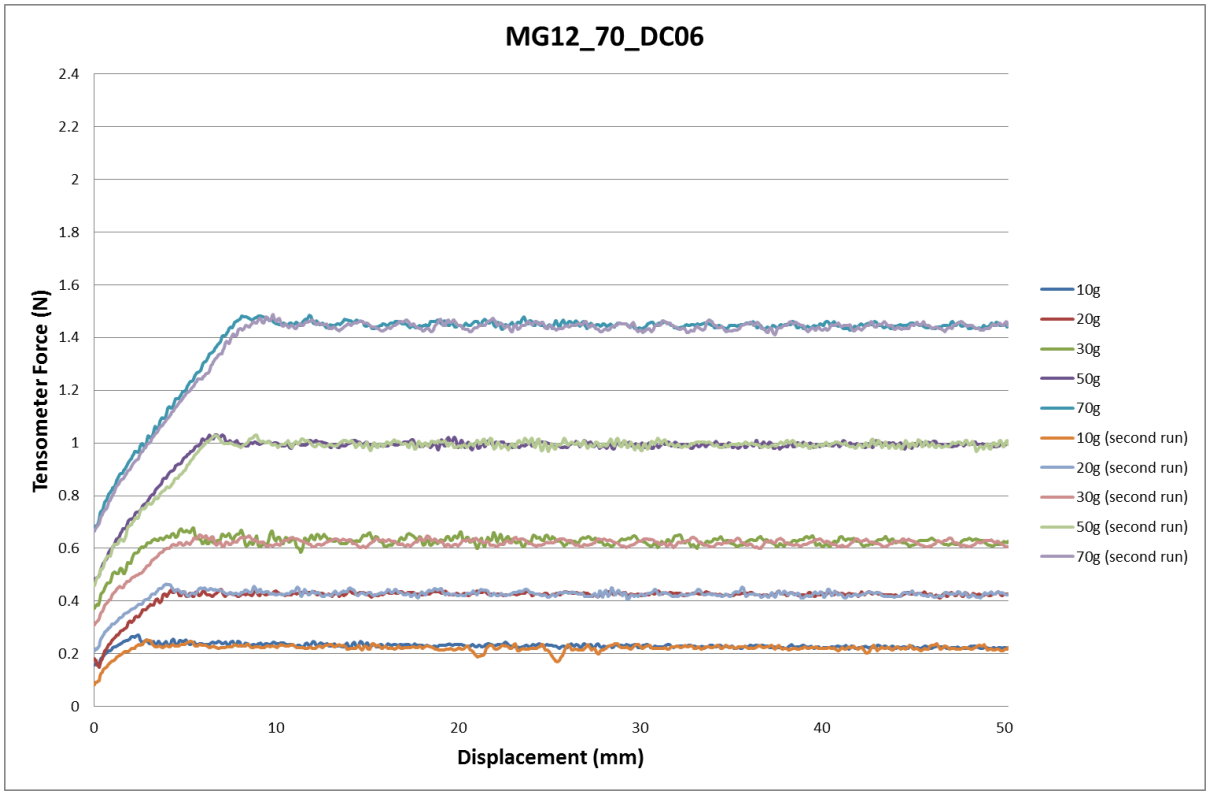
MG12_70_DC06
Tensometer Force (N)
Displacement (mm)
0
0.2
0.4
0.6
0.8
1
1.2
1.4
1.6
1.8
2
2.2
2.4
0
10
20
30
40
50
10g
20g
30g
50g
70g
10g (second run)
20g (second run)
30g (second run)
50g (second run)
70g (second run)

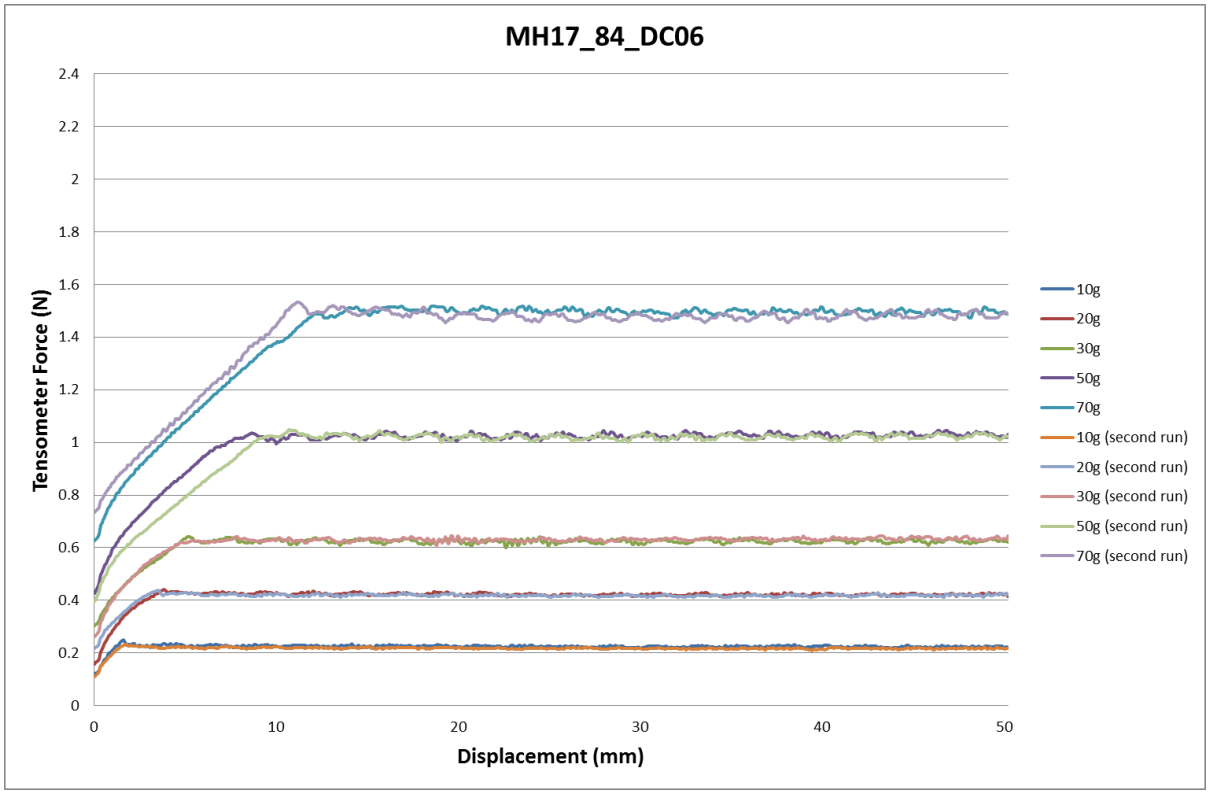
MH17_84_DC06
Tensometer Force (N)
Displacement (mm)
0
0.2
0.4
0.6
0.8
1
1.2
1.4
1.6
1.8
2
2.2
2.4
0
10
20
30
40
50
10g
20g
30g
50g
70g
10g (second run)
20g (second run)
30g (second run)
50g (second run)
70g (second run)

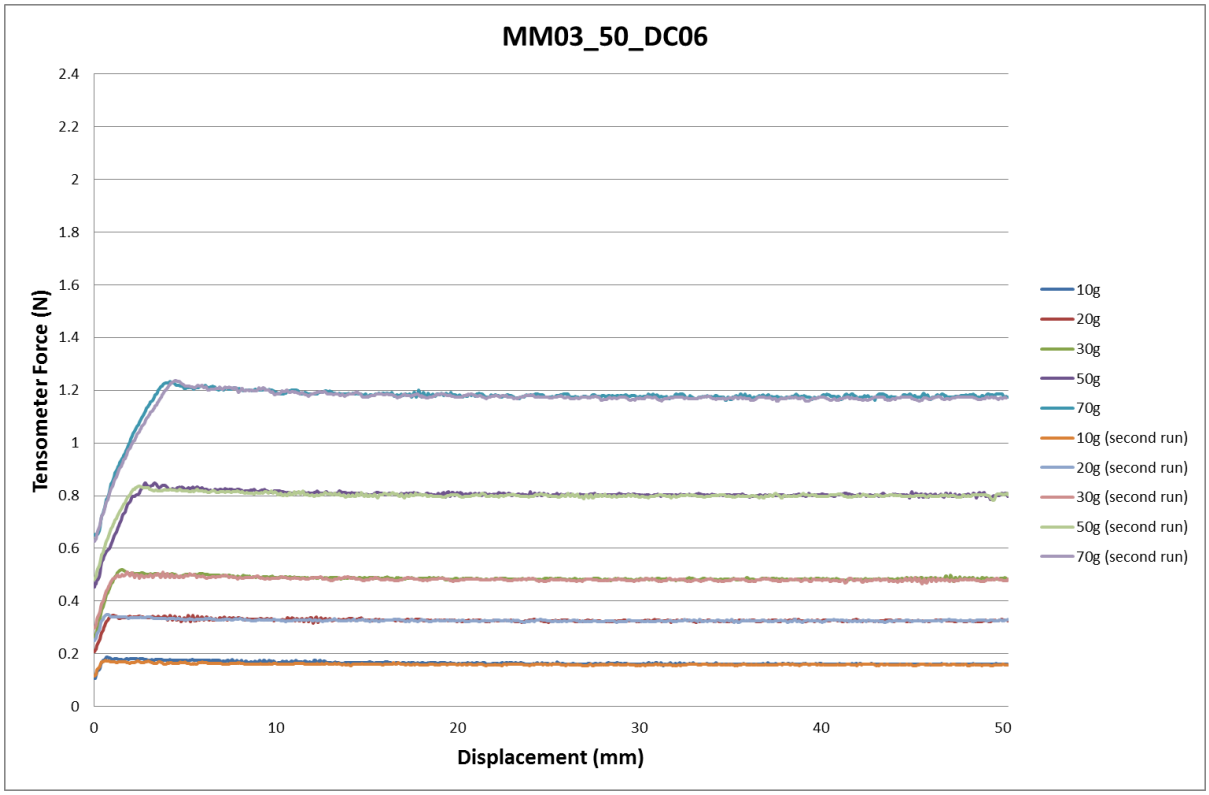
MM03_50_DC06
Tensometer Force (N)
Displacement (mm)
0
0.2
0.4
0.6
0.8
1
1.2
1.4
1.6
1.8
2
2.2
2.4
0
10
20
30
40
50
10g
20g
30g
50g
70g
10g (second run)
20g (second run)
30g (second run)
50g (second run)
70g (second run)

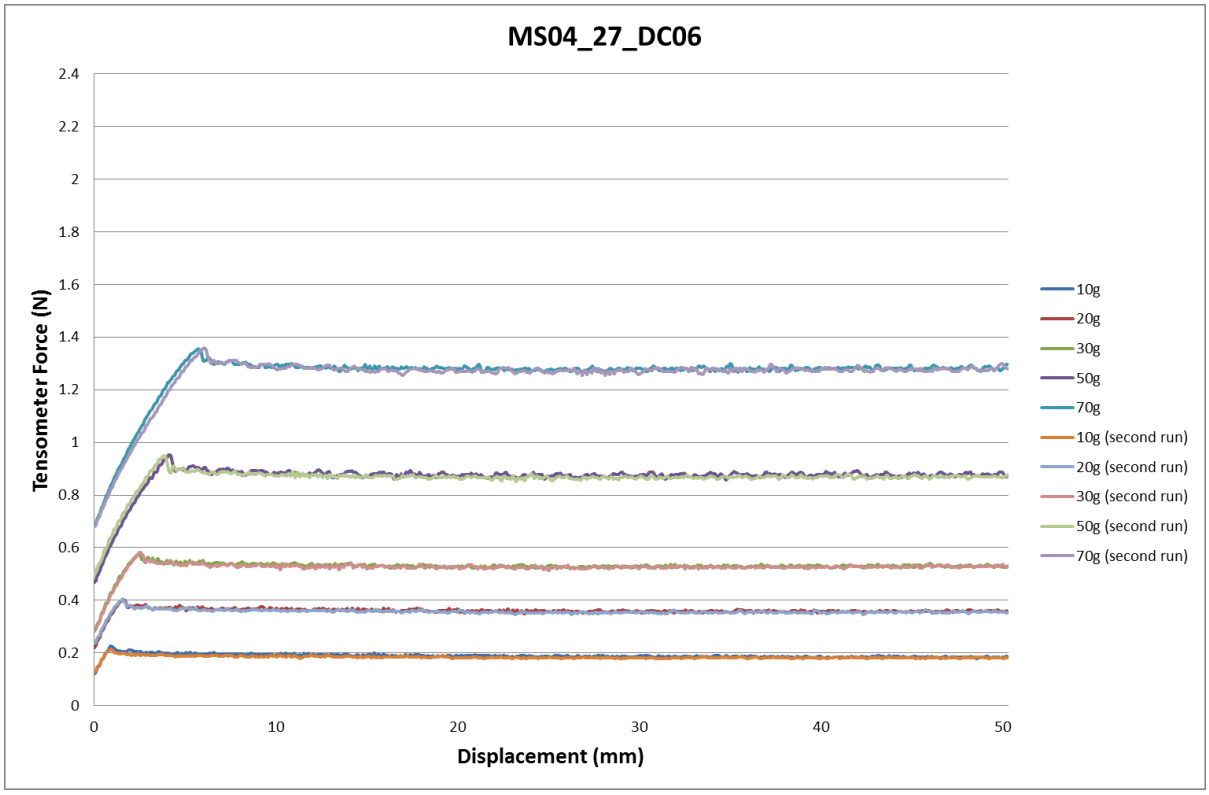
MS04_27_DC06
Tensometer Force (N)
Displacement (mm)
0
0.2
0.4
0.6
0.8
1
1.2
1.4
1.6
1.8
2
2.2
2.4
0
10
20
30
40
50
10g
20g
30g
50g
70g
10g (second run)
20g (second run)
30g (second run)
50g (second run)
70g (second run)

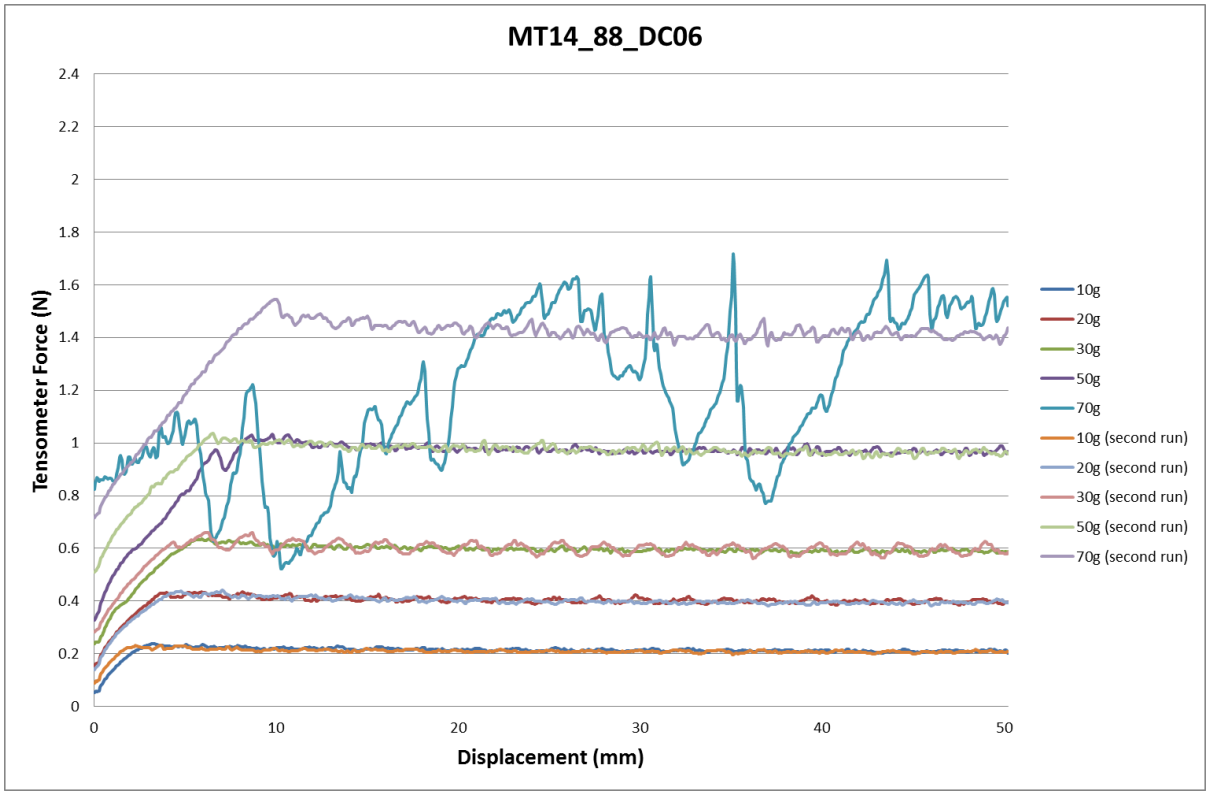
MT14_88_DC06
Tensometer Force (N)
Displacement (mm)
0
0.2
0.4
0.6
0.8
1
1.2
1.4
1.6
1.8
2
2.2
2.4
0
10
20
30
40
50
10g
20g
30g
50g
70g
10g (second run)
20g (second run)
30g (second run)
50g (second run)
70g (second run)

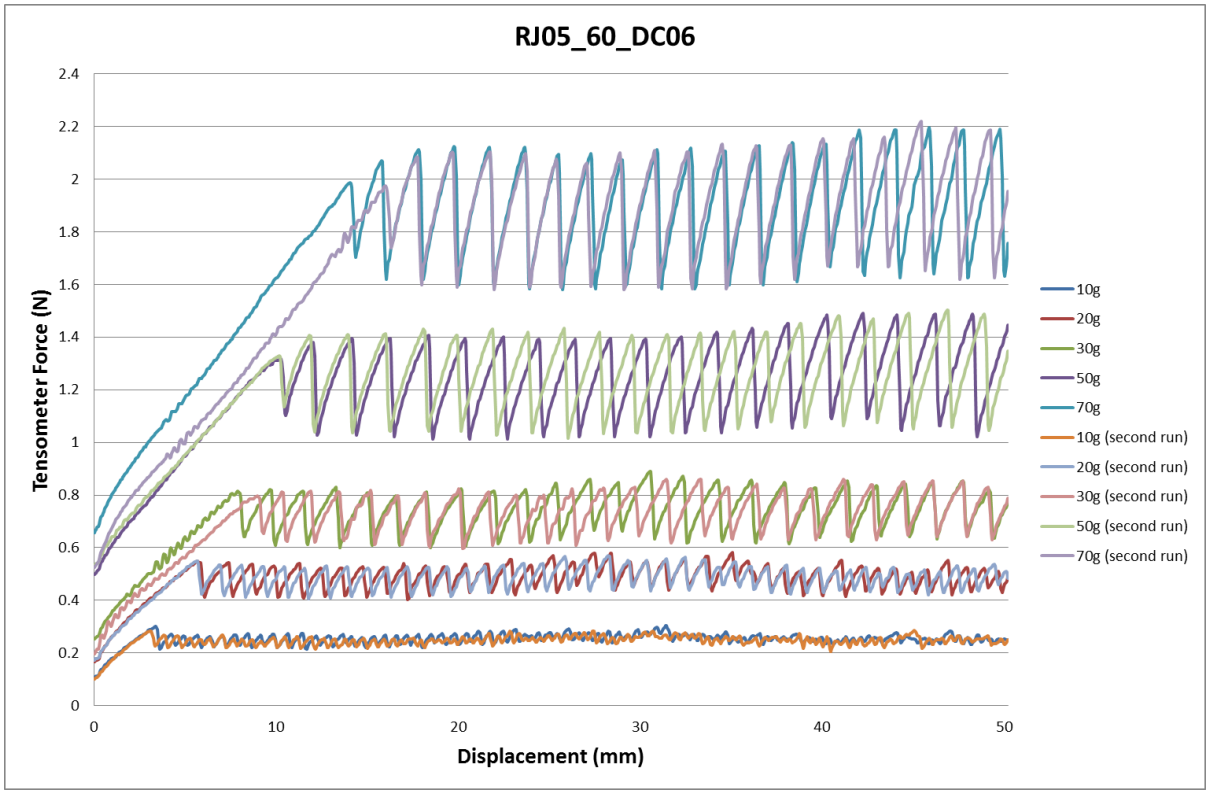
RJ05_60_DC06
Tensometer Force (N)
Displacement (mm)
0
0.2
0.4
0.6
0.8
1
1.2
1.4
1.6
1.8
2
2.2
2.4
0
10
20
30
40
50
10g
20g
30g
50g
70g
10g (second run)
20g (second run)
30g (second run)
50g (second run)
70g (second run)

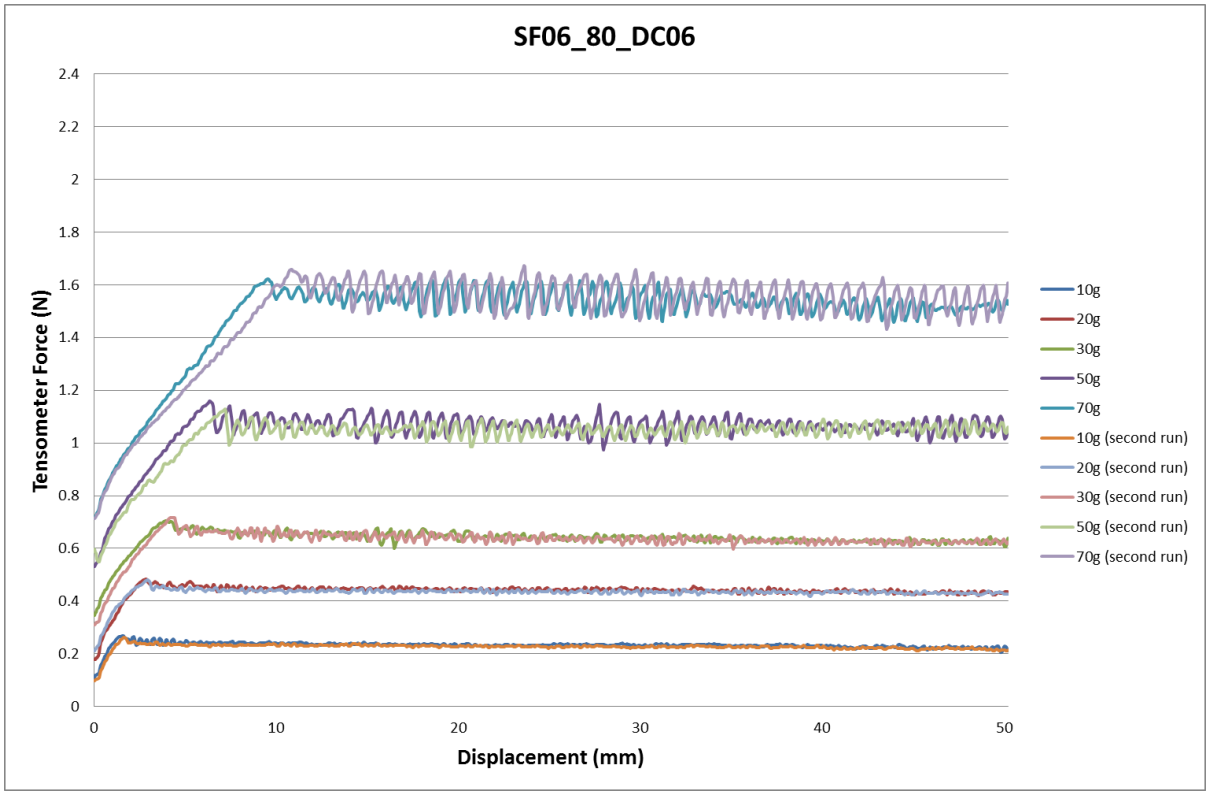
SF06_80_DC06
Tensometer Force (N)
Displacement (mm)
0
0.2
0.4
0.6
0.8
1
1.2
1.4
1.6
1.8
2
2.2
2.4
0
10
20
30
40
50
10g
20g
30g
50g
70g
10g (second run)
20g (second run)
30g (second run)
50g (second run)
70g (second run)

APPENDIX C

Library of tensometer curves from all friction measurements on compliant and rigid cylinders

This appendix contains the tensometer curves for all the compliant arm friction experiments discussed in Chapter 5. These were five fabrics (SF03, SF14, SF17, SF18 and DC06) and two compliant arms. The title of each graph is the kind of silicone gel (S) and the fabric (F) which corresponds at each measurement (SSSSSSSS_FFFF). For all the compliant arms two runs were made for each dead weight load, for each fabric. For the rigid cylinders the title of each graph is the cone of each fabric and the number of membrane I use, for instance (FFFF_1st membrane)

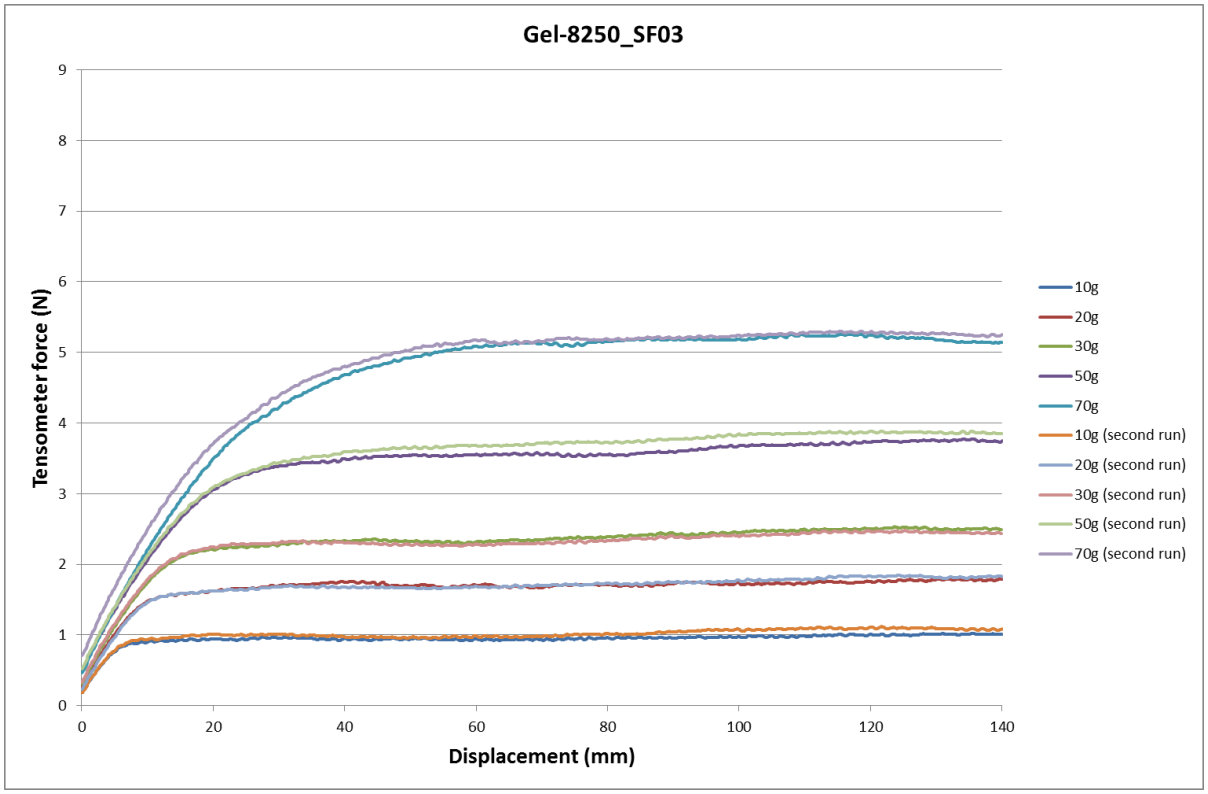
Gel-8250_SF03
Tensometer force (N)
Displacement (mm)
0
1
2
3
4
5
6
7
8
9
0
20
40
60
80
100
120
140
10g
20g
30g
50g
70g
10g (second run)
20g (second run)
30g (second run)
50g (second run)
70g (second run)

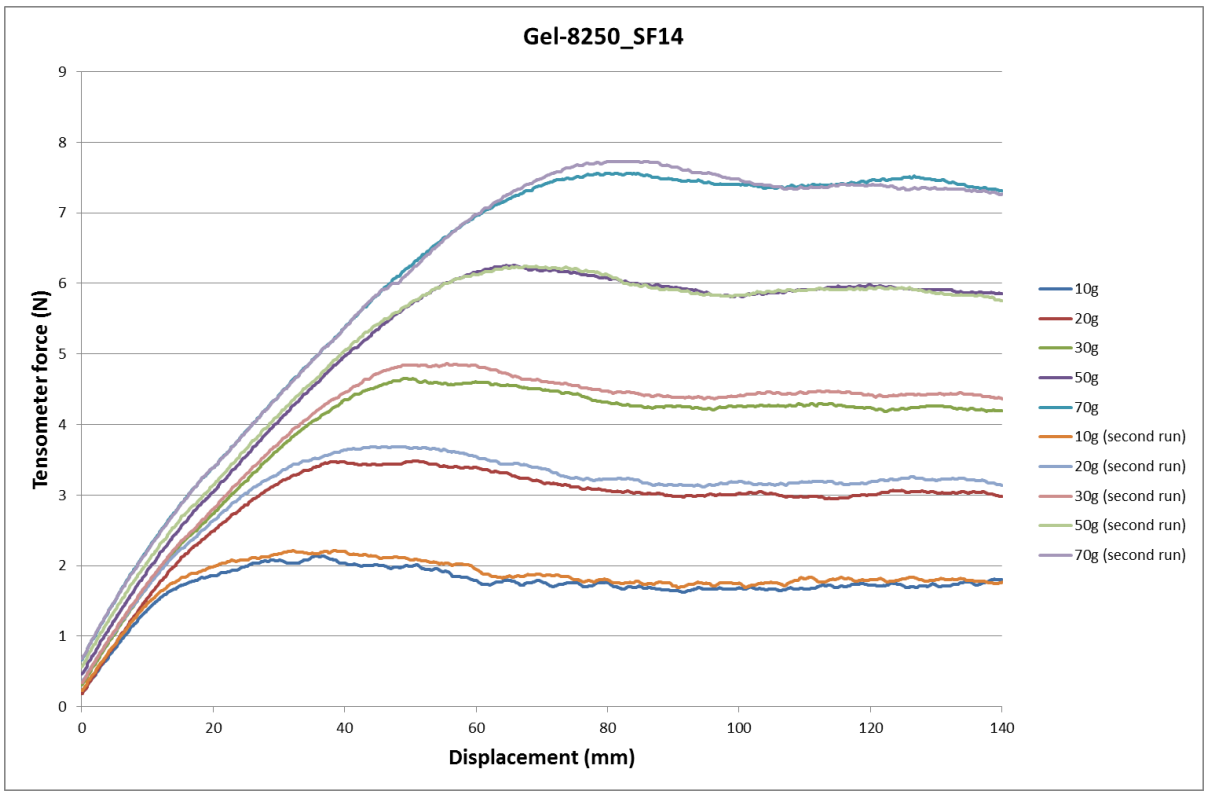
Gel-8250_SF14
Tensometer force (N)
Displacement (mm)
0
1
2
3
4
5
6
7
8
9
0
20
40
60
80
100
120
140
10g
20g
30g
50g
70g
10g (second run)
20g (second run)
30g (second run)
50g (second run)
70g (second run)

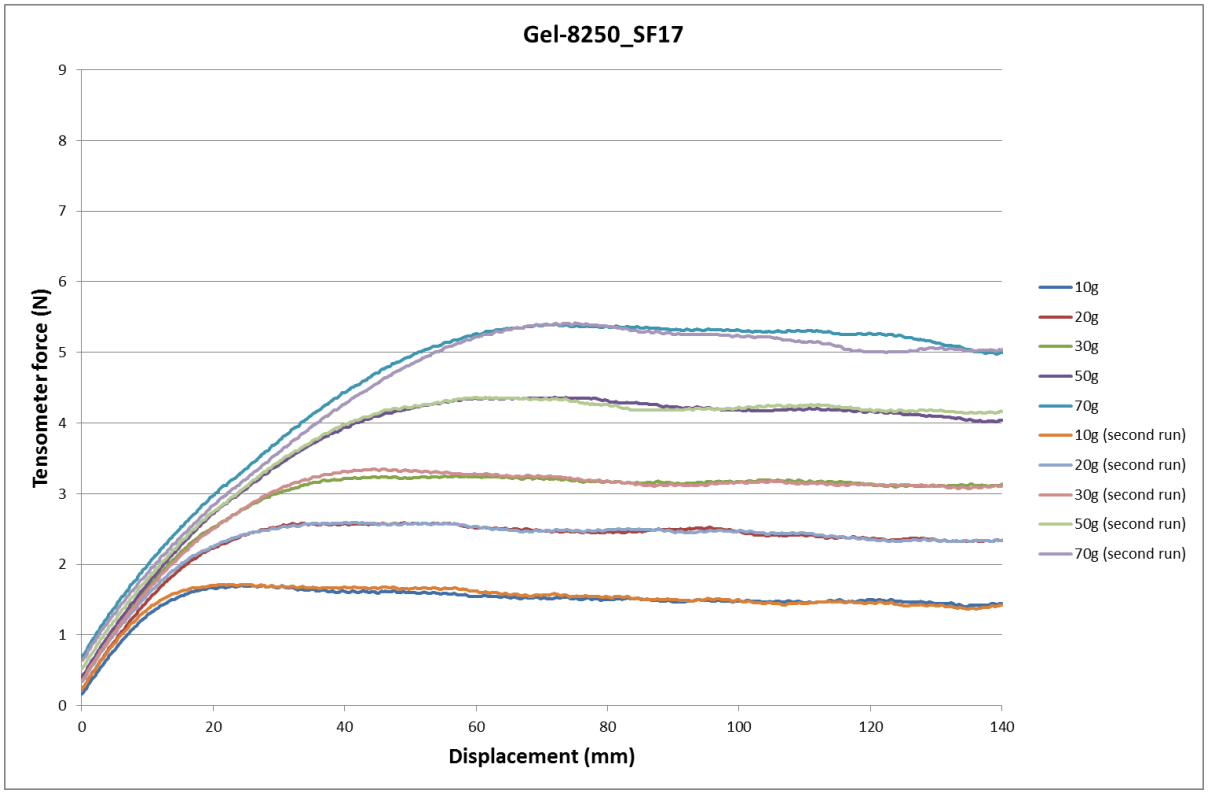
Gel-8250_SF17
Tensometer force (N)
Displacement (mm)
0
1
2
3
4
5
6
7
8
9
0
20
40
60
80
100
120
140
10g
20g
30g
50g
70g
10g (second run)
20g (second run)
30g (second run)
50g (second run)
70g (second run)

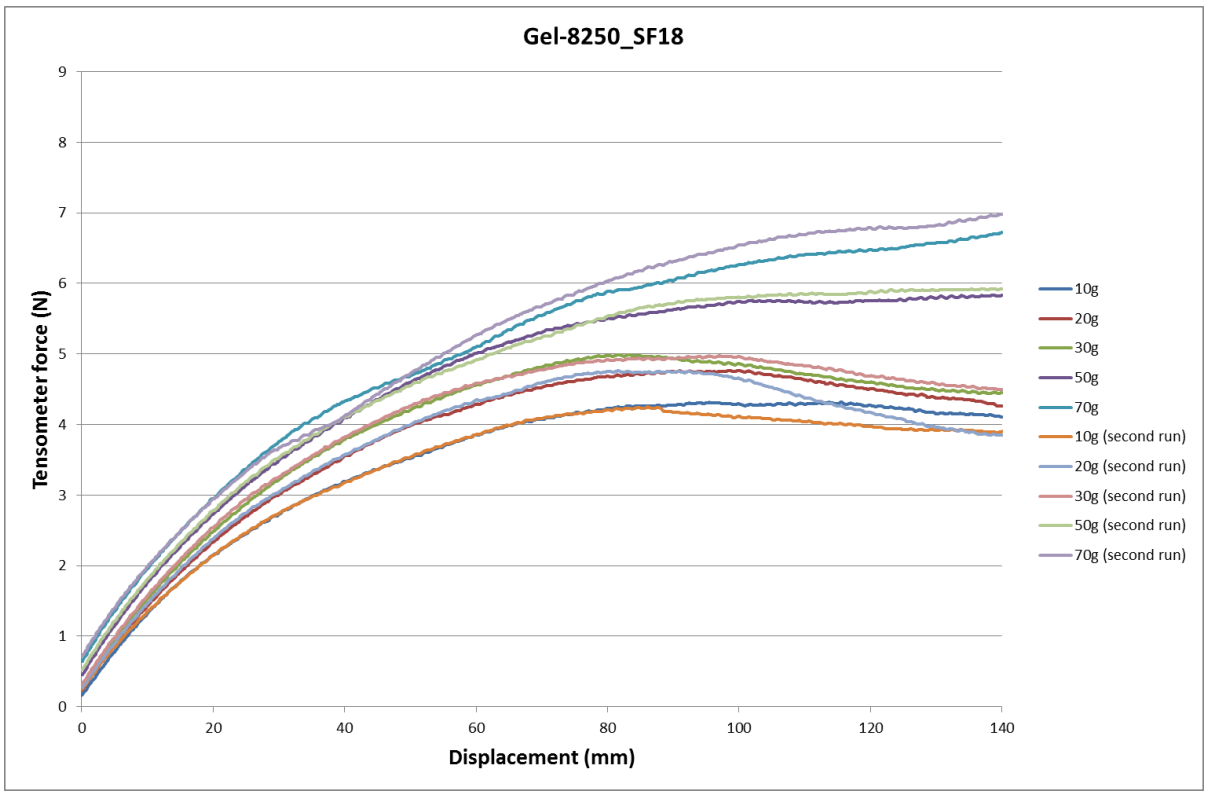
Gel-8250_SF18
Tensometer force (N)
Displacement (mm)
0
1
2
3
4
5
6
7
8
9
0
20
40
60
80
100
120
140
10g
20g
30g
50g
70g
10g (second run)
20g (second run)
30g (second run)
50g (second run)
70g (second run)

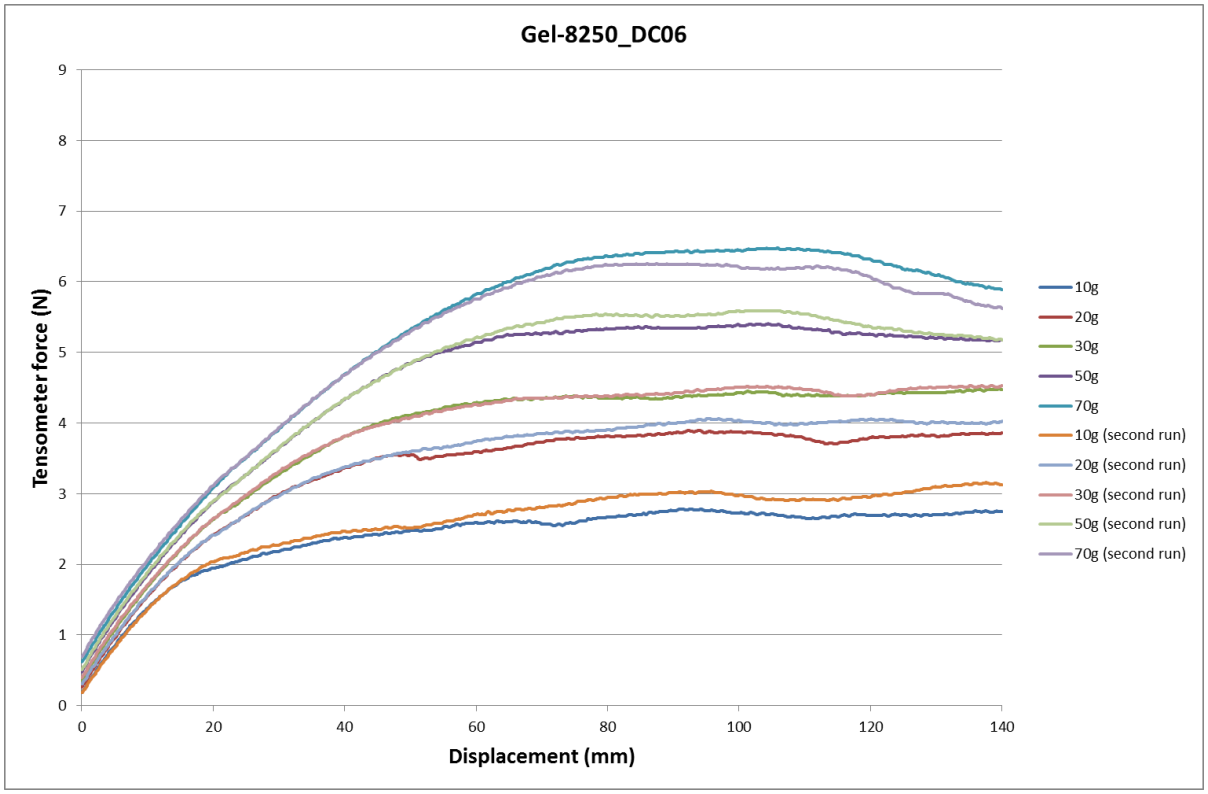
Gel-8250_DC06
Tensometer force (N)
Displacement (mm)
0
1
2
3
4
5
6
7
8
9
0
20
40
60
80
100
120
140
10g
20g
30g
50g
70g
10g (second run)
20g (second run)
30g (second run)
50g (second run)
70g (second run)

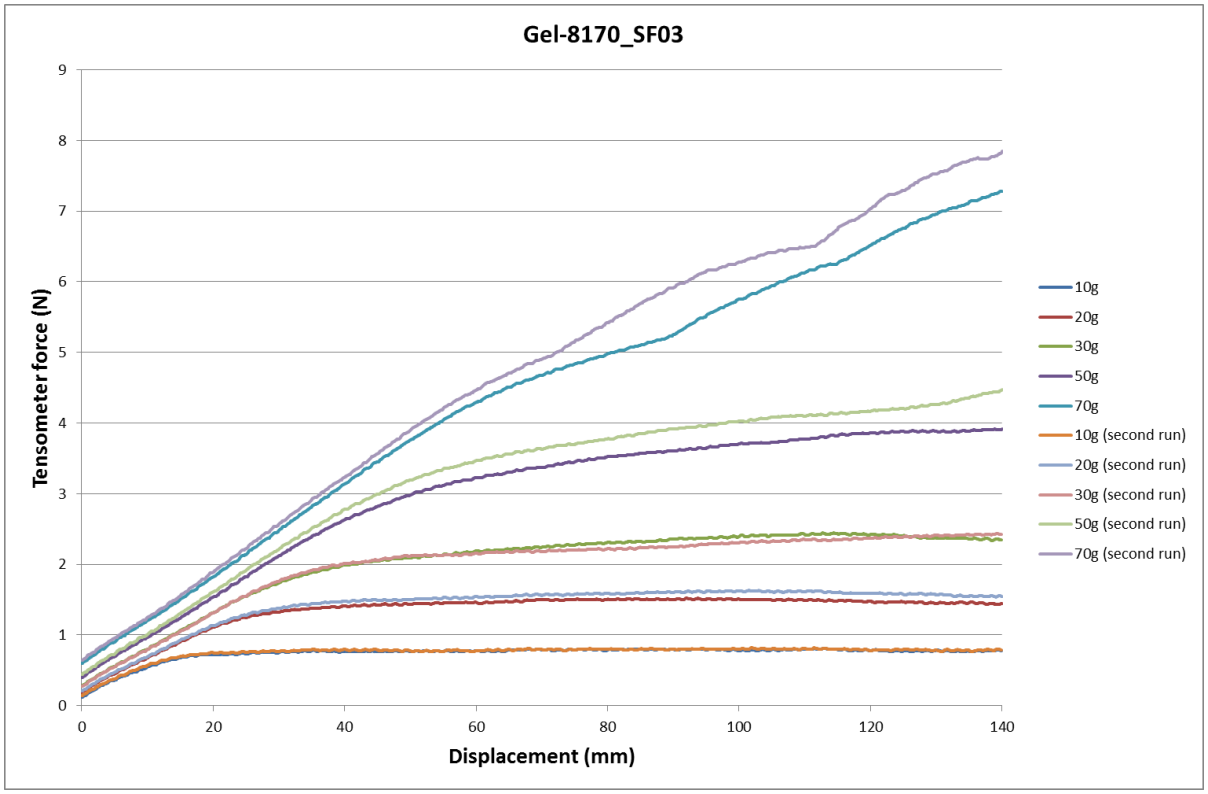
Gel-8170_SF03
Tensometer force (N)
Displacement (mm)
0
1
2
3
4
5
6
7
8
9
0
20
40
60
80
100
120
140
10g
20g
30g
50g
70g
10g (second run)
20g (second run)
30g (second run)
50g (second run)
70g (second run)

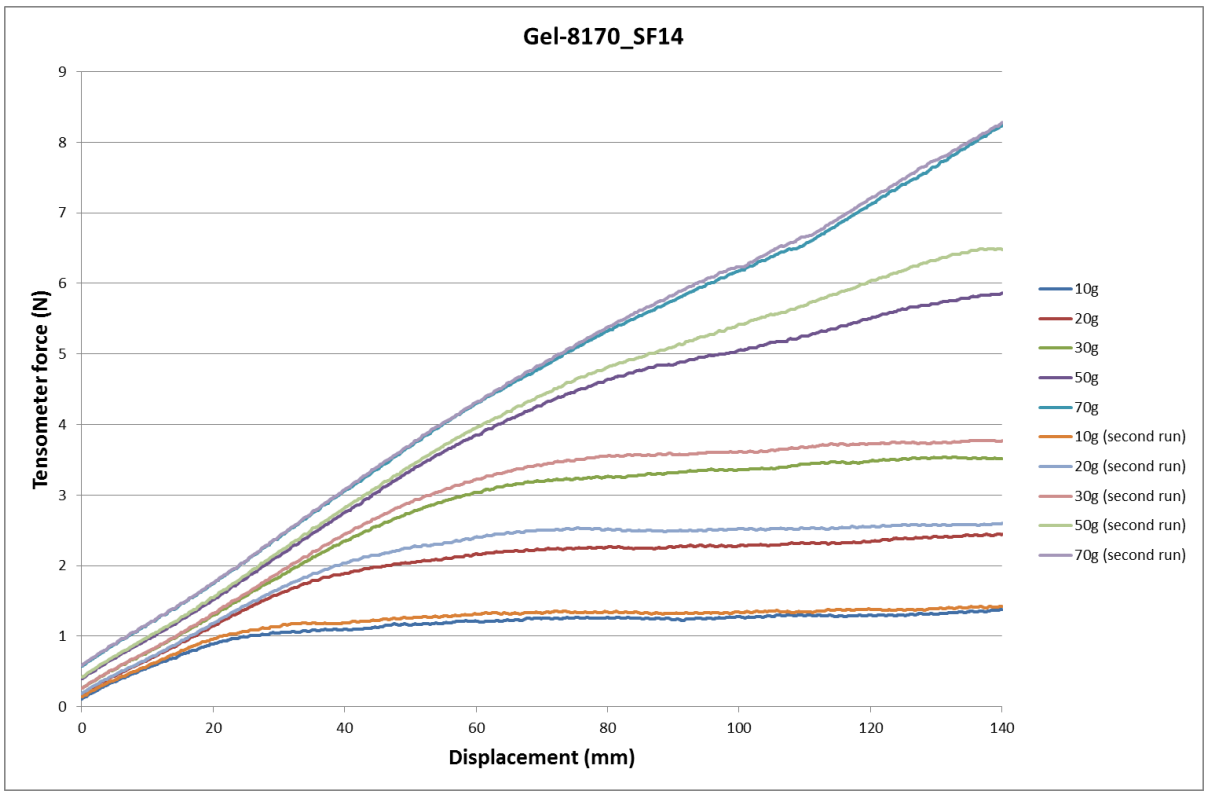
Gel-8170_SF14
Tensometer force (N)
Displacement (mm)
0
1
2
3
4
5
6
7
8
9
0
20
40
60
80
100
120
140
10g
20g
30g
50g
70g
10g (second run)
20g (second run)
30g (second run)
50g (second run)
70g (second run)

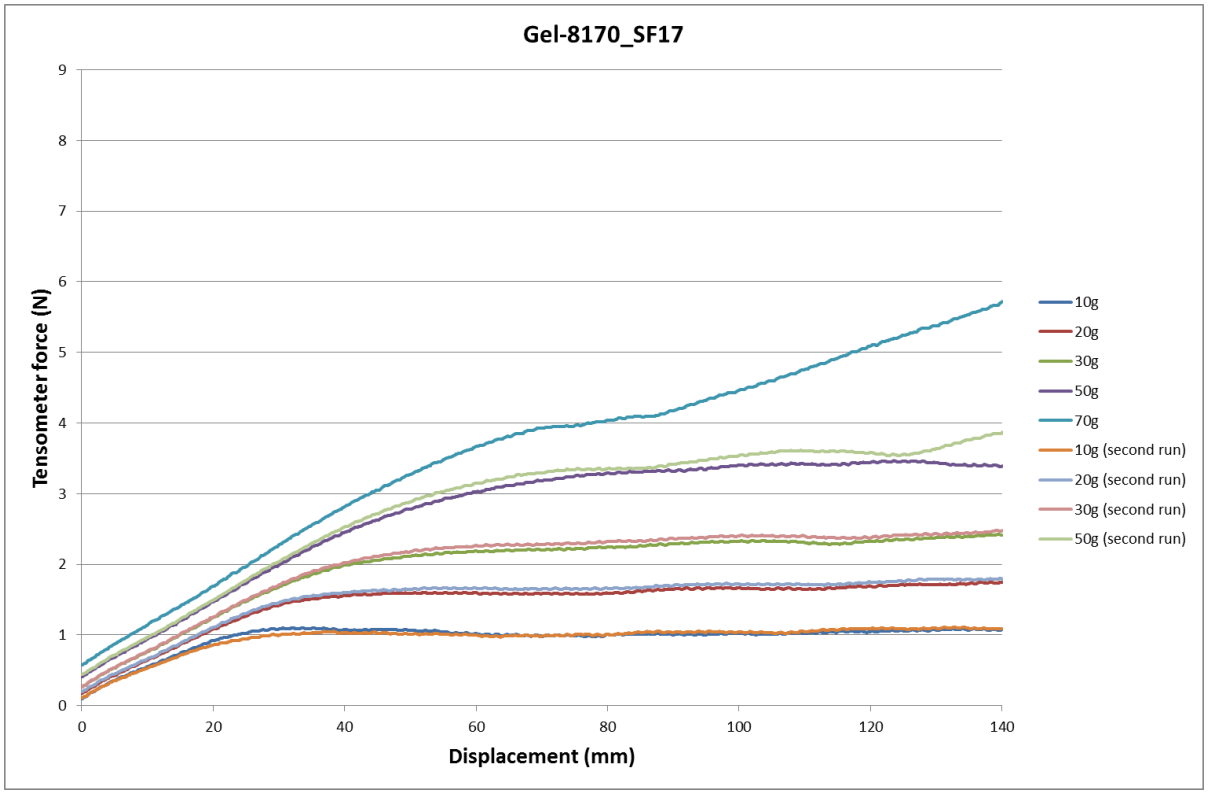
Gel-8170_SF17
Tensometer force (N)
Displacement (mm)
0
1
2
3
4
5
6
7
8
9
0
20
40
60
80
100
120
140
10g
20g
30g
50g
70g
10g (second run)
20g (second run)
30g (second run)
50g (second run)


Gel-8170_SF18
Tensometer force (N)
Displacement (mm)
0
1
2
3
4
5
6
7
8
9
0
20
40
60
80
100
120
140
10g
20g
30g
50g
70g
10g (second run)
20g (second run)
30g (second run)
50g (second run)
70g (second run)

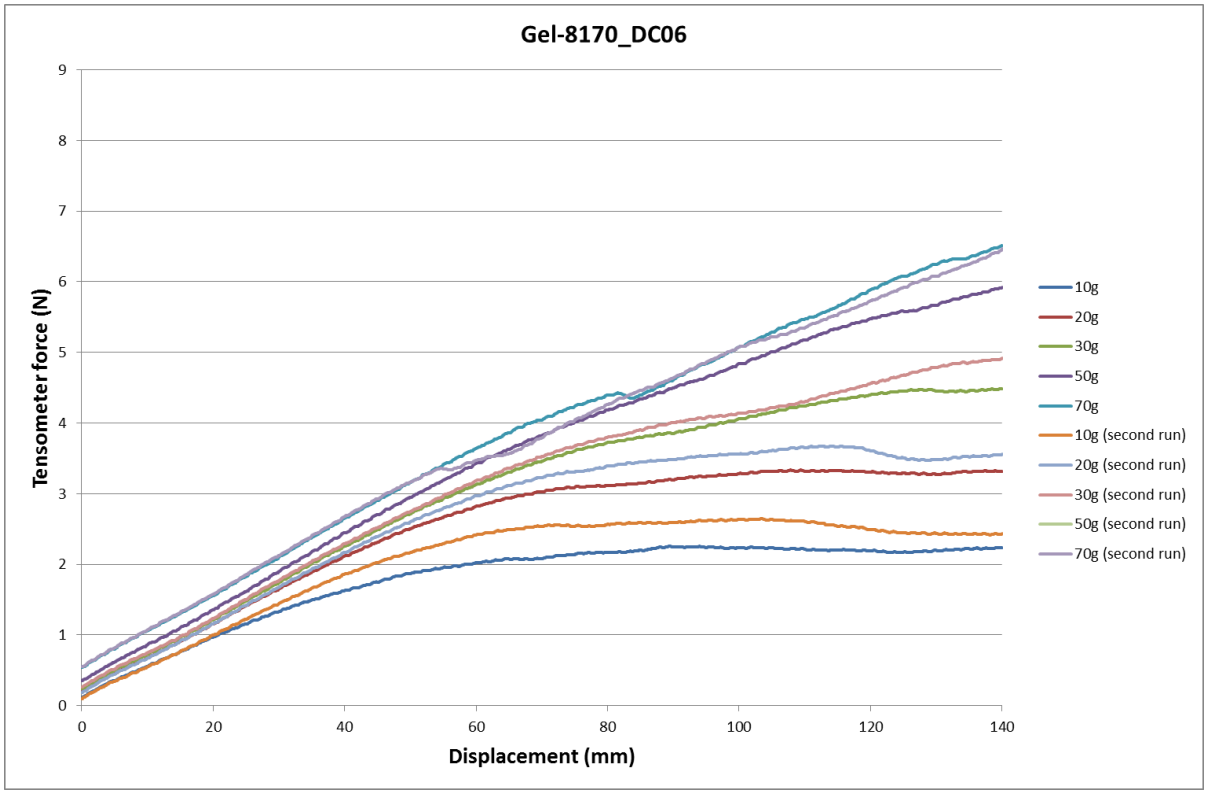
Gel-8170_DC06
Tensometer force (N)
Displacement (mm)
0
1
2
3
4
5
6
7
8
9
0
20
40
60
80
100
120
140
10g
20g
30g
50g
70g
10g (second run)
20g (second run)
30g (second run)
50g (second run)
70g (second run)

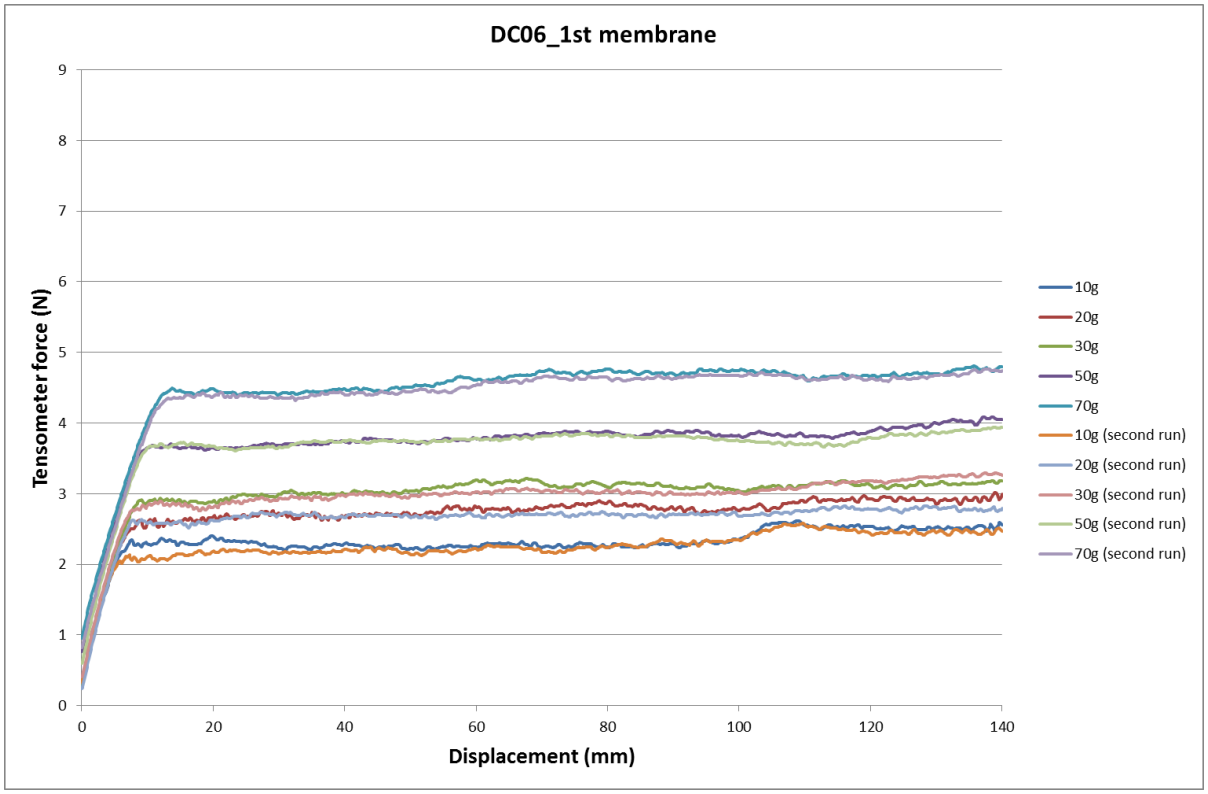
DC06_1st membrane
Tensometer force (N)
Displacement (mm)
0
1
2
3
4
5
6
7
8
9
0
20
40
60
80
100
120
140
10g
20g
30g
50g
70g
10g (second run)
20g (second run)
30g (second run)
50g (second run)
70g (second run)

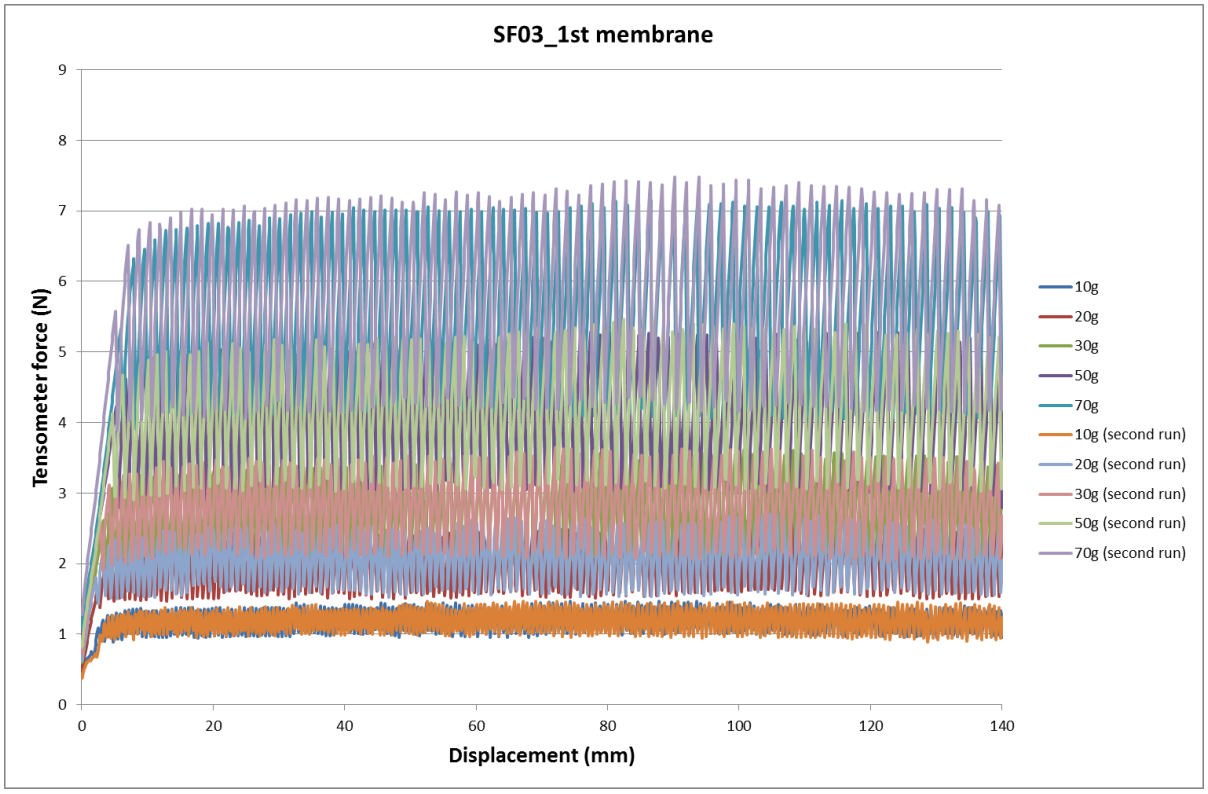
SF03_1st membrane
Tensometer force (N)
Displacement (mm)
0
1
2
3
4
5
6
7
8
9
0
20
40
60
80
100
120
140
10g
20g
30g
50g
70g
10g (second run)
20g (second run)
30g (second run)
50g (second run)
70g (second run)

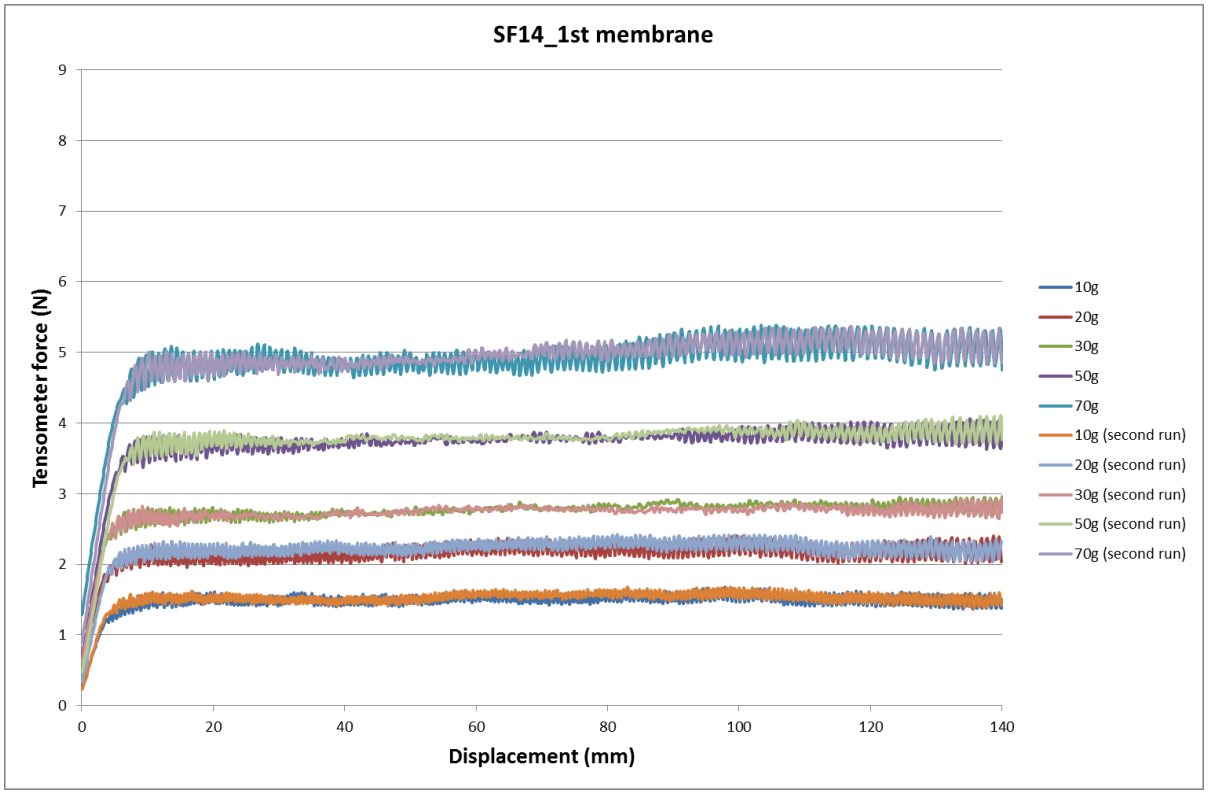
SF14_1st membrane
Tensometer force (N)
Displacement (mm)
0
1
2
3
4
5
6
7
8
9
0
20
40
60
80
100
120
140
10g
20g
30g
50g
70g
10g (second run)
20g (second run)
30g (second run)
50g (second run)
70g (second run)

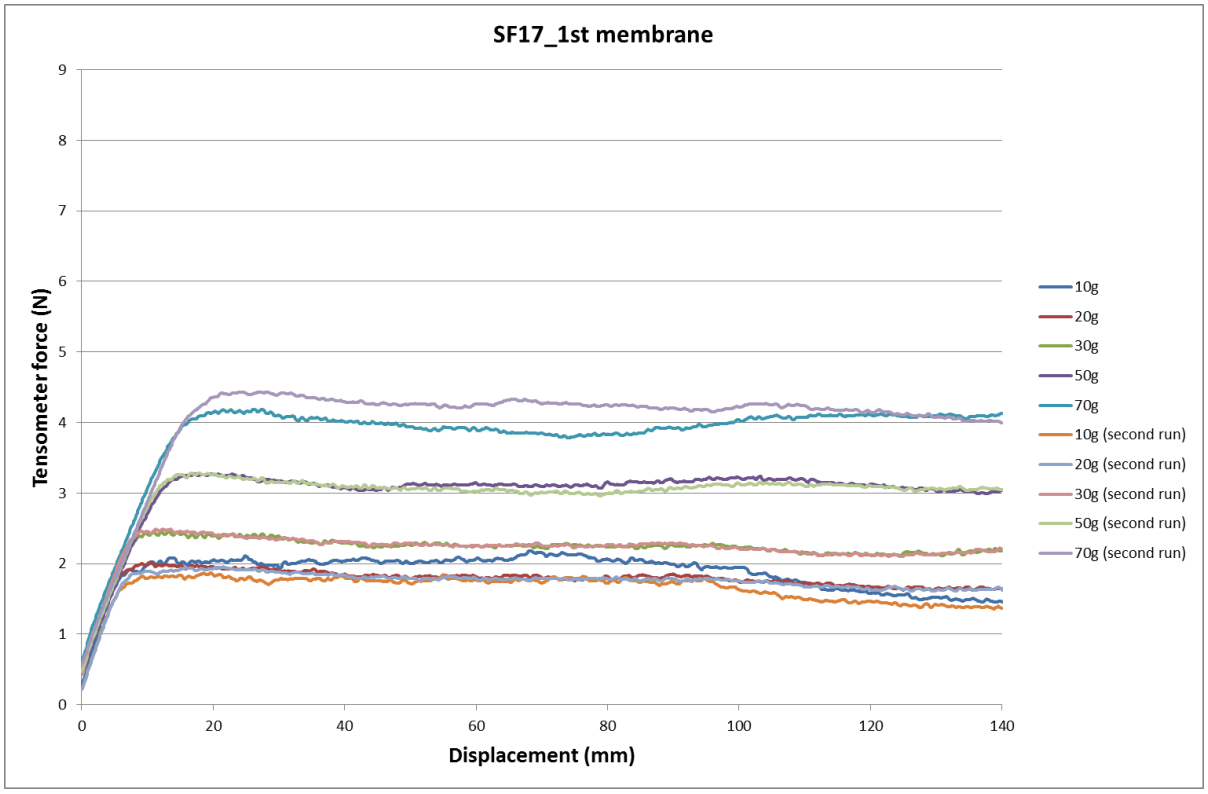
SF17_1st membrane
Tensometer force (N)
Displacement (mm)
0
1
2
3
4
5
6
7
8
9
0
20
40
60
80
100
120
140
10g
20g
30g
50g
70g
10g (second run)
20g (second run)
30g (second run)
50g (second run)
70g (second run)

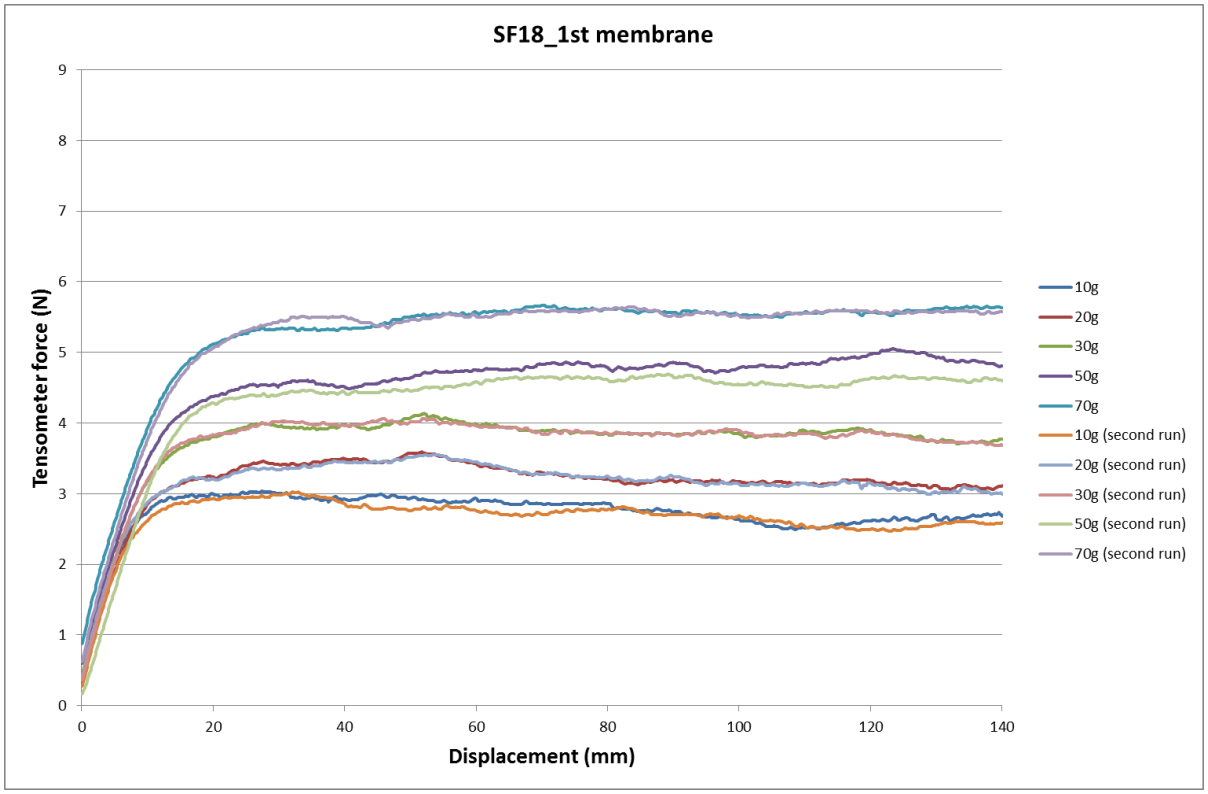
SF18_1st membrane
Tensometer force (N)
Displacement (mm)
0
1
2
3
4
5
6
7
8
9
0
20
40
60
80
100
120
140
10g
20g
30g
50g
70g
10g (second run)
20g (second run)
30g (second run)
50g (second run)
70g (second run)

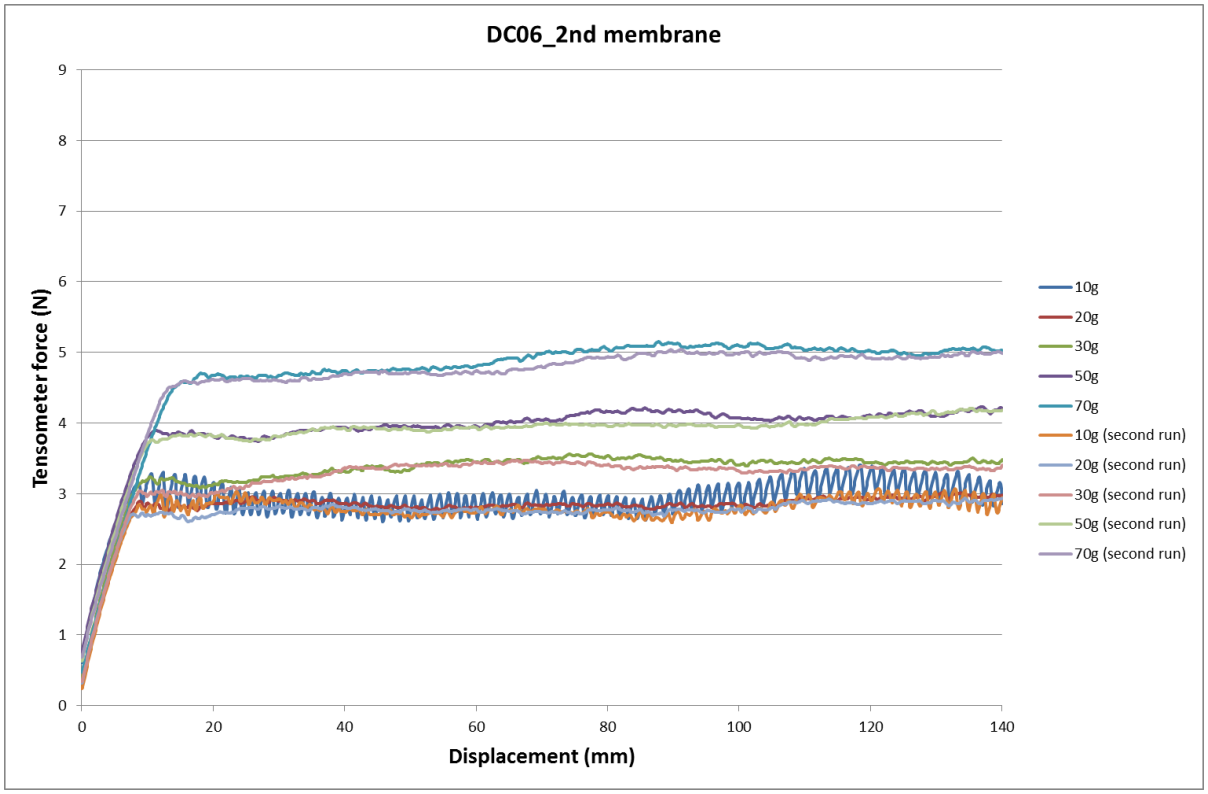
DC06_2nd membrane
Tensometer force (N)
Displacement (mm)
0
1
2
3
4
5
6
7
8
9
0
20
40
60
80
100
120
140
10g
20g
30g
50g
70g
10g (second run)
20g (second run)
30g (second run)
50g (second run)
70g (second run)

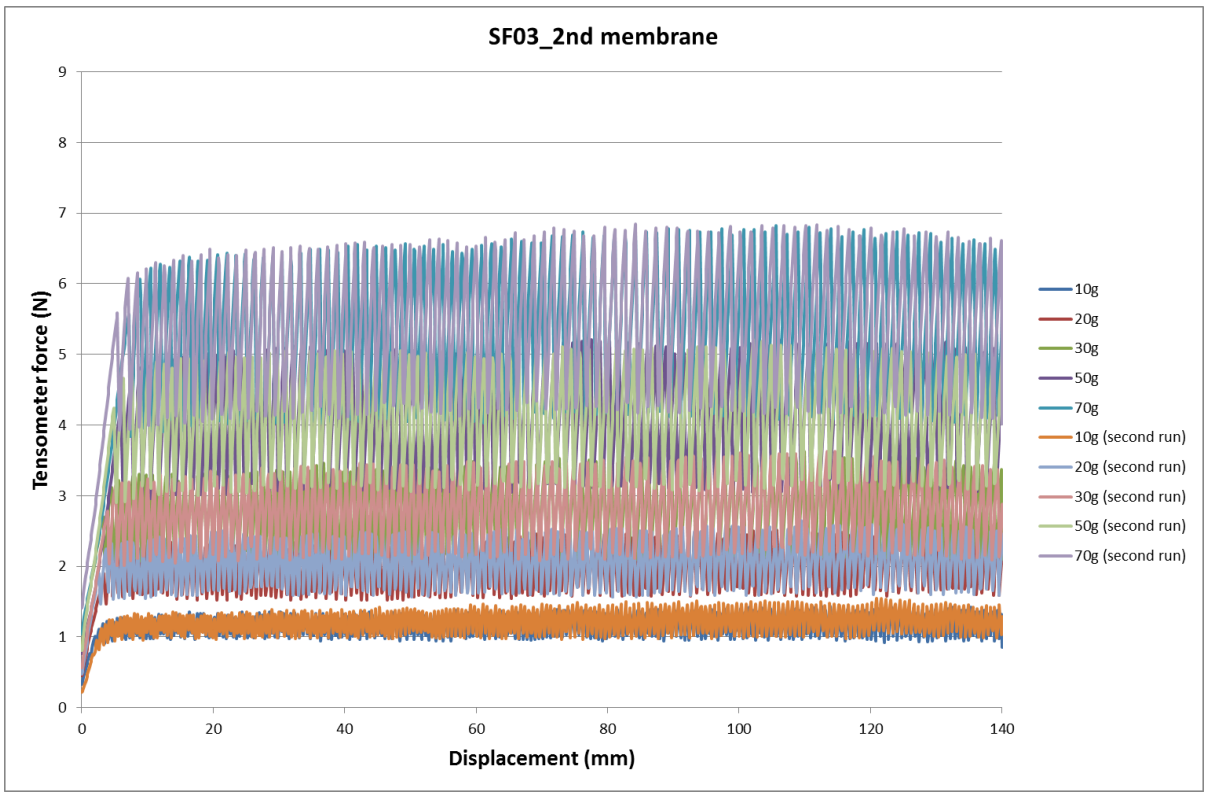
SF03_2nd membrane
Tensometer force (N)
Displacement (mm)
0
1
2
3
4
5
6
7
8
9
0
20
40
60
80
100
120
140
10g
20g
30g
50g
70g
10g (second run)
20g (second run)
30g (second run)
50g (second run)
70g (second run)

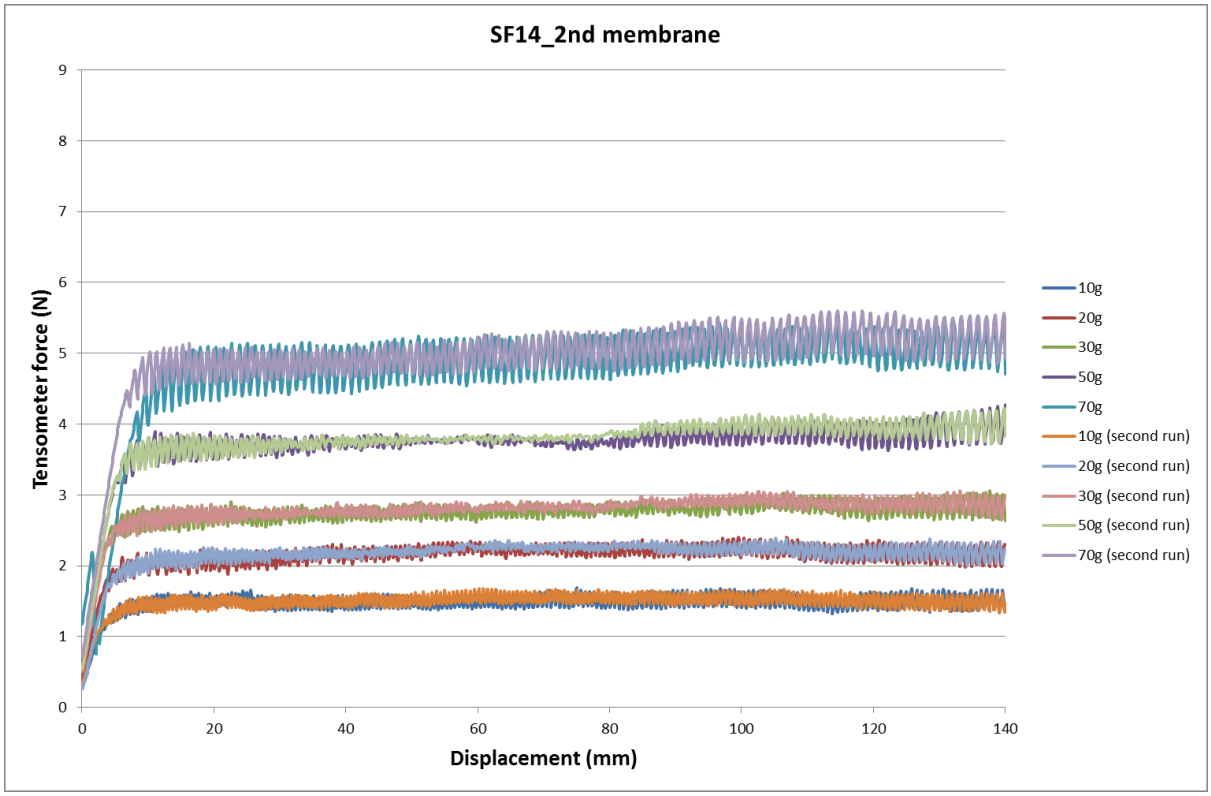
SF14_2nd membrane
Tensometer force (N)
Displacement (mm)
0
1
2
3
4
5
6
7
8
9
0
20
40
60
80
100
120
140
10g
20g
30g
50g
70g
10g (second run)
20g (second run)
30g (second run)
50g (second run)
70g (second run)

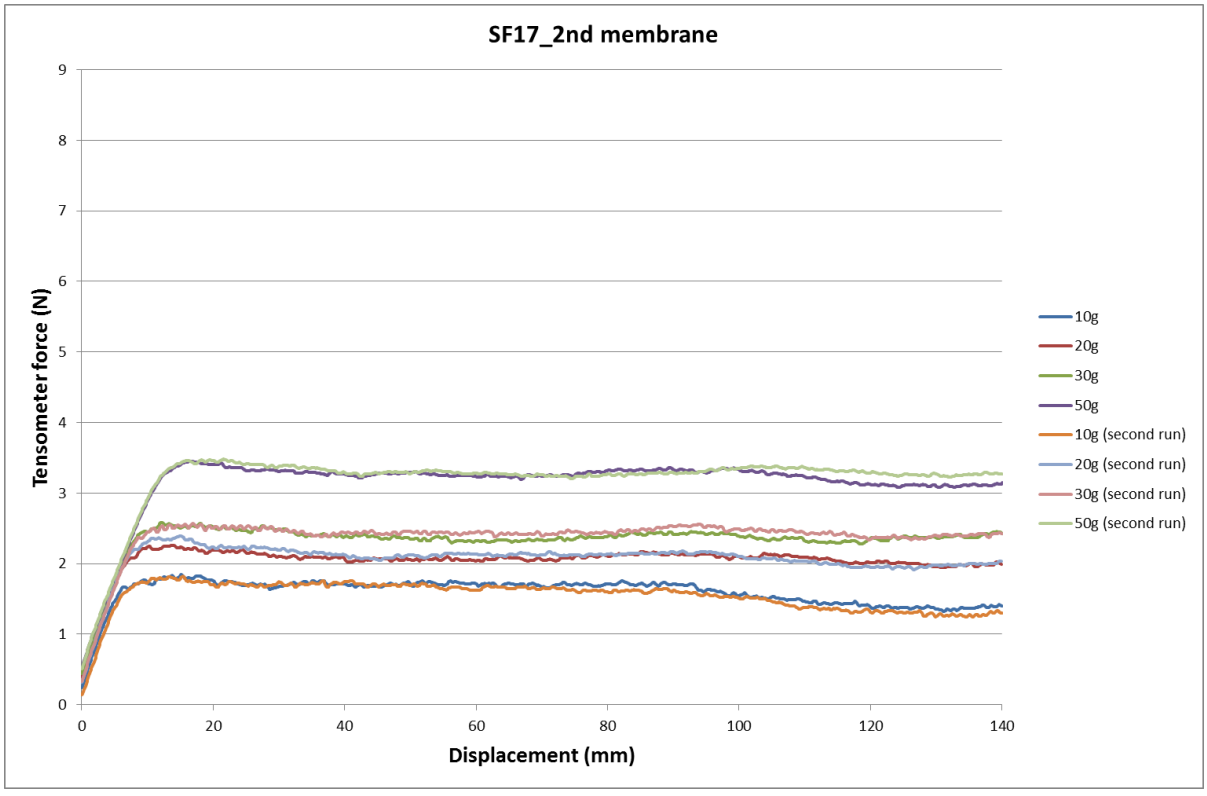
SF17_2nd membrane
Tensometer force (N)
Displacement (mm)
0
1
2
3
4
5
6
7
8
9
0
20
40
60
80
100
120
140
10g
20g
30g
50g
10g (second run)
20g (second run)
30g (second run)
50g (second run)

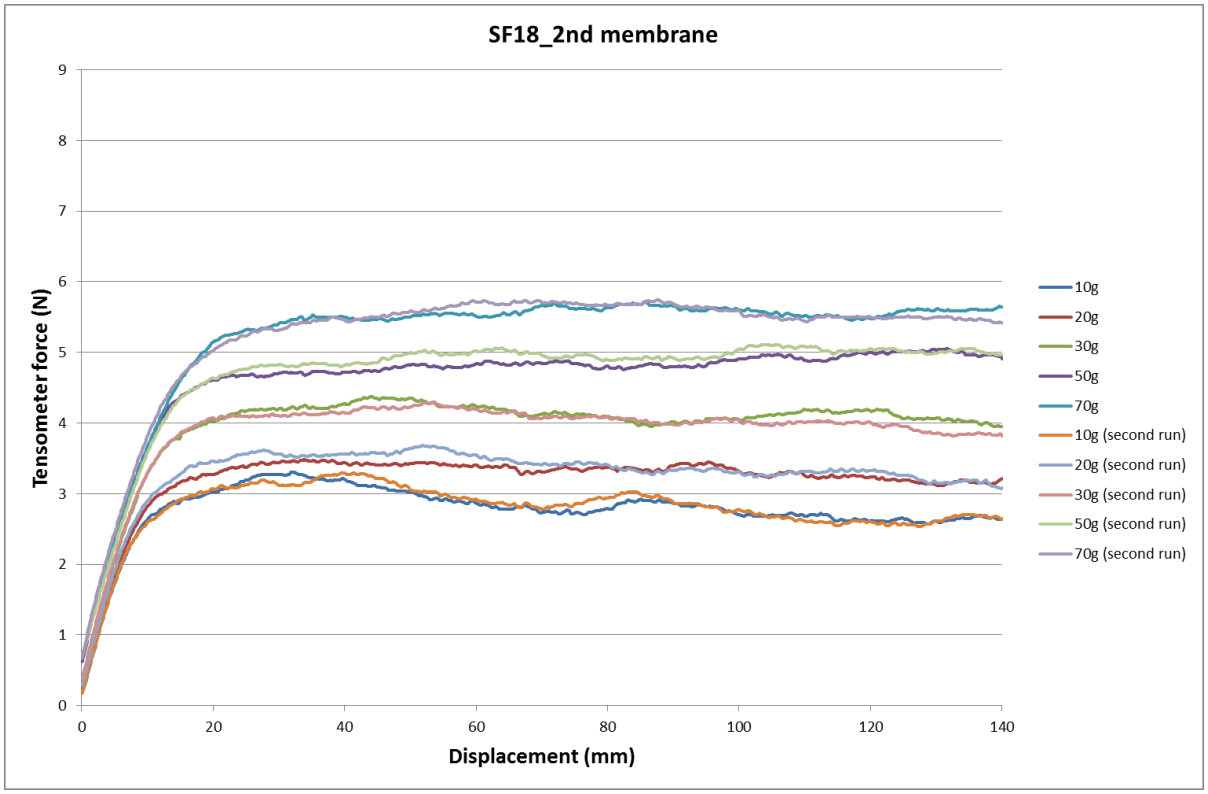
SF18_2nd membrane
Tensometer force (N)
Displacement (mm)
0
1
2
3
4
5
6
7
8
9
0
20
40
60
80
100
120
140
10g
20g
30g
50g
70g
10g (second run)
20g (second run)
30g (second run)
50g (second run)
70g (second run)

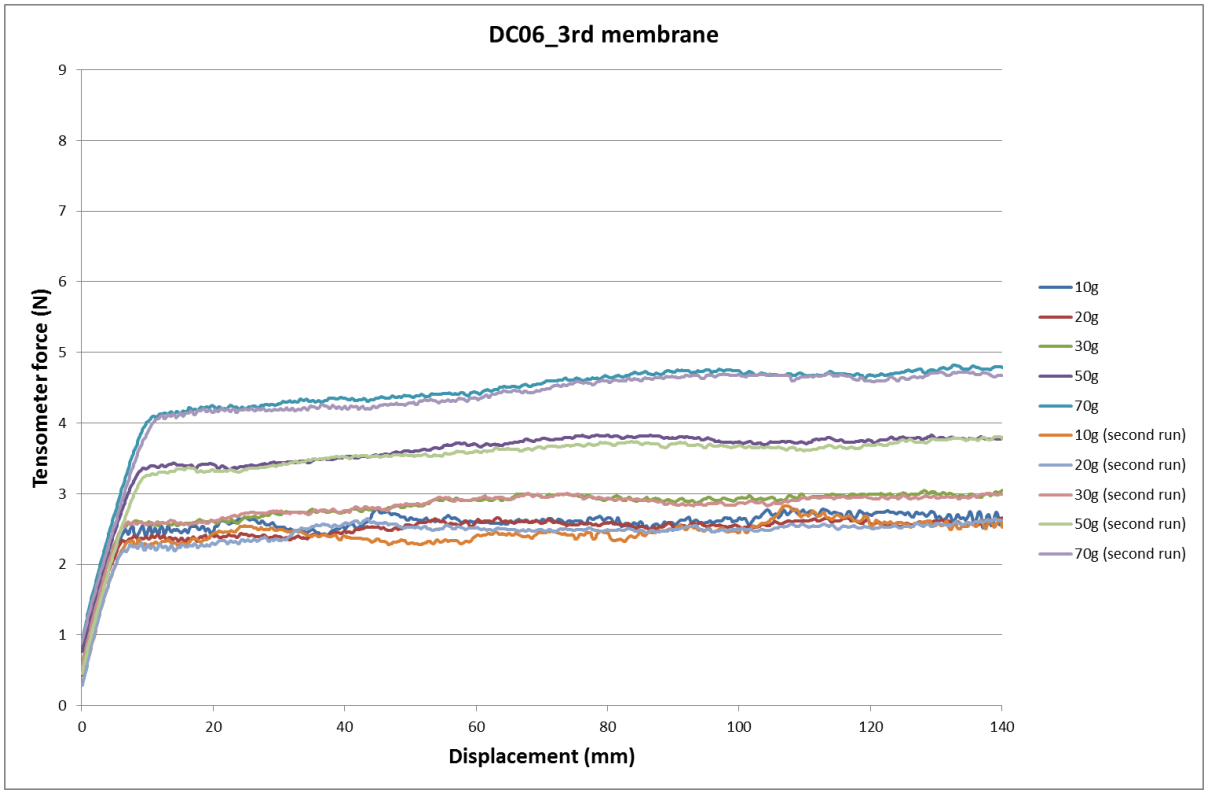
DC06_3rd membrane
Tensometer force (N)
Displacement (mm)
0
1
2
3
4
5
6
7
8
9
0
20
40
60
80
100
120
140
10g
20g
30g
50g
70g
10g (second run)
20g (second run)
30g (second run)
50g (second run)
70g (second run)

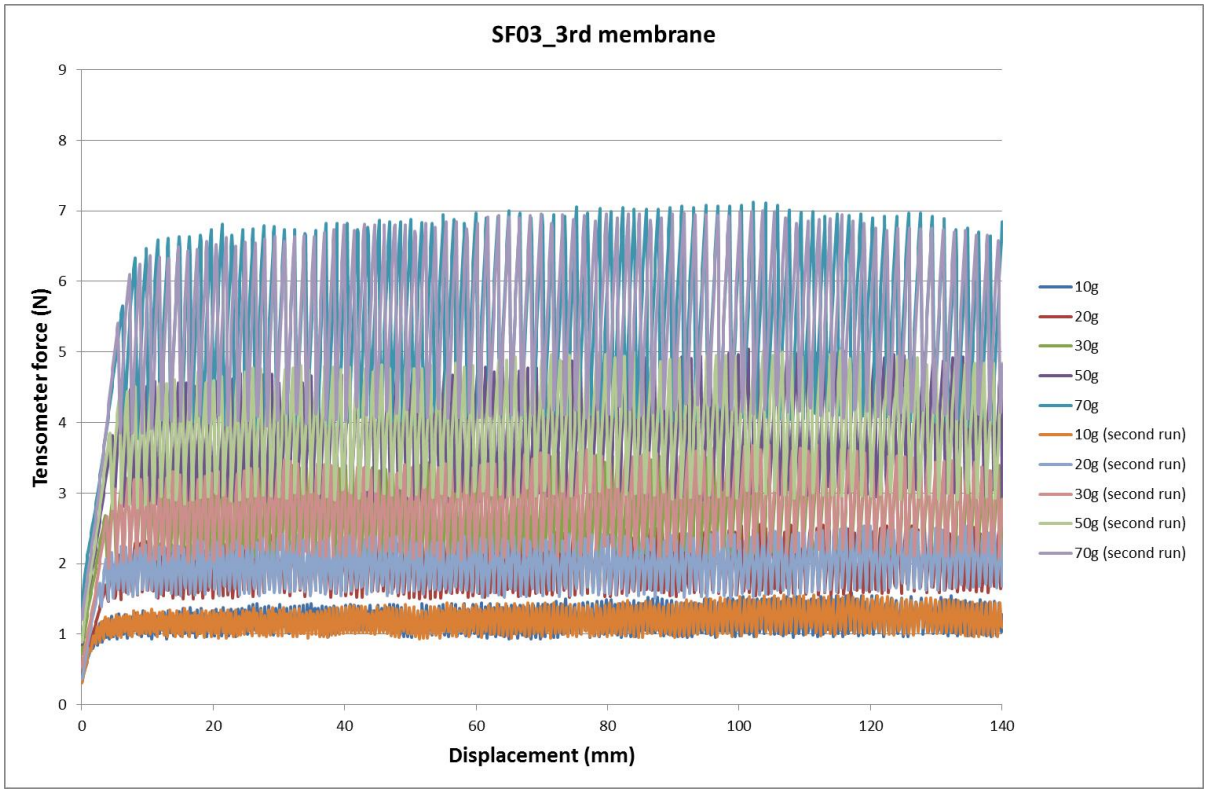
SF03_3rd membrane
Tensometer force (N)
Displacement (mm)
0
1
2
3
4
5
6
7
8
9
0
20
40
60
80
100
120
140
10g
20g
30g
50g
70g
10g (second run)
20g (second run)
30g (second run)
50g (second run)
70g (second run)

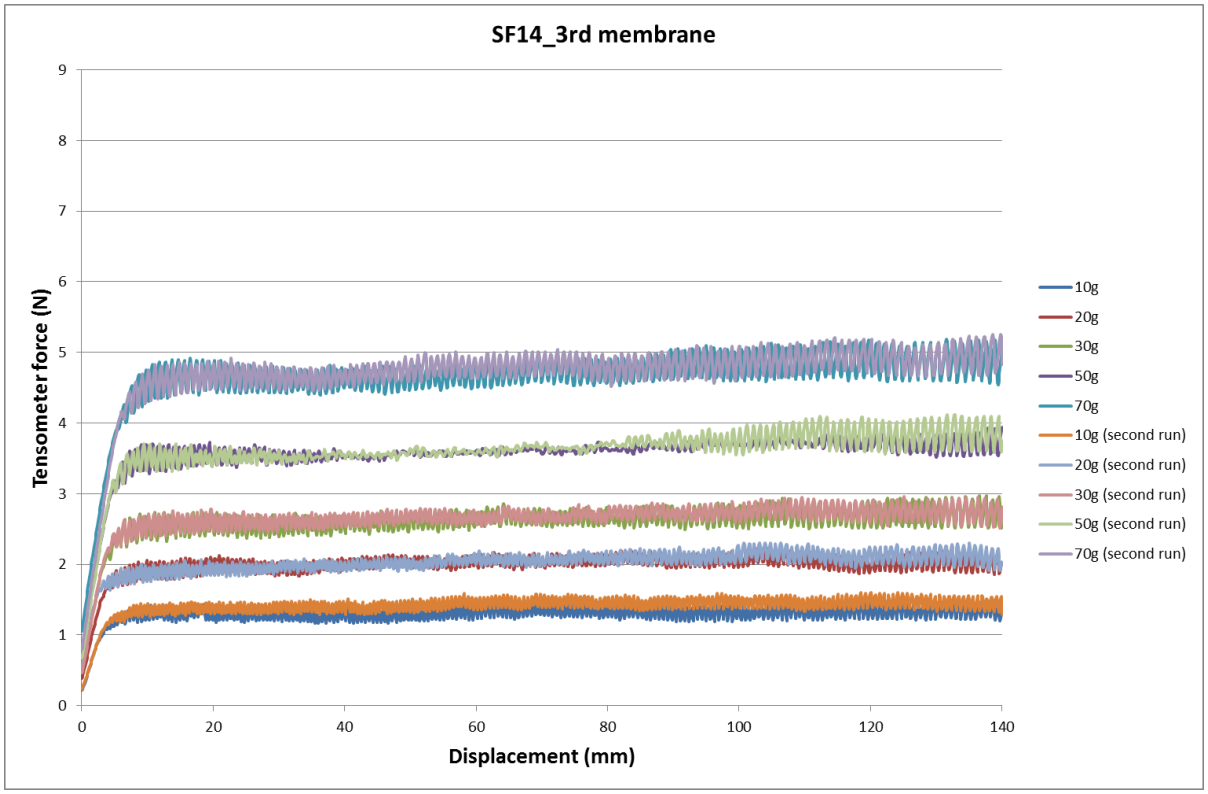
SF14_3rd membrane
Tensometer force (N)
Displacement (mm)
0
1
2
3
4
5
6
7
8
9
0
20
40
60
80
100
120
140
10g
20g
30g
50g
70g
10g (second run)
20g (second run)
30g (second run)
50g (second run)
70g (second run)

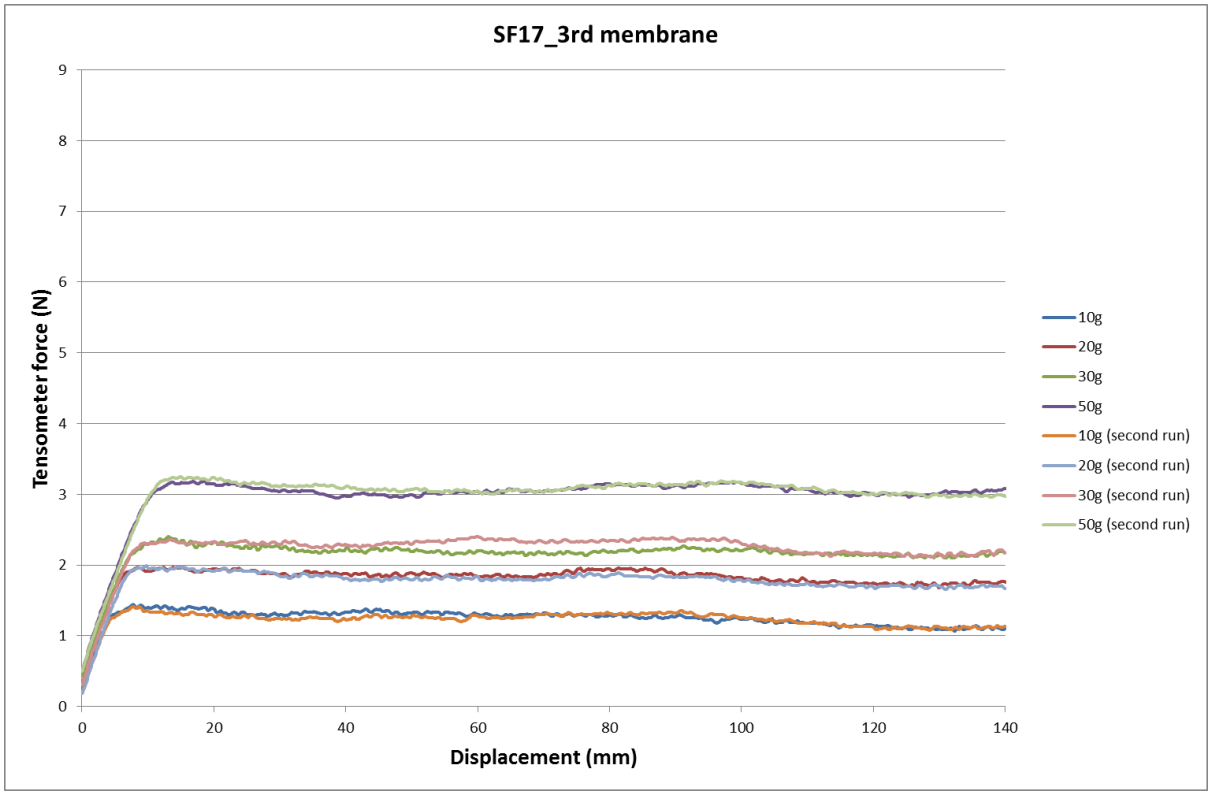
SF17_3rd membrane
Tensometer force (N)
Displacement (mm)
0
1
2
3
4
5
6
7
8
9
0
20
40
60
80
100
120
140
10g
20g
30g
50g
10g (second run)
20g (second run)
30g (second run)
50g (second run)

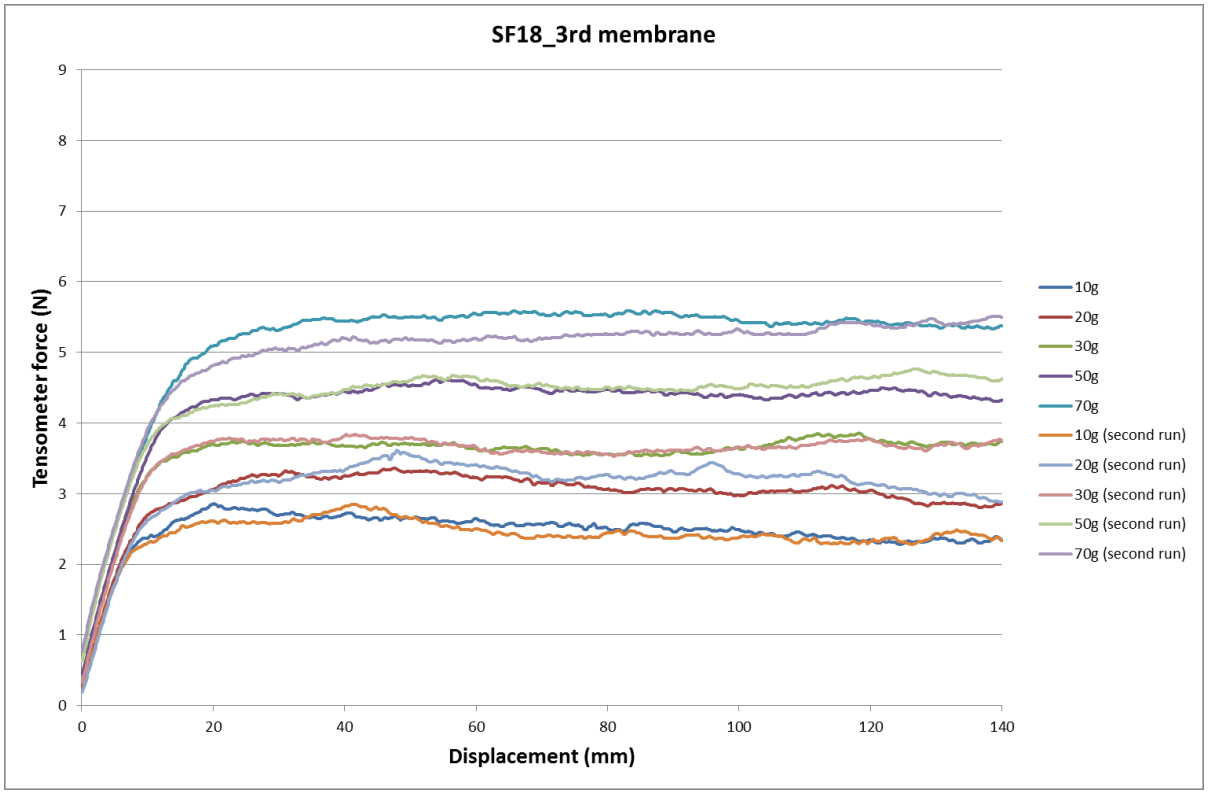
SF18_3rd membrane
Tensometer force (N)
Displacement (mm)
0
1
2
3
4
5
6
7
8
9
0
20
40
60
80
100
120
140
10g
20g
30g
50g
70g
10g (second run)
20g (second run)
30g (second run)
50g (second run)
70g (second run)

Bibliography

Adams, M.J., Briscoe, B.J. and Johnson, S.A. (2007) 'Friction and lubrication of human skin', *Tribology letters*, vol. 26, pp. 239-253.

Altman, D., Lapitan, M.C., Nelson, R., Sillen, U. and Thom, D. (2009) 'Epidemiology of urinary (UI) and feacal (FI) incontinence and pelvic organ prolapse (POP)', in Abrams, P., Cardozo, L., Khoury, S. and Wein, A. *Incontinence*, Paris: Health Publication Ltd.

Amontons, G. (1699) 'De la resistance causée', in Amontons, G. *Les Mémoires de Mathématique et de Physique*, Paris: l'Academie Royale des Sciences.

Asserin, J., Zahouani, H., Houmbert, P., Couturaud, V. and Mougin, D. (1999) 'Measurement of the friction coefficient of the human skin in vivo. Quantification of the cutaneous smoothness', *Colloids and surfaces B*, no. 19, pp. 1-12.

Bertaux, E., Lewandowski, M. and Derler, S. (2007) 'Relationship between friction and tactile properties for woven and knitted fabrics', *Textile research journal*, vol. 77, pp. 387-396.

Bhushan, B. (1999a) 'Solid-solid contact', in Bhushan, B. *Introduction to tribology*, John Wiley and Sons.

Bhushan, B. (1999b) 'Friction', in Bhushan, B. *Principles and applications to triboogy*, John Wiley and Sons.

Charalambous , S. and Triantafilidis, A. (2009) 'Impact of urinary incontinence of quality of life', *Pelviperineology*, pp. 51-53.

Comaish, S. and Bottoms, E. (1971) 'The skin and friction: Deviations from Amonton's laws and the effects of hydration and lubrication', *British Journal of Dermatology*, no. 84, pp. 37-43.

Comaish, J.S., Harborow, P.R.H. and Hofman, D.A. (1973) 'A hand-held friction meter', *British journal of dermatology*, vol. 89, pp. 33-35.

Cottenden, D.J. (2010) *A multiscale analysis of frictional interaction between human skin and nonwoven fabrics*, London: University College London.

Cottenden, D.J. and Cottenden, A.M. (2009) 'An analytical model of the motion of a conformable sheet over a general convex surface in the presence of frictional coupling', *Q. Jl Mech. Appl. Math*, pp. 345-364.

Cottenden, A.M., Cottenden, D.J., Karavokiros, S. and Wong, W.K.R. (2008a) 'Development and experimental validation of a mathematical model for friction between fabrics and a volar forearm phantom', *Journal of engineering in medicine*, vol. 222, pp. 1097-1106.

Cottenden, A.M., Wong, W.K., Cottenden, D.J. and Farbrot, A. (2008b) 'Development and validation of a new method for measuring friction between skin and nonwoven materials', *Proceedings of the Institution of Mechanical Engineers, Part H: Journal of Engineering in Medicine*, pp. 791-803.

Cua, A.B., Wilhelm, K.-P. and Maibach, H.I. (1990) 'Frictional properties of human skin: relation to age, sex and anatomical region, stratum corneum hydration and transepidermal water loss', *British journal of dermatology*, vol. 123, pp. 473-479.

Darden, M.A. and Schwartz, C.J. (2009) 'Investigation of skin tribology and its effects on the tactile attributes of polymer fabrics', *Wear*, vol. 267, pp. 1289-1294.

Derler, S., Gerhardt, L.-C., A. Lenz, E.B. and Haddad, M. (2009b) 'Friction of human skin against smooth and rough glass as a function of the contact pressure', *Tribology international*, vol. 42, pp. 1565-1574.

Derler, S., Huber, R., Feuz, H.-P. and Hadad, M. (2009a) 'Influence of surface microstructure on the sliding friction of plantar skin against hard substrates', *Wear*, no. 267, pp. 1281-1288.

Derler, S., Schrade, U. and Gerhardt, L.-C. (2007) 'Tribology of human skin and mechanical skin equivalents in contact with textiles', *Wear*, vol. 263, pp. 1112-1116.

Diane Kaschak Newman, A.J.W. (2002) *Managing and Treating Urinary Incontinence.*, Baltimore: Springer-Verlag.

Egawa, M., Oguri, M., Hirao, T., Takahashi, M. and Miyakawa, M. (2002) 'The evaluation of skin friction using a frictional feel analyzer', *Skin research and technology*, no. 8, pp. 41-51.

Elkyat, A., Courderot-Masuyer, C., Gharbi, T. and Humbert, P. (2004) 'Influence of the hydrohobic and hydrophilic characteristics of sliding and slider surfaces on friction coefficient: in vivo human skin friction comparison', *Skin research and technology*, vol. 10, pp. 215-221.

Gere, J.M. (2004) *Mechanics of materials*, Belmont, California: Thomson - Brooks/Cole.

Gerhardt, L.-C., Lottenbach, R., Rossi, R.M. and Derler, S. (2013) 'Tribological investigation of a functional medical textile with lubricating drug-delivery finishing', *Colloids and surfaces B: Biointerfaces*, pp. 103-109.

Gerhardt, L.-C., Strassle, V., Lenz, A., Spencer, N.D. and Derler, S. (2008) 'Influence of epidermal hydration on the friction of human skin against textile', *Journal of the royal society interface*, vol. 5, pp. 1317-1328.

Gray, M., Bliss, D.Z., Doughty, D.B., Ermer-Seltun, J., Kennedy-Evans, K.L. and Palmer, M.H. (2007) 'Incontinence-associated dermatitis, a consencus', *J Wound Ostomy Continence Nurs*, pp. 45-54.

Gwosdow A. R., S.A.C..B.L.G..S.J.A.J. (1986) 'Skin friction and fabric sensationin neutral and warm environments', *Textile Research Journal*, vol. 56, pp. 544-550.

Gwosdow, A.R., Stevens, J.C., Berglund, L.G. and Stolwijk, J.A.J. (1986) 'Skin friction and fabric sensations in neutral and warm environments', *Textile research institute*, vol. 56, pp. 574-580.

Hendriks, C.P. and Franklin, S.E. (2010) 'Influence of surface roughness, material and climate conditions on the friction human skin', *Tribology letters*, vol. 37, pp. 361-373.

Hills, R.J., Unsworth, A. and Ive, F.A. (1994) 'A comparative study of the frictional properties of emollient bath additives using porcine skin', *British journal of dermatology*, vol. 130, pp. 37-41.

Hong, K.H., Kim, S.C. and Kang, T.J. (2005) 'Effect of abrasion and absorbed water on the handle of nonwovens for disposable diapers', *Textile research journal*, no. 75, pp. 544-550.

Karavokiros, S. (2007) *Skin friction: validating a mathematical model with a simple laboratory model*, London: University College London.

Kenins, P. (1994) 'Influence of fiber type and moisture and measured fabric to skin friction', *Textile research journal*, vol. 64, pp. 722-728.

Kondo, S. (2002) 'Part 1: Factors of human skin characteristics affecting the frictional properties between fabrics and the human skin.', *Journal of the Japan Research Association for Textile End-Uses*, pp. 264-275.

Koudine, A.A. and Barquins, M. (2000) 'Frictional properties of skin: proposal of a new approach', *International Journal of Cosmetic Medicine*, vol. 22, pp. 11-20.

Kwiatkowska, M., Franklin, S.E., Hendriks, C.P. and Kwiatkowski, K. (2009) 'Friction and deformation behaviour of human skin', *Wear*, vol. 267, pp. 1264-1273.

Lima, M., Vasconcelos, R.M., Abreu, M.J. and Silva, M.E.C. (2008) 'Comparative study of friction coefficient in nonwovens applied for non active medical devices', *Tekstil ve Konfeksiyon*, vol. 18, pp. 258-262.

Li, W., Pang, Q., Jiang, Y., Zhai, Z. and Zhou, Z. (2012) 'Study of physiological parameters and comfort sensations during friction contactsof the human skin', *Tribology letters*, pp. 12-23.

Nakajima, K. and Narasaka, H. (1993) 'Evaluation of skin surface associated with morphology and coefficient of friction', *International journal of cosmetic science*, vol. 15, pp. 135-151.

Naylor, P.F.D. (1955) 'The skin surface and friction', *The british journal of dermatology*, vol. 67, pp. 239-248.

Pailler-Mattei, C., Pavan, S., Vargioglu, R., Pirot, F., Falson, F. and Zahouani, H. (2007) 'Contribution of stratum corneum in determining bio-tribological properties of the human skin', *Wear*, no. 263, pp. 1038-1043.

Ramahlo, A., Szekeres, P. and Fernandes, E. (2013) 'Friction and tactile perception of textile fabrics', *Tribology international*, pp. 29-33.

Ramkumar, S.S., Umrani, A.S., Shelly, D.C., Tock, R.W., Parameswaran, S. and Smith, M.L. (2004) 'Study of the effect of sliding velocity on the frictional properties of nonwoven fabric substrates', *Wear*, no. 256, pp. 221-225.

Shao, F., Childs, T.H.C. and Henson, B. (2009) 'Developing an artifician fingertip with human friction properties', *Tribology international*, vol. 42, pp. 1575-1581.

Shigley, J.E. (1956) 'Clutches, brakes and couplings', in Shigley, J.E. *Machine design*, McGraw Hill book company.

Sivamani, R.K., Goodman, J., Gitis, N.V. and Maibach, H.I. (2003) 'Friction coefficient of skin in real-time', *Skin Research and Technology*, no. 9, pp. 235-239.

Sulzberger, M.B., Cortese, T.A., Fishman, L. and Willey, H.S. (1966) 'Studies on blisters produced by friction', *The journal of investigative dermatology*, vol. 47, pp. 456-465.

Tang, W., Ge, S.-r., Zhu, H., Cao, X.-c. and Li, N. (2008) 'The influence of normal load and sliding speed on frictional properties of skin', *Journal of bionic engineering 5*, no. 5, pp. 33-38.

Thibodeau, G.A. and Patton, K.T. (2000) 'Structure and function of the body', in Gary A. Thibodeau, K.T.P. *Structure and function of the body*, St Louis, Misouri: Mosby.

Veijgen, N.K., Masen, M.A. and Heide, E.v.d. (2012) 'A noven approach for measuring the frictional behaviour of human skin in vivo', *Tribology international*, pp. 38-41.

Veijgen, N.K., Masen, M.A. and Heide, E.v.d. (2013) 'Relating friction on the human skin to the hydration and temperature of the skin', *Tribology letters*, pp. 251-262.

Wong, W.K.R. (2008) 'A study of evaporation and friction on hydrated forearm skin', *PhD Thesis*.

Zhang, M. and Mak, A.F.T. (1999) 'In vivo friction properties of human skin', *Prosthetics and orthotics international*, vol. 1999, pp. 135-141.